DOCTOR OF PHILOSOPHY

Sedimentary processes in the Dwyryd estuary.

Mahamod, Yusuff

Award date:
1989

Awarding institution:
Bangor University

SEDIMENTARY PROCESSES IN THE DWYRYD ESTUARY

By

Yusuff Mahamod

A thesis submitted in accordance with the requirements of the University of Wales for the degree of Doctor of Philosophy.

School of Ocean Sciences

University College of North Wales

Menai Bridge

Gwynedd, WALES.

April 1989

To my wife Kamaliah, daughter Marina, and son Imran.

CONTENTS

ACKNOWLEDGEMENTS

I would like to thank Dr. C.F.Jago, for his enduring patience, advice and constructive critism throughout the period of my study.

I also would like to thank many students, technical and academic staffs of the School of Ocean Sciences for the help and assistance which they have given me during field expeditions.

I would like to acknowledge the provision of the basic equipment and facilities of the School of Ocean Sciences, UCNW, Bangor: in particular, the co-operation of A.Nield, D.Boon, G.Williams, and J.Moore.

I wish to acknowledge the financial support of the Government of the Malaysia (PSD and USM), which enabled me to carry out and complete my study.

ABSTRACT

This study aims to describe and quantify the important sedimentary processes which control the dispersal and accumulation of sediment in the Dwyryd Estuary, adjacent to Tremadog Bay in West Wales. It is shown that sedimentation in the estuary is dominantly control by fast tidal currents, and in the bay by weak tidal currents. Landward transport of coastal sediments by tidal currents is the residual sediment transport path. The spatial distribution of textural parameters of the estuarine sediments is related to the strength of tidal currents as well as the morphology and bathymetry of the study area.

The estuarine sediments, predominantly sand, are very similar in texture and mineralogy to the adjacent beach sediments but markedly different to the river sediments. However, the beach sediments are slightly coarser and more poorly sorted than the estuarine sediments. In contrast, sediment in the deeper parts of Tremadog Bay are finer than both the estuarine and beach sediments due to the presence of substantial admixture of mud. The grain size distributions of most of the sediments are neither log-normal nor log-hyperbolic reflecting the great variability of hydrodynamic conditions in the study area.

Using previously published flume data, a new sediment transport rate formula in the form of a power law has been developed for computation of total sediment load from the bed mean grain size and flow parameters:

$$q \propto \left(\frac{U - U_c}{U_c}\right)^n$$

The exponent n varies from 2.7 (for 0.93 mm sand) to 4.18 (for 0.19 mm sand). This is in contrast to the Bagnold (1966) formula which regards the exponent value (equal to 3) as constant for all grain sizes.

Sediment transport patterns depend on the asymmetry between flood and ebb tidal currents due to distortion of the tidal wave on entering the estuary. Estimates of sediment budgets from surveyed profiles suggest that large amounts of sand have been transported from coastal areas into the estuary, supporting the mineralogical evidence. The estimates are of the same order of magnitude as estimates using flow velocity data and the above sediment transport formula.

ONE

INTRODUCTION: A REVIEW AND THE AIM OF THE INVESTIGATION

1.1 Introduction

The word estuary comes from the Latin 'aestu' meaning tide. By common usage, it means a place where a river meets the sea. Estuaries constitute interface systems between rivers and ocean, often characterised by complex water masses, changing salinity, large seasonal variations, and by high sediment loads. A widely used definition is given by Pritchard (1952) which defines an estuary as 'a semi-enclosed coastal body of water which has a free connection with the open sea and within which sea water is measurably diluted with fresh water derived from land drainage'.

This definition attempts to define an estuary as an environment in which the fresh water dilutes the sea water and causes the formation of the density gradients which drive the familiar estuarine flow patterns. The weakness of this definition is that it emphasises the dilution of sea water rather than the dynamic influence of the tidal flow in an estuary. Another weakness with this definition

is that there are many estuaries in Texas and Western Australia in which the salinity of estuarine water exceeds that of sea water due to high water evaporation and low river discharge (Fisk,1959; Hedgpeth,1963).

An alternative definition is given by Fairbridge (1980) which defines an estuary as 'an inlet of the sea reaching into a river valley as far as the upper limit of tidal rise'. This definition differs from that given by Pritchard in taking the tidal influence rather than the presence of sea water as defining the upper limit of an estuary.

An estuary is a distinct sedimentary environment which functions either to trap sediment or to convey sediment from the land and the sea.Estuaries are among the most dynamically active of all coastal marine environments. The morphology of an estuary is continuously changing due to mobility of its sediment as can be seen from active movement of its bedforms. It is thought that estuaries will ultimately be filled with sediment and disappear, and as a consequence fluvial material will be discharged directly to the sea (Schubel and Meade,1977). An estuary is regarded as stable when sediment input is balanced by sediment output.

Estuarine morphology depends essentially on the long term average sediment supply from various sources and the direction and magnitude of the long term averaged sediment

transport. Abrupt changes in estuarine morphology may also be caused by storm surges or by engineering works (Dronkers,1986).

Sedimentary processes,such as erosion , transportation , deposition and consolidation of deposits are active in estuaries and create distinctive morphologic and sedimentary features. By studying the texture and morphology of the deposits, sedimentary processes operative in this environment can be understood. Such an understanding is very important in any effort to solve practical problems since estuaries are increasingly threatened by manmade interferences to their natural hydrodynamic regimes. The shape and size of estuaries and water circulation are among the contributory factors in determining the sedimentary processes. However, sedimentary processes of estuaries are basically similar in kind the world over; only their scale and intensity differ.

1.2 Areas of Research

Knowledge of sedimentary processes in estuaries over the past half-century has grown from many different fields of research. A variety of sediment types, sediment textures and sediment structures occurs, most of which are recognizable in ancient sedimentary rocks. Other reasons for a growing interest in estuaries are many: Estuaries are often the site for developing industry and its growing

population, they are recipients of discharges into their watersheds, and a source of pollutants to the sea. They are also recognised as the natural habitat of shellfish, and the nursery grounds for some species of fish. Naturally, understanding of such sedimentary systems is vital to the optimal use of an estuary.

The earliest studies of tidal environments began in this century when Kindle (1917) made a descriptive summary of ripple mark occurences from several environments and included data and illustrations from the tidal flats of the Bay of Fundy. However, intensive study on coastal zones and estuaries did not begin until the end of the Second World War, when there was an upsurge of research on tidal flat sedimentology. The first major study was by van Straaten directed specifically to sediment features and later expanding to include comparative studies of other areas (van Straaten, 1952, 1953,1954,1959,1961; and van Straaten and Kuenen, 1957). Similar studies were carried out along the northwest coast of Germany by Reineck (1963,1967,1972) and Reineck and Wunderlich (1968 a,b), and along the coast of eastern England (the Wash) by Evans (1965,1976). These studies emphasized the description of sedimentary structures, and the distribution of different sediment textural groups. Variation of tidal current velocity and its duration were recognised as being the major control for sediment distribution across a tidal flat.

The study of sedimentary processes was first carried out by Krumbein (1939) in Baratavia Bay of the Gulf Coast (USA), in which he showed that grain size distribution of sediments were sensitive to hydrodynamic conditions. Inman and Chamberlain (1955) demonstrated that particle size distributions result from different transport processes and from different amounts and types of sediment supply. The detailed results of Steward (1958) showed how textural and compositional properties are closely linked to environmental processes. In Europe, most of the published information on hydrodynamic controls of sediment distribution comes from literature on intertidal flats (Reineck,1973; Evans,1965; Pestrong,1972).

Recent studies emphasize the effects of the transporting fluid on sediment particles, and provide a basis for interpreting hydrodynamic conditions from grain size distributions (Middleton, 1976; Sagoa and Visher, 1977). Several techniques have been used to interpret sedimentary environments from grain size distributions such as plotting skewness versus standard deviation (Friedman, 1961), comparing the coarse fraction to the median size (Passega, 1964) and analysing log-probability cumulative curves (Visher,1969).

Intertidal parts of shoals that carry bedforms have received particular attention in the research literature (Klein, 1970; Dalrymple et al.,1978; Boersma, 1969; Gellathly, 1970; Allen and Friend, 1976). From the wide

range of hydrodynamic conditions encountered in these studies , it was shown that tidal current velocity, flow depth, and grain size are the controlling parameters for the occurrence of the different bedforms. The size, shape, and rate of migration of tidal bedforms is determined by the degree of time-velocity asymmetry . Study of the internal structures of bedforms under tidal flow conditions showed that the prevailing structure developed is cross-stratification demarked by sharp set boundaries (Reineck and Wunderlich, 1968a; Klein, 1963,1970). The internal organization of the cross-strata may be simple or complex. The most dominant structure is in the form of herringbone cross-stratification which forms in response to twice daily reversing flow (Reineck,1963).

The formation of mud or sand shoals is a common feature of estuaries. The study of sediment transport processes by direct observation of suspended sediment and water movement were carried out by Dutch workers in the Wadden Sea (van Straaten and Kuenen,1957; Postma,1954,1961,1967). These studies were followed by extensive research programmes in estuaries and lagoon inlets (Allen and Castaing, 1973; Nichols, 1974; Byrne, 1975; Evans and Collins, 1975). O'Brien (1969) suggested that the main controlling factor of the large accumulation of sediment in these environments was the tidal prism. The most dramatic manifestation of the fine sediment accumulation in estuaries known as turbidity maxima have been reported in a

large number of estuaries throughout the world (Postma and Kalle, 1955; Nichols and Poor, 1967; Schubel,1968; Conomos and Peterson, 1976). Their origin has been attributed to flocculation of mud (Ippen, 1966) and to deflocculation (Nelson,1959).

A number of studies have indicated the interactions between estuarine organisms and their surrounding environments (Rhodes and Stanley,1965; Edzwald and O'Melia, 1975; Coles, 1979). Burrowing in sediment deposit by organisms will affects physical characteristic of the sediment (Schafer, 1962). Rhoads (1974) outlined the changes of sedimentary characteristics brought about by benthic organisms including the effects they have on sediment transport processes, chemical reactions, particle aggregation, and nutrient recycling. Pryor (1975) studied the role of filter feeders on the rate of sedimentation and their relationship to the processes of pelletization of argillaceous material. Some deposit-feeders fractionate and sort sediment particles of different sizes (Myers,1977). Aller (1982) reported on physical and chemical changes taking place in the bottom water due to the biogenic activities of benthic organisms.

1.3 Controlling Parameters

An understanding of estuarine hydrodynamics is very important in studies of the sedimentary processes that affect sediment distribution. Water circulation,

stratification and mixing have to be considered . The relative roles of tidal current asymmetry, waves , tidal and fresh water discharge in estuarine dynamics need to be evaluated. Estuarine hydrodynamics have been described in the literature reviews by Prichard (1952), Bowden (1962, 1967) , Cameron and Prichard (1963) and Dyer (1973,1979 and 1986).

1.3.1 Tides

Tides play a very important role by keeping large amounts of sediments in active movement and by trapping the sediment in the estuary. The net rate of transport is largely dependent on the asymmetry of the tidal wave and currents (Allen et.al.,1980a). Variability of tidal current velocity is obviously one of the most important single parameters in sedimentary processes(Postma,1954; Inglis and Allen,1957; van Straaten and Kuenen, 1957; Terwindt et al., 1963 and Meade,1969).

Tidal currents are caused by the rise and fall of water level at the mouth of estuaries which varies according to local and global geographic constraints and proximity to amphidromic points. Fluctuations in tidal level during the spring-neap period cause a considerable variation in tidal intrusion, water depth and current velocity. The variation is regular and predictable in contrast to the considerable

fluctuations and sometimes unpredictable nature of river discharge. This variation will influence the transporting potential of individual tidal cycles (Sundborg, 1956; Jackson, 1964a). The changing of current direction has a significant effect on the morphology of the estuary.

In an estuary, both tidal range and current velocity decrease away from the mouth as tidal energy is slowly reduced by friction as the tidal wave propagates up the estuary. When the tidal wave travels into an estuary, it is commonly deformed in such a way that the time of flood is always shorter than the ebb period. This deformation produces higher current velocities during the flood then during the ebb (Postma,1961, 1967; Boon, 1975; Wright,1978; Allen et al., 1983),and thus can contribute to the landward transport of marine sediment into the estuary (Groen,1967). The differences between the flood and ebb velocities also depend on the volume of fresh water flow.

1.3.2 Waves

Wave activity has been shown to play an important role in estuarine processes. However, in large and shallow estuaries,it can contribute considerably to sedimentary processes (Allen, 1971; Krone, 1979; Anderson, 1972,1983). Waves tend to be small because fetch is limited, and they only affect intertidal sand bodies for short durations because water level changes rapidly (Lambiase, 1977,1980).

Sedimentary features such as sand spits across many estuaries,beaches and barriers are the result of wave activity in sorting and transporting sediments. The relative importance of waves depends on the wind strength and the length of fetch and resulting degree of exposure. Therefore, the dimension of the estuary and its orientation to the prevailing wind direction are important factors for wave activity.

Along a coast with high wave energy, large quantities of sediment are brought into suspension and longshore currents can move large amounts of sediment. Since waves activity is reduced by sand bodies at the mouth of the estuary, longshore transport is active only in the offshore area. Although waves are damped inside estuaries, the influence of wind waves (in tidal flat areas at high water) on the resuspension of sediment is very significant (Anderson, 1972; McDowel & O'Connor, 1977). Once resuspended, these fine sediments are redistributed by the prevailing currents either into the estuary or out into the sea. They tend to settle out in low energy environments.

1.3.3 Salinity

In estuaries the mixing between seawater and fresh water produces a distinct estuarine circulation. Salinity will affect sedimentation processes directly through water density changes and electrolyte strength, and indirectly

through circulation patterns established independently from tidal forces.

Density stratification has been observed in many estuaries throughout the world such as the Gironde in France (Allen, 1972) and Chesapeake Bay in the U.S.A (Haas, 1977). The fresh water, which is less dense than sea water, tends to flow outward over the sea water. On the other hand, the intruding sea water penetrates the estuary as a salt-wedge along the bottom. This circulation pattern is an important factor in the retention of fine sediment at the tidal limit of salinity intrusion (Simmon,1955 and 1966; Schultz and Simmons,1957; Einstein and Krone, 1962; Ippen, 1966). This landward flow of salt water at the bottom is partly responsible for the formation of a turbidity maximum in many estuaries (Nichols and Poor,1967; Nichols,1972; Schubel,1972; Conimos and Peterson, 1977; Inglis and Allen, 1957; Buller et al., 1975).

Salinity stratification in estuaries varies with tidal and seasonal river flow cyles. During a spring-neap period, the changes of tidal prism relative to river flow modifies the degree of mixing (Allen,1972). Such variations have been observed in many estuaries throughout the world, and can modify stratification characteristics from well-mixed during spring tides to partially-mixed during neap tides. Mixing also varies with the varying river discharge due to seasonal rains. For example, the river discharges into the Tay estuary are particularly

strong during the winter months and spring melts, although heavy storms occur occasionally during the summer months (Buller et al 1975). Seasonal variation of river discharge in the Vellar River is large which reflects monsoonal periods coincident with heavy precipitation (Dyer and Ramamoorthy, 1969).

The fluid density changes which occur as a result of mixing may interact directly with suspended sediment in the water and modify the depositional patterns. The change in density will change the settling velocity of sediment particles.However, the change is very small compared with the magnitude of the changes associated with turbulent mixing processes which maintain sediment transport.

Increased salinity in the estuary due to sea water intrusions will increase electrolyte strength of the estuarine water. This increase will affect flocculation of suspended sediment in the water (Einstein and Krone, 1962; Ippen,1966). The probability of flocculation of sediment particles into large aggregates in salt water is a function of sediment and electrolyte concentration (Welder, 1959; Whitehouse, Jeffrey and Debrecht, 1960). Complete flocculation of illite and kaolinite occurs above a salinity of about 4% . For montmorillonite, the floc size varies over the entire range of estuary salinity (Whitehouse et al., 1960) .

As the concentration is increased, the increased frequency of interparticle collision causes enhanced flocculation, resulting in larger but low density flocs. The net effect is to cause an increase in the settling velocity. This increase in settling velocity will favour deposition of fine grained sediments within the estuary. Once deposited cohesion will increase the critical erosion velocity necessary for the initiation of transportation (Sundborg, 1956).

1.3.4 Temperature

Estuarine water temperature can directly influence the processes of sedimentation by altering the viscosity and density of water and also by affecting floc formation.

Density changes in estuarine water due to variation of temperature are very small and are unlikely to affect the settling of particles from the flow. On the other hand, viscosity changes are significant between the summer and winter season where the temperature difference can be quite large. The change of viscosity can bring about a change in settling velocity of over 20% (Stokes,1851). Deposition during the summer period is higher due to lower viscosity. The influence of viscosity variation on sedimentation is, however, very small and unlikely to be a major factor. Inertial forces very likely dominate over viscous forces in a estuary and the existence of turbulence forces will

inhibit settling of fine sediment (Allen,1970; Raudkivi,1976).

It has been revealed that temperature might have an influence on the flocculation of fine material in estuaries (Jackson,1964a). A 14° C change in water temperature was found to cause a big increase of fine sediment deposition. The viscosity of the water only accounted for a fraction of the increase. A similar situation has been observed by Halliwell and O'Connor (1960).

1.4 Estuarine Morphology

Estuaries are difficult to classify, and there is no common ground where those interested in various aspects can agree upon the kinds of environments that are estuaries. Estuaries are often classified on the basis of geomorphological criteria. This method divides estuaries into three classes: drowned river valleys (or coastal plain) estuaries, deep estuaries (or fjords) , and bar-built estuaries (lagoon).

The drowned river valleys were formed by the rising sea-level after the last glaciation about 6000 years ago (Pritchard, 1952; Meade, 1969). Most estuaries fall into this class. The Chesapeake Bay system (east coast of North America), Thames estuary, Sydney Harbour and Gironde

(France) illustrate the main features of this type of estuary.

The fjords were formed by the submergence of glacial troughs resulting in the formation of very deep estuaries with steep rocky walls and parallel-sided courses. Fresh water discharge is small compared with the total fjord volume so that a typical fjord will have a thin layer of fresh water overlying a large quantity of sea water. This type of estuary may be found on the coasts of Canada, New Zealand, Greenland, Noorway, Scotland, Chile ,and Siberia.

The bar-built estuaries are formed by the build up of a sand spit, barrier island or sand bar. Bar-built estuaries may have several rivers flowing into them and several outlets between the bars into the open sea. They are typical of the southern states of USA and of parts of Australia. The origin and classification of this type of estuary in Mexico is disscussed by Lankford (1976).

Estuaries can also be classified by their tidal range, each sharing a common tidal range and therefore common processes and depositional shapes. Such a classification has been suggested by Davies (1964) and Hayes (1975). They are micro-tidal estuaries (when tidal range is less than 2 metres); meso-tidal estuaries (when tidal range is between 2 and 4 metres); and macro-tidal estuaries (when tidal range is in excess of 4 metres).

In micro-tidal estuaries the dynamical processes are dominated by fresh water discharge upstream of the estuary entrance and by wind-driven waves near the entrance. The dominant fresh water flow produces a salt-wedge characteristic. The position of the salt wedge will alter with the magnitude of the flow in the surface layer i.e with river discharge. Wind tides are commonly generated and extensive tidal flats may develop. Near the entrance wind-driven waves produce spits and barrier islands which enclose the estuaries. In some cases, extensive deltaic deposits may develop. The Mississippi is an example of a micro tidal estuary (Wright, 1971). When the river discharge is low the salt wedge extends over 150 km inland, but with high discharge the salt wedge only extends a kilometre or so above the river mouth.

In meso-tidal estuaries the dynamical processes are no longer dominated by salt wedge circulation; instead tidal flows are more effective and may significantly influence sediment transport in the lower parts of estuaries. These estuaries are characterized by a partially mixed circulation system, and comprise a broad funnel-shape entrance which passes upstream into an area of tidally influenced meandering channels before reaching the fluvial-dominated river channel (Ahnert, 1960). The main features include flood and ebb-tidal deltas (Boothroyd,1978; Wright and Sonu, 1975), transverse bars and spill-over lobes. Discrete flood and ebb tidal channels disect these features

and frequently exhibit sandwaves with superimposed dunes (Boothroyd and Hubbard, 1975). An example of this type of estuary is Chesapeake Bay, USA.

In macro-tidal estuaries the dynamical processes are dominated by the tidal flow which induces near-complete of the water bodies and the circulation system is therefore nearly vertically homogeneous. In this situation, longitudinal and lateral advection processes dominate. Vertical salinity gradients no longer exist but there does exist a steady upstream decrease in overall salinity.Tidal ranges in excess of 4 metres produce strong tidal currents which may reach hundreds of kilometres inland. Estuaries with such a tidal range do not posses the ebb-flood deltas of the meso-tidal ranges; instead the central main channel near the estuary mouth is occupied by long linear sand bars parallel with the tidal flow. Macro-tidal estuaries are characterized by a broad mouthed and funnel-shape channel (Langbein, 1963; Wright et al., 1973). Sediments deposited on intertidal flats are moulded into ripples and sandwaves. Examples of these estuaries are the Severn, and Thames in the UK, Gironde of France and Ord Estuary of Western Australia.

1.5 Estuarine Sediments

Estuaries act as sediment traps collecting sediments from various sources such as rivers,offshore and beaches as

well as from biological production within the estuary. As sediment accumulates in estuaries, the space available for deposition will decrease (Roy, Thom and Wright,1980). After reaching maturity, the estuary can be filled with intertidal deposits with little space left for further deposition. At this stage sediment carried by the river flow will be discharged directly to the sea. Theoretically, estuarine sediment may accumulate vertically to the highest tide level.

Sediments in estuaries range from very fine colloidal particles in suspension to very coarse grained in the main channel. Size distributions of both suspended and bedload sediment reflect the balance between supply of material and the prevalent hydrodynamic conditions. Sands are often found at the seaward ends of estuaries where wave action and tidal currents remove the finer particles such as fine sand, while muds are found in the upstream of an estuary near the limit of tidal wave intrusion (van Straaten, 1964). The precise composition of sediment deposits in any particular estuary depends upon the particular geological and social history of the estuary and its hinterland, as well as the sediment transport characteristics of the tidal currents.

1.5.1 River Source

The sediment supplied by rivers and streams, together with land surface drainage, consists of sand, silt and clay size material. Rivers also supply a substantial quantity of organic matter and dissolved mineral salts. The most common are salts of iron, aluminium, and silica. The amount of sediment and the distribution of grain sizes depend on relief, climate, human interference and geology of the drainage area.For instance, an intensive use of soil and a low vegetation cover can increase sediment supply to the estuary. On the other hand, the presence of dams or lakes can drastically reduce the supply of fluvial sediments. Abnormally high river runoff may transport more material into an estuary in a few days than normal runoff in years. An example is given by Schubel (1974a) for upper Chesapeake Bay.

1.5.2 In situ rewoking source

Guilcher and Berthois (1957) suggested that a possible source of sediment in an estuary from Pleistocene deposits outcropping on the slopes or in beds of the estuaries themselves. They showed that the muds of both saltmarshes and mudflats possessed identical physical and chemical properties to the periglacial sediments which bordered the estuary. Material dredged and discharged again within the estuary no doubt form important sources of sediment deposits. There is also the possibility of the return of

dredge spoil and of domestic wastes from depositional areas in the sea but too near the estuary entrance.

1.5.3 Marine source

Most estuaries probably receive some sediment from offshore. A low river discharge may be countered by fast landward tidal currents that bring offshore or beach sediment into the estuary on every flood tide. Evidence of the movement of sediment into estuaries has been reported from the Wash (Evans, 1965), the Taf (Jago, 1980) in Britain and the U.S East Coast (Meade, 1969). Jago (1980) uses evidence of sediment texture and mineralogy to show that the Taf estuary is filling with marine sand from Carmarthen Bay. Byrne and Kulm (1967) report material from beaches outside the entrance to Yanquina Bay, Oregon, more than six miles upstream. Such deposition is increased during the winter flood season when littoral drift and onshore winds are greatest.

Sediment in moderately stratified estuaries moves progressively landward along the bottom and accumulates near the limit of net landward flow (Prichard, 1967). In highly stratified estuaries coarse sediments are trapped near the toe of the salt wedge (Robert and Pierce, 1976).

1.5.4 Biogenic sources

Biogenic contribution in the form of dead marine and fluvial flora and fauna is secondary in importance compared to the much larger amounts of fluvial or marine terrigenous sediments in temperate regions. Living creatures, such as marine bivalves and filter-feeding zooplanton, can provide material indirectly. They have the ability to filter the finer particles from water and eject them later as larger sized agglomerate particles which are capable of settling from suspension (McDowell and O'Connor, 1977). In Charleston Harbor, for example, the organic component has been identified as constituting up to 15 percent of the finer sizes of sediment found in shoals, but in other places little is contributed by organic sources (Ippen,1966).

Upon entering estuarine water, sediment from various sources encounters the familiar estuarine circulation in its various forms. The sediments are dispersed to different parts of the estuarine system by this circulation. In addition, wave and current action within the estuarine environment locally distribute and rework the sediment supplied and sort it into well differentiated sediment sizes, each of which is relatively homogeneous. Spatial and temporal patterns in sediment parameters will reflect the interaction of the controlling parameters and any other factors with the sediments.

Coarse sediment, consisting mainly of grains with a diameter larger than 0.2 mm, is transported as bedload material (Yalin,1972; McDowell & O'Connor,1977; Heathershaw, 1981). Bedload sediments travel with a speed much smaller than the current speed. Coarse sediment can also be transported in suspension by fast tidal currents and can adapt to changes in the current speed rapidly in comparison with the time scale of the tide. Sediment load transported at a given current speed depends on particle size (Bruun,1978; Dyer,1980); thus, the local dominance of either flood or ebb currents will determine the nature of coarse material deposition.

Fine sediment is generally transported in suspension or as fluid mud. In many estuaries, the suspended sediment is composed mainly of particles with a size between 1 and 10 microns and aggregates with a size up to 100 microns (Meade,1972; Eisma et al., 1980). Suspended load moves about as fast as the current speed. However, the nature of transport is complicated due to the cohesive properties of the sediment. Cohesion is the result of interparticle attractions due to the presence of electric charges which make bed sediment more resistant to erosion. Most fine sediments in suspension are very responsive to the changes of current speed and settle only at very low current speeds in the period around slack water.

In areas where powerful tidal curents move up and down

an estuary, the sediments are usually sand, particularly in the channels, but the tidal flats between channels commonly have sediments consisting of poorly sorted, rather sandy muds becoming finer with distance from the channels (Emery, et al.,1957). Near the entrances of estuaries where strong tidal currents and waves are common, little mud is deposited. Study of sediment distribution is a valuable aid in the understanding of estuary dynamics and sedimentation (Postma, 1967; Wright, Coleman and Thom, 1973; Boothroyd and Hubbard, 1975).

1.6 Nature of the study

Estuarine sedimentary environments provide a wide range of scientific enquiry which have always been of some interest to scientists of various disciplines. There is a need for studies of the physical characteristics of estuarine water, its circulation, net exchange with the open sea and response to freshwater input which are a basis for understanding hydrodynamic conditions of estuarine environments. Understanding of the processes of water-sediment interaction, the transport processes and mobility of sediments, and the influence of natural forces is fundamental to the study of the behaviour of estuaries as sedimentary environments.

The main objective of this study was to identify and to assess the relative roles of various parameters and

processes controlling sedimentation in the Dwyryd estuary. This investigation was designed to obtain a broad scientific knowledge of the estuary and its neighbouring submarine area. The studies of water circulation, sediment distribution and sediment transportation and deposition processes form a significant part of the study.

The first part of the study was to establish the hydrodynamic conditions operative within the area, since little information was available. Tidal conditions are of the utmost importance in controlling estuarine sedimentation (Elliott,1978). Various circulation patterns develop within estuaries, depending on the manner in which the water bodies mix. The rate of mixing is mainly controlled by the strength of tidal current in relation to basin geometry and freshwater discharge. During weak tides, fresh water extends over a saltwedge as a distinct layer, and the water column is highly vertically stratified. Strong tides on the other hand cause turbulent mixing leading to a more homogeneous water column. Measurement of various hydrodynamic variables such as current velocity, salinity and temperature variation during tidal cycles were carried out at a number of sites and depths. These data are necessary to establish the circulation and stratification patterns and also enables the effect of seawater intrusion and fresh water input to be determined. By using the circulation-stratification of Hansen and Rattray (1966), it is possible to classify the

estuary and to compare it with other British estuaries.

An essential part of the study of sedimentary proceses must include a detailed examination of the spatial distribution of estuarine sediments and also sediment from nearby sedimentary zones, such as sand dunes along the coast, beaches, and seabed. The coastline and offshore areas are obviously related to the estuarine sedimentation processes. The volumes of sediment in estuaries vary widely , and particle size distributions differ both within and between estuaries. Such differences depend greatly on the sediment source and on the hydrodynamic conditions within estuaries. In this study, sediment samples have been collected along transect lines across the estuary. Detail statistical analyses of sediment samples were undertaken which include an assessment of grain size, sorting,skewness,and kurtosis.Combination of these parameters can be used to differentiate sedimentary environments. The study also examined grain size distributions and analysed the observed trends in textural parameters. The aims were to define the characteristics of grain size distributions that reflect hydraulics in the estuary, and then to use hydraulics to interpret existing grain size distributions.

In addition to the sediment distribution studies, the relationship between surface processes and sedimentary features was also studied, which is obviously significant to the understanding of the depositional and transportion

processes on intertidal flats. The external shape and configuration of the bedforms and their internal sedimentary structures depend mainly on current velocity, water depth, grain size, and sedimentation rate. As such they are critical to the understanding of the processes and conditions of deposition (Boothryoyd and Hubbard, 1975; Klein, 1970; Dalrymple et al.,1978; McCave and Geiser, 1978). It has been shown that the net migration of bedforms is in the direction of the dominant tidal current. This dominance not only reflects the magnitude of the peak current velocity of one tide compared with the opposite tide but more specifically the dominance of the sand transport. The morphology of intertidal bedforms found at the lower section of the Dwyryd Estuary was measured during a spring tide when the size of the bedforms was at a maximum.

There is evidence to suggest that the source of the major part of sediment deposited in the estuary appears to have been derived from a marine source. In view of the significance of this, an attempt has been made to estimate the transportation rate of the sediment. The assessment of sediment transport involves the selection of suitable sediment transport rate formulae from the many formulae currently available. Boundary-layer measuremants were made at a number of sites over spring and neap tidal cycles.In an attempt to improve the accuracy of the predicted load, use was made of Guy et al.,(1966) flume data. Rating

curves were fitted by least squares linear regression analysis on sediment discharge (total load) and mean velocity data.

In common with other high-latitude coasts, this area was glaciated during the Pleistocene, thus, the uppermost sediments should exhibit attributes of glacial and post-glacial processes and sedimentation. Only recently, continuous seismic profiling in the bay indicate the existence of presumably post-glacial sediments of varying thickness (Taylor Smith, 1975; Fenemore, 1976). In order to understand the sedimentary processes within the estuary and the bay a survey program which included sampling of the bottom sediment, side-scan sonar, and continuous seismic profiling in the bay was carried out . This survey aimed at providing the surface sediment distribution pattern which may be relevent to the sedimentary processes of the Dwyryd estuary. The response of the seafloor to tidal flow in the bay can be observed from sonar records and from grain-size frequency distributions of the sediments.

TWO

MORPHOLOGY OF THE DWYRYD ESTUARY AND TREMADOG BAY

2.1 Setting

Two small rivers, the Dwyryd and the Glaslyn form a small estuarine system at the northern corner of Cardigan Bay. This estuary system is located along latitude 52°53′ to 52°56′N and longitude 4°3′ to 4°11′W as shown in Fig.2.1. The Dwyryd estuary extends about 8 km before meeting the Irish Sea. The length of an estuary is defined as the distance from the mouth of the estuarine basin to the upstream limit of tidal influence. This length varies with time in any given estuary in response to changes in river discharges and tidal input. The width of the estuary mouth is about 2 km and narrows down to less than 0.5 km near the Briwfad Bridge (Figure 2.3). This estuary, like those of the Mawddach and Dovey estuaries to the south, follows a general Northeast-Southwest axis, and is one of the drowned embayments of Cardigan Bay.

Much of the Glaslyn estuary has been reclaimed. Before the building of the embankment across the river in 1811, the tide reached nearly to the Aberglaslyn (Figure 2.2) situated 13 km from Portmadog, and the whole of the Glaslyn

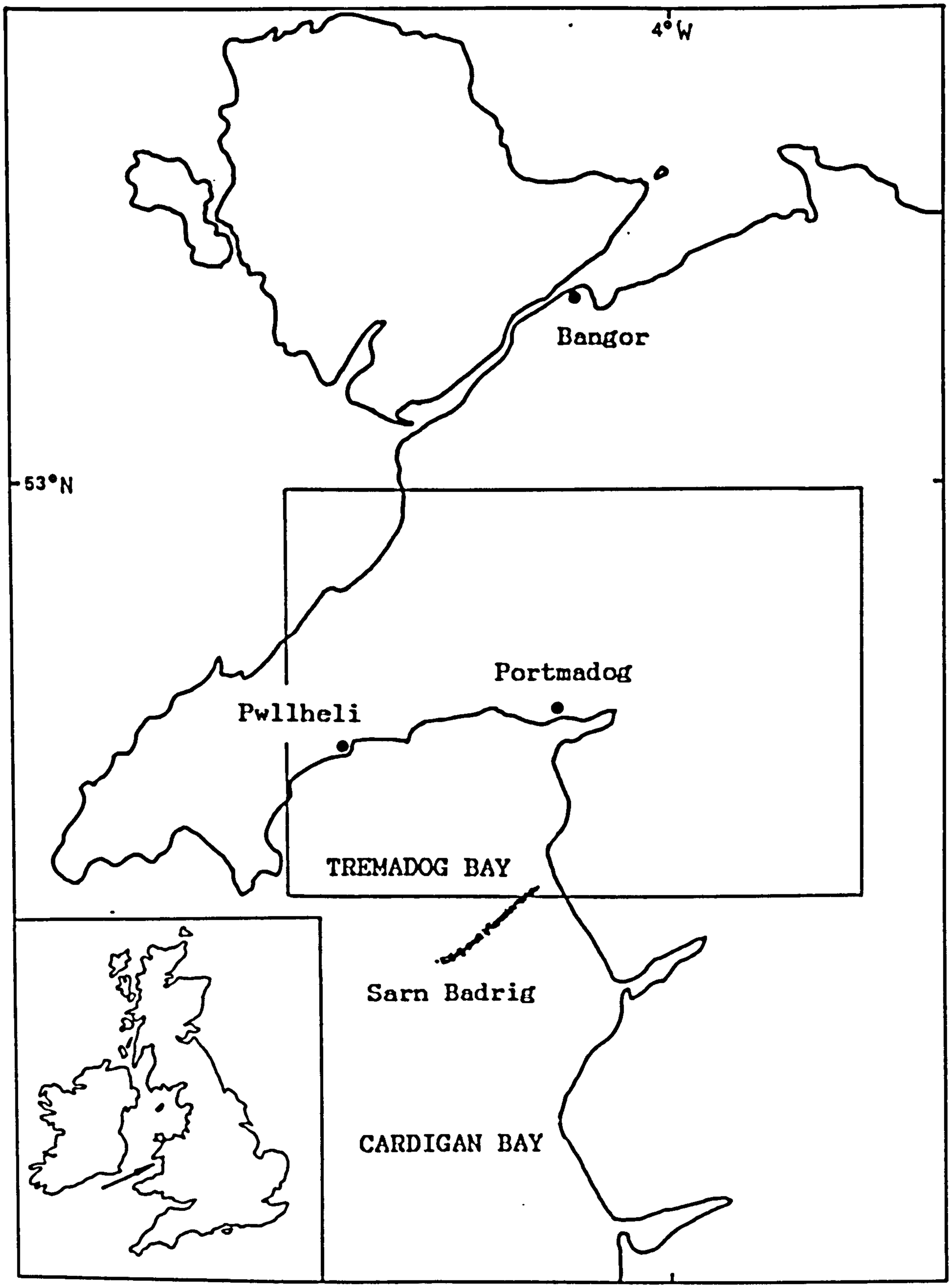

Figure 2.1. Location of the study area.

valley is said to resemble the Dovey estuary (Steers,1964). The Penrhyndendraeth peninsula (Figure 2.3) separates the Dwyryd estuary from the Glaslyn estuary. The coast of the peninsula is mostly rocky, with small sandy patches at various places.The Dwyryd river reaches the sea through a narrow glacial gorge. The Dwyryd valley is subject to tidal influence up to Maentwrog, about 8 km from the Briwfad Bridge. Most parts of the southern side of the estuary have been reclaimed for agricultural purposes (Figure 2.2), but a small portion of the marsh still exists.

The Dwyryd estuary receives most of its fresh water from a 300 km^2 catchment area which is largely mountainous with moderate relief (Figure 2.2). The river flows are partly regulated as the waters pass through reservoirs which suppress high discharges during wet weather flows. The flow rates for the past ten years are not available, but based on 1976 data, the volume of fresh water entering the estuary can vary one hundredfold. At Maentwrog gauging station, a minimum flows of 0.1 cumecs and maximum flows of 39.8 cumecs have been recorded. The annual mean flow was 4.3 cumecs. The volume of fresh water supply by the Prysor River, a tributary of Dwyryd River, is unavailable. Since the catchment areas of the two rivers which supplies fresh water into the estuary more or less of the same size, we can assume that the minimum, the maximum and the annual mean discharge rates of fresh water into the estuary were twice the values measured at Maentwrog station.

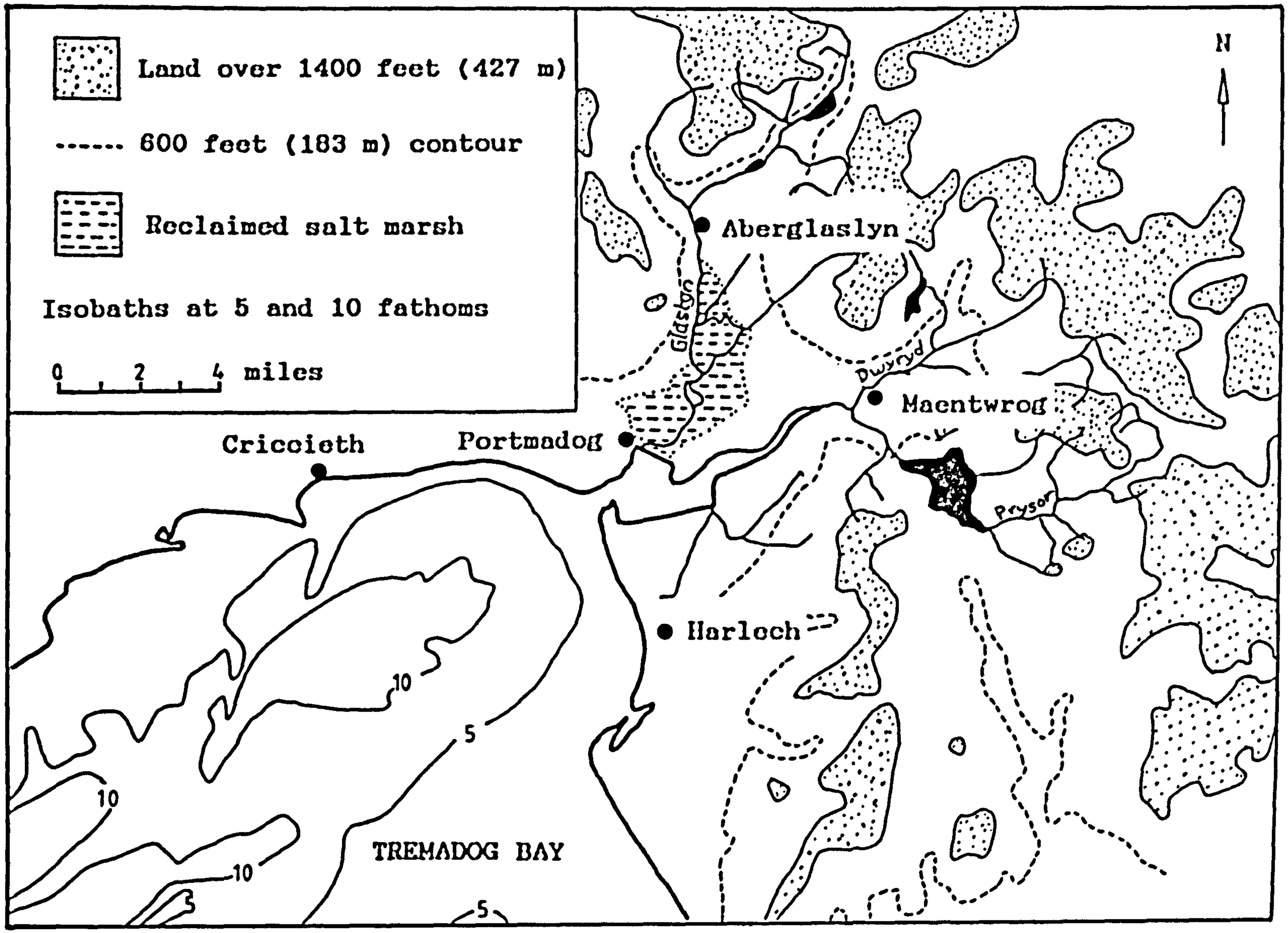

Figure 2.2. Topography of the study area.

The Penrhyndendreath peninsula reaches an elavation of 250 metres, but the eastern and southern highland reach elevations of 2000 metres, but in general form undulating hills of 1000 metres. Clearing of the river plain and other low-lying areas has led to changes in land-use. At present agriculture, principally dairying, is dominant, with a small percentage of the catchment still being forested.

The present topographic form of the estuary bears a resemblance to that of the original river valley, sharing many common features. The degree of modification that has been made relates mainly to the amount of sediment that has been deposited in it. This sediment must come from the sea, and/or local coast erosion, and/or from the land via the rivers. The estuary is constricted at the mouth by a beach-spit which extends from the southern side of the estuary. The Dwyryd estuary is also constricted at the centre by a small hill, Ynys Gifftan (Figure 2.3). During high tides, this hill becomes a small island in the middle of the estuary.

At the estuary mouth, the tidal range varies between 1.0 m for a neap tide, and 4.0 m for a spring tide measured at Portmeirion (Figure 2.3). At low tide the water level in the channels rarely exceeds 1.2m in depth, and in subsidiary channels it is centimetres in depth. Because of this shallowness, many of the channels are very variable in

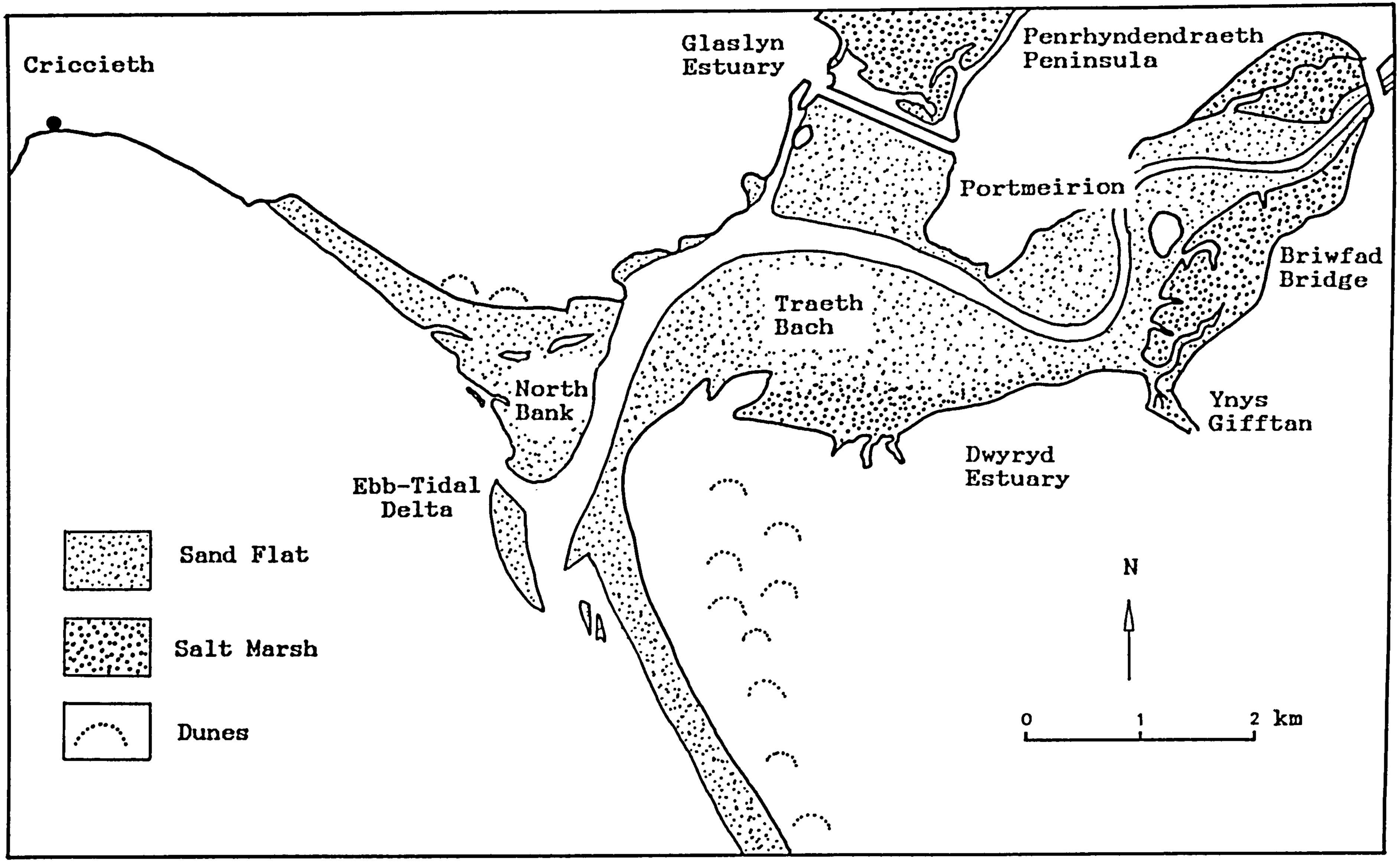

Figure 2.3. The Dwyryd estuary, including the intertidal flats, salt marsh and its ebb-tidal delta.

their position which can alter in a short time, although the major channels are more stable than the minor ones.

The shapes of the tidal curves are symmetrical at the estuary mouth, but further upstream the curve gradually become asymmetrical, the fall of water becoming longer than the rise (see chapter 3). This phenomenon is particularly noticeable in the upper estuary and at a spring tide. At Portmeirion, during spring tides, the fall of water lasts 9 hours and the rise only 2.5 hours (see chapter 3).

South-westerly winds prevail in both strength and frequency in the study area. The NE-SW fetch is the longest in Tremadog Bay, thus south-westerlies probably generate the largest windwaves on the north-east shores. Wind wave heights were found to exceed 3 m in the Irish Sea. Previous study in this area indicated that the wave having the greatest effect on sediment transport has a period of about 6 seconds (Simpkin, 1976). Waves are important by providing energy to keep sediment in suspension but transport of sediment is mainly accomplished by tidal currents.

2.2 Geological Evolution And Setting

The drainage basin of the Dwyryd river consist of a

rugged mountainous region with many high peaks, towering crags, and deep U-shaped river valleys which display thick layers of sedimentary and igneous rocks. The outcrops form a barren and desolate surface, much of it almost without vegetation. The tributaries of the Dwyryd river flow down to the main stream in steep and short gorges, in contrast to the long and gentle topographic profiles of many river valleys draining into England.

The geology of the Meirionnydd region is associated with the pattern of sedimentation and faulting along the Northwest region of Wales. The geological structure of North Wales,particularly in the Snowdonia National Park boundaries, is exceedingly complex, both in terms of the variety of its rocks and in the way in which these rocks are arranged (Figure 2.4). Subsidence and sedimentation occurred during Cambrian time, in which a sediment pile up to 5000 metres thick accumulated on top of an ancient platform of Pre-Cambrian rock in a wide ocean that stretched from the North American coast eastwards across to Europe. This huge mass of sediment slowly rose to form a series of huge wave-like folds and was elevated above sea level where erosion is strong.

The Pre-Cambrian basement is exposed at the surface outside the boundaries of the National Park, in the surface rocks of Anglesey and Lleyn and in two small areas between Bangor and Caernafon, and between Bethesda and Penygroes

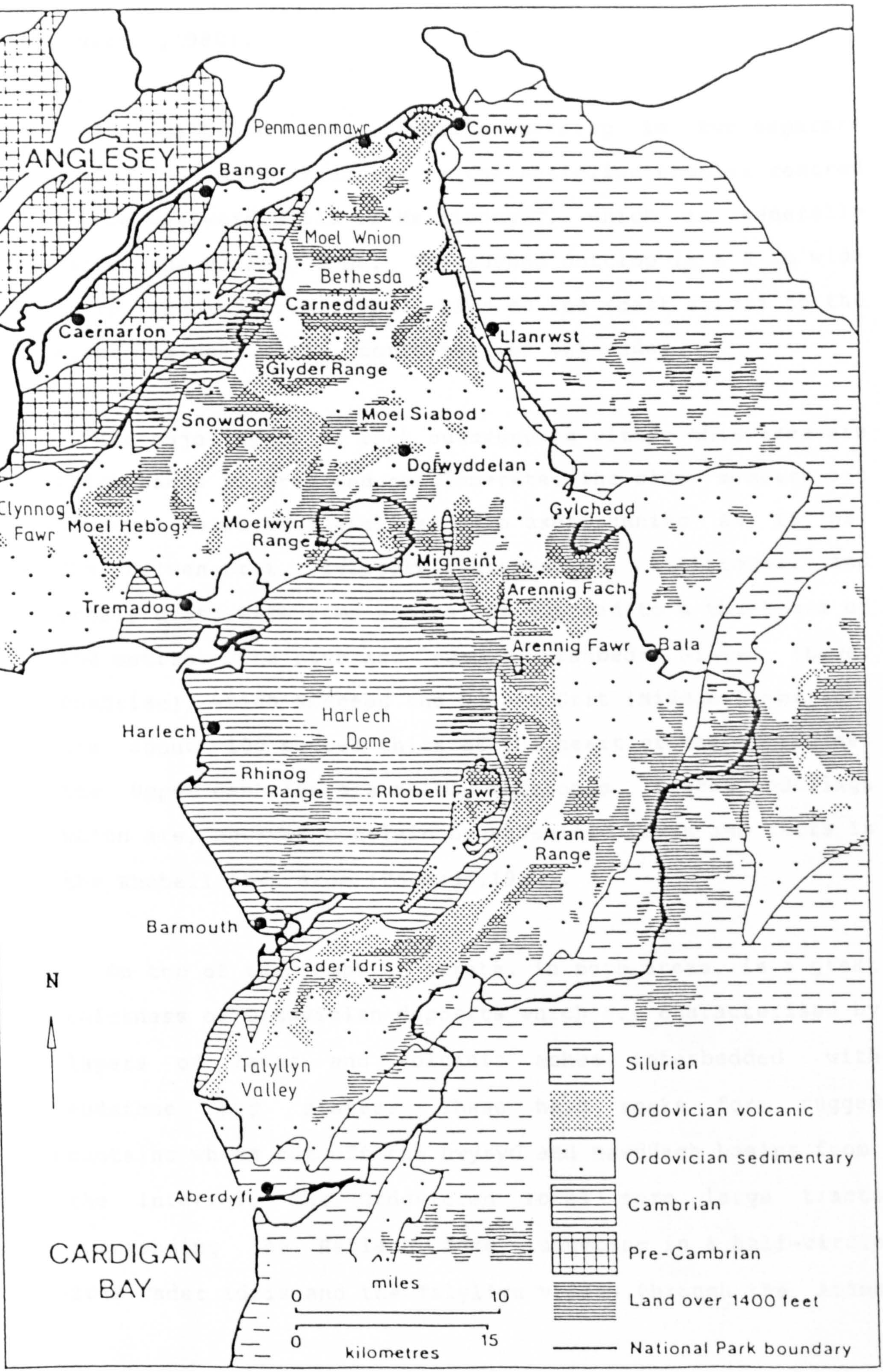

Figure 2.4. Outline map of the 'solid' geology of North Wales. (After Edwards, 1980).

(Edwards,1980).

The Cambrian rock deposits outcrop in two separate areas. The most extensive is the anticline complex centred on the westward hills of Meirionnydd, which is generally called the Harlech Dome. The second outcrop is a 8 km wide strip running from Clynnog Fawr on the coast across to the slopes of Moel Wnion, north-east of Bethesda.

The major types of rock outcropping within this area are thick bands of grit and conglomerate. The older members are found in cores of anticlines with axes running SE to NE. The Dolwen Grit, felspathic greywackes, siltstones, and pebbly grits with some shales, is exposed to a thickness of 150 metres. The blue and purple Llanbedr Slates (Lower Cambrian), which succeed the Dolwen Grit (Middle Cambrian), are about 100 metres thick at the heart of the anticline. The Upper Cambrian are mainly mudstones, slates and flags which are, however overlain by andesitic lavas and tuffs in the Rhobell Fawr area (Edwards,1980).

On top of the Cambrian strata, in both areas, is a great thickness of Ordovician deposits which are characterised by layers of lavas and volcanic ashes interbedded with mudstone and slates. These hard rocks form rugged mountains which cut off the Dwyryd and Mawddach basins from the interior. The Ordovician rocks form large tracts surrounding the Harlech Dome, sweeping in a half-circle from Cader Idris and the Talyllyn valley through the Arans

into the Bala county, the Arenigs, and the Moelwyns (Smith and George,1961). They occupy the complex syncline of Snowdonia, which extends north-eastwards to Conwy and Penmaenmawr, and westwards to the Lleyn Peninsula.

During the Pleistocene , a great ice-sheet spread over Scandinavia, the North Sea, and Scotland. This penetrated down the depression of the Irish Sea and across North Wales. At the same time small valley glaciers developed, which later coalesced into a single local sheet with a centre in Meirionnydd east of the Arenigs. This Welsh ice-sheet was able to push back and deflect the invading ice from the north. The ice-streams eroded and carried the weathered rock debris and dumped it in large quantity which remain now spread over the lowlands and over the foothills in Arfon, through the Caernafon-Pwllheli-Criccieth gap, and among the isolated hills of Lleyn. The sequence of boulder-filled silts and clays alternating with laminated sands and gravel is exposed in the cliffs of Cardigan Bay.

At the end of the ice-age,the outline of North Wales was already in very considerable detail much as it is at present, and the principal changes that have occured in post-glacial times have been due to the continuous eustatic rise of the sea level which started in late Devensian times (Kidson,1977). Evidence of the subsidence is provided by the drowned valleys of Cardigan Bay- the estuaries of the Glaslyn river, the Dwyryd river, the Mawddach, the Dovey,

the Conwy and the Dysinni. In all these estuaries the bedrock of the valleys is a few meters below sea-level.

2.3 The Dwyryd Estuary Environment

The intertidal area of the Dwyryd estuary shows similar morphological features, sediment types and vegetation to other estuaries along the coast of Cardigan Bay (Haynes & Dobson, 1969). The distribution and the size of depositional and erosional areas are dependent on the topography, as well as on location with respect to wave, current and sediment types and supply. Three major intertidal subenvironments are recognised within the estuary (Figure 2.3): salt marsh, sand flats, and channels.

2.3.1 Salt Marsh

The salt marsh occurs in the highest intertidal zone which is inundated only by spring tides or during high wind-driven tides. In many places this zone is colonised by Spartina townsendi, a similar species found in the Dovey estuary (Haynes & Dobson, 1969), although on their landward side these flats may contain bare mud patches. Salt marshes are developed mainly on the southern part of the estuary, but it is not areally extensive . The width of the marsh varies from a few metres to about 500 metres. On the sandier marshes grass may be dominant. Rapid expansion of Spartina townsendi toward low water mark on bare

mudflats is a common feature in the Wash, in eastern England (Evans, 1965), and in the Taf, south Wales (Jago, 1974).

Salt marsh sediments are mainly fine sands but at a few places the sediments are muddy sands. Near the mouth of the estuary, storm or wind-blown sands from the sand dunes and aeolian sand flat around Morfa Harlech may be deposited in the marsh . Normally only very fine sediments, primarily silts and fine sands in suspension are able to reach this zone.

The presence of vegetation on the intertidal flats impedes tidal flow across the flats and results in the trapping of fine sediments put into suspension during the rising tide. This leads to increase in the rate of deposition on the marsh surface which causes the marsh to grow gradually in height. The original colonisers find it difficult to adjust to the fast changing environment and to compete with new colonizers, such as Spartina townsendi. Thus a sequence or succession of plant communities develops both over time and, to a lesser extent, over the width of the marsh.

2.3.2 Sand Flat

In broad and shallow estuaries, the intertidal flats often occupy as much as half of the estuarine surface area. Long-term periodic surveys of estuaries have indicated that

intertidal flats are generally growing at the expense of the tidal channels and in turn are being engulfed by salt marsh vegatation (Redfield, 1967).

Intertidal sand flats in the Dwyryd estuary range in elevation from Irish Sea mean low water (O.D) to 3 metres, and thus the surfaces of these flats are inundated twice daily by tidal waters during high tides. The flats are exposed during low tides i.e less than 40% of the tidal cycle. In this estuary the area of the flat uncovered at low water of a spring tide is about 6.5 km^2.

These flats occupy about 70% of the estuary and consist mainly of sand flats. Gradients across the flats are very low except in those instances where they border the edges of channels, but topography and drainage may be complex in detail. Central ponds which do not completely drain may lie behind elevated channel banks where currents and waves have moved overwash sands from nearby channels.

The sediment in this environment consists of medium to fine-grained sands containing very small amounts of shell fragments (see chapter 6). The spatial distribution of the sands correlates with the strength of the tidal currents; the velocity over the tidal flats is higher than over the salt marsh since the tidal flats are lower than the salt marsh. Lower down the intertidal flats near low water mark, there is often a more sandy area probably due to active and prolonged wave activity, or, on the other hand,

the stronger tidal currents prevented deposition of finer material. Thin layers of mud have been observed on higher sandflats near the estuary mouth following stormy weather, probably due to storm surge which enhanced flood currents. Sedimentation of mud from suspension is appreciable only if current speeds drop below 20 cm/s (Einstein & Krone,1962).

Exposed areas of the estuary during low tide can be seen to be ornamented by an extremely diverse assemblage of bedforms. Ripples are the smallest bedforms observed; generally they are asymmetrical. During periods of moderate to strong winds the tidal flats are covered by straight-crested, short wavelength, symmetrical and asymmetrical ripples. These ripples are produced by local, short-period wind-driven waves generated in the shallow waters which cover the tidal flats during the high water period.(see later).

2.3.3 Tidal Channels

Numerous tidal channels can be seen cutting across the sand flats within the estuary complex.Most of them display extreme sinuosity, and a few abandoned meander scars can be seen on the active tidal flat surface. From observation during low water, it is obvious that the tidal channels tend to migrate and meander. Channel migration only occurs at an extremely slow rate. Bridges and Leeder (1976) have

described these processes from Solway Firth, Scotland, and they quote average rates of migration of between 3 and 15 mm per day.

The channel width averages 100 metres and exhibits minor variability except near the head of the estuary. Channel depths show a tendency to decrease upstream. Average depths range from 1.5 metres at the mouth to approxmimately 0.5 metres near the upstream limit of the tidal influence. In most instances these depths do not exceed the average tidal amplitude.

The channel sediments are generally coarser than associated tidal flat sediments, indicating that the strongest currents are mainly confined to the channels. A small dune field exists on the channel bed adjacent to the channel margin in the lower part of the estuary.(see below).

2.4 Morphology of Tremadog Bay

The bottom topography and the surface sediments of Tremadog Bay have been the subject of many investigations. Taylor Smith (1975) mapped the general sediment size distribution over most parts of the bay using samples that were obtained on a grid pattern. More recently, Fenemore (1976) compiled a Boulder Clay topography map of this area based on high-resolution seismic reflection records. A

series of boreholes by I.G.S have revealed that this reflector is the interface between modern and glacial deposits. Another slightly deeper reflector has been identified beneath the southern part of the bay at about 80 m below the sea bed and is interpreted as the interface between bedrock and the overlying glacial deposits (Fenemore, 1976).

Tidal currents and wind generated waves dominate the hydrodynamics of the area. Surface tidal currents flow in a northeastern direction with velocities between 25 and 75 cm/s (BRITISH ADMIRALTY Chart 368). West of Sarn Badrig the current splits into two prominent branches, one flowing to the east and the other flowing west into the Irish Sea (Figure 2.5). The tidal range is moderate with a mean of 3.25 m (quoted by the Admiralty for Pwllheli). The mean neap tide range is 2.2 m and the mean spring range is 4.3m.

Bathymetric contours of the bay are generally parallel to the shoreline, except at the western part where the topography of the sea bed is irregular as shown in Fig.2.6. Seaward of the estuary entrance, the sea bed has a gradient of 1:125 which is relatively steeper than the gradient at the northern and southern flank of the bay which have gradients of 1:160 and 1:450 respectively.

Sarn Badrig (welsh for "St. Patrick's causeway"), which is regarded as the southern limit of the bay, is a very

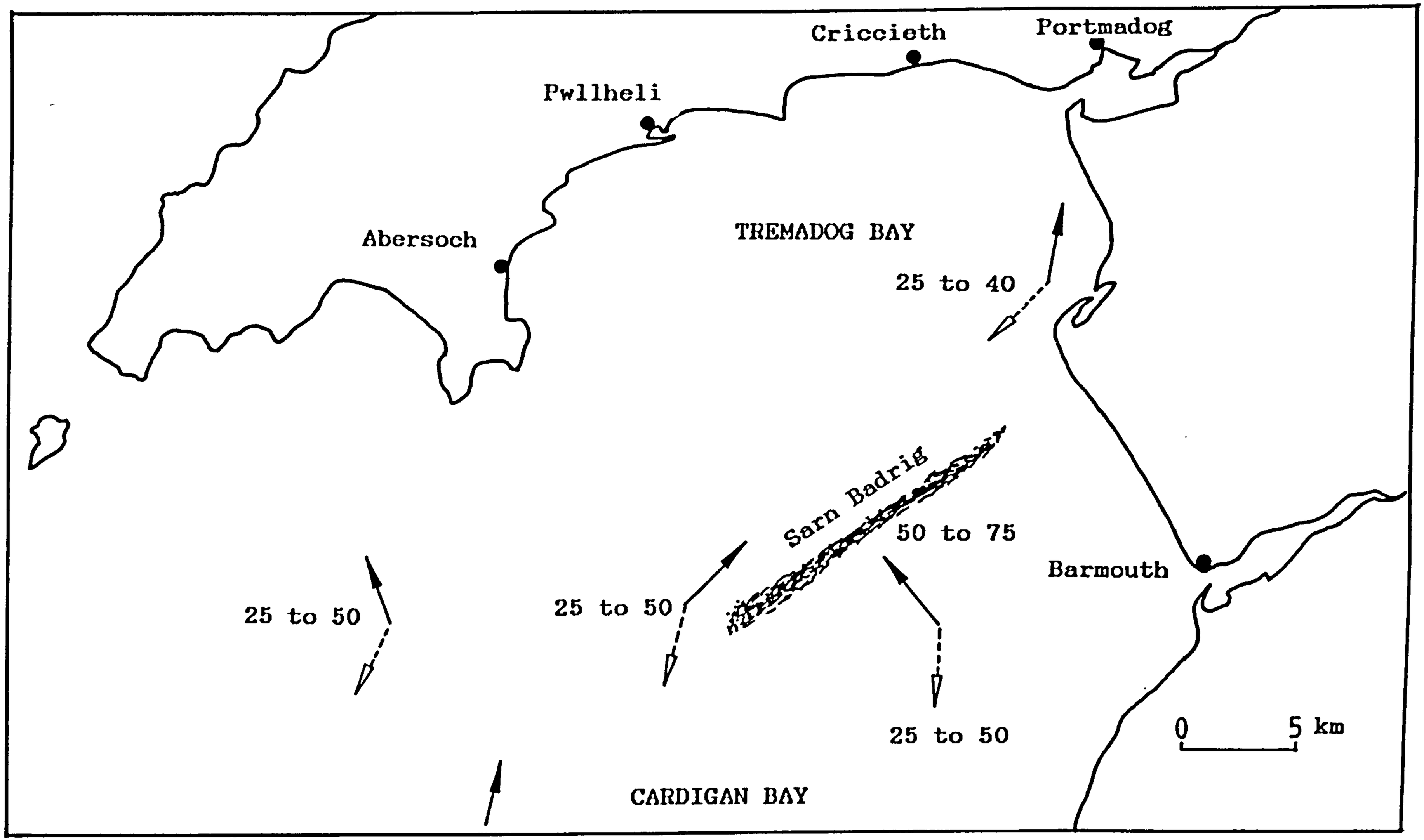

Figure 2.5. Inflow of water into the Tremadog Bay (number indicate cm/s) and the general surface water circulation, indicated by solid arrows (flood currents) and broken arrows (ebb currents).

shallow subtidal feature, roughly linear in shape and oriented parallel to the Llyn Peninsula. It stretches 17 km offshore and appears to be composed entirely of morainic material such as boulders, cobbles and pebbles. Sarn Badrig probably marks the line of contact between the local Welsh ice cap and the ice flowing southwards (Irish Sea ice) over the Llyn Peninsula (Foster, 1968). The Sarn breaks the surface of sea level at low water and must represent an effective barrier to current and sediment movement between Tremadog and Cardigan Bays (to the south). The effect of this barrier upon water circulation and sediment transport is not yet fully understood.

The present work was carried out as an integral part of an investigation aimed at understanding sedimentary processes in the Dwyryd estuary. The data used in this investigation are mainly from subbottom profiling surveys and sediment samples as well as from previous investigations of the geophysical and sedimentological characteristics of the area.

2.5 Bedform Morphology of the estuary

An understanding of bedforms and primary sedimentary structures resulting from bedform migration and their relation to water dynamics may lead to an understanding of the depositional environment. It has been proved in many studies that most sedimentary structures observed in the

geological record found world wide can be explained by present day processes (Terwindt, 1981; Allen, 1982a). Literature on bedforms and their internal structures have been accumulated from many studies along coastlines in most part of the world. In Britain, many estuaries and coastal intertidal flats have been studied and these have contributed enormously to an understanding of sedimentary processes of intertidal environments (Evans, 1965; Evans and Collins, 1975; Allen, 1976; Jago, 1980; Elliot and Gardiner, 1981; Collins et. al., 1981). Active movement of sand and the development of large-scale bedforms are restricted mainly to tide-dominated seas and intertidal areas such as estuaries.The development of bedforms has been described from many estuaries around the world (van Straaten, 1950b; Boersma, 1969; Klein, 1970; Terwindt & Breusers, 1972; Boothroyd, 1978; Boersma & Terwindt, 1981a,b; Zarillo, 1982; Dalrymple, 1984; Terwindt et al., 1986).

The study area is an active and dynamic environment. Tidal currents with a maximum speed of 125 cm/s and tidal range of about 3.5 metres (see chapter 3) are responsible for the formation of the observed sedimentary features. Bedforms of different size ,shape ,and orientation are encountered on the intertidal sand flats. The major bedforms consist of small ripples, megaripples (or dunes), and sand waves. Small-scale ripples have been observed to respond rapidly to changing hydrodynamic variations while

large-scale sand waves remain fairly constant over the rapid changing of flow conditions.However, the relationships between bedforms and estuarine dynamical parameters and the significance of bedforms, particularly the larger ones, remains poorly understood. Distribution of large-scale bedforms in the lower section of the estuarine and North Bank intertidal flats is shown schematically in Fig.2.7.

Bedforms can be divided into two types according to their shape relative to flow direction - longitudinal and transverse bedforms (Swift,1976). Longitudinal bedforms include sand ribbons and sand ridges, where the extended orientation is parallel to the stream flow direction. Transverse bedforms include ripples, megaripples (or dunes), and sand waves whose crestlines are normal to the flow direction. Bedforms with a fairly straight crestline lacking local scour in the trough are called two-dimensional (2-D) bedforms, while those with sinuous,often discontinuous, uneven crestlines and local scour pits in the trough are called three-dimensional (3-D). During the survey, two and three dimensional megaripples and sandwaves have been observed on the intertidal flats in this study area.

There is a considerable confusion in the literature concerning the classification and terminology of transverse bedforms in tidal environments.In this study, bedforms will be classified on the basis of wavelength and not on the

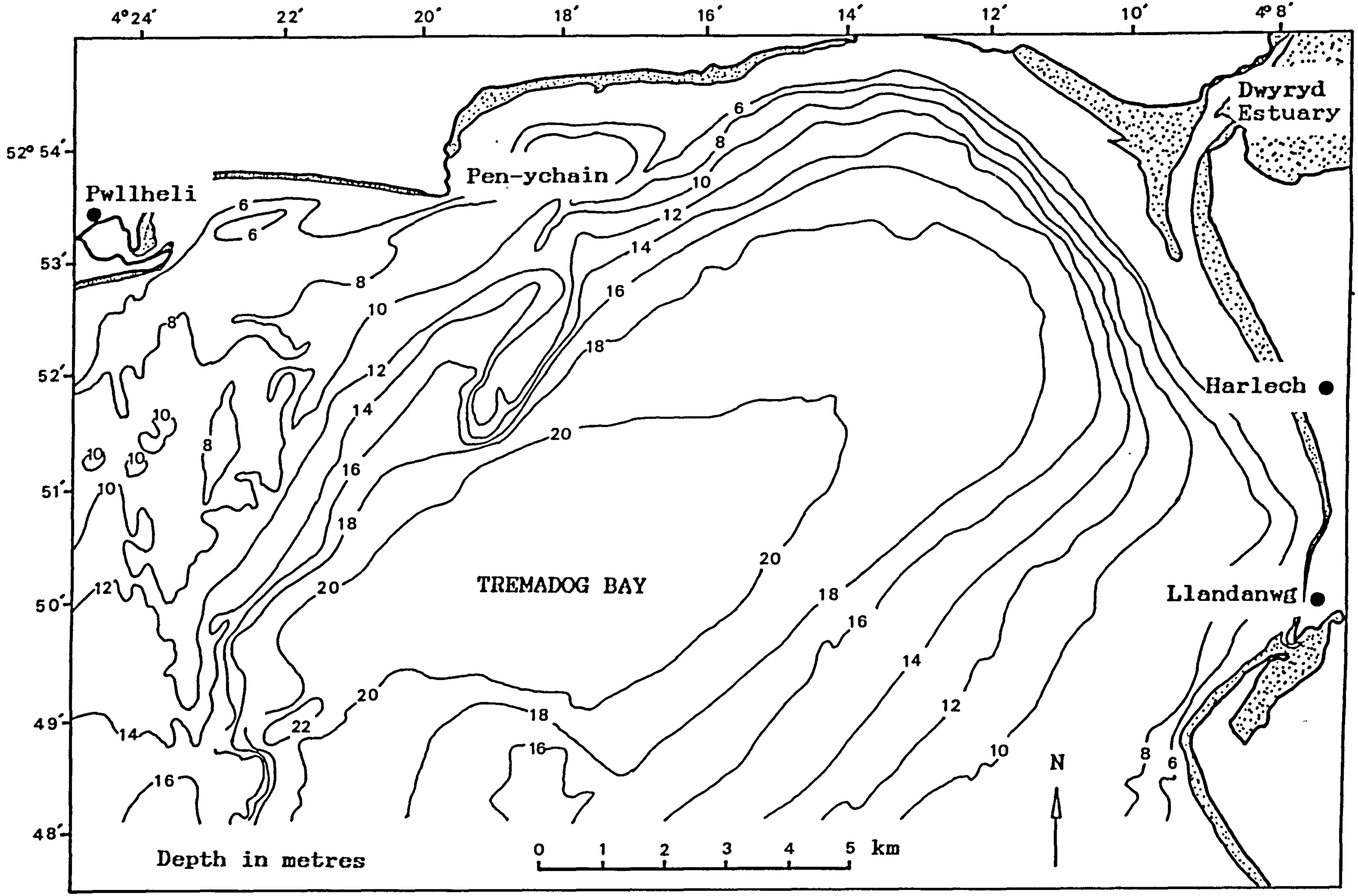

Figure 2.6. Bathymetric map of the Tremadog Bay (After Taylor Smith, 1976)

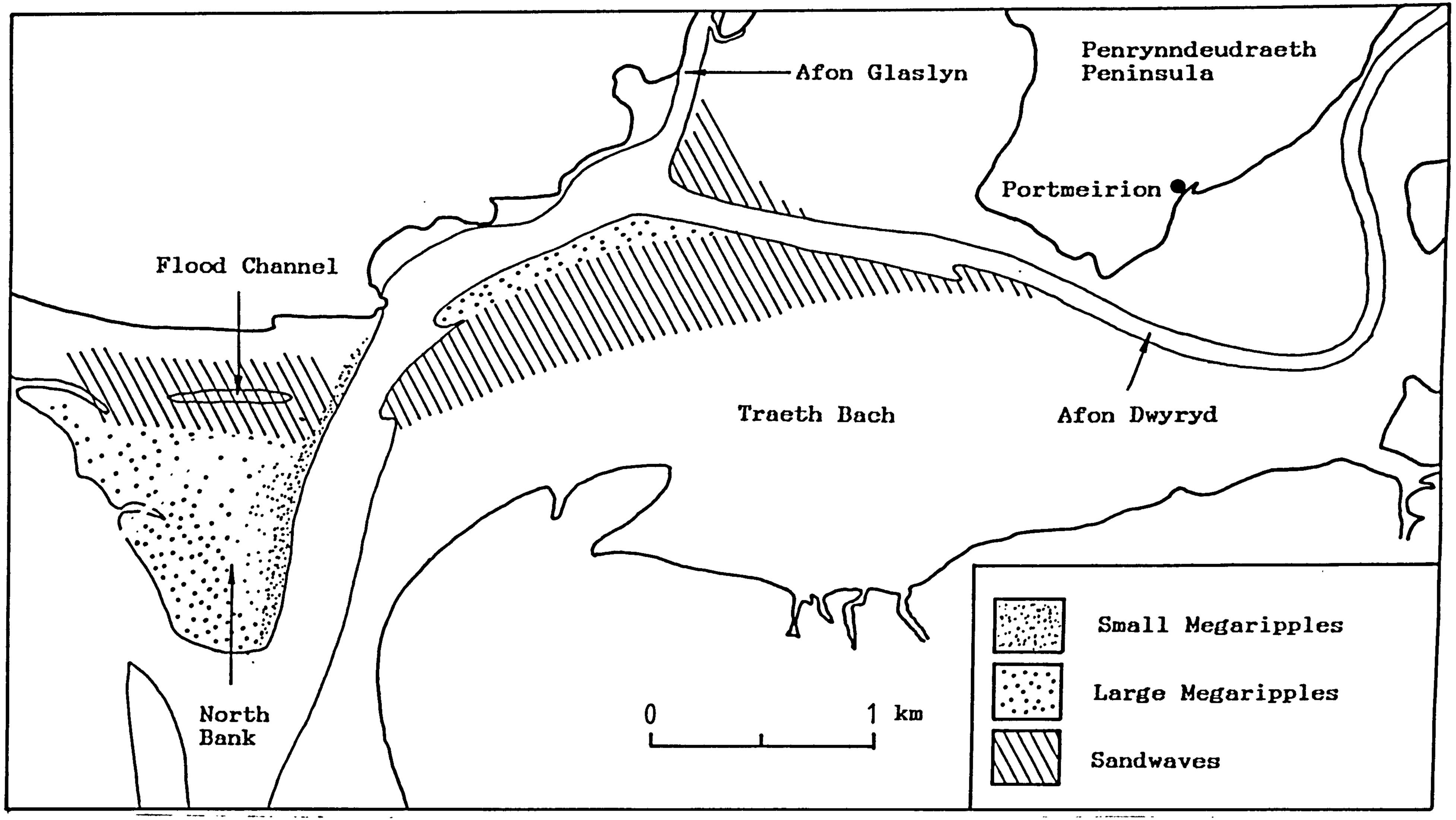

Figure 2.7. Map of intertidal bedforms on beach spit (North Bank) and on sand flats in the lower part of the Dwyryd estuary (Traeth Bach).

basis of height. The smallest ripples range up to 60 cm wavelength; megaripples,from 60 cm to 10 metres; and sand waves, greater than 6 metres wavelength (Hayes,1969; Boothroyd and Hubbard, 1975; Harms et al.,1975 and Dalrymple et al.,1978). The term "large bedform" is used to denote those bedforms of wavelength greater than 60 cm and height of more than 4 cm (Allen, 1968). The division between megaripples and sandwaves is somewhat arbitrary. The term megaripples using in this study are equivalent to bedforms termed "dunes" in other studies (Simons et al., 1965; Southard, 1971).

2.5.1 Estuarine intertidal flats (Traeth Bach)

The intertidal flats of the upper section of the estuary are in general devoid of any large bedforms probably due to the fineness of sediment in this area (chapter 5) and low current speeds (chapter 3). But the whole area is covered with small ripples with wavelengths and heights less than 20 and 5 cm respectively (Figure 2.8a). These ripples are found in most area where low current speeds are unable to produce large bedforms. Ripples generally form approximately transverse to the direction of water movement and have crests that are straight or sinuous (Figure 2.8b). Many studies have shown that ripples propagate rapidly downstream from any irregular bed because of flow separation (Raudkivi, 1963; Southard and Dingler, 1971).

Figure 2.8. Sinuous current ripples on sand flat at the head of the estuary.

Ripples can develop spontaneously on a plane bed by random turbulent vortices which scour the first irregularities (Williams and Kemp, 1971). Small ripples undoubtedly reverse with the changing tide direction , but ripples exposed during low tide are generally ebb-oriented.

In areas where the sand flats are exposed to moderate or strong winds, straight-crested, short wavelength and asymmetrical ripples have been observed (Figure 2.9). This type of ripple is formed by wind-driven waves generated in the shallow waters which submerge the sand flats briefly during high tide. Sometimes, water draining from higher flat to low water mark destroys some of the small ripples, leaving behind scattered patches of plane beds. These plane beds are different from plane bed developed by fast currents which are generally absent in this study area.

The lower section of the estuary which is dominated by sandwaves was surveyed on 20th and 21st. October, 1987 during low spring tide. As shown in Figure 2.10a, the frequency distribution of wavelengths was polymodal and asymmetrical. The majority of the bedforms have wavelengths between 15 to 30 metres and a secondary mode occurred at wavelengths between 5 to 10 metres. Most of the large bedforms are flood-oriented (Figure 2.10b). The distribution of lee-slope orientation varies from 30° to 80° (flood orientation) and from 220° to 280° (ebb orientation). The flood oriented bedforms showed large variations in lee-slope direction because the flood current on entering the

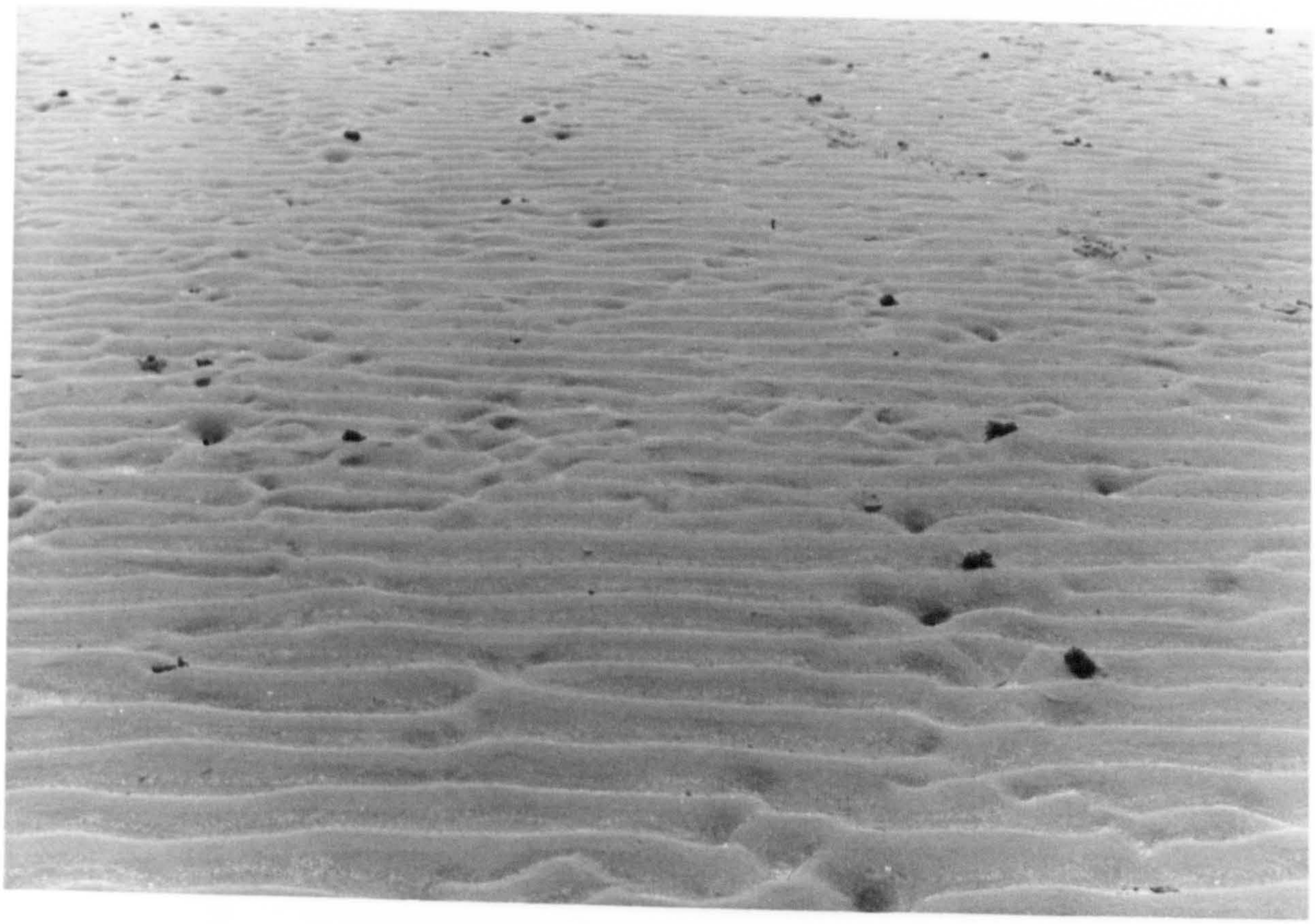

Figure 2.9. Straight-crested current ripples.

TEXT BOUND INTO

THE SPINE

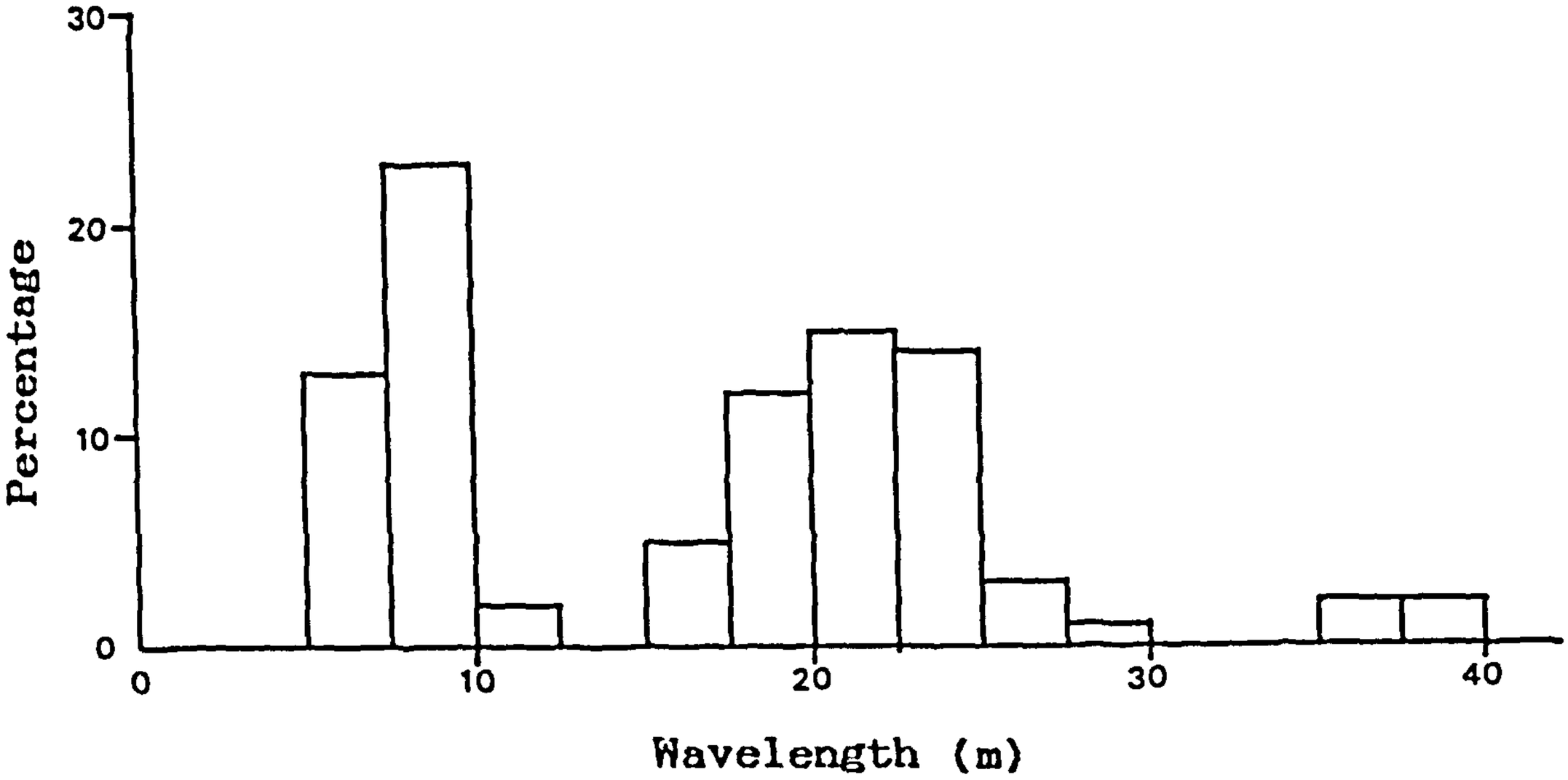

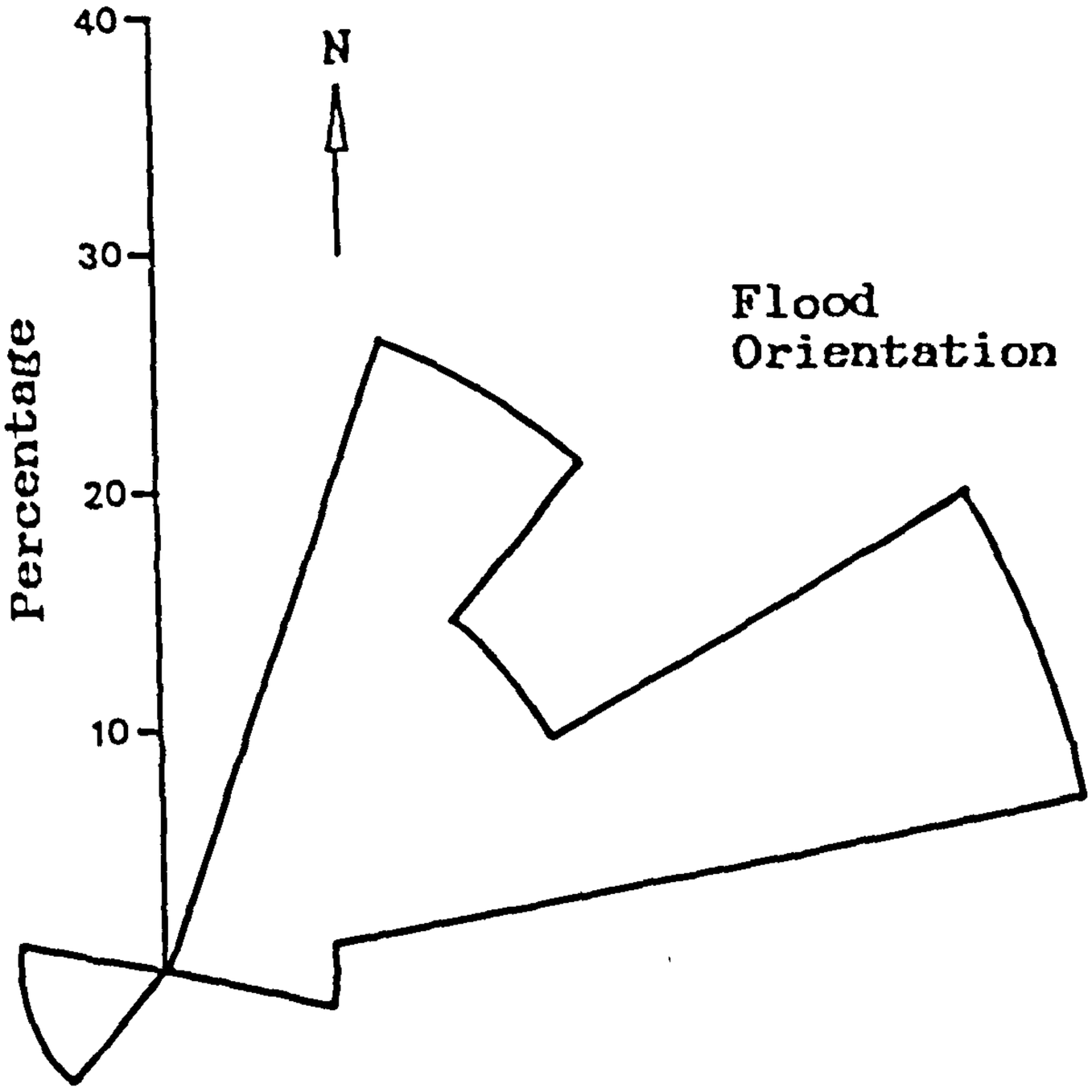

Figure 2.10. Frequency distribution of wavelengths (A) and the distribution of lee-slope orientation of large bedforms (megaripples and sandwaves) on the Traeth Bach.

estuary disperses toward the northeast to the Glaslyn estuary and toward the east to the Dwyryd estuary.

The largest bedforms developed in this area are tidal current formed two dimensional sandwaves. These sandwaves are generally asymmetrical in cross-sectional profile and it is assumed that this asymmetry is an indication of both direction of bedform migration and net sediment transport. On higher topography (Figure 2.11) the sandwaves generally have a long-span with a simple two-dimensional shape. The troughs are generally devoid of scour pits and spurs are not developed on the slipfaces. Their crestlines are straight or of very low sinuosity . The height of the sandwaves, however, decreases away from low water mark. Heights vary only gradually along any individual sandwave because isolated scour pits are absent, and the spacing between adjacent crests also remains more or less constant along their span. The sandwaves in this area show a permanent asymmetry and do not appear to prograde or retrograde into different bedform types.On lower parts of the sandflats near the channel, lunate high-energy current flood-oriented megaripples occur (Figure 2.12). Many studies have shown that 2-D bedforms may change into 3-D forms with increasing current velocity (Rubin & McCulloch, 1980; Costello & Southard, 1981; Harms et.al., 1982; Dalrymple, 1984). These megaripples increase in size towards low water mark probably in response to the increase in grain size (Collins et al., 1981).

Figure 2.11. Typical appearance of 2-D sandwaves (Flood-oriented).

Figure 2.12. Typical 2-D (A) and 3-D (B) magaripples.

2.5.2 North Bank

The sand spit at the mouth of the Dwyryd estuary which is known as North Bank is a sand-body of area about 1.5 km^2 (Figure 2.7). The northern part of the bank consists of a digitating system of flood-channels (van Straaten, 1952; Robinson, 1960). The southern part consists of relatively very large sandwaves where the wavelengths and heights vary up to 50 m and 0.7 m respectively (Figure 2.13).

The major topographic feature of the North Bank is the diversity of its bedforms. On 19th October, 1987 wavelengths and lee-slope orientations of well-formed megaripples and sandwaves were measured. The frequency of distribution of wavelengths was bimodal and asymmetrical (Figure 2.14a). The primary mode had wavelengths less than 10 metres and a secondary mode occurred at wavelength between 10 to 20 metres. The frequencies of ebb-oriented and flood-oriented bedforms are approximately the same. The distribution of lee-slope orientation (Figure 2.14b) vary from 60°to 100°(flood orientation) and from 160°to 240° (ebb orientation). The flood-oriented bedforms showed less diversity in lee-slope direction because their formation is affected probably by a uniform flow direction during the early and middle stages of the flood-tide. The ebb-oriented bedforms on the other hand showed more diversity because of the curvature of the main or ebb channel.

Figure 2.13. Large sandwaves.

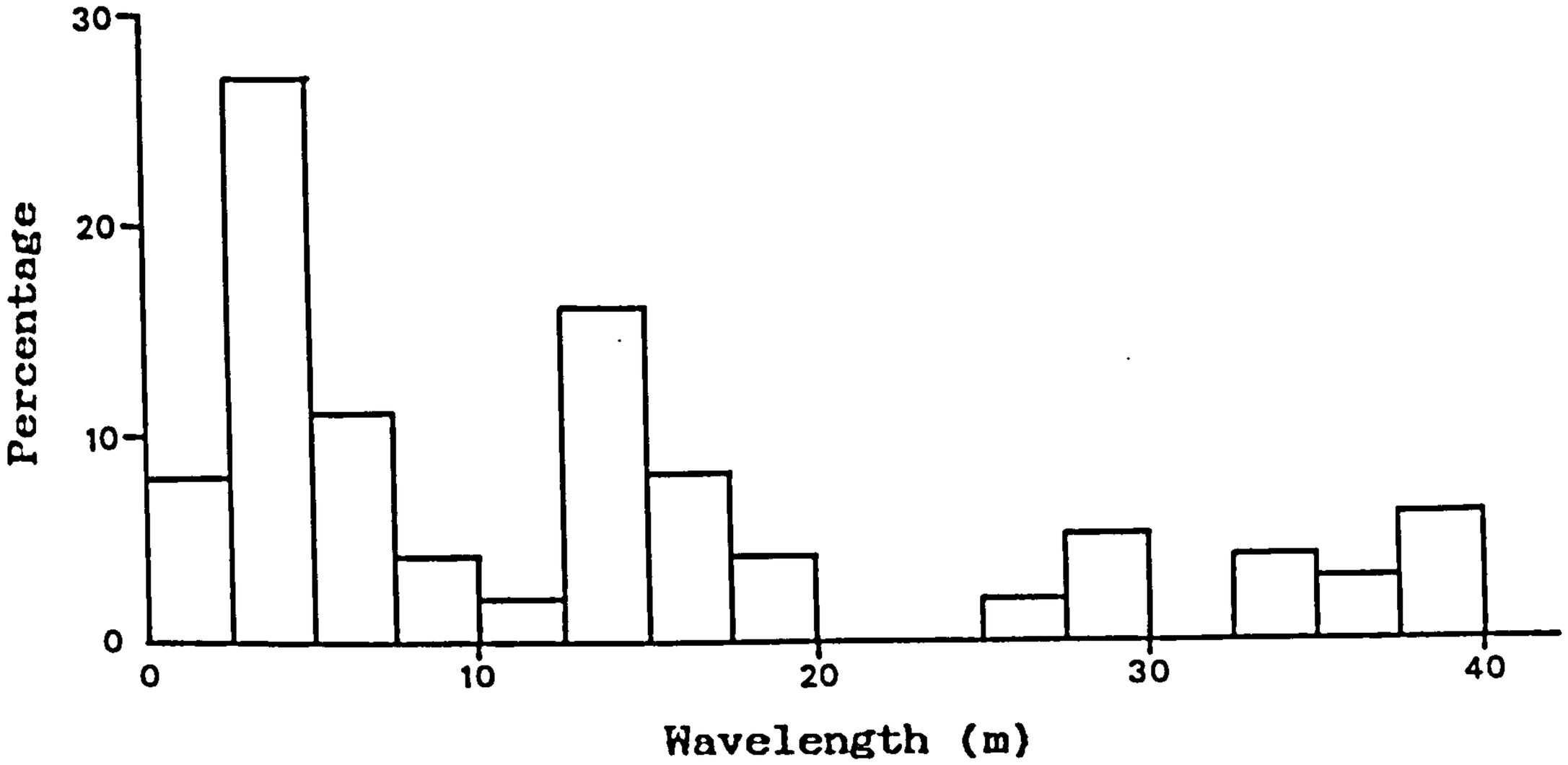

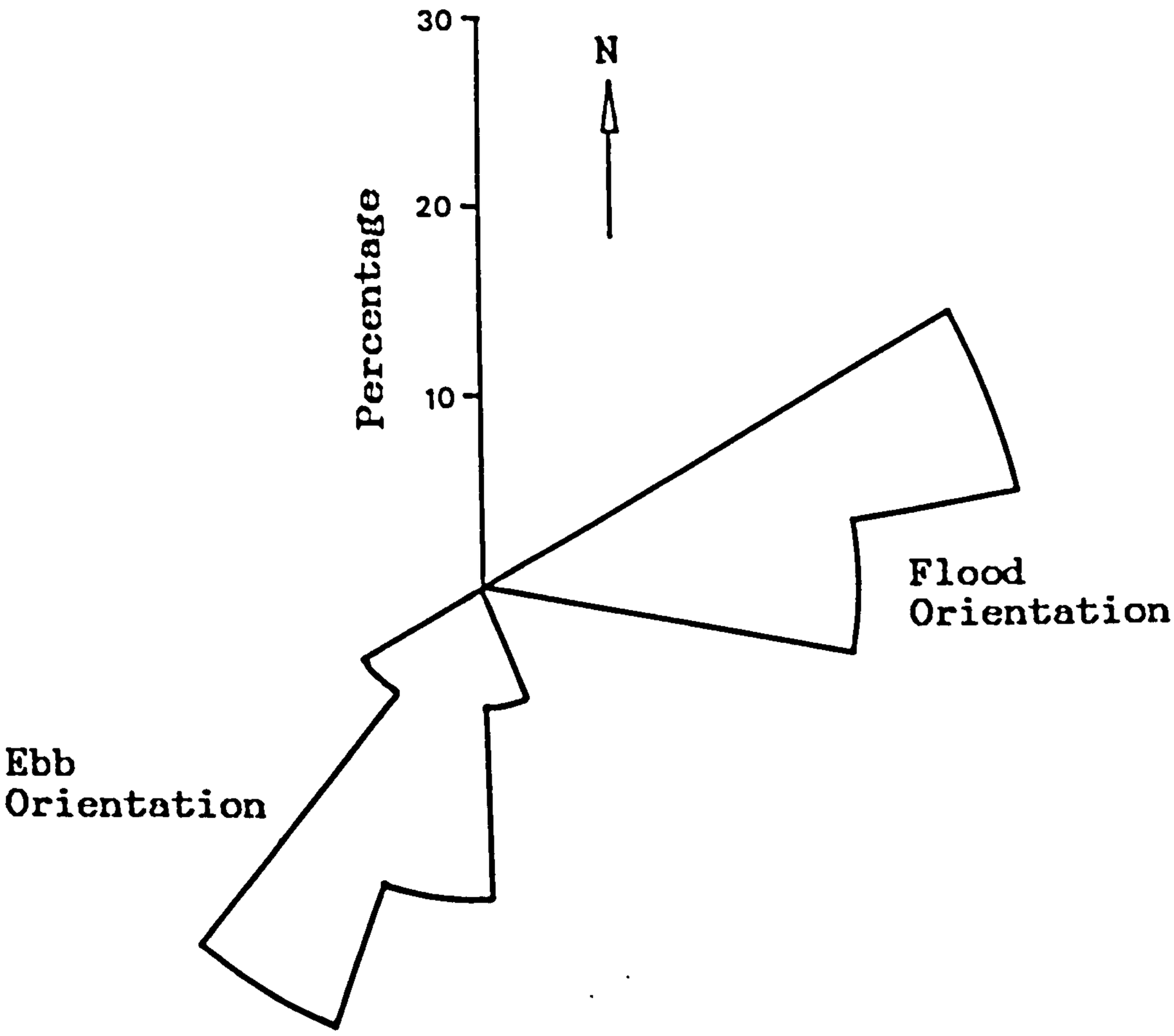

Figure 2.14. Frequency distribution of wavelengths (A) and the distribution of lee-slope orientation of large bedforms (megaripples and sandwaves) on North Bank.

Most of the bedforms in areas close to the main channel are ebb-oriented megaripples with wavelengths varying from 1.9 to 4.5 metres, but the majority of the megaripples have a relatively constant wavelength around 3 metres. Large megaripples occur mostly on topographically low areas near the seaward end of the spit as shown in Figure 2.15. These lunate megaripples are associated with fast currents (Boothroyd and Hubbard, 1975), probably developed when the flood current tends to move in a straight line across the sand spit. These megaripples are best developed during spring tidal conditions when tidal currents are at their maximum. Small megaripples are generally found along the low water mark of the main channel. Their shapes vary from straight crested (2-D) (Figure 2.16a) to lunate (3-D) megaripples (Figure 2.16b).

Most of the flood channel area is covered with nearly symmetrical two dimensional sandwaves (Figure 2.17). The wavelength to height ratio is very small ranging from 1:40 to 1:100. They occur at current strengths below that of the dune (Harms et al., 1975). Such bedforms occur abundantly in nearshore and shallow marine tidal environments because of the unique processes associated with reversing tidal currents (Allen et al., 1980a,b).

The bedforms found in this study area bear a close resemblance to those of the Loughor estuary recently described by Elliott and Gardiner (1981) where bed deposits

Figure 2.15. Flood-oriented megaripples with sinuous crests, fluctuating crest height and well-developed scour pits.

Figure 2.16. Ebb-dominated 2-D (A) and 3-D (B) megaripples with superimposed current ripples.

Figure 2.17. Large flood-oriented 2-D sandwaves in the blind flood channel (North Bank).

consist of fine sediment (0.20 to 0.25 mm) which is slightly coarser than sediment found in this area (chapter 5). The bedforms observed in this area are also similar to those occuring in the Bay of Fundy where heights and wavelengths average 0.81 and 37.9 metres respectively (Dalrymple, 1984). But, in the Bay of Fundy, Dalrymple et al. (1978) showed that sandwaves developed only in medium size sand coarser than 0.3 mm which is obviously in contradiction to the finding in this study.

The relationship of these sandwaves to the unidirectional (non-tidal shallow marine and fluvial) bedforms remains unclear despite extensive research (Coleman, 1969; Harms et. al., 1974; Jackson, 1976; Flemming, 1978; Swift et. al., 1979). Under constant flow the bedform may adjust until an equilibrium dimension is reached, which implies that the wavelength and wave height of the bedform become constant. But under changing flow conditions as found in estuarine environments, there is a continuous creation, change and vanishing of individual bedforms (Allen, 1982a,b,c; Costello and Southard, 1981 ; Wijbenga and Klassen, 1983), so equilibrium bedforms cannot be formed

As shown in this study, megaripples and sandwaves exposed during the low water period present obvious evidence of residual sediment transport on intertidal flats in this estuary. The variations of current speed, water

depth and current direction during the short period flood-ebb cycle as well as over the longer neap-spring-neap cycle have some influence on the type of bedforms observed. Because bedforms are sensitive to flow velocity and water depth (Boothroyd and Hubbard, 1974, 1975), bedform type is a powerful tool in differentiating areas of high and low energy (current strength) without actually making detailed measurements.

2.6 Surface and Subbottom features of Tremadog Bay

2.6.1 Survey and equipment

The study of the surface and subbottom structures of Tremadog bay was carried out during a cruise from July 6 to 7, 1987, involving the UCNW research ship 'Prince Madog' where about 80 line kilometers of uniboom, pinger, and side-scan sonar records were collected. In addition, 25 sediment samples were also collected during the survey using a Shipek grab sampler. The survey profiles which run parallel and normal to the bathymetric contours and sediment sampling stations are presented in Figure 2.18.

The positions of the lines and the sampling stations were obtained using a Decca Hifix with positional accuracy of about 10 m depending on weather conditions. During the survey, the position of the ship was taken at 15 minute intervals and at every time the ship changed its course. At

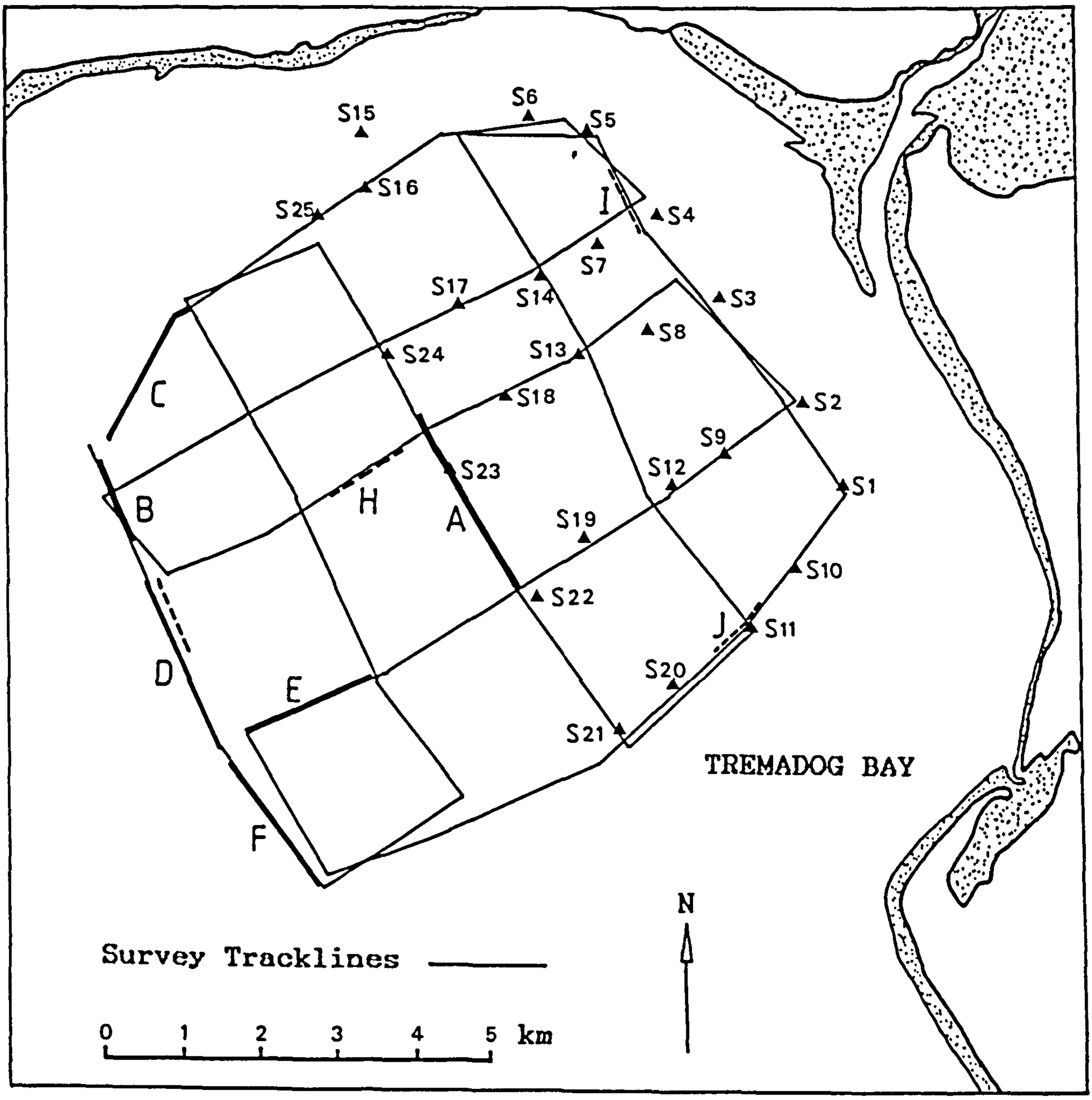

Figure 2.18. Map of Tremadog Bay showing locations of surveying tracklines and sediment sampling stations. Tracklines with letters locate survey records shown in Figures 2.20 to 2.30.

the same time position marks on the recorder charts were also printed to indicate the position of the ship.

Subbottom profiling was carried out simultaneously with EG&G uniboomer model 230 and ORE pinger model 140. The uniboomer is a system consisting of a separate source and detector which are towed behind the ship. The energy source consists of an insulated metal plate and rubber diaphragm adjacent to a rigidly-held electric coil; all these components are mounted within a towfish. The uniboomer operates by releasing an acoustic pressure pulse from the metal plate. The stored electrical energy is discharged from a bank of capacitors. During the discharge, the resultant electromagnetic force induced by the coil forces the metal plate explosively which generates a broad band acoustic pulse in a frequency range of 400 Hz to 14 kHz. Most of the energy is directed towards the sea bed. The detector is a linear array of eight element hydrophones spaced at 3.8 m interval detect the reflected signal by the reflector and recorded it on the charts.

The ORE pinger system consists of a fixed transducer mounted on the hull of the ship. The sound source used is usually produced by a piezoelectric or magnetostrictive transducer. The transducer is designed to produce a focoused beam of sound to reduce energy loss to the surface. A variable range of frequency between 3.5 to 7 kHz can be generated thus allowing a choice between

penetration and resolution. The lowest frequency (3.5khz) was chosen for the entire survey since it can produce the best resolution with an adequate penetration.

The side-scan sonar used in the survey is an ORE model 170-B dual channel system with output power of 2 kWatts, operating at 97 kHz frequency. A continuous series of sound pulses is projected into the sea bed. The returned signals are picked up by a receiving transducer and continuously recorded on paper. The resolution and clarity of the records are dependent on a variety of factors, such as sediment type and the size of bedforms on the sea bed.

2.6.2 Interpretation of Subbottom Profiles

The seismic profiling records are dominated by the appearance of a diffuse reflector at a shallow depth beneath the sea bed which apparently masks the underlying reflectors. The masking of reflectors by strong attenuation of high frequency acoustic signals is characteristic of gas-charged sediments. In Tremadog Bay the gas-charged sediments zone occurs mainly in the central part of the bay comprising about 75 km in area as shown in Fig.2.19 (Fenemore, 1976). These sediments are similar to the 'turbid' sediments found in other shallow water environments (Reeburg,1969; Schubel and Schiemer,1973; and Schubel,1974b). Schubel (1974b) attributes the turbid character to the attenuation and scattering of acoustic

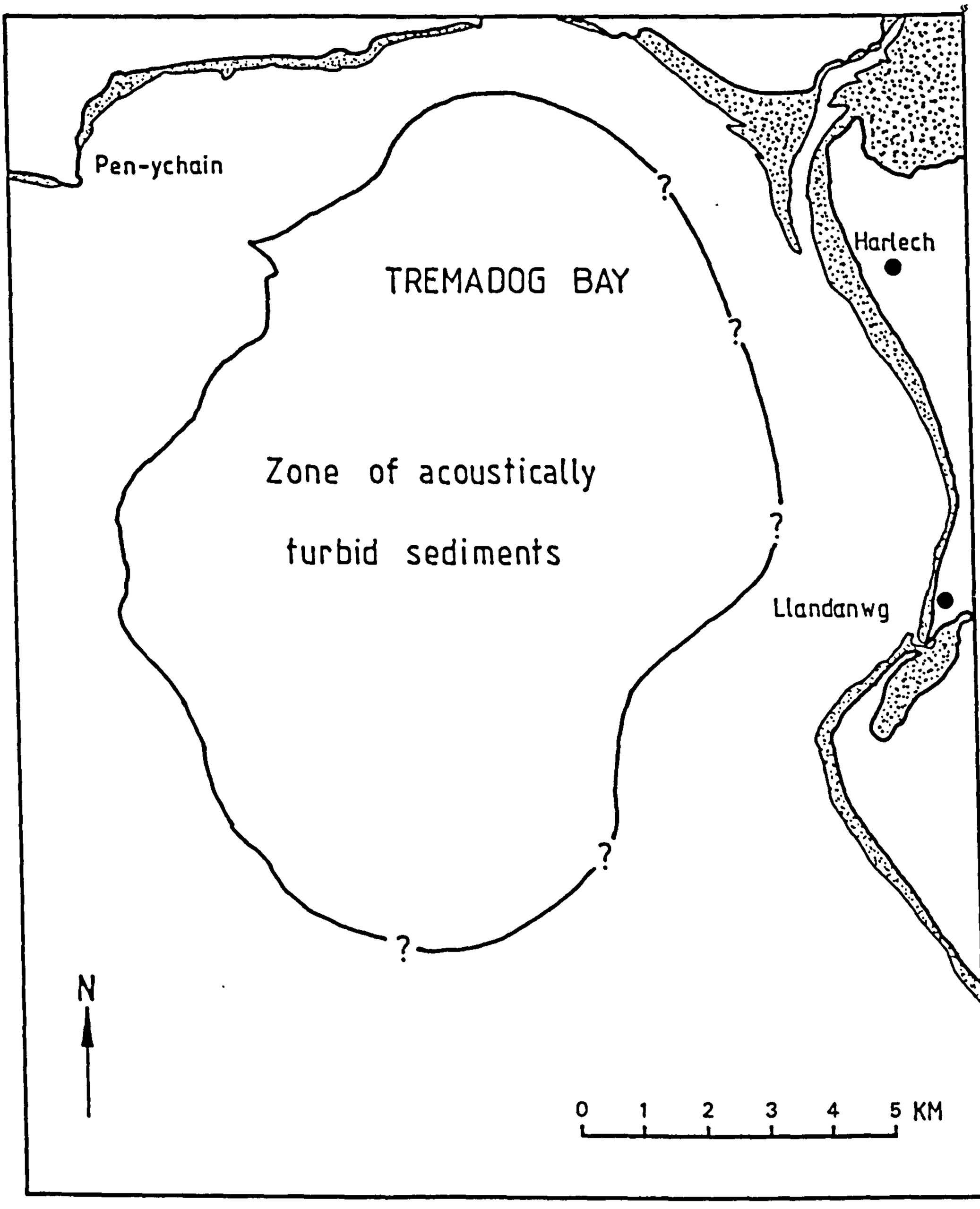

Figure 2.19. The distribution of accoustically turbid sediments (After Fenemore, 1976).

Figure 2.20. Uniboom profile A across the thick sediment accumulation in the central part of the bay showing the turbid layer below which accoustic energy attenuates. Arrows indicate the gas plumes. For position see Figure 2.18.

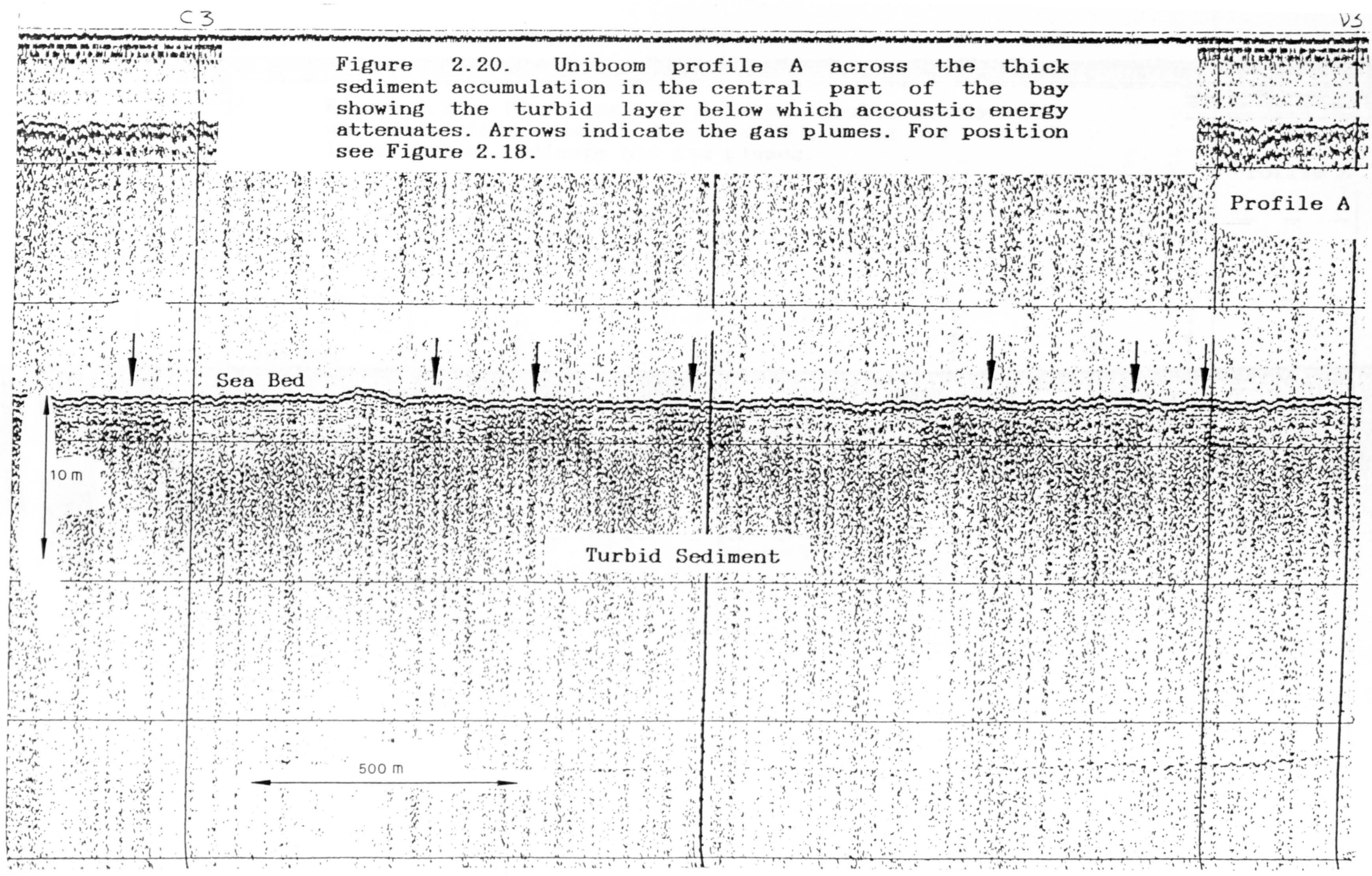

C3

D3

Figure 2.21. Pinger profile A taken simultaneously with uniboom profile shown in Figure 2.20 showing the turbid layer. Arrows indicate the gas plumes.

Profile A

Sea Bed

10 m

Turbid Sediment

500 m

energy in sediments which contain gas bubbles in their interstices.

The origin and constitution of the gas is still unknown. One possible explanation is that the gas may originate from the decomposition of organic matter buried with the sediments. Only geochemical analysis of the gas will possibly provide the answer to its origin and constitution. Obvious evidence of gas seepage and migration through the upper layers of modern sediment is provided by observations of gas bubble plumes under the sea bed in the uniboomer and pinger records (Figure 2.20 and 2.21).

Out of the 80 line kilometers of subbottom records collected during the survey, only about 5 line km revealed the presence of a more or less continous reflector. A strong single reflector has been recorded from the western part of the survey area. The quality of the records are good since the conditions of the sea during the survey was perfect for the survey with slight ripple and low swell. Wind strength was around Force 2.

In order to convert the vertical time scale of the records into actual depths of the reflectors it is necessary to know the velocity of sound for the modern deposits in this area. Information concerning this parameter is currently available (Taylor Smith, 1975; Simpkin,1976; Fenemore,1976). For the interpretation of the

records in this investigation, a value of 1700 m/s has been chosen for the mean velocity of sound in the modern sediment above the subbottom reflectors. The depth of modern sediment to the reflector is given by

$$d = \left[\frac{v^2 (t_1 - t_0)^2 - \Delta x}{4} \right]^{1/2}$$

where d is the depth of the subbottom reflector from the sea bed, v is the sound velocity through the sediment, t_1 is the two way travel time to the subbottom reflector, t_0 is the two way travel time to the sea bed and Δx (equal vt) is the distance from the source to the detector which is equal to the product of sound velocity in sea water (1500 m/s) and the time elapsed which can be estimated from the records.

Original records which show the subbottom reflector are shown in Figures 2.22 to 2.26. The positions of each section of the record are indicated in Figure 2.18. Strong reflectors are encountered only at the northwest section of the study area (Figures 2.22 and 2.23) and are interpreted as the top of boulder clay deposits. The depth of this reflector is very variable and boulder clay emerges from the sea bed to reach the surface to the west of survey area. The boulder clay surface seems to descend toward the centre of the bay (Figure 2.24) to form a broad depression which is infilled by modern sediment. It is impossible to trace the boulder clay surface from the rest of the record

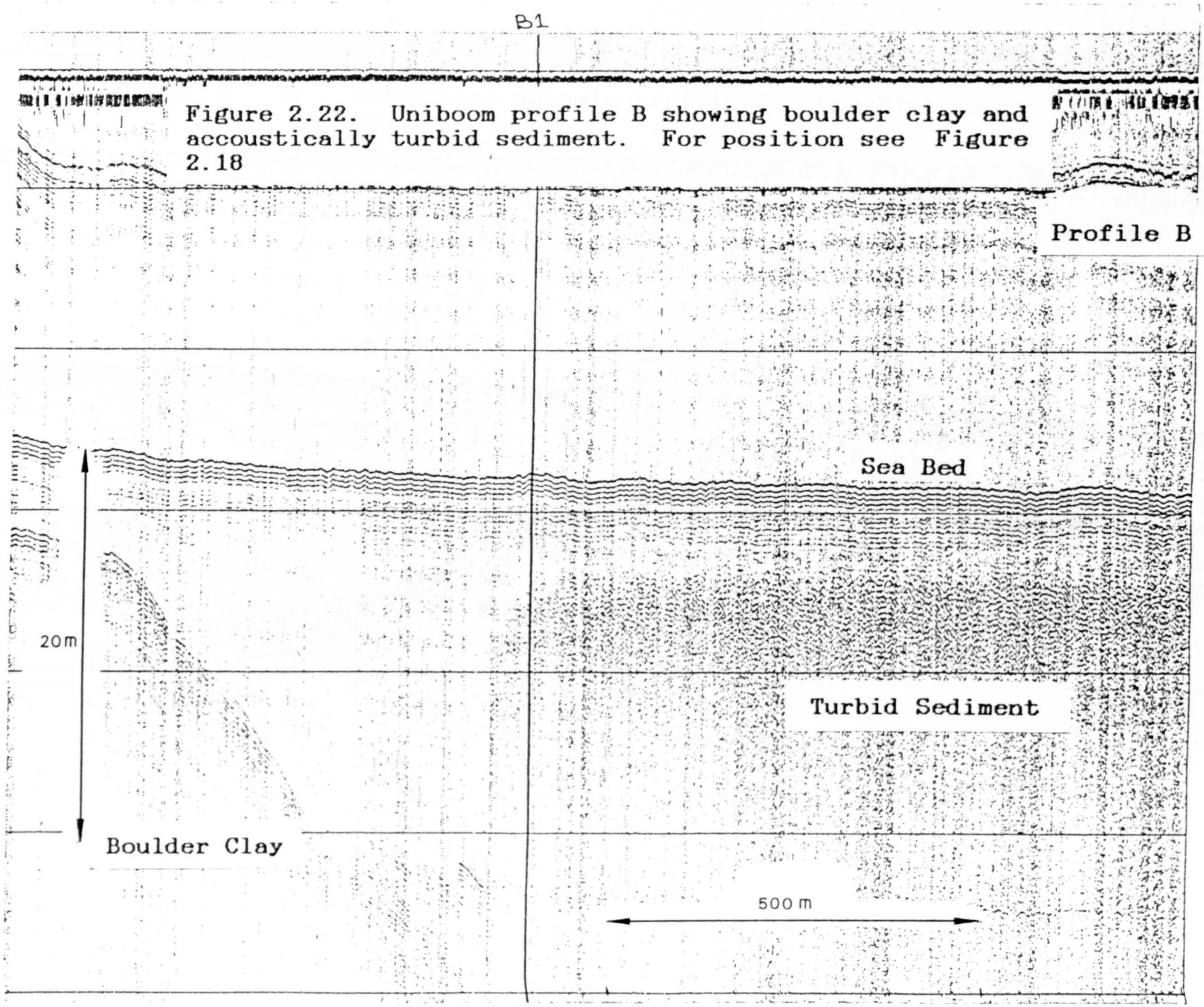

Figure 2.22. Uniboom profile B showing boulder clay and accoustically turbid sediment. For position see Figure 2.18

Figure 2.23. Reflection seismic profile C. Location is indicated on Figure 2.18.

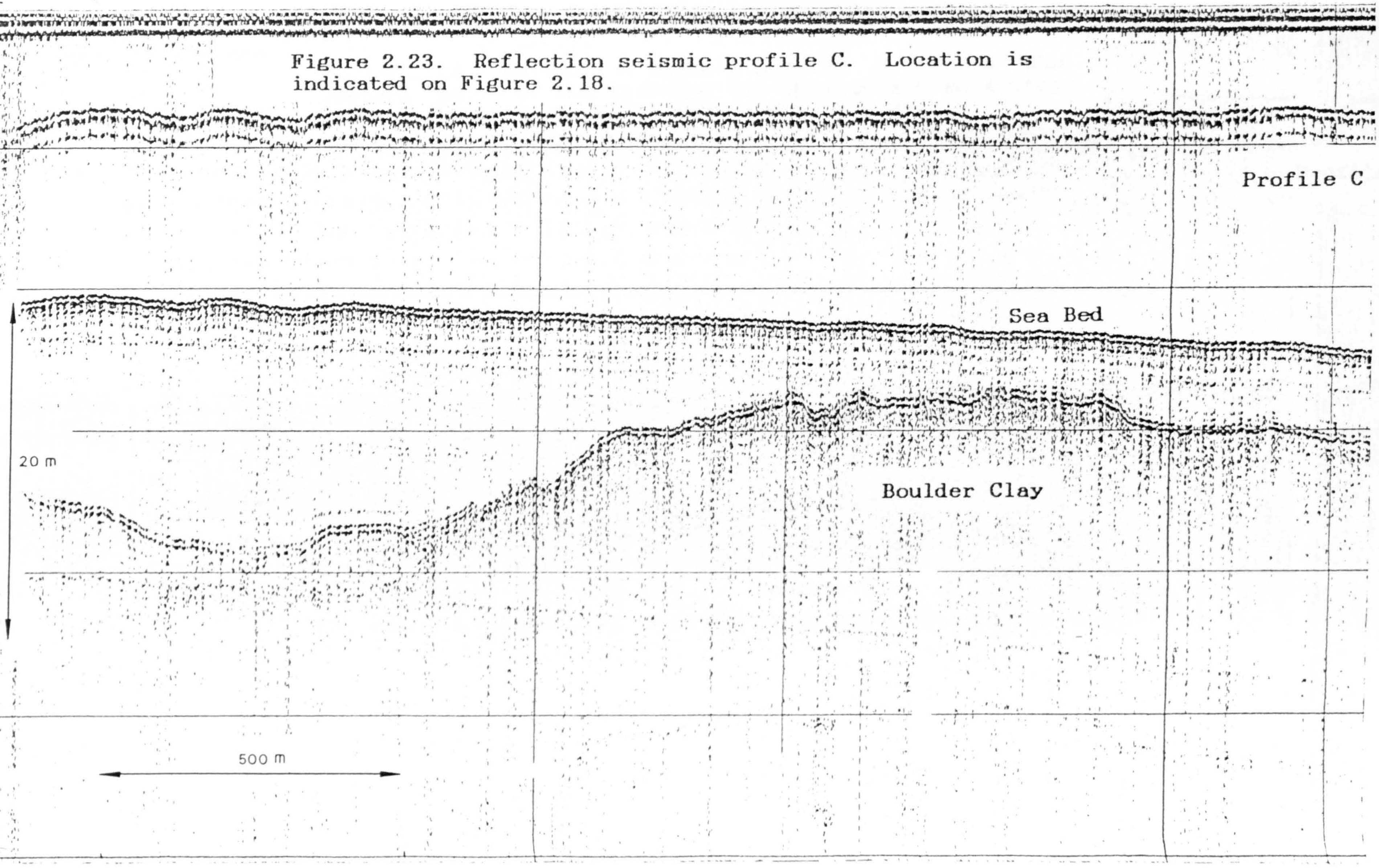

78
D1

Figure 2.24. Reflection seismic profile D across the western part of the Tremadog Bay showing mid-reflector (arrow). Location is indicated on Figure 2.18.

Profile D

Sea Bed

10 m

Turbid Sediment

Boulder Clay

500 m

Figure 2.25. Reflection seismic profile E. Location is indicated on Figure 2.18.

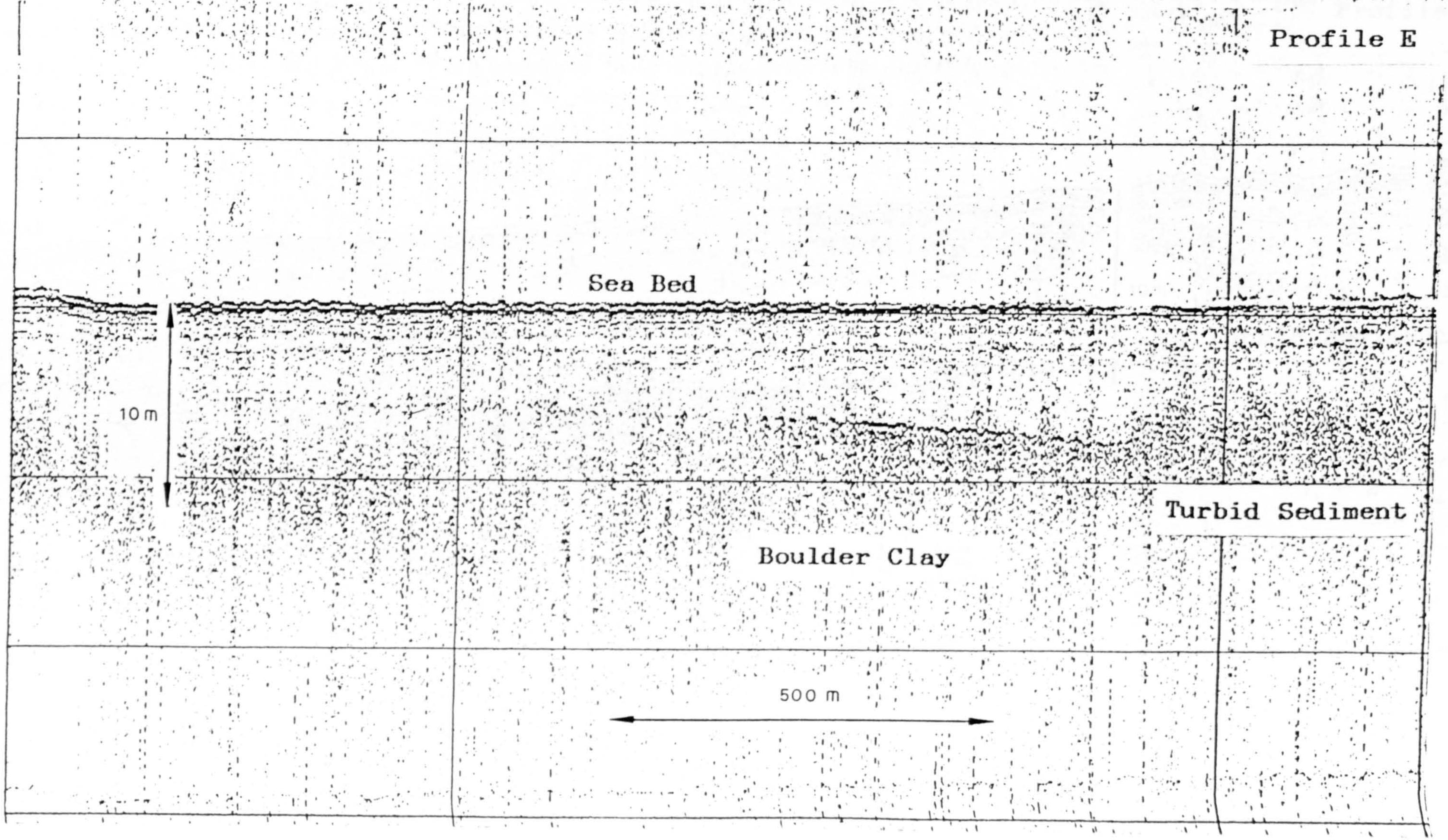

Figure 2.26. Reflection seismic profile F. Location is indicated on Figure 2.18.

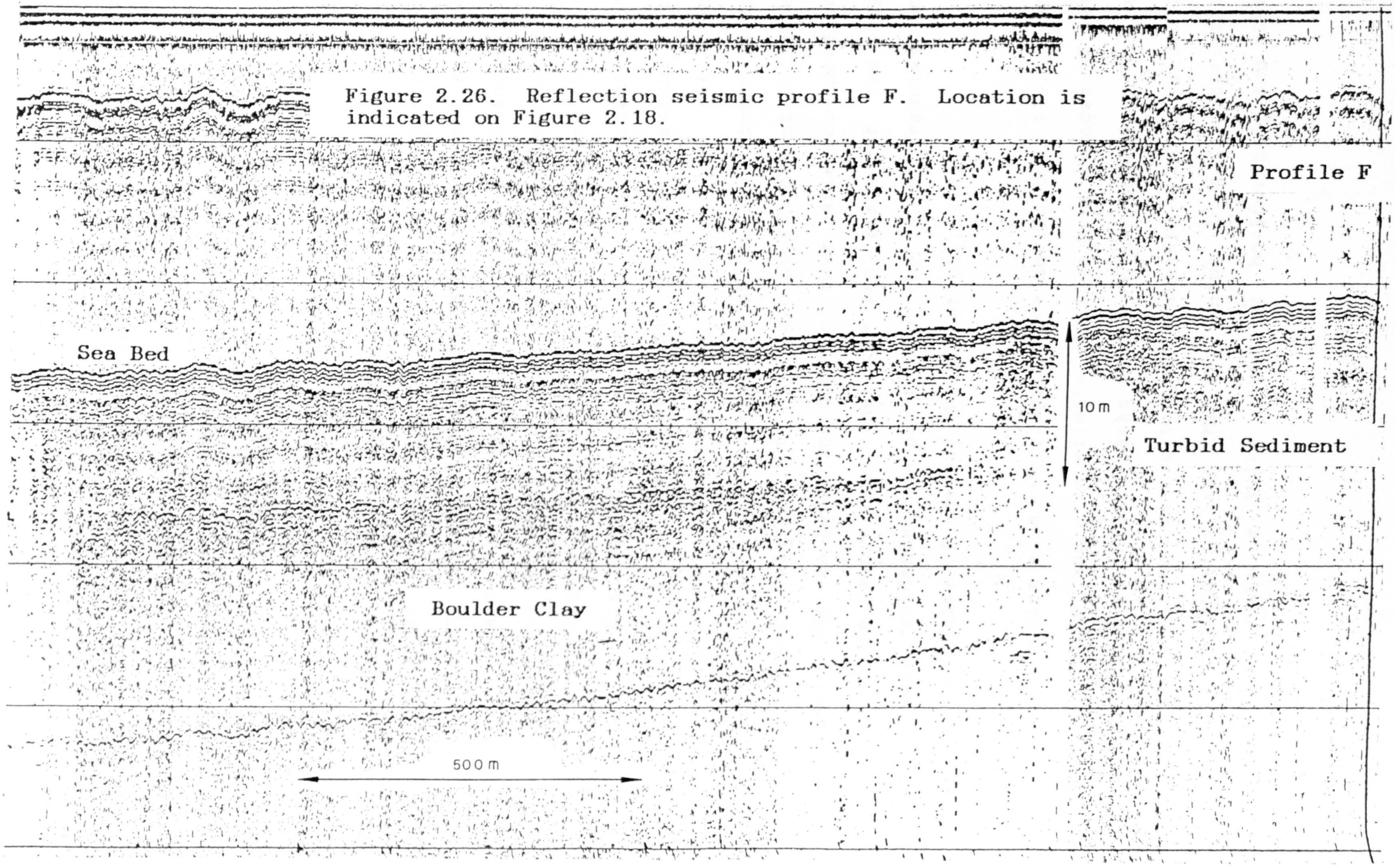

due to the inpenetrable nature of the turbid sediment at the top.However,in the south part of the area, the masking effect is not continous,and a reflector was detected at a few places. The thickness of modern deposits in the depression varies from a few centimeters to about 30 metres.

Detailed descriptions of the distribution of the boulder clay layer , and the nature of Sub-Pleistocene and Pleistocene geology of the bay,have been given by Fenemore (1976) based on a seismic reflection profiling survey carried out during 1976. Three different sedimentary units of the presumably lower Palaeozoic, Jurassic and Tertiary can be distinguished from the reflection records on the basis of their acoustic characteristics. The presence of a lower Palaeozoic reflector was confirmed by refraction seismics in the northeastern part of the bay which measured a seismic velocity of 4345 m/s at a depth of 80 meters beneath the sea bed. The depth of this reflector increases toward the centre from the northern flank of the bay. Further evidence was provided by the I.G.S boreholes sunk in the centre of the bay (Wright et al.,1971).

The entire area overriden by ice during the Pleistocene glaciations and the effects of subsequent changes of sea-level have left their marks in the morphology of the area. The Irish Sea glaciers moved southward a large volume of Tertiary deposits into the bay which form a depression infilled with a thick layer of boulder clay and other

deposits. Retreat of the Irish Sea glaciers was followed by partial reworking of the deposit by local Welsh glaciers which eroded the boulder clay westward from Portmadog across the Tertiary and Lower Palaeozoic rocks to form a broad depression which partially closed at its south-western extreme. The southern section of this depression is exposed at the surface of sea bed to form a distinct linear moraine, Sarn Badrig. The northern flank of the depression is exposed at the sea bed as a distinct boulder clay ridge which has been recorded during this survey. Much of the modern topography of this embayment bears a similar feature to the old boulder clay topography.

The rise of sea level resulted in a decrease of wave disturbance and turbulence and probably also in a reduced current speed close to the sea bed. When the present-day circulation pattern was established (probably around 6000 BP), fine material was transported from the Irish Sea via Cardigan Bay to Tremadog Bay by tidal currents and subsequently deposited in relatively quiet water areas of the bay. This resulted in a gradual decrease in grain size of the bottom sediments since that time. This is confirmed by the presence of a transition record from freshwater glacial to fluviatile to estuarine and ultimately to marine sediments in the I.G.S boreholes sunk in this area (Fenemore, 1976).

The occurrence of turbid sediments in the central part

of the Tremadog bay are an indication of low energy levels in these areas. The absence of bedforms in the deeper part of the bay (see later) is probably due to low velocity currents which provide the most favourable condition for the deposition of fine suspended sediment. The presence of a high percentage of mud and marine fauna (foraminifera, bivalves and gastropods) is responsible for the formation of turbid sediments (chapter 5). In general, the central part of the bay can be regarded as a depositional environment with little net sediment movement. Sediment movement is taking place in areas of relatively high energy which includes the southern part of the bay just north of Sarn Badrig and nearshore areas along the coast of the bay. In these areas the sediments probably move parallel to the coastline.

2.6.3 Interpretation of Sonar Records

Geophysical evidence suggests that most parts of Tremadog Bay are areas of sediment deposition. Most of the sonar records consist of broad variations in shading which indicates the absence of large bedforms on the bed. The shading varies from light to moderate tonality indicating a relatively weak acoustic reflection from the sea bed . The changes of shading are probably due to textural changes in the sediments.Such changes have been observed from shallow shelf areas around the British Isles (Belderson & Stride, 1966; Kenyon and Stride, 1970). In these areas, the dark

colour is due to coarse sand,whereas the surrounding light areas are fine-grained sand. Featureless records were found mainly within bathymetric lows in the central part of the bay which corresponds with the zone of muddy sand. However, this environment is likely to contain small-scale bedform features not detectable by the side-scan sonar or seismic techniques employed.

A few sections of the sonar records,however, indicate the existence of strong acoustic reflections from the sea bed, and also reveal that large scale bedforms are present on the sea bed at the northwestern part of the study area which produce a strong reflection of acoustic waves (Fig. 2.27 to 2.30). Large-scale bedforms such as sandwaves (wavelength greater than 6 m) with wavelength in the range 25 to 140m have been observed at a few places from the records. Their areal distribution is limited to zones of sandy sediment in shallow water near the coast. The presence of such bedforms on topographic highs and their absence elsewhere implies that the direction and intensity of sediment transport are controlled by the interaction of topography and tidal currents. They also could be caused by strong currents generated during the occasional severe storms experienced in the area.

The shape of the sandwaves seen from the shading pattern of the bedforms in genaral are markedly asymmetrical (Figures 2.27 and 2.29) and indicate mass sediment movement to the northeast in the western section of the bay. Near

Figure 2.27. Side-scan sonar record (profile G) showing patterns produced by bedforms and featureless seabed.

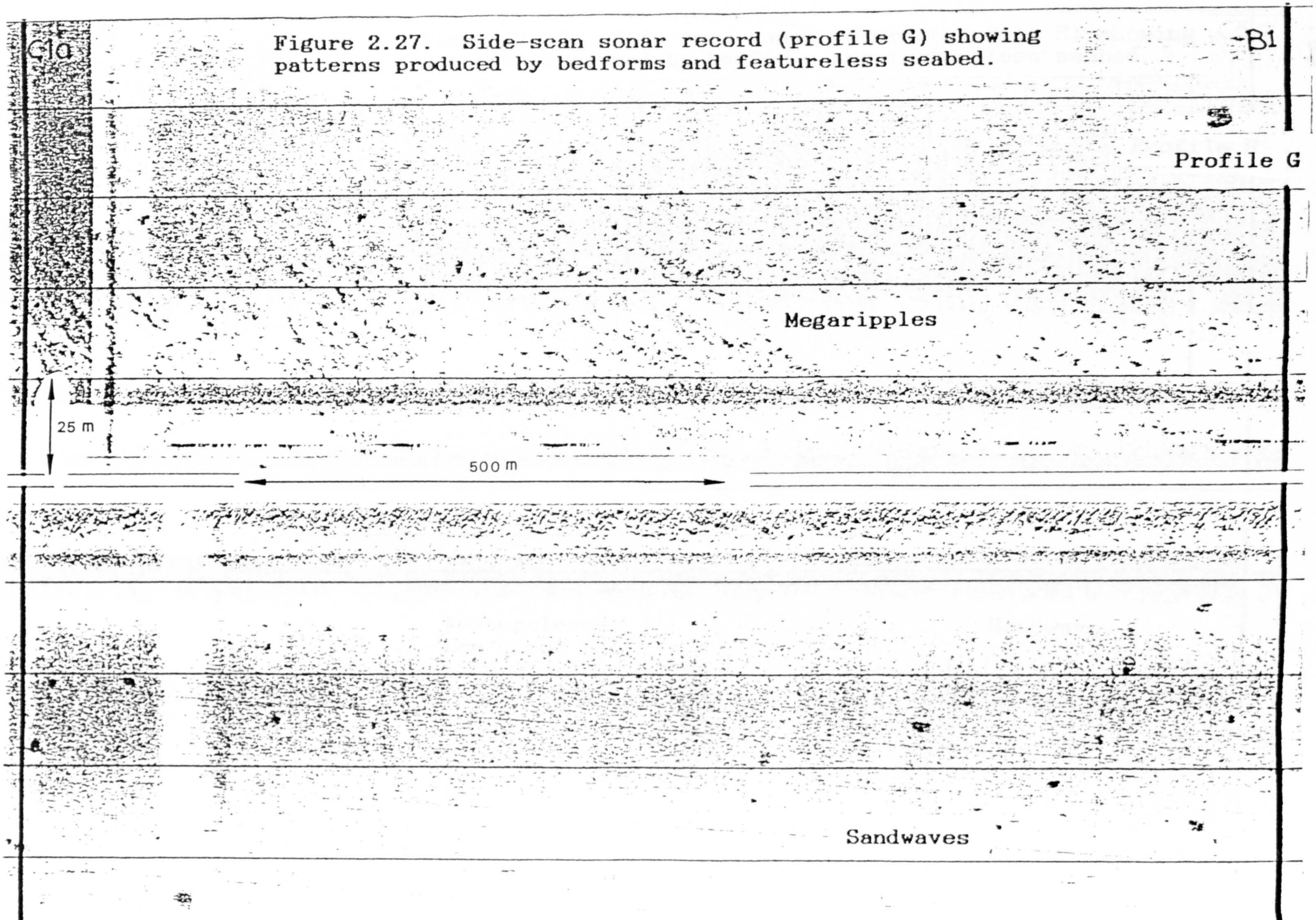

Figure 2.28. Side-scan sonar record (profile H) showing patterns produced by bedforms and featureless seabed.

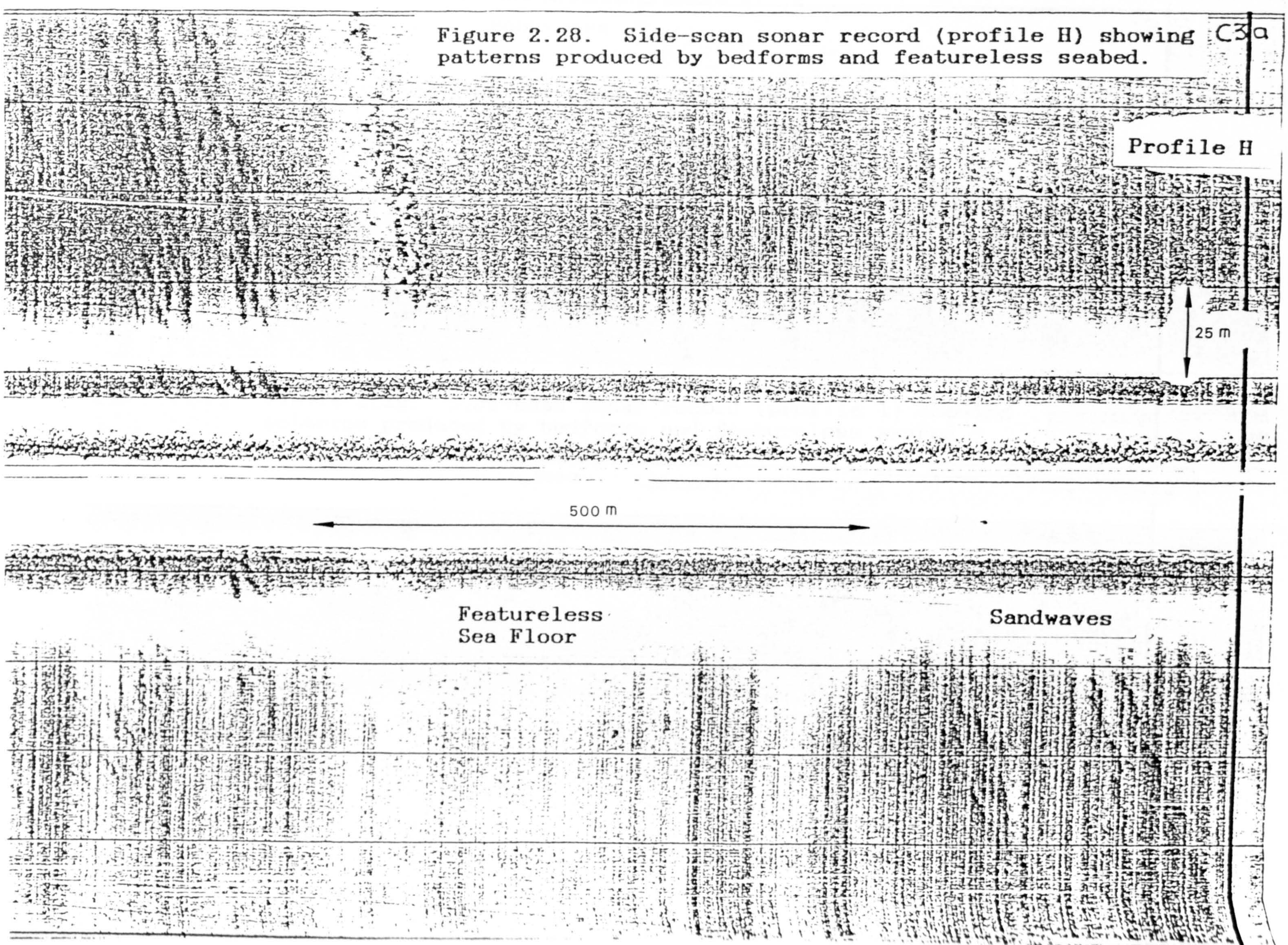

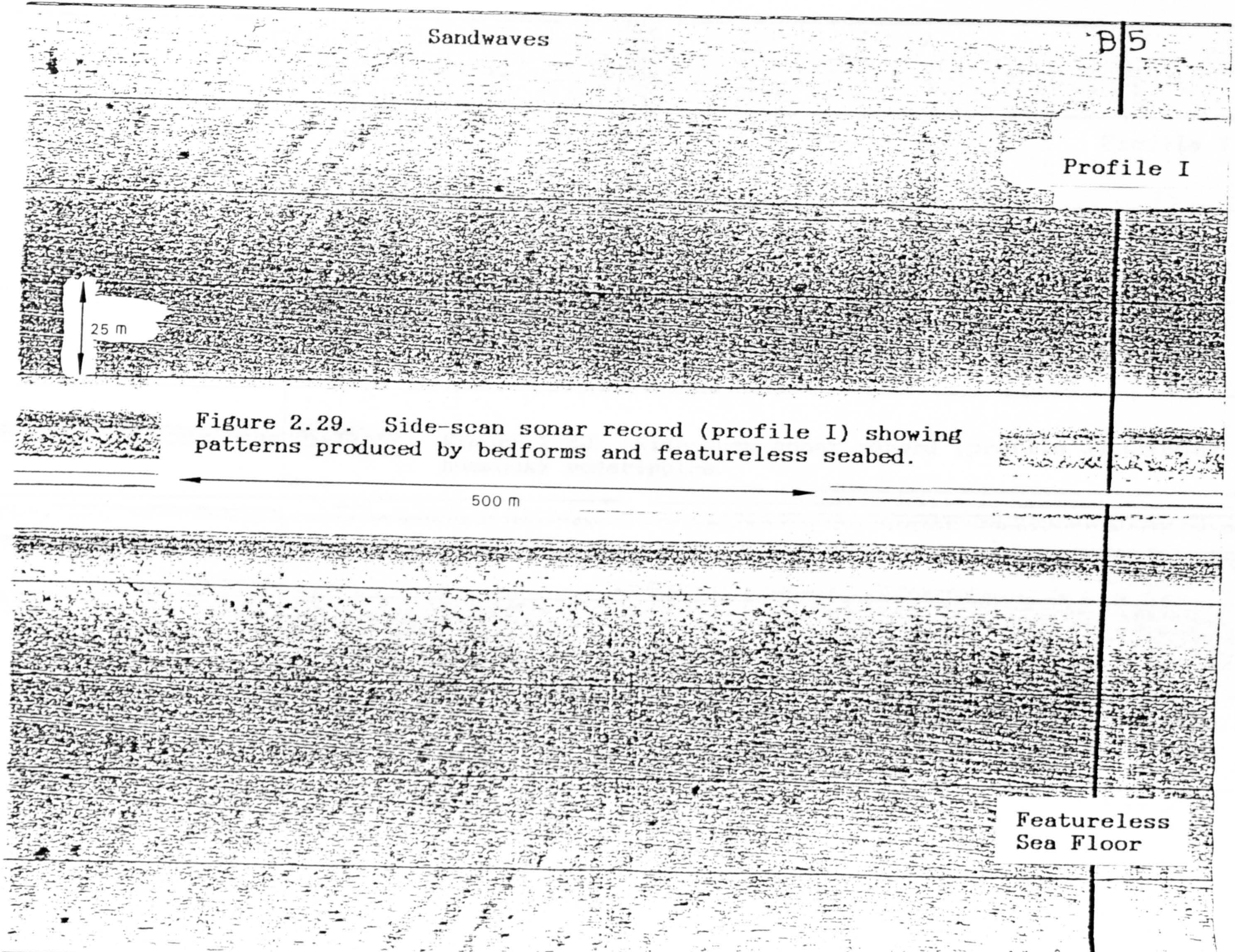

Figure 2.29. Side-scan sonar record (profile I) showing patterns produced by bedforms and featureless seabed.

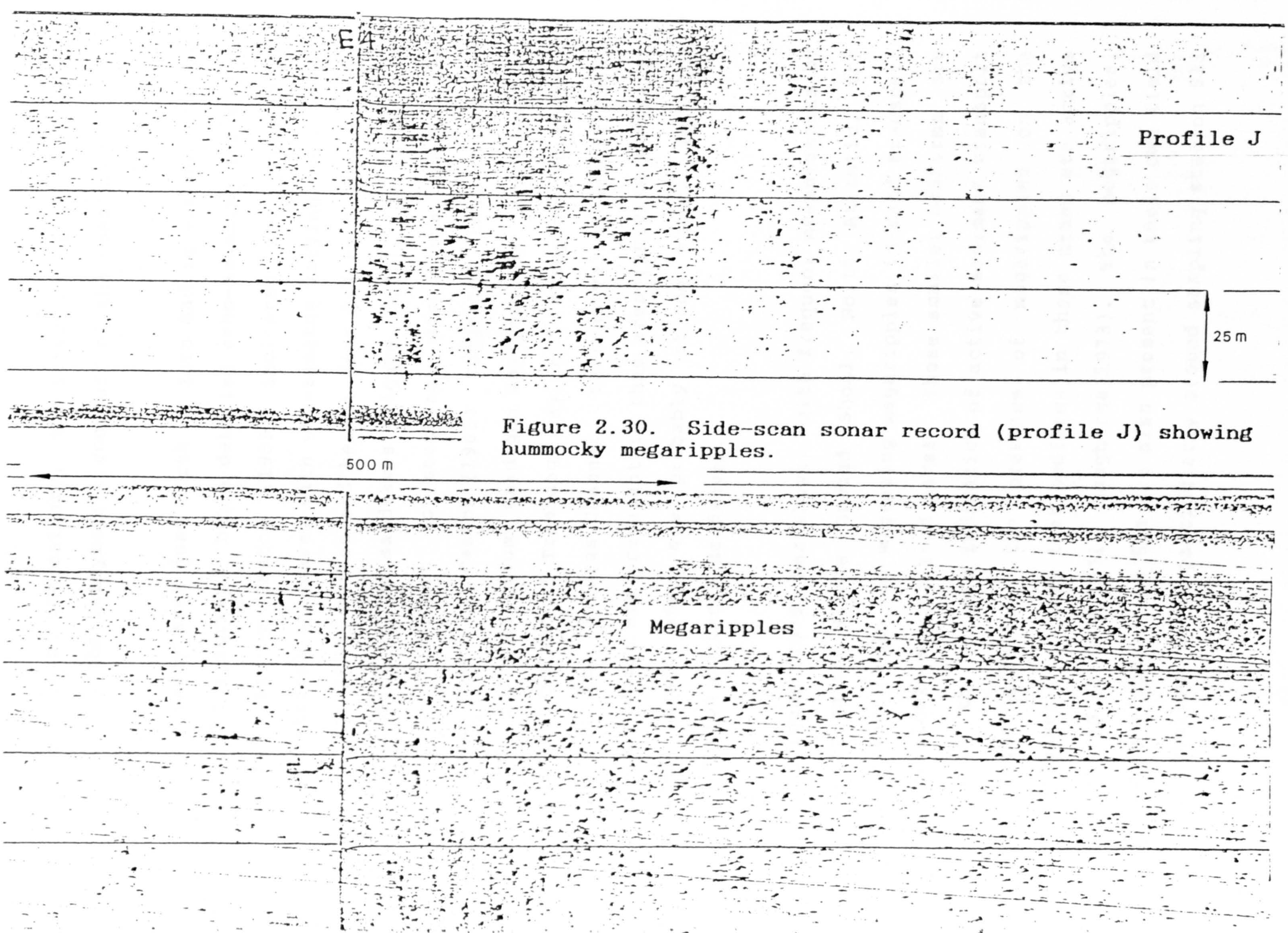

Figure 2.30. Side-scan sonar record (profile J) showing hummocky megaripples.

the mouth of the estuary, the direction of movement tends to follow the bathymetric contours of the coastlines.

The sandy area just north of Sarn Badrig was not covered during the survey, but a detailed echo-sounding survey in this area by Caston (1965) indicated the presence of asymmetrical sandwaves with wavelengths varying from about 700 to 1000 metres and height from 0.7 to 2 metres. The orientation of the sandwaves (Figure 2.31) indicates the genaral transport to southeast directions toward the Mochras Channel. Caston (1965) suggested that northward tidal currents from Cardigan Bay possibly "ponded-up" at the eastern end of Tremadog Bay and escaping southwards through the Mochras Channel. Current velocities of about 50 cm/s which are prevalent in this area (BRITISH ADMIRALTY 1896, chart 368) are probably strong enough for the formation of these sandwaves.

Brigges (1979) has shown, with frequent measurements by divers on the Middle Ground Shoal, North Atlantic, the important role of migrating megaripples in sand transport over slowly moving sand waves. These smaller bedforms are likely to be more indicative of active sediment transport (Langhorne,1977). The presence of megaripples on the sandwaves indicate that bedforms in these areas are active features (McCave,1971; Langhorne,1973). The megaripples, having a spacing of 5 m are also present in their own field in shallow water particularly around sampling station S11

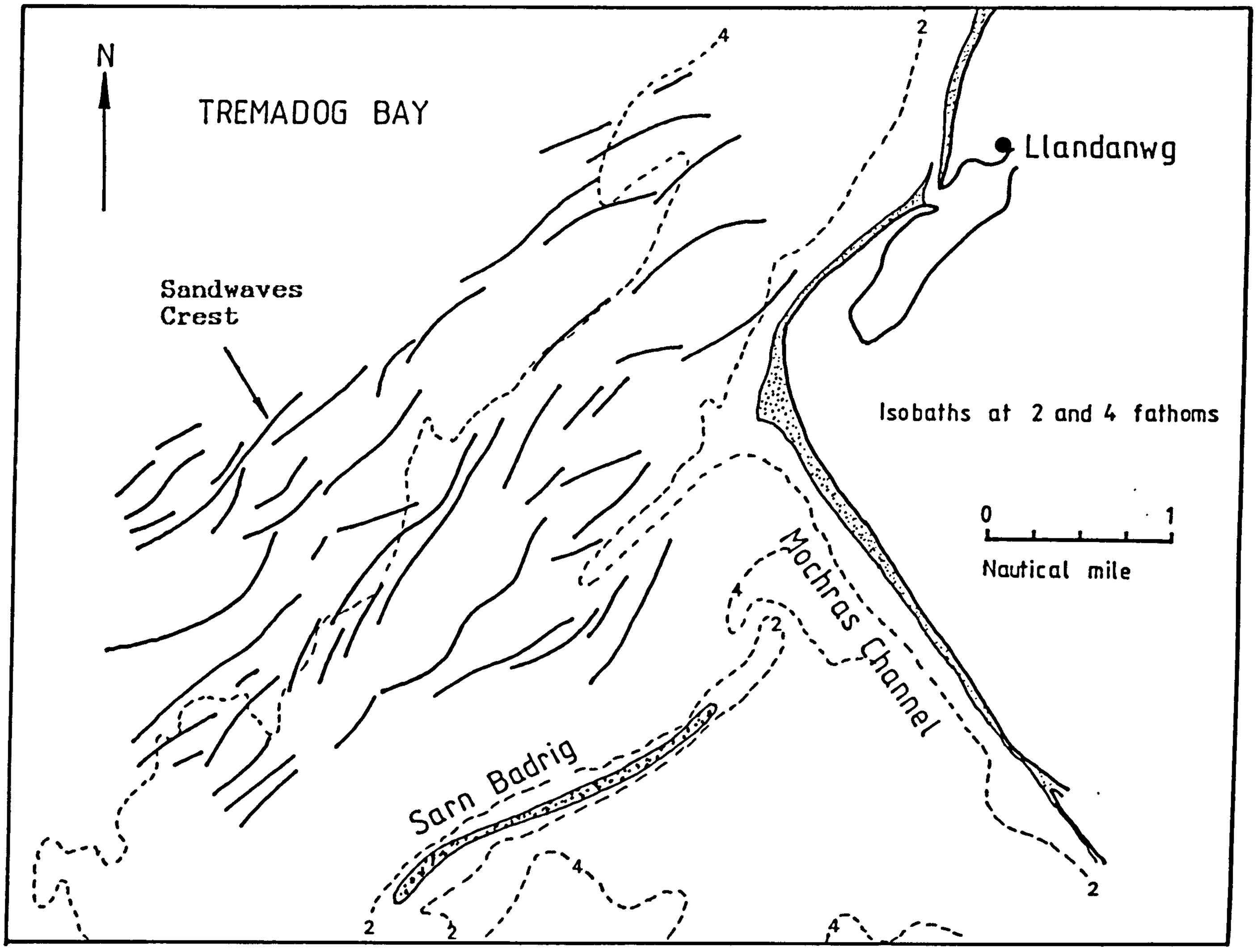

Figure 2.31. Offshore tidal sandwaves in the southern portion of Tremadog Bay. (After Caston, 1965).

(Figure 2.18). The presence of the sand waves may also be caused by strong currents generated during storms. Transport directions can be resolved from these large features and is at right angles to the strike of the bedforms. The directions inferred from these features show the importance of northeastward currents at the western and southern part of the bay and the longshore current near the shore with direction generally conforming to the coastal alignment.

The morphology of the sea floor and shallow structure of Tremadog Bay are strongly related to glacial and post-glacial events. Up to about 20 m thickness of muddy sand overlies the older rocks (boulder clay). Recent deposits have buried nearly all older rocks except for a few ridges associated with morainic deposits at the north and south. The different sediment types and distributions have been influenced by the variation of climatic conditions accompanying the changing of sea level during the Quartenary Period. Recent sediment supply and deposition have been superimposed on the older sediment to produce the present-day sediment distribution. Tidal currents have built large bedforms, suggestive of sediment transport processes at the sea bed at various places in the bay, especially in the shallow areas adjacent to the coastline. The lack of sedimentary structures in most of the records reflects the fineness of the sediment size (see chapter 6) and is probably an indication of deposition from suspension.

Evaluation of bedform orientation on the seabed of Tremadog Bay and on the intertidal flats of the estuary indicates the existence of general sediment dispersal patterns from the southwest to northeast along the shallow sublittoral areas of the bay (Figure 2.32). Comparison of the mapped distribution of the bedforms with the general direction of tidal currents (Figure 2.5) supports the sedimentary evidence that sediment transport directions are controlled by the tidal currents. The locations of bedforms also reflect control by the strength of the tidal currents. Since these bedforms indicate transport processes, their presence on high topography seabed, and absence elsewhere in areas of deeper water, implies that the direction and intensity of sedimentation are controlled by an interaction of relative water depth, tidal currents and (possibly) wave-induced currents. Sandwaves with wavelengths larger than 100 metres found in this area are normally associated with higher currents velocities which probably occur in shallow waters where sediment supply is generally abundant (Kenyon & Stride, 1970; Belderson et al., 1971; Caston, 1974; Owen, 1981). The featureless area which corresponds with the zone of deposition of fine and muddy sediments is likely to contain small-scale bedform features not detectable by the sonar-techniques employed.

The presence of flood-oriented lunate megaripples and sandwaves (Figure 2.11 and 2.12) on the intertidal flats of

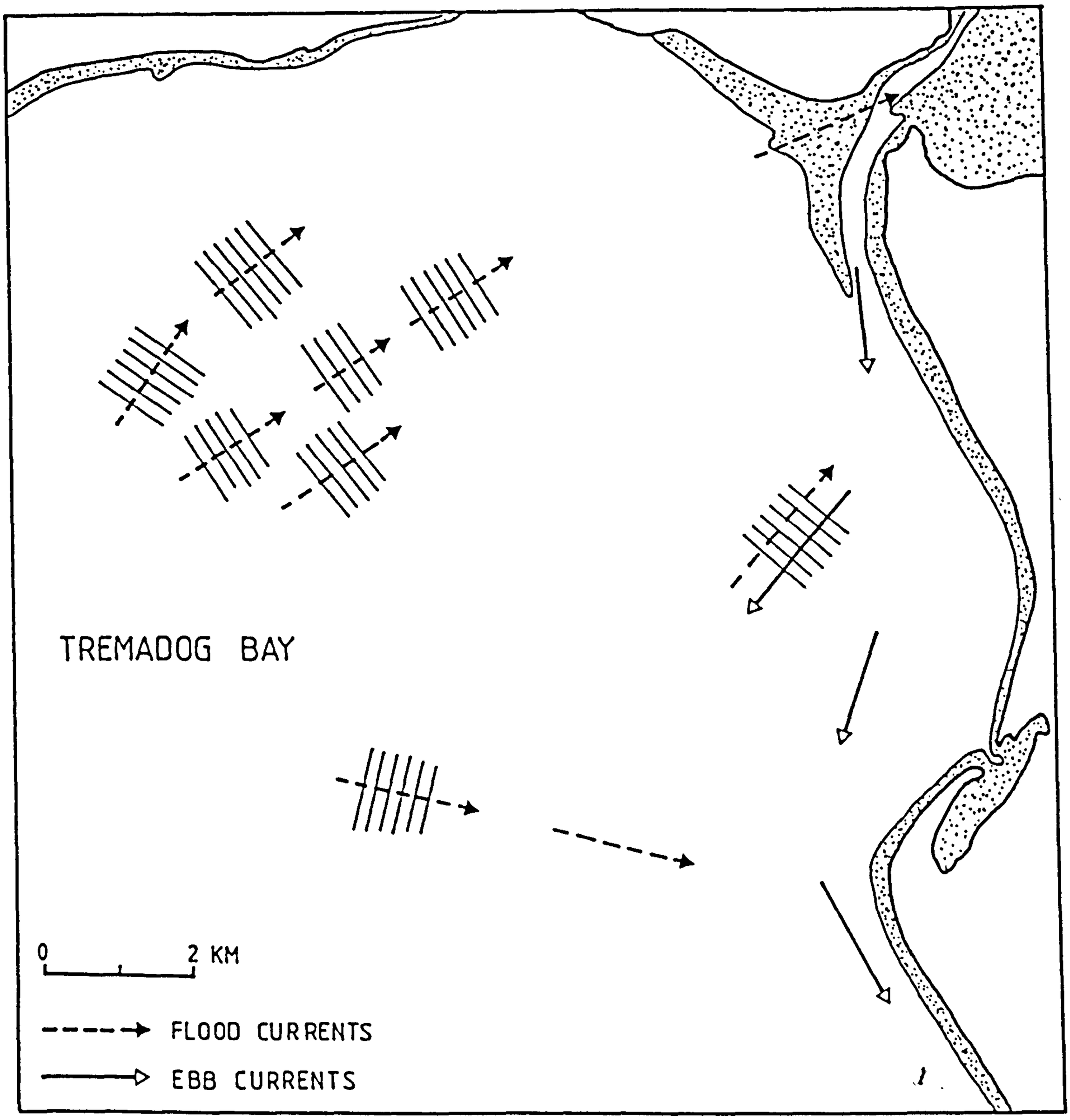

Figure 2.32. Off-shore large bedform distributions and the flood and ebb current pattern. The directions are identified from bedform orientations from side-scan sonar records.

the estuary prove the domination of flood tidal currents which tend to flow straight across the sand spit into the estuary. The trends in grain-size distribution characteristics along the nothern and southern coastline (chapter 6) correlates quite well with the assumed dispersal pattern. The littoral sediment transport is possibly interruped at the tidal inlet, where strong currents force their way into the estuary . As practically no sand finer than 3.0 phi (chap. 6) deposited in the areas of strong currents, most finer material must be transported into and deposited in the estuary and the coarser material deposited directly on the flat across the tidal inlet. A dramatic change in grain-size distribution characteristics of sediment found along the tidal inlet possibly indicates the area where strong flood currents jet their way into the estuary (see chapter 6).

The strong tidal currents in the main channel during the ebb stages are also important agents of inlet sediment dispersal. The main channel which is deflected southward by the sand spit is ebb-dominated as indicated by the presence of mostly ebb-oriented 2-D and 3-D megaripples (Figures 2.16). The strength of ebb currents and hence the capacity for net seaward transport of sediment by ebb currents rapidly diminishes as the flow finally reaches the sea. This is accompanied by deposition of sediment and the formation of a spillover (or terminal) lobe right across the end of the main channel.

THREE

ESTUARINE HYDRODYNAMICS

3.1 Introduction

Water dynamics in estuaries are very complex and vary both spatially and temporally. Mixing processes and circulation patterns within estuaries are related to physical factors such as river flow, tidal range, density differences between fresh and sea water, and estuarine topography. The effective influence of the tide decreases away from the mouth because of the hydraulic gradient which is itself controlled by the tidal range. Changes in channel cross section will change the hydraulic geometry so bringing about increases and decreases in current velocity for any given discharge. A short term variation such as a semi-diurnal tidal cycle will always mask a longer term variation such as seasonal or annual variation. A spatial and temporal variability of controlling parameters will be reflected in the resulting patterns of sedimentary deposit.

Sediment characteristics are directly related to a variety of processes that control sedimentation and these can be physical, chemical or biological. The most important are those which produce water movement and turbulence such as tides, waves, wind and river flow. As a result, sediment

is transported and morphology is changed in response to the changing flow dynamics.

Before the initiation of this study, little was known about either dynamics or sedimentation within the Dwyryd estuary and its adjacent Bay. Previous observations of the estuary are given by Steers (1964). Short descriptions of Tremadoc Bay and its dynamical environment are given by Caston (1965).

Some of the physical processes of the Dwyryd Estuary are described below. Not only do they provide a basis on which to classify, and so allow comparison with other estuaries, but they also conveniently summarise the forces available for sediment dynamics, and so provide a basis for understanding of sediment distribution.

3.2 Measurement techniques

Detailed investigations were made of various hydrographic parameters- temperature, salinity and current velocity- at six different stations spaced over a distance of about 6 km from the mouth of the estuary to the Bridwar Bridge. The stations were chosen so as to provide a representative coverage of the estuary. Station locations are shown in Figure 3.1.

A 13 feet Dory was used for all survey work. This type

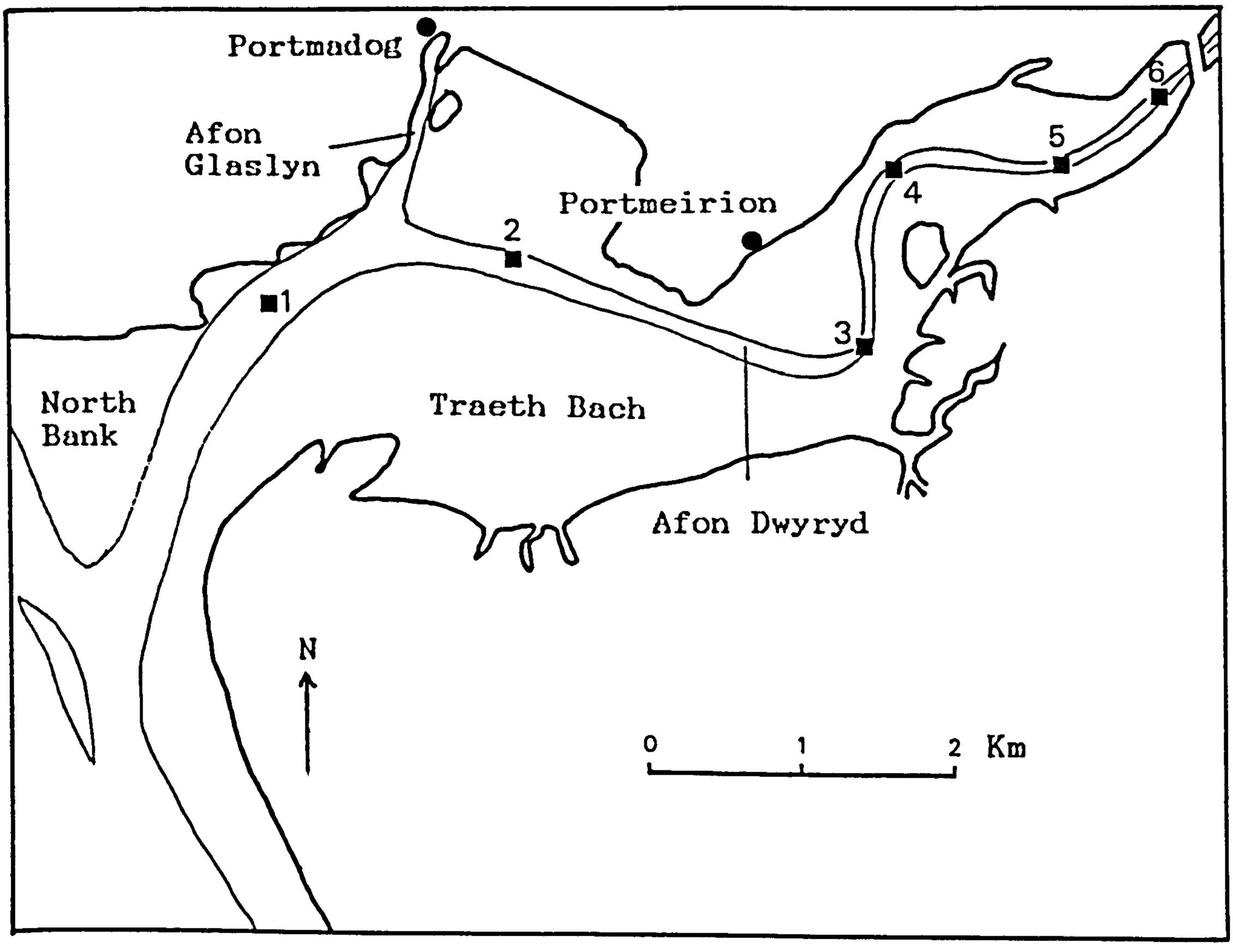

Figure 3.1. Locations of CTD and current meter stations.

of boat is ideal for shallow water survey work since the inherent stability of its hull increases measurement accuracy. The boat was anchored in the main ebb channel. Current measurements were made using a Braystroke type B.F.M 002 current meter, capable of measuring flow speed from 0.04 to 5.00 m/s, with a standard error of 0.03 m/s. Flow speed is sensed by a propellor which is directed into the current by vanes. The in situ values of salinity and temperature in the water column were determined by using a Valeport MkII CTD (conductivity-temperature-depth) probe. The temperature is accurate to within 0.02°C and the salinity to within 0.03 ‰.

It was not feasible to follow the preferred procedure of monitoring all six stations simultaneously; instead stations were monitored individually at different times and at different stages of the lunar cycle. All six stations were occupied during the summers of 1985 and 1986 when the weather was suitable for a long stay in an open boat.

The current and CTD meters were attached to a stainless steel tackle and weighted with a streamlined-mass. The whole assembly could be raised and lowered from the boat by means of a small hand-winch attached to the boat's derrick. Once in the water the assembly swung about its support rod and was kept pointing into the current by a vane.

Measurements were began just before the onset of the flood tide and took from 8 to 10 hours to complete. The

assembly was lowered into the water until the weight just touched the bottom. The approximate depth of the instruments from the surface was read from a deck unit. At this depth, current speed, salinity and temperature were taken. The measurements were repeated at depth intervals of about 20 cm or 50 cm between bottom and surface depending on the water depth. The whole process was repeated every 15 minutes. The read-outs of current speed, salinity and temperature were obtained manually from two deck units, one for measuring speed only and the other for salinity, temperature and depth. One disadvantage arises from this technique. The time taken for reading at each level in the water column produces time lapses between observations and so reduces their comparability in this tidally changing system (though this is a matter of minutes).

Current speeds obtained using the Braystoke current meter were read as the number of impeller revolutions over 10 seconds. These readings were reduced to give a value in revolutions per second, which was subsequently converted to meters per second, using the calibration chart supplied with the instrument. There was intermittent interference from fouling by seaweed. This produced almost immediately noticeable effects on the counters enabling those results to be rejected and the measurement to be repeated.

3.3 Mixing index

If a conservative estimate of 1.5m is taken for the average water-depth in the estuary at high spring tide and the surface area of the estuary at high spring tide is about 9 km^2 , the total volume of water (tidal prism) is of the order of 13.5 million m^3. Of this amount, under average river discharge 8.7 m^3 /s (see chapter 2), approximately 0.125 million m^3will be supplied by the river Dwyryd. The ratio of the volume of fresh water to the total volume of water entering the estuary during the period of a flood tide (Schubel, 1971) may be used as a mixing index which is a crude guide to the classification of the estuary in terms of Pritchard's (1955) categories. The mixing index for the Dwyryd estuary during spring tide is 0.009, a value which places the estuary in Pritchard's type D category. Type D estuaries according to Prichard's classification scheme are estuaries which have very low mixing index (<0.05), very high width/depth ratio, and very high mixing energy due to large tidal energy.

During a neap tide, when the tidal prism is small (about 3.0 million m^3), the mixing index is 0.031, which also places the estuary during a neap tide in Pritchard's type D category. Compared to the mixing index of the Dovey estuary which has a mixing index for an average spring tide of about 0.016 (Hayes and Dobson, 1969), the mixing index of the Dwyryd estuary is slightly higher than that of the Dovey estuary. The difference in mixing index of the two estuaries must be due to the amount of sea water and fresh water intruded into them . The Dovey estuary has a higher

river discharge of 22.5 m^3/s (Hayes and Dobson, 1969). The tidal prism entering the Dovey estuary is higher than for the Dwyryd estuary because of the higher tidal range of about 4.5 m compared to 3.5 m for the Dwyryd estuary.

The theoretical mixing index applies to the estuary as a whole, but in the natural environment the degree of mixing between fresh and salt water varies from section to section within the estuary, and, as pointed out by Hansen and Rattray (1966), no single value of a mixing or circulation parameter can adequately characterise an estuary.

3.4 Velocity Observations

There are several factors which determine the current velocity at different elevations above the bed and distances from the mouth. Directional variation between near-surface and near-bottom flow at a particular station is attributable to three factors:

a) the interaction tidal currents with river flow,
b) the development of spiral flow, and
c) the conflict between water confined to a channel in the lower part of a column and unconstrained water in the upper part of a column.

The effective influence of tidal rise and fall decreases away from the mouth because of the hydraulic gradient which

is itself controlled by the tidal range. Changes in the channel cross section will alter the hydraulic geometry so bringing about increases and decreases in velocity for any given discharge. Density layering may induce reversed flows at the base of the water column and the potential energy of fresh water entering at the head of the estuary may cause premature seaward movement of surface water (Ippen and Harleman, 1966).

Station 1:

This station was occupied on June 24th,1986 about five tidal cycles after a spring tide (ST+5) near the mouth of the estuary. The tidal wave at this location indicate that it has an asymmetrical form (Figure 3.2). It took 5.25 hours for the flood tide to reach its highest level while it took 7.5 hours for the ebb tide. In the first hour after the onset of the flood, the highest velocity was at approximately two-thirds depth of the water column (Figure 3.8a) due to the interaction with fresh water flow at the surface and also due to strong underthrusting of sea water at the bottom of the water column. During the remainder of the flood, however, the maximum velocities occured near the surface. The maximum recorded velocity was 125 cm/s at the onset of the flood.

During the ebb tide surface velocities were always in excess of those near the bed, and maximum velocities occured

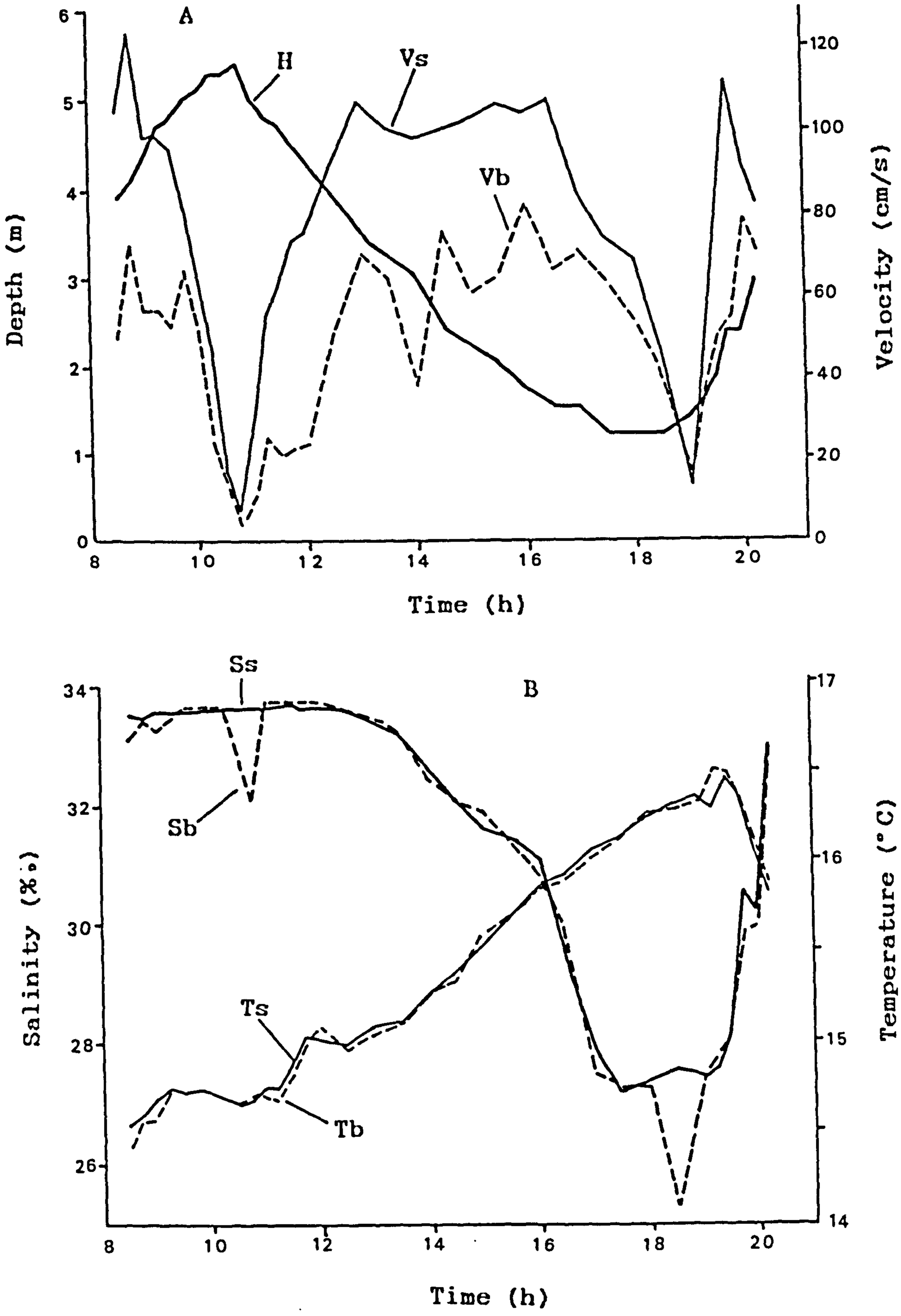

Figure 3.2. Station 1 (Five tidal cycles after spring tide, ST+5). A) Measured water depth (H), surface and bottom velocities (Vs, Vb). B) Measured surface and bottom salinities (Ss, Sb) and surface and bottom temperatures (Ts, Tb) during a tidal cycle.

5 hours after high water. Maximum ebb surface currents recorded at this station were 107 cm/s, and those near the bed were about 80 cm/s.

Station 2:

This station was occupied on May 16th, 1986 at neap tide (NT-2) north of station 1. The tidal curve for this station (Figure 3.3) was similar to the station 1 curve where the flooding period was about 5 hours and the period of falling water level 7.75 hours. Flood flow velocities slowly reached a maximum value of 40 cm/s which occured 2.5 hours after the onset of the flood.

The highest flood velocities within the water column occured not at the surface but at about 0.5 m below the surface (Figure 3.8b). This may be the result of bed friction and salinity stratification. Bed friction slows down the flood current near the bed while the fresh water flow decreases the near surface flood currents. Ebb velocities were on average higher than flood velocities and velocities of 60 cm/s were recorded near the surface 1.5 hours after high tide. The flow became stratified 2 hours after the onset of the ebb flow where velocities of 30 cm/s were recorded near the bottom.

Station 3:

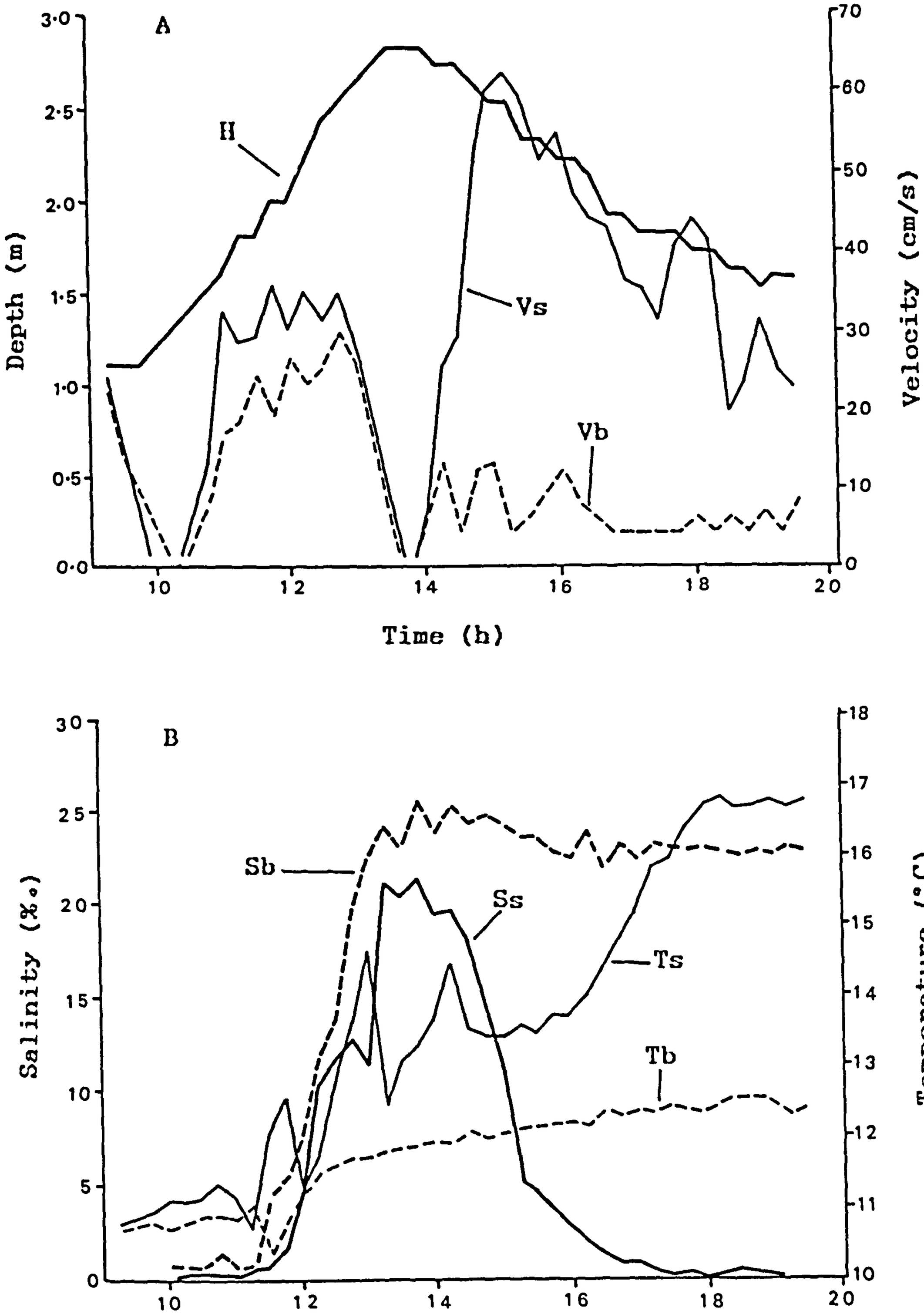

Figure 3.3. Station 2 (Two tidal cycles before neap tide, NT-2). A) Measures water depth (H), surface and bottom velocities (Vs, Vb). B) Measured surface and bottom salinities (Ss, Sb) and surface and bottom temperatures (Ts, Tb) during a tidal cycle.

This station was occupied on June 20th,1985 at spring tide (ST+4) in the middle of the main channel opposite Portmeirion. The tidal curve for this station (Figure 3.4) was strongly asymmetrical with the rise in the water level, taking only 2.0 hours and the period of falling water being 10.75 hours. Figure 3.9a shows that the highest flood velocity recorded was 102 cm/s at the surface 1.25 hours after the beginning of the flood.

The highest flood velocity may be higher than the recorded value which was not recorded due to a delay in setting up the equipment. Ebb velocities reached maximum values of 127 cm/s at the surface and 112 cm/s near the bed about 4 hours after high water.

Station 4:

This station was occupied on July 24th, 1985 between spring and neap tides. The tidal curve at this station was strongly asymmetrical (Figure 3.5 and 3.9b) where high water was achieved 1.5 hours after the begining of the flood while the ebb extended over 11.25 hours. The CTD measurements were begun 1.5 hours before the onset of the flood. About 0.5 hours before the beginning of the flood, the ebb velocity fell abruptly from a steady value of 80 cm/s to a standstill. The flood velocity increased very fast reaching a maximum value of 46 cm/s in 45 minutes. After high water the ebb flow increased steadily from zero

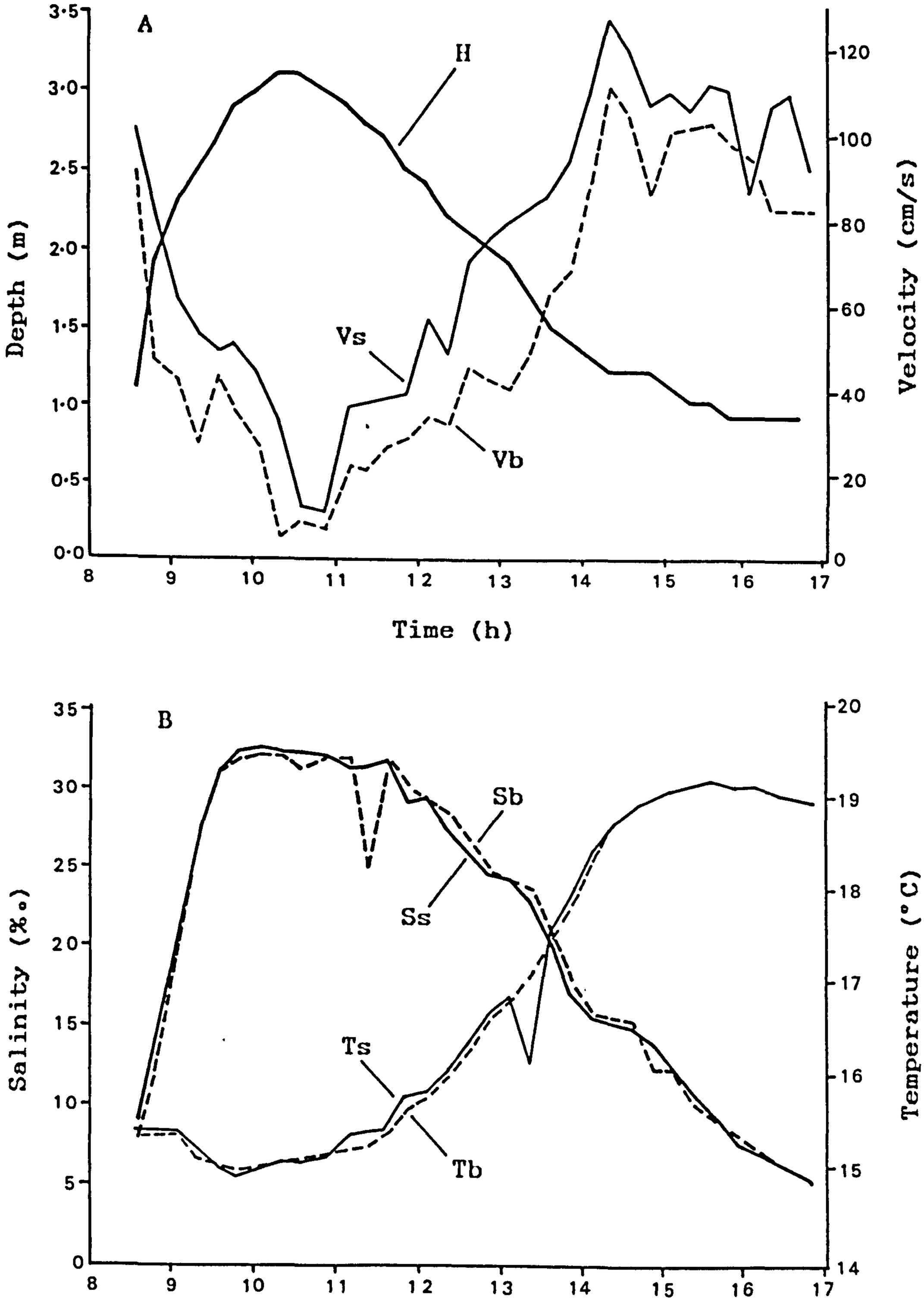

Figure 3.4. Station 3 (Four tidal cycles after spring tide, ST+4). A) Measures water depth (H), surface and bottom velocities (Vs, Vb). B) Measured surface and bottom salinities (Ss, Sb) and surface and bottom temperatures (Ts, Tb) during a tidal cycle.

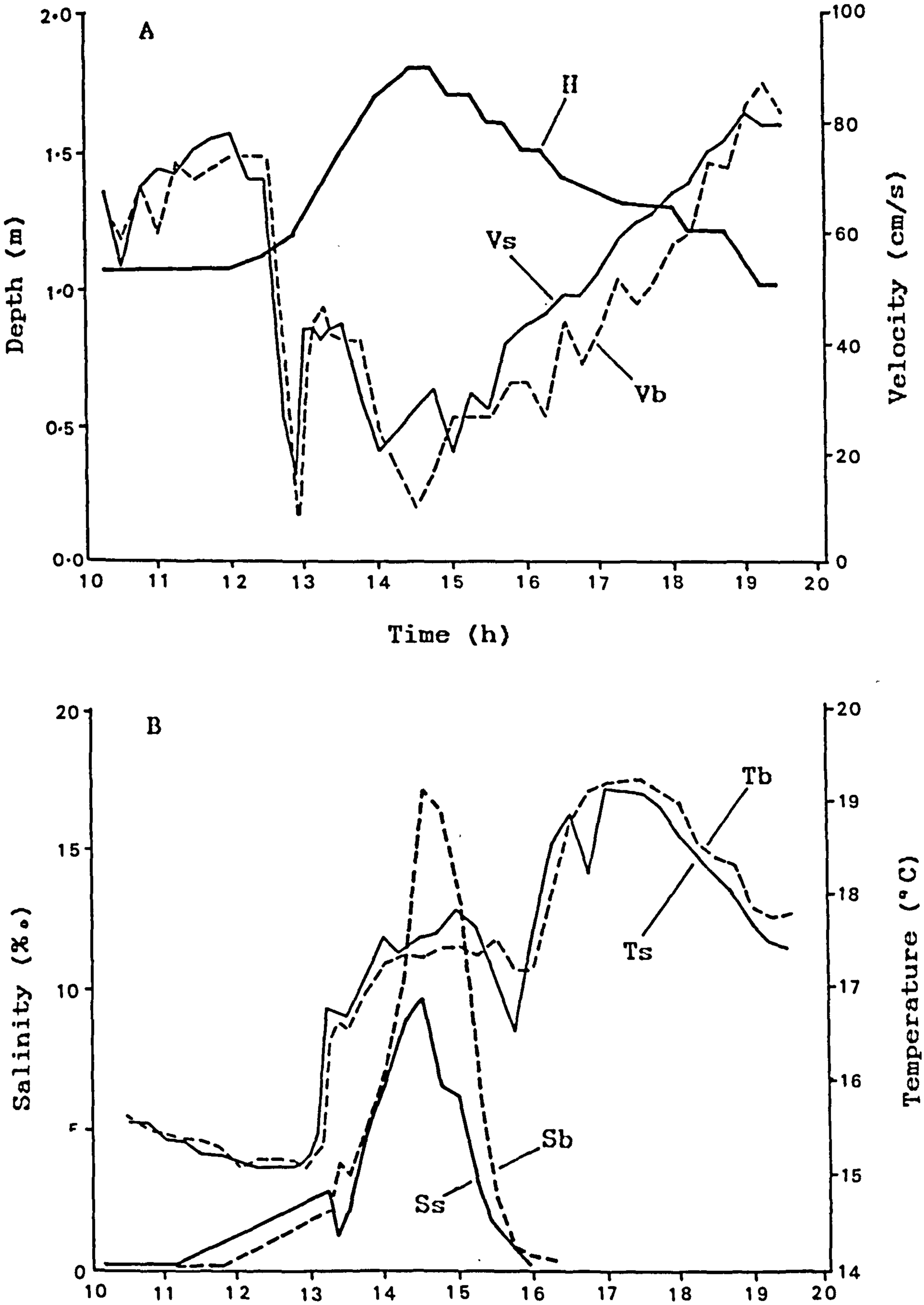

Figure 3.5. Station 4 (Four tidal cycles before neap tide, NT-4). A) Measured water depth (H), surface and bottom velocities (Vs, Vb). B) Measured surface and bottom salinities (Ss,Sb) and surface and bottom temperatures (Ts, Tb) during a tidal cycle.

to about 80 cm/s in 5 hours and then decreased.

Station 5:

This station was occupied on October 18th,1986 between spring and neap tides. Within the first half-hour of the measurement the flow direction was reversed and the flow increased rapidly to a maximum value of 68 cm/s at the surface in 0.5 hours after the onset of the flood (Figure 3.6 and 3.10) . The velocities then decreased to standstill one hour later. Similar to the ebb flow recorded at station 4, the ebb velocities increased steadily to a maximum value of 103 cm/s at the surface and then decreased rapidly to a value of about 60 cm/s when measurements were terminated.

A velocity-depth-time diagram for station 6 was not drawn due to an incomplete velocity record owing to instrument failure. However, it was observed that the pattern of velocity variation was similar to that observed at station 5 (Figure 3.7).

3.4.1 Vertical Velocity Profiles

Enough measurements were taken to enable construction of vertical velocity profiles for each half-hour from the velocity data. Time-averaged velocities were computed for the non-dimensionalised depths, z/d= 0, 0.25, 0.50, 0.75 and 1.0 for each tidal cycle, where z is the distance above the

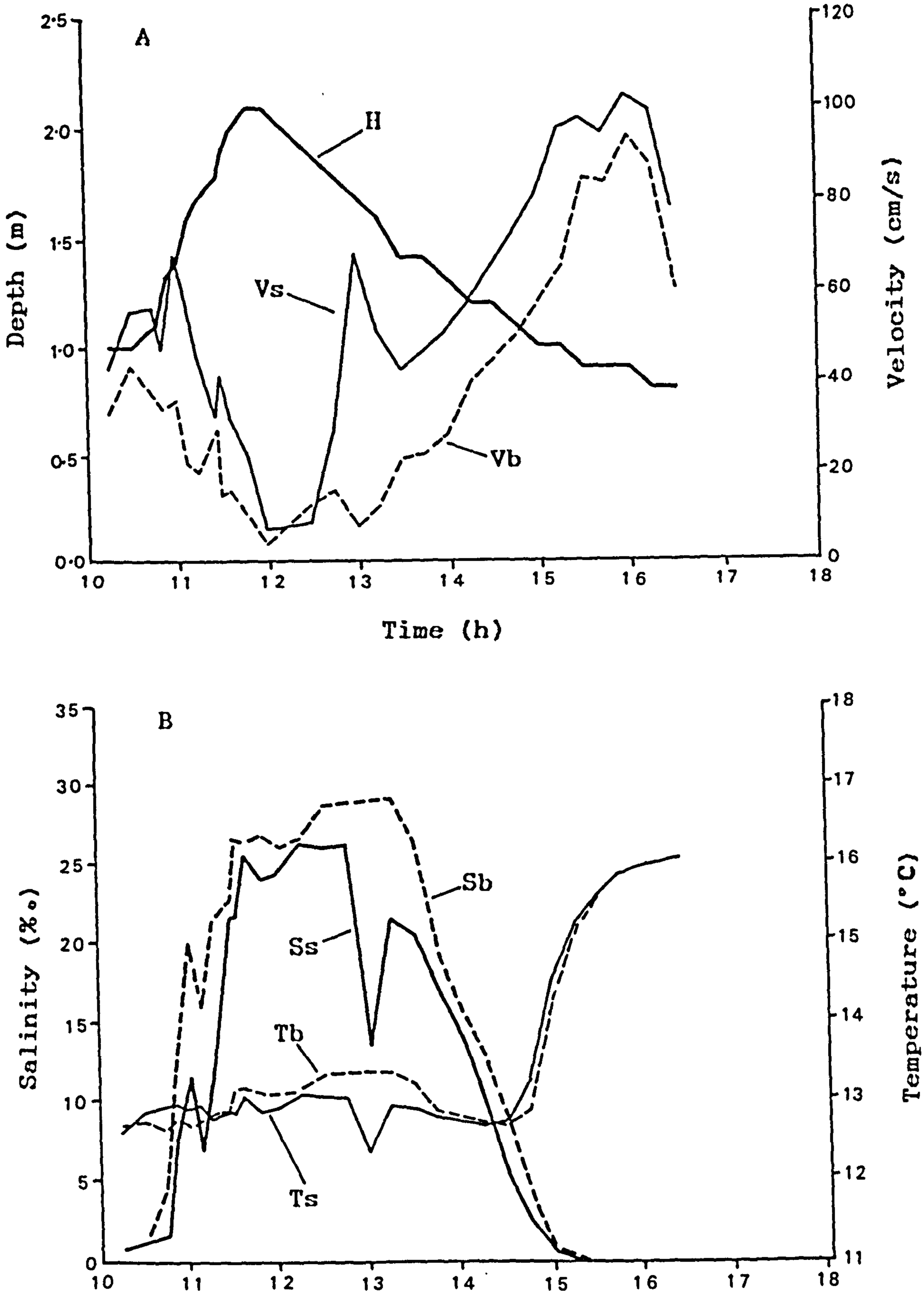

Figure 3.6. Station 5 (Eight tidal cycles after spring tide, ST+8). A) Measured water depth (H), surface and bottom velocities (Vs, Vb). B) Measured surface and bottom salinities (Ss, Sb) and surface and bottom temperatures (Ts, Tb) during a tidal cycle.

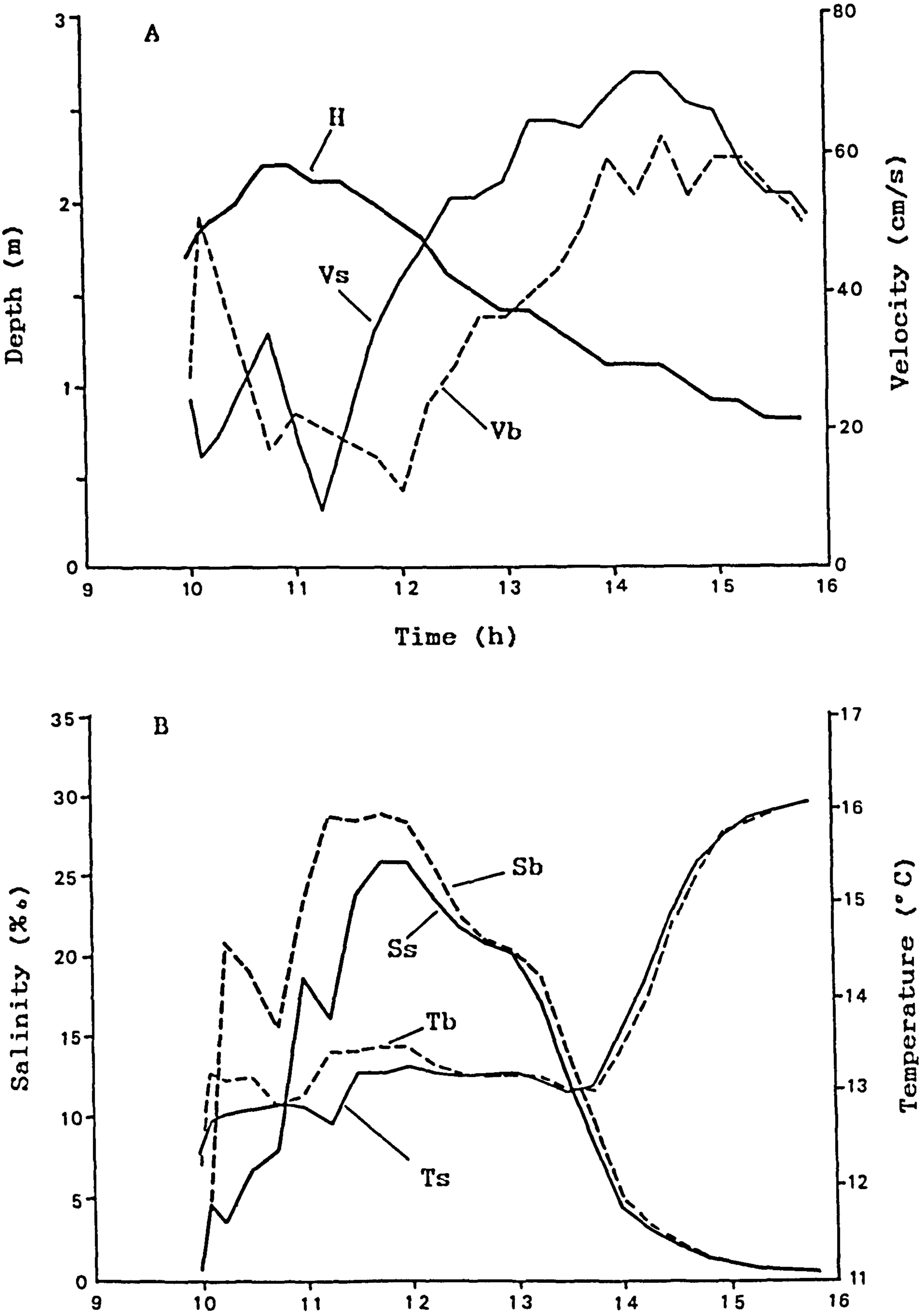

Figure 3.7. Station 6 (Six tidal cycles after spring tide, ST+6). A) Measured water depth (H), surface and bottom velocities (Vs, Vb). B) Measured surface and bottom salinities (Ss, Sb) and surface and bottom temperatures (Ts, Tb) during a tidal cycle.

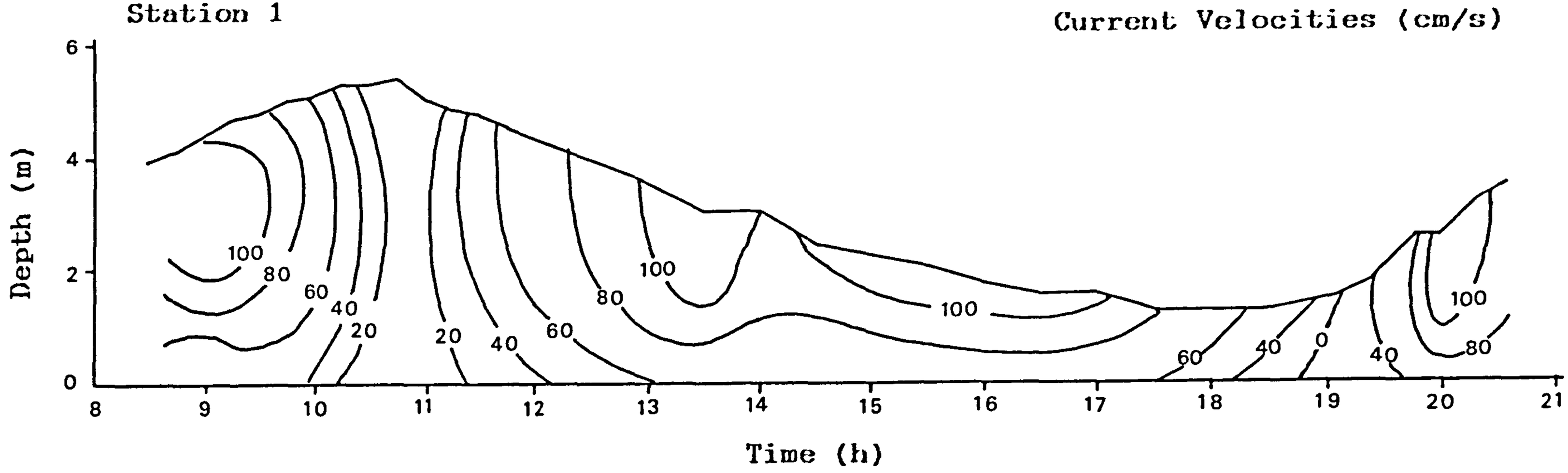

Figure 3.8. Distribution of velocity at stations 1 and 2 as a function of depth and time.

Station 3

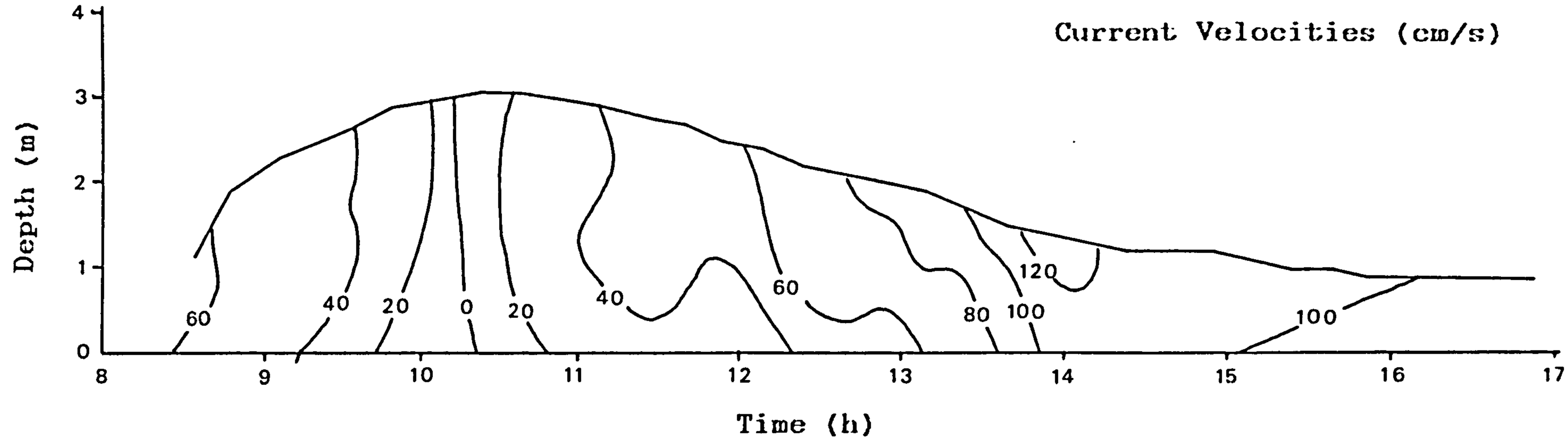

Station 4

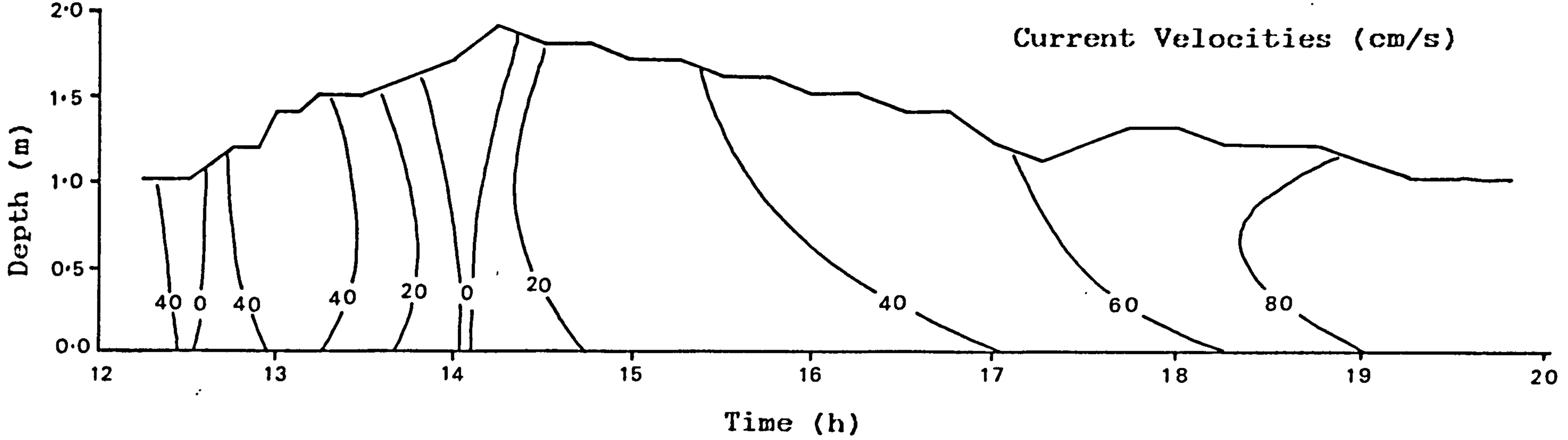

Figure 3.9. Distribution of velocity at stations 3 and 4 as a function of depth and time.

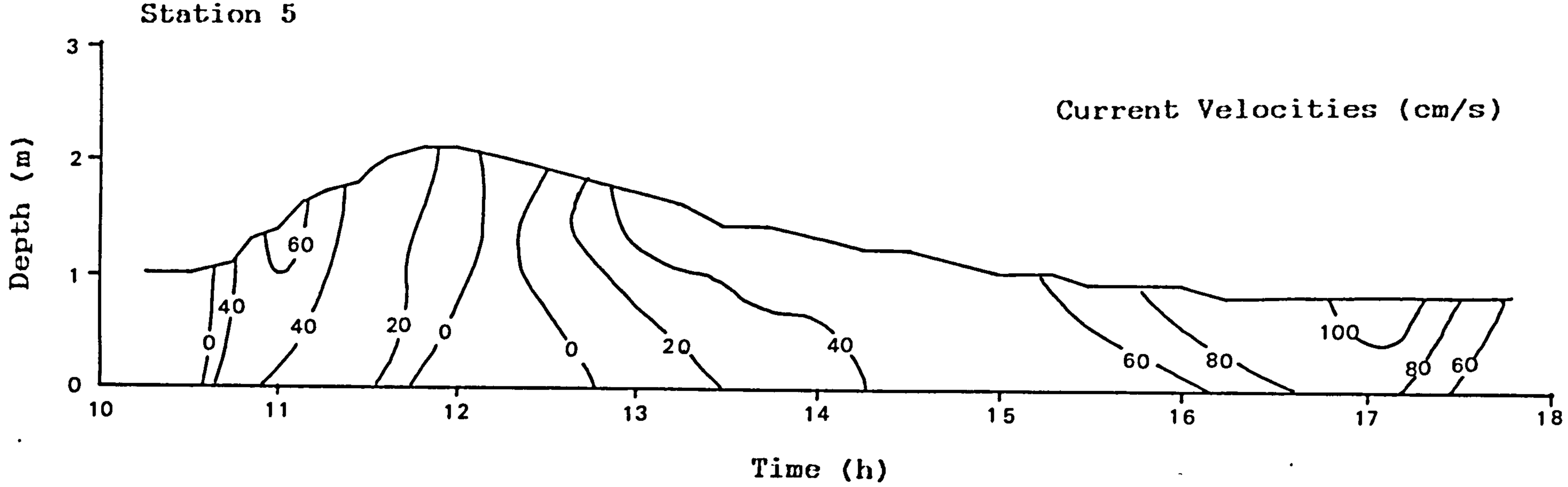

Figure 3.10. Distribution of velocity at station 5 as a function of depth and time.

bed and d is the depth of the water column. As discussed by Kjerfve (1975), this averaging technique conserves the shape of the profiles, and allows net profiles to be constructed even when the tidal range is an appreciable fraction of the mean water depth.

The time-averaging of velocity was done vectorially. The usual convention is to consider the ebb-flow to be positive and flood-flow to be negative. The balance of flow is in favour of the ebb because of the boost provided by river flow.

Near bottom observations (Figures 3.8 to 3.10) showed consistently slower current speeds than the points above. This observation is expected from theoretical considerations of fluid motion over solid boundaries. The fluid must have no net motion over the interface and the magnitude of the velocity gradient perpendicular to the bed is a function of the mean flow velocity of the main stream (Raudkivi, 1976; Allen, 1970).

The vertical velocity profiles of the mean flood and mean ebb currents for five stations are shown in Figure 3.11. In general, the mean ebb velocity was greater than the mean flood velocity except at Station 2. As shown in Figures 3.8 to 3.10 the maximum flood velocity occurred during the mid-stage of flood period when a considerable portion of the tidal flats had been submerged. Consequently flood currents tend to flow straight across the tidal flats avoiding the

main channel, thus reducing the flood current in the main channel. The existence of flood-oriented sandwaves on a large portion of the tidal flats near the mouth of the estuary (chapter 2) provides strong evidence of the presence of fast flood currents on the tidal flats during the flood period. Figure 3.8 to 3.10 also indicate that strong ebb current occurred during the last stage of the ebb period. Boon & Byrne (1981) and Speer & Aubrey (1985) suggest that large tidal flats may enhance the maximum ebb current. The tidal wave propagates faster in the channels than on the tidal flats. Therefore, the decrease in water-level during the ebb takes place later on the tidal flat than in the channel. This leads to water-level inclination and a strong current during the last stage of the ebb period. Also the ebb becomes channelised as the tidal flats emerge, so currents increase.

At Station 2, the mean flood was found to be higher than the mean ebb except at the surface layer where the mean ebb was slightly higher than the mean flood. This station was occupied near the mouth of the estuary during a neap tide where the flood and ebb currents were confined in the main channel throughout the tidal cycle. Since the flood period was shorter than the ebb period, the mean flood current was higher than the mean ebb as expected. As shown in Figures 3.8b and 3.17b, there was a strong flow stratification during the ebb stage. Small tidal range and probably greater than average river discharge were responsible for the formation of flow stratification. The position of the

station close to the sea may also be a contributing factor to the formation of flow stratification. Strong fresh water currents tend to flow toward the sea in the top layer while the slower sea water tends to flow in the bottom layer.

As shown in Figure 3.11, the mean flood velocities were dependent on tidal height and the longitudinal position of the stations along the estuary profile, being greatest on a spring tide (Stations 1 and 3) and least on neap tides (Station 2). The mean flood velocity profiles generally have maximum flood currents occurred not at the surface but at a certain depth below the surface (Stations 2 and 4). The opposition from seaward fresh water flow in the surface layer was responsible for the decrease of flood currents at the surface.

Since the mean ebb currents were generally stronger than the mean flood currents at all stations, the mean velocity averages over the tidal cycle have a net ebb direction as shown in Figure 3.12. It should be remembered that these net velocity profiles are not representative of the whole cross-section at the stations. It is possible that the velocity profiles on the tidal flats have a net flood direction as indicated by the presence of flood-oriented sandwaves on the tidal flats, while the velocity profiles in the main channel have net ebb directions.

3.4.2 Discussion

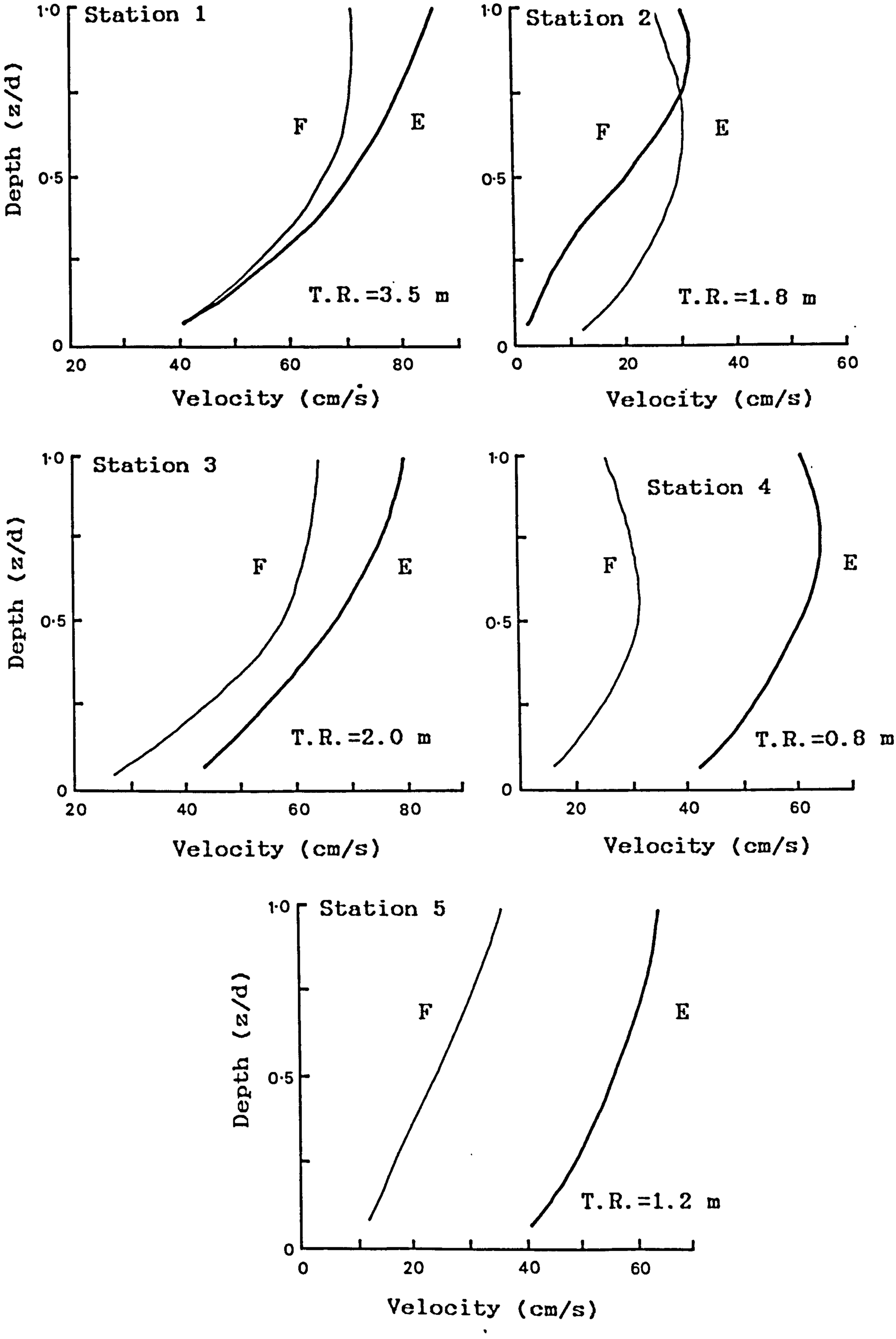

Figure 3.11. Mean flood (F) and mean ebb (E) velocities at stations 1 to 5. (T.R.= Tidal Range).

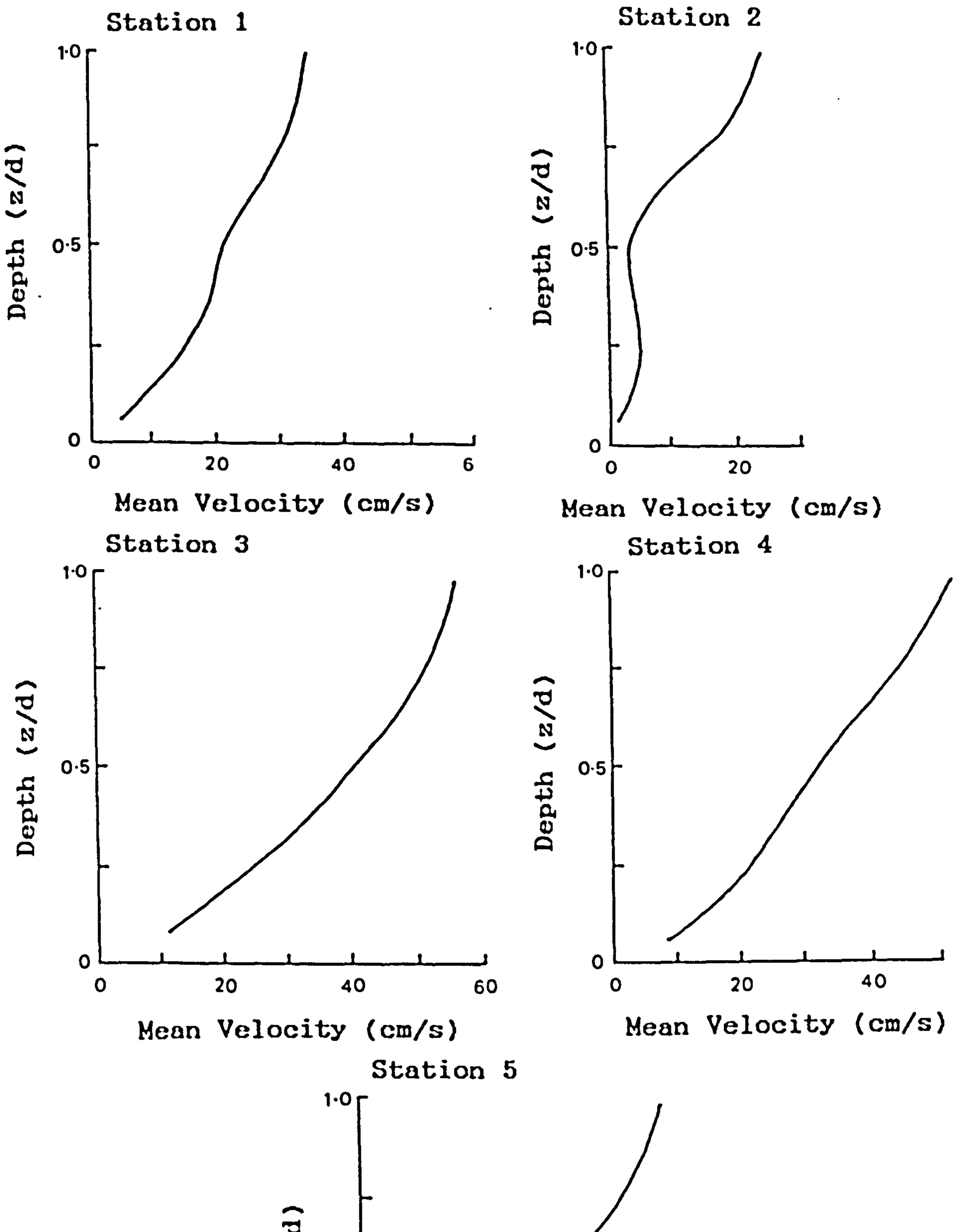

Figure 3.12. Mean velocity profiles at stations 1 to 5.

Throughout Dwyryd estuary tidally induced flows are recognised as the dominant velocity component, as tidal fluctuations are closely related to the current speeds observed. Tidal range at the mouth of the estuary can reach 4 m during the peak spring tide, but only about 1.5 m during neap tide. Since the average depth of the river at low-water is about 1.0 m, such tidal variations must play a major role in controlling flow patterns within the estuary. Tidal phase influence on tide dominated estuaries is well-documented, particularly in Europe, where the tidal prism is relatively larger than fresh water input (e.g. Thames, Severn, Seine and Gironde - Inglis & Allen, 1957; Kirby & Parker, 1977; Avoine et al., 1981; Allen et al., 1977).

The first important characteristics recognised from the observations were the respective durations of flood and ebb. The pattern observed is similar to that present in most estuaries.The degree of asymmetry of the velocity curves increases in the landward direction with the period of rising water-level becoming shorter, for example 5.25 hours at the mouth (Station 1, Figure 3.2) and about 3 hours at the head of the estuary (Station 6, Figure 3.7). Generally, surface currents vary from zero during slack water to about 125 cm/s during the sampling period. The time of maximum flood currents is consistently around 1.5 hours before high-water. Maximum ebb currents occur between 1.5 to 4 hours after high-water.

Tidal range has a considerable influence on the observed maximum flood and ebb current velocities at all depths. The tidal wave is strongly asymmetric, the rise to high water being achieved at station 5 in 1.5 hours. Flood tide energy is therefore concentrated into a small time interval. Maximum flood currents generating strong turbulence occur immediately post low-water . Maximum ebb currents, also with some associated turbulence, occur near the end of the salt-water flushing time; ebb currents then decline to a minimum, approaching the velocity of the seaward flow of river water.

The Dwyryd estuary as measured in the main channel was found to be ebb-dominated (Figures 3.2 to 3.7). The greatest current velocities occurred at the surface, invariably decreasing near the bottom due to friction. For most stations, the maximum deviation of surface and bottom currents occurred on the accelerating ebb tide. Details of the reversing tidal motion are significant for bottom sediment motion because of the non-linear relationship between water and sediment movement. The influence of the wind on the tidal motion is probably of secondary importance and will not be considered in this study.

The velocity measurements in the main channel indicate that the ebb currents dominate over the flood currents except at spring tide. Strong flood currents force their way across the sand flats while strong ebb currents follow the curved channel-bend. This is because the peak flood

currents occur after the submergence of the sand flats; they are less confined by meandering channels and may flow directly over the sand flats. During the ebb, drainage of water becomes concentrated in the channel. This may explain why at most stations ebb velocities exceed flood velocities.

Current-meter data obtained from the VGU (velocity gradient unit) have been analysed to provide information on bottom velocities at stations B and C (Figure 3.1) during the neap-spring cycle (see chapter 5 for detailed descriptions of the instruments). These measurements were designed to estimate the rate of sediment transport; however, the data collected also provide useful information on tidal conditions at each station. At each station, an array of five current meters was used for both flood and ebb directions, but only data recorded by the lowest current meter (about 10 cm above the bed) was used for this analysis because it provided the longest current records. Current velocities versus time for approximately one week duration have been plotted in Figures 3.13 to 3.16 to illustrate the general nature of the bottom currents at each station.

Measured tidal-current characteristics show significant differences, not only between stations but also between flood and ebb magnitudes at particular stations. Over a spring-neap cycle, although the peak current velocities at each station vary in magnitude considerably, the basic current pattern and the tidal asymmetry at individual stations show little change. Strong tidal currents occur

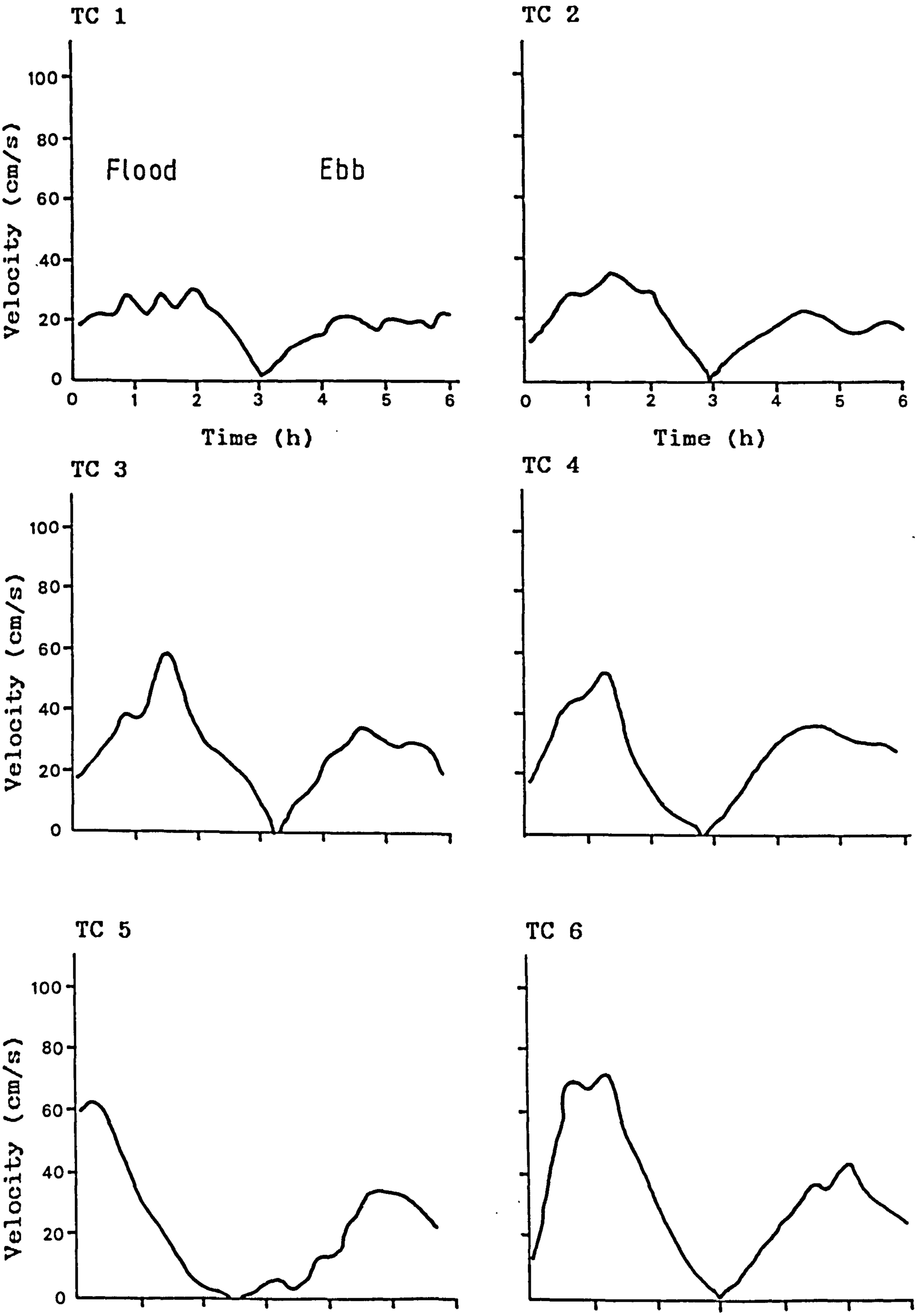

Figure 3.13. Variations in the velocity asymmetry from neap to spring tide at Station B. Continue in Figure 3.14.

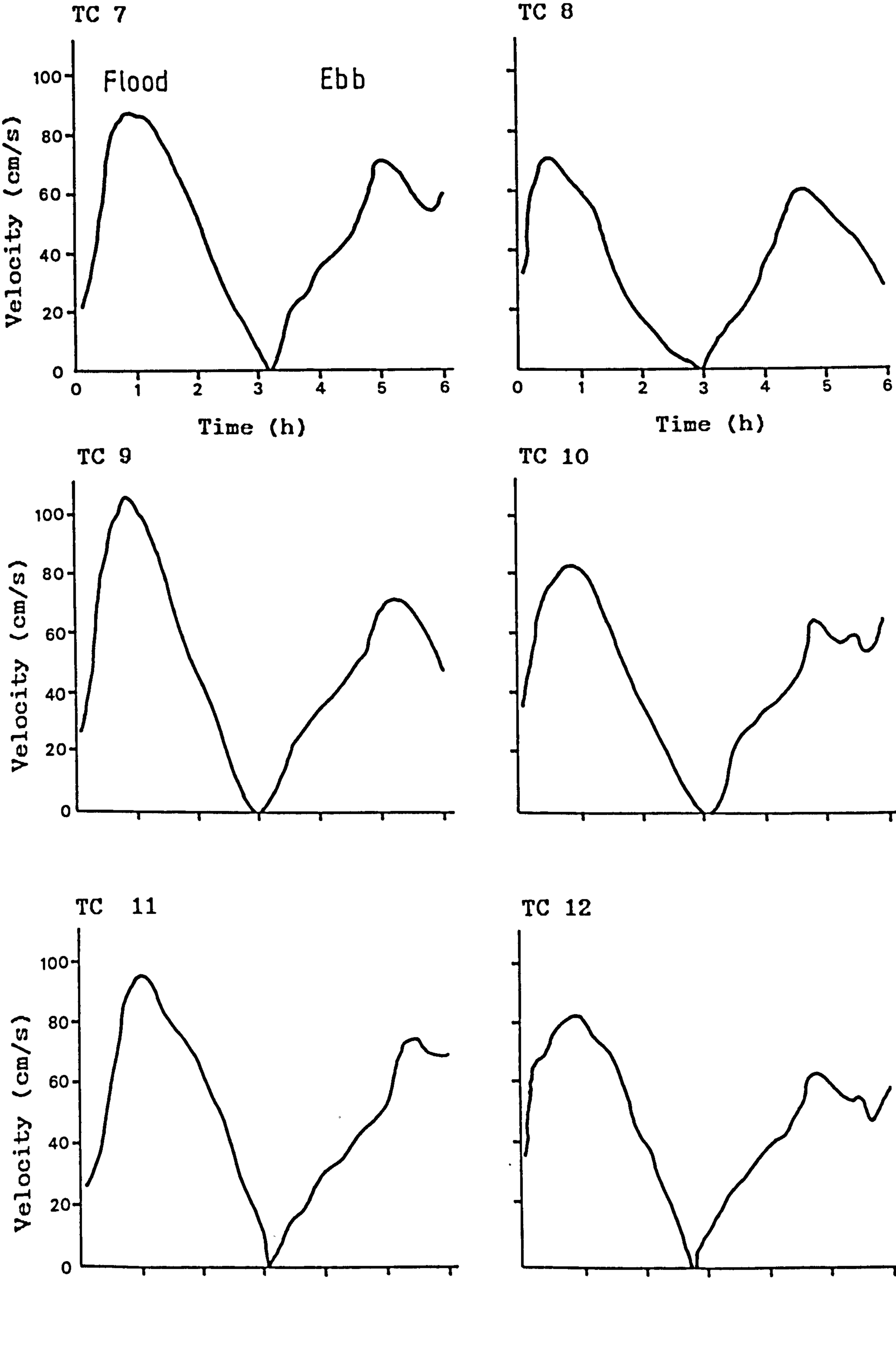

Figure 3.14. Continuation from Figure 3.13.

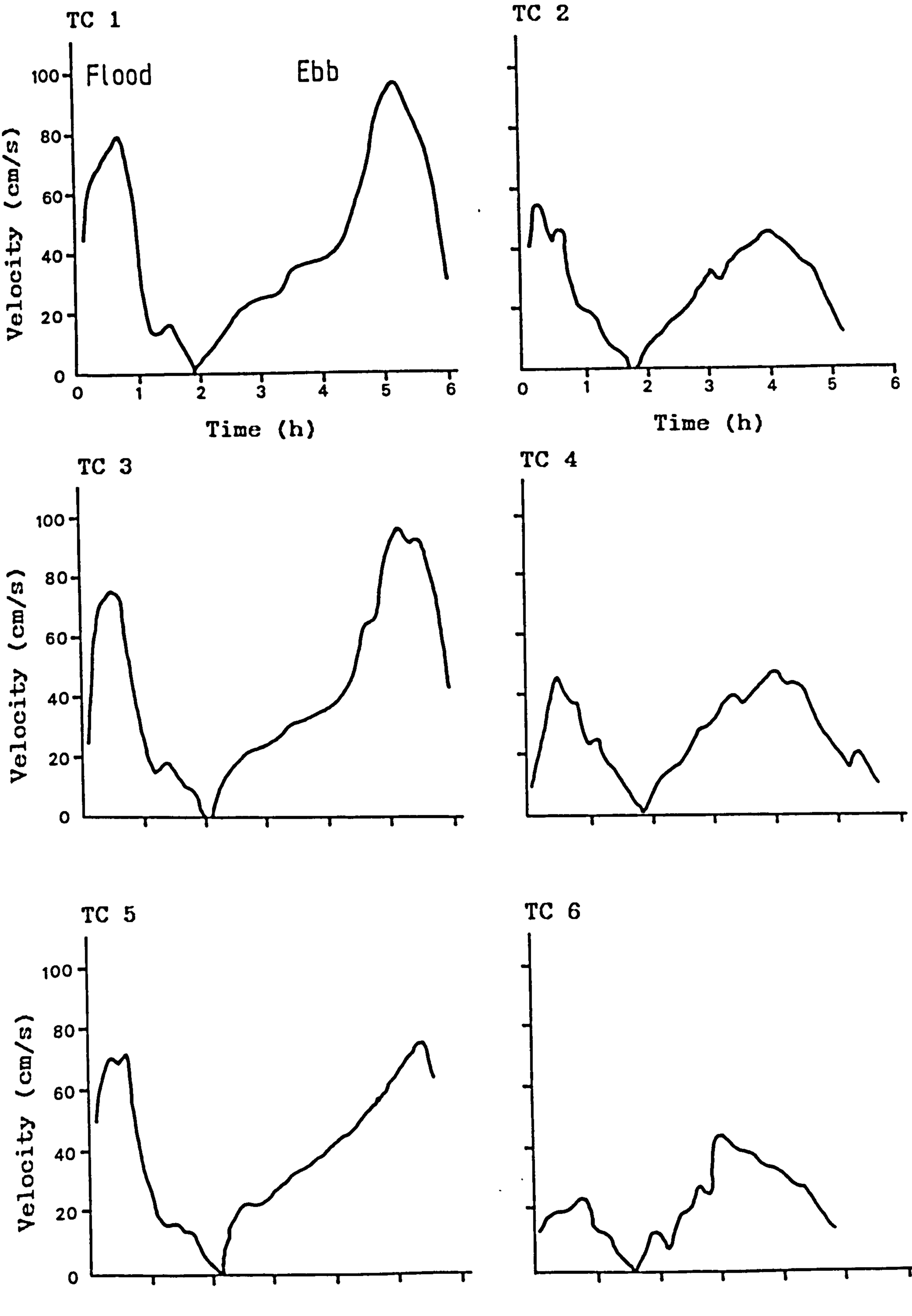

Figure 3.15. Variations in the velocity asymmetry from spring to neap tide at Station C. Continue in Figure 3.16.

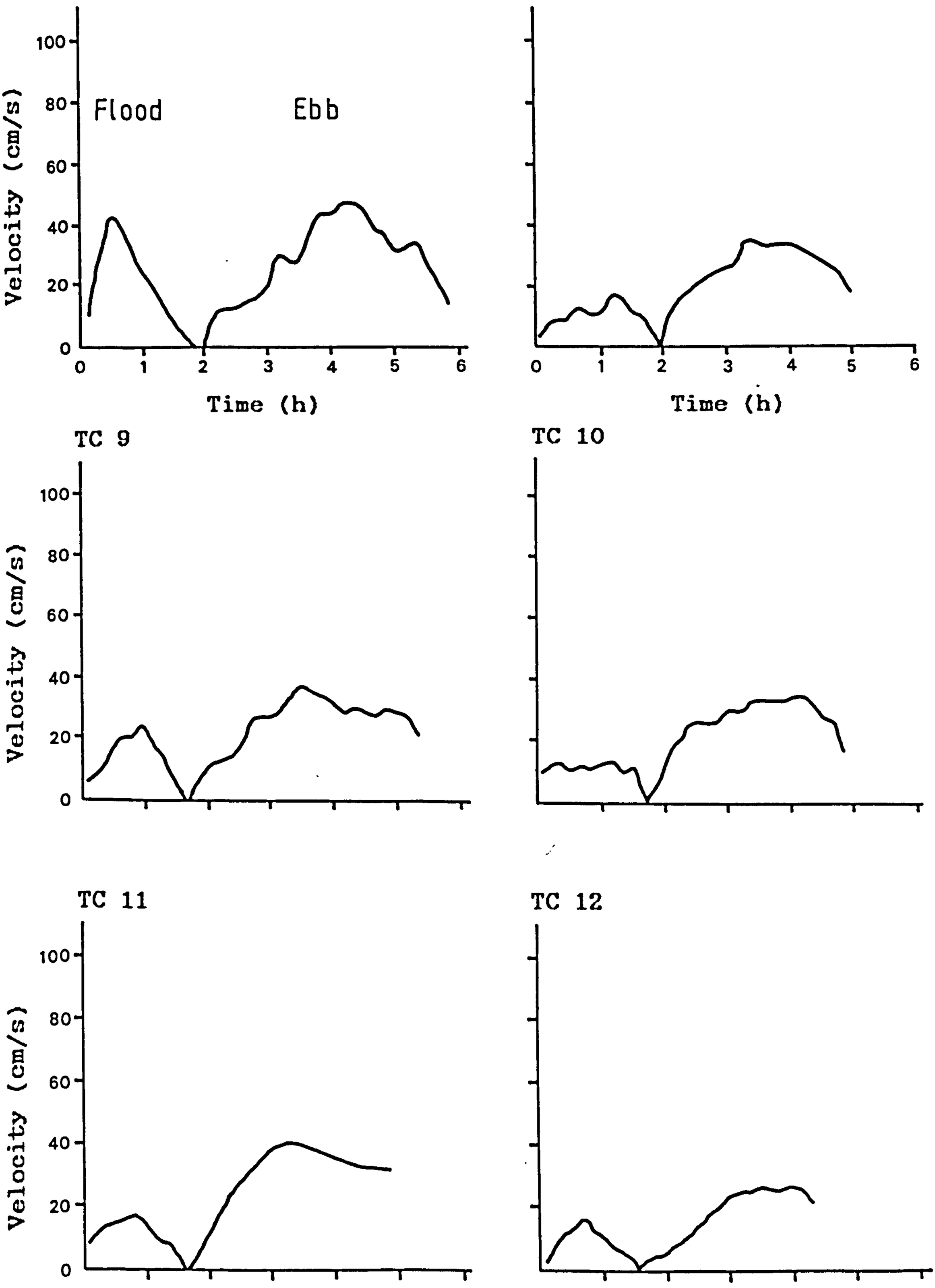

Figure 3.16. Continuation from Figure 3.15.

only during spring tides, while weak tidal currents usually occur during neap tides. Flood dominance was observed on the lower part (mouth) of the estuary throughout the neap-spring cycle (Figures 3.13 and 3.14). Ebb flow seems to dominate in the upper part (head) of the estuary (Figures 3.15 and 3.16). These patterns seem to be controlled by local conditions, such as the position in the channel, the bottom topography, and the bend of the channel. Wind stress acting on the surface of water may be an important factor, especially in intertidal areas, but has not been considered in the present measurements.

3.5 Salinity Observations

Salinity stratification in the Dwyryd Estuary obviously varies according to the stage of the tide and the magnitude of river discharge. During the neap-spring fortnightly tide cycle, the varying ratio between the river flow and tidal prism modifies the intensity of mixing in the estuary. Such variations, also observed in the estuary of the Aber Dovey (Haynes and Dobson, 1969), can change stratification from well-mixed during spring tides, to partly-stratified during neap tides.

Station 1:

The salinity range at this station was very small i.e

from 27.0‰ at low water to about 33.6‰ at high water (Figure 3.2 and 3.17a). Throughout the time of measurement the salinity was almost uniform throughout the water column, with less than 0.1‰ difference between surface and bottom water indicating strong mixing between the small amount of fresh water at the top and the bottom sea water. At high-water the salinity of the water column was very close to the salinity of the sea water which showed that the water column at station 1 (Figure 3.17a) was largely influenced by seawater intrusion.

Station 2:

The salinity-time diagrams in Figure 3.3b and 3.17b show that the salinity measured during a neap tide at this station increased gradually during the flood reaching a salinity of 21.3‰ near the surface and 25.3‰ at the bottom at high water. A slight stratification characterised the flood with water near the surface approximately 4.0‰ less saline than the water at the bottom. Immediately after high water salinity at the surface decreased rapidly from 21.0‰ to about 5.0‰ in 1.5 hours, whereas in the bottom layers salinity decreased only slightly from 25.0‰ to 20.0‰ within this time and then remained at 20.0‰ for the rest of the ebb. Maximum stratification occured before the beginning of the flood when the surface water was almost fresh while the bottom salinity remained at 22.0‰ .

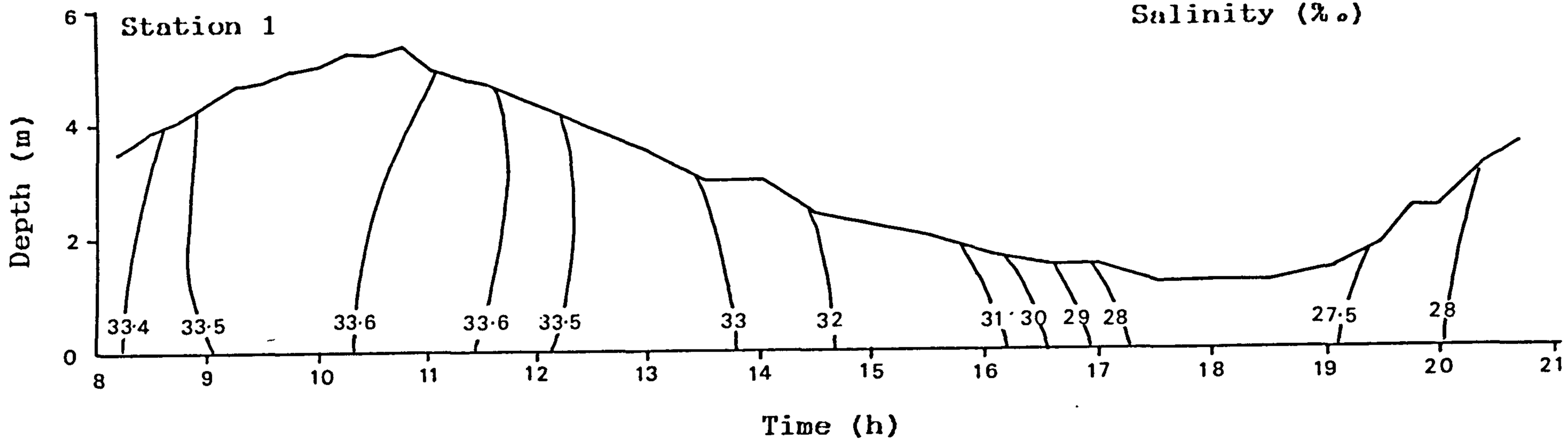

Figure 3.17. Distribution of salinity against depth and time at Stations 1 and 2.

After 1700 h (Figure 3.17b) shows a well-developed halocline, similar to a salt-wedge situation. Before 1700 h, the halocline is less distinct or absent, indicating that some mixing between the top fresh water and the bottom sea water had occurred. These observations can mostly be explained in terms of the influence of the tide on water movements within the estuary. During the late stage of the ebb tide, there was relatively little movement of bottom waters due to tidal influence and, as a result, little mixing between bottom and top waters. In the halocline salinity changes abruptly from 0.2‰ to 20.5‰ over a depth interval 0.5 meters.

Station 3:

The depth-salinity-time diagram shown in Figure 3.18a illustrates the abrupt increase in salinity during the 1.5 hours of the flood tide from 8.0‰ to about 30.0‰ , increasing further towards high water. During the ebb salinities decreased slowly to 8.0‰ in 6 hours after high water. There was little difference between near surface salinity and bottom salinity. The water column was well mixed with respect to salinity with a maximum variation of 1.0‰ .

Station 4:

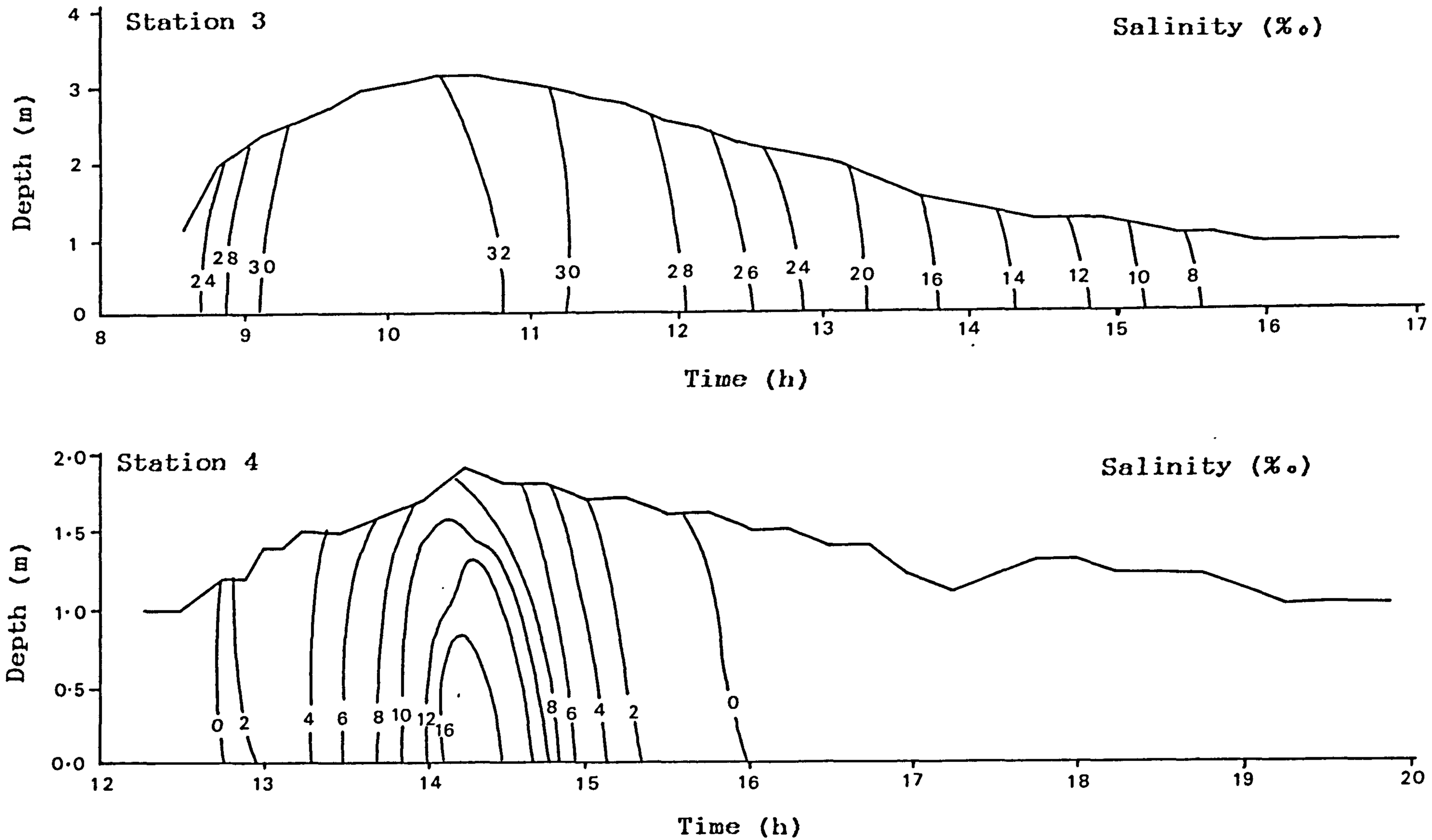

Figure 3.18. Distribution of salinity against depth and time at Stations 3 and 4.

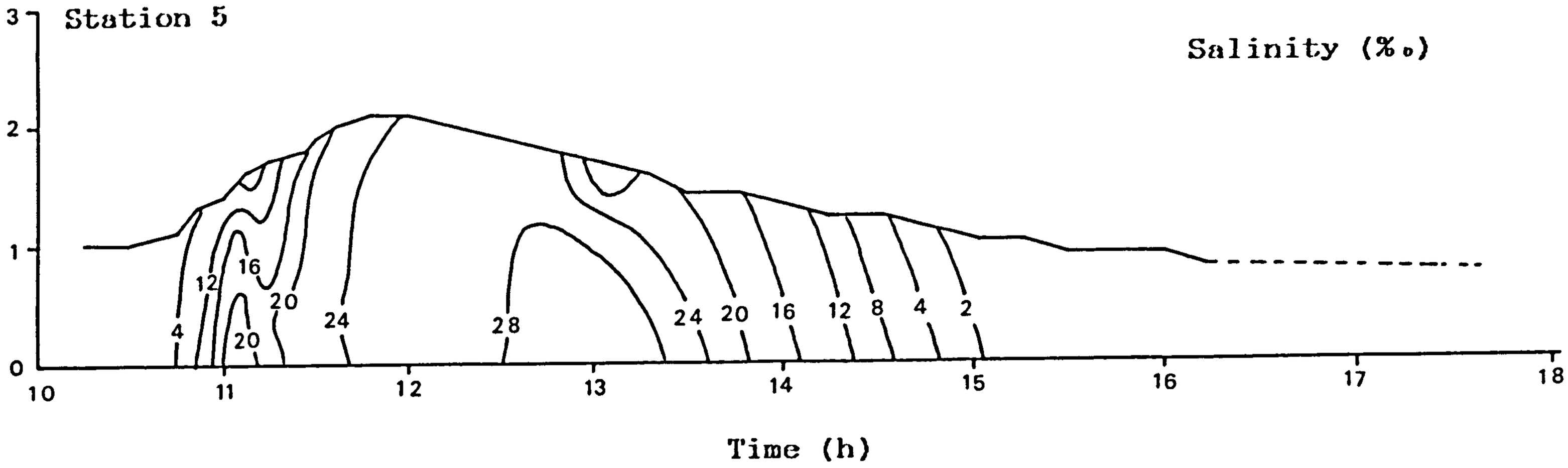

Figure 3.19. Distribution of salinity against depth and time at Station 5.

Salinity increased gradually during the period of the flood tide from 0‰ at the beginning of the flood to about 10.0‰ at the surface and 16.0‰ at the bottom at the time of high water (Figure 3.5 and 3.18b). Salinity stratification developed during the flood flow reaching maximum stratification at high water when the surface to bottom salinity difference was about 6.0‰ . The salinity decreased during the ebb to fresh water in 1 hour after high water.

Station 5:

Salinity stratification was more marked at station 5, even over the high water period (Figure 3.6 and 3.19). Maximum stratification occurred at the middle of the flood tide where a difference between surface and bottom salinity of about 10.0‰ was recorded. Immediately after high water, salinity throughout the water column decreased rapidly to 2.0‰ in 3 hours, and slowly reduced to fresh water for the rest of the ebb tide. It can be seen from the diagram that the maximum bottom salinity was recorded at about an hour after high water.

3.5.1 Vertical Salinity Profiles

The salinity in the Dwyryd estuary is determined by mixing of the tidal prism and fresh water discharged by the

river. The hydrodynamic conditions contrasted strongly between spring and neap tides. There are obvious changes of salinity in the estuary on various time-scales: flood and ebb tides, spring and neap tides, and probably during high and low river flows.

Salinity observations usually showed regular fluctuations in response to tidal currents with two peaks and two troughs in one day. The salinity peak value usually occurred during high water. For example at station 1 the salinity maximum can reach 33.5‰ with little difference between surface and bottom throughout the tidal cycle (Figure 3.17a). Thus, water is fully mixed during a spring tide. A similar situation also occurred at station 3 (Figure 3.18a). At station 2 (Figure 3.17b), the salinity maximum reached 25.0‰ . The salinity difference between surface and bottom was small during the flood but quite big during the ebb. Differences between 2 to 4 ‰ have been observed during the early phase of flood tide, and a difference of about 20.0 ‰ during most of the ebb. Thus, water is highly stratified during the ebb.

As with the vertical velocity profiles, time-averaged salinities were also computed for the non-dimensionalised depths for each half-hour from the CTD data. The mean salinity values of z/d= 0, 0.25, 0.5, 0.75 and 1.0 (where z is the distance above the bed and d is the depth of the water column) were determined for each station, as shown in Figure 3.20.

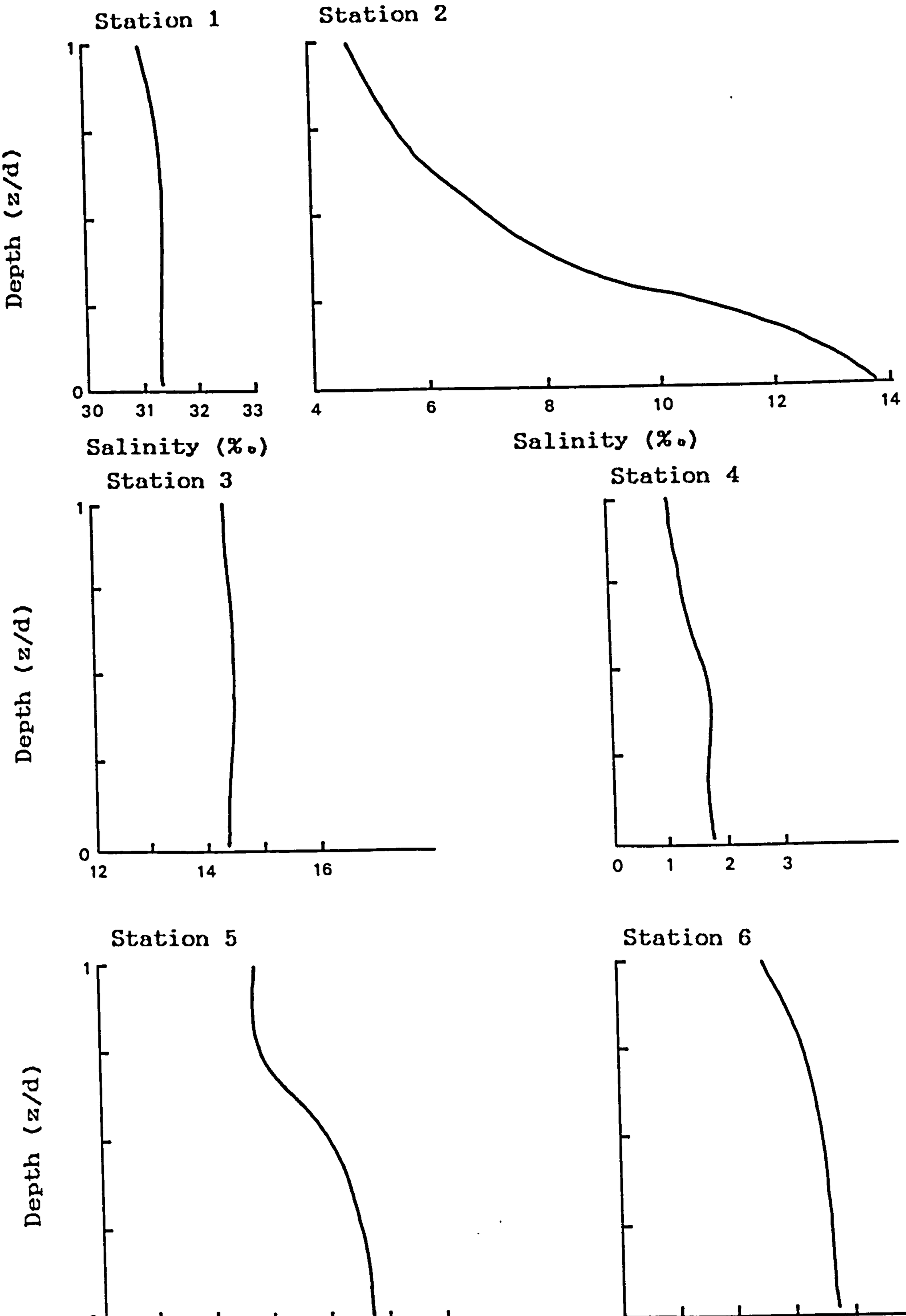

Figure 3.20. Mean salinity profiles at Stations 1 to 6.

During a spring tide,the estuary was vertically mixed, with maximum salinities at high-water. In contrast, the estuary during a neap tide was fairly stratified. The fluctuation of daily salinity is relatively large during a neap tide and very small during a spring tide. In most cases, the salinity gradually reduces to totally fresh at the end of ebb phase except during the spring tide at Station 1.

As can be seen in Figure 3.20, the mean salinity profiles over a tidal cycle for station 1,3,4 and 6 were to some degree rather similar since mixing processes were very active. For these four stations, the difference between the surface and bottom salinities was very small i.e less than 1‰ .Station 5 showed a small stratification with a difference between surface and bottom salinities of about 2.2‰ .Complete mixing caused by intense turbulence produced by tidal currents created near vertical salinity profiles, with mixing being most complete in the near surface. Mixing was most developed on spring tides, especially at station 1 and 3.

At station 2, the situation was very different from those at other stations. Here, the difference between the surface and bottom salinities was very large- about 15‰ .Thus the flow during this tidal cycle was strongly stratified indicating strong underthrusting of sea water at the bottom of the water column. This means tidal turbulence was

dominant only in the lower regions of the flow, due to the frictional effect of bed topography. Low salinity at the surface was due to the strong fresh water flow forcing its way to the sea.

3.5.2 Discussion

The mixing of salt and fresh water in estuaries is related to the balance between river discharge and tidal volume. The degree of mixing depends also upon estuary size and bottom morphology. Salinity will affect sedimentation patterns directly, through increased electrolyte strength and fluid density changes, and indirectly, through any circulation patterns established independently of tidal rise and fall and induced by saline or nonsaline density differences.

In the Dwyryd Estuary the most immediate and obvious effects of a cyclic sea water incursion are a flood increase and an ebb decrease in salinity at each station. An interesting feature of these tidal salinity curves is a tendency for asymmetry about the high slack water value, where the rates of increase of salinity during the flood were larger than the rates of decrease. This is most noticeable at the downstream stations 1,2 and 3. The time of maximum salinity consistently occured at high-water i.e always in phase with water level.

The curves for salinity also reflect the asymmetry of the tidal wave, with a steep rise in values on the flood and slower decline on the ebb. The lowest salinities were reached just prior to the flood surge. Salinity ranges were small at the mouth and increased upstream due to a decrease of mixing between fresh water and sea water.

The greatest salinity was measured in the bottom waters, surface waters being 0 - 12 ‰ fresher. This inevitably follows from density differences between river water and seawater, and indicates that, at these times (i.e during calm weather), mixing of fresh and saltwater was not always complete. Generally, at high water, the surface water began to ebb before the bottom waters, sometimes even while the final stages of the flood continued in the bottom waters.

3.6 Temperature Observations

The temperature of the water in the estuary on a particular occasion will be expected to depend primarily upon the temperature of the fresh water entering the estuary and the temperature of the sea water with which it mixes (and also on meteorological conditions) (Postma, 1950; Pritchard, 1952). The shapes of the temperature curves vary for each station. Water temperature closely follows local air temperature, depending on the degree of exposure of the water surface to sun light, rising during the daytime and falling during the night. Water temperatures are always at

a minimum at the beginning of the flood tide and increase steadily during the flood tide (Figures 3.2 to 3.7).

The distribution of temperature is influenced by the same factors which determine the salinity distribution. However, the temperature variations are in genaral not as regular as the salinity variations because temperature is not a conservative property and can be modified by heating and cooling within the channel.

3.7 Mixing Types

The mixing of river and sea water in estuaries is a complex process, depending on the topographic and dynamic characteristics of each estuary. A useful way to classify an estuary is through the stratification-circulation diagram suggested by Hansen & Rattray (1966), using mean cross-sectional values (Figure 3.21). The longitudinal coordinate of the diagram is a stratification parameter, (Sb - Ss)/Sv and the lateral coordinate is a circulation parameter, Us/Uf, where Sb is the bottom salinity, Ss is the surface salinity, Sv is the depth average salinity, Us is the net surface velocity, and Uf is the mean flow due to river discharge. All parameters are averaged over a tidal cycle (Table 3.1). However,it is difficult to calculate the value of Uf due to the lack of data over the cross-section and due to the large variation of cross section area between low water and high water. Kjerfve (1979) used depth-average

Table 3.1. The value of stratification and circulation parameters and the classification of stations 1 to 5.

Station no	$\frac{Sb - Ss}{Sav}$	$\frac{Us}{Uf}$	Classification
1	0.010	2.69	partially-mixed
2	1.150	3.13	salt-wedge
3	0.009	2.90	partially-mixed
4	0.500	2.33	partially-mixed
5	0.270	3.33	partially-mixed

velocity estimated from velocity profiles instead of mean flow for the calculation of circulation parameter, Us/Uav. Since river discharges are unavailable, the depth-average velocities are used for the calculation of circulation parameters for each CTD station.

Figure 3.21 suggests that in terms of mixing types, the Dwyryd estuary is a partially mixed estuary. The mixing strength at the head of the estuary is less than that in the mouth of the estuary. Mixing is probably stronger during spring tides at the same station than during neap tides, and stronger during low runoff than during high runoff.

It should be mentioned that, even if we had cross-sectional values, the usefulness of the stratification-circulation diagram in analysing circulation and mixing in a shallow estuary such as the Dwyryd estuary might be limited. As Fischer (1972) has pointed out, the application of Hansen and Rattray's analysis to wide and shallow estuaries is restricted. In wide estuaries the circulation will not be evenly distributed across estuaries due to the effect of Coriolis force where there is a tendency for the seaward-flowing fresh water to deviate toward the right bank of estuaries (in Northern Hemisphere). The cross-sections of wide estuaries are not consistent longitudinally and vary considerably during a tidal cycle, therefore the mean flows vary considerably along estuaries. The effect of estuarine shape and topography on circulations has been discussed by Fischer (1972, 1976), Okubo (1973), Prych (1970), and Smith

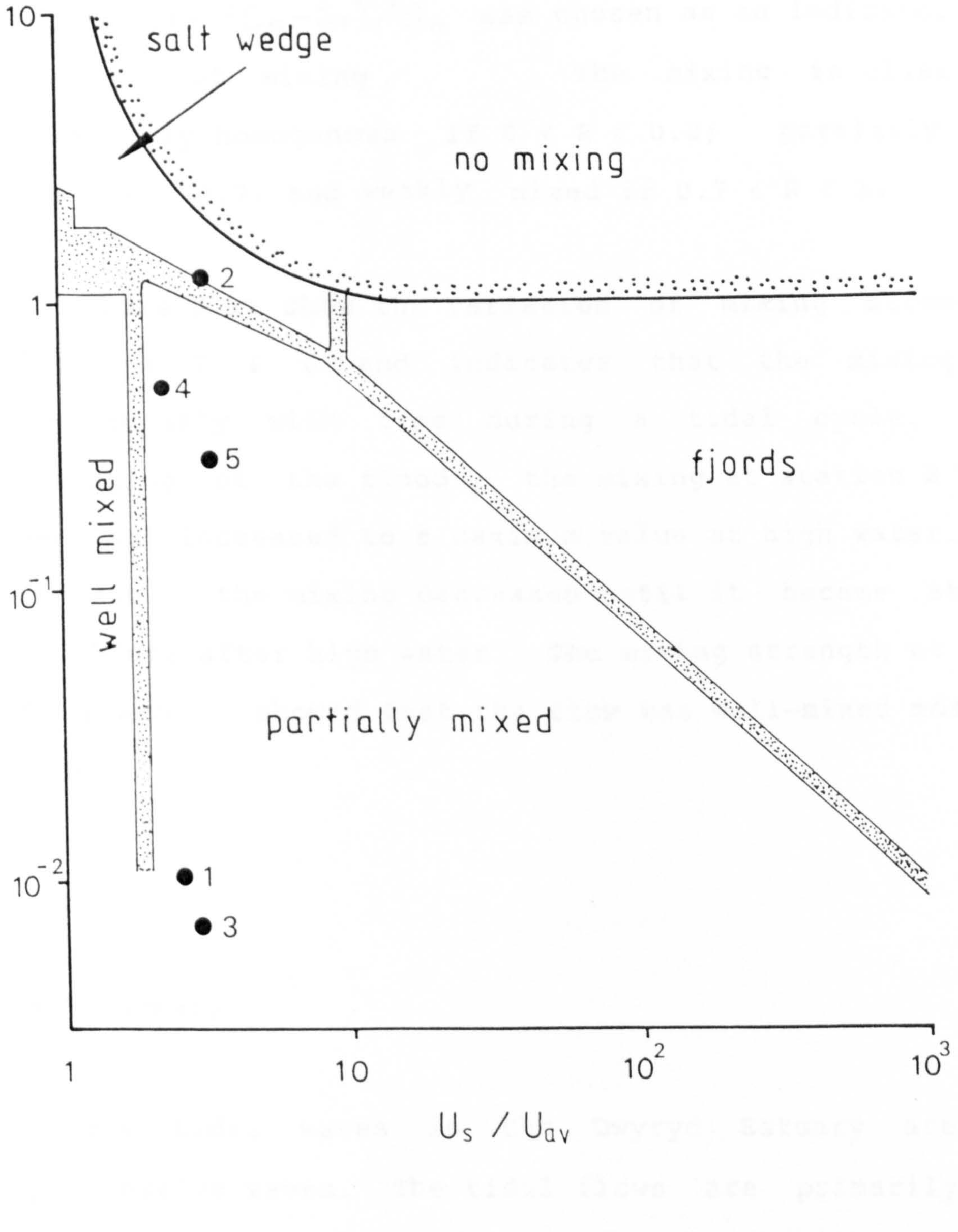

Figure 3.21. Estuarine classification diagram of Hansen & Rattray (1966) with the Dwyryd estuary points plotted.

(1978).

Huanting et al.(1984) suggest a method to show the variation of mixing strength during a tidal cycle. The relation $R = (S_b - S_s)/S_b$ was chosen as an indicator of the strength of mixing. The mixing is classified as vertically homogenous if $0 < R < 0.2$; partially mixed if $0.2 < R < 0.7$; and weakly mixed if $0.7 < R < 1$.

Figure 3.22 show the variation of mixing strength for stations 2 & 6 and indicates that the mixing varied continuously with time during a tidal cycle. At the beginning of the flood, the mixing at station 2 was very weak but increased to a maximum value at high water. During the ebb, the mixing decreased until it became stratified two hours after high water. The mixing strength at station 6, however, showed that the flow was well-mixed most of the time.

3.8 Summary

The tidal waves in the Dwyryd Estuary are modified progressive waves. The tidal flows are primarily regular lunar semidiurnal tides with a period of about 12 hours and 45 minutes. This estuary changes its character considerably during changes in tidal phase. In general, the water in this estuary has a wide range of salinity and other physical

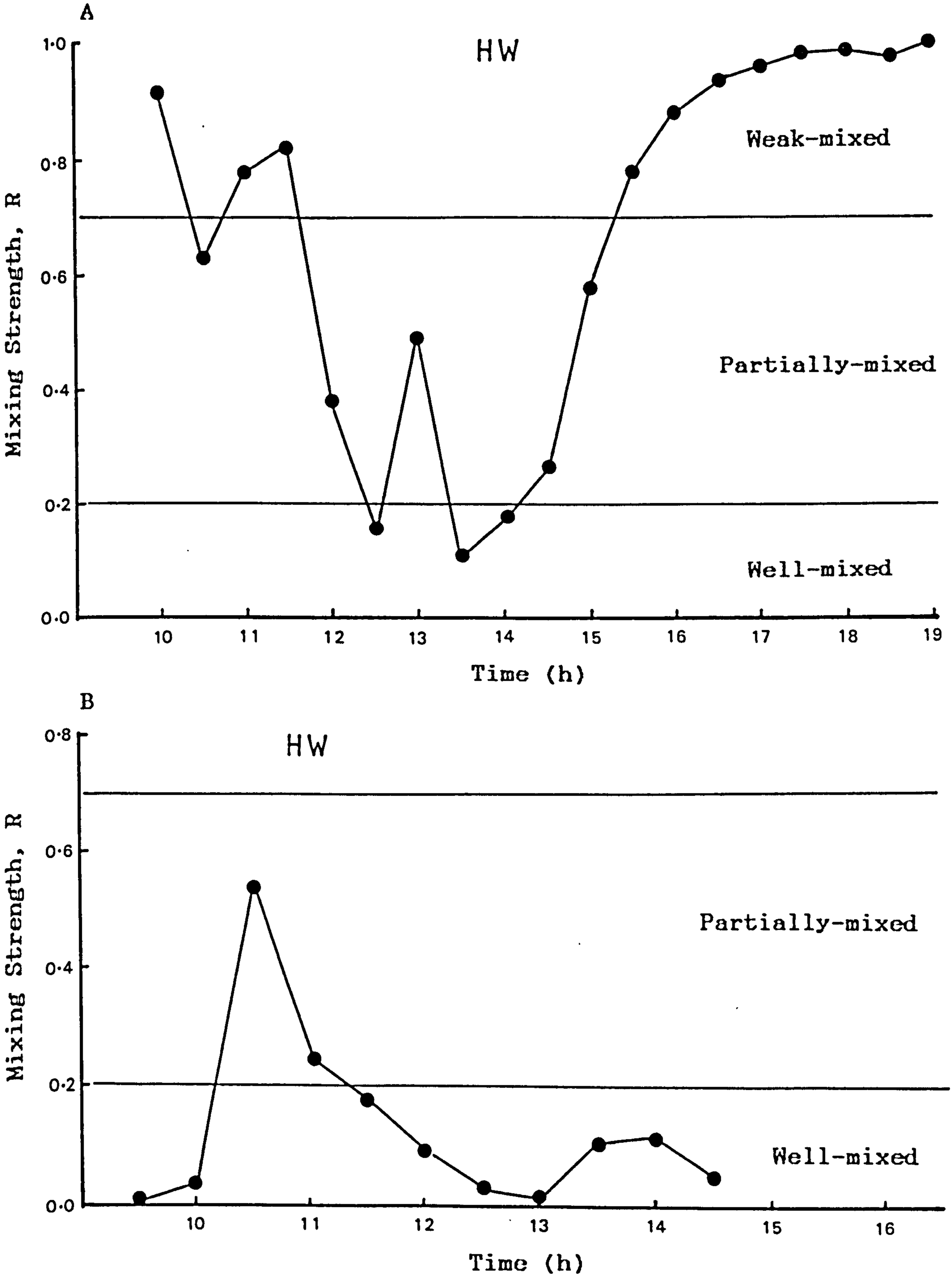

Figure 3.22. Variations of mixing strength (R) at Stations 2 (A) and Station 6 (B).

properties. At a particular station, these properties show regular periodic changes in synchrony with the excursions of water during tidal cycles.

The temporal and spatial variations of hydrodynamic variables in the estuary are relatively complex, partly because of the changes in the volume of fresh water entering the estuary and partly because of the large spatial changes in mixing due to tidal currents. The general effects of all these variables are evident in the data obtained during the work in this estuary.

These studies show that the mixing processes in the Dwyryd estuary were very variable during the sampling period when tidal ranges varied from approximately 1 to 4 meters. The degree of asymmetry of the tidal wave increased in the landward direction with the flood phase becoming shorter, e.g. 5.25 hours near the mouth of the estuary and 1.25 hours at the upper section of the estuary. Currents during a spring tide were higher compared with a neap tide in both flood and ebb directions. The time of maximum flood currents consistently occured immediately after the onset of the flood tide. Maximum ebb currents occured near the end of the sea water flushing time when the water was confined to the Dwyryd channel. Maximum ebb current velocities were generally greater then maximum flood current velocities.

The vertical salinity and velocity variation of the water column are also very variable. Variations from well mixed

to highly stratified conditions occured from time to time. At a neap tide, especially during high river discharge, the estuary was usually highly stratified but some variation in the degree of vertical mixing occurs on some occasions at all stages of the tide. The significance of these variations lies in the relationship that exists between salinity, river discharge and tidal ranges. Discharge is low for much of the year making the Dwyryd estuary a tide-dominated estuary where mixing processes largely destroy stratification (Simmons, 1955; Hansen & Rattray, 1966). As this is a small estuary wind-induced mixing processes will not significantly influence the salinity distribution (Ketchum et al., 1951).

FOUR

BOUNDARY LAYER STRUCTURES

4.1 Introduction

The transport of estuarine or marine sediments which are frequently taken into traction and/or suspension and deposited on the bed depends largely on the nature of the flow near the bed and the grain size of the sediment. It is well known that transport rates over rippled beds are substantially different from those over flat beds, probably due to differences of the flow characteristics over the ripples and flats beds. The nature of flow near the bed (or boundary layer) as shown in chapter 3 is very complex. There has been considerable interest in recent years in establishing the nature of flow regimes, the effect of various types of bedform on the flow, and the distribution of shear stresses within the water column (Sternberg, 1968; Heathershaw, 1979; Dyer, 1980; Soulsby and Dyer, 1981; Soulsby, 1983).

The water flows interact with the bed physically by means of friction forces which are expressed in terms of bed shear stress (or force per unit area of bed),usually denoted by τ_o , which is related to the nature of the bed

and to the geometry of the bed . The lowest part of the boundary layer where the shear stress is nearly constant is referred to as the viscous sublayer and is characterised by laminar flow (Wimbush and Munk,1971) . Within this laminar flow the velocity gradient is linear. The rest of the boundary layer is characterised by turbulent flow in which the velocity gradient is logarithmic with respect to height from the bottom. Within turbulent flow, the shear stress is related to the shear velocity, u_* , by $\tau_o = \rho u_*^2$ (ρ is water density) which has an important influence on the rate of sediment transport (Channon & Hamilton, 1971; Mc Cave,1973).

Many studies have verified the existence of a logarithmic velocity profile in the lower region of fully-developed turbulent flows (Sternberg,1968; Dyer,1970; Bowden,1962; Langhorne,1981). For steady two dimensional unstratified flow, the law of the wall relates and the time average velocity u_z by

$$u_z = \frac{u_*}{k} \ln\left(\frac{z}{z_o}\right) \qquad 4.1$$

where z is the depth of the flow and z_o is the roughness length (conceptually, the elevation at which u=0) and K is von Karman's constant, taken as 0.4 (though this ignores a variation in this value during the tidal cycle as

demonstrated by Vanoni & Nomicos (1959), McCave (1974) and Thorn & Parsons (1980) from shallow marine and estuarine environments, and by Einstein & Chein (1955) from laboratory measurements). Although this boundary layer equation was developed for steady uniform flows, it has been shown that it accurately describes the velocity profile in the marine environment in the vicinity of the bed (Bowden,1962; Sternberg,1968).

Equation 4.1 has been used under a great variety of experimental conditions in the sea to calculate the bed shear stress from near-bottom velocity measurements over various types and sizes of bedforms. The bed shear stress can be calculated quite easily from the measured velocity profile in the turbulent part of the constant stress layer within the bottom 1 meter of the flow. The profile is normally fitted to data using a least squares technique.

The technique of fitting velocity profile data to a logarithmic model by a least square method has become so common in boundary layer studies that it is a natural tendency to apply this technique to any near bed velocity profiles. However, this can be misleading, as a slight curvature in the profile, due perhaps to surface irregularities of different scales (Soulsby, 1983; Chriss & Caldwell, 1982), stratification (Adam & Weatherly, 1981), wave and current interaction (Grant & Madsen, 1979), and flow acceleration /deceleration (Soulsby & Dyer, 1981) can cause the measured u_* and z_o to be very different from the

true values. Soulsby and Dyer (1981) estimated that in accelerating and decelerating flow the values of u_* may deviate by about 20% from the steady state value.

Another important parameter frequently used in sediment transport formulas is mean velocity which can be calculated from the known values of shear velocity and roughness length by the equations

$$U = \frac{1}{d}\int_0^d u(z)\,dz \qquad 4.2$$

or

$$U = 2.5\, u_* \ln\left(\frac{d}{2.718\, z_0}\right) \qquad 4.3$$

where U is the mean velocity, d is the flow depth, and u_* is the shear velocity.

An alternative but practical approach is to estimate the bed shear stress from a single current velocity measurement made at a single fixed elevation above the bed (Sternberg,1972; Ludwick,1975a). This can be done using the quadratic friction law of the form

$$\tau_0 = \rho C_D U \qquad 4.4$$

where C_D is the drag coefficient which is usually taken as constant over the study area. Current velocity measurements for use in sediment transport calculations are commonly made at a height 100 cm above the bed, and the corresponding drag coefficient C_{D100} is somewhat larger than C_D based on U. The value of C_{D100} can be calculated from

$$C_{D100} = \left[\frac{k}{\ln(100/z_o)}\right]^2 \qquad 4.5$$

The value of the roughness length z_o must be estimated from velocity profiles,or from formulas suggested by many people (Lettau, 1969; Wooding et al., 1973; and Kamphuis, 1974). Once the value of C_{D100} has been determined for the local roughness and flow conditions, it is possible to calculate shear stress from a single current meter measurement.

Much research has been focussed towards the evaluation of the value of roughness length in order to determine the nature of the flow and its relation to sediment transport. The problem related to sediment transport is to estimate, for a given flow condition , the residual energy that is available to the sediment. How much energy is available for sediment transport and how much is used to overcome bed resistance is linked to the friction factor or on the value of roughness length, a parameter that appears in most sediment transport calculations. Roughness length is basically an empirical parameter associated with the nature

of the boundary layer and is expressed in terms of either the grain size or ripple size. It is used to overcome the lack of detailed knowledge of events in the boundary layer.

Many studies have been carried out to determine the value of this parameter for different sea bed types. Values of roughness length ranging from 0.02 cm for a muddy bed to about 0.6 cm for a rippled sandy bed have been suggested (Soulsby, 1983). Over a rippled sand bed, the roughness length varies considerably throughout a tidal cycle (Dyer, 1980), while over sandy gravels it remained relatively constant throughout a tidal cycle (Heathershaw & Langhorne, 1988). The variation of the roughness length over a tidal cycle is probably due to changes in bedform geometry and also to the changes in the characteristics of the flow over the bed (Sternberg, 1968; Heathershaw, 1979; Dyer, 1980).

4.2 Measurements

A current meter rig (velocity gradient unit) for measuring the current velocity at various distances from the bed was constructed and its general arrangement during the deployment on the tidal flat can be seen in Figure 4.1. It consisted of ten Ott current meters mounted in a vertical configuration with a logarithmic spacing from 10 to 105 cm above the bed, five current meters each for flood

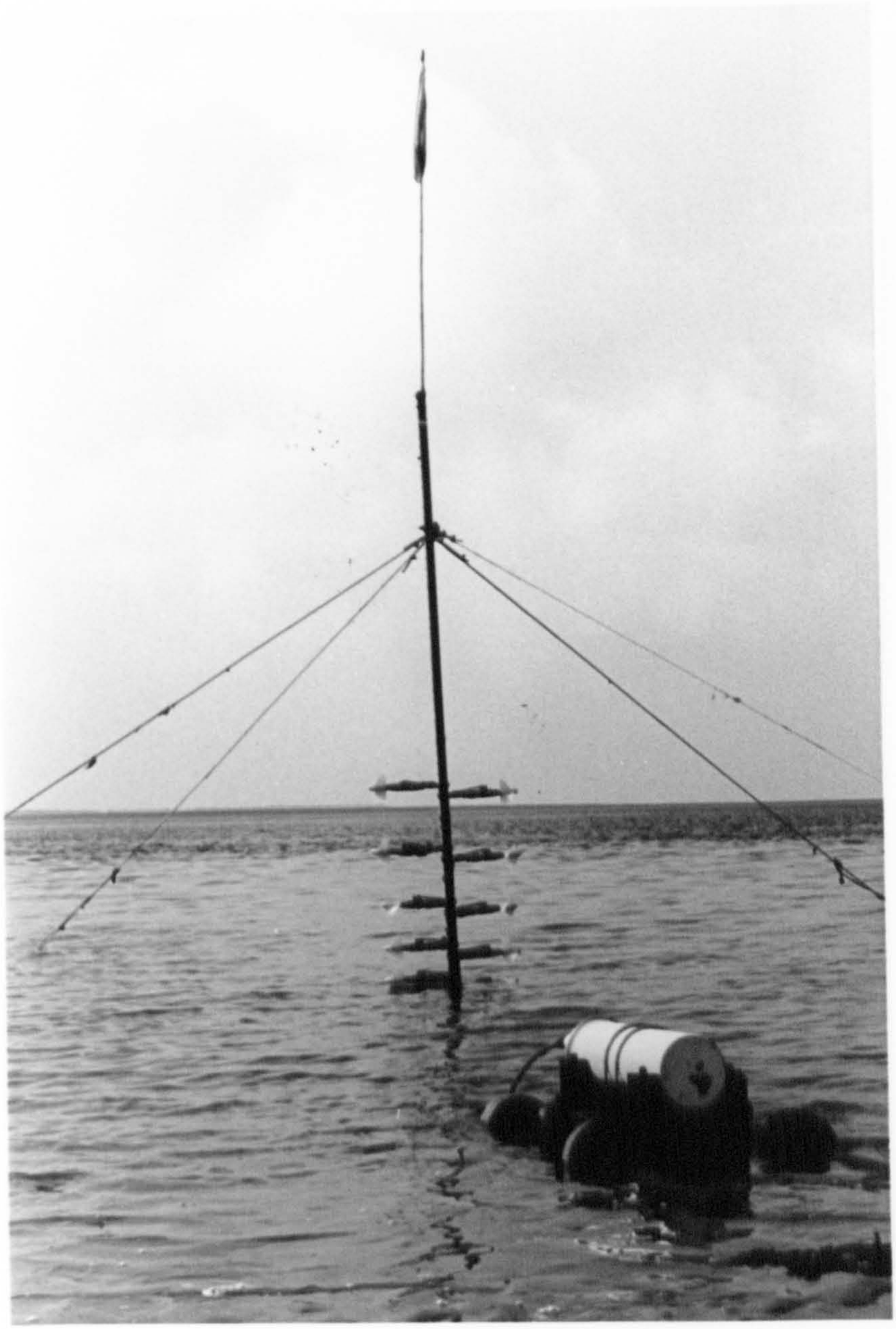

Figure 4.1. A velocity gradient unit and a data logger (yellow cylinder).

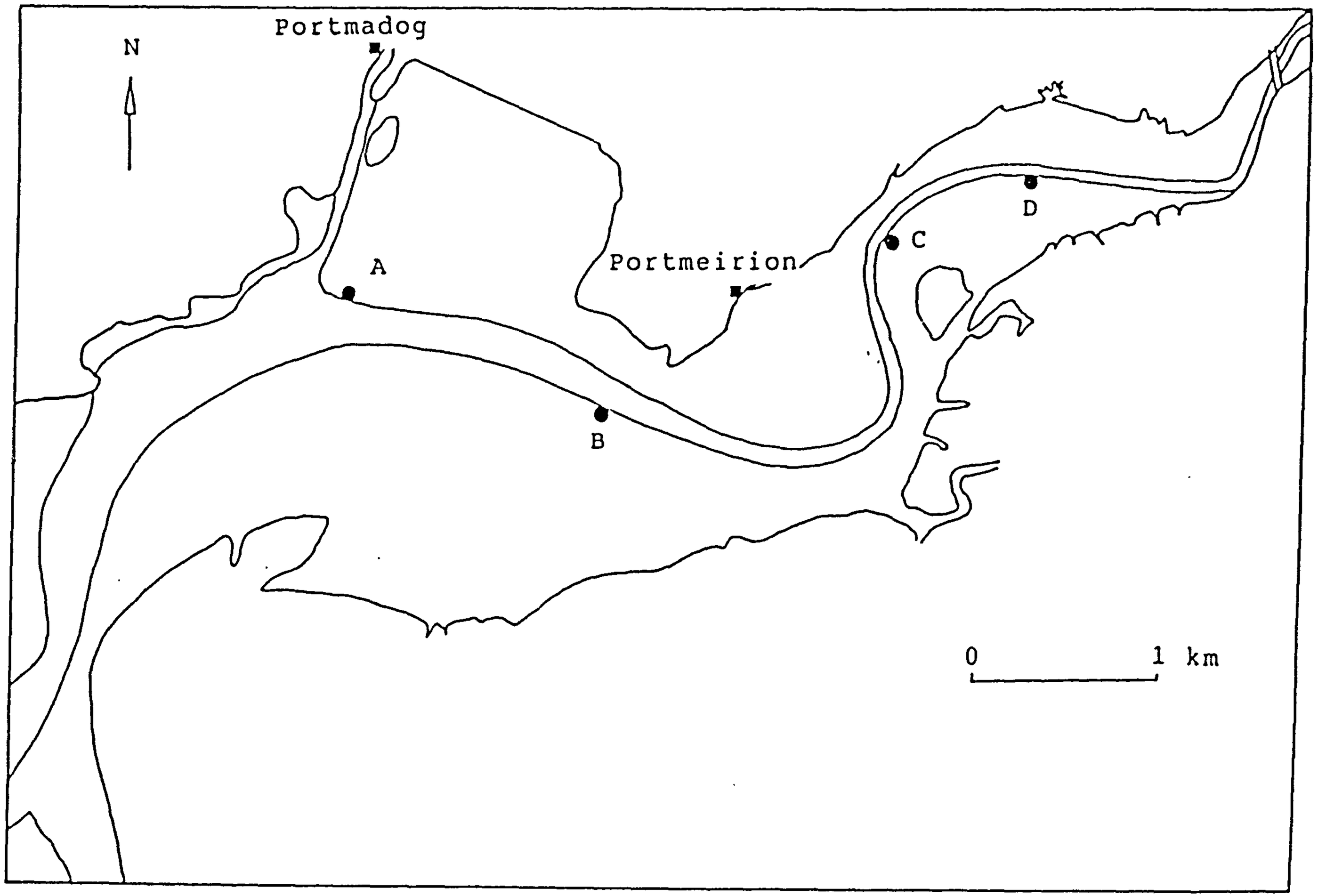

Figure 4.2. Position of the current meters rig.

and ebb directions. The vertical steel pole which supports the current meters is bolted to an iron bar which is hammered into the sand. Extra stability is provided by four guy ropes tied to four metal stakes.

The electrical cables from the curent meters were connected to a data logger via a junction box which was attached to a lead block. This junction box was buried into the sand to reduce the disturbance around the current meters. The speeds of the propellor were recorded by an automatic data logger capable of storing the data for a period of about 8 days. The logger was programmed to record current velocity for about eight hours for each tidal cycle,four hours before and four hours after high water. Rotor counts were measured at 2 minutes intervals and were averaged over 2 minutes. The rig was stationed adjacent to the main channel at four different locations (Fig. 4.2). All the stations were located near the main channel at the lower, middle, and upper sections of the estuary. As shown in chapter 3, the tidal range at the lower section varies from less than 1 m during the neap tides to about 3.5 m during spring tides. This range decreased slightly toward the estuary head. Area around station A is composed of small flood-oriented megaripples, whereas area around station B is composed of flood-oriented sandwaves. Repeated visits to these areas reveal that these bedforms are permanent, but not static in response to contrasts between spring and neap tidal flow. Areas around stations C and D, however, are composed of small current

and wave ripples only.

4.3 Results and discussion

Most of the profiles were approximately logarithmic but on many occasions discrepancies could possibly be explained as due to turbulent fluctuations, flow unsteadiness especially at and near the high water, but also to fouling of propellors by seaweed which is common in this area. The velocity distribution was considered logarithmic if the square of the correlation coefficient was larger than 0.8. High values of R^2 do not necessarily mean that the profiles are strictly logarithmic but Figures 4.3, 4.5, 4.7 and 4.9 show that only those measured near slack water depart much from this ideal, probably because of the unsteadiness of the flow (or to errors in measurement).

The number of points available for the regression plot varies from zero to five points. This is because the number of current meters submerged in the water depends on the tide level. During and near spring tides when tide level is higher than 1.1 m, all current meters are submerged, but during neap tides and at the early stages of flood tides and at the end of ebb tides when the tide level is very low, the number of current meters submerged under the water is reduced. In cases when data from only one

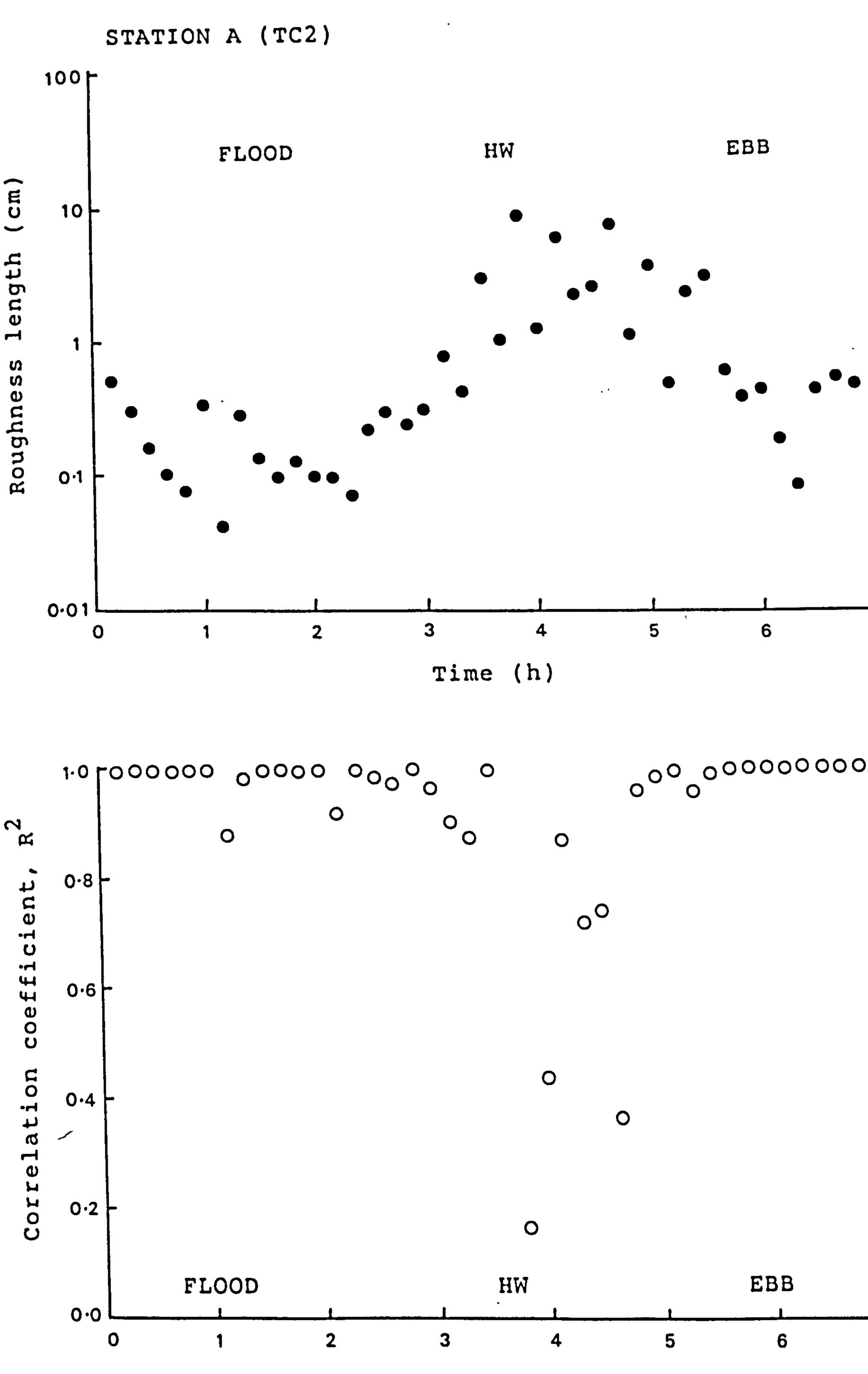

Figure 4.3. Variations of roughness length (Z_o) and correlation coefficient (R^2) using four or five data sets over a typical tidal cycle.

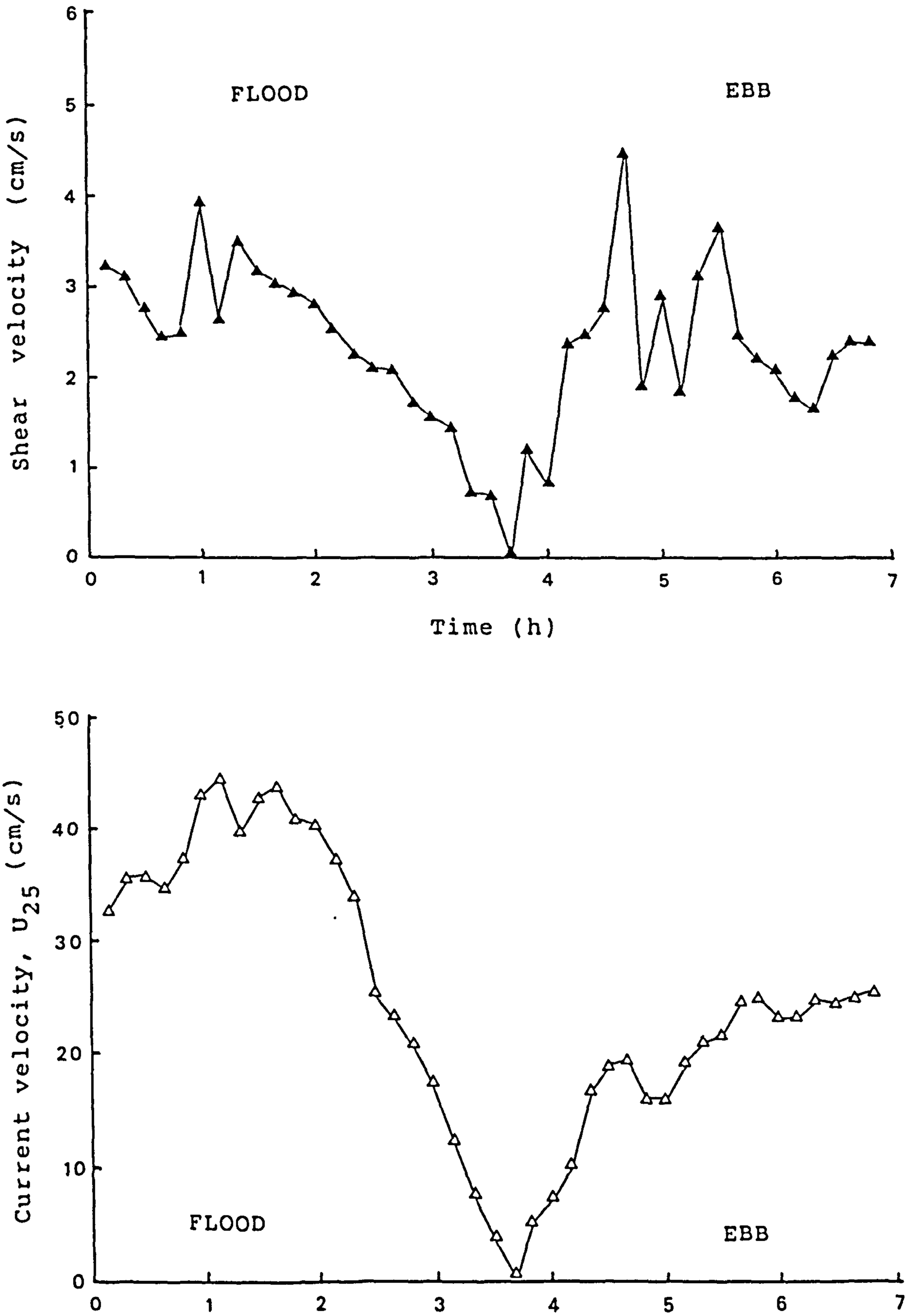

Figure 4.4. Variations of shear velocity, U_* and current velocity measured by current meter 25 cm above the bed (U_{25}) over a typical tidal cycle.

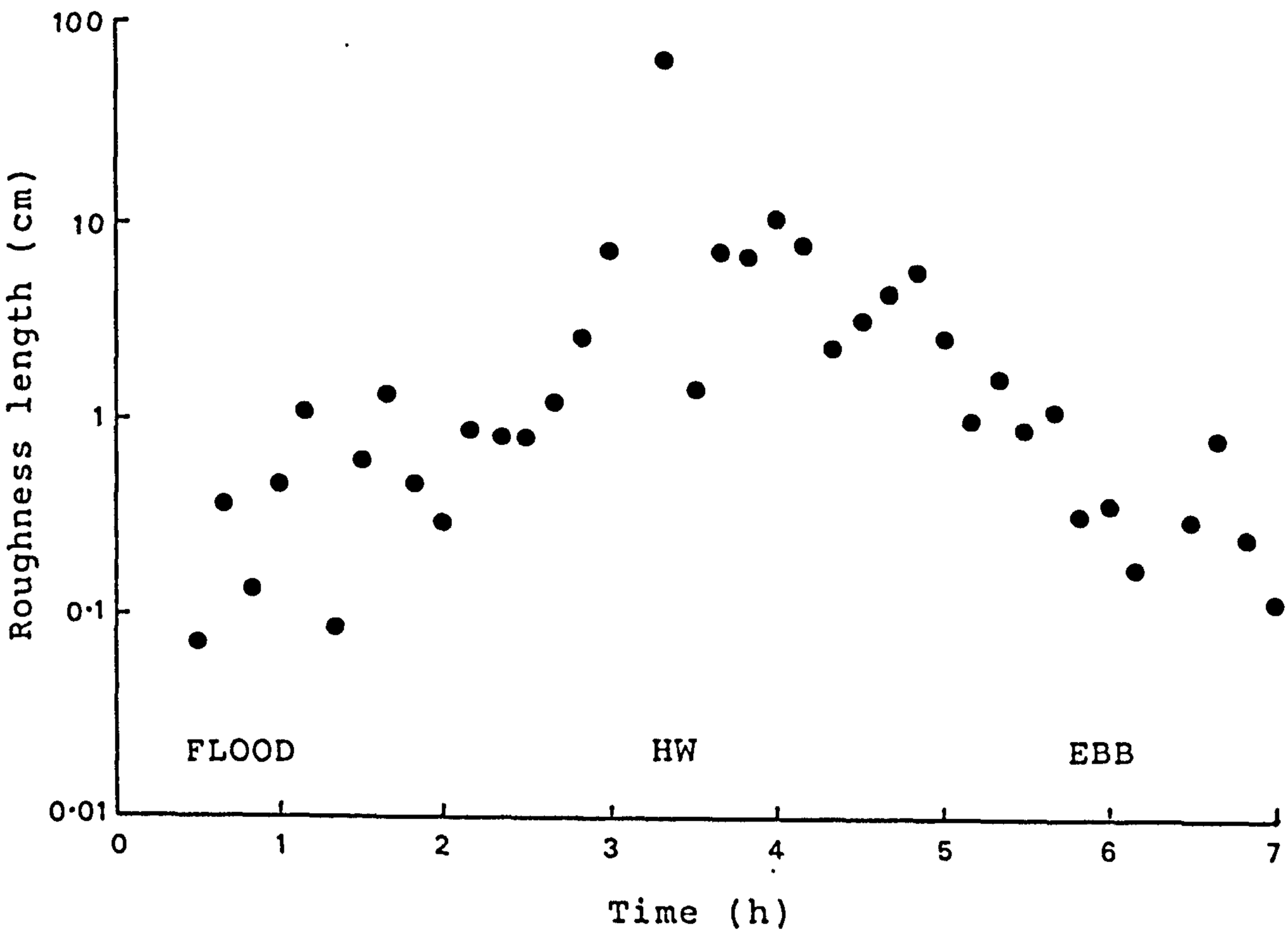

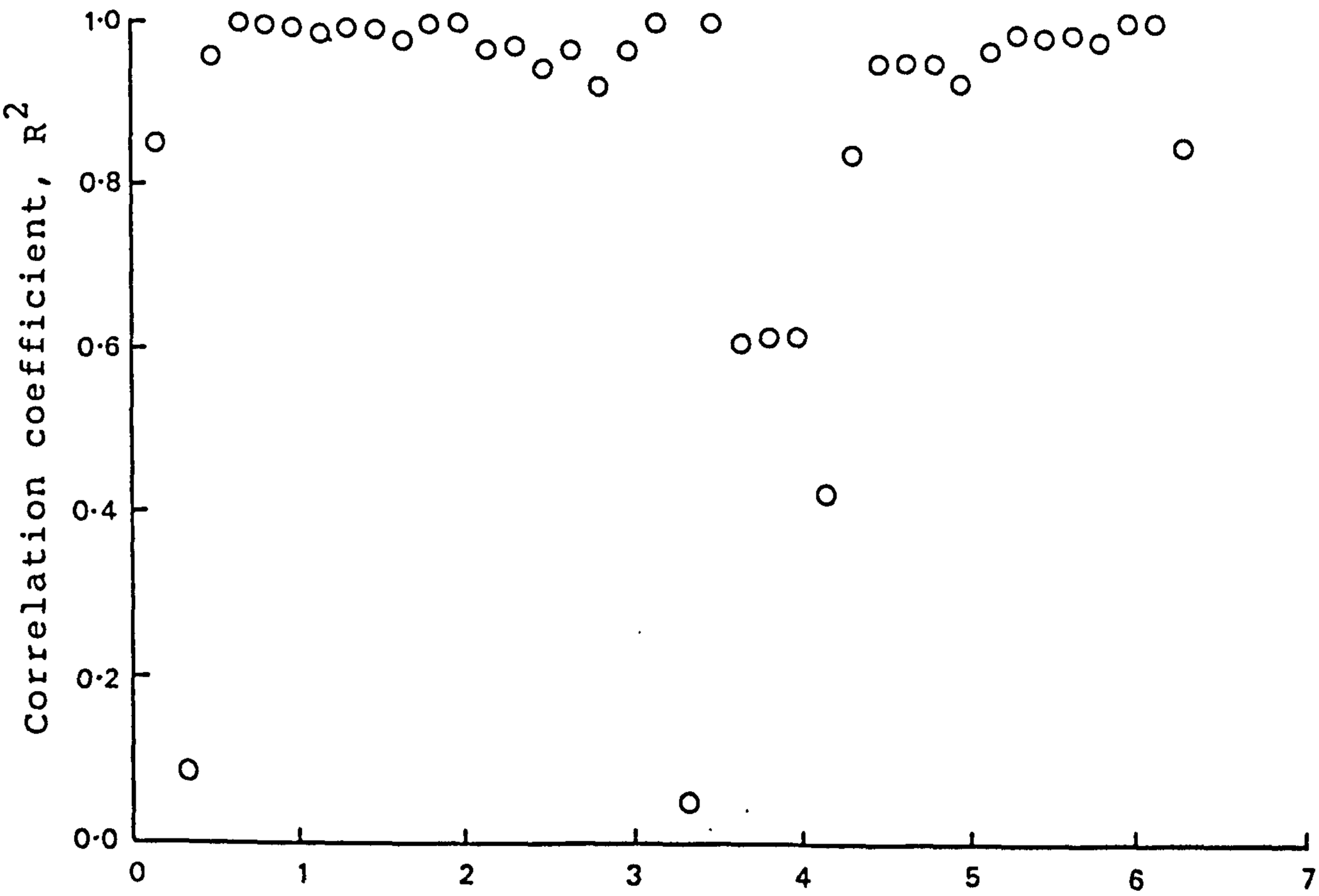

Figure 4.5. Variations of roughness length (Z_o) and correlation coefficient (R^2) using four or five data sets over a typical tidal cycle.

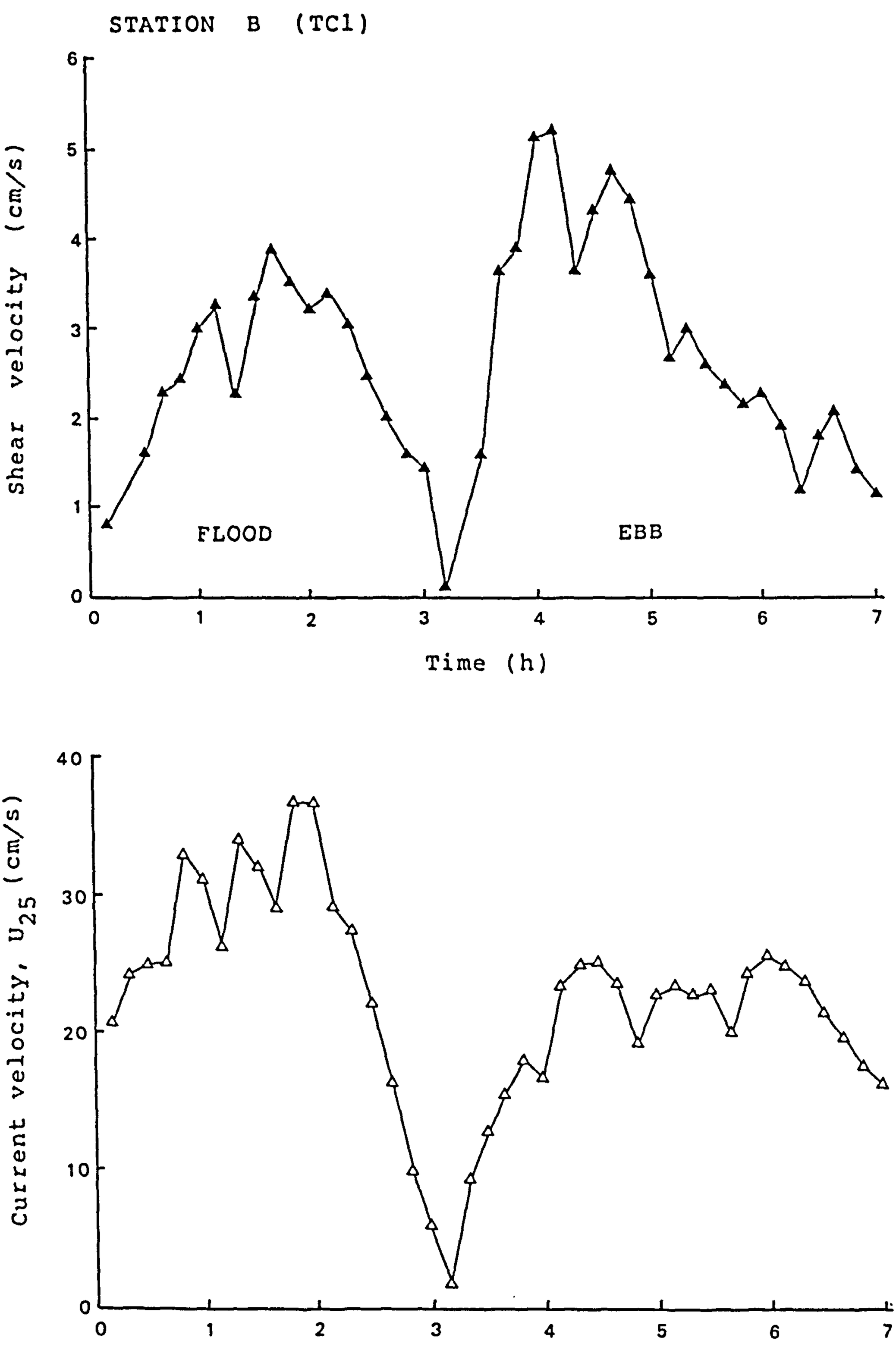

Figure 4.6. Variations of shear velocity, U_* and current velocity measured by current meter 25 cm above the bed (U_{25}) over a typical tidal cycle.

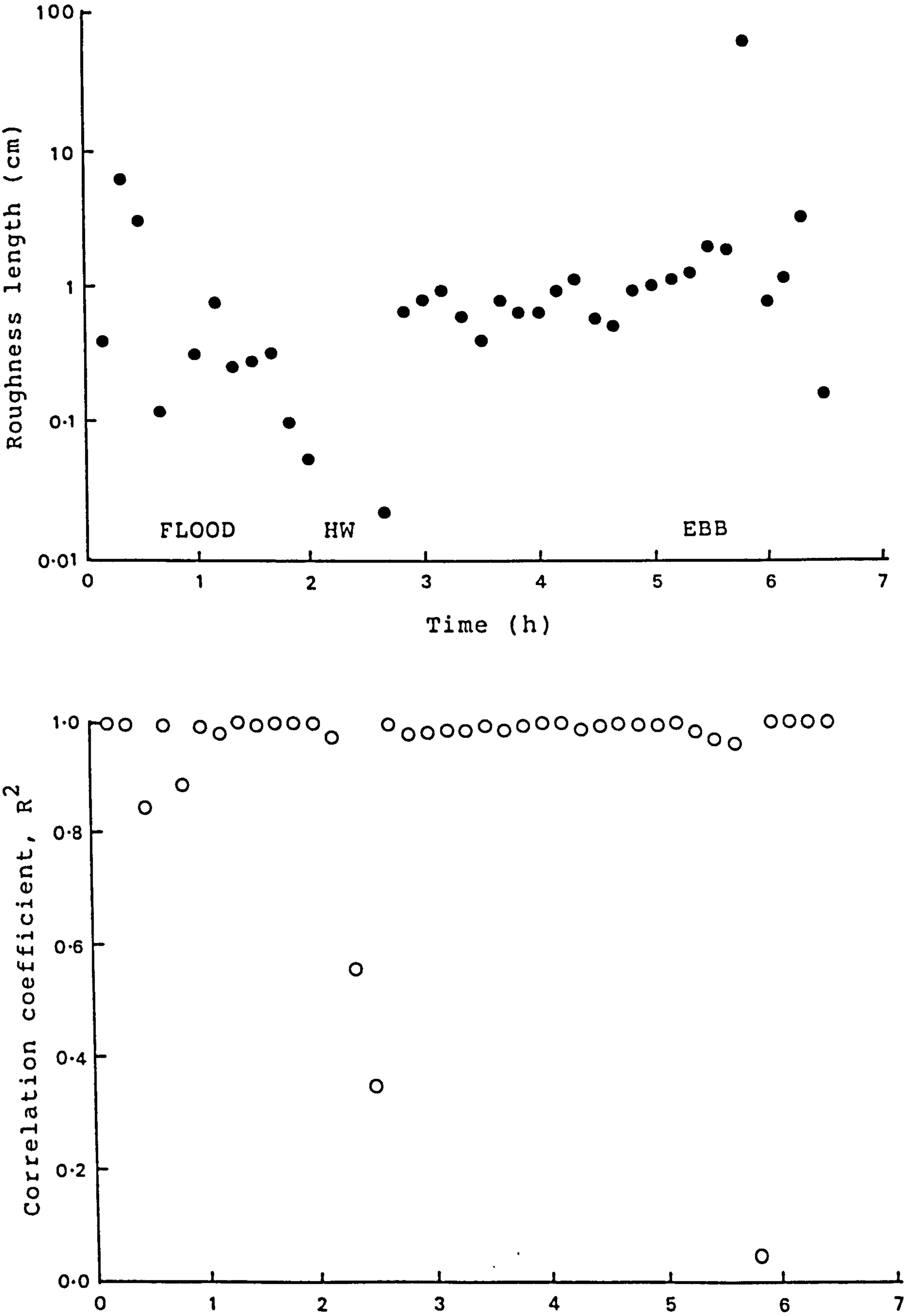

Figure 4.7. Variations of roughness length (Z_o) and correlation coefficient (R^2) using four or five data sets over a typical tidal cycle.

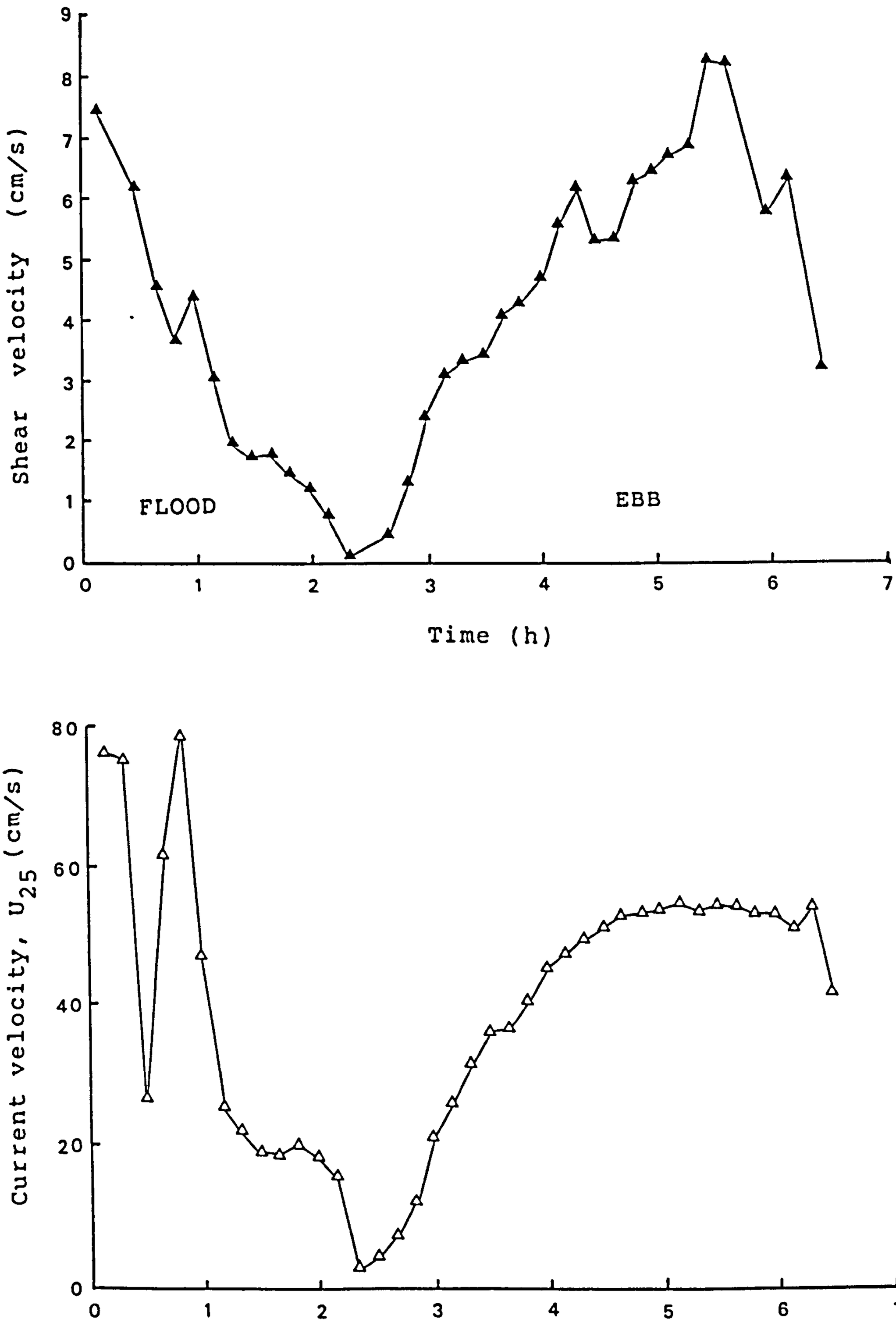

Figure 4.8. Variations of shear velocity, U_* and current velocity measured by current meter 25 cm above the bed (U_{25}) over a typical tidal cycle.

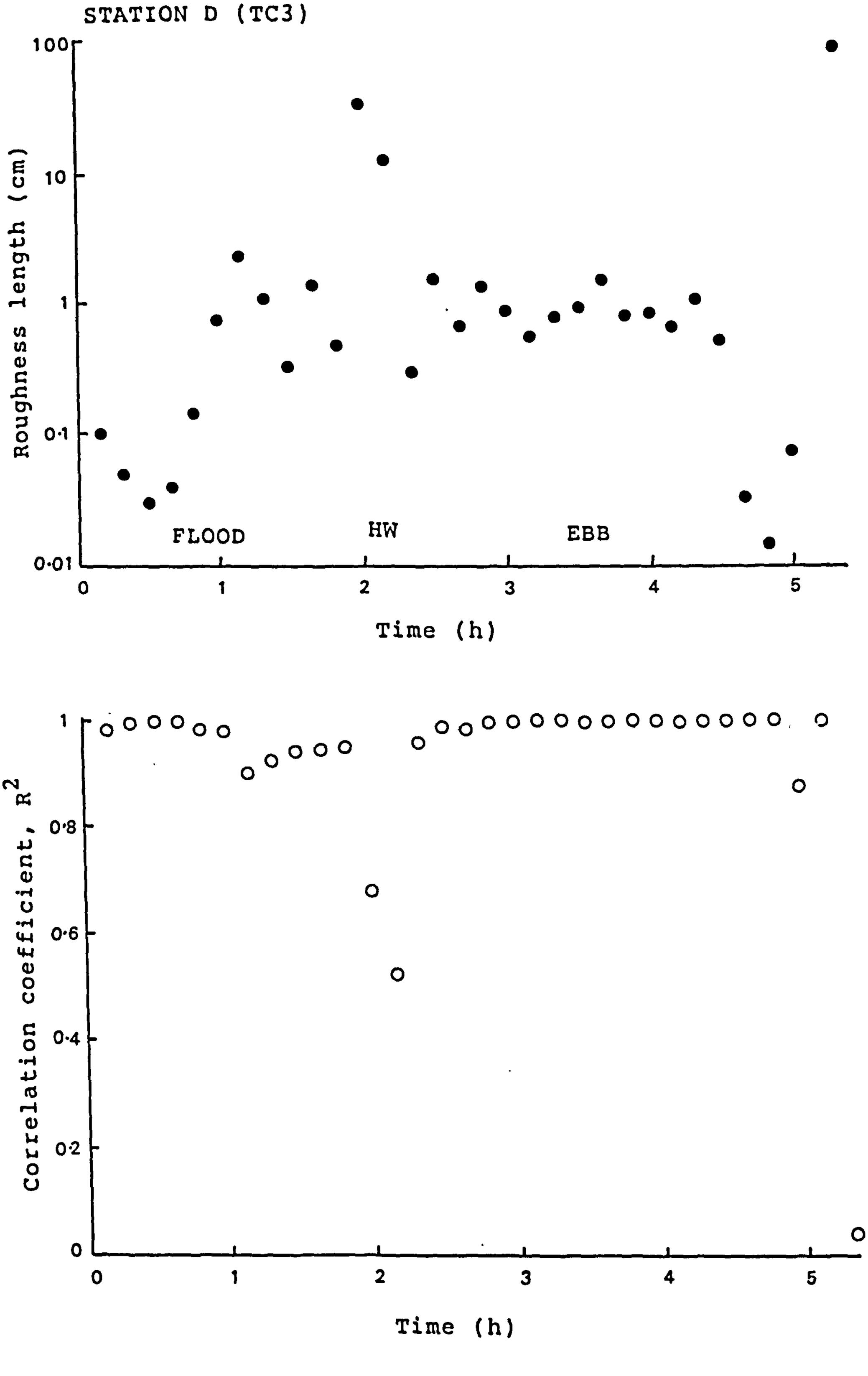

Figure 4.9. Variations of roughness length (Z_o) and correlation coefficient (R^2) using four or five data sets over a typical tidal cycle.

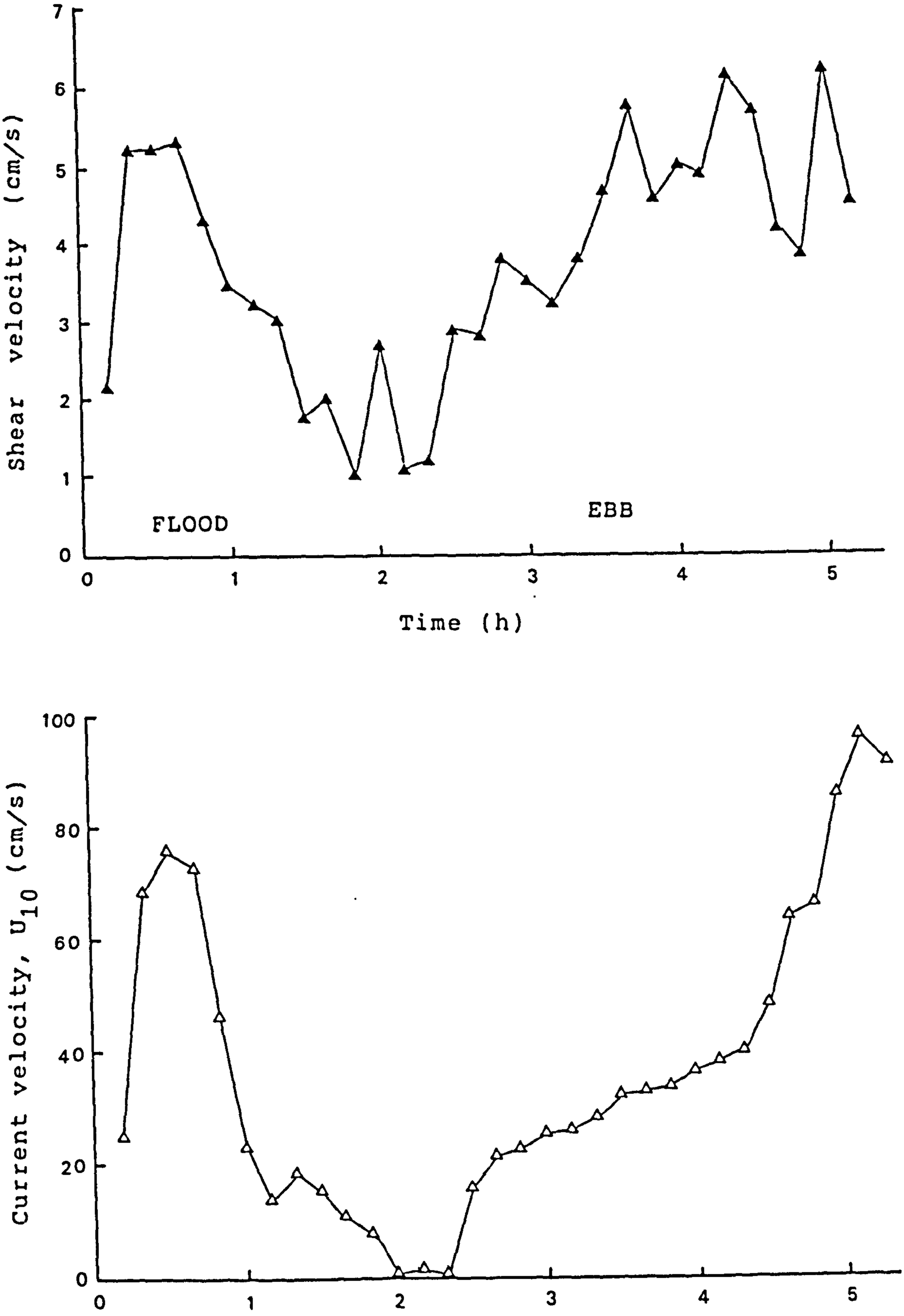

Figure 4.10. Variations of shear velocity, U_* and current velocity measured by current meter 10 cm above the bed (U_{10}) over a typical tidal cycle.

current current meter were available, the shear stress can only be estimated using the quadratic friction law of equation 4.4. The equivalent values of u_{100} were calculated from the following equations

$$u_z = \frac{u_*}{k} \ln\left(\frac{z}{z_o}\right) \qquad 4.6$$

and

$$u_{100} = \frac{u_*}{k} \ln\left(\frac{100}{z_o}\right) \qquad 4.7$$

Where u_z is the current velocity z m above the bed. The value of roughness length in this equation is based on the average value for the whole spring-neap tidal cycle.

The roughness length and the correlation coefficient were determined for every profile which have two or more points for linear regression. The mean roughness was estimated for each flood and ebb tide. This was done for every tidal cycle. The results are shown in Figures 4.11 to 4.14 for station A to D respectively. The mean value of z_o varies from 0.542 to 1.278 cm at individual locations. However, the mean z_o for the flood tide is always less than the mean value for the ebb tide.

This mean value of roughness length reflects the possible effects of the bedforms and the stratification on the velocity profiles. It is comparable with a value calculated from theoretical considerations. Wooding,

STATION A

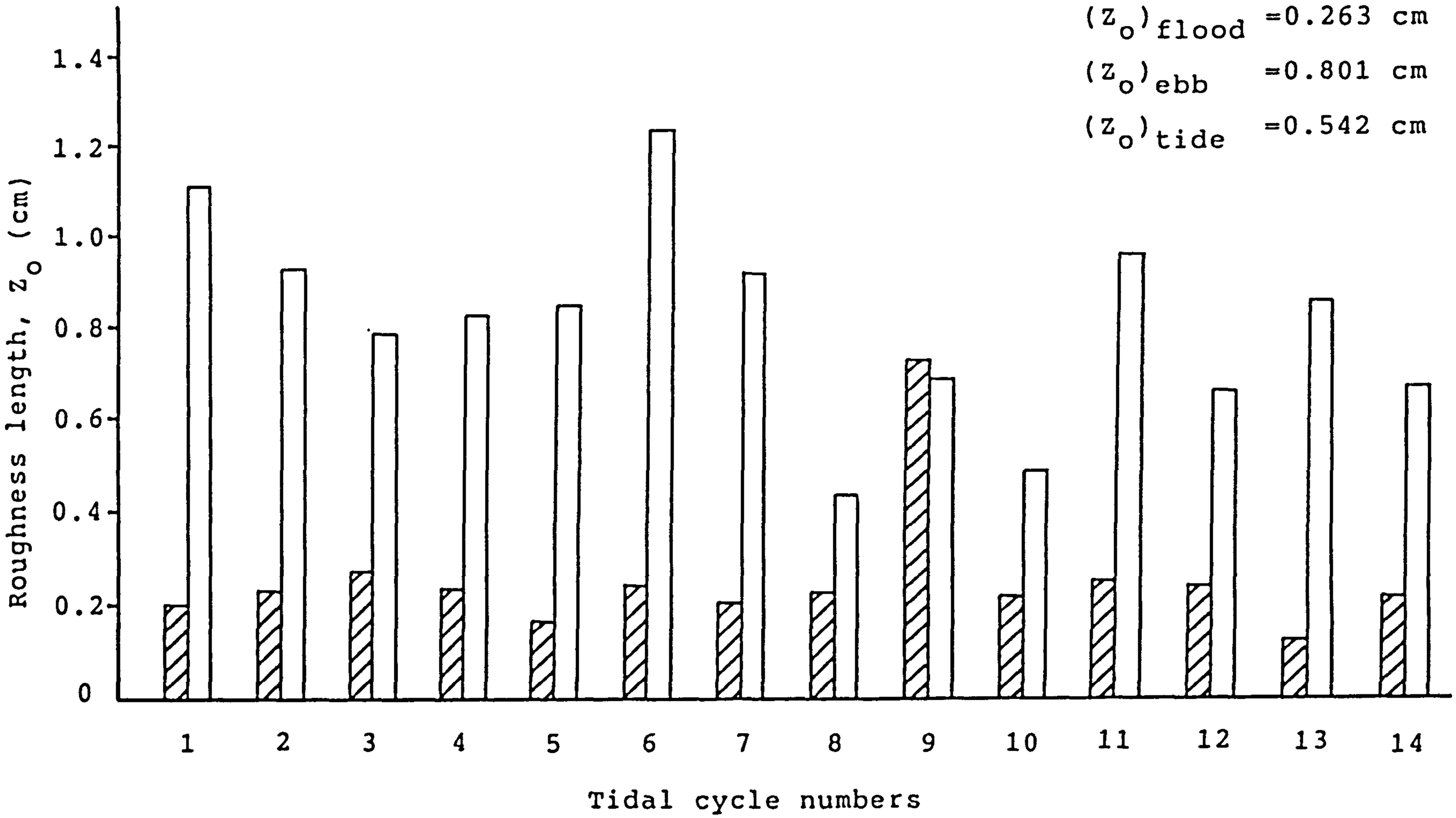

Figure 4.11. Mean flood (shaded) and ebb (unshaded) roughness length for each tidal cycle at station A.

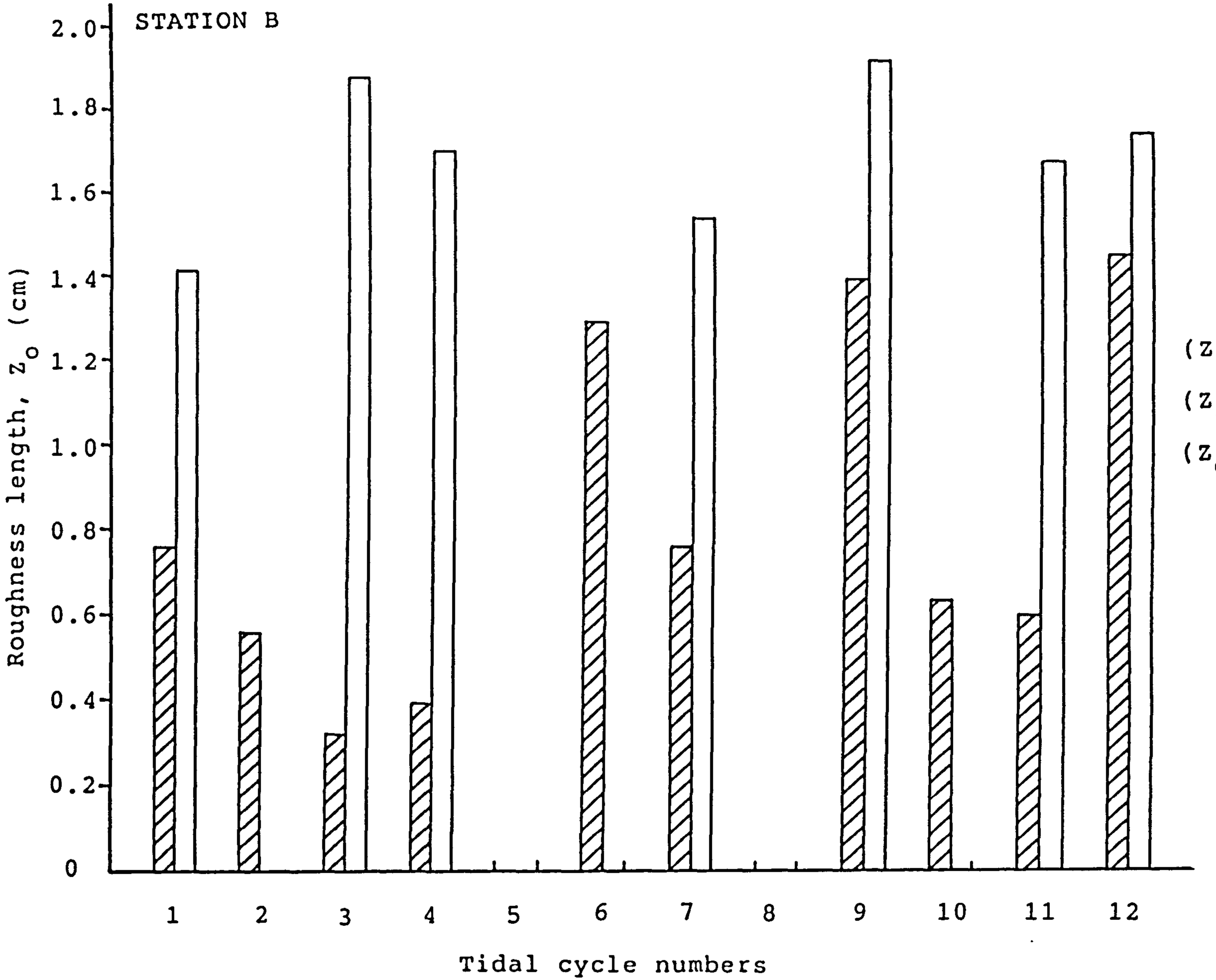

Figure 4.12. Mean flood (shaded) and ebb (unshaded) roughness length for each tidal cycle at station B.

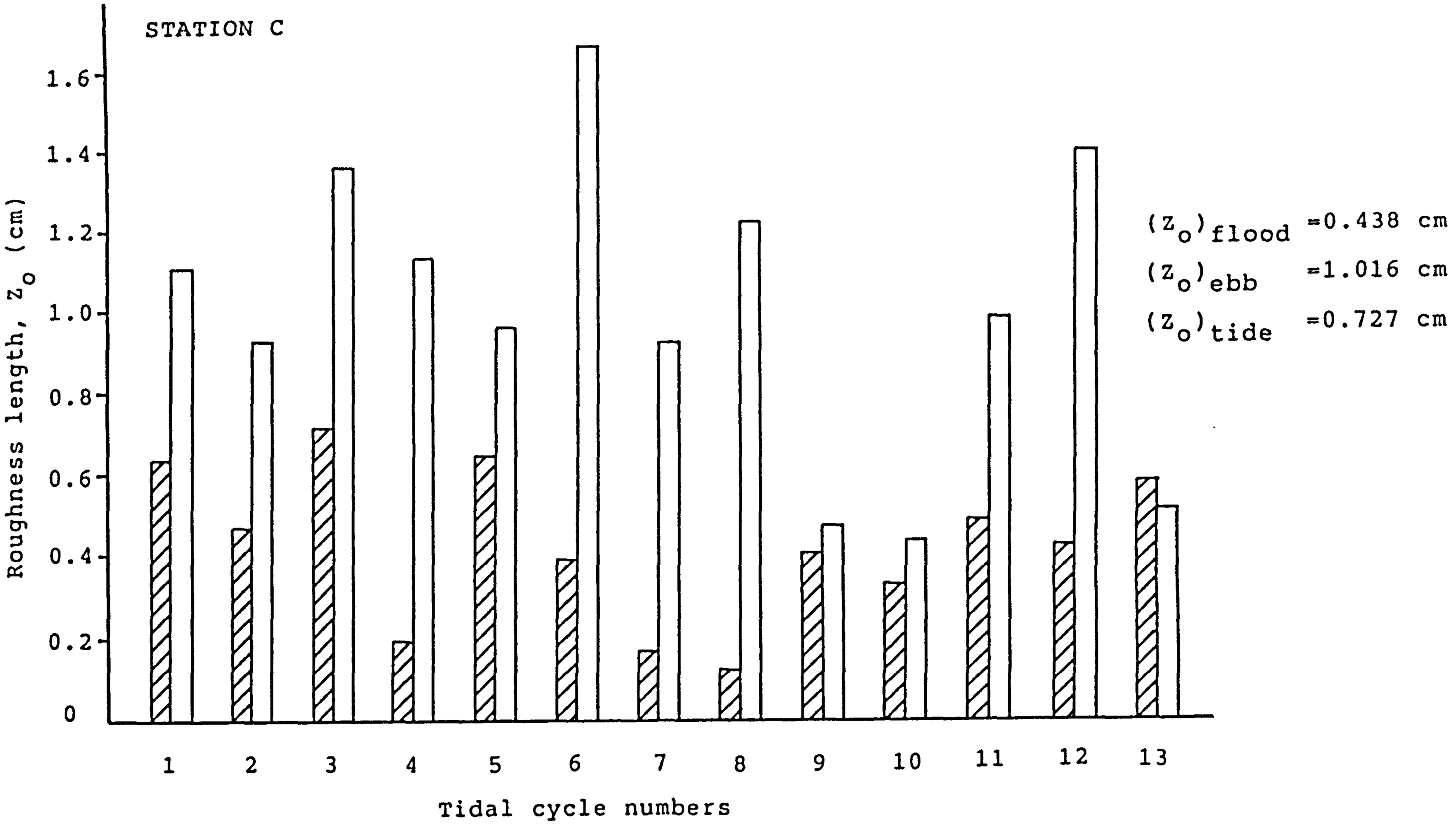

Figure 4.13. Mean flood (shaded) and ebb (unshaded) roughness length for each tidal cycle at station C.

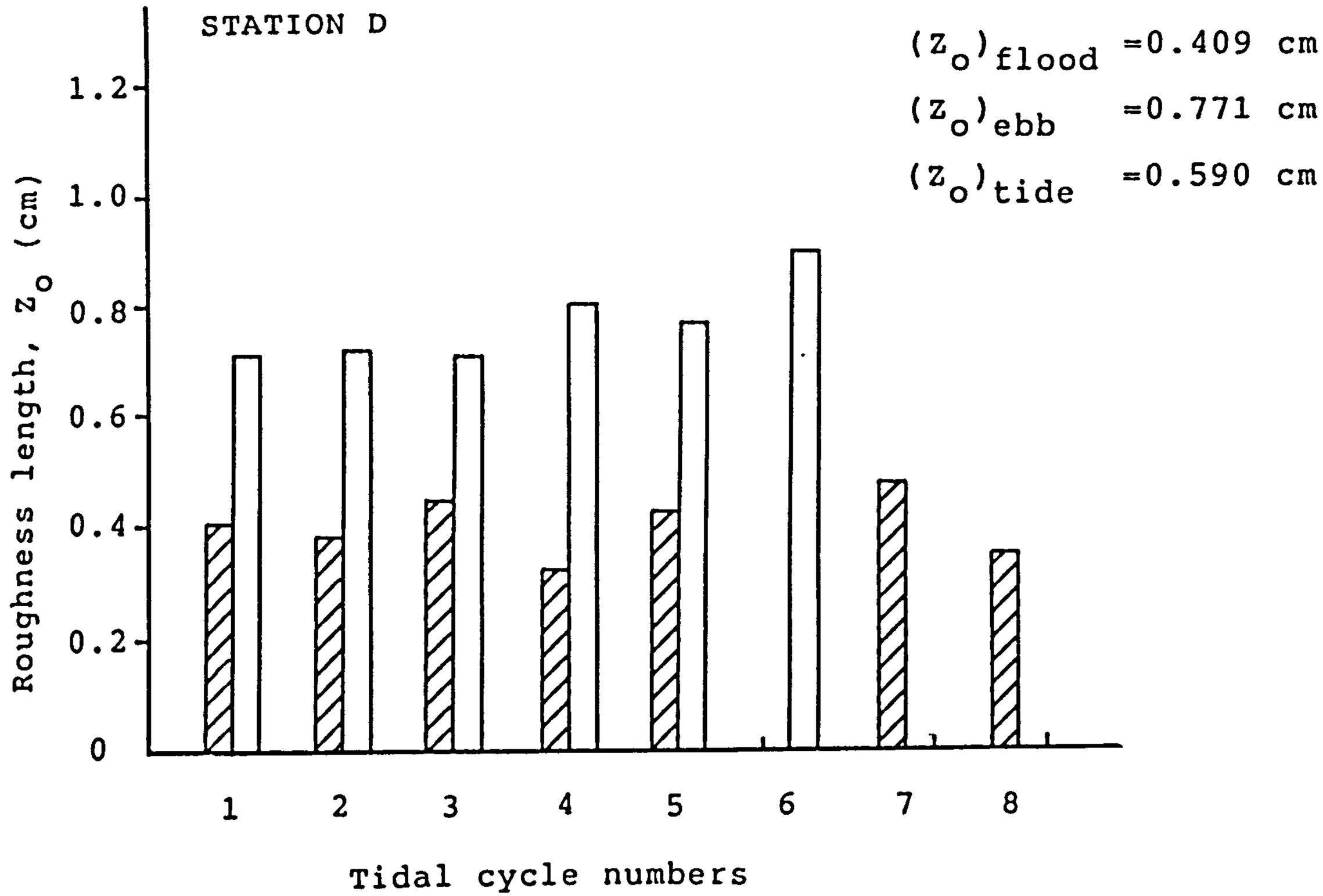

Figure 4.14. Mean flood (shaded) and ebb (unshaded) roughness length for each tidal cycle at station D.

Bradley & Marshall (1973) proposed the relationship

$$z_o = 2.0\ H \left(\frac{H}{\lambda}\right)^{1.4} \qquad 4.8$$

between roughness length and bedform dimensions where H is bedform height and λ is bedform wavelength. Using equation 4.8, ripples with heights of 3 cm and wavelengths of 20 cm, as commonly observed in this study area, should have a roughness length of 0.4 cm. This is in agreement with the value calculated at station A,C, and D. Station B,however, was located in the sandwave field with heights up to 50 cm and wavelengths of about 16 meters, should have a roughness length of 0.78 cm which is smaller than the estimated value of 1.27 cm.

The individual values of z_o calculated from each profile,however, still vary considerably during each tidal cycle. Time series of roughness length and correlation coefficient (R^2) during the flood and ebb period are shown in Figures 4.3, 4.5, 4.7 and 4.9. The variability in z_o is quite large compared with the variability of R^2 . In areas with bedforms, and sometimes even for flatbed areas, a wide range in z_o between 0.001 to 10.0 cm is often found with accelerating and decelerating flows (Dyer,1972, 1980; Soulsby & Dyer, 1981; Bridge & Jarvis, 1982).

The use of a logarithmic velocity profile model in this study seems to be adequate since the relationship of the form of equation 4.1 fits the measured velocity profiles most of the time except a small portion of time near slack water. This is probably because of the unsteadiness of the flow as the current diminishes. This reflects an increase of non-logarithmic profiles during slack water as indicated by the reduction of R^2 values as shown in Figures 4.3, 4.5, 4.7, and 4.9. The excellent fit of the regression linear lines to the velocity data were obvious in the values of correlation coefficient (R^2) which were always greater than 0.98. Sternberg (1968) found that the model fits such velocity data 61% to 100% of the time. However, several workers have commented on the limitations of the logarithmic model (Smith,1969b; Nece & Smith, 1970; and Ludwick, 1974). The effects of unsteady flow on the logarithmic profiles have been studied by Soulsby & Dyer (1981). For a tidal flow, they estimated that the value of roughness length would be underestimated by 60% during accelerating flow and overestimated by 80% during decelerating flow. Consequently, the value of shear velocity would be underestimated and overestimated by 40% and 20% respectively. This is because during accelerating flow velocity profiles tend to curve upward, while during the decelerating flow, the velocity profiles tend to curve downward (Soulsby and Dyer, 1981).

In this study the differences between roughness lengths during the flood and ebb periods were very

noticeable in which the average roughness lengths measured during the flood were always less than the average value measured during the ebb period. The typical time series curves of shear velocity and roughness length calculated from velocity profiles for every 10 minute interval (Figures 4.3 to 4.10) show that there were apparently anomalous low and high values of shear velocity when compared to velocity recorded by any of the current meters. These correspond with low and high values of roughness length. As shown in Figures 4.4, 4.6 and 4.8 the estimated maximum value of the shear velocity during the flood tide is smaller than the maximum value during the ebb, but the velocity recorded by the current meter 25 cm above the bed showed that the maximum velocity occurred during the flood tide instead of the ebb. The cause of these anomalies may possibly be due to the variability of the velocity profiles.

The logarithmic and linear velocity profiles during two tidal cycles, one each at Stations A and B are plotted for comparison, as shown in Figures 4.15 to 4.18. The correlation coefficient, R^2, for each logarithmic and linear profile was calculated, and shown in Table 4.1. As shown, the velocity profiles deviated slightly from straight lines. In most cases, the profiles either curved upward or downward. The upward curvature has been observed only during the early stages of flood tide, while the downward curvature occurred during both flood and ebb

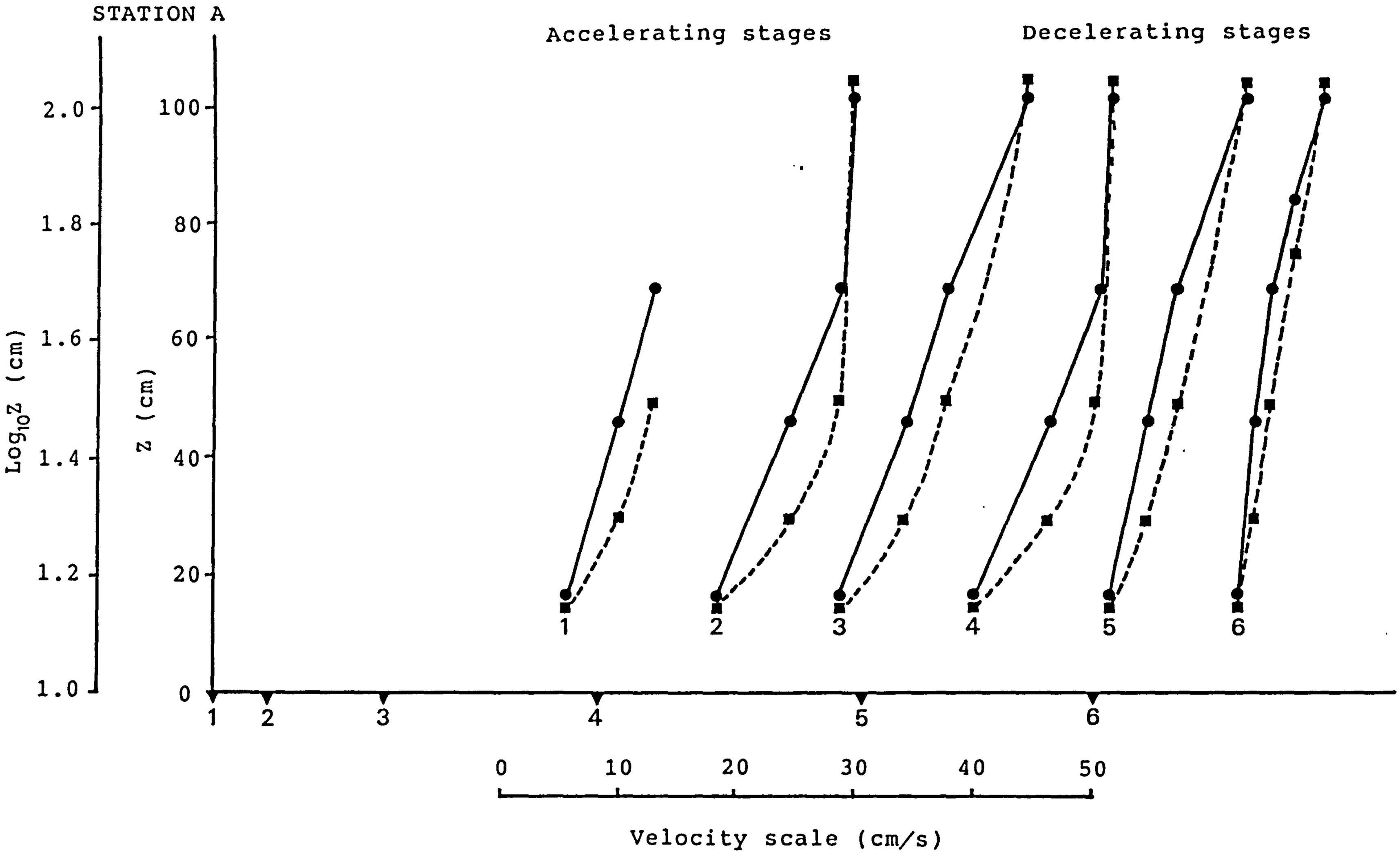

Figure 4.15. Linear (------) and logarithmic (————) velocity profiles at station A, on May 8, 1987, during flood tide.

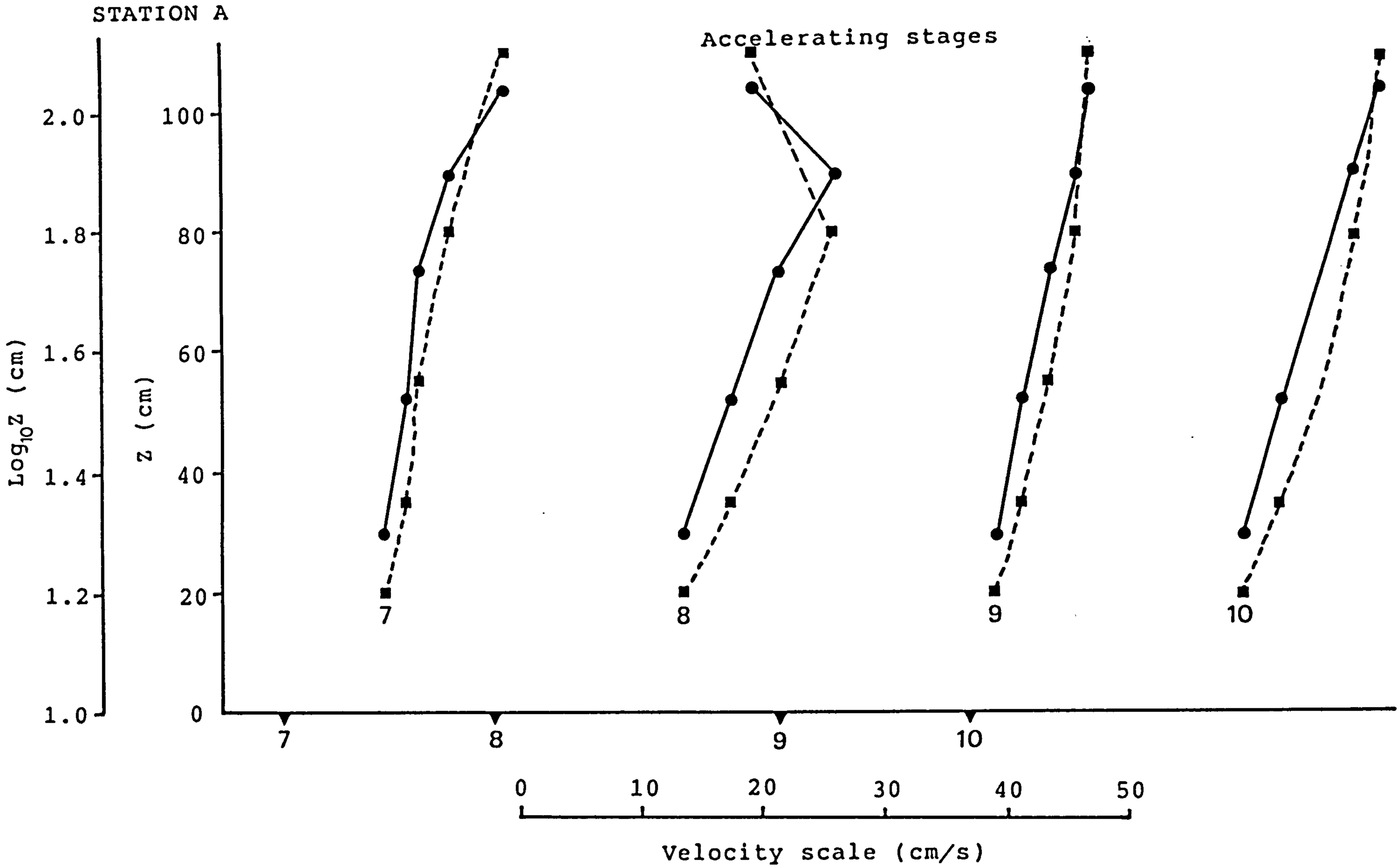

Figure 4.16. Linear (– – – – –) and logarithmic (————) velocity profiles at station A, on May 8, 1987, during ebb tide.

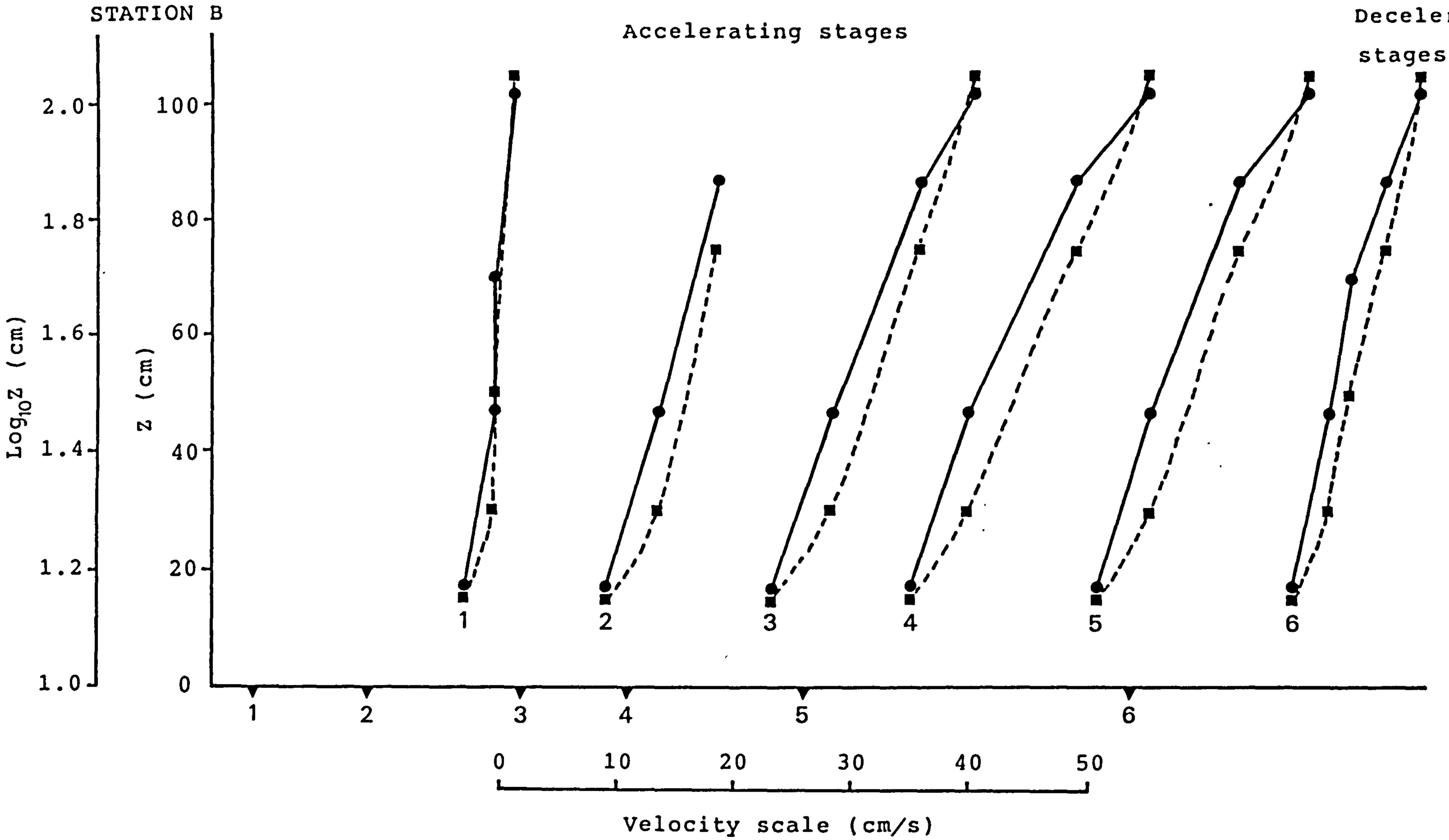

Figure 4.17. Linear (– – – – –) and logarithmic (————) velocity profiles at station B, on August 16, 1986, during flood tide.

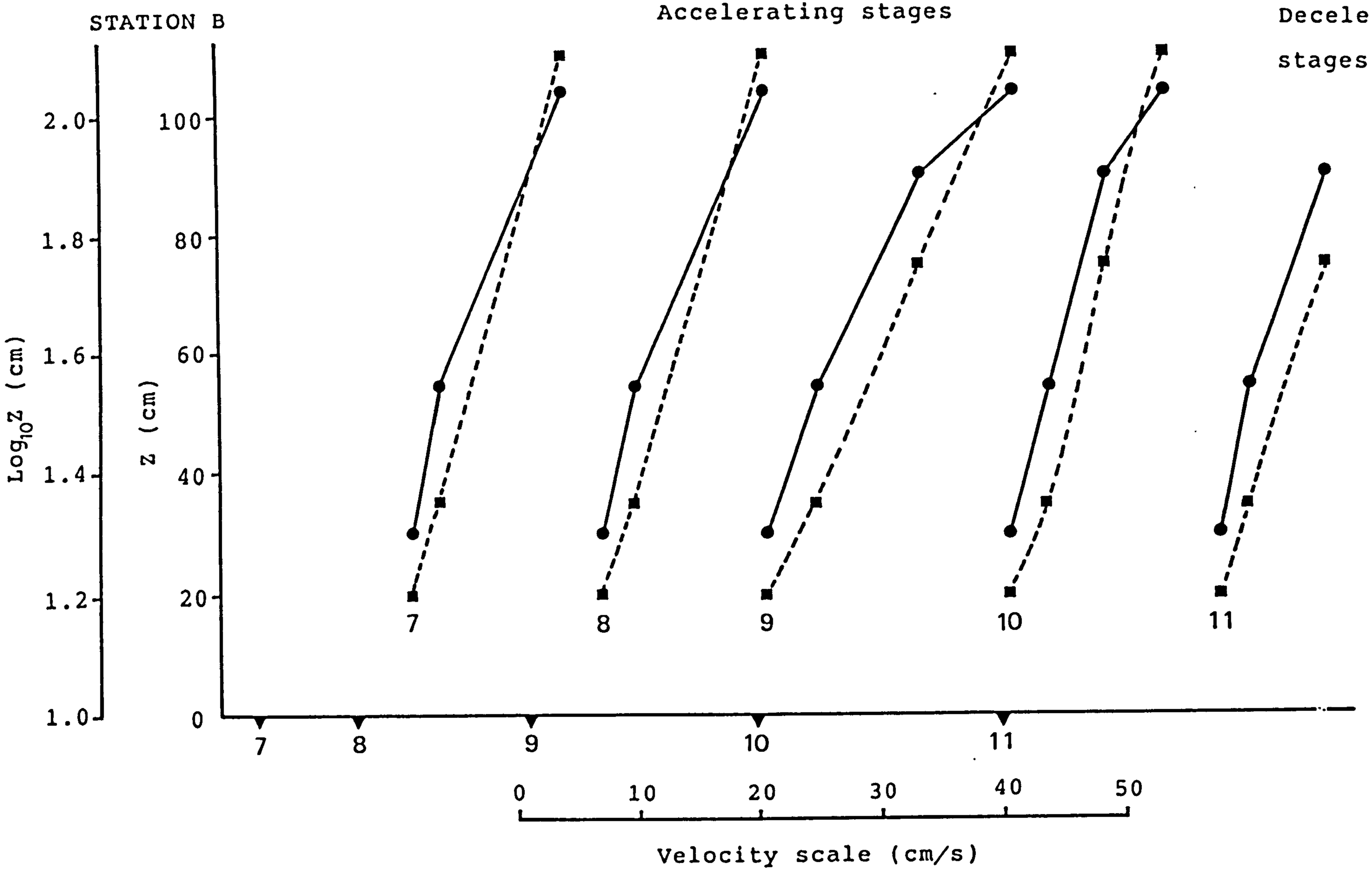

Figure 4.18. Linear (------) and logarithmic (————) velocity profiles at station B, on August 16, 1986, during ebb tide.

STATION A

Profile number	Correlation coefficient, R^2	
	Logarithmic model	Linear model
1	0.996	0.948
2	0.878	0.645
3	0.998	0.934
4	0.918	0.706
5	0.971	0.987
6	0.899	0.997
7	0.867	0.976
8	0·362	0·194
9	0.989	0.965
10	0.996	0.974

Table 4.1. The estimated values of correlation coefficients (R^2) of velocity profiles shown in Figure 4.15 and 4.16 fitted to logarithmic and linear models.

STATION B

Profile number	Correlation coefficient, R^2	
	Logarithmic model	Linear model
1	0.845	0.720
2	0.997	0.936
3	0.984	0.988
4	0.976	0.991
5	0.964	0.992
6	0.962	0.988
7	0.603	0.725
8	0.419	0.538
9	0.945	0.995
10	0.963	0.995
11	0.984	0.998

Table 4.2. The estimated values of correlation coefficients (R^2) of velocity profiles shown in Figure 4.17 and 4.18 fitted to logarithmic and linear models.

tides. The deviation from logarithmic profiles occurred at the top of the profiles. In many cases, the velocity profiles fit rather better to linear profiles instead of logarithmic as shown by high values of R^2 (Tables 4.1 and 4.2). The deviation from a linear model occurred at the bottom of the profiles, since near the bed the velocity profiles more likely to be logarithmic rather than linear.

The velocity profiles measured during CTD measurements in the main channel provided an opportunity for the study of velocity profiles for the whole water column. Two stations near the mouth of the estuary were chosen, and z(cm) vs. flow velocity (cm/s) and log z(cm) vs. flow velocity plotted for each station are shown in Figures 4.19 to 4.22. In most cases, velocity profiles were found to deviate from a logarithmic model, although in some cases they were found to be more or less logarithmic. Since only a single current meter was used for the profiling, the time lapses between consecutive measurements probably contributed to the deviation. As can be seen, deviation from the straight log line is higher near the surface layer. Generally, the velocity at the surface is slightly slower than velocity at a certain depth below the surface. Most of the profiles, however, are composed of two sections, the downward curved lower section and the upward curved upper section. This type of profile can be seen clearly during the neap tide at Station 2 (Figure 4.22) compared to the spring tide at station 1 (Figure 4.20). The possible effect of bedforms on these profiles, however,

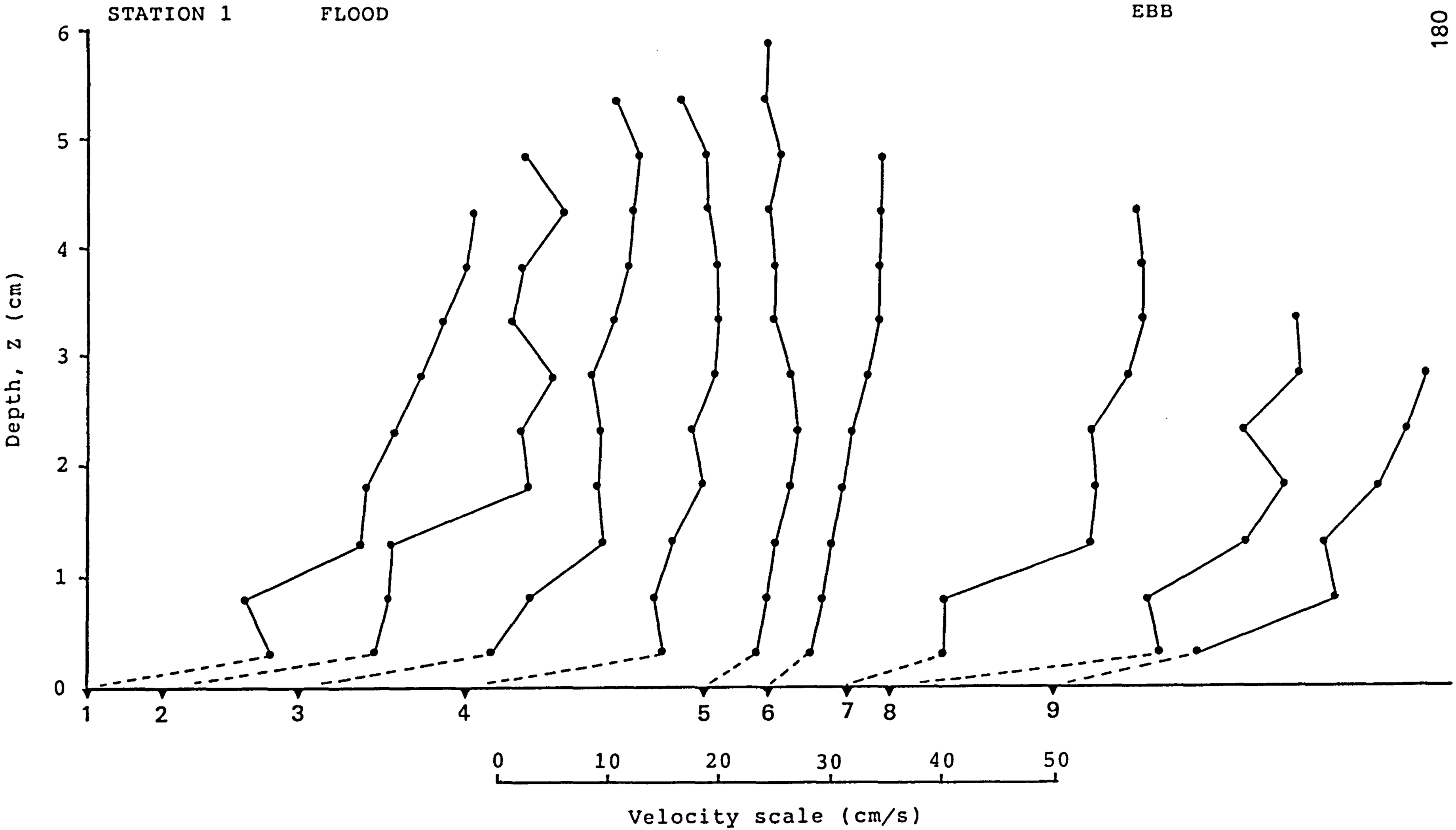

Figure 4.19. Typical velocity profiles for flood and ebb tides at Station 1, on June 24, 1986.

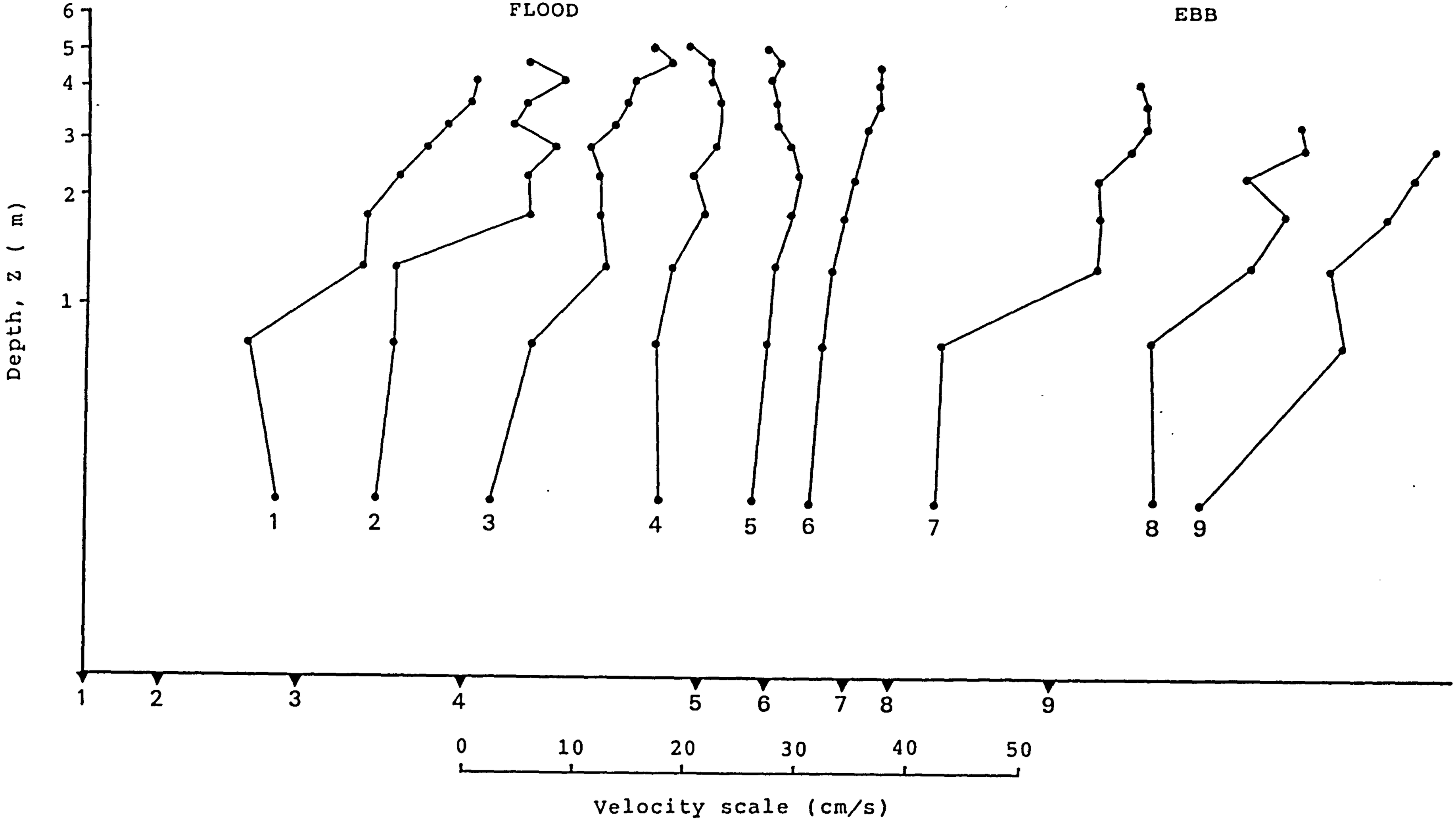

Figure 4.20. Typical logarithmic velocity profiles for flood and ebb tides at Station 1, on June 24, 1986.

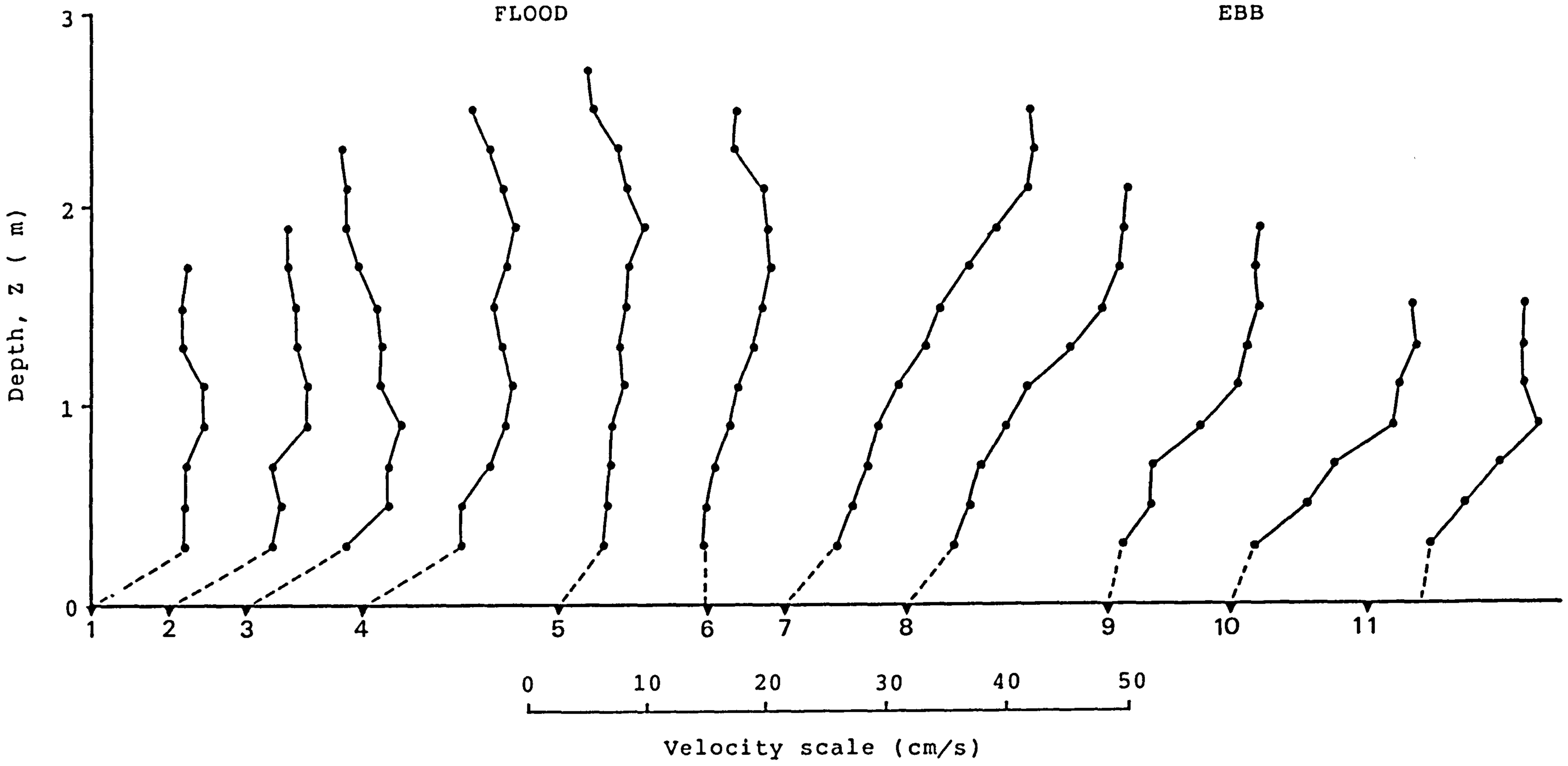

Figure 4.21. Typical velocity profiles for flood and ebb tides at Station 2, on May 16, 1986.

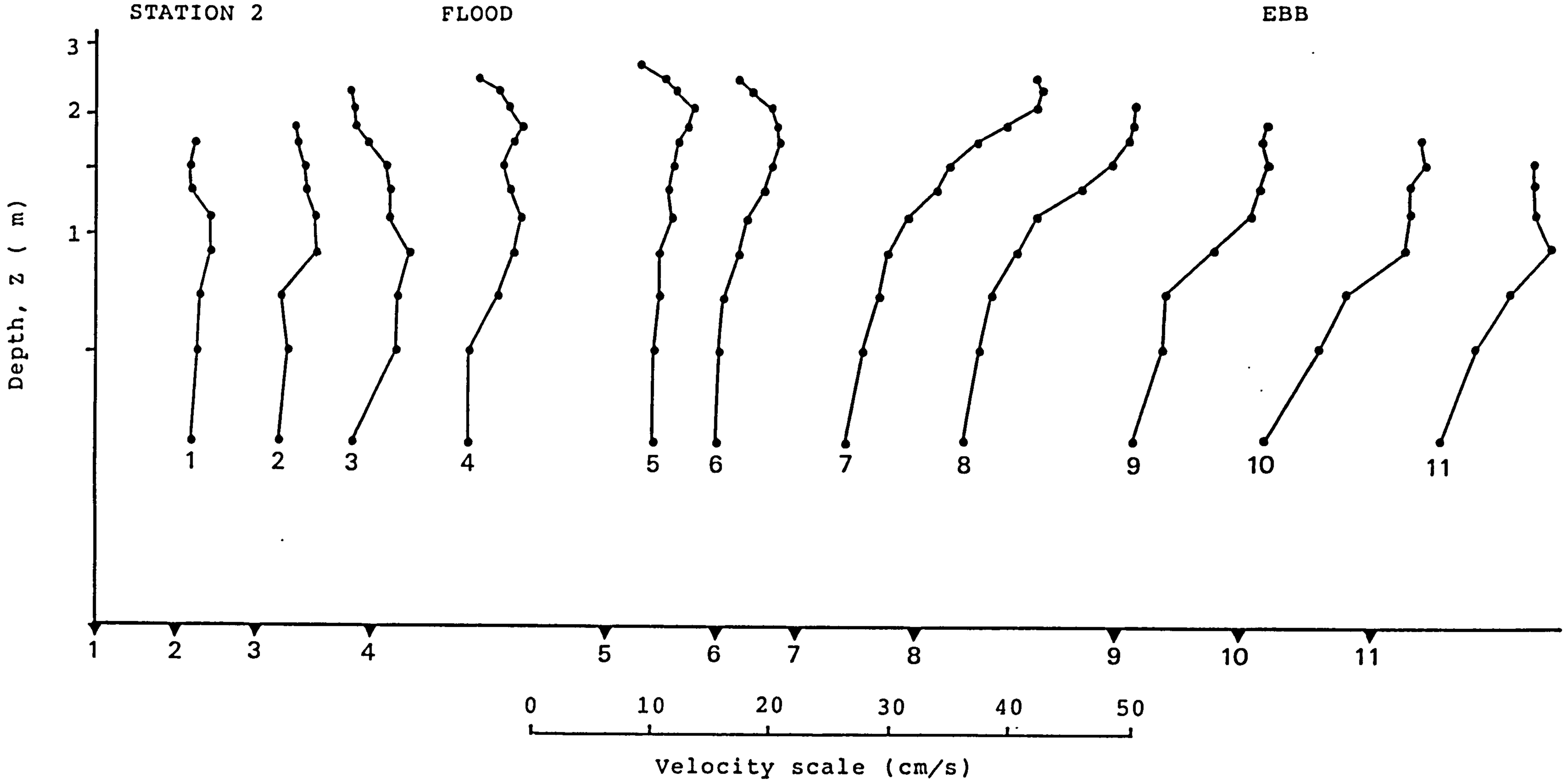

Figure 4.22. Typical logarithmic velocity profiles for flood and ebb tides at Station 1, on May 16, 1986.

could not be determined since the nature of bedforms was not studied during the CTD measurements.

As shown in Figures 4.20 and 4.22, the upward curvature in the upper section of the flow was most noticeable during the flood stages, while downward curvature was most noticeable during the ebb stages. The break in the slope of the velocity profiles which persistently occurred at about 50 to 100 cm above the bed is probably due to flow statification as shown in Figure 3.17B. The positions of the break (Figure 4.22) were seen to coincide with the position of the halocline (Figure 3.17B). Consequently, it is difficult to obtain values of roughness lengths and of bed stresses that adequately represent the stress operating on the bed.

The effect of velocity profile curvature on the estimated values of shear velocity and roughness length can be reduced if only the velocity data in the water column 35 cm above the bed is analysed. This means that only the two bottom current meters were considered. For the purposes of comparisons, two typical data sets from two tidal cycles were chosen; the estimated values of u_* and z_o are shown in Figures 4.23 and 4.24. These results indicate that the variation of u_* is consistent with velocity recorded by any of the current meters, probably the result of the lower part of the flow being less sensitive to any departure from logarithmic profiles. As shown in Figures 4.23 and 4.24

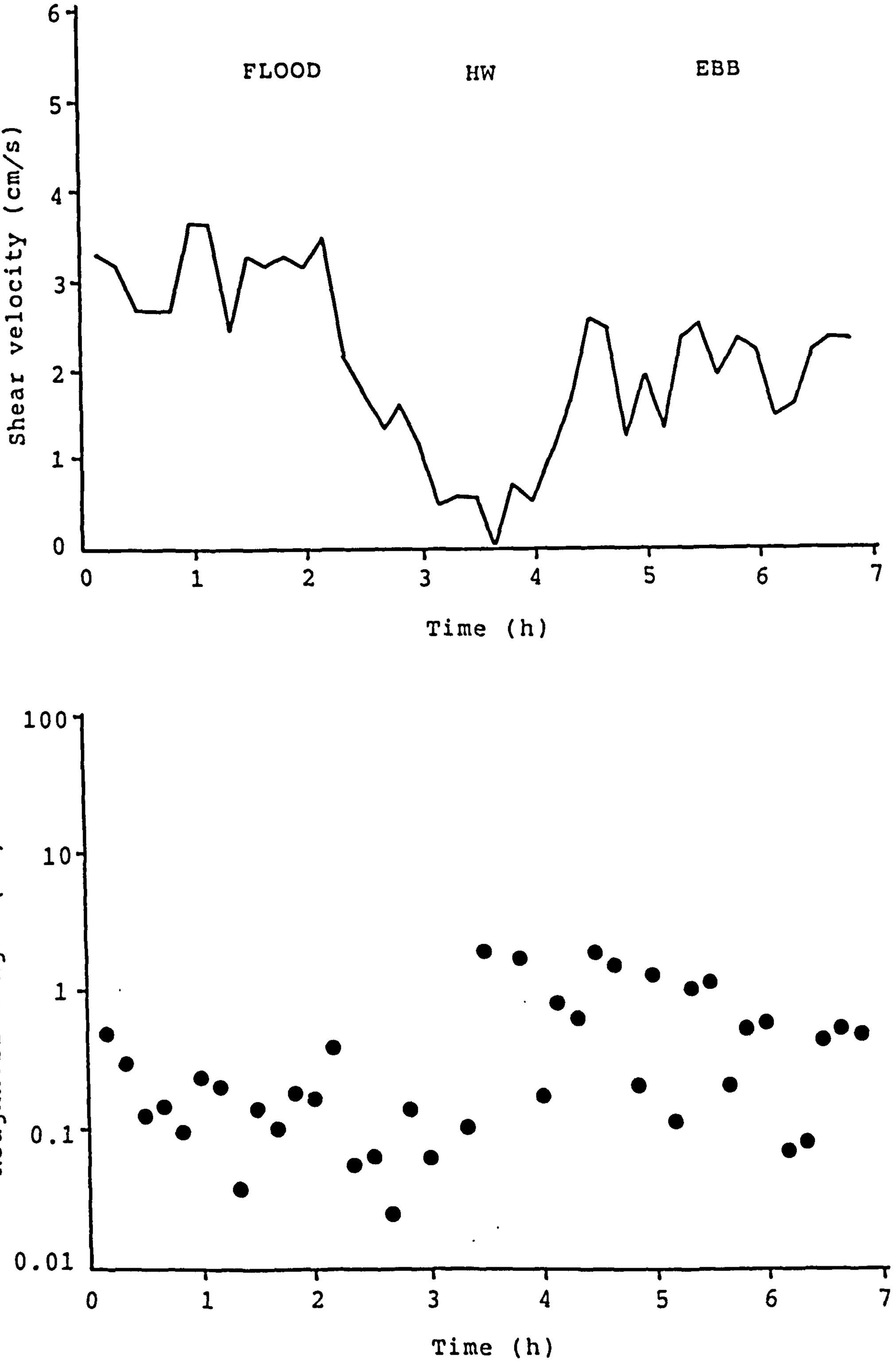

Figure 4.23. Variation of shear velocity (U_*) and roughness length (Z_o) during a tidal cycle on May 8, 1987, using the lowest two current meters data sets.

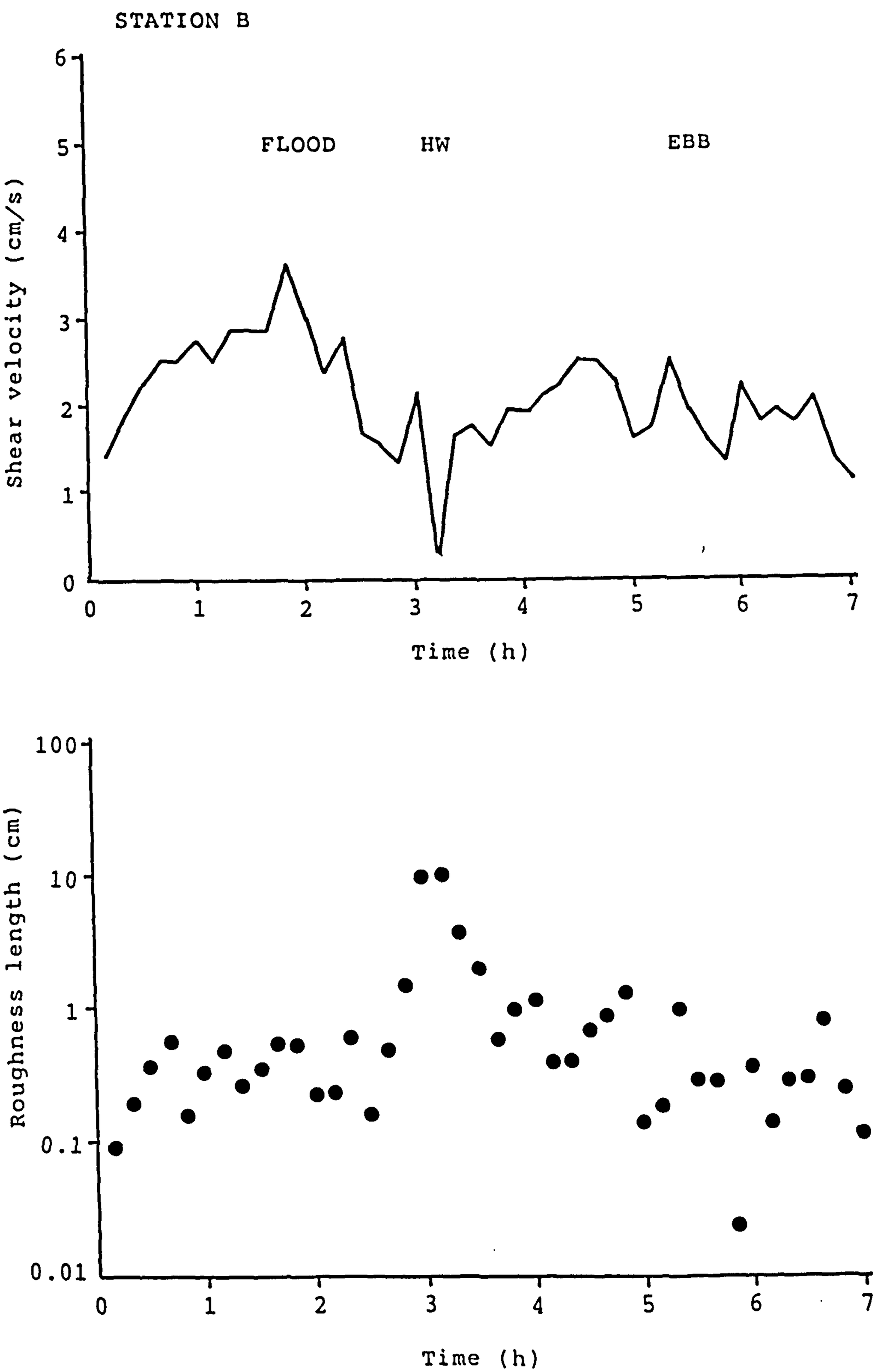

Figure 4.24. Variation of shear velocity (U_*) and roughness length (Z_o) during a tidal cycle on August 16, 1986, using the lowest two current meters data sets.

the variations of z_o during the tidal cycle are smaller than the variation of z_o measured using four or five data sets.

Compared to Figures 4.4 and 4.6 where u_* and z_o were calculated from four or five data sets and from the same tidal cycles, the apparently anomalously high and low values of u_* and z_o have dissapeared. The values of u_* and z_o calculated from the lowest two current meters are most likely to represent the friction drag on the boundary in the immediate vicinity of the rig (Dyer,1970). Heathershaw and Langhorne (1988) suggested that the consistent downward curvature of the velocity profiles may be attributed to the presence of form drag by the irregular topography upstream of the measurement position. The curvature of the velocity profiles may also be caused by error in the measurement of the heights of the current meters above the bed. If the height datum for the current meters is incorrectly set, the velocity profiles may be curved upwards or downwards depending on whether the datum is above or below the mean level of the bed. The movement of bedforms and the erosion of sand at the base of the rig were the main contributing factors to error in the measurement of the heights of the current meters above the bed.

The effects of height displacement on the curvature of velocity profiles and consequently on the values of u_* and z_o is shown in Figures 4.25 and 4.26 and Table 4.3 . The heights of the current meters were displaced up and down

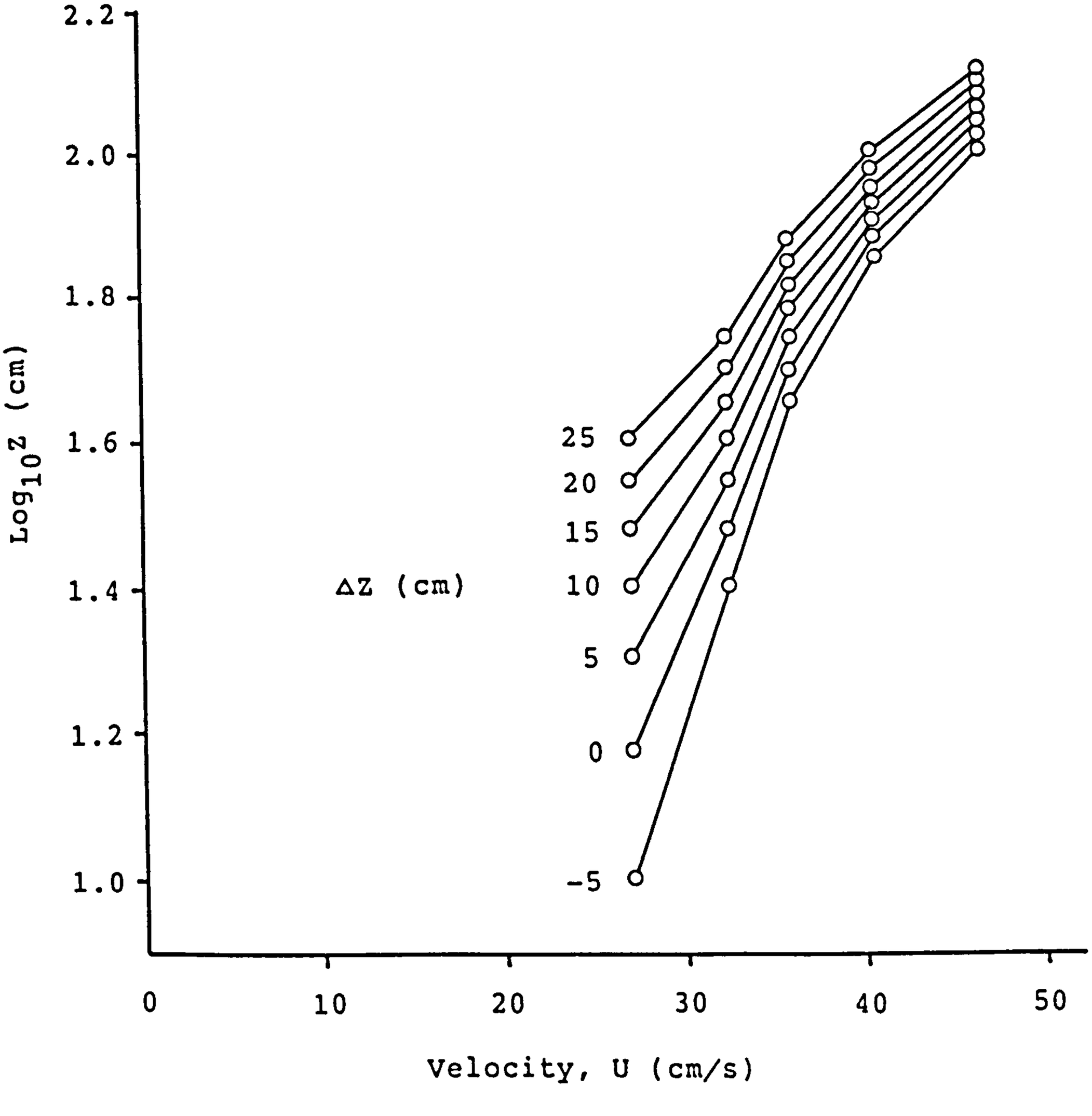

Figure 4.25. Changes in velocity profile shape due to displacement ΔZ. Variation of correlation coefficient with displacement is shown in Table 4.3.

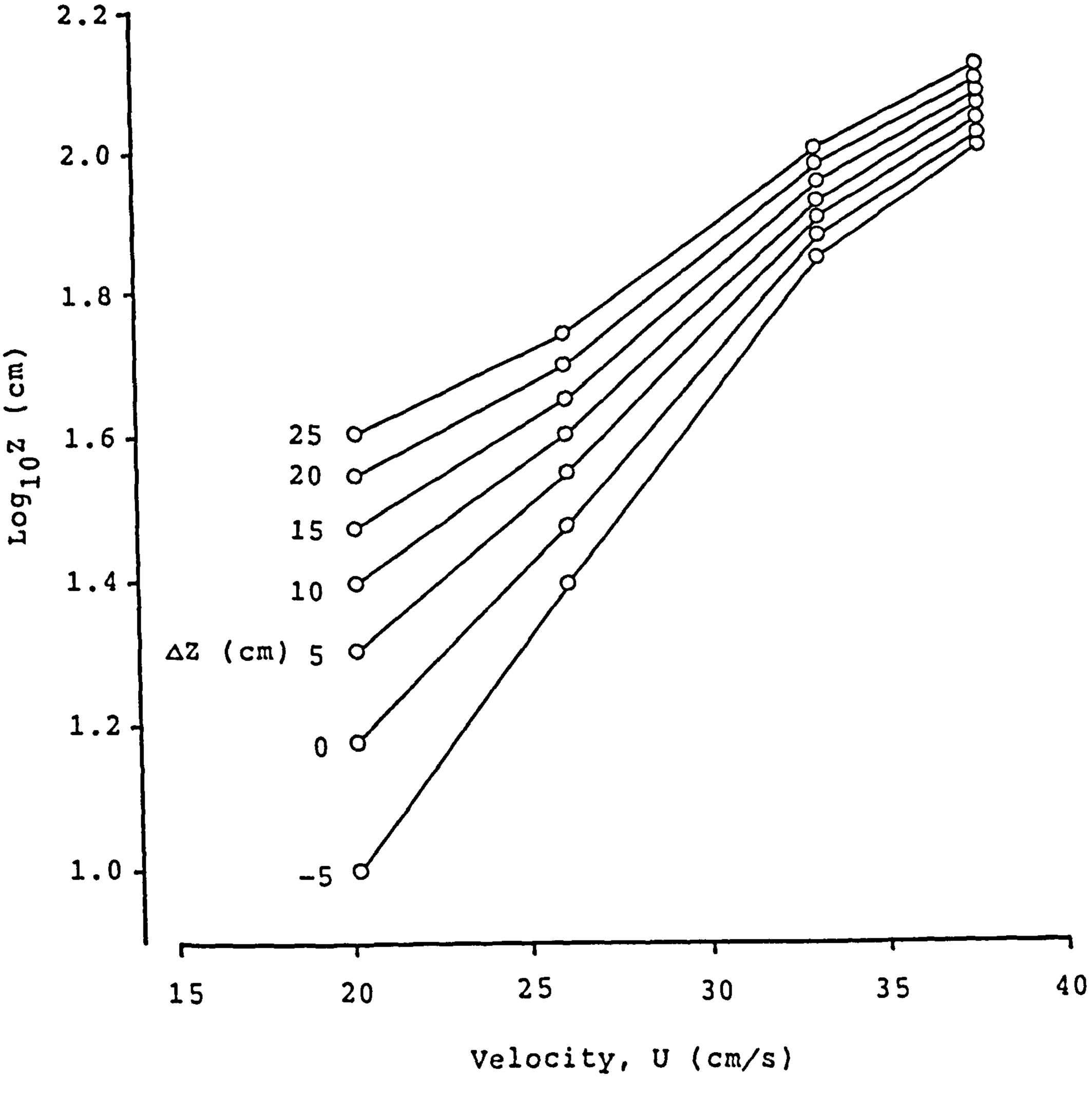

Figure 4.26. Changes in velocity profile shape due to displacement ΔZ. Variation of correlation coefficient with displacement is shown in Table 4.3.

STATION B

	Z (cm)	R^2	U (cm/s)	Z (cm)	U (cm/s)
	-5	0.973	2.78	0.51	32.1
	0	0.984	3.26	1.14	31.1
	5	0.989	3.70	2.02	30.0
Profile 3	10	0.992	4.12	3.14	28.8
	15	0.994	4.53	4.48	27.6
	20	0.995	4.92	6.05	26.3
	25	0.996	5.31	7.81	25.0
	-5	0.946	1.72	0.55	20.7
	0	0.962	2.01	1.20	20.4
	5	0.972	2.28	2.09	19.9
Profile 6	10	0.978	2.54	3.21	19.4
	15	0.982	2.80	4.57	18.9
	20	0.985	3.03	6.13	18.3
	25	0.987	3.27	7.89	17.6

Table 4.3. Values of R^2, U , Z , and U for velocity profiles shown in Figure 4.17 for each displacement height, Z from -5 to 25 cm. The mean velocities were calculated assumming depth=1.04 m for profile 3 and depth=1.85 m for profile 6.

from -5 to 25 cm. These results indicate that increases in displacement produces higher values of u_*, z_o and R^2. The best fit as indicated by the highest value of are obtained when the displacement is about 20 to 25 cm or higher, but the corresponding value of z_o is unrealistically large compared to the average value of z_o for this station (z_o=1.2 cm). If the displacement is increased to a very high value, it seems very likely that the value of R^2 will approach unity, i.e. all the points will lie in a straight line. Heathershaw and Langhorne (1988), however, showed that the value of R^2 has a maximum value at a certain displacement of between 15 to 22 cm. These results would in turn suggest that the values of u_* and z_o estimated from velocity profiles are dependent on the choice of height datum for the current meters and the good fit as indicated by high R^2 values does not mean that the velocity profiles are correct.

These problems highlight the main shortcoming of the velocity profile method in the calculation of shear velocity and sediment transport rate. An alternative is to calculate the mean velocity from the estimated values of shear velocity and roughness length using the equation

$$U = 2.5\, u_* \ln\left(\frac{d}{2.718\, z_o}\right) \qquad 4.9$$

where z_o is the roughness length and u_* calculated from

velocity profiles. In cases when only one current meter was in working order, the mean velocity could be calculated from a single velocity value u_z using equations

$$u_z = \frac{u_*}{k} \ln\left(\frac{z}{z_o}\right) \qquad 4.10$$

and

$$U = 2.5\, u_* \ln\left(\frac{d}{2.718\, \bar{z}_o}\right) \qquad 4.11$$

where $\bar{z}_o$ is the average value of roughness averaged over a spring-neap cycle for each station (Figures 4.11 to 4.14). For comparison, the same tidal cycle shown in Figures 4.3 to 4.10 were chosen. As shown in Figures 4.27 and 4.28 the mean velocities calculated from both equations are almost identical. We may conclude that the use of a single current meter value in the calculation of the mean velocity seems to be adequate in cases when only single current meter data were available. The choice of z_o =0.54 cm for station A, z_o=1.27 cm for station B, z_o=0.72 cm for station C, and z_o=0.59 cm for station D have proved to be adequate.

4.4 Conclusion

The above results show that the near bed logarithmic profiles in the Dwyryd estuary can be applied only in the region about 35 cm above the bed. Above this level,

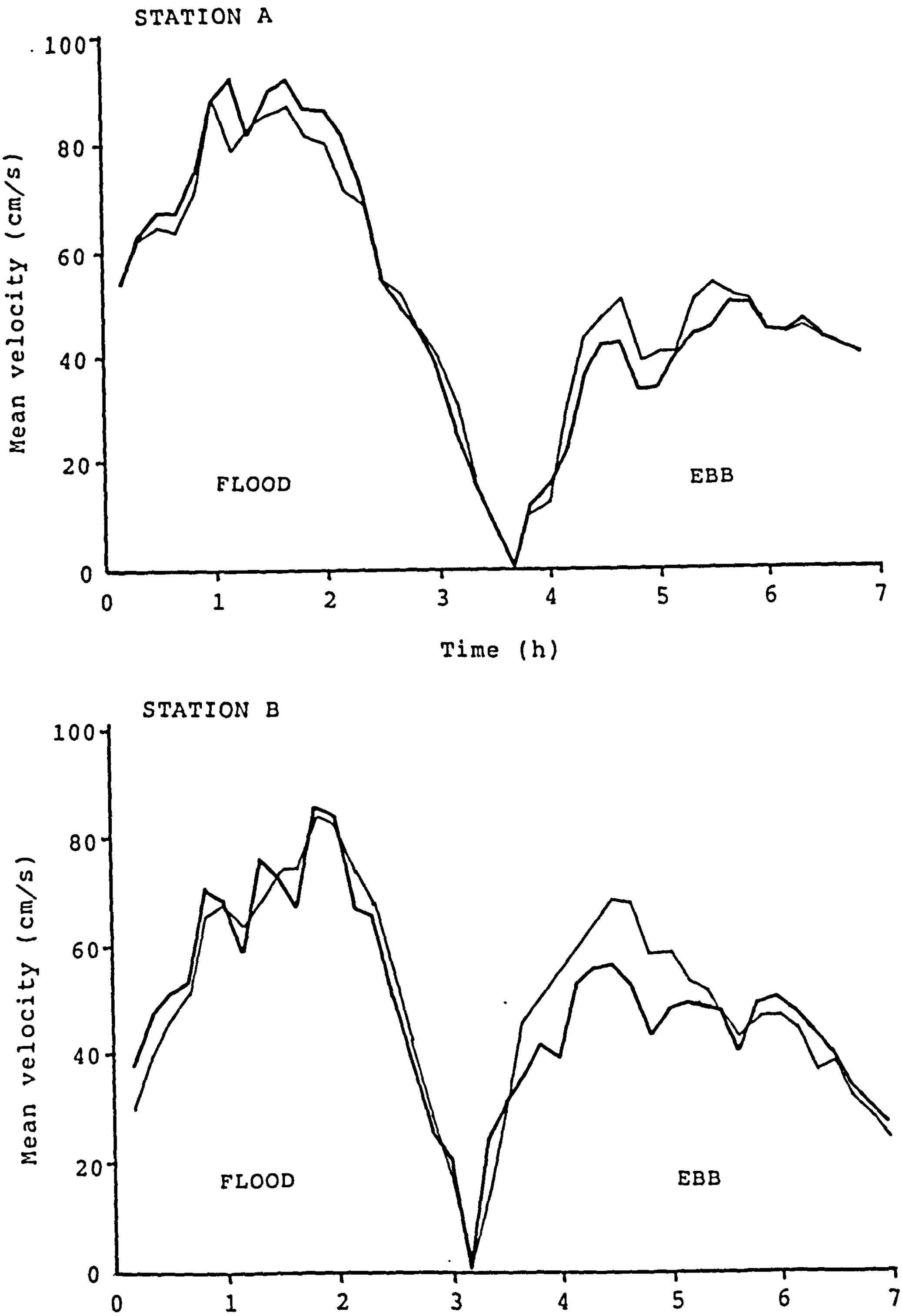

Figure 4.27. Variation of mean velocity at stations A and B calculated from velocity profiles (———) and mean velocity calculated from a single current meter data using an average roughness length value (———).

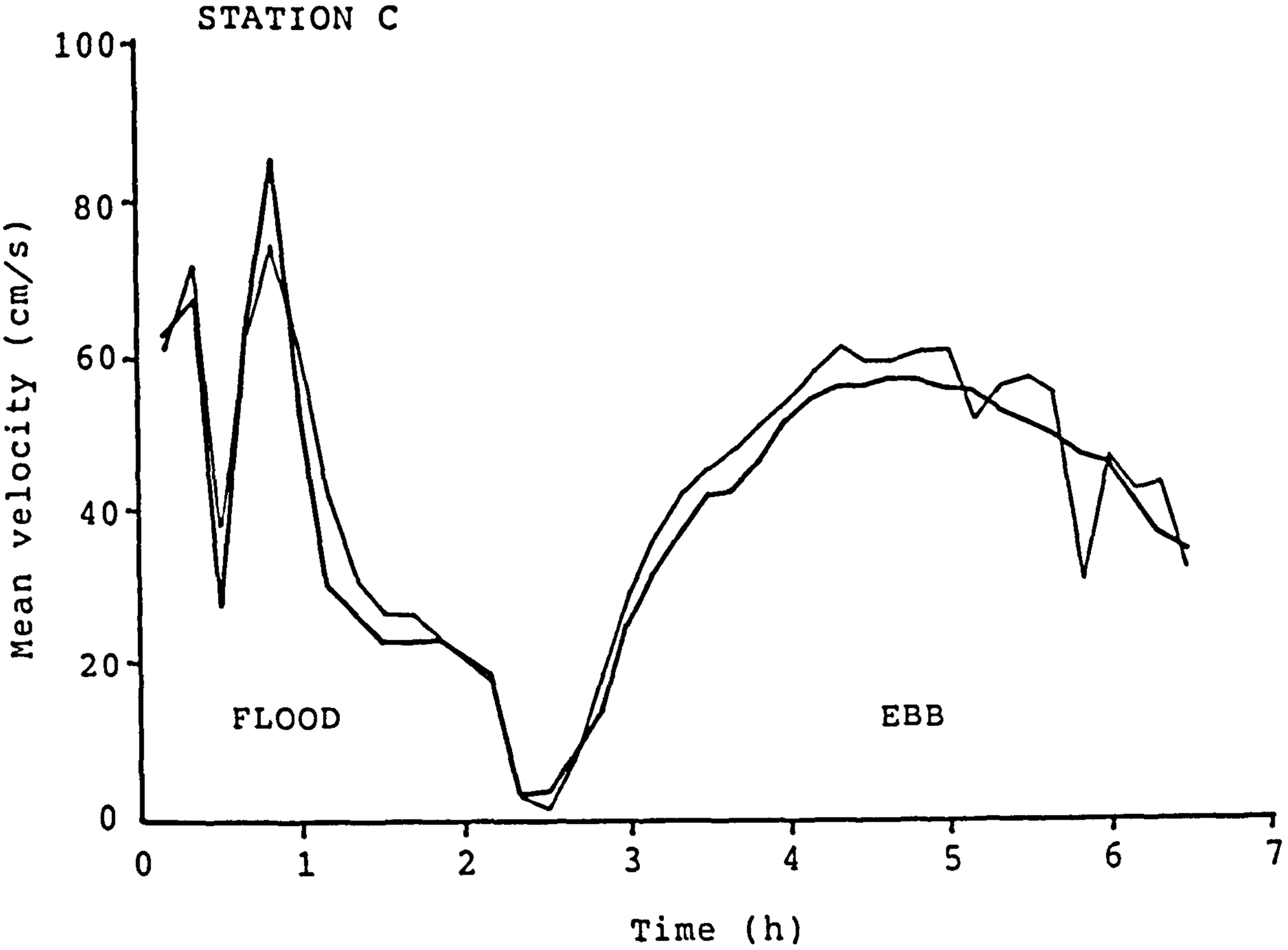

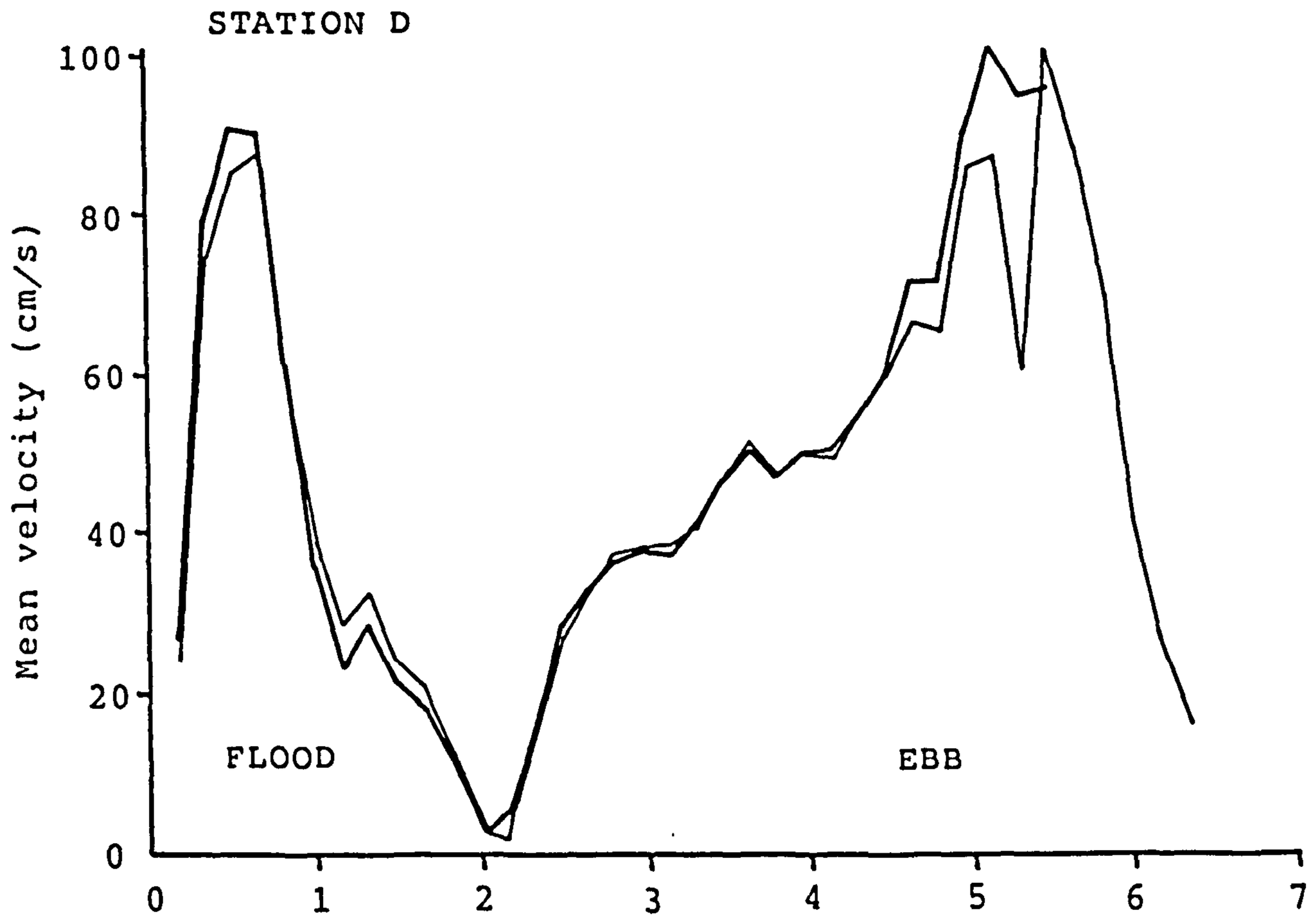

Figure 4.28. Variation of mean velocity at stations A and B calculated from velocity profiles (————) and mean velocity calculated from a single current meter data using an average roughness length value (————).

velocity profiles are found to deviate from logarithmic probably due to flow stratification. This study shows that the high value of correlation coefficient (r^2) should not be regarded as evidence for the existence of logarithmic profiles since high r^2 values also could be obtained by assuming linear velocity profiles. During the flood tide, velocity profiles tend to curve upward, consequently reducing the shear velocity and increasing the value of roughness length. During the ebb, velocity profiles tend to curve downward which is responsible for increase in the value of shear velocity and decrease in the value of roughness length. The effect of velocity profile curvature can be avoided by using data from the lowest two current meters only for the calculation of mean velocity. It has been shown that in cases where data from only one current meter are available, the mean velocity can be calculated by assuming a constant value of roughness length between 0.5 to 1.2 cm. These two methods of calculation of mean velocity have been shown to be equivalent to each other.

FIVE

SEDIMENT TRANSPORTS

5.1 Introduction

The movement of sediment in the estuarine environment is of great interest to both the sedimentologist and the marine engineer because estuaries are one of the most important sedimentary environments of a coastal system which serve to either trap or transfer sediment between the land and the sea. The evolution of an estuary depends essentially on the long-term time averaged sediment supply from inland or coast, and the direction and magnitude of the long-term time averaged sediment transport. Estuarine morphology is to a large extent determined by the residual sediment transport pattern. However, the inverse statement is also true (Dronkers, 1986). Sediment transport is a particularly difficult process to measure. Knowledge of sediment transport rates and patterns throughout the estuary can be very useful in the overall understanding of the estuary system and its relationship to the adjacent shoreface. A better understanding of sediment transport is also needed to enhance interpretation of sediment deposits.

The transport of sediment in estuaries can be as

suspended-load, i.e. sediment held in suspension above the bed by the turbulence of the fluid, and/or bed-load, i.e. grains that bounce or roll along the bed continuously or intermittently (depending on the grain size of the sediment and the flow strength). However,the distinction between suspended load and bed load is not as apparent in nature (Dyer,1986). Suspended load moves approximately as fast as the mean velocity of the tidal current, whereas bed load moves at a slower velocity than that of the mean flow since the velocity closer to the bed is slower than the mean velocity. Bed-load transport is limited chiefly to a relatively thin zone immediately above the bed and can occur in laminar as well as turbulent fluids (Bagnold, 1955,1966). Einstein (1950) suggested that the bed-load is two grain diameters thick but most other researchers prefer a somewhat larger thickness. Suspended motion involves grains moving rather higher up from the bed where the excess weight of the grain is supported wholly by a random succession of upward impulses imparted by eddy currents of fluid turbulence moving upwards relative to bed (Bagnold, 1977).

There is a lack of suitable and reliable devices for the measurement of transport rates in the field, although it is now possible to get some measure of bed load transport directly by means of sediment traps, and by studying the movement of bedforms and tracers (Ritter, 1972; Finley, 1978; Heathershaw, 1981; Langhorne, 1981; Lees, 1983;

Pickrill, 1986). A sediment trap, which has a rectangular orifice and perforated container mounted on a sledge frame, usually gives an unreliable estimate of bed-load transport rate due to local disturbance,uncertainty in the relative levels of orifice and bed, and the likelihood of dredging during the course of recovery. Several types of suspended sediment sampler collect suspended sediment in a container by natural settlement, but the most effective method entails the pumping and filtering out of the sediment. Interpretation as a rate of transport, however, requires the simultaneous recording of current velocity.

In areas where there are large bedforms present it might be possible to estimate the rate of sediment transport by periodic surveys along a line of bedform movement (Ludwick, 1972; Kelland & Bailey, 1975; Langhorne, 1982). In inter-tidal environments sufficiently detailed surveys can easily be carried out during low tide to reveal a consistent trend of bedform migration. Such a survey requires a high precision in position fixing and sufficiently detailed mapping to reveal a consistent trend.

Sediment grains may be labelled by attachment of certain radioactive tracers (Smith and Parson, 1965; Heathershaw and Carr, 1977). The movement and distribution of the tracer can be surveyed at intervals by means of a Geiger counter. Generally, the result will be of qualitative value only , but in certain circumstances it is possible to examine distribution of the tracer with respect

to depth and hence to make a quantitative interpretation, at least over a limited area. Many difficulties arise, however, due to wide differences in the total range of movement during a tidal cycle, between suspended-load transport and bed-load transport. Suspended-load will tend to become widely dispersed while the bed-load remains relatively concentrated, with resulting difficulty in designing the scheme for detection.

An alternative means of estimating sediment transport rates is to use the physical relationship between material transport and flow strength. There has been a remarkable progress in the study of boundary layers and sediment transport in recent years (Nowell,1983) which provides a good base for sediment transport estimations. Up to now many sediment transport formulae have been proposed. Faced with such a large number of transport rate formulae the most sensible way is to choose one or more which appear to give good results for conditions similar to those of interest (Sleath, 1984). These formulae try to correlate flow velocity with sediment transport but natural systems such as estuaries are quite variable and application of these formulae has been difficult.

Most of the formulae proposed were in fact completely based on empirical relationships between the rate of sediment transport and flow characteristics of the fluid such as mean velocity or shear velocity. Although some of

the formulae are derived from the basic principles of physics they are basically empirical since all of them involve experimentally determined coefficients . Examples of this are the methods of Einstein (1950) and Bagnold (1956, 1966). Transport rate formulae are probably a function of several parameters, including grain size distribution, flow velocity, water and sediment densities, terminal velocity, viscosity, temperature and surface roughness. Unfortunately, accurate information on these parameters is very difficult to obtain and even more difficult to include in the formulae. In practise, however, only a few of these parameters are considered while the rest are combined as a constant to be determined experimentally.

The basic framework in which to examine sediment transport in the Dwyryd estuary is provided by tidal currents. Data on tidal currents obtained from a current meter rig are used in this study to show that sediment movement is primarily related to tidal conditions. The degrees of variability of the transport rate during flood and ebb stages and also during spring and neap tides and the net movement of sediment at individual stations were determined but the limited number of stations precludes detailed discussion of the movement of sediment past cross-sections, and of overall sediment budgets.

The flow conditions at which sediment movement begins is of critical importance to the estimation of sediment

transport by tidal currents. In view of this, a short review of past studies carried out on this subject will be given.

5.2 Entrainment of Sediment by Unidirectional Flow

Basically, a stationary grain will begin to move when the shear stress at the sea bed exceeds a critical or threshold value. The sediment grain can be entrained either directly by the water or by being struck by another moving grain. The threshold or critical flow stress is dependent on the relative density of the grains and their diameter. Competency curves,defining the threshold of grain motion for variations in stream power and grain size have been suggested by several workers (Gilbert,1914; Shields, 1936; Hjulstrom, 1935, 1955; Sundborg, 1956; Bagnold, 1963 ; and Postma, 1967). All of them believed that the shear stress on the bed is the most important parameter in initiating grain motion and in sustaining the movement of coarse material along the bed and of suspended material in the flow. As regards the bed load, deposition occurs as soon as the flow causes the shear stress at the bed to fall below the critical value because friction at the bed and the viscosity of the water combine to overcome any inertia that the grains might have. For suspension, grains require greater critical shear stresses to transport grains above 200 micron diameter in suspension than to

support them in the bed load. Smaller grains lift directly into suspension when the value of the critical stress is reached. In general, for large grain sizes, the threshold stress seems to be linearly proportional to grain diameter.

All theoretical entrainment formulae start from a consideration of the balance of forces on a grain of sediment which is just at the limit of equilibrium. The forces on the grain include drag, gravity and lift forces and interparticle forces (cohesion). The drag (fluid) forces tend to drag the grain from the bed, whereas gravity tends to pull it back. The lift force, however, varies in a complicated way with flow and bed conditions and connot be straightforwardly predicted. Einstein (1950) indicates the importance of lift forces in the movement of sediment, whereas Helley (1969) and Inokuchi & Takayama (1973) explicitly include lift in their analyses of threshold conditions. Interparticle forces may be due to electrostatic forces which are known to be relatively more important for small grains (Iversen et al., 1976)

In practice, entraiment conditions are estimated using empirical correlations based on laboratory experiments. Krenter (1921), who was one of the earliest workers to investigate sediment transport by a fluid, suggested that the critical force required to initiate sediment movement is approximately 20% greater than that which is required to maintain this movement. A major breakthrough in threshold determination was provided by the

Shields diagram (Shields, 1936). Based on physical arguments, it may be expected that the begining of a grain's motion is dependent upon the diameter of the grain D, its specific weight $g(\rho_s - \rho)$, the bed shear stress and the fluid viscosity ν and fluid density ρ. Thus

$$f(D, g(\rho_s - \rho), \tau_o, \nu, \rho) = 0 \qquad 5.1$$

The parameters in this equation can be rearranged into non-dimensional groups for the purpose of plotting experimental results. It follows that

$$\Theta = \frac{\tau_c}{(\rho_s - \rho) g D} = f_1\left(\frac{u_* D}{\nu}\right) \qquad 5.2$$

where τ_c is the critical or threshold value of for which grains just begin to move. The term on the left hand side of this equation is known as the Shield's entraiment function, Θ .It may be thought of as representing the relative magnitudes of the inertial force and gravitational force acting on the grain. The term on the right hand side is the dimensionless grain Reynolds number, generally denoted by R_{e_3}. The threshold curve based on the relationship of equation 5.2 is shown in Figure 5.1. The shape of the curve which Shields originally proposed was

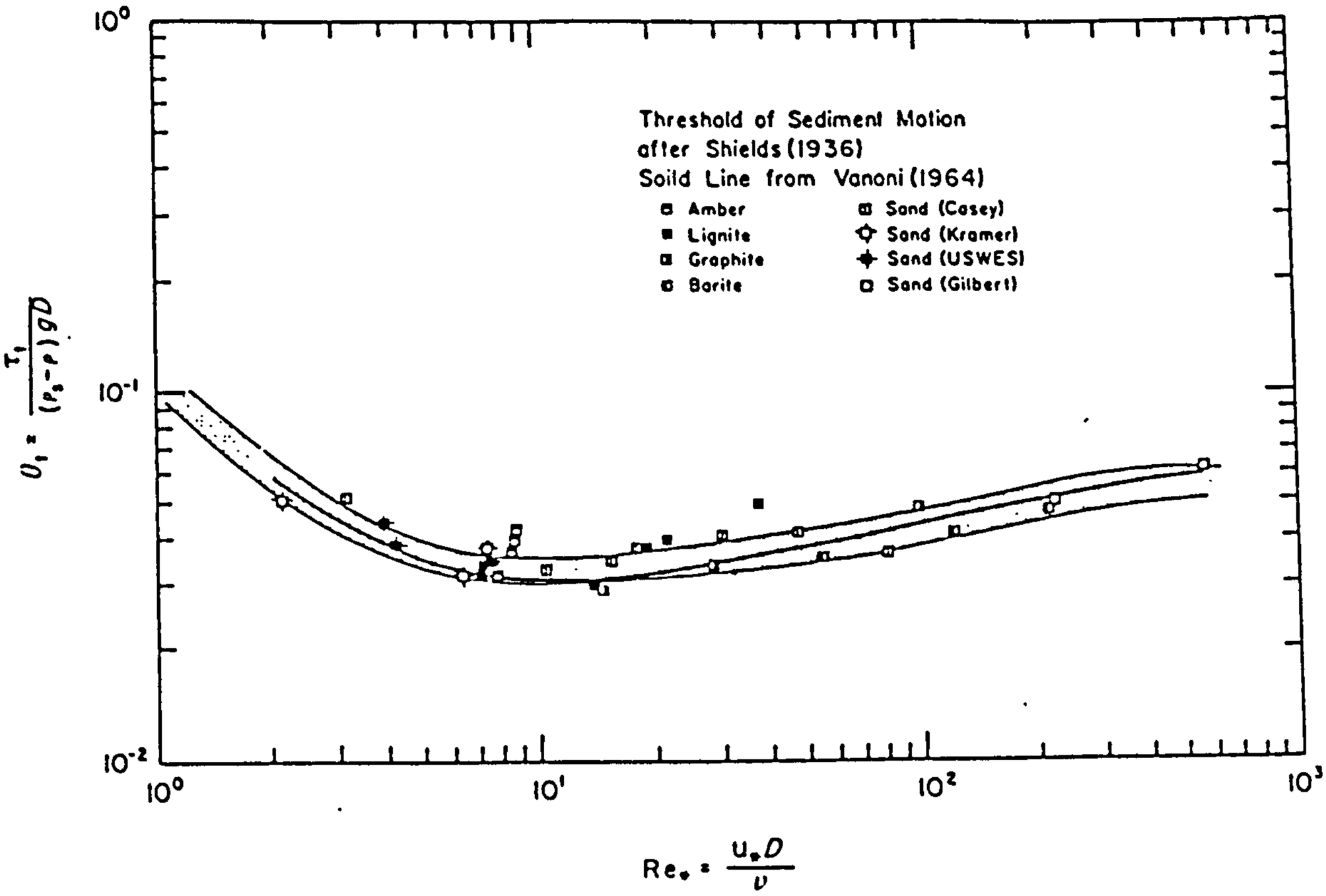

Fig. 5.1 The original Shields threshold curve of the grain Reynolds number Re_* versus the Shields threshold criterion θ_t. The heavy solid line was added by later investigators.
(after Miller et al. 1977).

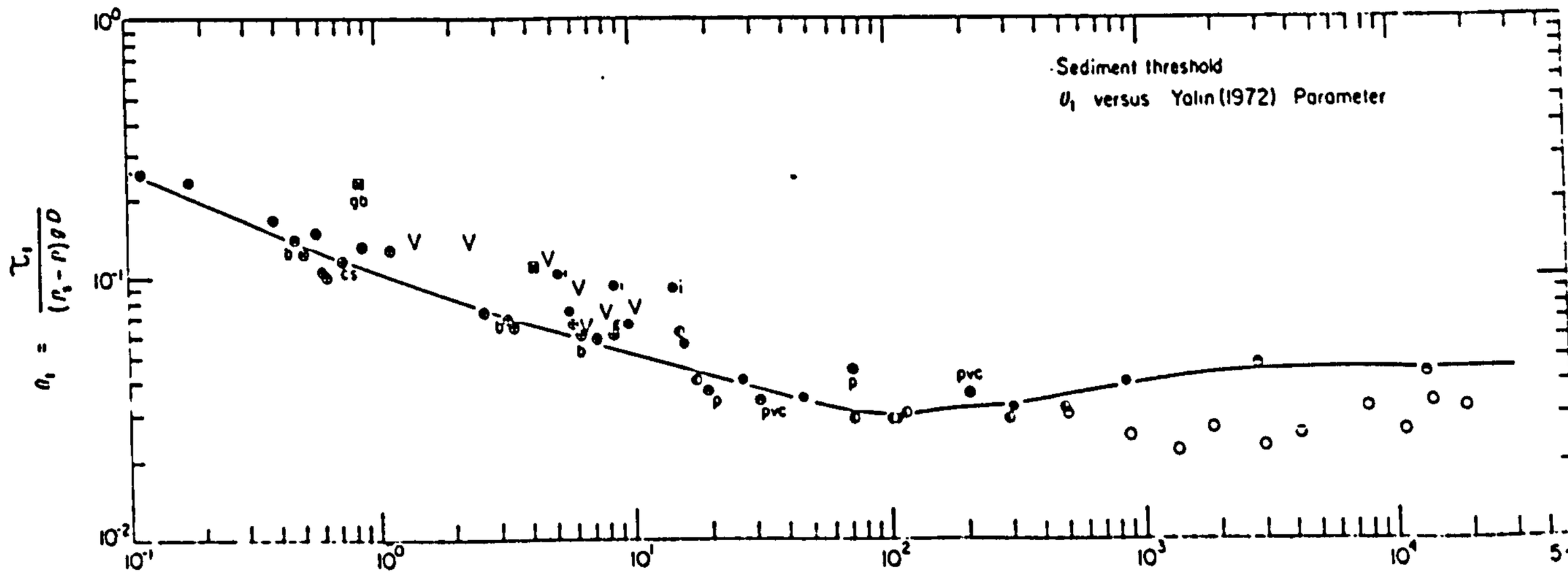

$$\sqrt{\Xi} = \frac{Re_*}{\sqrt{\theta_t}} = \left[\frac{(\rho_s - \rho)gD^3}{\rho\nu^2}\right]^{1/2}$$

Fig. 5.2 The Yalin parameter $\sqrt{\Xi}$ versus the Shields threshold criterion θ_t. The solid curve is calculated from the curve given in Fig. 3. See Table I for identification of symbols. [modified from Yalin (1972)] .
(after Miller et al. 1977)

purely speculative at lower values of the Reynolds number (Re_3) because the lowest value of Reynolds number in the data used by Shields was 1.9. Mantz (1977) showed that for Reynolds numbers between 0.03 to 1.0, the experimental results actually follow the equation

$$\frac{\tau_c}{(\rho_s-\rho)gD} = 0.1\left(\frac{u_* D}{\nu}\right)^{-0.3} \qquad 5.3$$

In producing the threshold diagram, Shields assumed that sediment grains were non-cohesive and the flow was assumed to be steady and uniform, with a fully developed turbulent boundary layer, over a flat bed of sediment of grains of single size. It is very unlikely that natural sediments approach such a narrow grain size distribution; nor are the beds generally flat. Furthermore, marine currents are not normally steady and uniform, although it does not appear that they are so variable as to invalidate completely the general predictions that can be made from such curves. Sternberg (1971, 1972) finds a Shields-type criterion to be helpful in marine environments where currents can be regarded as unidirectional.

Yalin (1972) proposed the combination of Θ_t and Re_3 to eliminate u_* from the equation. This allows a more direct determination of the grain diameter from other variables by yielding the Yalin Parameter,

$$\equiv = \frac{Re_g}{\theta_t} = \frac{(\rho_s - \rho) g D^3}{\rho \nu^2} \qquad 5.4$$

Experimentation has revealed the form of both θ_t and Re_g with respect to the grain size for initiation of grain movement. The graph of Yalin (Figure 5.2) is more easily used in application than the curve of Shields (Figure 5.1).

Figure 5.3 shows another widely used entrainment curve proposed by Bagnold (1966). This diagram applies only to quartz-density solids in water, and shows medium and coarse sands are more easily entrained than any other grade. It is also apparent that when $D < 0.170$ mm, suspension of sand grains is likely to occur at the threshold of the movement. Threshold conditions for suspension of sand were postulated by Bagnold (1966). He obtained the criterion for sediment suspension as

$$\theta \geqslant C \frac{\omega^2}{gD} \qquad 5.5$$

where θ is the Shields entraiment function, ω is the fall velocity of a grain diameter of D and C is a constant equal to 0.4. This diagram suggested that material finer than

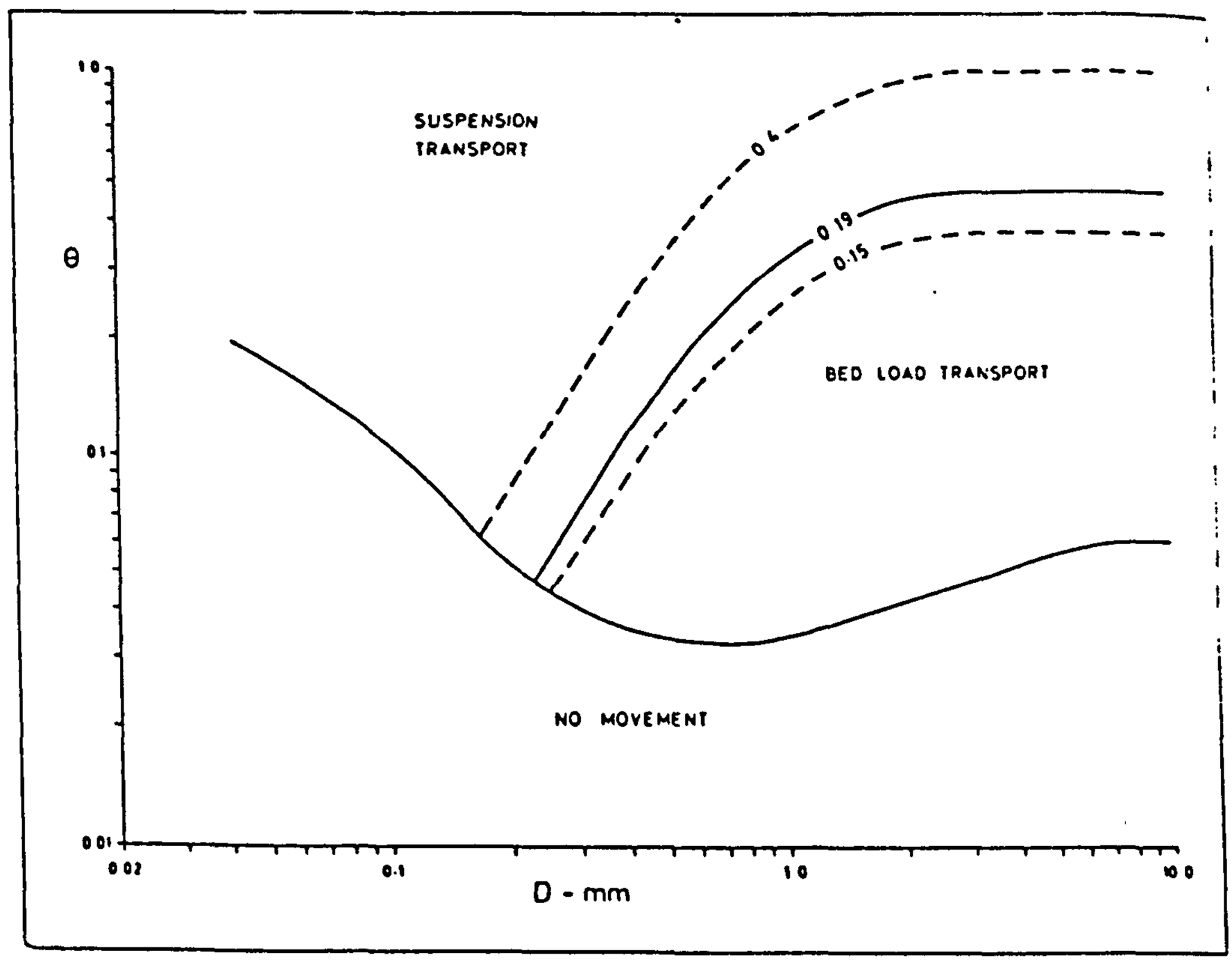

Fig. 5.3 .. Dimensionless shear stress (θ) versus grain diameter (D, in mm) showing revised critical suspension curves (0.4, 0.19, 0.15). These numbers refer to the constant C in eq.2.

(After McCave, 1971)

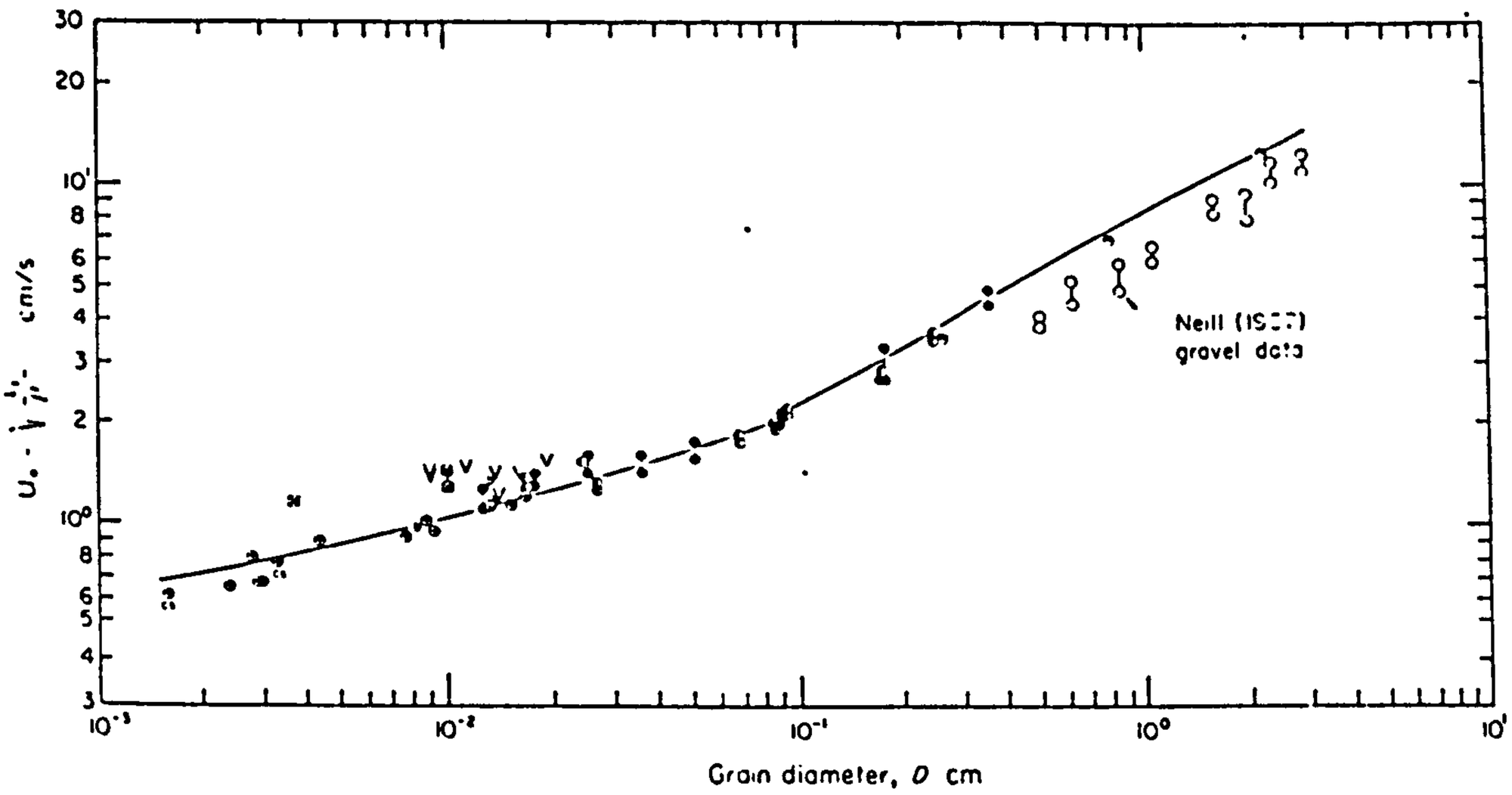

Fig. 5.4 The grain diameter D versus the friction velocity u_* necessary for the threshold of quartz density material ($\rho_s = 2{\cdot}65$ g/cm³) in water at 20° C (ρ 1·0 g/cm³; ν 0·01 cm²/s): [modified from Inman (1949)]. (after Miller et al. 1977)

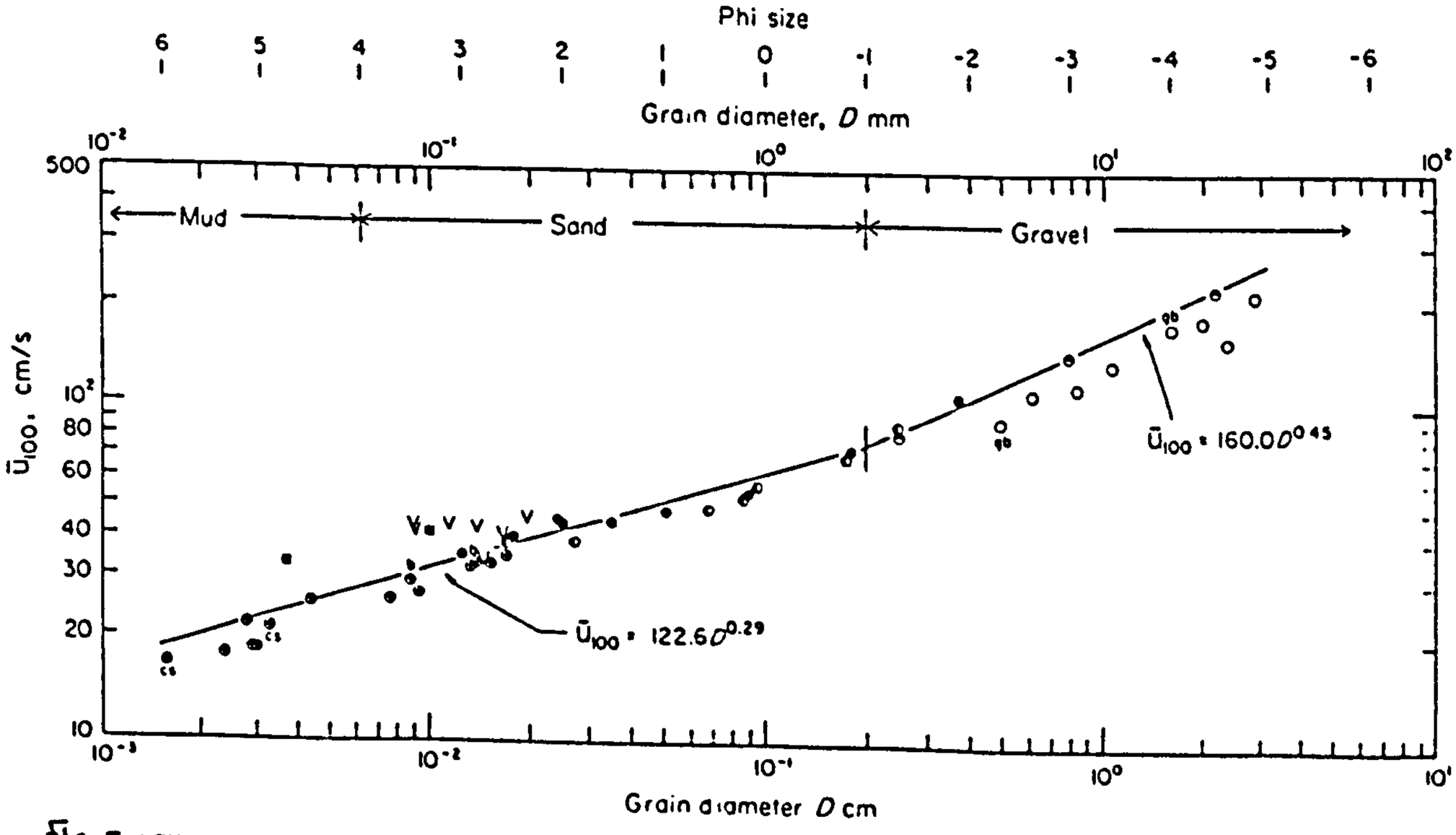

Fig. 5.5 The grain diameter D versus the flow velocity 100 cm above the bed u_{100} necessary for threshold for quartz density material in water of temperature 20° C. (modified from Sundborg 1956)
(after Miller. et al. 1977)

0.230 mm will be largely transported in suspension, and that full suspension may occur for material finer than 0.17 mm. The onset of full suspension can be estimated by assuming that the vertical components of the turbulent velocity fluctuations close to the bed begin to exceed the fall velocity of the grains (Bagnold, 1956). Under natural conditions, it has ben found empirically that if suspension is to occur, the settling velocity, w must be less than 1.25 times the shear velocity, u_* (Leeder, 1982; Dyer, 1986). In other words,

$$w \leq 1.25\, u_* \qquad 5.6$$

Bagnold's criterion has been proved valid by Leeder (1983). An important effect from this criterion is that when the grain diameter is less than 0.15 mm, suspension of sand grains is likely to occur at the threshold of movement.

Since the velocity and grain diameter parameters appear in both ordinate and abscissa (Figures 5.1 to 5.3), the relationship between the two is less obvious. Miller et al. (1977) has produced a more useful threshold curves of u_* versus D (Figure 5.4) and u_{100} versus D (Figure 5.5).

5.3 Sediment Transport Equations

There are a large number of sediment transport rate formulae which have been proposed to predict the transport rate in terms of bedload and total load, largely as a result of experimental work in flumes and natural water courses. Many of the formulas are very similar in form, some include a critical or threshold condition below which no sediment transport takes place (Sternberg, 1972; Gadd et al., 1978; White, 1979; Langhorne, 1981; Hardisty, 1983; Yang, 1986) whereas others do not (Einstein, 1950; Bagnold, 1956, 1963, 1966; Yalin, 1963; Engelund and Hansen, 1967; Ackers & White, 1973). A few of these formulae have been tested for their applicability in tidal marine environments (Kachel & Sternberg, 1971; Gadd et.al., 1978; Heathershow & Hammond, 1979; Siegenthaler, 1982).

There is a general agreement that the rate of bedload transport is approximately proportional to u_*^3 (Bagnold, 1941) and the total load (including suspension) goes to some higher power, perhaps u_*^5 as in the expression of Engelund & Hansen (1967). The non-linear dependence of transport rate on u_* means that small errors in u_* result in large errors in transportation rate.

5.3.1 Bagnold Transport Equations

The most frequently used transport rate equation is that of Bagnold (1966). According to him, the fluid may be

regarded as a transporting agent in which the principle of energy conservation can be applied. It is assumed that the rate of mass transport of sediment is proportional to the power expended on the bed by the fluid. Because of the limited efficiency of the transport process only a fraction (e) of the available power (W) is used to carry the sediment within the flow.

Bagnold (1966) assumes the total stream power available to be divided between the bedload and suspended load so that only $\omega(1-e_b)$ is available for the latter. For bedload transport, the work required is equal to the product of bedload transport rate and $\tan\alpha$, where $\tan\alpha$ is the coefficient of dynamic solid friction. Equating the required work to the available work gives the following equation for the bedload transport rate

$$\frac{(\rho_s-\rho)}{\rho} q_b \tan\alpha = \tau_o U e_b \qquad 5.7$$

where q_b is the bed load transport rate, e_b is the bed load transport efficiency, $\tan\alpha$ is the coefficient of dynamic bed load friction, U is the mean velocity, τ_o is the bed shear stress, ρ_s is the density of the sediment and ρ is the water density.

For suspended load transport, the suspended load work rate is $q_s\omega/U$, and the suspended load transport rate is

given by

$$\frac{(\rho_s-\rho)}{\rho} q_s \frac{\omega}{U} = \tau_* U (1 - e_b) e_s \qquad 5.8$$

where e_s is the efficiency of the suspended load transport process and ω is the fall velocity.

Adding both equations 5.7 and 5.8 will give an expression for the total load transport rate q as

$$\frac{(\rho_s-\rho)}{\rho} q = \left(\frac{e_b}{\tan\alpha} + \frac{e_s U(1-e_b)}{\omega} \right) W \qquad 5.9$$

Bagnold (1966) suggests that $(1-e_b)e_s$ should be taken equal to 0.01. The ratio $e_b/\tan\alpha$ is assigned the value of 0.17 in the case of sand size $D < 0.5$ mm and dimensionless shear stress $\Theta < 1$. Consequently Bagnold's total load equation is

$$\frac{(\rho_s-\rho)}{\rho} q = (0.17 + 0.01 \frac{U}{\omega}) W \qquad 5.10$$

Generally bedload and suspended load transport modes from

different origins should not be mixed unless the assumptions made are similar. However, since the distinction between the bedload and suspended load is not well defined this procedure is commonly accepted.

The application of the stream power concept to sediment transport has considerable potential, as stream power is highly sensitive to slight changes in water discharge (Bull,1979). Changes in stream power ω should be reflected in the sediment transport rate, as suspended sediment concentrations are highly sensitive to changes in discharges (Leopold et.al.,1964; Dyer, 1980).

Sternberg (1972), proposed a relationship which included a threshold shear stress term (τ_c) in the form of excess shear stress $(\tau_o - \tau_c)/\tau_c$:

$$q = A \exp\left[B\left(\frac{\tau_o - \tau_c}{\tau_c}\right)\right] u_*^3 \qquad 5.11$$

where coefficient A and exponent B can be estimated according to grain size. For sediment with grain size of 0.19 mm diameter, the constants A and B are equal to 0.005 and 0.69 respectively.

A similar equation was proposed by Langhorne (1981), based on sediment transport rates measured across a sandwave crest in Start Bay, Devon, U.K:

$$q = 0.18 \frac{(\tau_0 - \tau_c)}{\tau_c} u_x^3 \qquad 5.12$$

which has a weaker dependence on excess shear stress than that of Sternberg (1972).

Gadd et al., (1978) compared a number of transport equations with the Bagnold equation and found that the transport rate could be represented by

$$q = K_1 (u_{100} - u_{100c})^3 \qquad 5.13$$

where u_{100} is the velocity measured at the standard height of 100 centimeters above the sea bed, u_{100c} is the threshold velocity, and K_1 was quoted as 7.22×10^{-4} g cm^{-4} s^2 for 0.18 mm and 1.73×10^{-5} g cm^{-4} s^2 for 0.45 mm sand.

One other equation incorporating a threshold condition was proposed by Hardisty (1983), following a suggestion by Vincent et al.(1981), where Bagnold's equation is written as

$$q = K_2 (u_{100}^2 - u_{100c}^2) u_{100} \qquad 5.14$$

where K_2 is the calibration coefficient which is strongly related to the grain size of the sediment. For grain sizes between 0.18 mm and 1.45 mm K_2 varies as

$$K_2 = (6.6\, D^{1.23})^{-1} \times 10^{-5}\ g\,cm^{-4}\,s^2 \qquad 5.15$$

where D is in millimeters.

5.3.2 Engelund & Hansen Transport Rate Formula

Engelund & Hansen (1966, 1967) put forward a formula for estimating total load sediment transport in streams. The relationships are as follows:

$$C_f \phi = 0.1\, \theta^{5/2} \qquad 5.16$$

where

$$\phi = \frac{q}{\rho_s \left[g \left(\frac{\rho_s - \rho}{\rho} \right) D^3 \right]^{1/2}} \qquad 5.17$$

and

$$\theta = \left(\frac{\tau}{(\rho_s - \rho)\, g\, D} \right)^{5/2} \qquad 5.18$$

A. Ali

and $$C_f = 2\frac{u_*^2}{U} \qquad 5.19$$

where C_f = a friction factor

ϕ = a dimensionless sediment discharge

Θ = a dimensionless bed shear stress.

The above equations can be combined to produce

$$q = \frac{0.1}{C_f}\beta\left(\frac{\rho_s-\rho}{\rho}D^3 g\right)^{1/2}\left(\frac{\tau}{(\rho_s-\rho)gD}\right)^{5/2} \text{A.Ali} \qquad 5.20$$

Recently, Engelund and Fredsoe (1982) suggested that the coefficient 0.1 of this equation should be reduced to 0.08.

Derivation of this formula was based on the assumption that the sediment moves at a velocity proportional to the shear velocity u_* and is calibrated for material coarser than 0.15 mm (Raudkivi, 1976). However, both Graf (1971) and A.S.C.E (1975) recommended its use for estimating sediment transport in rivers.

5.3.3 Flume Data Equations

Some of transport rate formulae which have been proposed were calibrated using the flume data of Guy et al (1966).

Among them are Kachel & Sternberg (1971), Gadd et. al (1978), Hardisty (1983) ,and Yang (1986). These formulae will only be as good as the data used to calibrate them, and will be restricted in the range by the calibration data. These formulae are valid for bedload only, except the formulae of Yang (1986) which have separate formulae for both bedload and suspended load. The formulae of Gadd and Hardisty were restricted to low flow velocity only, since they were calibrated for flow velocity less than 55 cm/s. In view of the fineness of the sediment in this study area (see chapter 6) which can be easily transported in suspension by a relatively strong tidal current which ranges up to 120 cm/s (see chapter 3) appropriate transport equations which include both bedload and suspended load and are valid for both low and high flow velocity must be used.

Guy et al (1966) flume data provides extensive information on transport variables and parameters for a large range of conditions most commonly found in natural streams and artificial channels. In these experiments sediment transport rates were measured for 10 sets of conditions in a wide recirculating flume. Each set covered flow phenomena ranging from a plane bed and no movement of sediment to antidunes. For each run data were collected after the equilibrium conditions had been established. The runs were considered as established when the bed configuration was consistent in the full length of the flume and the average water and bed-surface slope remained

constant with respect to time. Data relating to the mean velocity and suspended load discharge rate and total load discharge rate for four different grain sizes were used in this study. These experimental data are the most suitable for calibration of sediment transport formulae or for testing the validity of a new formula for predicting sediment transport rate.

In this study the flume data of Guy et.al (1966) will be reanalysed to find the relationship between total load and suspended load transport rates and mean velocity for different grain sizes. The data used in this analysis are shown in Table 5.1 to 5.4. Instead of a cubic power such as suggested by Bagnold (1966), let us for the purposes of discussion assume an equation of the form

$$q = A U^n \qquad 5.21$$

where A is a numerical coefficient and n is an empirical exponent. If tranport rate q is plotted against mean velocity on a logarithmic scale, the value of n can be estimated from the slope of the regression line if it is possible to fit a straight line to the data points. However, if it is not possible, we may be able to see how n varies with flow speed.

The values of the total load transport rate from Tables

5.1 to 5.4 have been plotted against the corresponding value of mean velocity on logarithmic scales for material with the grain size 0.19 mm, 0.28 mm, 0.45 mm, and 0.93 mm. These plots are shown in Figures 5.6 and Figure 5.7. It can be clearly seen that the data points plotted do not follow a linear trend but instead curve slightly. The slopes of the four curves vary from a higher value at low mean velocities to a smaller value at higher mean velocities. For sediment with grain size 0.19 mm the value of n varies from 9 to 5; for sediment with grain size of 0.28 mm the value of n varies from about 8 to 4.5; for sediment with grain size of 0.45 mm the value of n varies from 9 to 3.5 and for sediment with grain size 0.93 the value of n varies from 17 to 3.

These flume data have been replotted to include the threshold condition where the mean velocity U is replaced by $(U - U_c)/U_c$. For each data set the correlation coefficient between logq versus $\log(U - U_c)/U_c$ was then determined for a narrow range of threshold mean velocities. The effect of varying the value of threshold mean velocity on the value of correlation coefficient (R^2), the slope and the constant A are shown in Table 5.5. The critical mean velocities which produce the maximum values of R^2 are considered as the correct critical mean velocities. As shown in Table 5.5 the critical mean velocity for sediment with grain size 0.19 mm , 0.45 mm, and 0.93 mm are 17.0 cm/s, 19.0 cm/s, and 38.0 cm/s respectively. For sediment

Table 5.1. Total load (q) and suspended load (q_s) transport rates from Guy et al (1966) flume experiments for 0.19 mm diameter sand.

U cm/s	q g/cm/s	q_s g/cm/s	U cm/s	q g/cm/s	q_s g/cm/s
26.5	0.000148	-	51.2	0.401760	0.31220
26.5	0.000223	-	81.9	3.273600	2.36430
33.8	0.002860	0.00728	50.9	0.818400	0.52040
22.5	0.000476	-	54.2	1.383800	0.63910
39.6	0.035700	-	55.1	0.877920	0.63910
28.3	0.001930	-	117.0	6.993600	3.46470
46.9	0.177070	0.15460	88.0	3.422400	1.15980
25.9	0.000699	-	64.0	1.160640	0.66910
54.5	0.446400	-	126.2	11.904000	10.40900
60.6	0.892800	0.86240	131.9	23.808000	18.73600
31.7	0.017850	-	131.9	33.182000	34.49840
59.7	1.621900	1.44230	139.5	41.961000	52.04500
34.4	0.032700	0.01829	140.8	61.454000	59.92610
35.9	0.050590	-	122.8	47.169000	41.04120
71.6	3.124800	1.88840	144.4	68.001000	80.74410
94.2	3.124800	1.96280	116.1	63.984000	70.03770
98.1	3.868800	2.43860	128.0	119.932000	145.27990
105.4	5.059200	2.84010			

Table 5.2. Total load (q) and suspended load (q_s) transport rates from Guy et al (1966) flume experiments for 0.28 mm diameter sand.

U cm/s	q g/cm/s	q_s g/cm/s	U cm/s	q g/cm/s	q_s g/cm/s
29.2	0.002380	-	74.6	1.443360	0.61006
26.8	0.000476	-	93.2	2.499840	0.99696
40.8	0.014880	-	47.5	0.312480	-
51.2	0.117550	0.15475	94.7	2.663520	0.75886
47.5	0.063980	-	65.2	1.175520	0.58032
31.6	0.011450	-	102.1	5.952000	1.94926
56.6	0.610000	0.68448	115.5	6.844800	2.47006
54.8	0.595200	0.59520	108.8	5.059200	1.36896
48.1	0.124990	0.06249	114.9	5.654400	2.26176
53.0	0.297600	0.13392	118.2	9.076199	3.13966
65.8	1.071360	0.72912	142.9	26.486000	23.95680
62.7	1.175520	1.02672	137.1	20.683000	14.73120
72.5	1.726080	1.24992	145.0	32.140000	40.62240
57.9	0.639840	0.49104	150.2	68.448000	78.71520
64.3	1.101120	0.87792	106.0	19.344000	7.58880
92.0	3.124800	1.56240	145.3	63.537000	59.96640
58.5	0.580320	0.29760	142.9	105.350000	117.70080
66.1	1.294560	0.78864			

Table 5.3. Total load (q) and suspended load (q_s) transport rates from Guy et al (1966) flume experiments for 0.45 mm diameter sand.

U cm/s	q g/cm/s	q_s g/cm/s	U cm/s	q g/cm/s	q_s g/cm/s
24.3	0.000505	-	53.6	0.922560	-
24.0	0.000714	-	101.1	6.100800	2.276640
24.0	0.000416	-	143.5	9.523200	1.785600
23.7	0.000163	-	163.9	7.737600	-
36.5	0.008630	-	107.2	5.505600	5.208000
35.3	0.009225	-	57.6	0.982080	-
26.8	0.000624	-	129.2	8.184000	-
37.4	0.020980	-	91.1	3.720000	-
40.2	0.024840	-	62.1	0.505920	0.117552
21.3	0.000105	-	153.9	10.862400	2.276640
43.8	0.084810	-	75.2	2.202240	-
28.3	0.003422	-	85.3	2.990880	1.740960
43.5	0.248490	-	113.6	5.505600	0.669600
22.8	0.003571	-	140.2	7.886400	-
32.6	0.019046	-	163.9	15.475200	1.815360
25.9	0.000223	-	168.8	12.201600	1.651680
39.6	0.102672	-	153.3	10.713600	-
48.1	0.535680	0.266352	76.2	6.249600	0.162192
51.8	0.863040	-	145.6	19.046400	3.794400
44.8	0.215760	-	163.3	17.707200	6.993600
51.2	0.476160	0.372000	188.3	28.569600	-
78.3	1.324320	0.863040			

Table 5.4. Total load (q) and suspended load (q_s) transport rates from Guy et al (1966) flume experiments for 0.93 mm diameter sand.

U cm/s	q g/cm/s	q_s g/cm/s	U cm/s	q g/cm/s	q_s g/cm/s
44.8	0.003860	-	62.1	0.535680	0.057990
40.2	0.000505	-	81.6	1.383840	0.728600
45.4	0.000565	-	65.2	0.967200	0.416360
50.5	0.032700	-	84.7	2.842080	1.115250
53.3	0.047600	-	92.0	3.035520	1.576220
41.4	0.002630	-	74.9	1.934400	0.401490
58.8	0.122000	0.007732	95.0	4.910400	1.695180
45.7	0.018890	-	102.7	6.993600	3.048300
44.5	0.009960	-	88.0	3.422400	0.654280
48.7	0.053560	-	104.5	5.952000	5.353200
49.9	0.059520	-	124.9	10.416000	9.814200
61.8	0.273790	0.023490	158.4	15.772800	5.948000
54.8	0.178560	-	116.7	9.225600	4.312300
64.0	0.416640	0.057990	135.6	17.260800	4.014900
55.7	0.241056	0.013230	177.0	17.409600	3.866200
67.3	0.580320	0.151600	155.7	18.451200	2.646800
57.3	0.357120	0.012340	178.6	16.814400	5.948000
77.4	1.577280	0.684020	185.0	16.963200	5.650600

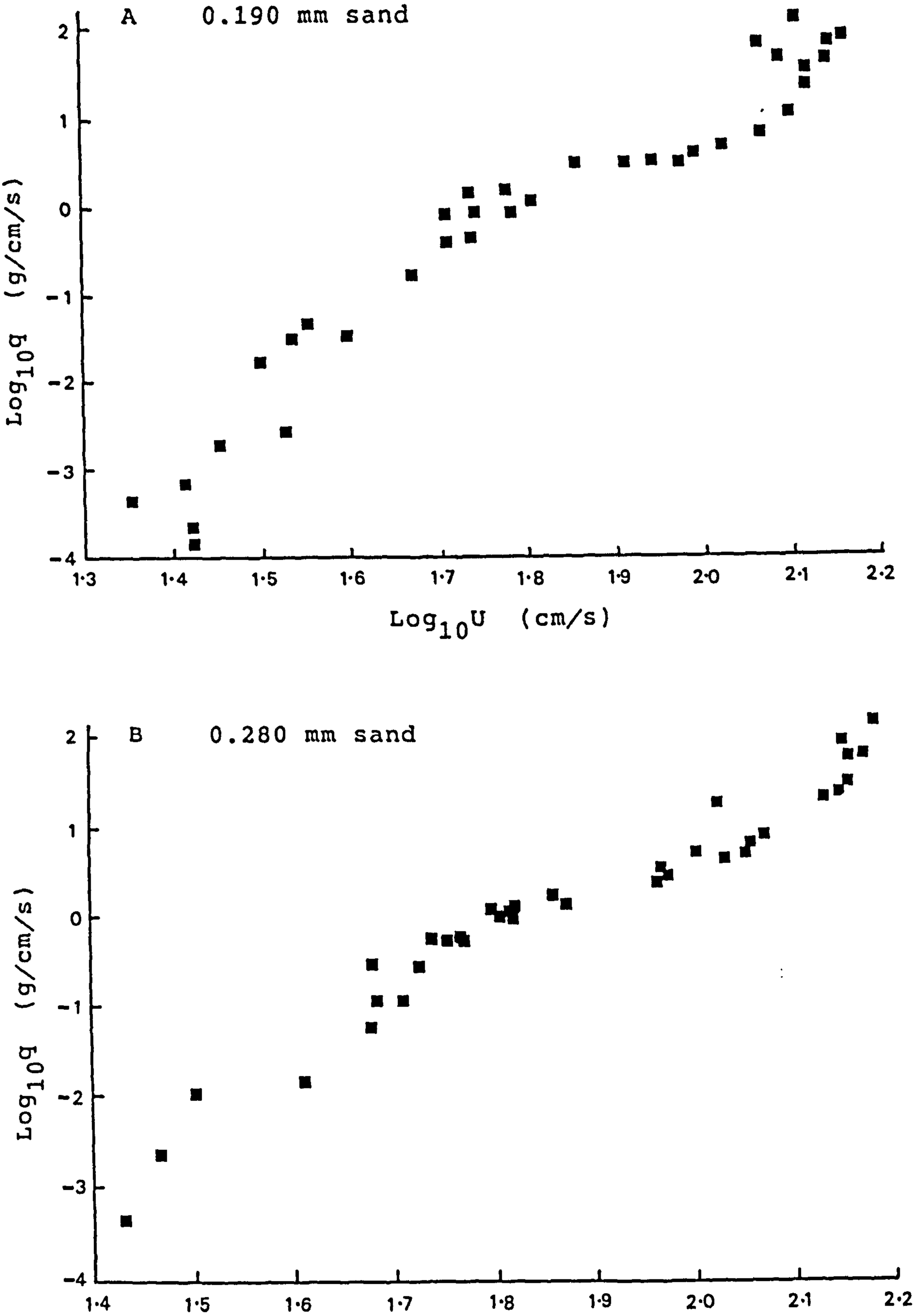

Figure 5.6. Plot of the measured transport rate against flow velocity for 0.190 mm diameter sand (A) and for 0.280 mm diameter sand (B). Data from Guy et al (1966) flume experiments.

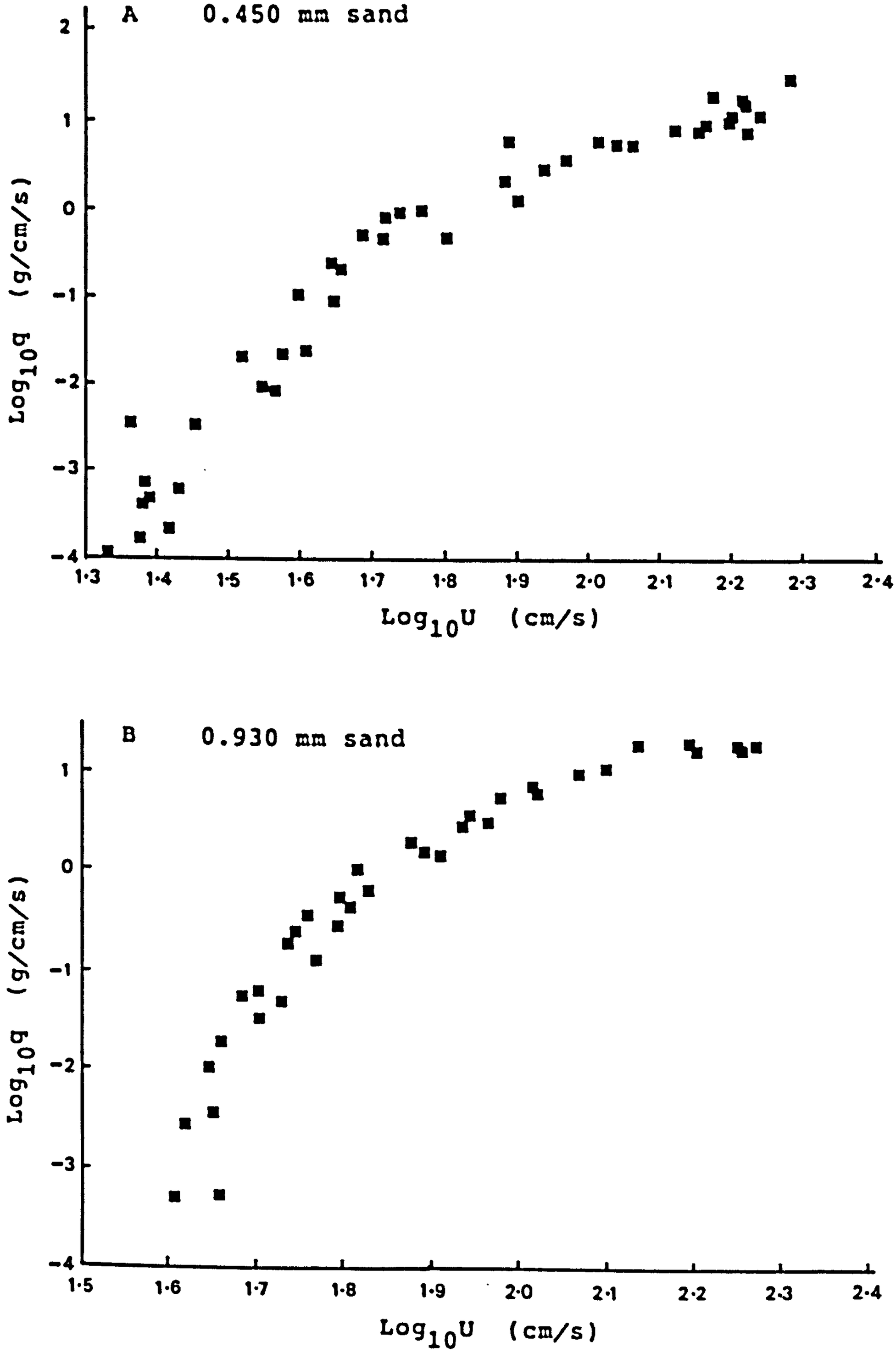

Figure 5.7. Plot of the measured transport rate against flow velocity for 0.450 mm diameter sand (A) and for 0.930 mm diameter sand (B). Data from Guy et al (1966) flume experiments.

Table 5.5. Variation of the coefficient A, exponent n and the correlation coefficient (R^2) with threshold velocity (U_c) from regression analysis of guy et al (1966) flume experiments.

D (mm)	Uc (cm/s)	A g/cm/s	n	R^2
0.19	15.0	0.00438	4.49	0.944
	16.0	0.00789	4.34	0.946
	17.0	0.01383	4.18	0.947
	18.0	0.02663	4.01	0.947
	19.0	0.03952	3.82	0.946
	20.0	0.06608	3.61	0.942
0.28	18.0	0.01783	3.92	0.957
	19.0	0.02742	3.80	0.958
	20.0	0.04140	3.68	0.959
	21.0	0.06152	3.54	0.959
	22.0	0.09022	3.40	0.959
	23.0	0.13100	3.24	0.958
0.45	17.0	0.01612	3.43	0.942
	18.0	0.02595	3.28	0.944
	19.0	0.04146	3.10	0.946
	20.0	0.06660	2.88	0.943
	21.0	0.11422	2.52	0.917
0.93	36.0	0.69240	3.03	0.936
	37.0	0.85640	2.89	0.941
	38.0	1.04790	2.72	0.945
	39.0	1.26230	2.51	0.943
	40.0	1.43700	2.09	0.904

with mean grain size of 0.28 mm the critical mean velocity as indicated by the maximum value of R2 was 20 cm/s, but instead the value of 18.0 cm/s was chosen since it lies between the critical mean velocities for sediment with grain size of 0.19 and 0.45 mm. Figures 5.8 and 5.9 do show a strong linear trend. The curve slopes, however, are different for different grain sizes. A straight line calculated by a least squares method in the form of

$$\log q = \log A + n \log\left(\frac{U - U_c}{U_c}\right) \qquad 5.22$$

can be fitted to all sets of data as shown in Fig. 5.8 to 5.9. The coefficients A and n are given in Table 5.6 together with the correlation coefficients R^2 and the number of data points used in each data set. The excellent fit of these total load transport rate models to the flume data are reflected in the values R^2 which are very high and all are higher than 0.94. The relationship is significant at the 99% confident level for all the data sets.

In contrast with the published transport rate formulae, the striking feature of the plots in Figures 5.8 and 5.9 is the range of slopes of the regression lines. Instead of an exponent 3, the value of exponent n varies from 2.7 for sediment with grain size of 0.93 mm to 4.0 for sediment with grain size of 0.19 mm. The variations of exponential

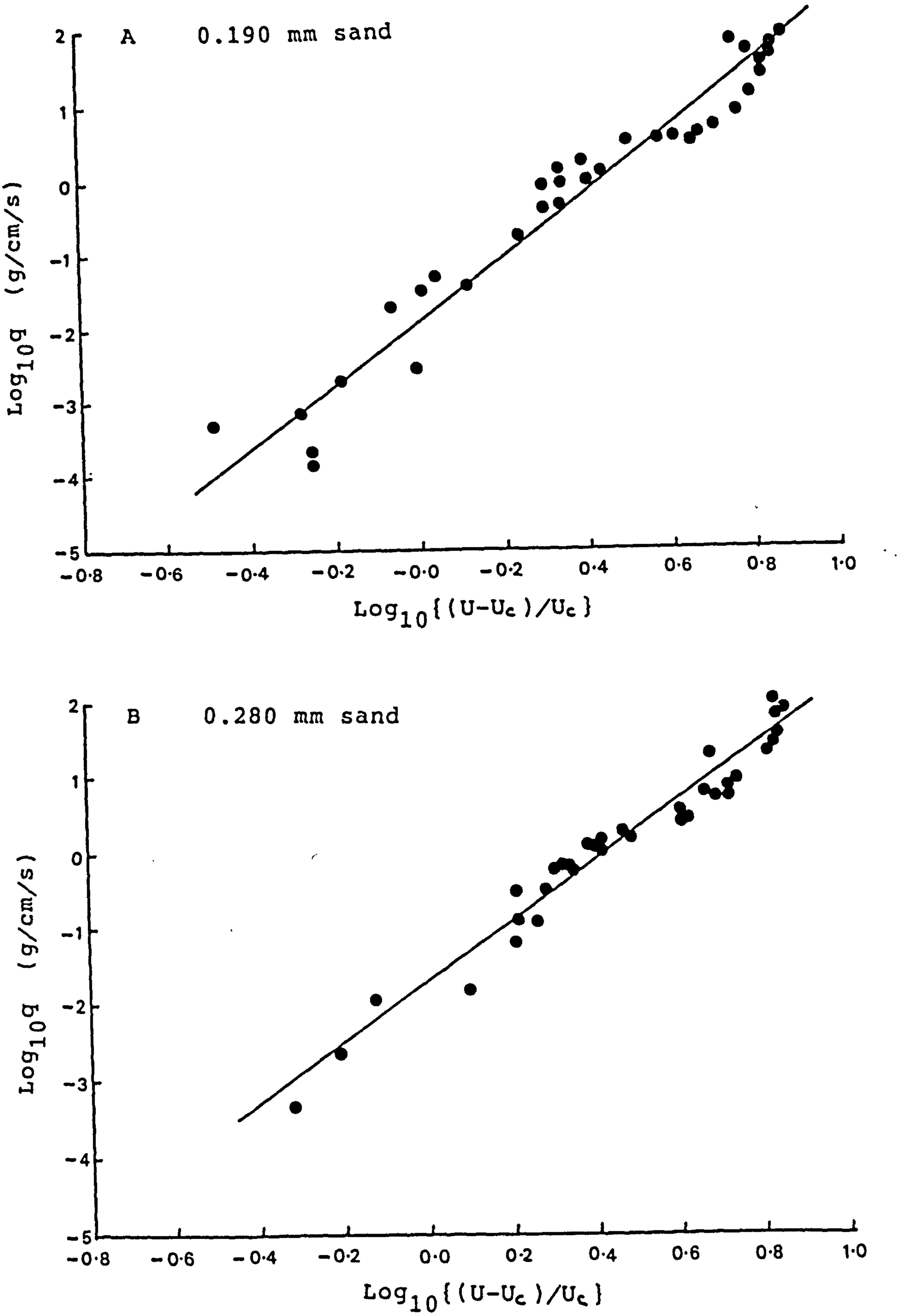

Figure 5.8. Plot of the measured transport rate against $(U-U_c)/U_c$ for 0.190 mm diameter sand (A) and for 0.280 mm diameter sand (B). The lines are derived from the regression analysis of the flume data.

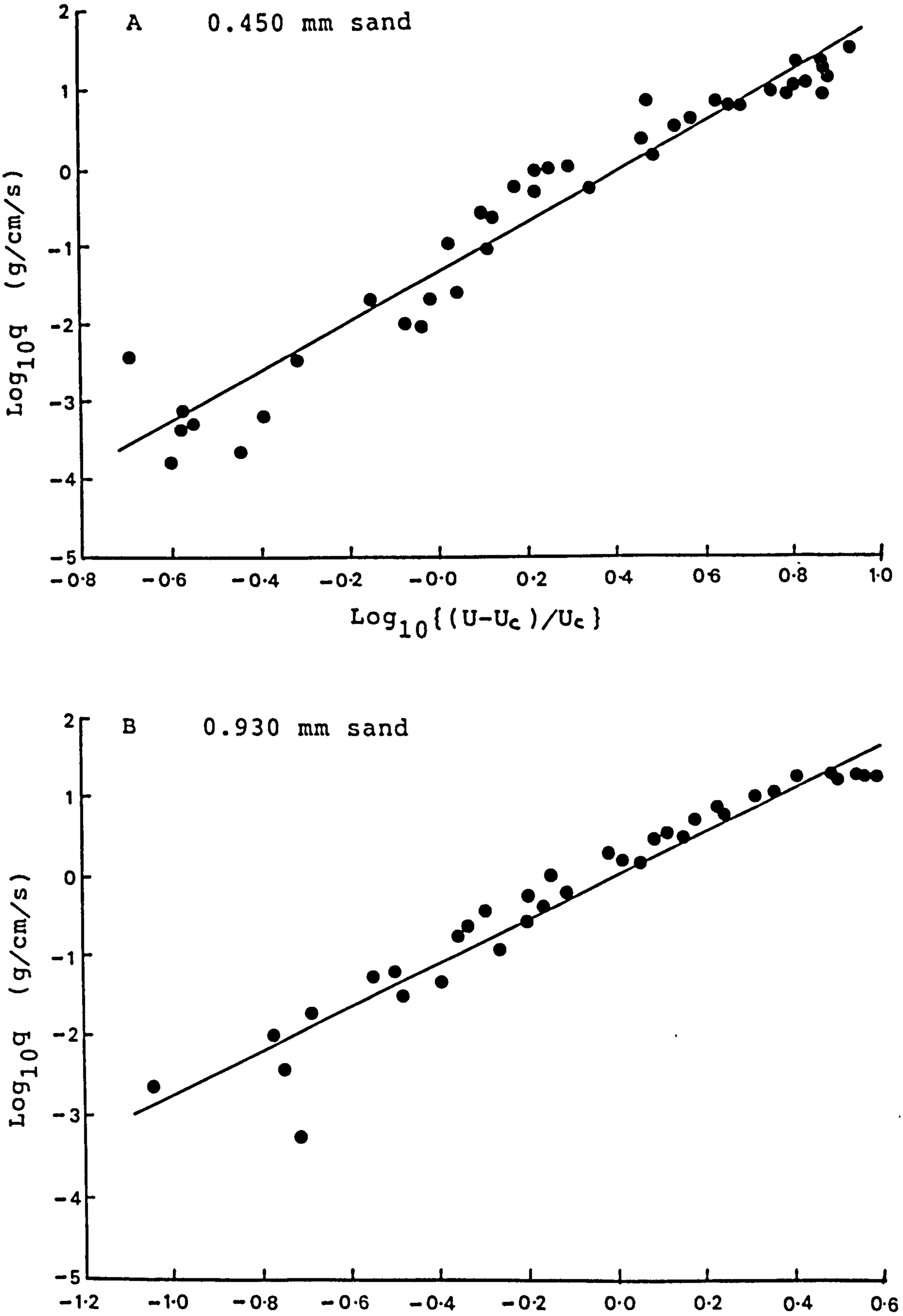

Figure 5.9. Plot of the measured transport rate against $(U-U_c)/U_c$ for 0.450 mm diameter sand (A) and for 0.930 mm diameter sand (B). The lines are derived from the regression analysis of the flume data.

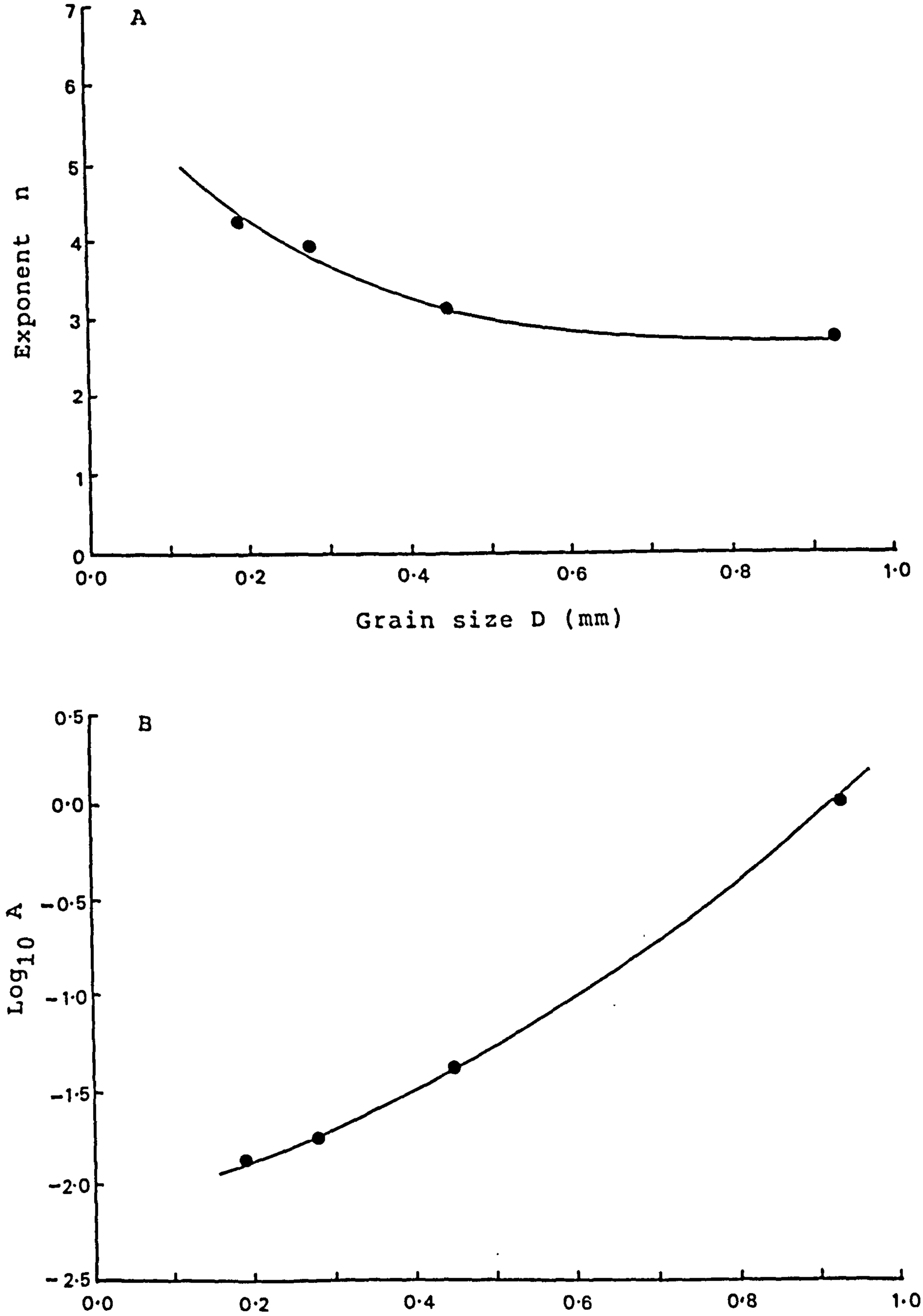

Figure 5.10. A) Plot of the exponent n against sand grain size D. B) Plot of the coeffient A against sand grain size D.

Table 5.6. Coefficient (logA), Exponent (n) and correlation coefficients (R^2) obtained from regression analysis of Guy et al.'s (1966) total load data.

Grain Size (mm)	Exponent n	Coefficient LogA	Correlation Coefficient (R^2)	Number of Data Points
0.19	4.18	-1.859	0.947	35
0.28	3.92	-1.748	0.957	35
0.45	3.10	-1.382	0.946	43
0.93	2.72	0.020	0.945	36

Table 5.7. Coefficient (logA), Exponent (n) and correlation coefficients (R^2) obtained from regression analysis of Guy et al.'s (1966) suspended load data.

Grain Size (mm)	Exponent n	Coefficient LogA	Correlation Coefficient (R^2)	Number of Data Points
0.19	3.90	-1.781	0.884	26
0.28	3.57	-1.752	0.800	29
0.45	1.71	-1.019	0.584	15
0.93	3.00	-0.575	0.836	25

n and coefficient A with the grain size are shown in Figure 5.10. These two figures show that the exponential n decreases with increasing grain size. However, the rate of this decrease reduces drastically for grain sizes larger than 0.4 mm.

Since the average mean grain size commonly found in the study area is about 0.15 mm or 2.75 phi (see chap.6), it is neccesary to extrapolate the curves of Figure 5.10 beyond the range covered by the experimental data. For the grain size 0.15 mm, the value of n is 4.5 and the value of A is 0.0132. The transport rate equation for this size of sediment can be written as

$$q = 1.32 \times 10^{-2} \left(\frac{U - U_c}{U_c} \right)^{4.5} \qquad 5.23$$

A high value of n in this equation may probably be due to the dominant influence of suspended material (see later) in the flow especially for very fine sand. Equation 5.23 will be used for the calculation of total load transport rate of sediments in this study in addition to the Engelund & Hansen (equation 5.20) formula.

In addition, suspended load transport rates from the flume data of Guy et al.(1966) were also analysed to find the relationship between the suspended load transport rate

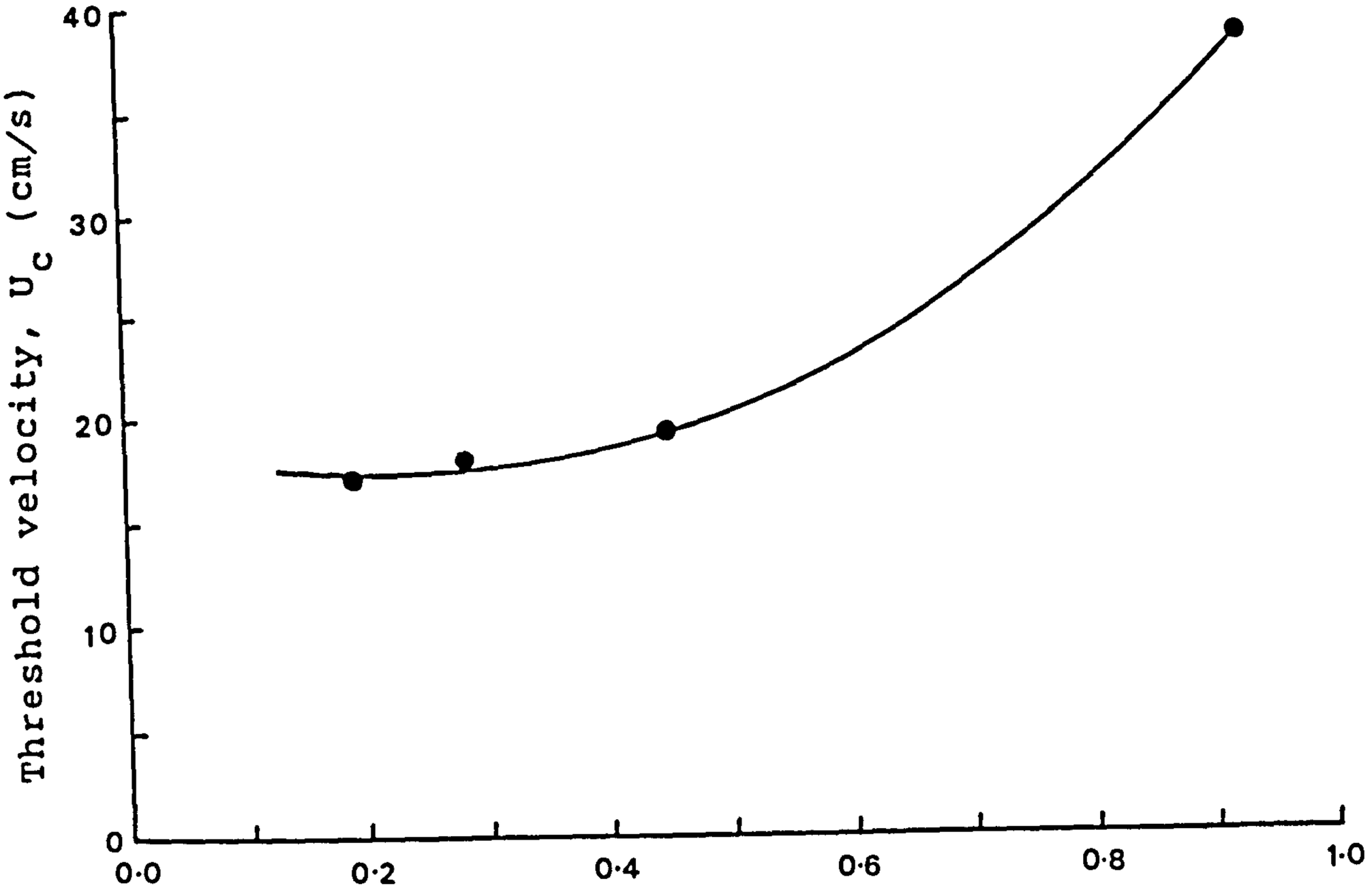

Figure 5.11. Plot of the threshold velocity, U_c against sand grain size D.

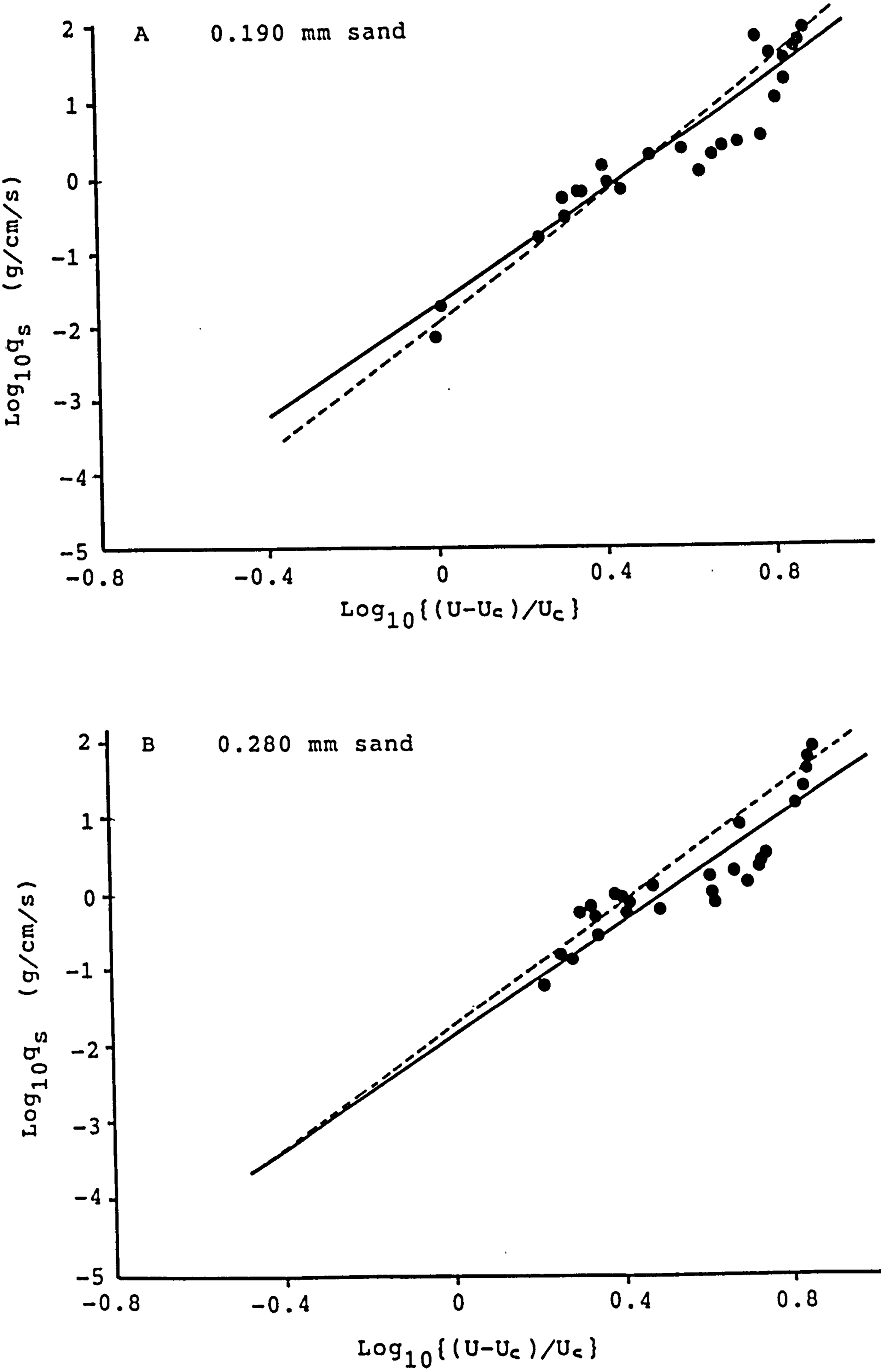

Figure 5.12 Regression lines based on the Guy et al (1966) suspended load flume experiments (————). Superimposed are the regression lines based on Guy et al (1966) total load flume experiments (- - - - -). A) 0.190 mm sand and B) 0.280 mm sand.

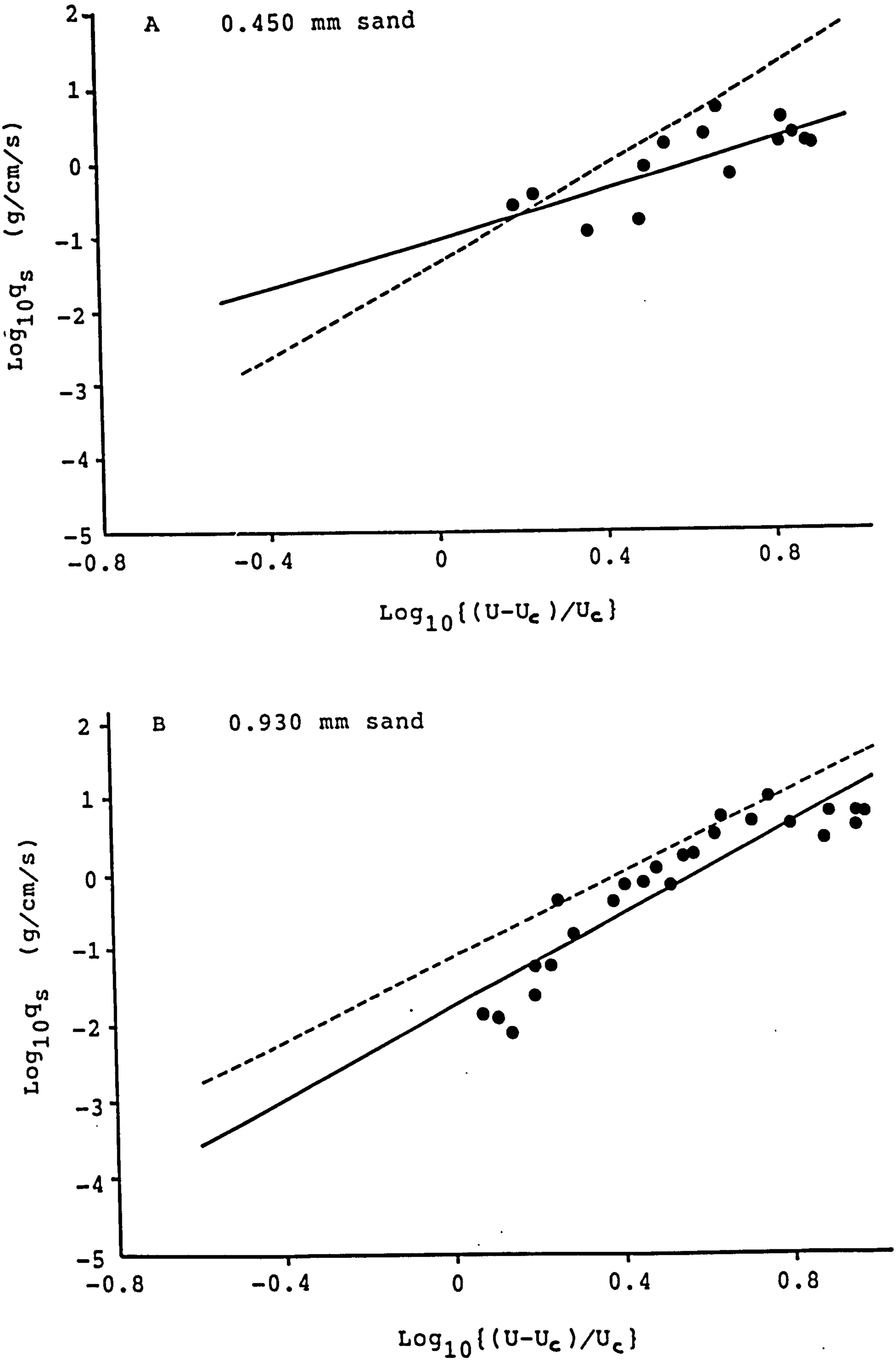

Figure 5.13 Regression lines based on the Guy et al (1966) suspended load flume experiments (———). Superimposed are the regression lines based on Guy et al (1966) total load flume experiments (- - - - -). A) 0.450 mm sand and B) 0.930 mm sand.

and the mean velocity for the same grain size. Both parameters were also plotted on log-log axes as shown in Figures 5.12 and 5.13 for four grain sizes (0.19, 0.28, 0.45, 0.93 mm). A simple power relationship in the form of a straight line was determined by a least squares method. The coefficients A and n are given in Table 5.7 together with the correlation coefficient and the number of data points used in each data set. The correlation coefficients for suspended load data are smaller than for total load data. The poor fits are due to a large deviation in the suspended load data compared to total load data (Guy et al., 1966). As shown in Table 5.6 and 5.7 some suspended load transport rates were found to be larger than corresponding total load transport rate. This difference was attributed partly to the inadequate number of suspended sediment samples, and partly to the possibility that the samples were taken in a region of flow where local concentrations were much greater than the average (Guy et al., 1966).

For comparison, the predicted total load transport rates for the same grain size are also plotted in the same figures, which clearly show that the suspended load transport rates are generally smaller than total load transport rates for the same grain size. The difference between these two transport rates depends on the magnitude of the mean velocity. A small deviation from this generalization is that for sand grain size of 0.19 and 0.45 mm the predicted suspended load transport rates are higher

than total load transport rate at low mean velocity, probably due to a large deviation in the suspended sediment data. Figures 5.12 and 5.13 show that the difference between suspended load and total load transport rates is smaller for fine sediment than for coarser sediment indicating the increasing domination of suspended load in the total sediment transport rate for fine sediment.

5.3.4 Discussion

The main difficulty in predicting sediment transport is its variability and non-linearity. In general, the sediment transport rate can be summarised as (Heathershaw,1981)

$$q_b \propto u_*^3 \quad \text{(at higher velocity)} \qquad 5.24$$

$$q_b \propto u_*^5 \quad \text{(at lower velocity)} \qquad 5.25$$

and $$q_s \propto u_*^{n+3} \qquad 5.26$$

where q_b and q_s are bedload and suspended load respectively and n is a constant (n=1,2,.....). A Recent

study suggested that may be proportional to u_*^7 (Dyer,1980).

Although sediment transport rate equations of the type proposed by Bagnold (1966) and the modified equations of Gadd et.al.(1978), Sternberg (1972), and Hardisty (1983) are useful for the prediction of bedload transport, they should not be relied on for the prediction of total transport for fine sediment. Failure to include the suspended meterial in sediment transport prediction may lead to errors in the predictions. The dominance of suspended material in a tidal environment has been observed in the Wash (Kestner,1975) where 90% of the total sediment transport was attributed to suspended material and the remaining 10% was attributed to bedload.

Bagnold (1956) has argued that suspension occurs when the upward components of the turbulent velocity fluctuations exceeds the fall velocity of the grains, and effective suspension occurs at a transport stage (U*/U*c)

$$\frac{u_*}{u_{*c}} = 0.8 \frac{w}{u_{*c}} \qquad 5.27$$

For sand with mean grain size of 0.7 mm, full suspension occurs when the transport stage reaches 3.6 and for fine sand with mean grain size of 0.15 mm full suspension occurs at the threshold of movement (Dyer,1986). Abbott and

Francis (1977) showed that near the threshold, rolling is dominant, but the proportion of grains rolling decreases very rapidly as the transport stage increases and suspension increases. Because of the intermittency in the shear stress there is considerable variability in sediment movement above the threshold condition.

The most striking result from the reanalysis of the flume experimental data of Guy et.al.(1966) is the variation in the value of the exponential power of the velocity. The total load transport rate can be expressed as

$$q = A\left(\frac{U - U_c}{U_c}\right)^n \qquad 5.28$$

The value of n increases from 2.7 for D=0.93mm to about 4.0 for D=0.19 mm. For fine sediments with a mean grain size commonly found in this area, the value of n is 4.5. As can be seen in Figure 5.10a, if we extrapolate the curve to the region of material finer than 0.06 mm, the value of n increase to about 5.5 . The value of n is almost constant for D>0.7 mm and this may indicate the lack of suspended material in the total load.

To examine the applicability of the new total load transport formula, it is useful to compare it with other

well known transport rate formulae. To do this, the sediment transport formulae of Bagnold (1966), Engelund & Hansen (1967), Gadd et al. (1978) and Hardisty (1983) were chosen , and the variations of transport rate with velocity for sediment of grain size 0.19 mm are shown in Figure 5.14. These comparisons indicate a variations in the magnitude of the predicted sediment transport rates given by these five formulae. Relative to the new formula which undoubtedly give the best fit to the flume data of Guy et al. (1966), the Gadd and Hardisty formulae predict smaller transport rates at high velocity, whereas the Bagnold formula predicts a higher transport rate. For mean velocities greater than 70 cm/s the transport rate predicted by Engelund & Hensen is almost equal to the values predicted by the new formula.

The formula proposed by Gadd et al.(1978) was calibrated over a range of mean velocity from 22.0 to 55 cm/s, i.e. in the lower flow regime only; therefore its application in high tidal currents is limited. Since the Hardisty formula was calibrated using Gadd's data , its applicability in a high flow regime is also limited. A least squares analysis of the flume data used by Gadd was performed in order to re-evaluate the transport rate equation in the form of a simple power relation between $\log q$ and $\log(U-U_c)$. For a grain size of 0.18 mm, the values which yield a best fit to the data were found to be $A = 4.772 \times 10^{-4}$ and $n=2.1$ or

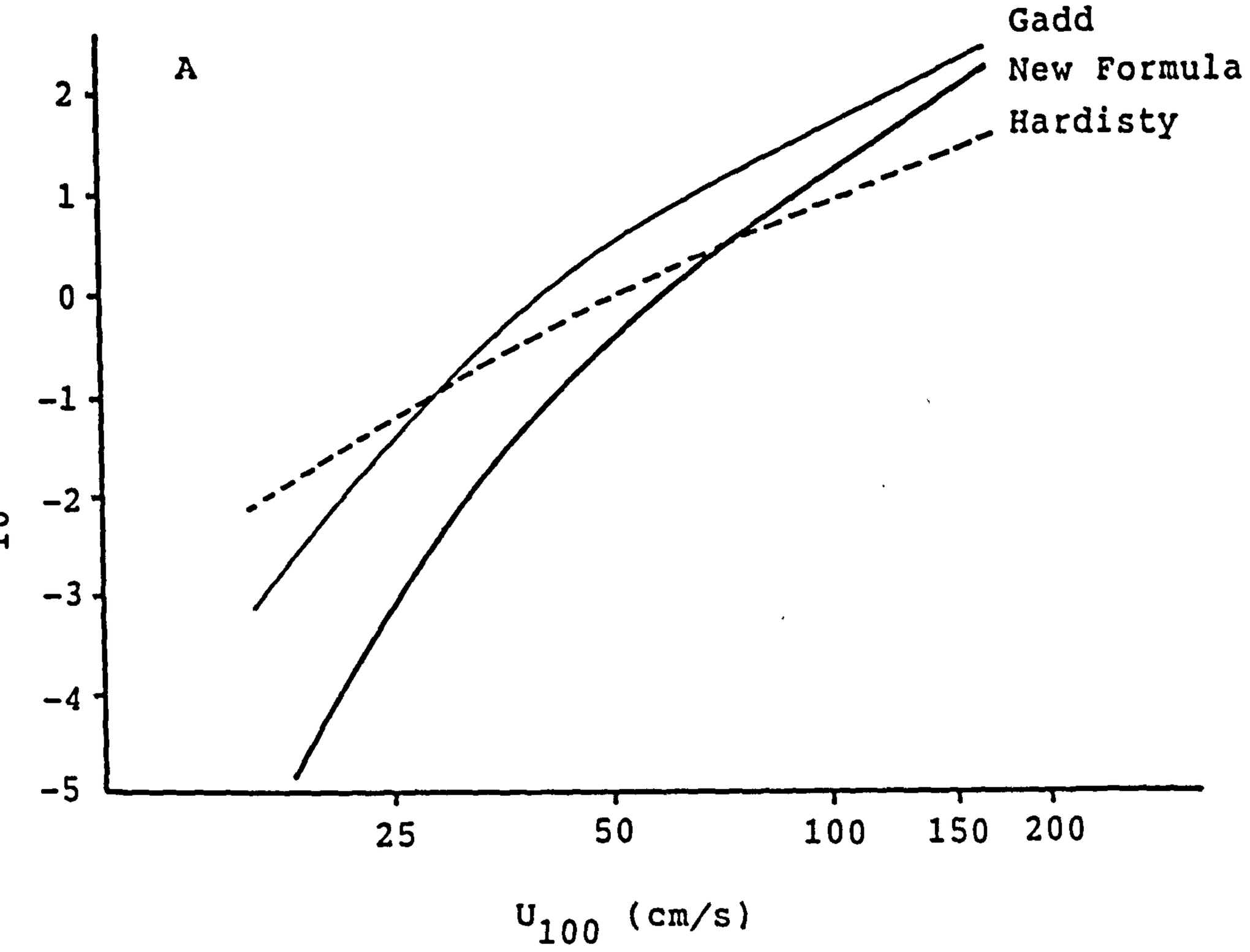

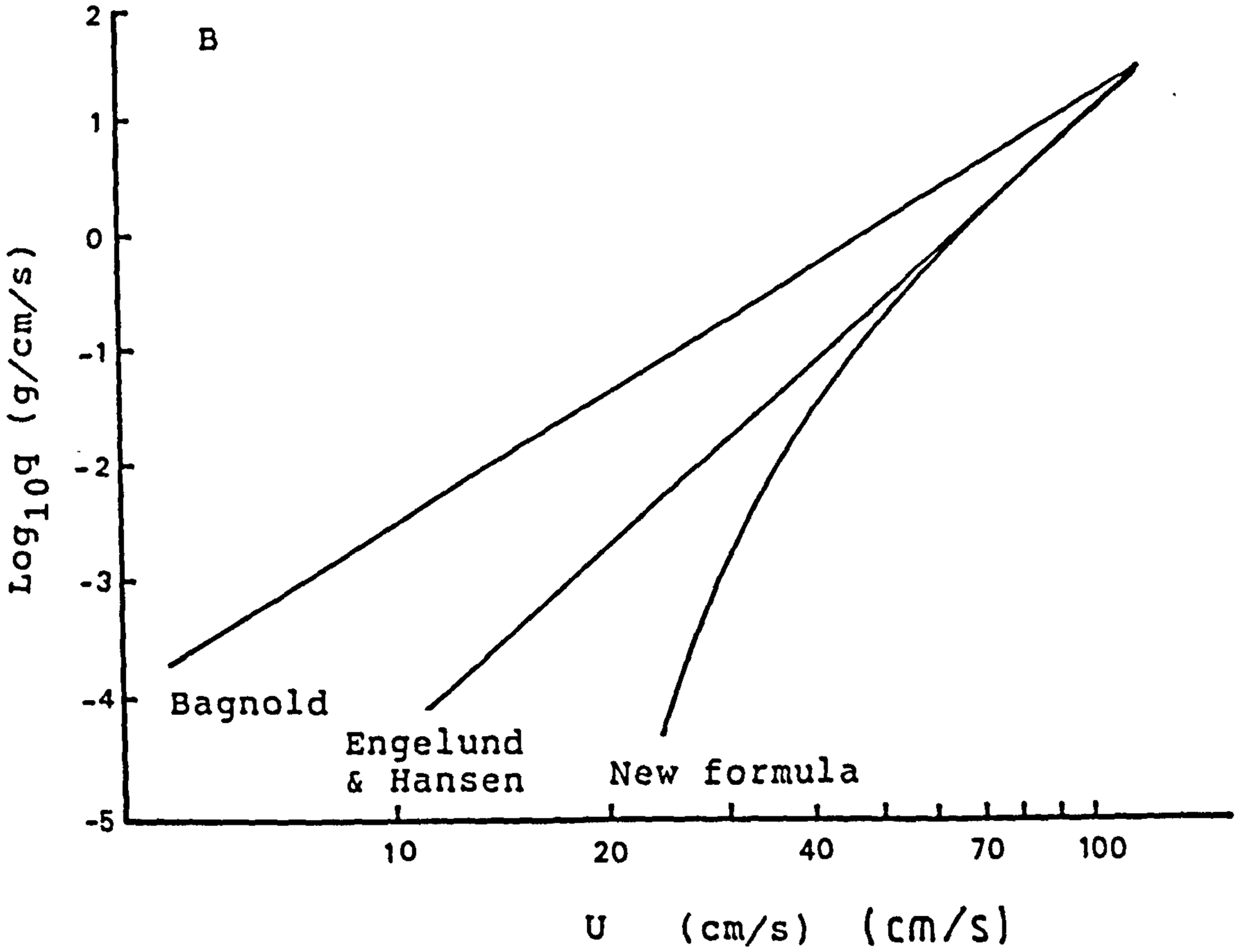

Figure 5.14. A) Plot of the transport rates against U_{100} calculated from Gadd et al (1978), Hardisty (1983) and the New Formula (eqn.5.23). B) Plot of the transport rates against U calculated from Bagnold (1966), Engelund & Hansen (1967) and the New Formula (eqn.5.23).

$$q = 4.772 \times 10^{-4} (U_{100} - U_{100c})^{2.1} \qquad 5.29$$

The correlation coefficient (r^2) is 0.838. Graphical representation of the this power relation formula is shown in Figure 5.15 in association with curves derived from the Gadd and Hardisty formulae. As shown, the Gadd curve does not agree well with the data; instead it appears as a rapidly rising curve which shows a large deviation from the calibration data at low and high flow velocities, whereas Hardisty's curve does agree with the experimental data because its calibration coefficient was calculated from regression analyses of the data.

The transport rate in the form of a simple power relation with the exponent n=2.1 obtained from flume data used by Gadd et al.(1978) is less sensitive to velocity changes when compared to the transport rate formula obtained from reanalysis of Guy et al.(1966) flume data where the exponent n is equal to 4.1 for the similar grain size. This discrepancy arises because the flume data used by Gadd et al. were for low velocity flow only whereas the data used in this reanalyses were for low and high velocity flow. As shown in Figures 5.5 and 5.6 the flume data scatter more widely for low flow velocities than for high flow velocities, indicating that the error in measuring transport rate is higher for low velocity than for high velocity. Therefore, the low and narrow range of flow

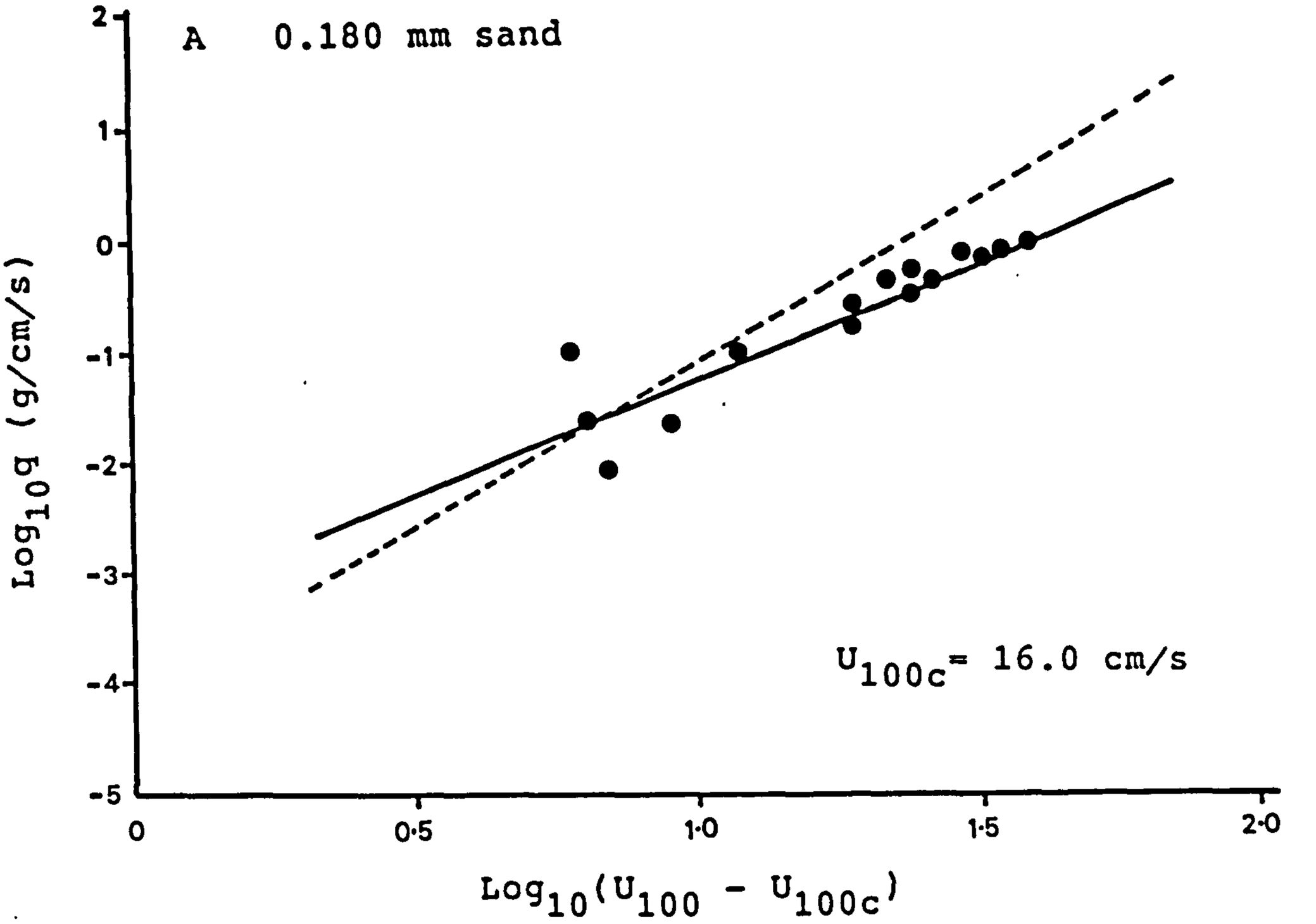

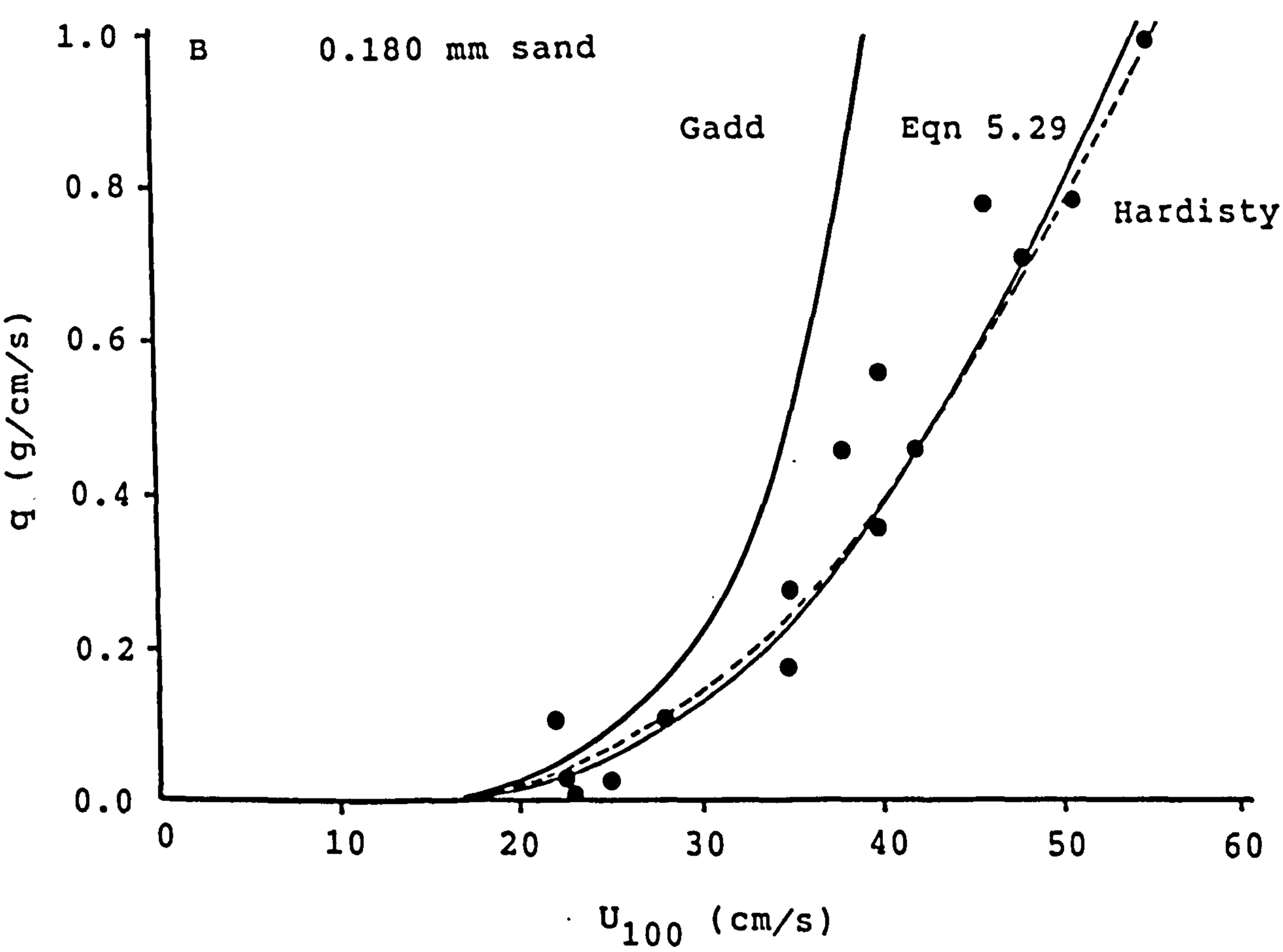

Figure 5.15. Plot of transport rate against (U_{100} - U_{100c}): data from Guy et al (1966) flume experiments and those predicted by the Gadd et al (1978) equation (- - - -), and the power regression line (———).

velocities used by Gadd et al. and Hardisty cannot give a valid relationship between the transport rate and flow velocity for flow velocities greater than 55 cm/s (which are commonly measured in tide dominated estuaries).

From this comparison, it is clear that only the transport rate of Englund & Hansen was found to be suitable for the calculation of sediment transport rate in addition to the new formula derived from the Guy et al. (1966) flume data, even though the Engelund & Hansen formula predicts a higher rate at low velocity than the new formula. Both formulae predict almost the same transport rate at velocities higher than 55 cm/s which are commonly observed in this study area.

5.4 Measured sediment transport in the Dwyryd estuary

The new sediment transport formula will be tested in the intertidal environment of the Dwyryd Estuary. Transport rates calculated from this formula have been compared with the Engelund & Hansen formula (equation 5.20).The relevent parameters used in these calculations are:

sediment density, = 2.65 g/cm

water density, = 1.02 g/cm

mean grain size,D = 0.15 mm

gravitational acceleration,g = 980 cm/s

threshold velocity, = 19.0 cm/s

The value of the threshold velocity was estimated from the Shield threshold diagram (Figure 5.1); for fully turbulent flows the threshold shear stress is

$$\frac{\tau_c}{(\rho_s - \rho)gD} = 0.045 \qquad 5.30$$

where ρ_s is the sediment density and ρ is the water density. ρ_s and ρ are given the values of 2.65 g/cm^3 and 1.02 g/cm^3 respectively. From this equation, the threshold shear stress, τ_c is found to be 1.079 dynes/cm and using a mean drag coefficient C_{100} =0.003 (Sternberg, 1972; Collins et al., 1981), the threshold mean velocity was found to be 19.0 cm/s.

Sediment transport rates were calculated using the estimated mean velocity (see chapter 4) for 10 minute intervals and the total transports for each flood and ebb cycle were obtained by summation of values of each interval over that portion of the cycle. Results are shown in Tables 5.8, 5.10, 5.12 and 5.14 for stations A to D. The most striking observation to be made at each station is the considerable differences in values between the flood and ebb of both spring or neap tides. Transport is greatest

where the currents are strongest, which usually occurs in the lower part of the estuary, particularly on the sand bank near the main tidal channels. Transport of sediment is generally low at stations located in the upper part of the estuary and on higher intertidal sand flats.

Station A:

This station was occupied for the whole neap-spring period beginning from May 8 to 15,1987 on the sandbank which separates the Dwyryd channel from the Glaslyn channel (Figure 5.16). The current meters which measured the flooding phase were oriented parallel to the channel while the current meters which measured the ebb phase were oriented slightly at an angle to the main channel because of the curvature of the main channel. During the period of deployment the station was visited three times to free the current meters from seaweed. There was little erosion around the pole so that the heights of the current meters above the bed were not altered.

The neap tides occurred on 8 and 9 May followed by spring tides on 14 and 15 May. At the neap tide, the maximum depth-mean velocity during the flood was 43 cm/s which is slightly larger than the ebb maximum depth-mean velocity of 25 cm/s, as shown in Figure 5.18. At the spring tide (Figure 5.17), the maximum depth-mean velocity during the flood was 110 cm/s while the ebb maximum depth-

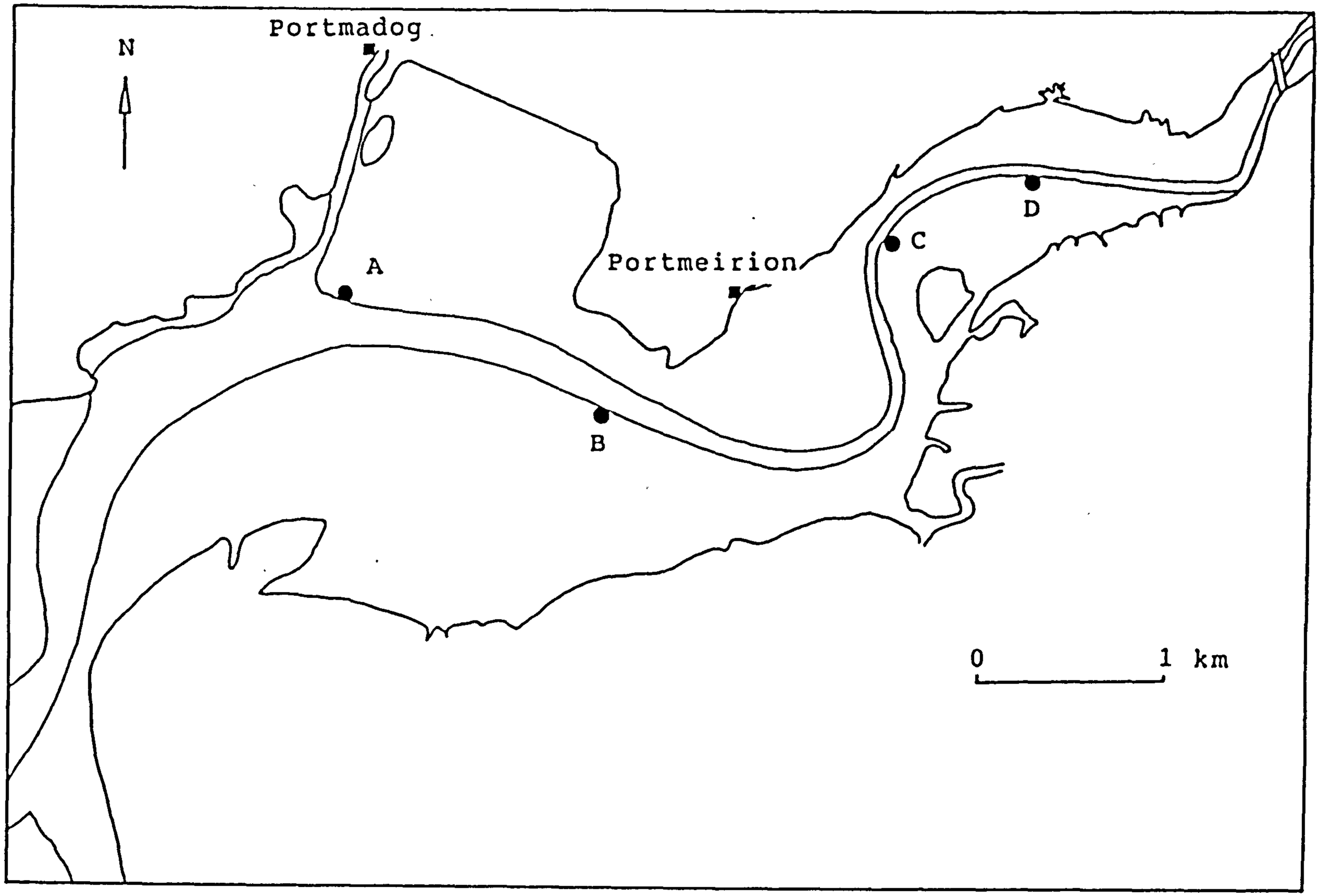

Figure 5.16. Position of the current meters rig.

mean velocity was about 40 cm/s which means that the flood current dominated the ebb by a factor of three during the spring tide.

The variation of sediment transport rate during a spring and a neap tide at station A are shown in Figures 5.17 and 5.18 respectively. The transport rates are very variable during a tidal cycle which range up to 28.4 g/cm/s and typically increase with flow velocities. Therefore, the pattern of sediment transport rate depends on the variation of flow velocity at this station. Estimated transport rates using the new formula are lower than the rate estimated using the Engelund & Hansen method. From both figures it appears that the general transport rate variations involve low values around high water and high values in the hours around low water. The importance of the early stage of flood is very apparent which shows that the greatest amount of sediment transport at this station occurred during these earlier stages of the tidal cycle.

The rates of sediment transport estimated by both methods for every 10 minutes interval have been integrated to give the total transport per flood and ebb stages for each of the 14 tidal cycles monitored at this station. The results are shown in Table 5.8 and Figure 5.19. As shown, total transport rates per flood and ebb are highly variable. The amount of sediment transport during the flood is generally higher than during the ebb.

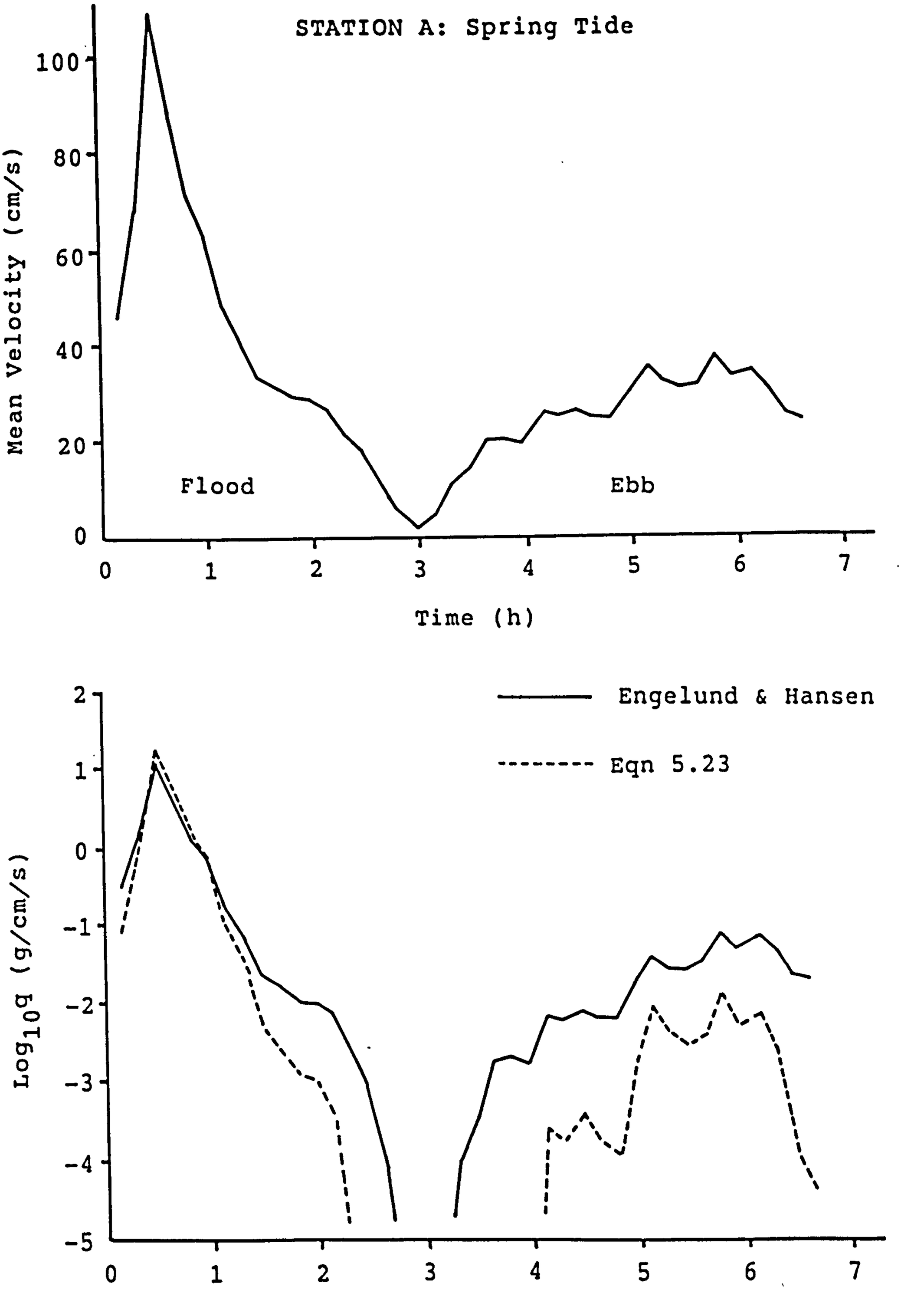

Figure 5.17. Typical spring tide velocity (A) and sediment transport curves (B) at station A over a tidal cycle predicted by Engelund & Hansen formula (———) and by the New Formula (------).

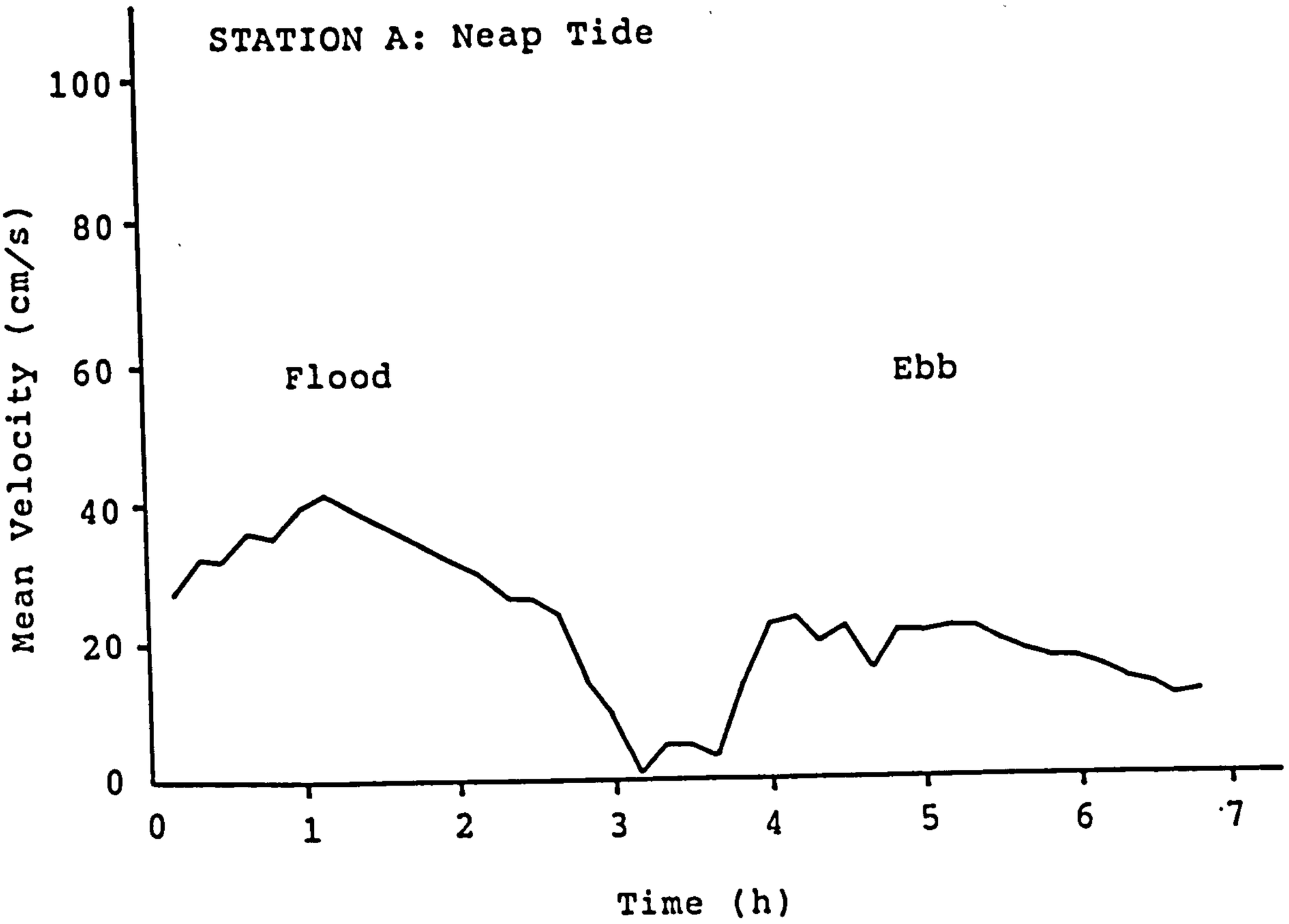

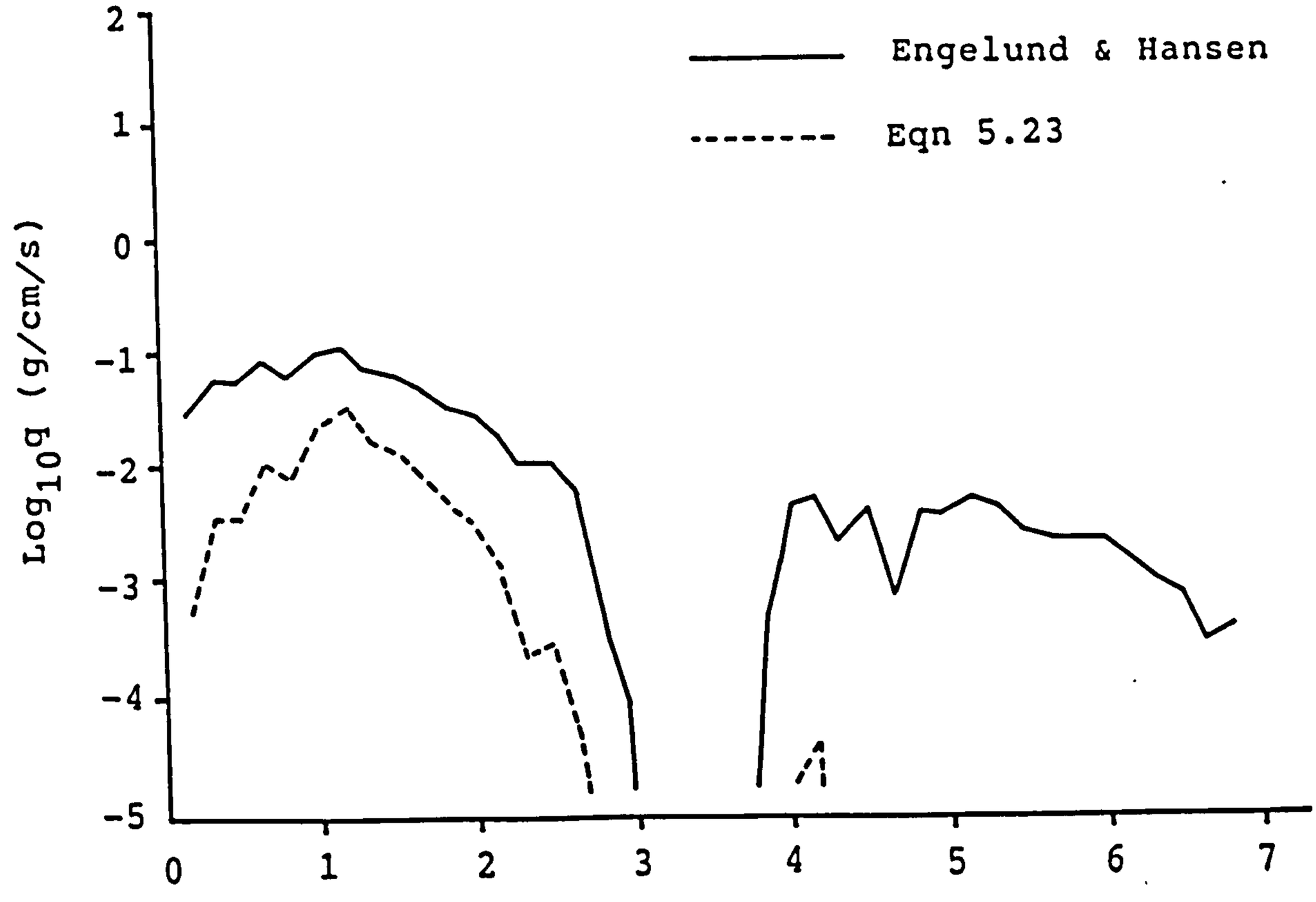

Figure 5.18. Typical neap tide velocity (A) and sediment transport curves (B) at station A over a tidal cycle predicted by Engelund & Hansen formula (————) and by the New Formula (--------).

Table 5.8. Total load computations at Station A.

Tide	Direction	Mean Velocity cm/s	Sediment Discharge, g/cm/tide	
			Engelund & Hansen	New Formula
1 (NT)	Flood	41.6	499	83
	Ebb	23.6	28	0
2	Flood	44.5	710	192
	Ebb	27.2	65	1
3	Flood	54.1	1,404	640
	Ebb	26.4	76	0
4	Flood	55.9	1,520	805
	Ebb	33.6	171	12
5	Flood	64.3	3,022	1,949
	Ebb	35.8	218	22
6	Flood	65.8	3,117	2,292
	Ebb	36.4	237	36
7	Flood	72.9	3,223	2,320
	Ebb	36.6	245	28
8	Flood	75.1	3,840	3,226
	Ebb	37.7	240	32
9	Flood	84.0	6,281	6,239
	Ebb	34.7	247	25
10	Flood	86.3	6,251	5,952
	Ebb	34.4	253	30
11	Flood	96.4	7,311	7,669
	Ebb	39.9	392	72
12	Flood	83.5	6,212	5,854
	Ebb	34.6	203	19
13	Flood	98.7	11,266	11,569
	Ebb	40.1	326	63
14 (ST)	Flood	108.5	12,772	15,074
	Ebb	37.0	281	28
Total	Flood		67,428 (96%)	63,864 (99%)
	Ebb		2,982 (4%)	368 (1%)

(NT=Neap tide and ST=Spring tide)

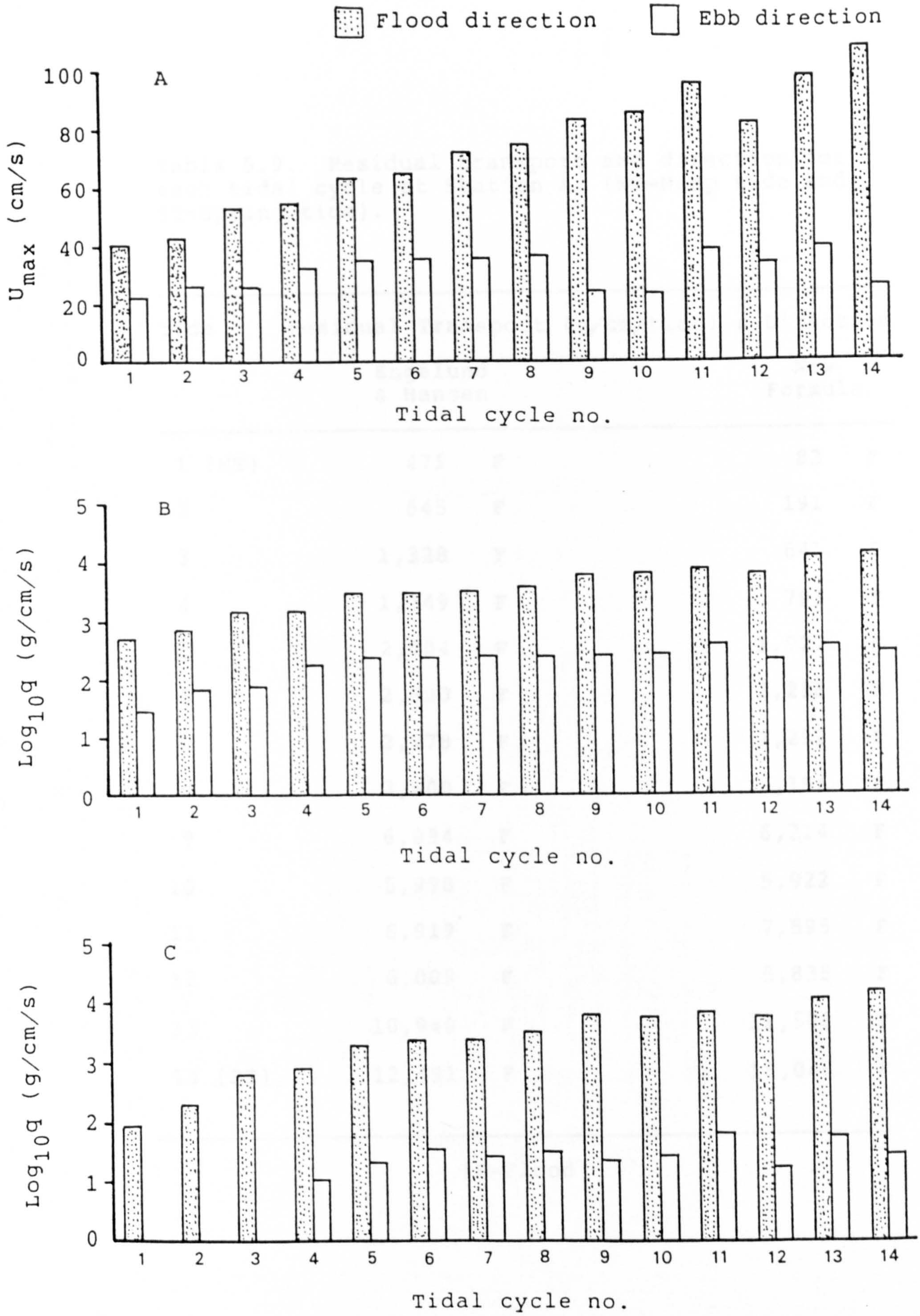

Figure 5.19. A) Variations of maximum mean flood and ebb velocities for each tide over a neap-spring period. B) Variation of sediment transport in the flood and ebb directions for each tide over a neap-spring period predicted by Engelund & Hansen formula and the New Formula (C).

Table 5.9. Residual transport and direction for each tidal cycle at Station A. (NT=Neap tide and ST=Spring tide).

Tide	Residual Transport (g/cm/tide) & Direction			
	Engelund & Hansen		New Formula	
1 (NT)	471	F	83	F
2	645	F	191	F
3	1,328	F	641	F
4	1,349	F	793	F
5	2,804	F	1,927	F
6	2,880	F	2,256	F
7	2,978	F	2,292	F
8	3,600	F	3,194	F
9	6,034	F	6,214	F
10	5,998	F	5,922	F
11	6,919	F	7,595	F
12	6,009	F	5,835	F
13	10,940	F	11,506	F
14 (ST)	12,491	F	15,046	F

(F=Flood)

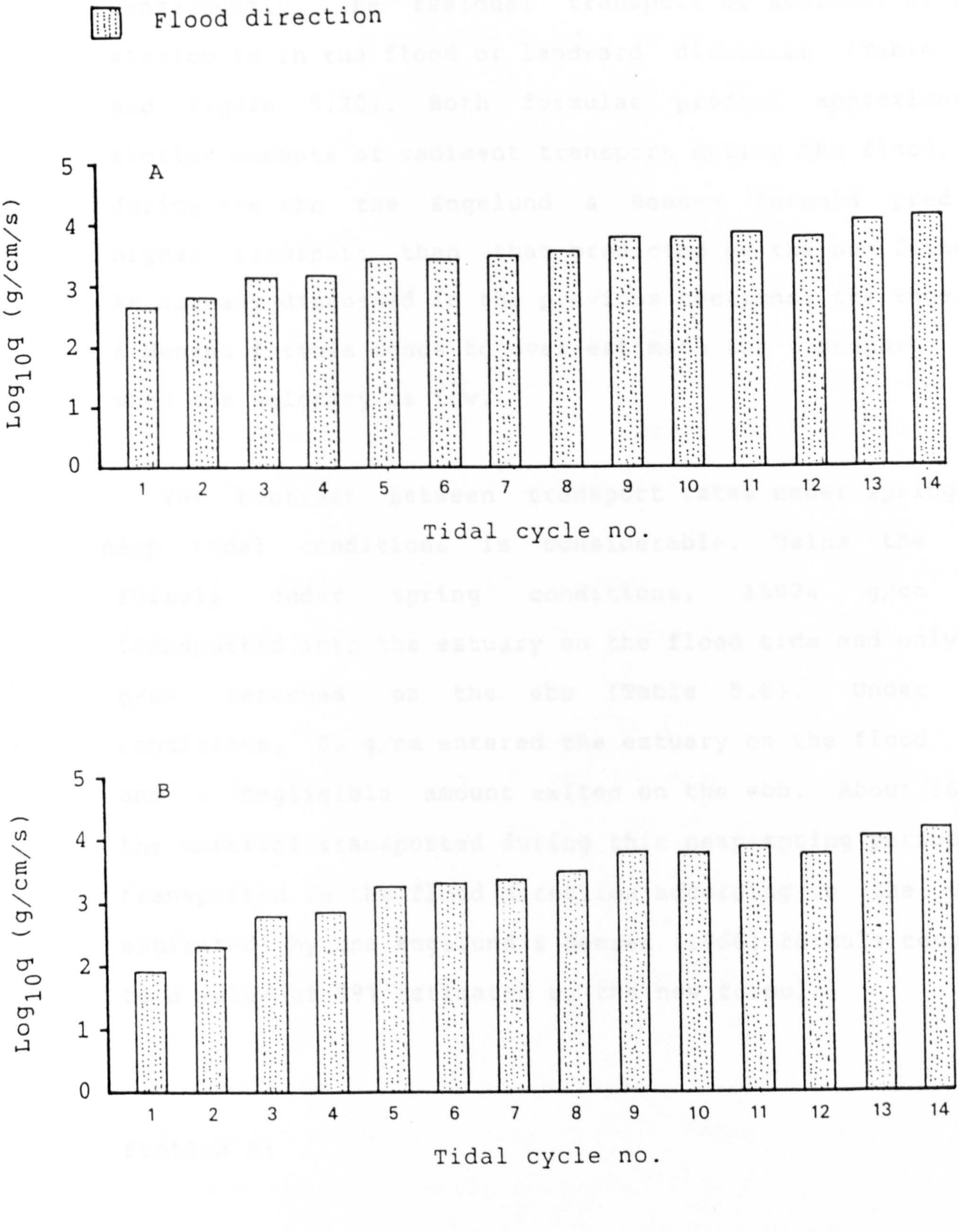

Figure 5.20. Variations of the amount of sediment transported for each tide over a neap-spring period predicted by the Engelund & Hansen formula (A) and the New Formula (B).

PAGE

MISSING

IN

ORIGINAL

Consequently, the residual transport of sediment at this station is in the flood or landward direction (Table 5.9 and Figure 5.20). Both formulae predict approximately similar amounts of sediment transport during the flood, but during the ebb the Engelund & Hansen formula predicts higher transport than that predicted by the new formula. As already discussed in the previous sections, the Engelund & Hansen formula tends to over-estimate the transport rate when the velocity is low.

The contrast between transport rates under spring and neap tidal conditions is considerable. Using the new formula under spring conditions, 15074 g/cm were transported into the estuary on the flood tide and only 28 g/cm returned on the ebb (Table 5.8). Under neap conditions, 83 g/cm entered the estuary on the flood tide and a negligible amount exited on the ebb. About 96% of the material transported during this neap-spring period was transported in the flood direction according to the value estimated by the Engelund & Hansen (1966) formula compared to a value of 99% estimated by the new formula.

Station B:

This station was occupied for six days beginning August 16 to 22,1986 on a channel bank approximately in the middle of the estuary (Figure 5.16). The sandflats around this station were covered with large sandwaves of about 16 m

length and 0.4 m height. The instruments were set up on the middle of the stoss side of a sandwave and the current meters were oriented parallel to the direction of migration of the sandwaves.

The velocity of the flood current during a neap tide reached a maximum value of 43 cm/s while the ebb velocity was less than 35 cm/s. Compared to station A, the difference between the maximum flood and maximum ebb current is smaller at station B. The duration of the flood was about 3 hours, and slightly less than 4 hours for the ebb phase, as seen in Figure 5.22. The maximum mean flood velocity during the spring tide was 105 cm/s and the maximum mean velocity for the ebb was 85 cm/s (Figure 5.21).

Asymmetry in water flows through this area produces asymmetry in sediment transport in favour of the flood direction. At this station the transport rates ranged up to 16.8 g/cm/s (Figure 5.21). The amount of material transported during the neap tide was small compared to the amount of sediment transported during the spring tide. At this station the flood transport dominates the ebb transport during all 12 tidal cycles measured. The relative amount of material transported during this neap-spring cycle is shown in Tables 5.10 and 5.11. The differences between the material transport in the flood and ebb directions were high. Under spring conditions, as

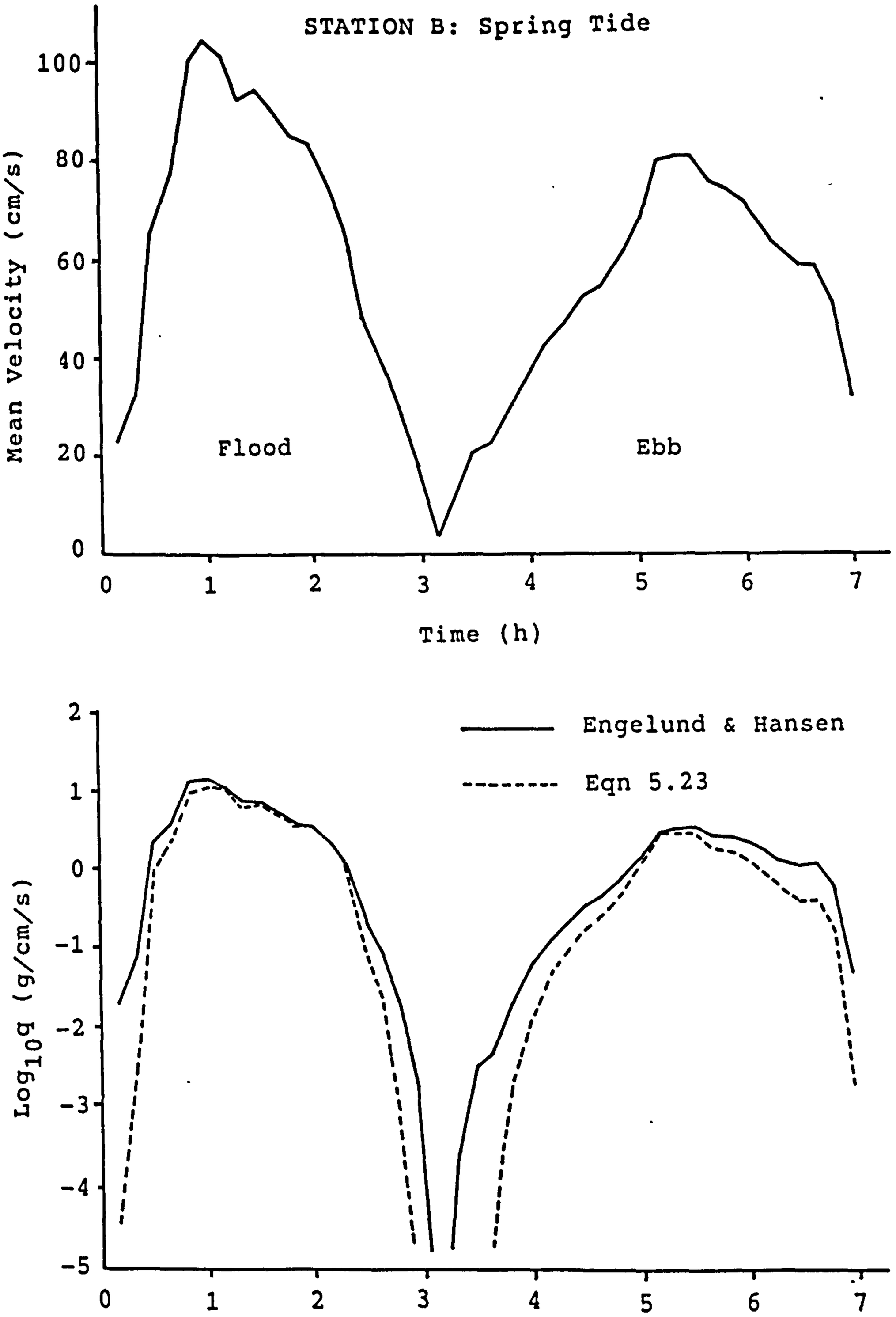

Figure 5.21. Typical spring tide velocity (A) and sediment transport curves (B) at station A over a tidal cycle predicted by Engelund & Hansen formula (————) and by the New Formula (------).

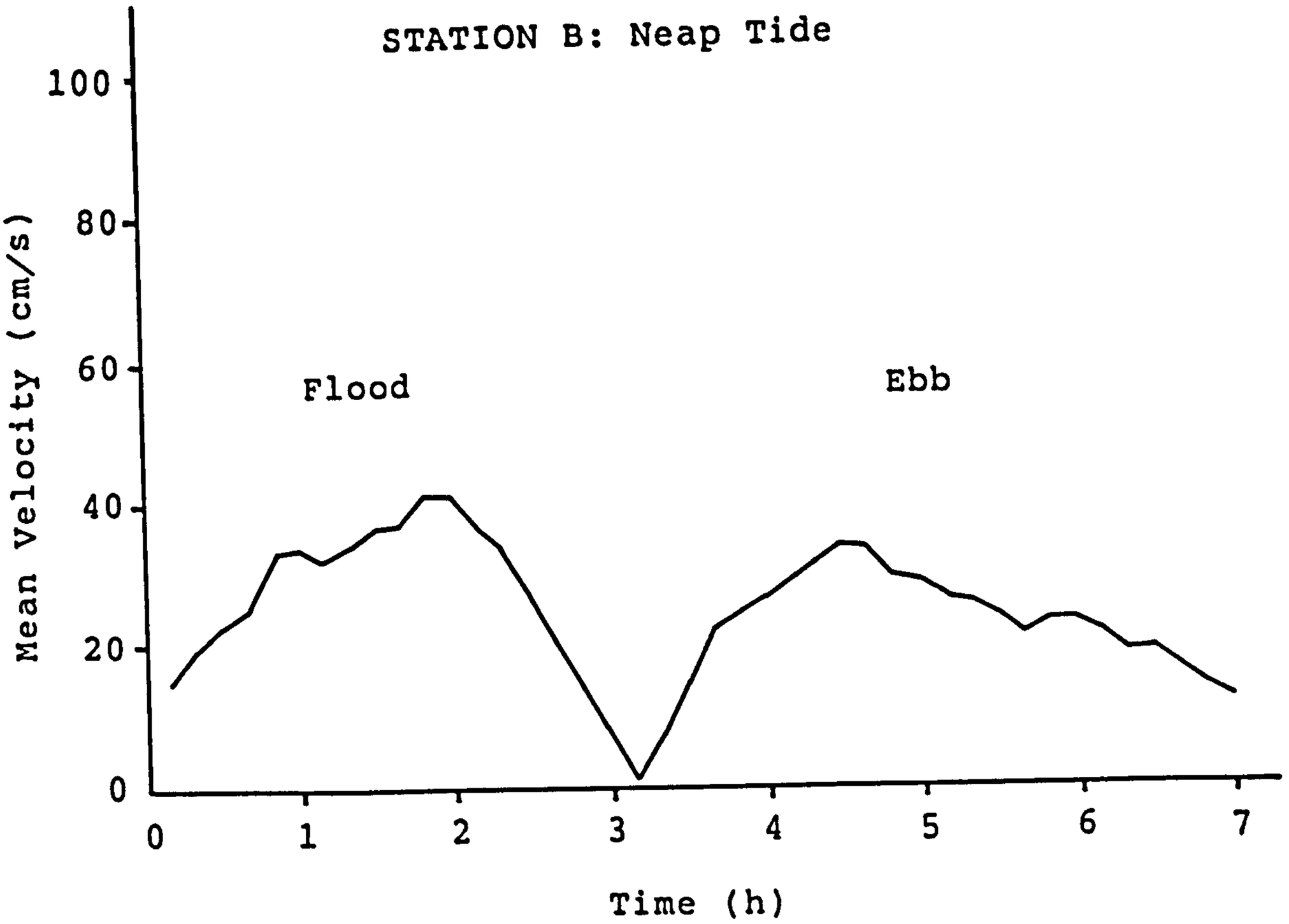

Figure 5.22. Typical neap tide velocity (A) and sediment transport curves (B) at station A over a tidal cycle predicted by Engelund & Hansen formula (————) and by the New Formula (-------).

Table 5.10. Total load computations at Station B.

Tide	Direction	Mean Velocity cm/s	Sediment Discharge, g/cm/tide	
			Engelund & Hansen	New Formula
1	Flood	41.8	542	80
	Ebb	34.2	233	12
2	Flood	48.5	869	207
	Ebb	28.7	79	1
3	Flood	66.6	3,817	1,757
	Ebb	44.0	788	141
4	Flood	83.6	7,442	4,741
	Ebb	44.6	874	184
5	Flood	95.5	22,052	14,228
	Ebb	70.8	11,651	5,065
6	Flood	97.0	20,312	14,102
	Ebb	66.0	3,798	1,666
7	Flood	99.3	38,808	26,843
	Ebb	81.4	20,056	12,881
8	Flood	95.9	29,887	22,206
	Ebb	72.9	8,294	4,932
9	Flood	108.5	54,537	44,425
	Ebb	84.6	19,831	13,275
10 (ST)	Flood	111.2	56,146	52,991
	Ebb	77.0	12,967	7,288
11	Flood	104.3	48,222	41,536
	Ebb	80.9	18,143	11,697
12	Flood	90.3	25,564	20,724
	Ebb	70.9	9,185	4,880
Total	Flood		308,198 (74%)	243,840 (80%)
	Ebb		105,899 (26%)	62,022 (20%)

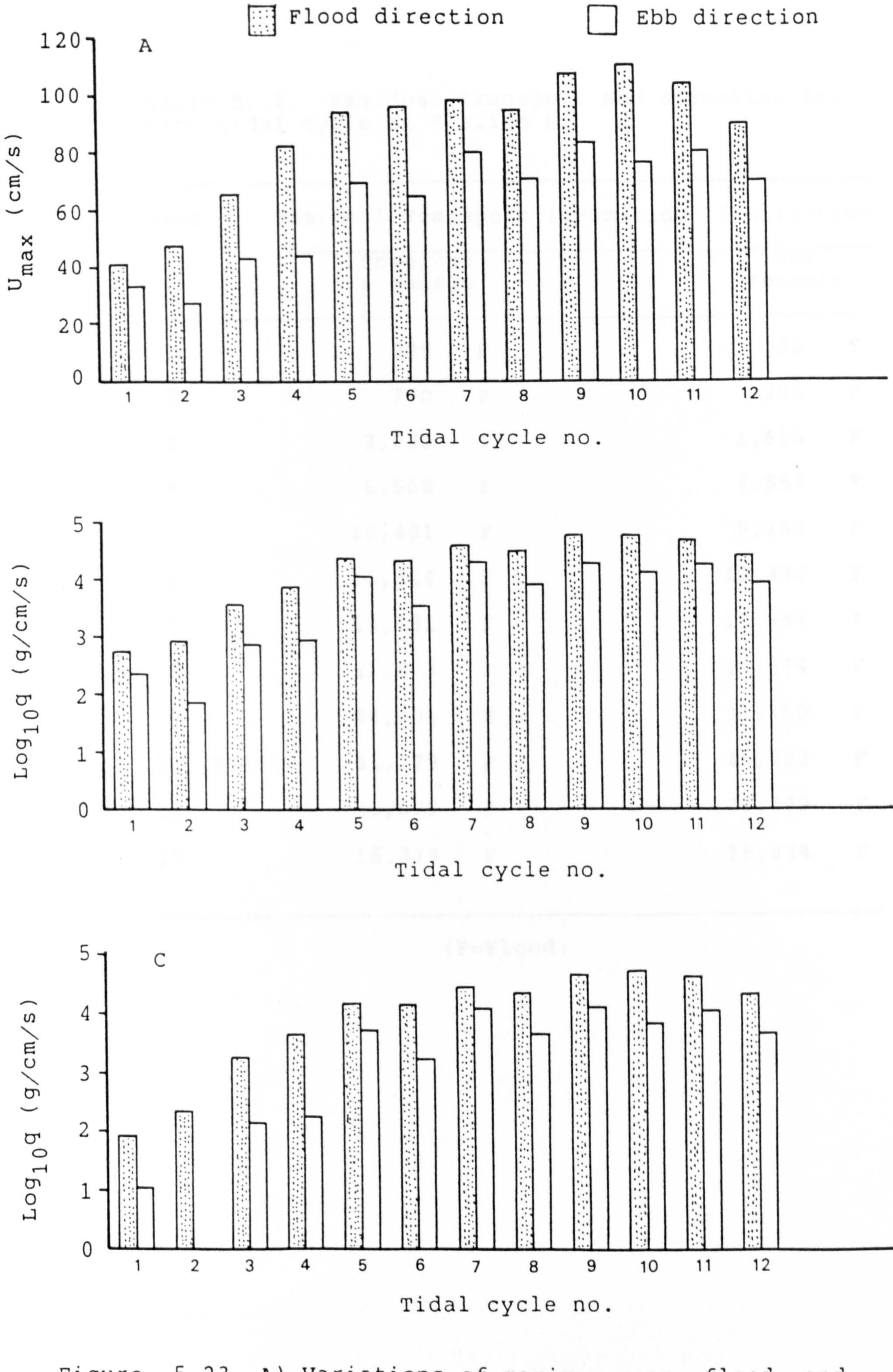

Figure 5.23. A) Variations of maximum mean flood and ebb velocities for each tide over a neap-spring period. B) Variation of sediment transport in the flood and ebb directions for each tide over a neap-spring period predicted by Engelund & Hansen formula and the New Formula (C).

Table 5.11. Residual transport and direction for each tidal cycle at Station B.

Tide	Residual Transport (g/cm/tide) & Direction			
	Engelund & Hansen		New Formula	
1	309	F	68	F
2	790	F	206	F
3	3,089	F	1,616	F
4	6,568	F	4,557	F
5	10,401	F	9,163	F
6	16,514	F	12,436	F
7	18,752	F	13,962	F
8	21,593	F	17,274	F
9	24,906	F	31,150	F
10 (ST)	43,179	F	45,703	F
11	30,079	F	29,839	F
12	16,379	F	15,844	F

(F=Flood)

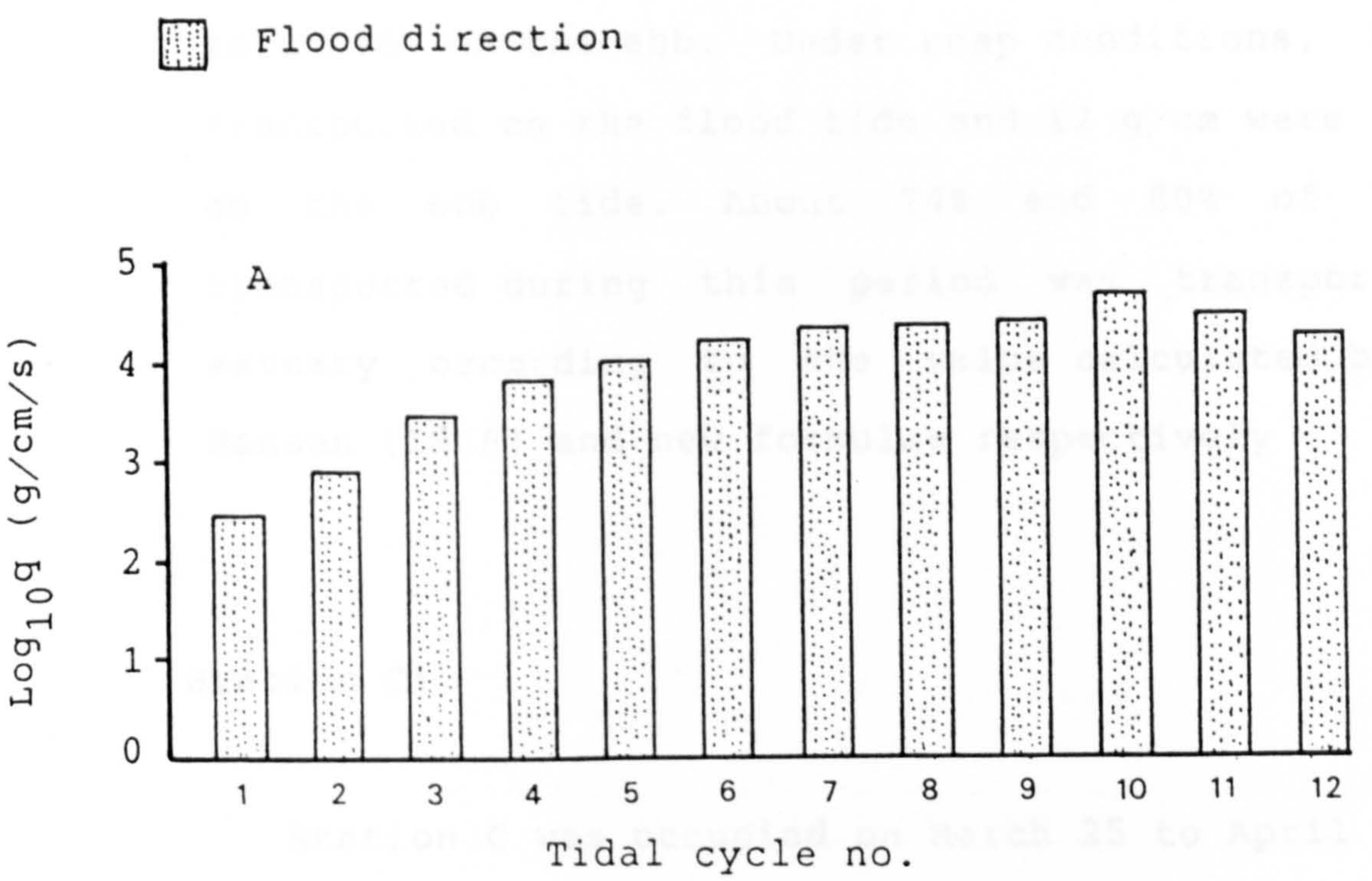

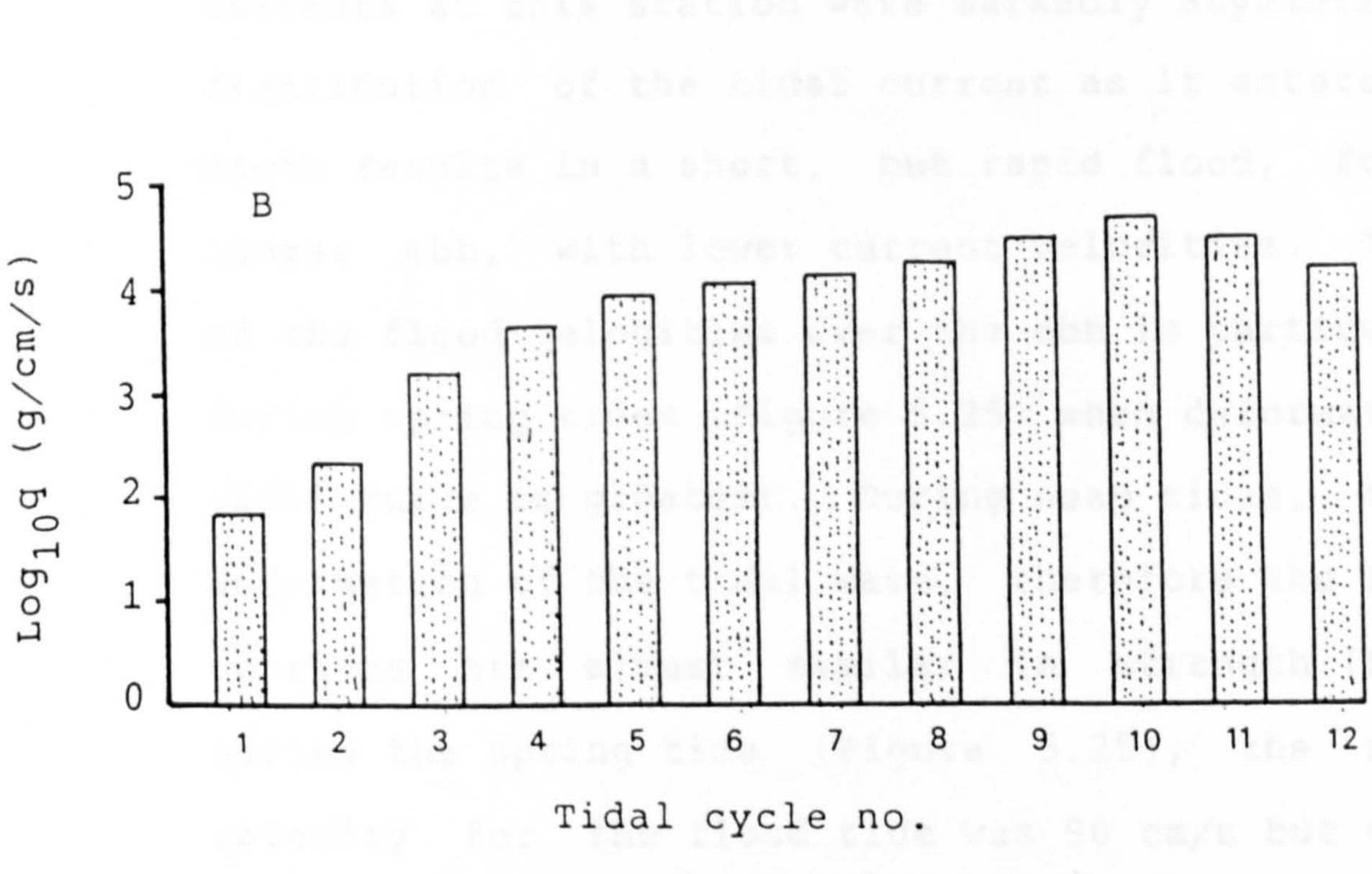

Figure 5.24. Variations of the amount of sediment transported for each tide over a neap-spring period predicted by the Engelund & Hansen formula (A) and the New Formula (B).

estimated using the new formulae, 52,991 g/cm were transported landward on the flood tide and 7,288 g/cm returned on the ebb. Under neap conditions, 80 g/cm were transported on the flood tide and 12 g/cm were transported on the ebb tide. About 74% and 80% of the material transported during this period was transported up the estuary occording to the value calculated by Engelund & Hansen (1966) and new formulae respectively .

Station C:

Station C was occupied on March 25 to April 2, 1986 for 15 tidal cycles. The spring tides occured on March 24 and 25, followed by neap tides on April 1 and 2. Tidal currents at this station were markedly asymmetrical,and the distribution of the tidal current as it enters the estuary mouth results in a short, but rapid flood, followed by a longer ebb, with lower current velocities. The dominance of the flood velocities over the ebb is particularly marked during spring tides (Figure 5.25) when deformation of the tidal curve is greatest. During neap tides, there is less deformation of the tidal wave, therefore the flood and ebb currents are almost similar in strength (Figure 5.26). During the spring tide (Figure 5.25), the maximum mean velocity for the flood tide was 90 cm/s but was lower for the ebb tide, being 60 cm/s. The maximum mean velocities during the neap tide (Figure 5.26) were almost similar for flood and ebb with velocities of 40 cm/s.

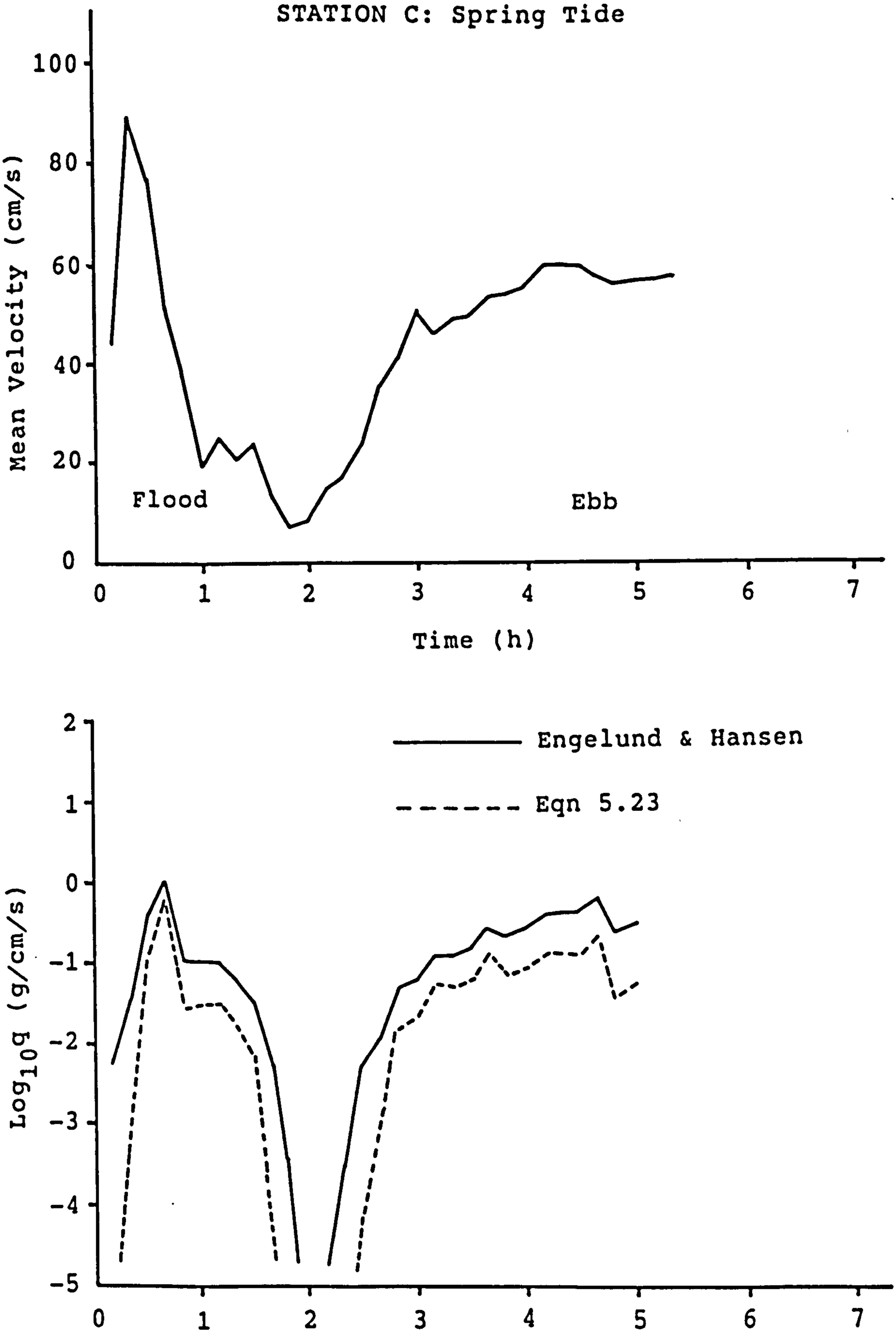

Figure 5.25. Typical spring tide velocity (A) and sediment transport curves (B) at station A over a tidal cycle predicted by Engelund & Hansen formula (————) and by the New Formula (- - - - -).

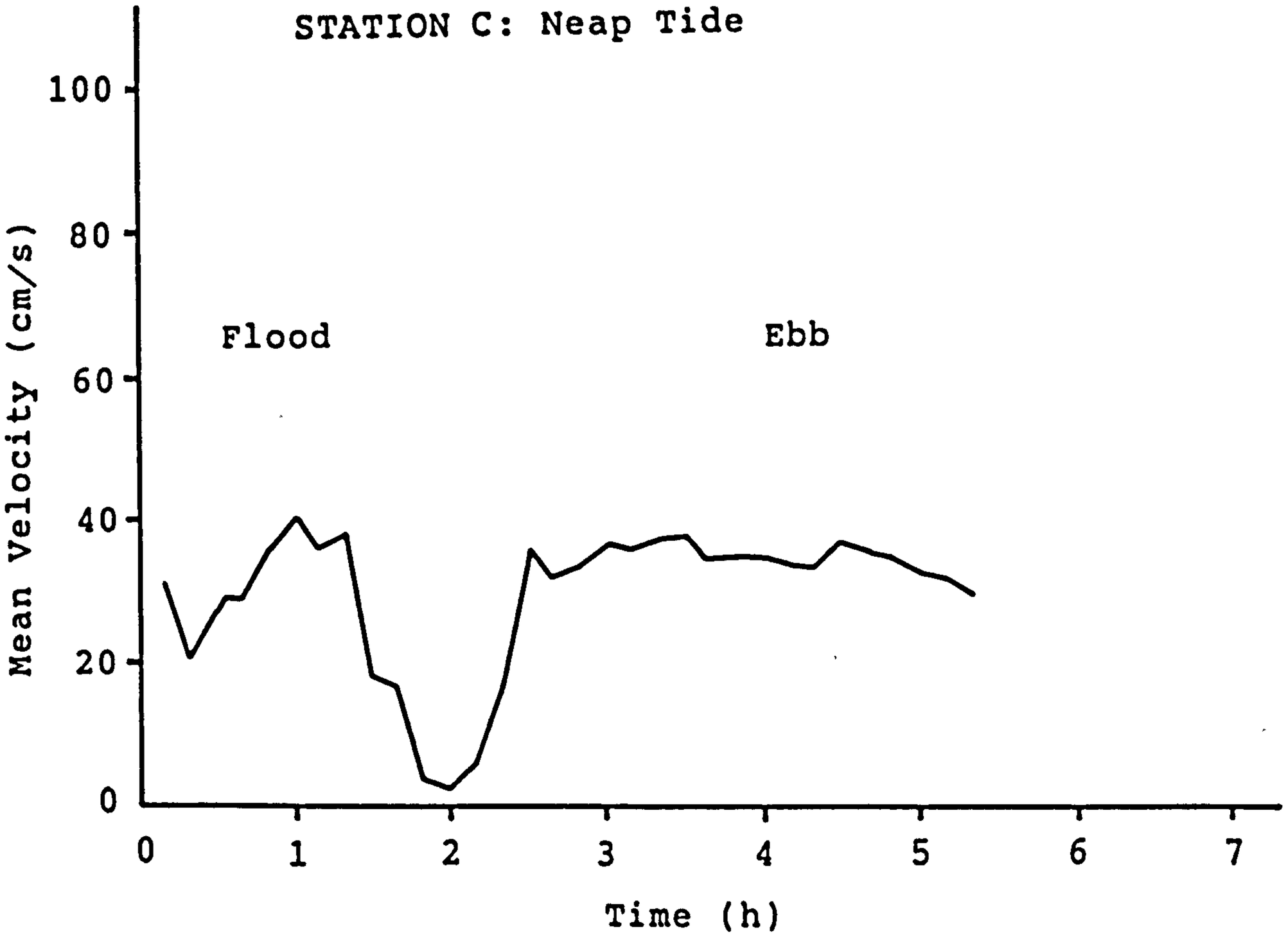

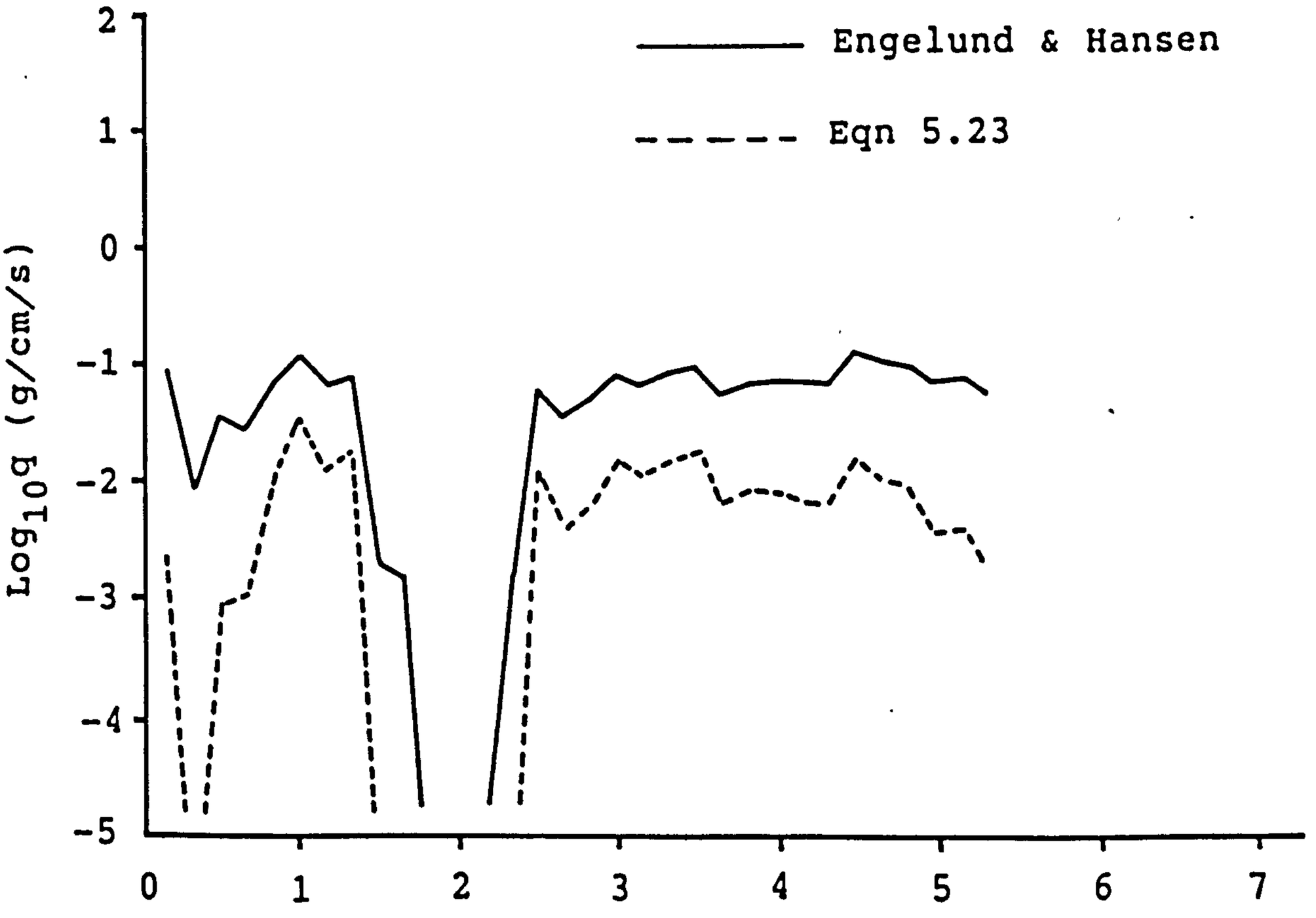

Figure 5.26. Typical neap tide velocity (A) and sediment transport curves (B) at station A over a tidal cycle predicted by Engelund & Hansen formula (————) and by the New Formula (- - - - -).

Table 5.12. Total load computations at Station C.

Tide	Direction	Mean Velocity cm/s	Sediment Discharge, g/cm/tide	
			Engelund & Hansen	New Formula
1	Flood	62.8	1,170	548
	Ebb	53.0	2,356	751
2	Flood	72.7	6,628	3,497
	Ebb	61.5	6,312	4,695
3	Flood	89.3	7,150	4,869
	Ebb	60.4	8,041	3,417
4 (ST)	Flood	93.4	7,029	5,312
	Ebb	64.7	9,263	4,654
5	Flood	86.9	8,379	5,625
	Ebb	62.7	6,969	3,199
6	Flood	65.7	2,757	1,113
	Ebb	63.4	7,798	4,137
7	Flood	79.0	3,338	2,247
	Ebb	62.5	6,318	3,148
8	Flood	91.4	7,167	5,338
	Ebb	56.3	4,719	2,008
9	Flood	67.8	2,594	1,320
	Ebb	50.0	2,200	886
10	Flood	80.0	3,255	2,382
	Ebb	47.6	1,992	481
11	Flood	77.0	3,084	1,843
	Ebb	56.2	2,557	528
12	Flood	41.9	277	35
	Ebb	41.4	1,217	190
13	Flood	41.6	315	50
	Ebb	38.7	855	158
14	Flood	16.4	5	0
	Ebb	29.0	92	2
15	Flood	18.2	5	0
	Ebb	29.2	112	1
Total	Flood		53,153 (47%)	34,175 (56%)
	Ebb		60,801 (53%)	26,391 (44%)

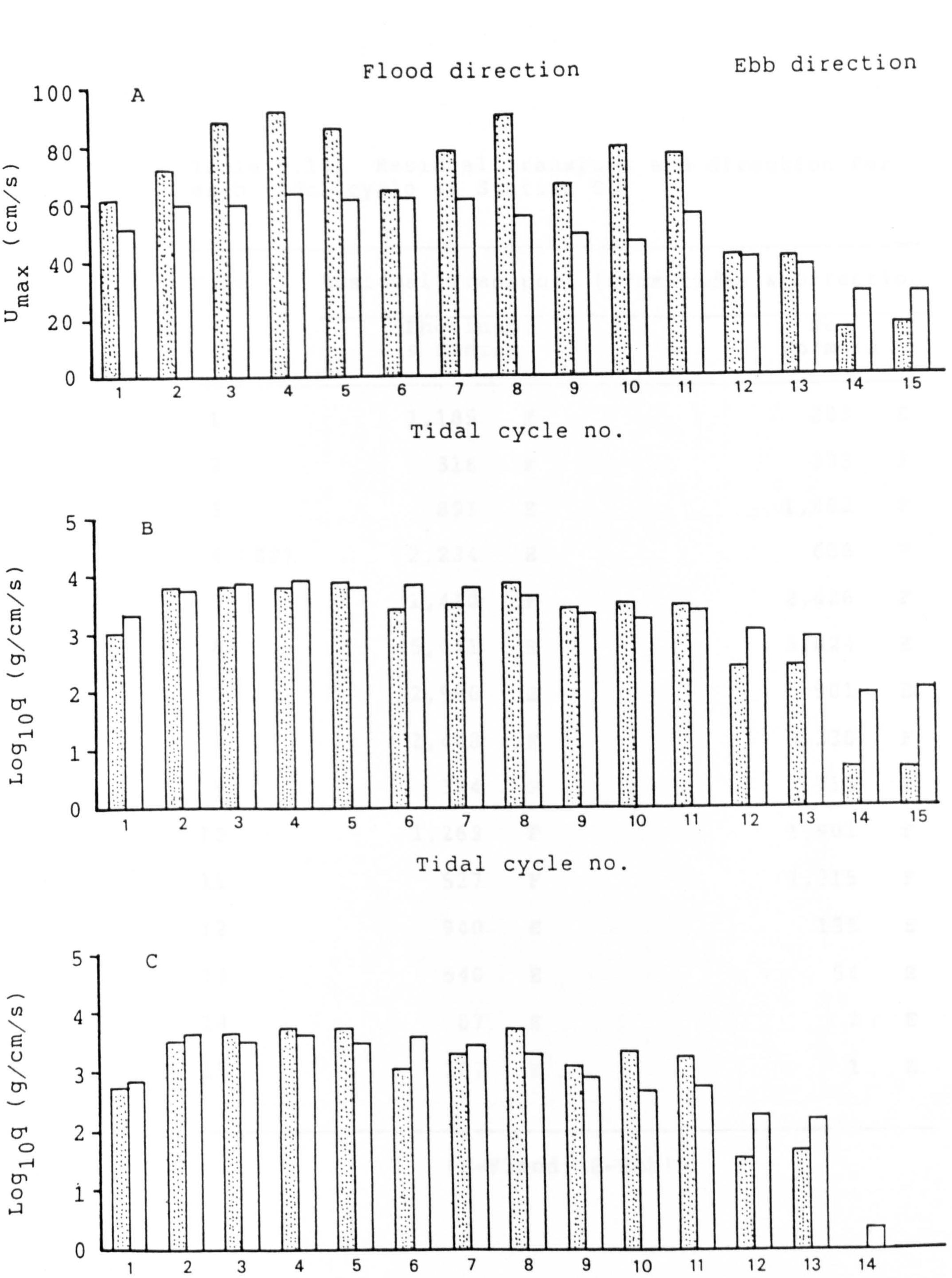

Figure 5.27. A) Variations of maximum mean flood and ebb velocities for each tide over a neap-spring period. B) Variation of sediment transport in the flood and ebb directions for each tide over a neap-spring period predicted by Engelund & Hansen formula and the New Formula (C).

Table 5.13. Residual transport and direction for each tidal cycle at Station C.

Tide	Residual Transport (g/cm/tide) & Direction			
	Engelund & Hansen		New Formula	
1	1,185	E	203	E
2	316	F	333	F
3	891	E	1,452	F
4 (ST)	2,234	E	658	F
5	1,410	F	2,426	F
6	5,041	E	3,024	E
7	2,980	E	901	E
8	2,448	F	3,330	F
9	394	F	713	F
10	1,263	F	1,901	F
11	527	F	1,315	F
12	940	E	155	E
13	540	E	54	E
14	87	E	2	E
15	107	E	1	E

(F=Flood, E=Ebb)

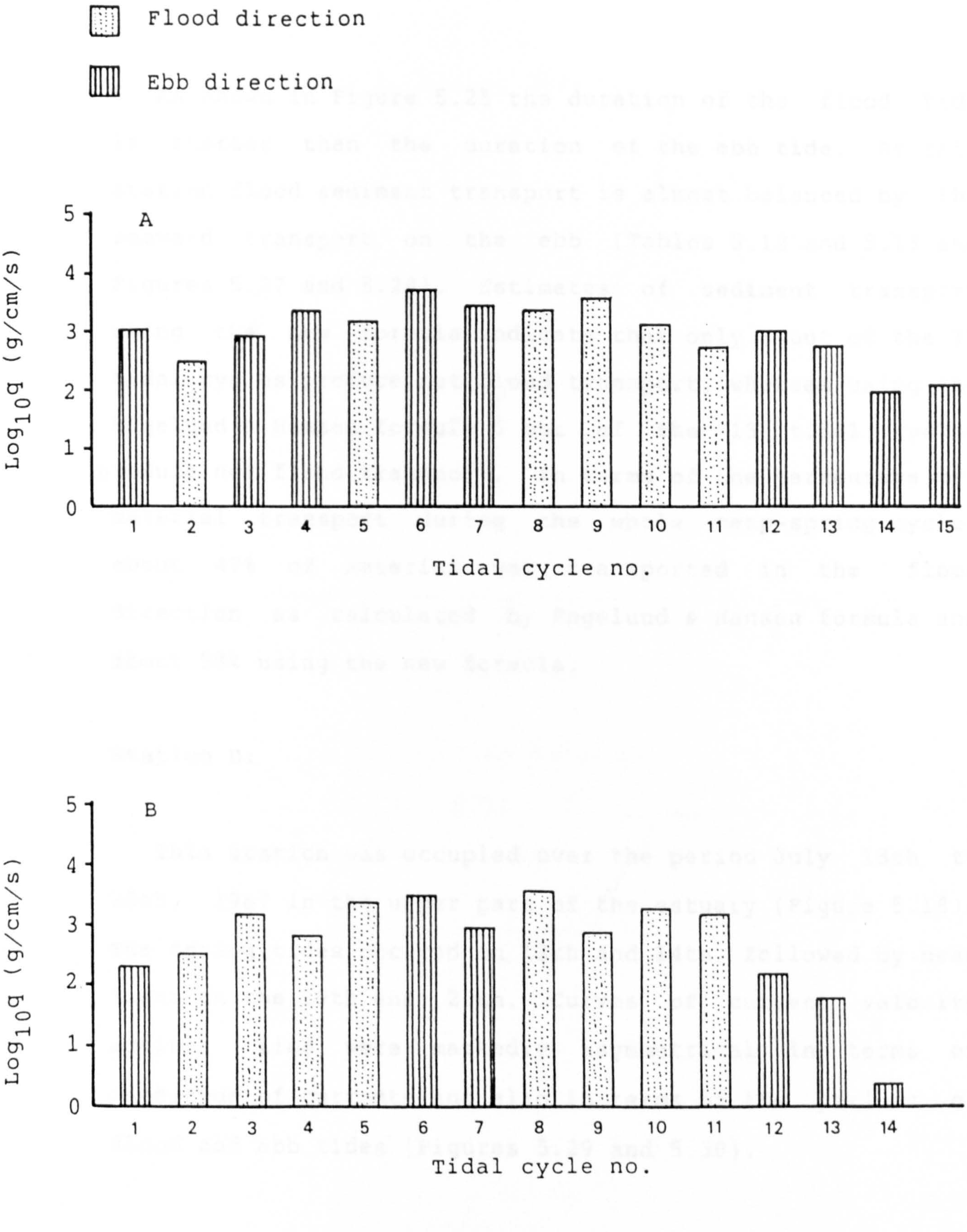

Figure 5.28. Variations of the amount of sediment transported for each tide over a neap-spring period predicted by the Engelund & Hansen formula (A) and the New Formula (B).

As shown in Figure 5.25 the duration of the flood tide is shorter than the duration of the ebb tide. At this station flood sediment transport is almost balanced by the seaward transport on the ebb (Tables 5.12 and 5.13 and Figures 5.27 and 5.28). Estimates of sediment transport using the new formula indicate that only 8 out of the 15 tidal cycles produce net flood transport, whereas using the Engelund & Hansen formula 6 out of the 15 tidal cycles produce net flood transport. In terms of the percentage of material transport during the whole neap-spring cycle, about 47% of material was transported in the flood direction as calculated by Engelund & Hansen formula and about 58% using the new formula.

Station D:

This station was occupied over the period July 13th to 20th, 1987 in the upper part of the estuary (Figure 5.16). The spring tides occured on 13th and 14th, followed by neap tides on the 19th and 20th. Curves of current velocity against time were markedly asymmetrical in terms of magnitude of currents and also in terms of the periods of flood and ebb tides (Figures 5.29 and 5.30).

During the spring tide (Figure 5.29), the mean velocity of the flood current rapidly reached a maximum value of 100 cm/s, then dropped rapidly to zero in just over 2 hours;the

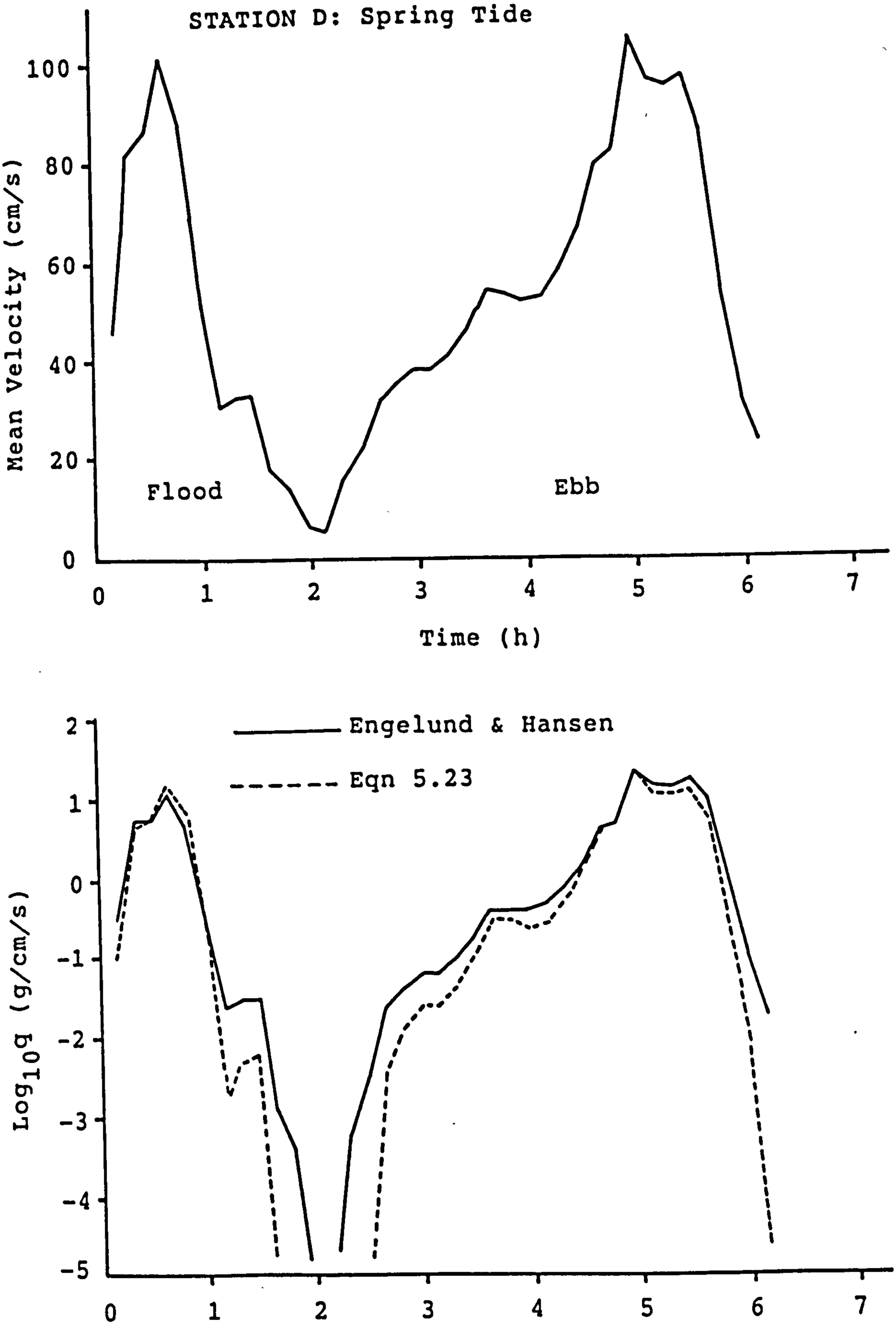

Figure 5.29. Typical spring tide velocity (A) and sediment transport curves (B) at station A over a tidal cycle predicted by Engelund & Hansen formula (———) and by the New Formula (- - - -).

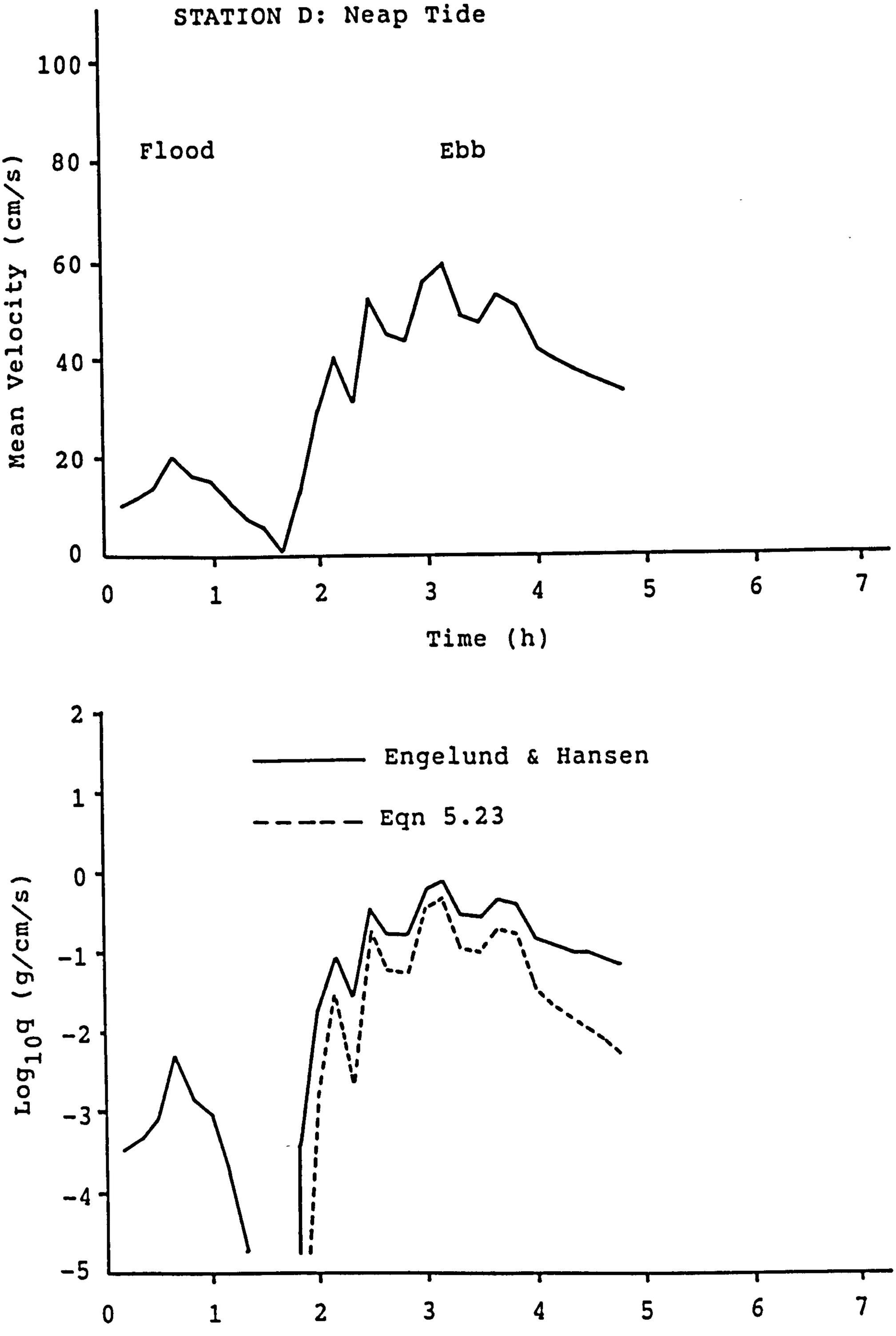

Figure 5.30. Typical neap tide velocity (A) and sediment transport curves (B) at station A over a tidal cycle predicted by Engelund & Hansen formula (———) and by the New Formula (- - - -).

Table 5.14. Total load computations at station D

Tide	Direction	Mean Velocity cm/s	Sediment Discharge, g/cm/tide	
			Engelund & Hansen	New Formula
1 (ST)	Flood	101.1	12,795	14,535
	Ebb	105.0	39,133	31,590
2	Flood	62.5	1,890	1,204
	Ebb	75.8	4,767	3,866
3	Flood	87.5	7,905	7,023
	Ebb	100.5	30,622	17,835
4	Flood	56.9	909	545
	Ebb	60.1	2,924	1,594
5	Flood	83.3	5,574	4,766
	Ebb	82.4	17,211	8,285
6	Flood	29.4	29	1
	Ebb	54.7	1,512	608
7	Flood	63.4	1,088	621
	Ebb	66.0	4,471	2,497
8	Flood	19.2	4	0
	Ebb	52.8	1,388	445
9	Flood	31.7	35	2
	Ebb	52.2	1,161	342
10	Flood	20.4	6	0
	Ebb	40.9	711	99
11	Flood	20.8	5	0
	Ebb	59.9	2,528	1,127
12	Flood	-	-	-
	Ebb	-	-	-
13	Flood	11.5	0	0
	Ebb	28.7	118	2
Total	Flood		30,240 (22%)	28,697 (30%)
	Ebb		106,546 (78%)	68,290 (70%)

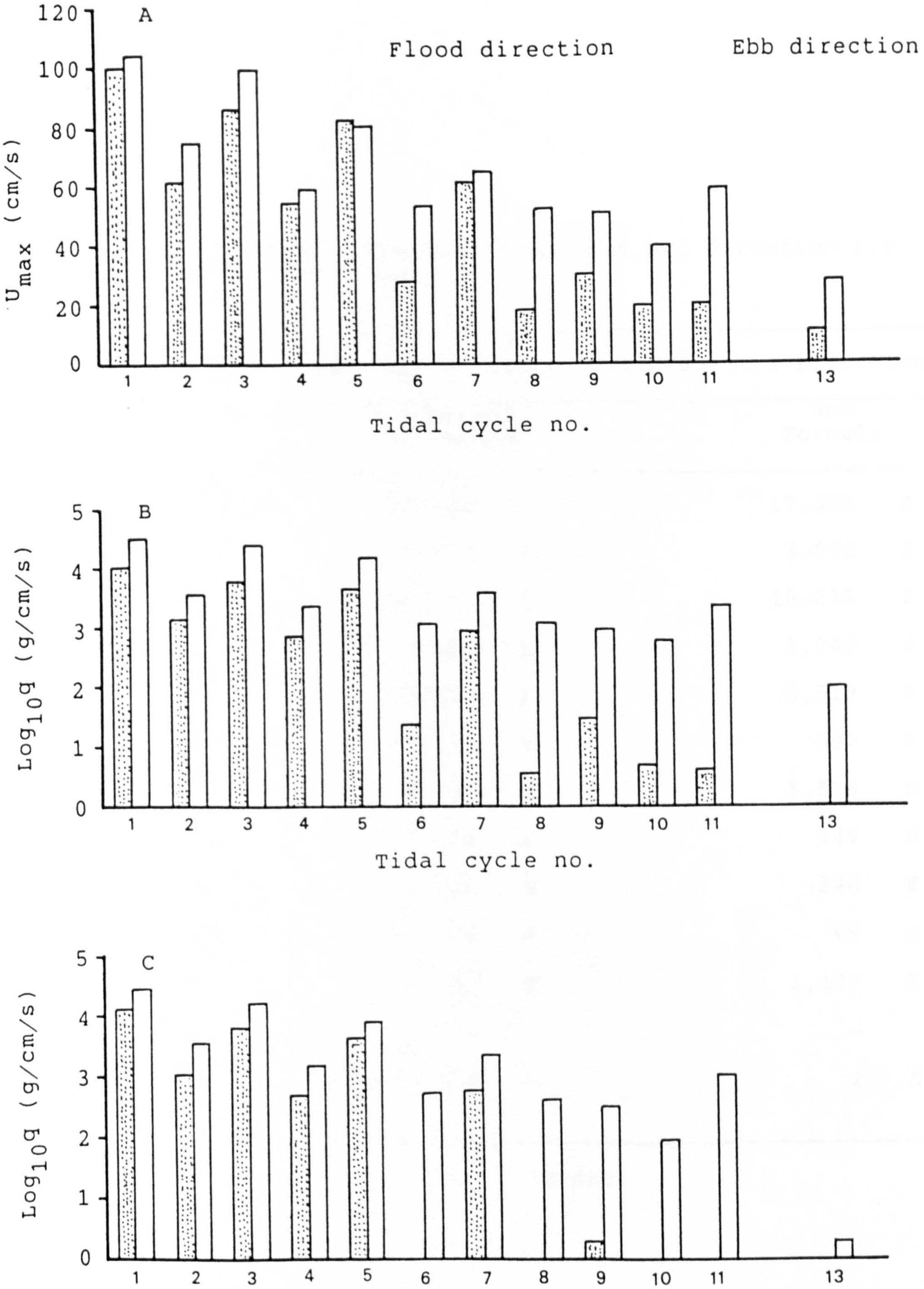

Figure 5.31. A) Variations of maximum mean flood and ebb velocities for each tide over a neap-spring period. B) Variation of sediment transport in the flood and ebb directions for each tide over a neap-spring period predicted by Engelund & Hansen formula and the New Formula (C).

Table 5.15. Residual transport and direction for each tidal cycle.

Tide	Residual Transport(g/cm/tide) & Direction			
	Engelund & Hansen		New Formula	
1 (ST)	26,338	E	17,055	E
2	2,877	E	2,662	E
3	22,717	E	10,812	E
4	2,015	E	1,049	E
5	11,637	E	3,519	E
6	1,483	E	607	E
7	3,384	E	1,876	E
8	1,384	E	445	E
9	1,126	E	340	E
10	705	E	99	E
11	2,523	E	1,127	E
12	-		-	
13	118	E	2	E

(E=Ebb)

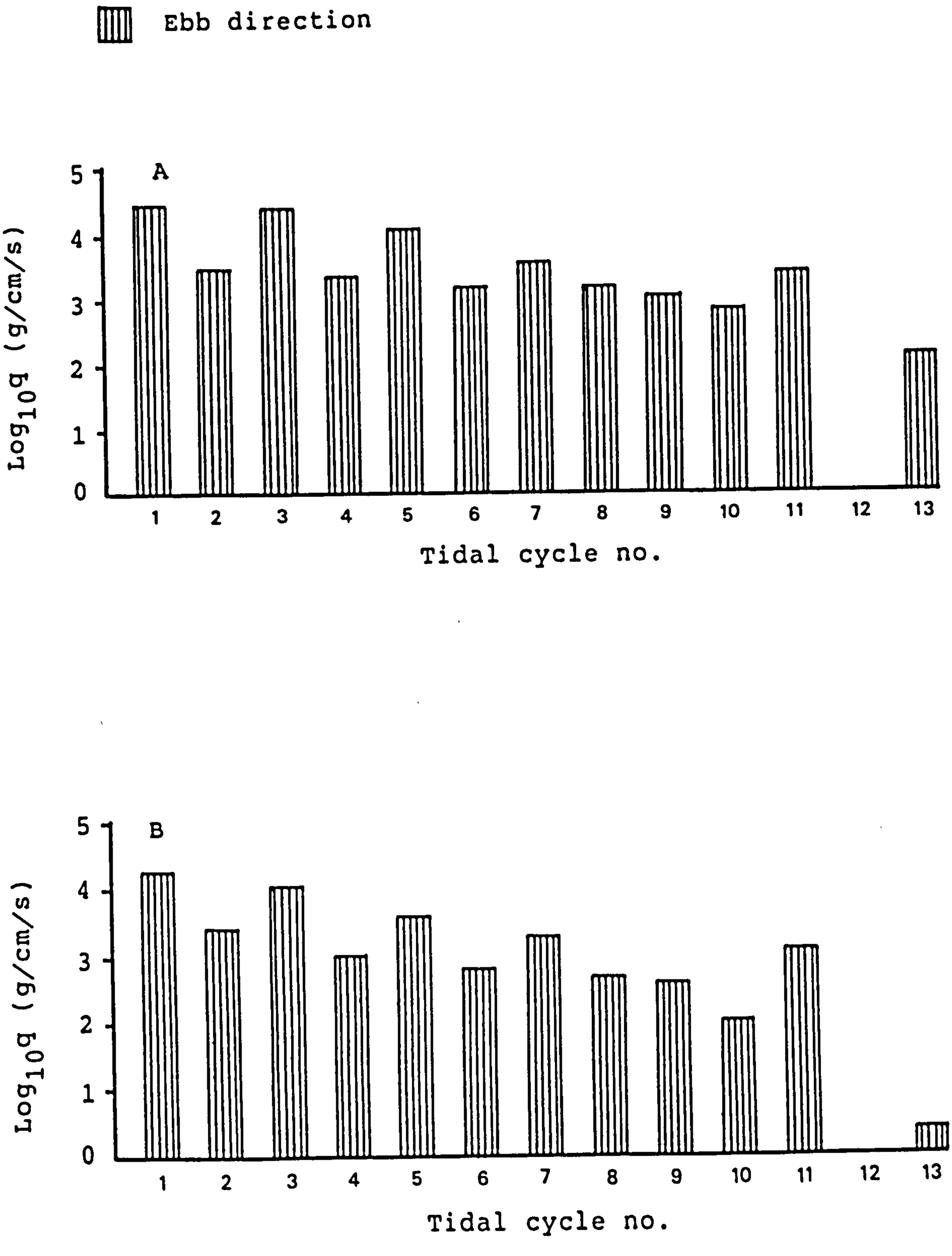

Figure 5.32. Variations of the amount of sediment transported for each tide over a neap-spring period predicted by the Engelund & Hansen formula (A) and the New Formula (B).

ebb tide then increased slowly to 100 cm/s. The dominance of ebb velocities was particularly marked during the neap tide when the maximum depth mean velocity of the neap current was 60 cm/s i.e three times larger than maximum mean velocity of the flood tide which reached 20 cm/s (Figure 5.30). With the reduction of flow after spring tides, the influence of the flood tide on sediment transport reduced rapidly, and as a result the dominant ebb tide transported most of the sediment in the ebb direction (Tables 5.14 and 5.15).

Figures 5.29 and 5.30 show that the maximum transport rates at this station occurred during the ebb tides on both spring and neap conditions in contrast with the other three stations closer to the estuary mouth. Since the duration of the ebb tide is longer than the flood tide, it is very obvious that at this station the net sediment transport was in the ebb direction for every tidal cycle (Table 5.15 and Figure 5.32). Under spring conditions, as estimated using the new formula, 14,535 g/cm were transported upstream on the flood tide and 31,590 g/cm were transported downstream on the ebb tide. Under neap conditions, the amounts of sediment transported on both flood and ebb tides were negligible. Engelund & Hansen's formula predicts 22% of the total load transported in the flood direction, while the new formula predicts 30%. In terms of the quantity of material transport, there is a close agreement between the value predicted by the Engelund & Hansen and the new formulae as shown in Table 5.15.

5.4.2 Discussion

Sands found in this estuary are so fine grained that they are not carried along the bed but instead are swept up into the flow by the upward component of the turbulent eddies within the lower boundary layer and are held there in suspension (Dyer,1986). Sediment transport and the resulting sedimentation patterns in this estuary are probably due to the complex interaction of currents and waves. However, the influence of waves on sediment transport was ignored due to the inability of the recording system to monitor wave activities. The neglect of wave activity, probably does not invalidate the order of magnitude of transport rate calculations reported in this study. Waves are probably of importance at the estuary mouth only.

Difficulties may arise in the application of transport rate formulae to tidal environments due to uncertainties of the values of the various parameters involved in the calculation. These may include the current velocity, the critical velocity for sediment movement, the mean grain size, the flow depth, the bed roughness and the sediment and water densities. In this study only current velocities were monitored continuously during the period of deployment of current meters, while the rest of parameters were

assumed to be constant.

The most obvious observation which has been made from the study of sediment transport in this estuary is the considerable variation in values when comparing the flood or ebb of a spring or neap tide. Strong tidal currents recorded in this estuary resulted in intense sediment transport. Transport rates ranging up to 20 g/cm/s have been measured for current velocities up to 120 cm/s. Peak current velocities of 100 cm/s are not uncommon in this study area. Residual sediment transport depends on differences in magnitude and duration between flood and ebb tidal currents. Such differences, i.e. tidal asymmetry, are produced by the distortion of the tidal wave propagating in the estuary due to high friction by this shallow estuary and offshore area on tidal currents. This tidal asymmetry produces asymmetry in sediment transport rates.

Across the estuary, sediment transport rates are probably highly variable. Transport is probably higher in the areas where the current is strong, that is in the main channel and on intertidal flats adjacent to the channel. Transport is probably low on higher flats far away from the main channel.

One interesting feature of sediment transport in the estuary is the relatively strong landward transport in the lower and middle sections of the estuary. The dominance of

the strong flood current is reflected in the size of bedforms on the sandflats which are commonly covered by megaripples and sandwaves (chapter 2). Intense sediment movement in the flood direction nourishes intertidal flats. Considerable variations in the intertidal flat profiles have been measured as shown in Figures 5.34 to 5.38. The upper section of the estuary shows a dominance of ebb flow. Also the ebb tide duration exceeds the flood tide duration by approximately 8 hours, which would again mean that more sediment would be transported during the ebb. At the middle section of the estuary where the currents are equal but in opposite directions, large quantities of material may be moved landward and seaward but there will be no preferential direction.

This estuary is subjected to ebb flow conditions for a longer period of time than to the flood flow conditions. At first this appears to favour net seaward sediment transport. However, the capacity of a channel to transport sediment is related in part to the estuary cross-sectional area which in turn is related to channel water level. Because the water level in this estuary is very low during much of the excess ebb flow time, ebb transport capacity will be greatly reduced for much of the ebb duration. The lack of a well-developed ebb tidal delta at the mouth of the estuary is evidence that the amount of sediment transported out of the estuary is small compared with the amount of sediment transported into the estuary by the

flood currents.

Estimating a budget for the sediment input is very difficult, as the measurements were conducted at four locations only. Assuming that the transport rates are representative of the area on either side of the stations, a crude estimate of the amount of sediment transported into the estuary can be made. Near the mouth, about 450 kg/m/tide were transported into the estuary on the flood tide and 2.6 kg/m/tide were transported seaward on the ebb. Assuming that the width and surface area of the estuary were 1 km and 8.0 km respectively, the amount of sediment deposited in the estuary is about 1.62×10^{11} g/year or in terms of unit area, it is about 2.2 g/cm^2/year. Assuming a porosity of 0.40 and a grain density of 2.65 g/cm^3, this represents a deposition rate of 1.38 cm/year. The actual magnitude of sediment deposited in the estuary is probably smaller than this estimated value. A recent study on intertidal sedimentation rates in the Bury inlet, South Wales by Carling (1981) found that the average deposition rate was 5.5 cm/year, that is twice the value estimated in this study.

5.5 Changes of estuarine topography

In the preceeding section, it was shown that a large amount of sediment has been transported into the estuary from offshore. Six profiles, running perpendicular to the

estuarine axis (Figure 5.33) were surveyed for about a year beginning from April 1986 to March 1987. Steel poles, firmly erected into the stable area of the marsh were used as reference points for each profiles. For transect 1 to 3, steel poles were set up on both sides of the channel close to the estuarine margin, so that all surveys of the transects were between two fixed points where the accuracy of the surveys could be checked. In the case of transects 4 to 6, the transects were terminated at the edge of low-water channel since the depth and the width of the water prevented further extension of the transects to the other side of the channel. In such cases, the surveys were not checked by completing a closed loop and therefore the profiles are possibly subject to error. Surveys were carried out at varying intervals during the study period; in all, the profiles were surveyed four or five times.

The profiles were surveyed with an engineer's level and leveling rod. Along a transect, elevational readings were taken at intervals of about 50 m unless a visible change in transect topography was present at which place the interval was decreased so as to include the feature. The survey programme, however did not progress smoothly as planned due to shortage of manpower and on a few occasions, bad weather prevented field work. Therefore, data from these surveys is far from complete and could not hope to establish any long-term trends of sediment accumulation. However, an attempt has been made to relate changes in estuarine

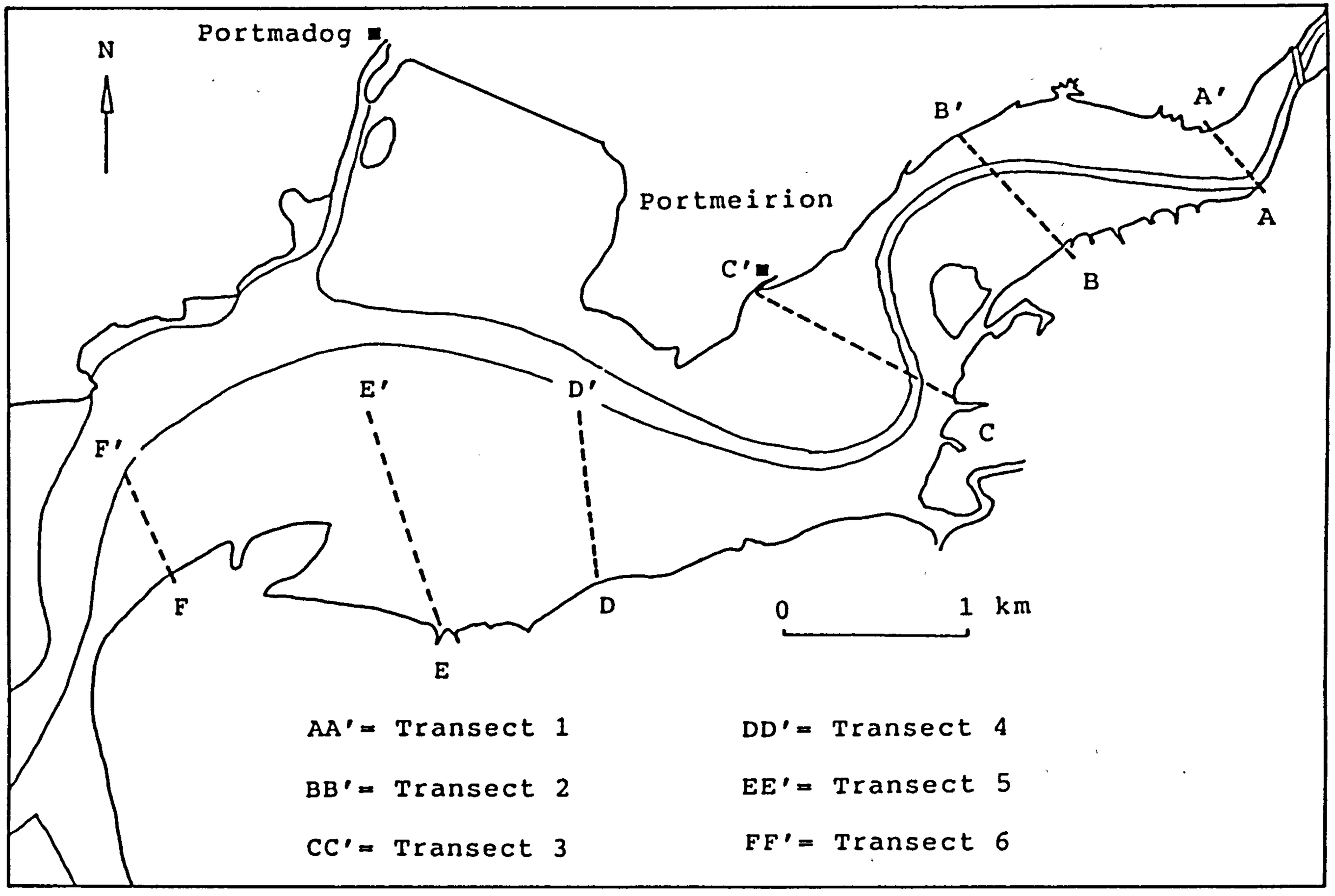

Figure 5.33. Position of Transects 1 to 6.

topography to the changes of energy level along each transect. The profile changes during the period of the surveys are shown in Figures 5.34 to 5.38.

The volume of sediment eroded and eccreted across the estuary between two successive survey dates have been calculated for each transect and are shown in Figures 5.39 to 5.43. The amounts of erosion and accretion were expressed in terms of the bottom elevation change along the transects. The volume of sediment which is eroded or accreted from each transect as obtained from comparison of the profiles of two successive surveys are listed in Table 5.16. It seems that the volume of sediment eroded or deposited during the survey period varied considerably for all six transects.

Table 5.16 shows that volumes of sediment accreted exceed the volumes of sediment eroded from the lower (transects 5 and 6) and upper estuary (transects 1 and 2), while the opposite is true for the middle estuary (transect 3 and 4). As shown in Figures 5.41 to 5.43 the changes of topography for transects 4 to 6 were considerable on intertidal flats adjacent to the main channel, but the stability of the profiles appears to increase with increasing distance from the main channel, since the amount of sediment eroded was small and seems to be matched by the amount of sediment accreted. Figures 5.36 to 5.38 show no obvious change of topography in this area compared to the area close to the main channel. The channels themselves

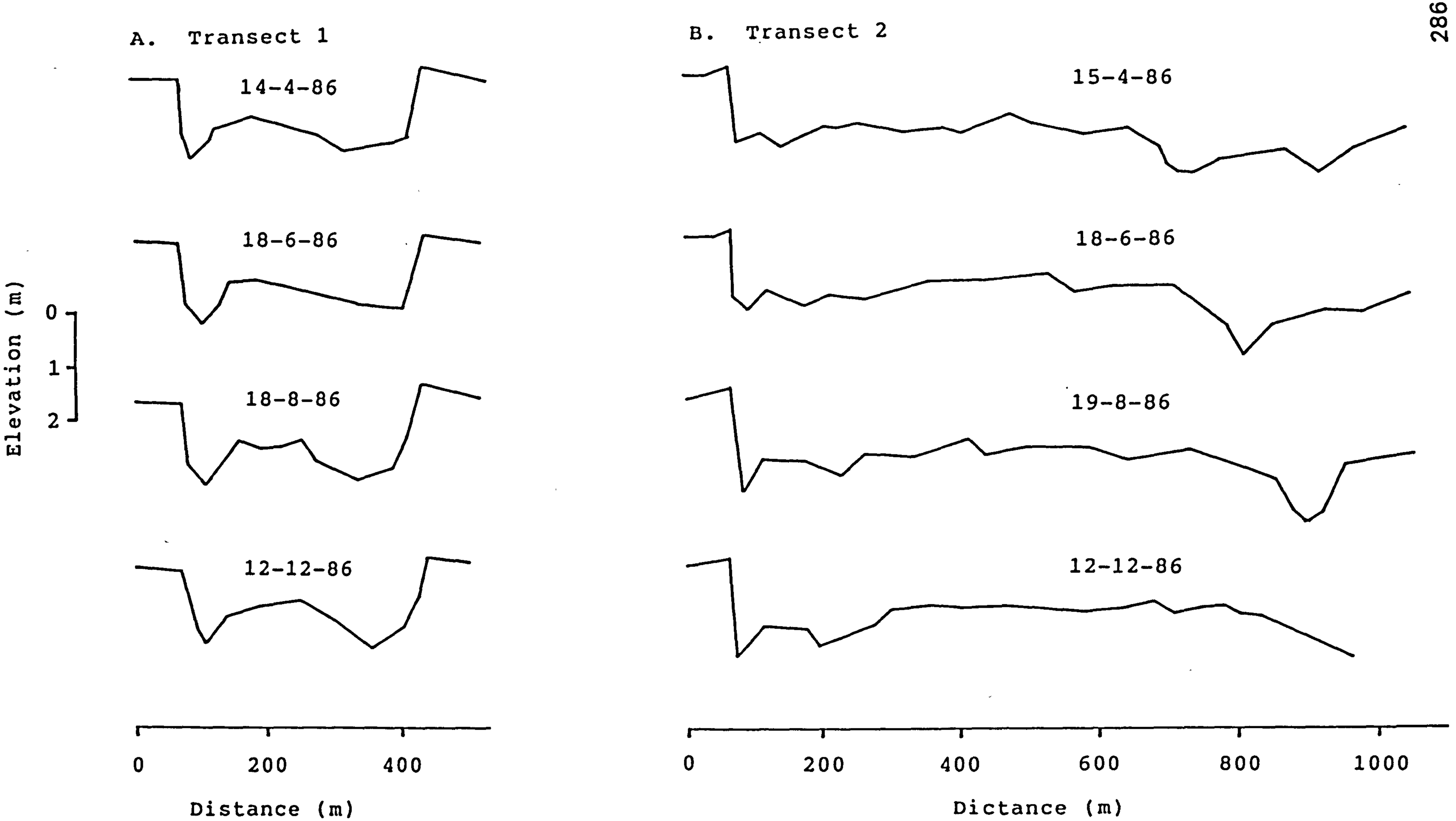

Figure 5.34. Profile variations along Transects 1 (A) and 2 (B).

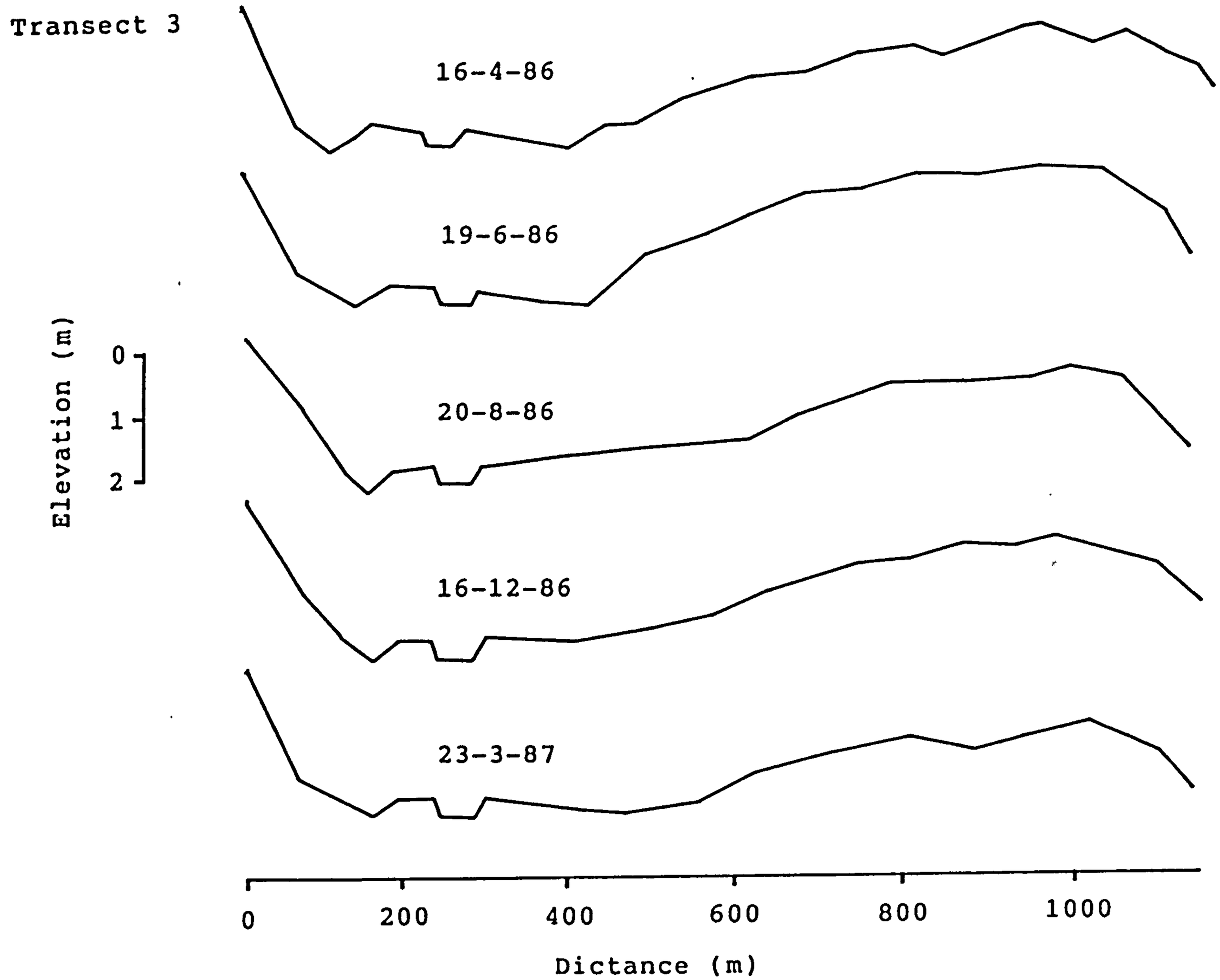

Figure 5.35. Profile variations along Transect 3.

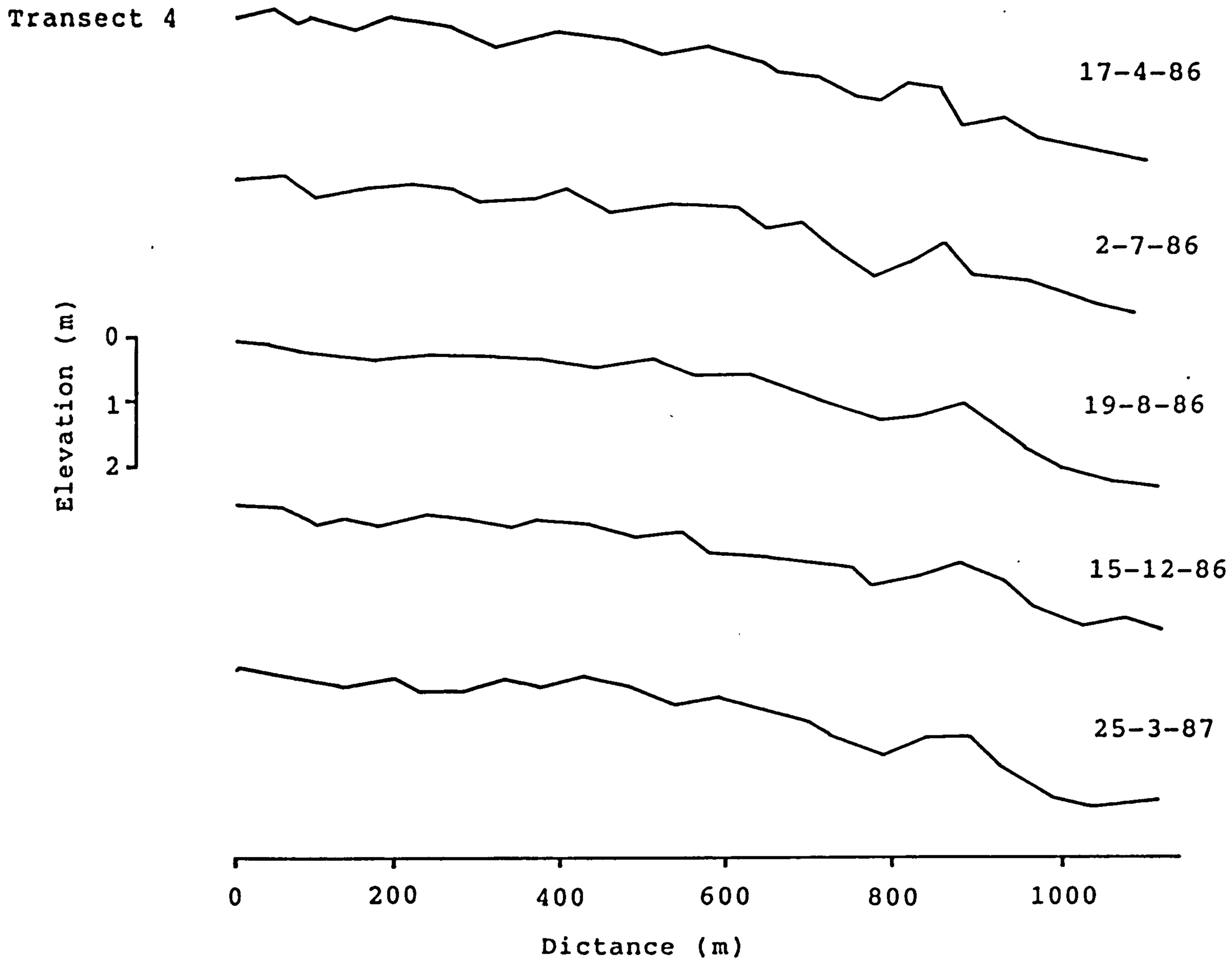

Figure 5.36. Profile variations along Transect 4.

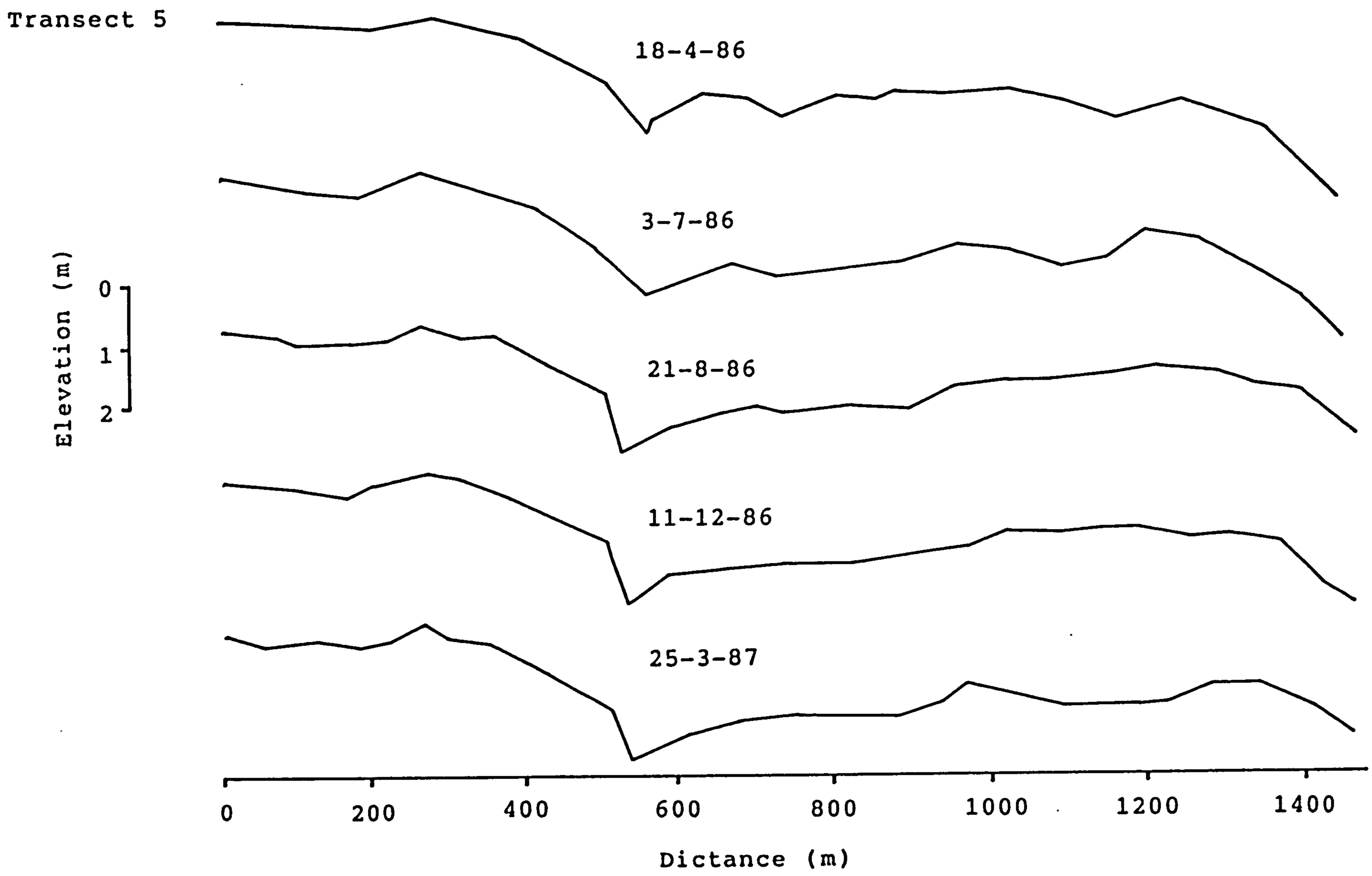

Figure 5.37. Profile variations along Transect 5.

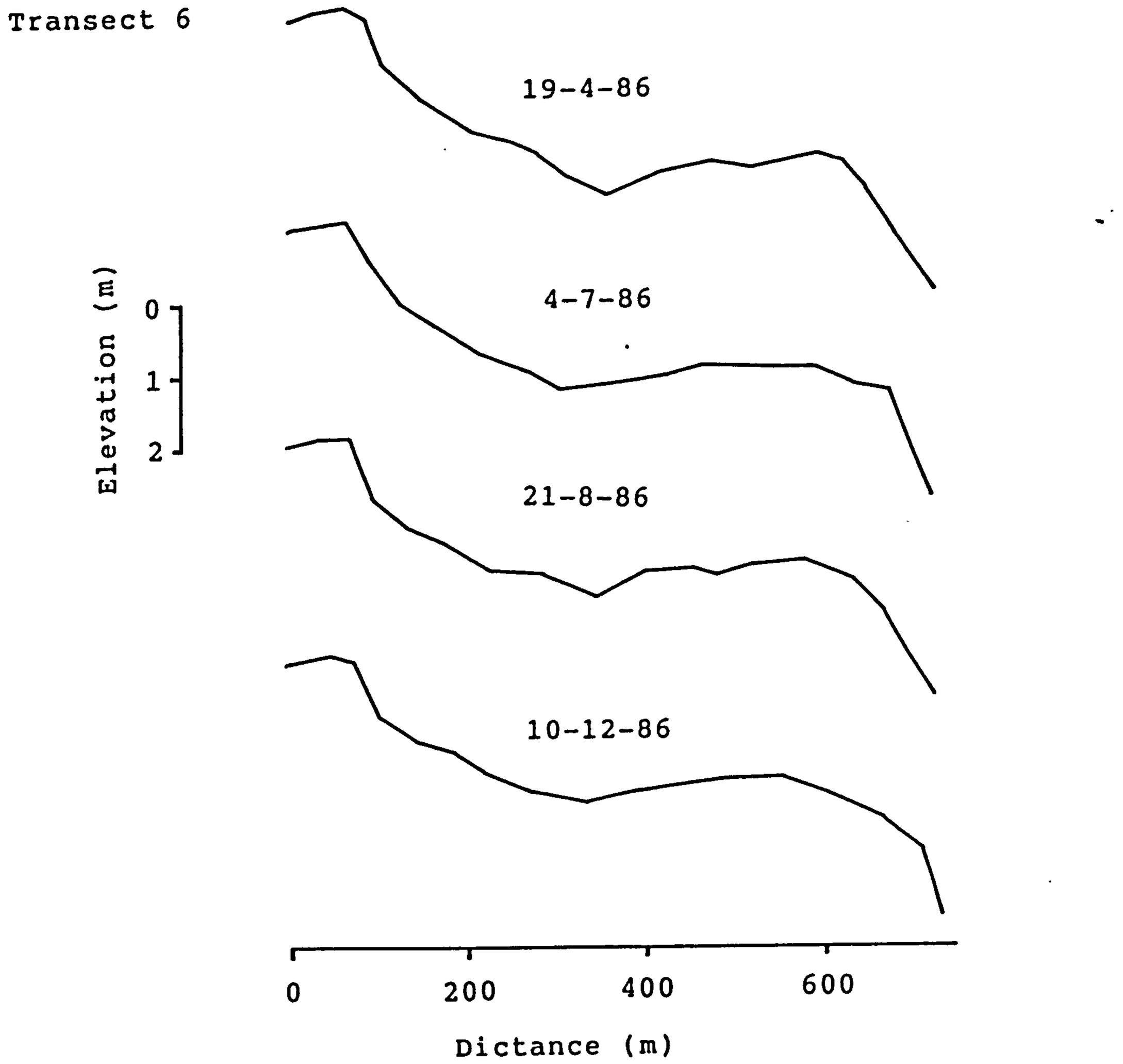

Figure 5.38. Profile variations along Transect 6.

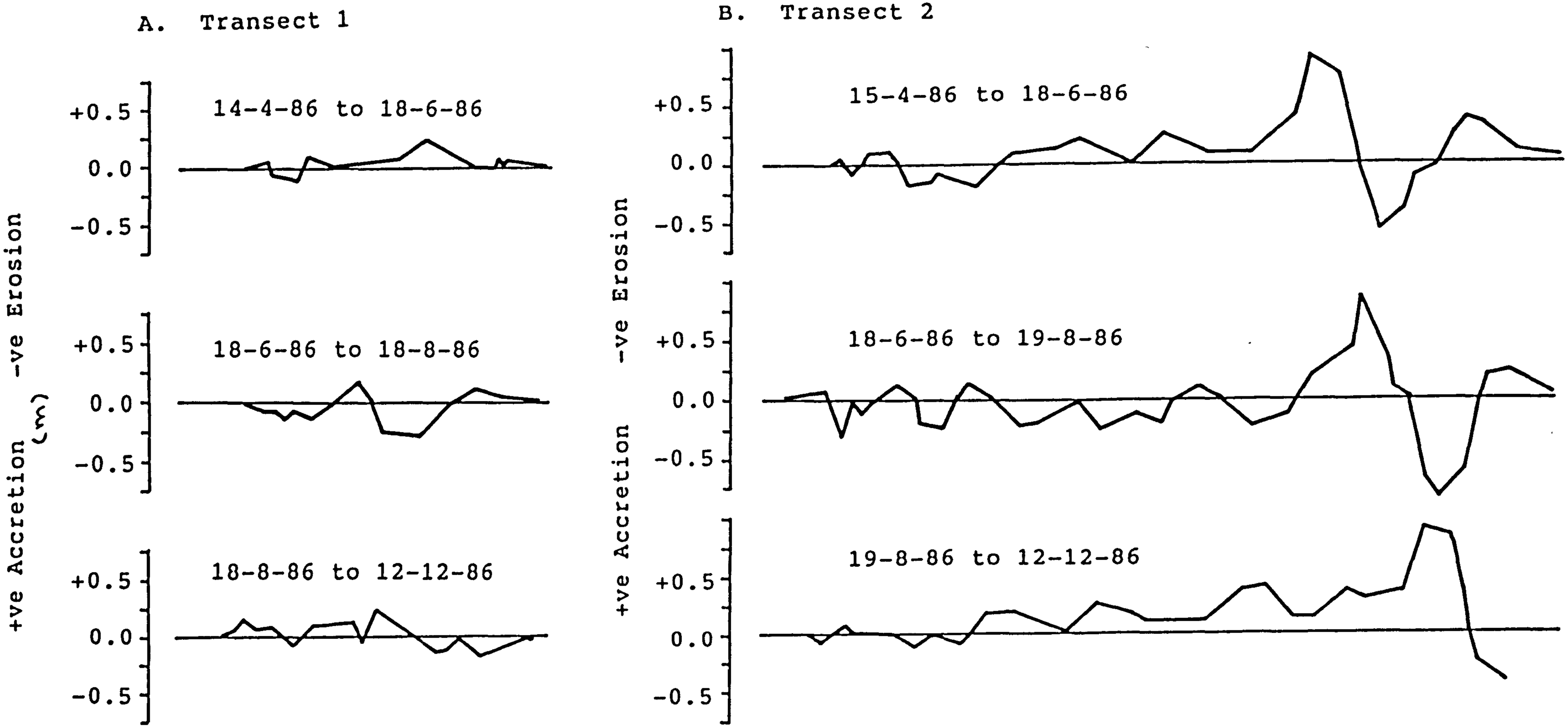

Figure 5.39. Erosion and accretion patterns along Transects 1 (A) and 2 (B).

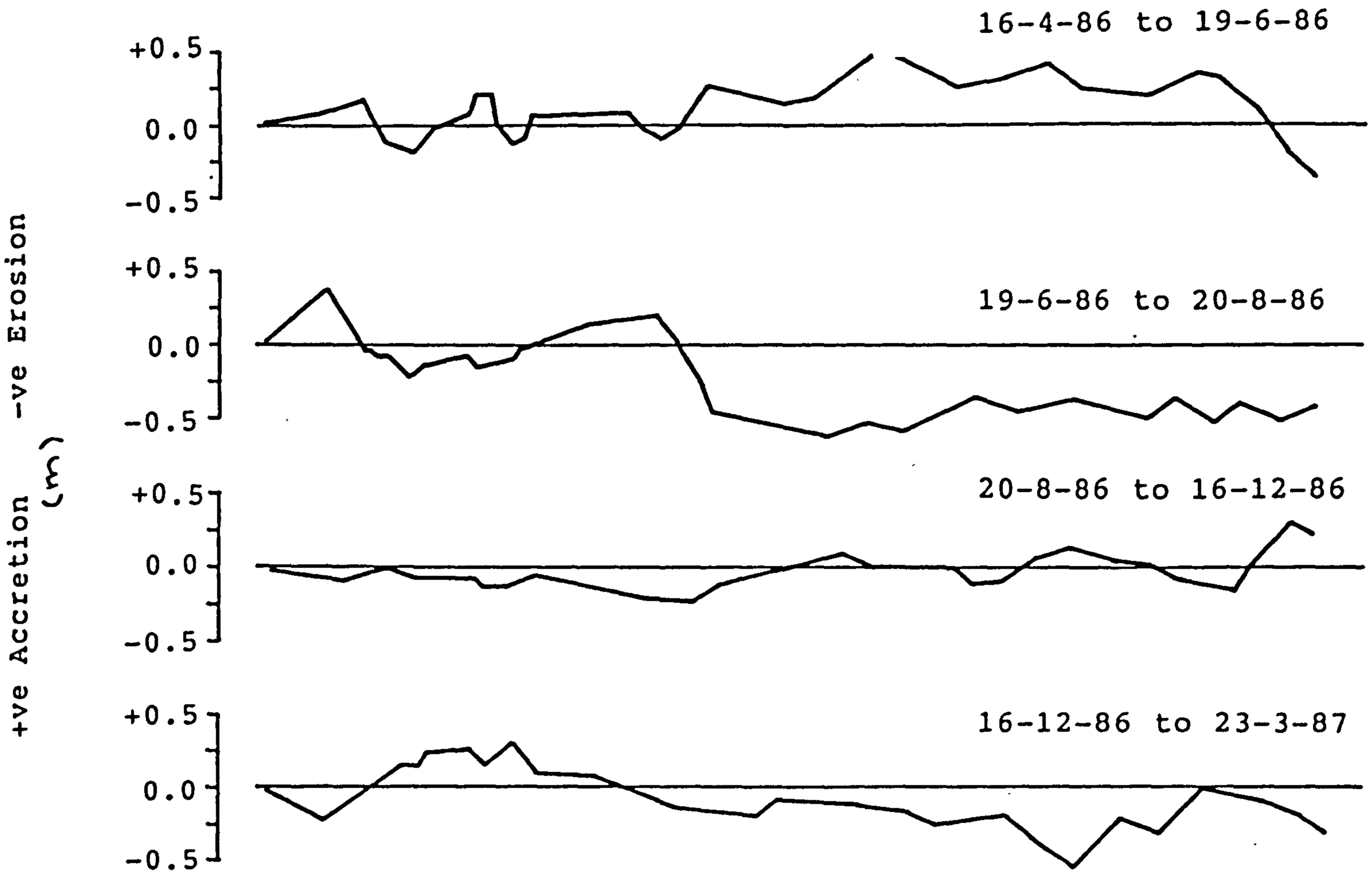

Figure 5.40. Erosion and accretion patterns along Transect 3.

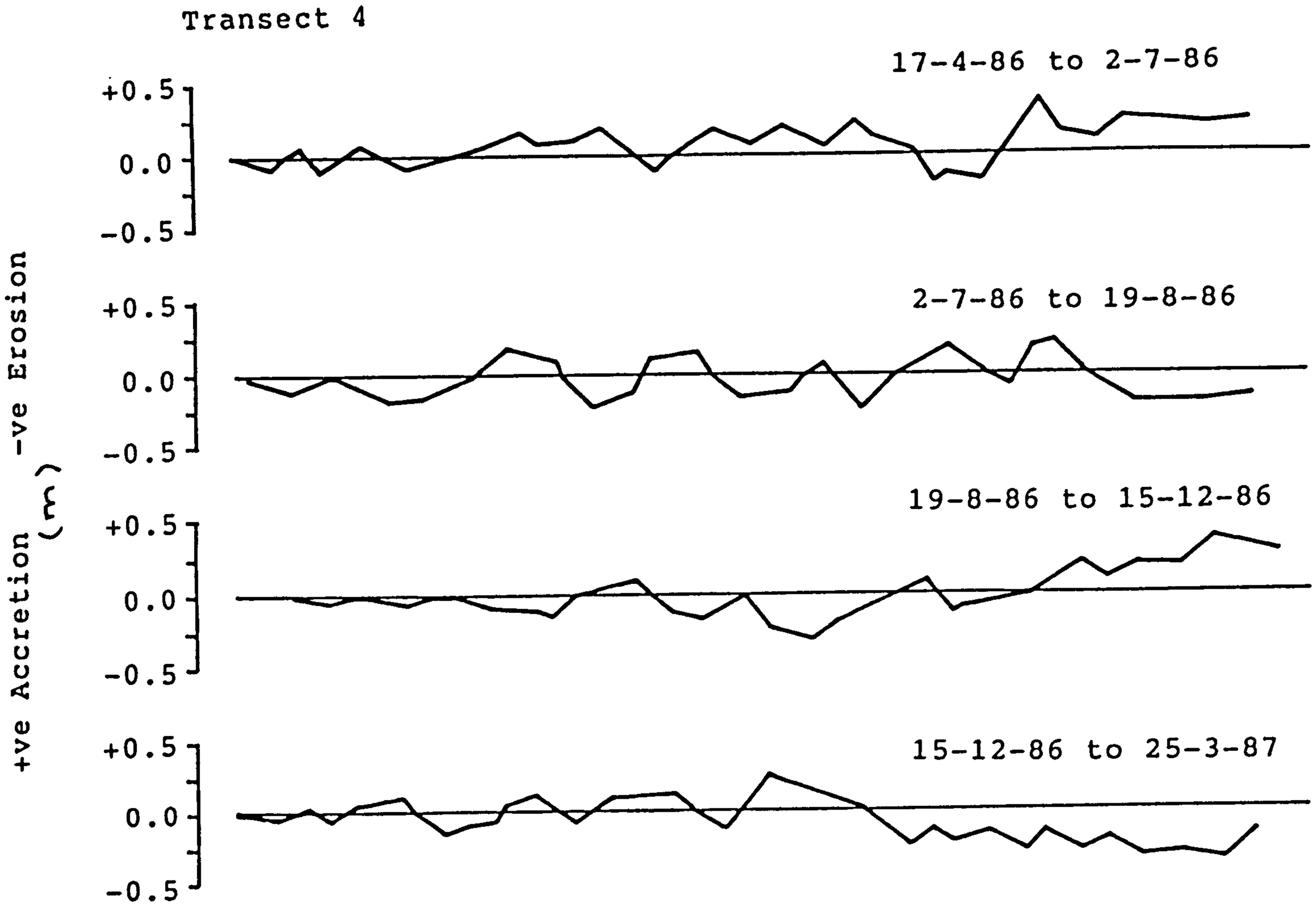

Figure 5.41. Erosion and accretion patterns along Transect 4.

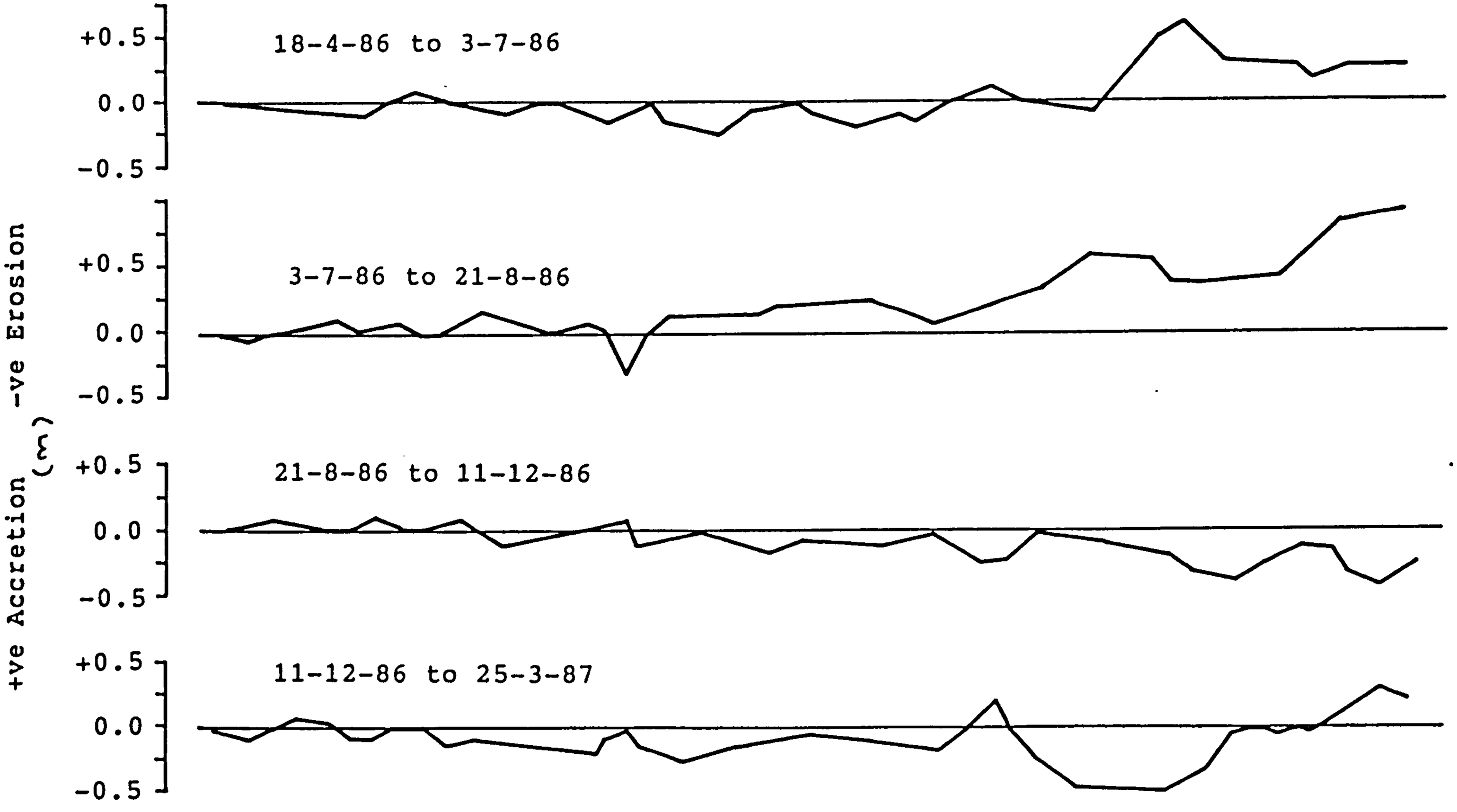

Figure 5.42. Erosion and accretion patterns along Transect 5.

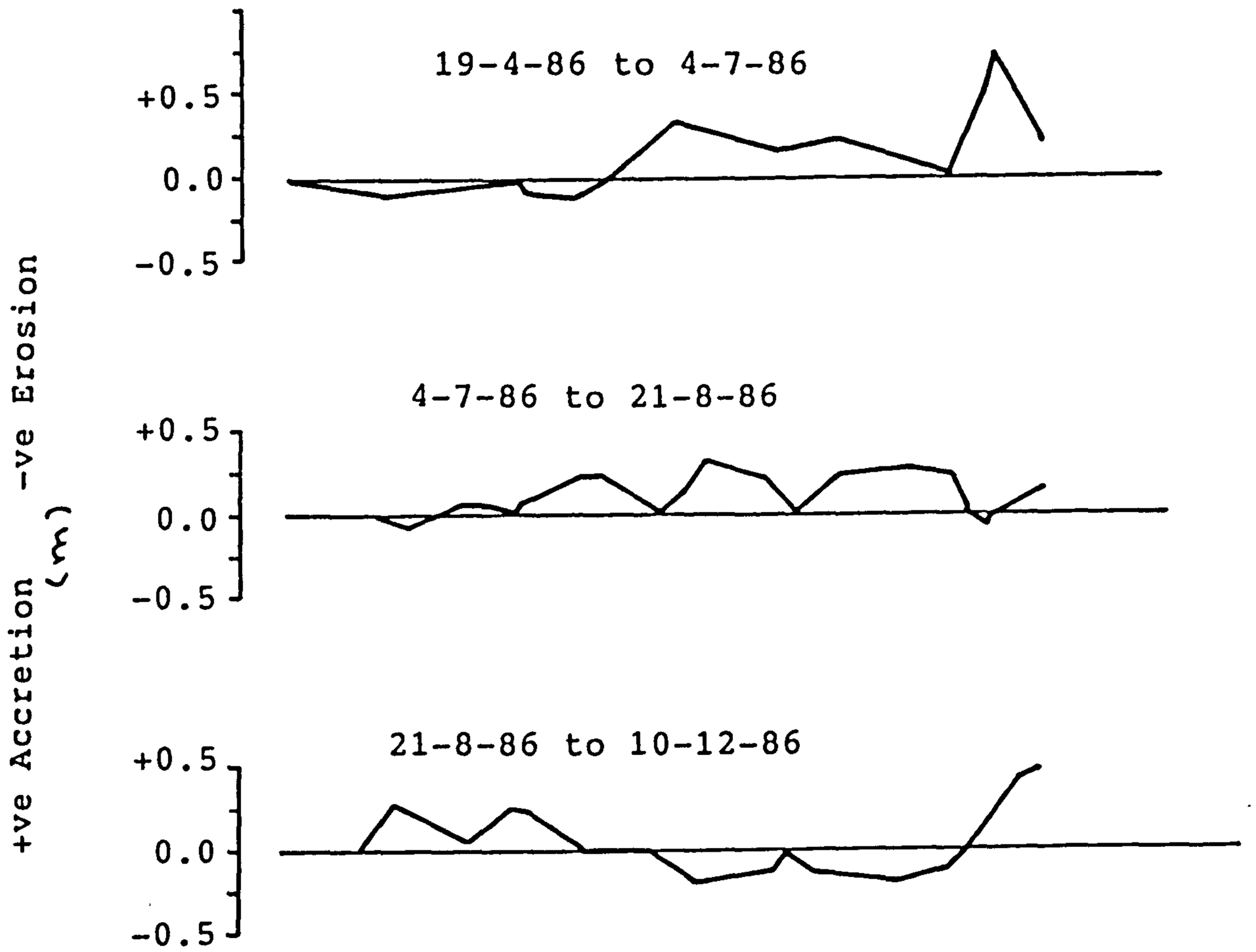

Figure 5.43. Erosion and accretion patterns along Transect 6.

Table 5.16. Erosion and accresion volume along the transects 1 to 6.

Transect no.	Survey 1 to Survey 2	Survey 2 to Survey 3	Survey 3 to Survey 4	Survey 4 to Survey 5	Total Accretion & Erosion
1	+ 27	+ 20	+ 22	-	+ 69
	- 5	- 37	- 16	-	- 58
2	+158	+101	+278	-	+537
	- 55	-106	- 22	-	-183
3	+192	+ 50	+ 27	+ 41	+260
	- 17	-309	- 48	-135	-509
4	+ 94	+ 38	+ 51	+ 35	+218
	- 25	- 63	- 52	- 90	-230
5	+124	+366	+ 19	+ 33	+542
	- 70	- 17	-165	-191	-443
6	+118	+ 55	+ 52	-	+225
	- 24	- 5	- 47	-	- 76

Note: m^3 (+ sign shown accretion, - sign shown erosion)

seem to be relatively stable, but the sides of the channels, and the adjacent sand flats were genarally highly variable. In terms of the amount of sediment eroded and accreted, transect 5 was the most unstable, though the net change of volume during the survey period was relatively small.

Transects 1 to 3, however, were unstable for the whole length of the profiles. The greatest instability occurred at the edge of the main channel of transect 2 due to the migration of the channel (Figure 5.39). Sediment eroded from the outer bank was partially compensated by an cccumulation of sediment on the inner bank. The amount of sediment eroded and accreted at the channel edges depends on the strength of the flow and on the hydraulic gradients set up by the flow. Transect 1 was relatively the most stable of all transects in terms of the volume of sediment eroded and accreted. In general, there seem to be no linear trend of variation with distance from the mouth. Away from the sand flats, the salt marsh surfaces were the most stable area, where no apparent changes in elevation were measured.

5.5.1 Discussion

The great local variability of the sediment eroded and accreted and the small number of surveys prevent any

meaningful generalizations from this data. Although data on the changes of estuarine profiles were limited and the duration of the surveys was short for the determination of seasonal or annual trends of the estuarine morphology, it provided some valuable information on the relative stability or activity at various parts of the estuary. Since the interval between transects were rather large, it could not be certain whether these small number of transects were representative of the estuary. Furthermore, because of the lack of data on short term variations (e.g., daily or weekly), it is probably invalid to assume the results of long term surveys to be representative of the magnitude of sediment eroded and accreted during these survey periods.

The lateral variations of erosion and accretion described for all the transects indicate that most part of the estuarine sand flats are areas of poor stability due to active movement of sediments. However, the most active are those close to the main channel which experience fast tidal currents and turbulence. In the lower estuary, this area seems to coincided with the sand flats which contain large flood-oriented bedforms where tidal currents must be strong for these bedform to exist. It has been shown that the flow dynamics of this estuary are dominated by tidal currents, so it is very unlikely that river flow has a major influence on sediment transport. Sediment transport and the resulting changes of topography may occur on both flood and ebb currents, therefore it is impossible to

determined the direction of net transport from the variation of profiles alone.

Results show that the middle part of the estuarine sand flats experienced loss of sediments during the study priod, while both lower and upper parts of the estuarine sandflats gained considerable amount of sediments. Sediment eroded from the middle part of the estuary may be transported and deposited at the lower and/or upper part of the estuary. It is also possible that this sediment was transported and deposited in the coastal area. These results seem to contradict the results of the sediment transport rate calculations which indicated that sediment transport in the lower part of the estuary was in the flood direction, while in the upper part the direction of transport was in the ebb direction (see section 5.4). In other words, based on sediment transport rate calculation sediment might be accumulating in the middle part of the estuary. However, this contradiction is probably not true because the sediment transport rate at each station may not be representative of the cross-section.

The considerable variation in the values of the amount sediment eroded and accreted along all the transects reflects the complexity of estuarine sediment budgets. Results indicate that some parts of the estuary gain sediment, while other parts lose sediment. As shown in Table 5.16, the total amount of sediment accreted for all

the transects was about 1851 m , while the total amount of sediment eroded for all the transects during the same period was about 1499 m . The difference between these two volumes reflects the amount of material being accumulated within the estuarine environment since there was a net gain of sediment amount to some 352 m , a vertical rise of 4.9 cm per year. This value was calculated based on the assumption that the variations occurring on the transects were representative of the variation occurring between the transects. This result was almost double that based on the sediment transport rates from currents data (see section 5.4) but closer to Carling's (1981) estimate.

5.6 Conclusion

This study shows that sediment transport rate equations based on Guy et al., (1966) flume data are better represented by a power law with variable exponent which depends on the grain size of the sediment. The sediment transport rate equation in the form of

$$q = A\left(\frac{U - U_c}{U_c}\right)^n \qquad 5.31$$

where n is the exponent and A is a numerical coefficient is therefore recommended. The value of n varies from 2.7 for sediment with mean grain size of 0.93 mm to 4.0 for

sediment with mean grain size of 0.19 mm. The applicability of many transport rate equations derived from flume data to the tidal marine environment is well supported by experimental data; therefore the application of the above equation in tidal environment can be justified.

The intertidal flats of the Dwyryd estuary are areas of active sedimentation. Sediment is transported into the estuary from the neighbouring submarine areas. The strong tidal currents measured at various locations in this estuary are the primary agents of estuarine sediment dispersal. The dynamics of estuarine sediments are also a function of tidal current asymmetry. This study shows that directional and temporal asymmetry is marked at all stations monitored. This estuary is dominated by flood tidal currents where the maximum value of 110 cm/s has been recorded at the estuary mouth. Dominance of flood tidal currents may be the result of negative asymmetry in the duration of the rising tide versus the falling tide. At the mouth, the flood duration is 4 hours shorter than the ebb. The flood duration is reduced toward the estuary head. The net sediment transport is mainly in the flood direction at the central and lower (mouth) parts of the estuary, while at the estuary head the net transport is in the ebb direction.

The value of transport rate estimates using the new and

Engelund & Hansen equations are in good agreement with each other. The amount of sediment transported per tidal cycle at each location estimated from both equations are of the same order of magnitude and in the same direction. The sediment transport estimate must be interpreted with much caution due to the limited amount of data available. In natural tidal environments, many complicating factors influence sediment transport; for example sediment transport is also affected by changes in wind conditions (storms) or by the changes in river discharges. Any complete sediment transport determination should carefully consider these factors. Obviously more long-term and detailed studies are required to determine water and sediment movements in many critical areas such as on the higher intertidal flats, salt marsh areas and also along the flood and ebb transport paths at the mouth of the estuary.

SIX

SEDIMENT ANALYSIS AND SEDIMENT CHARACTERISTICS

6.1. Introduction

Estuarine sedimentary evvironments are unique due to the variability and interaction of various processes which include the shape of the estuary, the strength of tidal currents , river discharge, the intensity of wind-induced waves, the accessibility of intruding oceanic swell, and the availability of sediment for transport and deposition. Some of these parameters have been considered in the previous chapters. Estuarine morphological features could not exist unless rocks of the drainage basin, local cliffs or nearby sea bed were broken down by various weathering agents to small pieces capable of transportation from place to place by water flow and wind (Guilcher, 1967). Rock fragments vary greatly in composition, size, and shape and respond differently to local water dynamics. The evolution of an estuary depends mainly on the long-term sediment supply, the direction and magnitude of the long-term sediment transport, and also on the abrupt changes in estuarine morphology caused by storm surges or by engineering works (Dronkers, 1986).

It has been recognized that grain size distributions should reflect the hydrodynamic environment in which the grains were transported and deposited. Several methods have been used to interpret deposional environments from grain size distributions, such as plotting skewness versus sorting (Friedman, 1961), comparing the coarsest fraction to the median size (Passega, 1964) and analysing cumulative curve shape (Visher, 1969). Recent workers have examined the relationships between grain size distributions and estuarine hydrodynamics (Middleton, 1976; Sagoe & Visher, 1977).

The analysis of estuarine sediment samples is an important part of any estuarine study which seeks to provide information about estuary hydrodynamics. This knowledge will become the basis of interpretation of past sedimentary processes and also in the prediction of future movement of sediment and therefore the development of the estuarine morphology. It also will enhance our overall understanding of the estuary system and its relationship with adjacent submarine environments. By examining the textural characteristics of the sediments and their distribution ,the interrelationships between the sediments and the hydrodynamics in the estuary can be established.

The present study examines grain size distributions in a small tide-dominated estuary and to a lesser extent along

the coastline and the embayment adjacent to it, and analyses the observed trends in textural parameters and cumulative weight percentage (in terms of coarse or fine fractions) profiles of some of the sediments samples with respect to the measured hydrodynamic parameters (chapter 3). The aims are to recognize the characteristics of grain size distributions that reflect hydrodynamics in the Dwyryd estuary. Hopefully, the results of this study will provide a useful contribution to our knowledge of Welsh estuaries.

6.2. Sediment Sampling and Analysis

Special attention was paid to the planning of sample collection in this study. Sampling was carried out in such a way that it would represent the whole environment under consideration. As pointed out by Folk (1974), one should search for and sample the coarsest and finest sediment obtainable as well as the sediments most typical of the area studied. It is a well known fact that sediment transported and deposited along the bed by water currents is subjected to sorting and abrasional processes which produce systematic changes in grain size distribution curves as specified by textural parameters. Among the objectives of most sedimentological studies is to determine whether there are any interpretable trends and to relate them to the physical processes of the of the study area (Krumbein, 1953).

About 140 sediment samples were collected at low water

from the upper three centimeters of the sediment bed at stations along six transects across the estuary (Figure 6.1) . The exact position of each sample was located with reference to a temporary reference point set up at one or both end of each transect line. Because of the length of the transect lines it was impractical to employ a fixed sampling interval; instead the sampling points were chosen on the spot to include as great a variety of bed features as possible. In addition 8 samples were collected further upstream between transect 1 and the limit of tidal intrusion, and 8 more samples were collected from the river bed (Figure 6.1). 74 samples were collected along the beach and on the sand spit at low water level (Figures 6.2 and 6.3). 25 grab samples were collected from the nearshore part of Tremadog Bay (Figure 6.4). The intervals between sample stations on the beach were estimated by pacing. Seabed samples were taken from the top 10cm layer of sediments using a Shipek grab sampler.

Each estuarine sample consisted of approximately 250g of sediment. This was obtained by pushing a PVC sampling ring, 8cm in diameter into the sediment, and excavating its contents with a trowel. As the sediment texture may vary with depth and the depositional units are usually difficult to recognise, the top 3 cm layer was used for sampling in order to reduce such complications. In the case of river samples, about 1 kg of material was collected for each sample with a spade since the deposits consisted

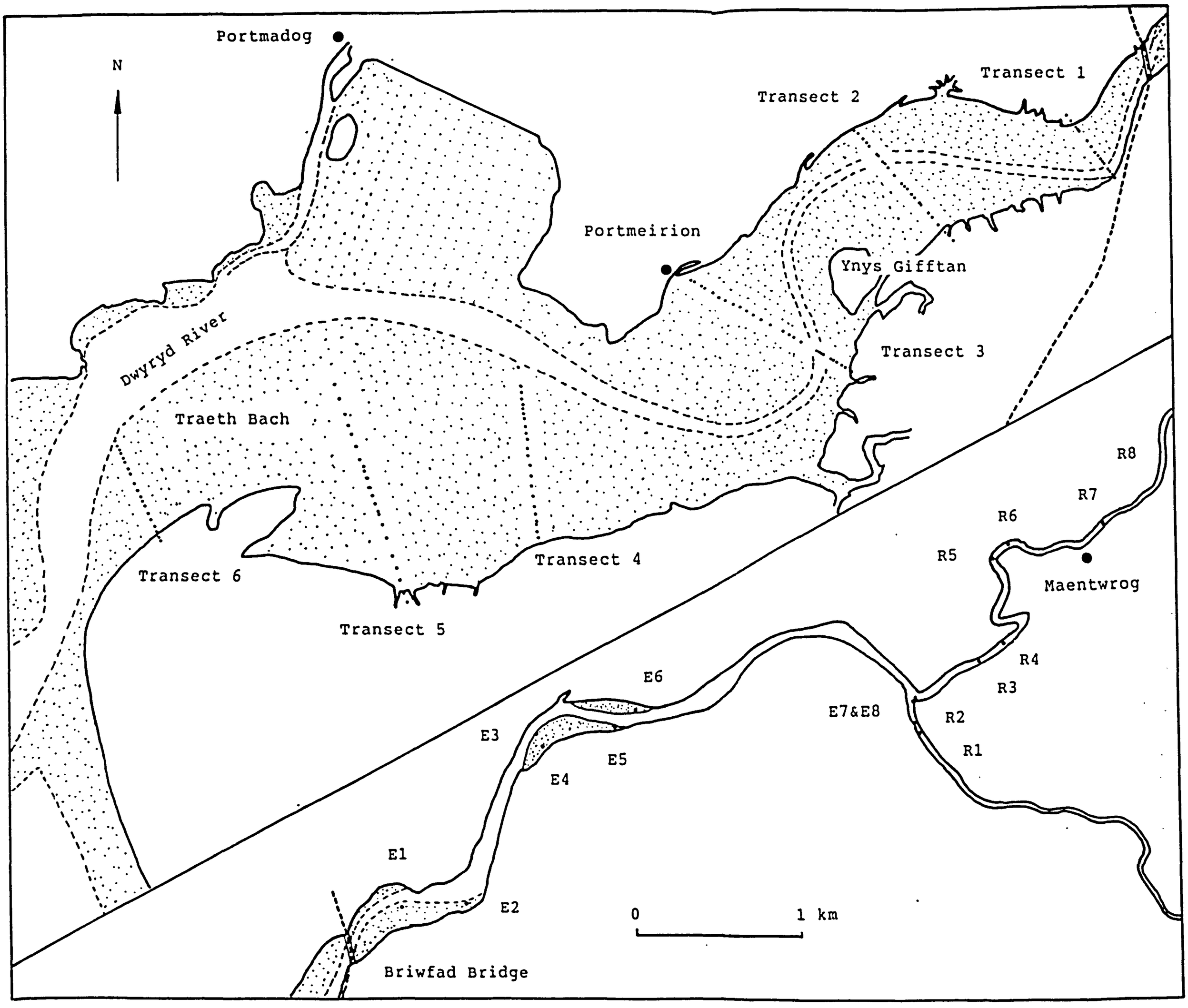

Figure 6.1. The Dwyryd estuary with positions of sampling transects and stations.

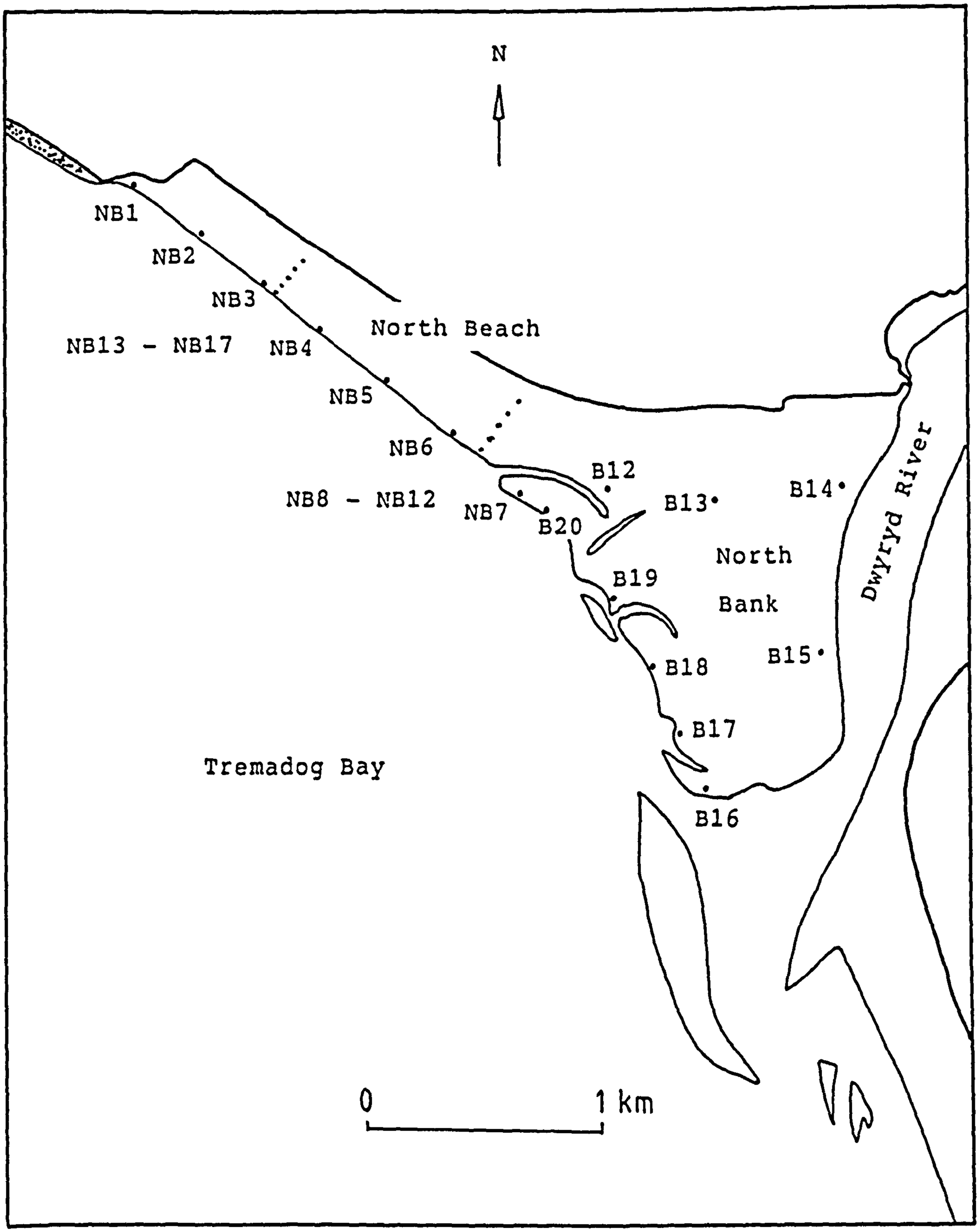

Figure 6.2. The positions of sampling stations along the north beach and North Bank (sand spit).

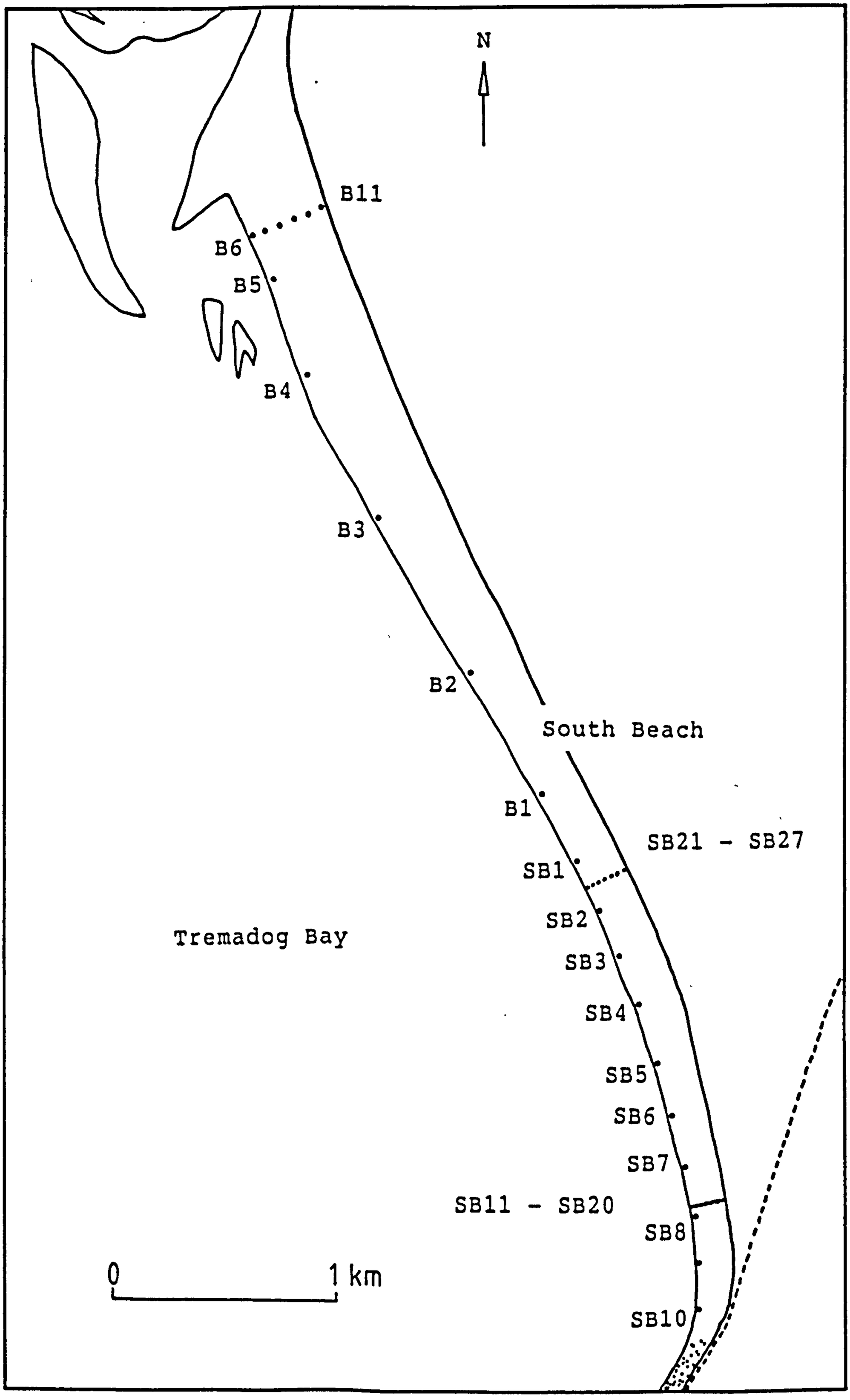

Figure 6.3. The positions of sampling stations along the south beach.

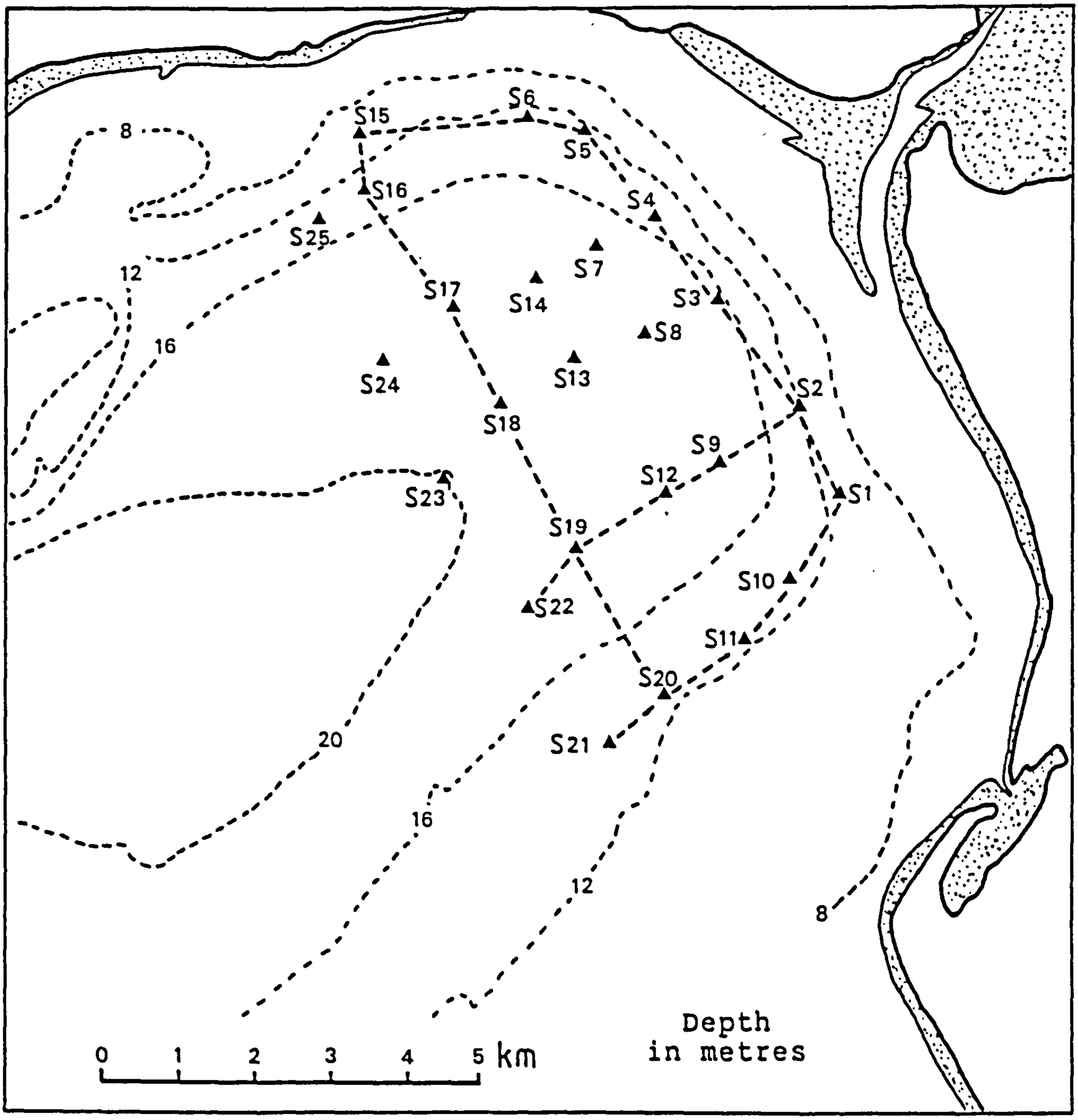

Figure 6.4. The positions of sampling stations in the Tremadog bay.

of a mixture of coarse and fine material.

The methods used here are based on the standard techniques which are described in detail in the literature concerned with petrological techniques such as Krumbein & Pettijohn (1938), Irani & Collis (1963), Muller (1967), Griffiths (1967), Allen (1968), Carver (1971) , Hutchison (1974), and Dyer (1979).

Samples were washed, separated into sand and mud fractions by wet sieving through a 63 micron sieve. The sand fractions were then split and sieved with a set of 1/4 phi sieves which ranged in size from 1.25 ϕ to 4.0 ϕ for estuarine samples. For the beach and river samples, the coarsest sieve was extended to -1.5 ϕ for the beach samples and -4.5 ϕ for river samples. The mud fractions were analysed by the pipette sedimentation technique in the usual manner. In order to assess the quantity of shell fragments in the estuarine samples, about 30 random samples were selected for further analyses. After an initial sieving, the material was immersed in dilute hydrochloric acid to dissolve the calcium carbonate particles in the sample and then resieved.

There has been no general agreement for dealing with the carbonate component of a sediment. Some researchers retain all the carbonate, others remove it. In this study the carbonate material finer than the coarsest lithic fragment was retained on the assumption that it was in hydrodynamic

equilibrium with its associated terrigenous components.It has been suggested that shell fragments and quartz particles with diameters less than 0.6mm (0.73ϕ) are relatively similar in their settling velocities . Shell fragments and quartz particles of diameter greater than 0.6mm diverge in their settling velocity because of the influence of the shape factor (Braithwaite,1973).

In this case, since it may be assumed that small shell fragments and quartz particles have a similar response to a given set of hydrodynamic conditions, it may then be permissible to include carbonate material of sieve diameter less than 0.6mm in the calculation of grain size statistical parameters. Shell fragments coarser than the coarsest sand components were excluded from the size analysis. This procedure was advocated by Frank and Friedman (1973) although they presented no factual support for the adoption of such a measure.

6.3. Sediment Distributions and Textural Parameters

A computer programme was used for the calculation of cumulative weight percent and textural parameters. For each sample mean grain size, standard deviation, skewness and kurtosis were obtained using graphical-statistical formulae put forward by Folk and Ward (1957). The basic formulae are:

Mean Diameter:

$$M_z = \frac{\phi 84 + \phi 50 + \phi 16}{3}$$

Standard deviation:

$$\sigma = \frac{\phi 84 - \phi 16}{4} + \frac{\phi 95 - \phi 5}{6.6}$$

Skewness:

$$S_k = \frac{\phi 16 + \phi 84 - 2\phi 50}{2(\phi 84 - \phi 16)} + \frac{\phi 5 + \phi 95 - 2\phi 50}{2(\phi 95 - \phi 5)}$$

Kurtosis:

$$K_g = \frac{\phi 95 - \phi 5}{2.44(\phi 75 - \phi 25)}$$

Each of these statistical parameters may be useful in an interpretation of the physical processes acting on the sediment. The mean diameter gives a simple indication of the magnitude of the energy, applied by water or wind, which will move the sediments. The standard deviation (or sorting) indicates the range of energy which has affected the sediment. The degree of sorting depends on the conditions under which the sediment is deposited. A very

well sorted fine sand, for instance, indicates that it is produced by the selective action of water or wind currents which transport and deposit only a limited range of grain sizes. A poorly sorted sediment indicates that little selection of grains has taken place during transport or deposition. The skewness of a sediment distribution is a particularly useful indicator of the history of the sample. A negative skew is indicative of a dominance of coarser grains over finer grains, whilst a positive skew indicate the dominance of finer material in the sample. However, care must be taken in interpreting grain size parameters since they may reflect source as well as hydrodynamic controls.

The phi (ϕ) scale which is a log-transformation of millimeters as defined by

$$\phi = -\log_2 D \qquad (D \text{ in mm})$$

was used throughout the present study. Krumbein (1934) introduced this scale to rationalise the geometric grain size scale devised by Udden (1914) and subsequently modified by Wentworth (1922). The phi scale is now used almost exclusively for classification of sediments and for computation of various statistical parameters.

The results of sieve analyses of all samples are tabulated in Appendix (Tables A1 to A9). The results

of sieve analyses of decarbonated samples are tabulated in Table A10.

6.4. Grain size Distributions

The use of grain-size distribution curves to describe and/or characterize specific sedimentary environments has been a major goal of sediment grain-size analyses. This, however, requires a suitable model for the grain-size distribution. Many grain-size distribution curves are so closely similar to the normal (or Gaussian) probability curve that it has become a common practice to assume that the size distribution of natural sediments are normal distributions. The size frequency data are said to be log-normally distributed when cumulative weight percent data, plotted on normal probability paper, yield a straight line. In reality, however, the log-normal distribution has rarely been observed (Friedman,1962; Bagnold, 1983; Flenley, 1985; Philip and Watson, 1987; Christiansen and Hartmann, 1988); in most cases the size frequency distribution curve is basically made up of three or more linear segments, each with a different mean and standard deviation. A recent study of single sand laminae shows that their grain size distributions are neither normal nor lognormal (Grace et al., 1978).

The deviations from the log-normal model have been given various environment interpretations. For example, Moss

(1962) and Visher (1969) related the segmented shape to sorting processs related to different modes of sediment transport. Middleton (1976) suggested that the segments and the break points between the segments were indicative of specific hydraulic and sedimentation conditions. Each segment is interpreted either as a truncated normal distribution or as part of an overlapping system of normal distributions. Other workers attribute the segmented curve to a mixing of several log-normal populations (Fuller, 1962; Spencer, 1963; Tanner, 1964). The usefulness of the shape of the cumulative frequency curve on probability paper for environmental classification, however, has recently been questioned by Reed et.al., 1975, Jackson (1977) and Sedimentation Seminar (1981).

Indeed, recent works by Bagnold (1941), Barndorff-Nielsen (1977), Bagnold & Barndorff-Nielsen (1980), Barndorff-Nielsen et.al.(1982), and Barndorff-Nielsen et.al.(1983) have shown that grain size probability distribution from a wide variety of environments approximate far more closely to the hyperbolic distribution than to the normal distribution. The theory and the applicability of such distributions have been the subject of a number of recent investigations. A number of possible explanations of the hyperbolic distribution are presented by Bagnold & Barndorff-Nielsen (1980).

6.5. Normal and hyperbolic probability curves

The best way to show whether grain-size distribution follow log-normal or log-hyperbolic distributions is to plot cumulative weight percentage against phi diameter on both normal and hyperbolic probability papers. If a sample is log-normal (sample X, Figure 6.5) then the cumulative percentage plot is a straight line on normal probability paper, but has a 'Z' shape on hyperbolic paper. However, if a sample is log-hyperbolic (sample Y, Figure 6.5) then the cumulative percentage plot is a straight line on hyperbolic probability paper, but has an 'S' shape on normal probability paper. If a sample is neither log-normal nor log-hyperbolic, then the degree of straightness of both curves could be used to judge whether the grain-size is best represented by a normal or hyperbolic distribution.

Nine samples from the river, the estuary, and the beach were selected to illustrate the difference between the normal and hyperbolic distributions. For each sample both normal and hyperbolic cumulative curves were plotted as shown in Figures 6.6 to 6.14. Examination of the normal and hyperbolic distribution curves of the estuarine sediments (Figures 6.6 to 6.9) reveal a diversity of the shape of distribution curves in all of the samples. Not a single curve plots as a straight line on normal and hyperbolic probability papers; as a result none the estuarine samples can be regarded as truely log-normal or log-hyperbolic; the distributions are either positively or

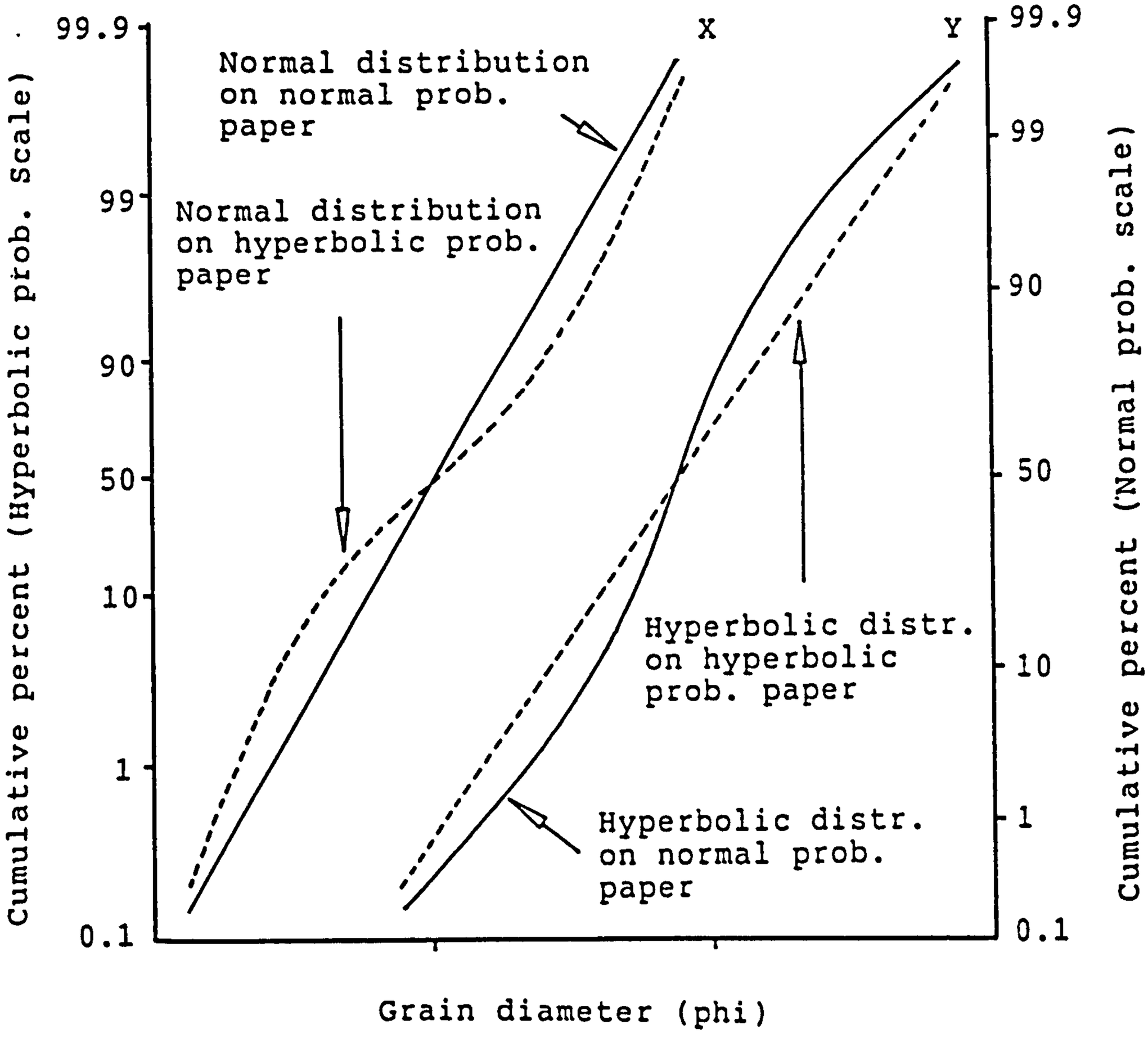

Figure 6.5. The hyperbolic and normal distributions plotted on hyperbolic and normal probability scales.

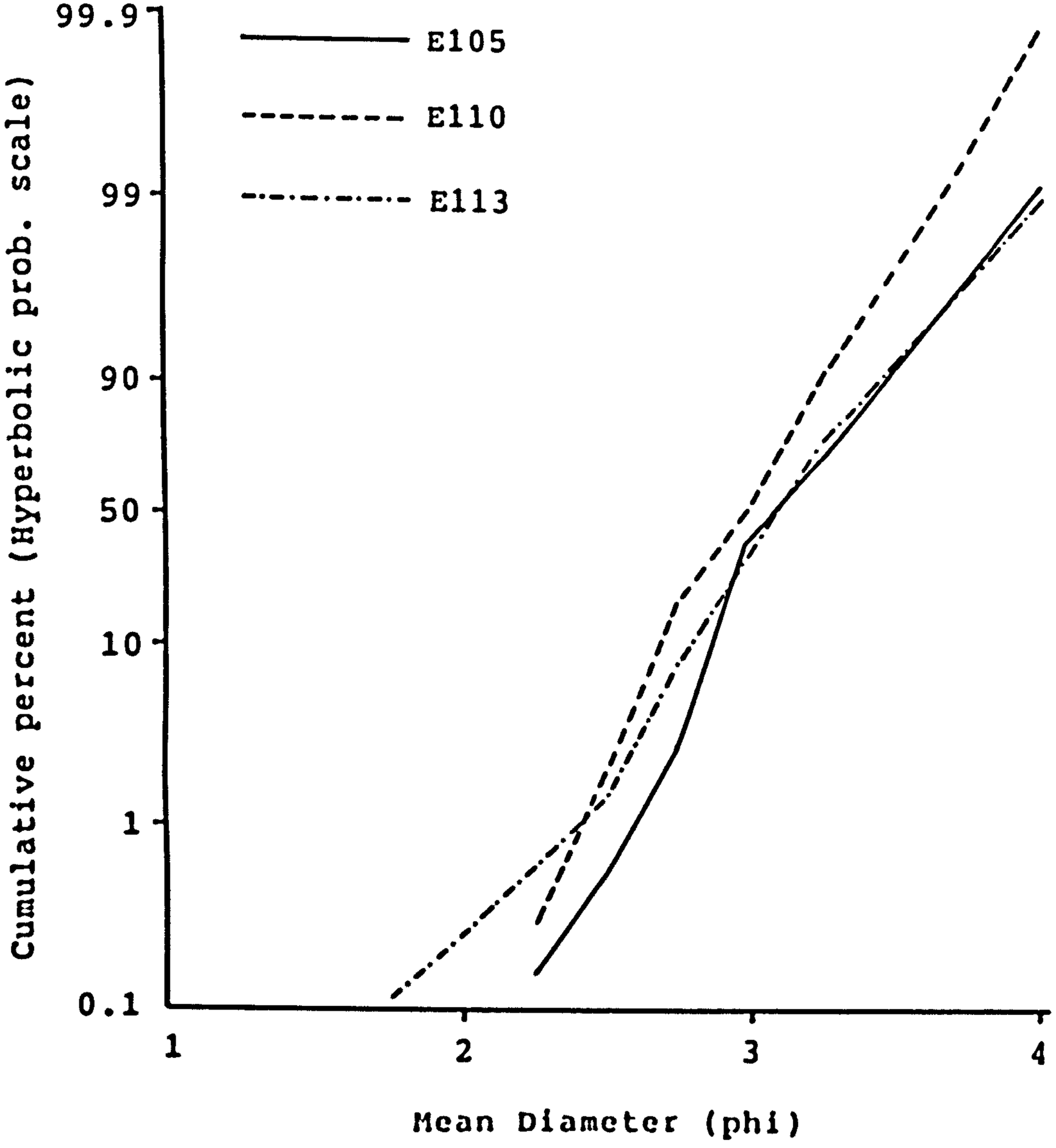

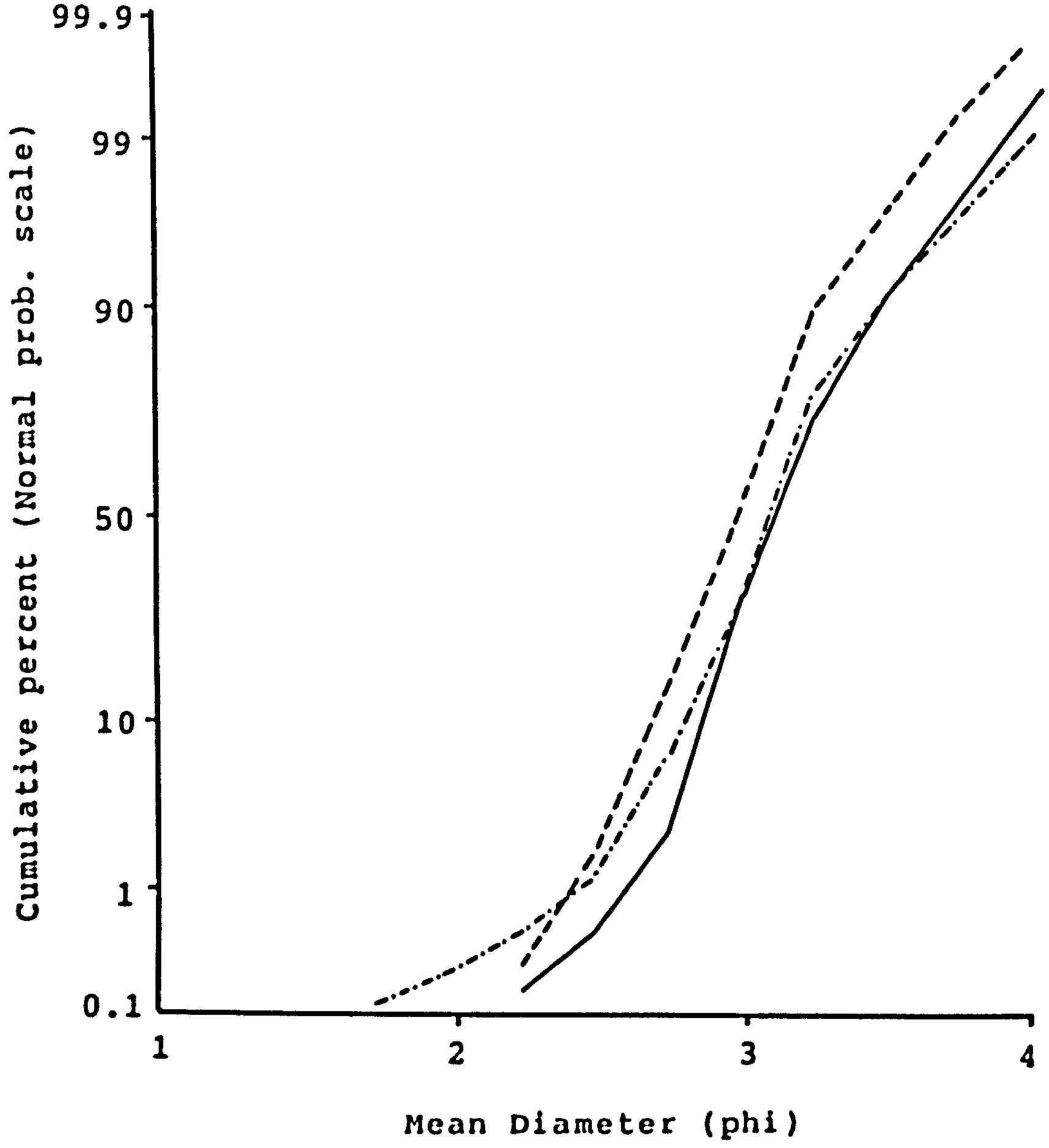

Figure 6.6. Grain size distribution curves on hyperbolic and normal probability papers typical of sediments from transect 1.

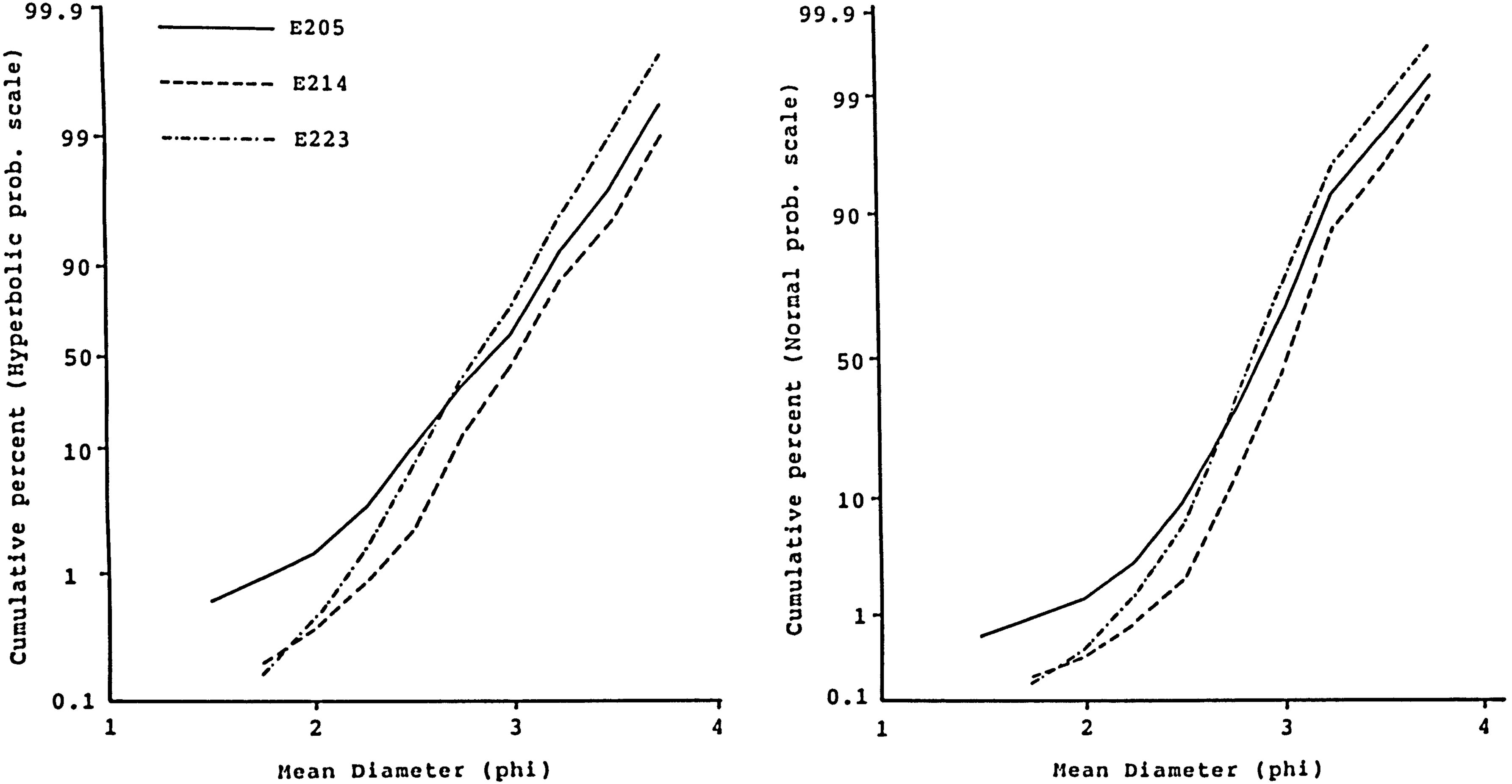

Figure 6.7. Grain size distribution curves on hyperbolic and normal probability papers typical of sediments from transect 2.

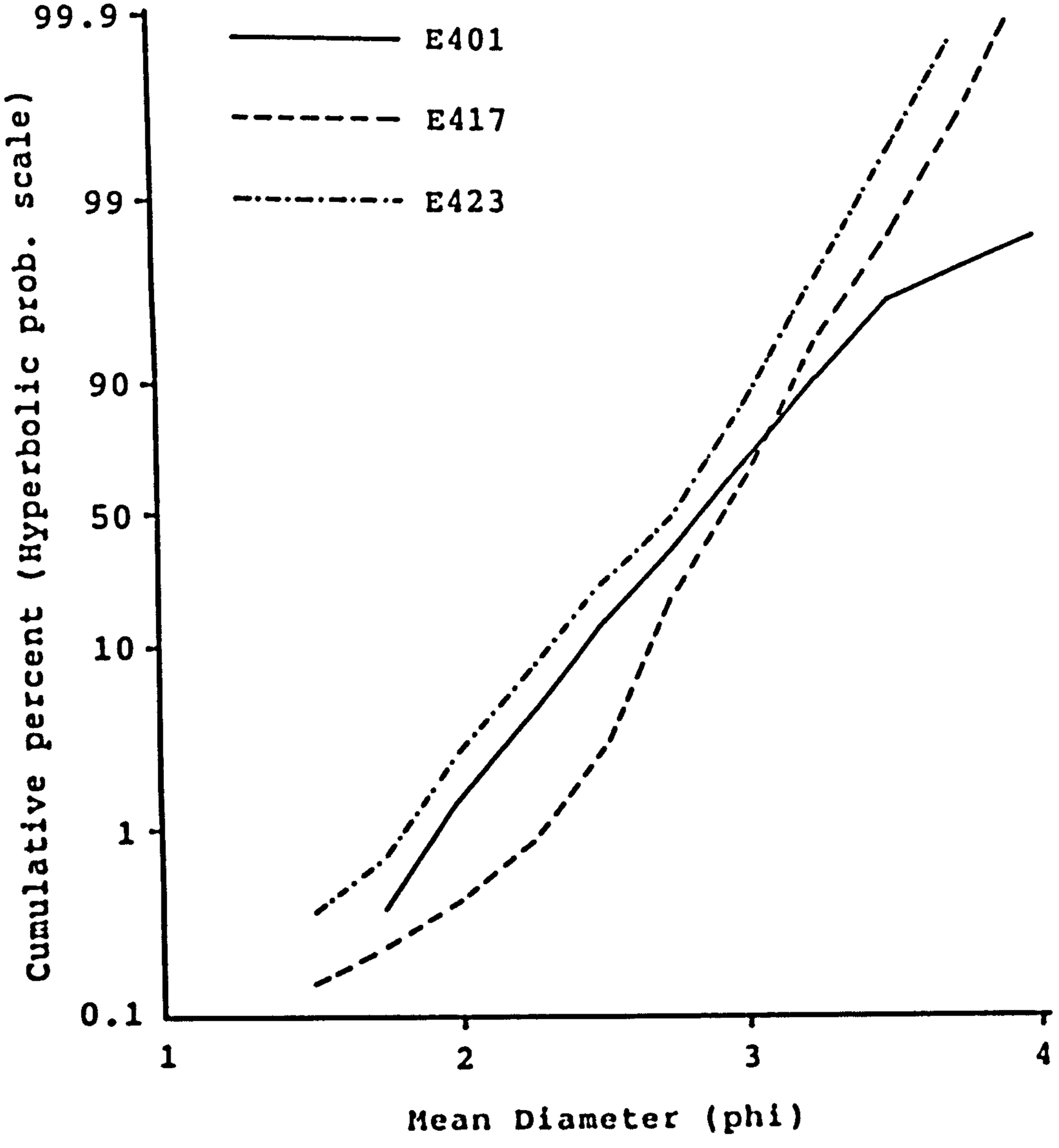

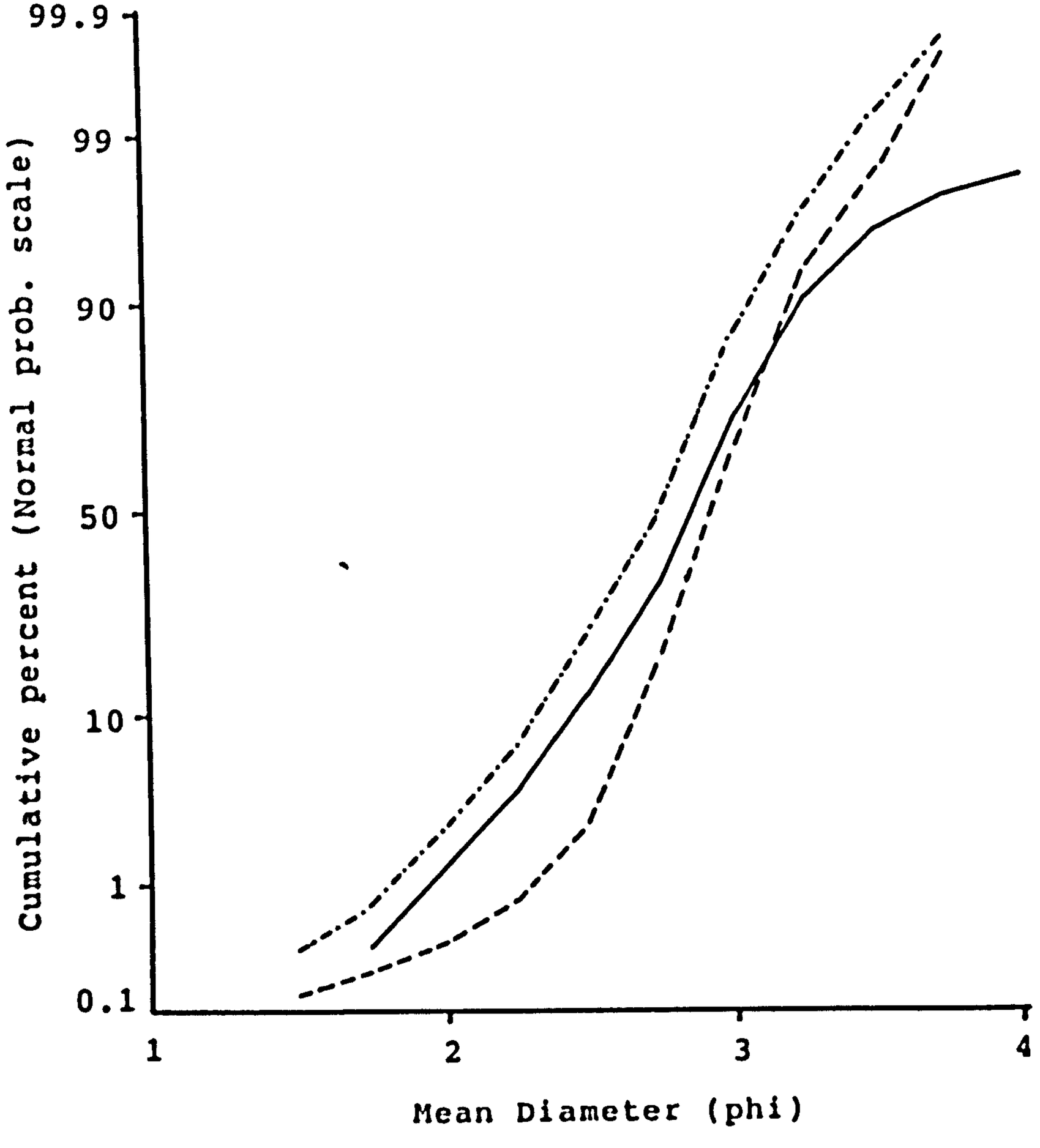

Figure 6.8. Grain size distribution curves on hyperbolic and normal probability papers typical of sediments from transect 4.

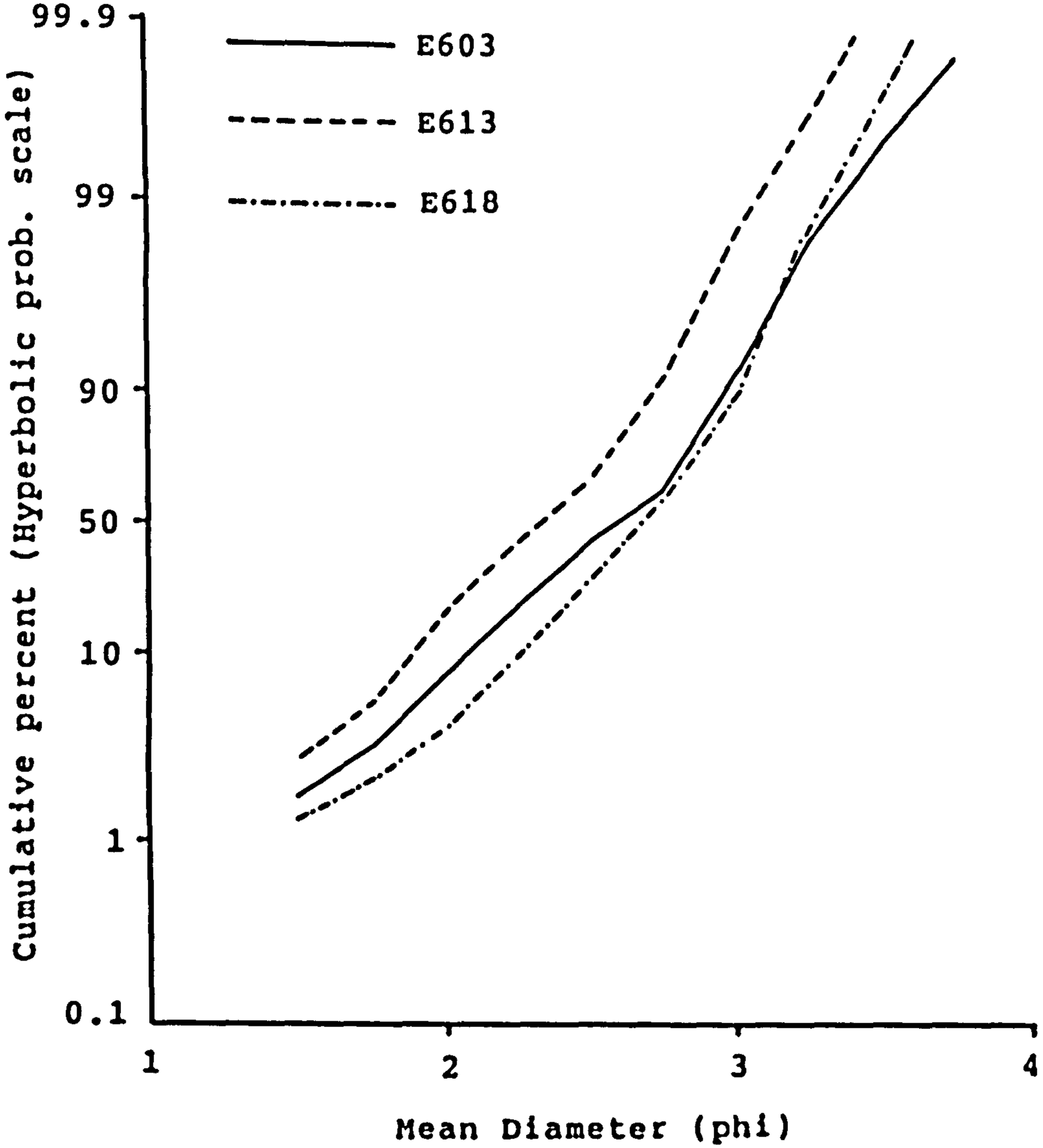

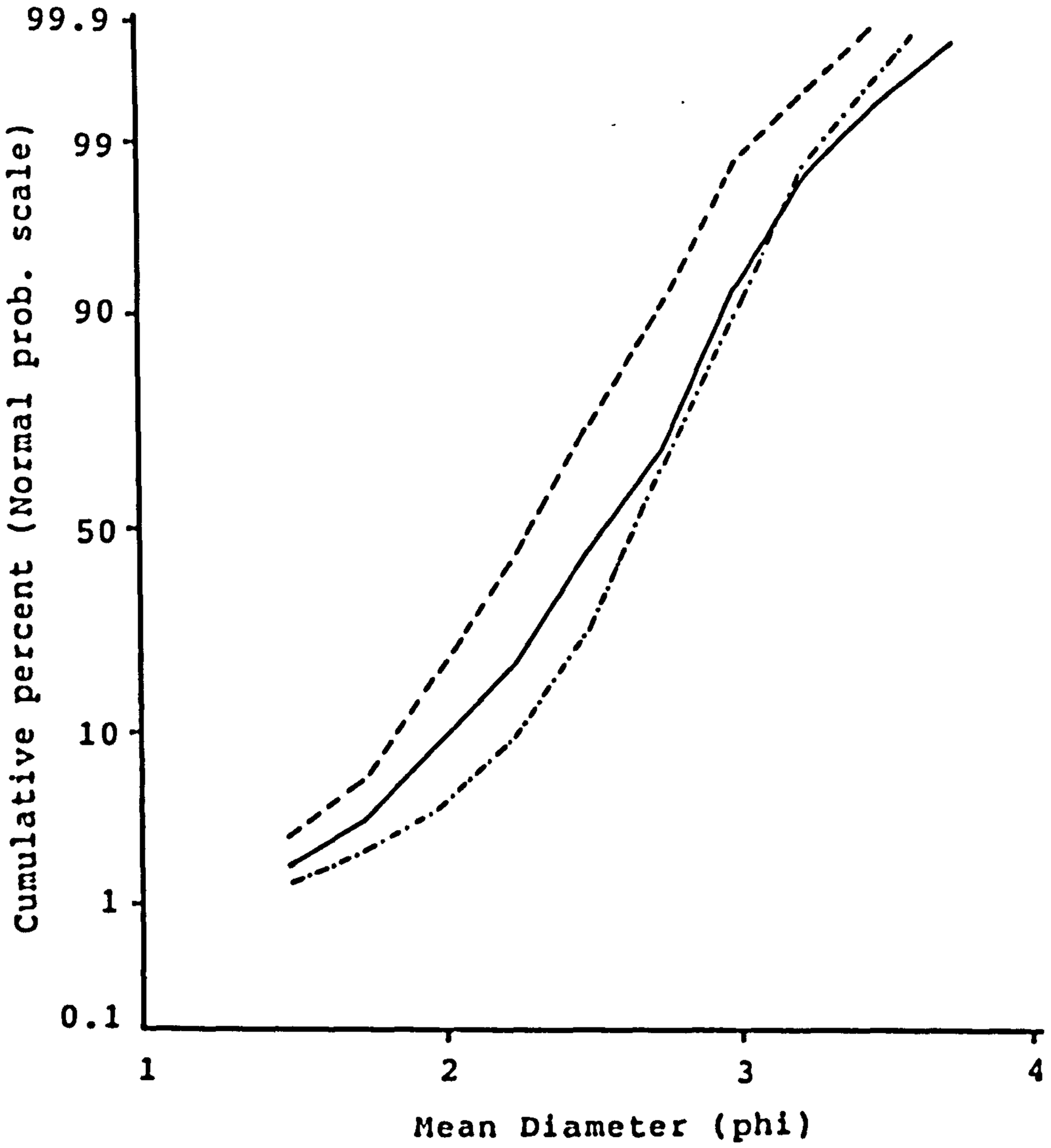

Figure 6.9. Grain size distribution curves on hyperbolic and normal probability papers typical of sediments from transect 6.

negatively skewed. On hyperbolic probability paper, however, the cumulative curves of a few of the samples yield almost straight lines. In most cases the tails of the cumulative hyperbolic probability curves are relatively linear compared to the cumulative normal probability curves where the usual deviations from log-normality have been observed in all the samples.

For the river (Figures 6.10 to 6.12) and the beach samples (Figures 6.13 to 6.14), the differences between the normal and hyperbolic curves are less obvious . The difference lies in the slope of the curves where the slope of the central section of the cumulative curves are generally smaller on hyperbolic probability paper compared to the curves on normal probability paper. But the slope of the tail sections are generally larger on hyperbolic probability paper than the normal probability paper.

The straighness of the distribution curves of some of the estuarine samples when plotted on hyperbolic probability paper compared to the similar curves plotted on normal probability paper strongly suggests that the hyperbolic distribution curve is the best approximation to the grain-size distribution of the sediments. The degree of straighness was used by Bagnold & Barndorff-Nielson (1980) to prove that the hyperbolic distribution is the best approximation to the true distribution of grain-sizes.

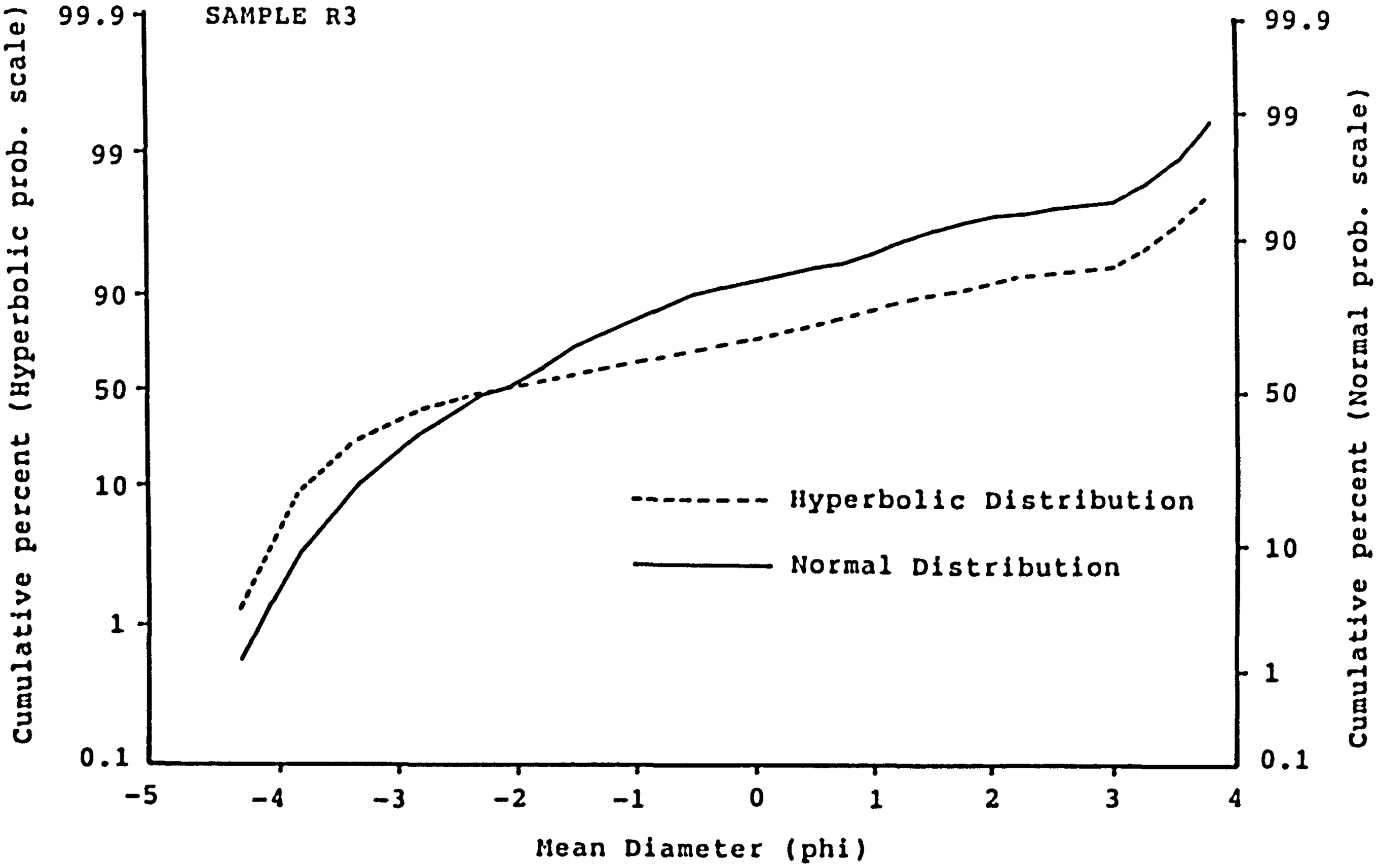

Figure 6.10. Grain size distribution curves of a river sample (R3) on hyperbolic and normal probability scales.

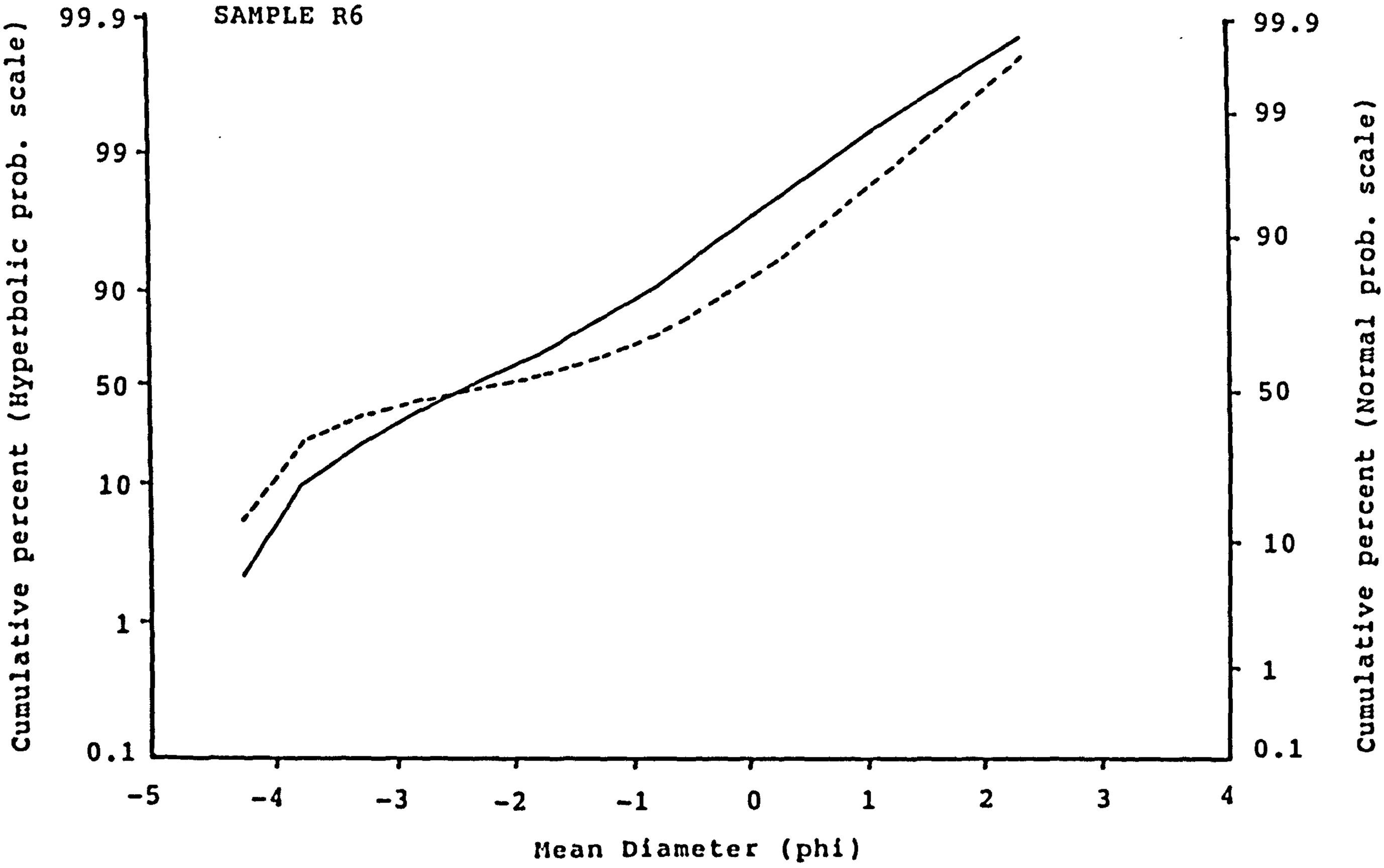

Figure 6.11. Grain size distribution curves of a river sample (R6) on hyperbolic and normal probability scales.

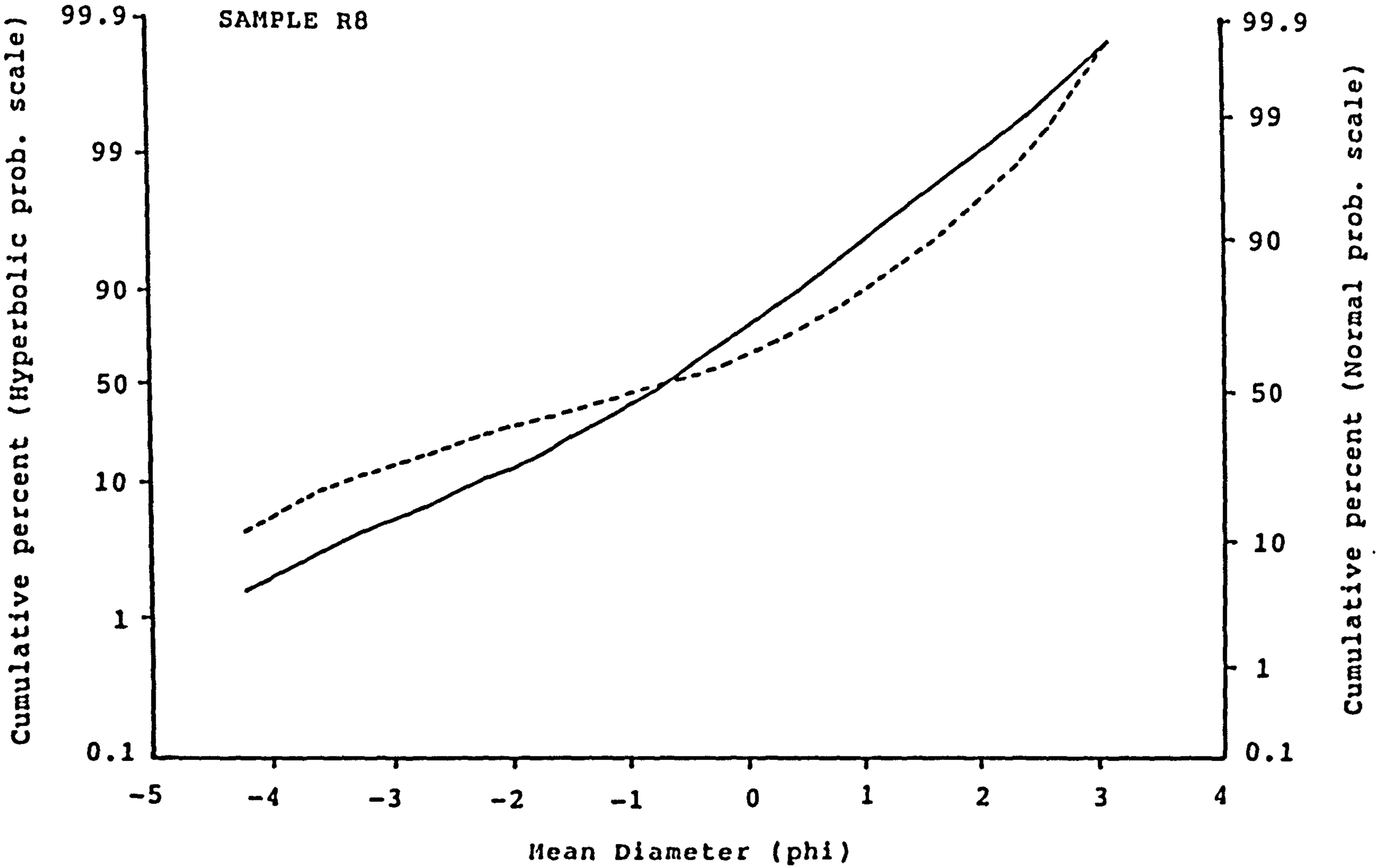

Figure 6.12. Grain size distribution curves of a river sample (R8) on hyperbolic and normal probability scales.

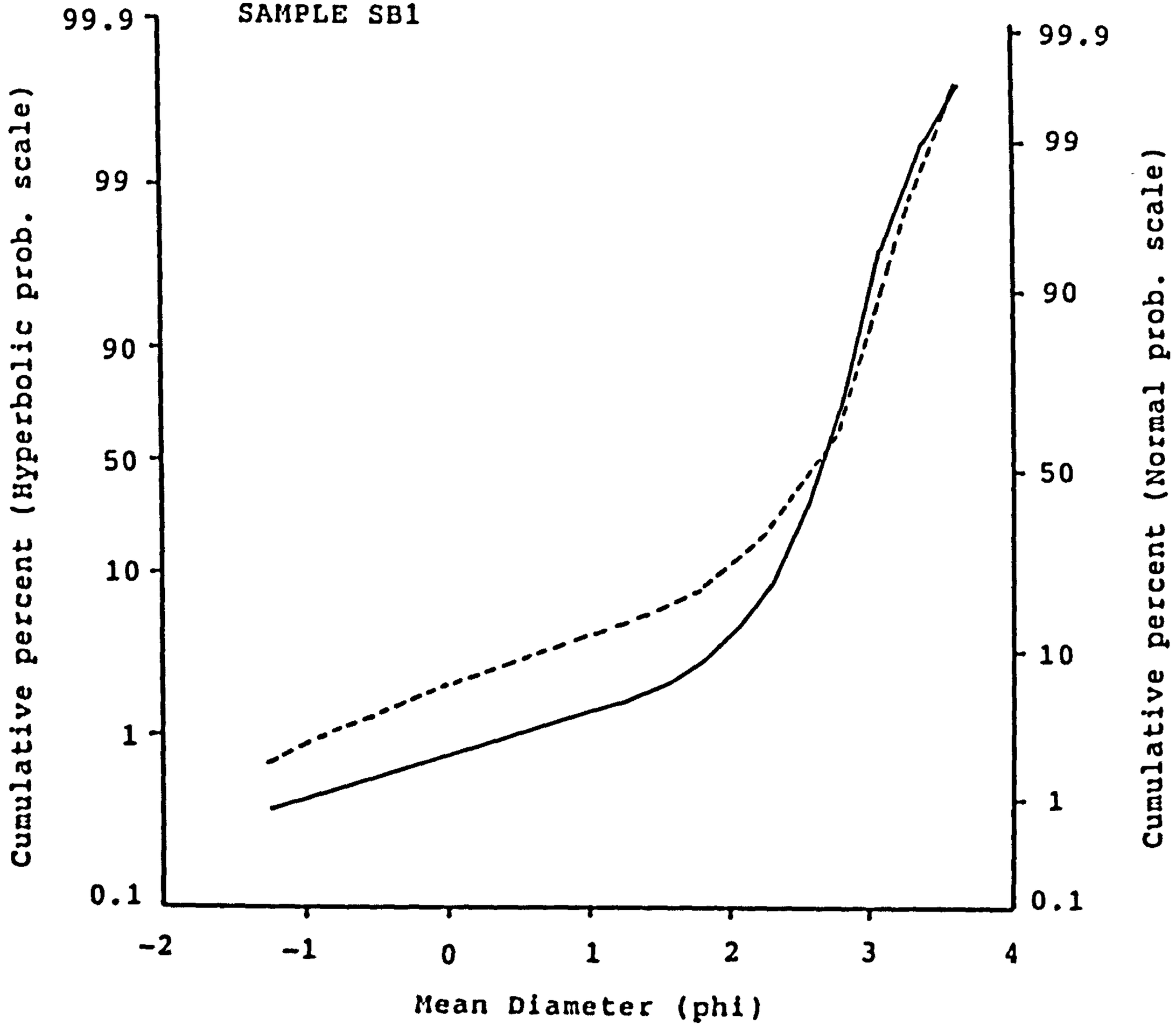

Figure 6.13. Grain size distribution curves of a beach sample (SB1) on hyperbolic and normal probability scale.

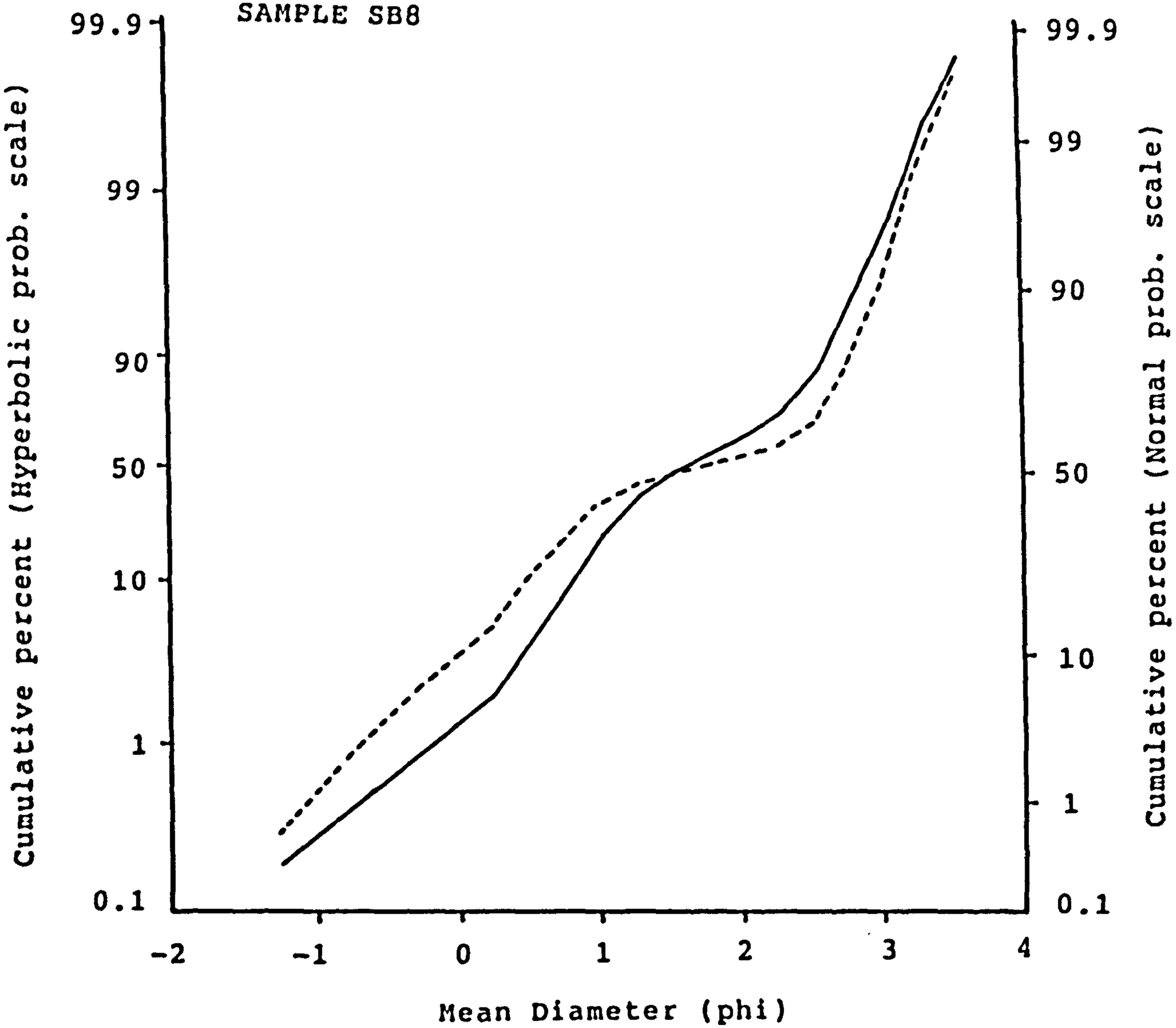

Figure 6.14. Grain size distribution curves of a beach sample (SB8) on hyperbolic and normal probability scales.

As shown in Figure 6.5 the log-hyperbolic distribution when plotted on normal probability paper exhibits a shape which can be misinterpreted as consisting of segments, as suggested by LeRoy (1981) and Christiansen et.al.(1984). The usual interpretation of the curve shape as resulting from normally distributed subpopulations each of which should reflect a mode of transport must be reexamined if grain-size distributions are better described as hyperbolic distribution rather than as normal distributions.

6.6. Source of estuarine sediments

The Dwyryd Estuary is apparently being filled by sediment which obviously must come either from the River Dwyryd or from Tremadog Bay or from both (chapters 2 and 5). Qualitative evidence of large bedform migration near the mouth of the estuary, together with the similarity of the estuarine and some of the beach sediments strongly suggests that the source of the estuarine sediments is probably marine rather than fluvial. As shown in Figures 6.6 to 6.9, the estuarine sediments are composed almost exclusively of a narrow range of grain-size from 4.0ϕ (0.063mm) to 1.5ϕ (0.355mm). However, approximately 90% of the samples consist of material within a size range of 3.5 (0.090mm) to 2.25ϕ (0.212mm). The same size range represents about 40 to 90% of the grain size range of beach sediments (Figures 6.13 and 6.14), and less than 5% of the size range of the river sediments (Figures 6.10 to 6.12).

The lack of sand within the size range of 3.5ϕ to 2.25ϕ in the river deposits suggests that the river may not be able to supply a large volume of sand of this size into the estuary. Only the sub-littoral areas of Tremadog Bay are likely to be a source of supply.

The source of estuarine sediment can be easily proven by the identification of various mineralogical types of sand grains within the river, the estuarine ,and the beach samples. A few selected samples from each environment were examined under an optical microscope to estimate the relative amount of quartz, lithic and biogenic calcium carbonate grains. The grains vary in appearance, ranging from translucent, through clear and tinted, to transparent, and may have angular, subangular, subrounded,or rounded shapes. Two size ranges were chosen for the analyses, i.e., the 0.090 to 0.212 mm range and the 0.212 to 0.424mm range. The summary results of the relative frequency percentages of the quartz, lithic fragments, and biogenic (calcium carbonate) components are given in Table A13 (Appendix). The biogenic materials are represented mainly by shell fragments of gastropods, bivalves, foraminifera and other unidentified fragments. Microscopic examination revealed that most of the shell fragments are severely micritized which could be responsible for the breakdown of coarse biogenic particles to finer particles which would then be moved away by tidal currents.

As shown in Figure 6.15a, the estuarine (samples E7, E213 and E 610) and marine (samples S1, NB2 and SB1) sediments within the size range of 0.090 to 0.212mm are composed almost entirely of quartz with a small amounts of lithic and carbonate grains . The percentages of quartz particles within the grain size range of 0.090 to 0.212mm in estuarine samples vary from 83 to 93% , while beach samples vary from 89 to 93% and seabed samples vary from 86 to 89% . The river sediments within the same size range, however, are composed of variable amounts of quartz in the range of 33 to 78%, while the rest consist of lithic fragments probably derived from upstream erosion. The percentage of carbonate component in this size range is very small making up less than 2% in estuarine samples , less than 3% in beach samples and less than 6% in seabed samples, while in the river samples the carbonate fragments are generally absent.

The percentage of carbonate within the size range of 0.090 to 0.212mm as estimated by counting the number of grains in the samples are smaller than the values estimated from the acid-digestion method which showed that the values vary from 1.2 to 7.5% (Figure 6.32). These high values as estimated by acid-digestion are due to the higher percentage of carbonate in the coarser grain size range as shown in Figure 6.15b. Within the coarser size range between 0.212 to 0.424mm, the percentage of carbonate are slightly higher varying from 6 to 21% in estuarine samples, from 4 to 20% in beach samples, while in seabed samples the

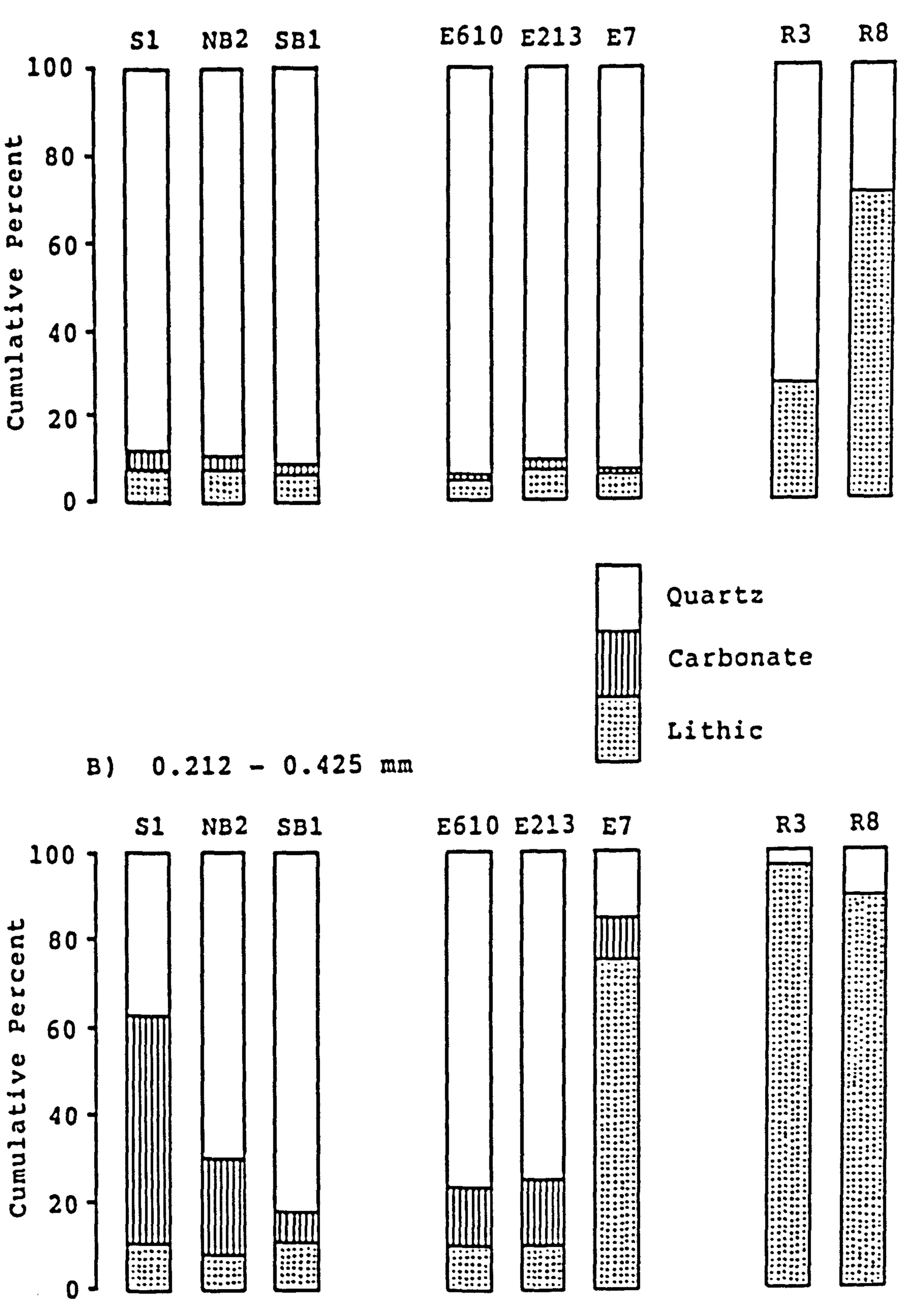

Figure 6.15. Bulk mineralogy of marine, estuarine, and river sediments. A) For material of the 0.090 - 0.212 mm grade. B) For material of the 0.212 - 0.425 mm grade.

percentages are very high, from 39 to 97% . The lack of quartz sand coarser than 0.212mm in some of seabed samples may explain the very high percentage of carbonate in this size range.

As shown in Figure 6.15a, the relative amounts of lithic fragments within the size range of 0.090 to 0.212mm vary from 6 to 15% in estuarine samples, from 8 to 11% in beach and seabed samples, but in river samples lithic material dominates the whole population ranging from 27 to 78% . The percentage of lithic material is even higher in the coarser size range of 0.212 to 0.424mm varying from 89 to 97% . Sample E7 which was taken from the upper part of the estuary probably marked the limit of tidal intrusion since the sediment is composed of a mixture of very fine sand from the sea and coarser material from the river.

This mineralogical evidence proves that estuarine sediments are derived mainly from a marine source which is consistent with the qualitative evidence from bedform migration (chapter 2) and the rate of sediment transport in and out of the estuary (chapter 5).

6.7. Estuarine sediments

Inspection of the spatial variation of coarse and fine fractions and the textural parameters of all estuarine

samples indicates that some general trends are observed. Figures 6.16 to 6.20 show the variations of cumulative percentage coarser than 2.0, 2.5, 3.0, and 3.5ϕ, while Figures 6.21 to 6.25 show the variarions of textural parameters (mean grain size, sorting, skewness, and kurtosis) along six transects (Figure 6.1) across the estuary. The distribution of estuarine sediment shows a trend of finer material upstream. Coarser material is more abundant in the lower part of the estuary, while the finest sediment can be found on the intertidal flat near the tidal limit of the estuary.

The percentages of material coarser than 2.5, 3.0, and 3.5 ϕ show striking variations across the intertidal flats (Figures 6.22 to 6.26). High percentages of coarse material are found on the higher sand flats while the lowest are found on the bank adjacent to the salt marsh and adjacent to the main channel because of the presence of significant amount of fine material. On the sand flats, as shown in Figures 6.16 to 6.20, material finer than 3.5 is present only in sediments upstream of transect 2, while generally absent downstream of this transect line. A small amount of fine material finer than 3.5ϕ is present at the margin of the estuary. Fast tidal currents on the sand flats downstream of transect 2 presumably prevent deposition of material finer than 3.5ϕ.

In areas where the sediments contain a considerable

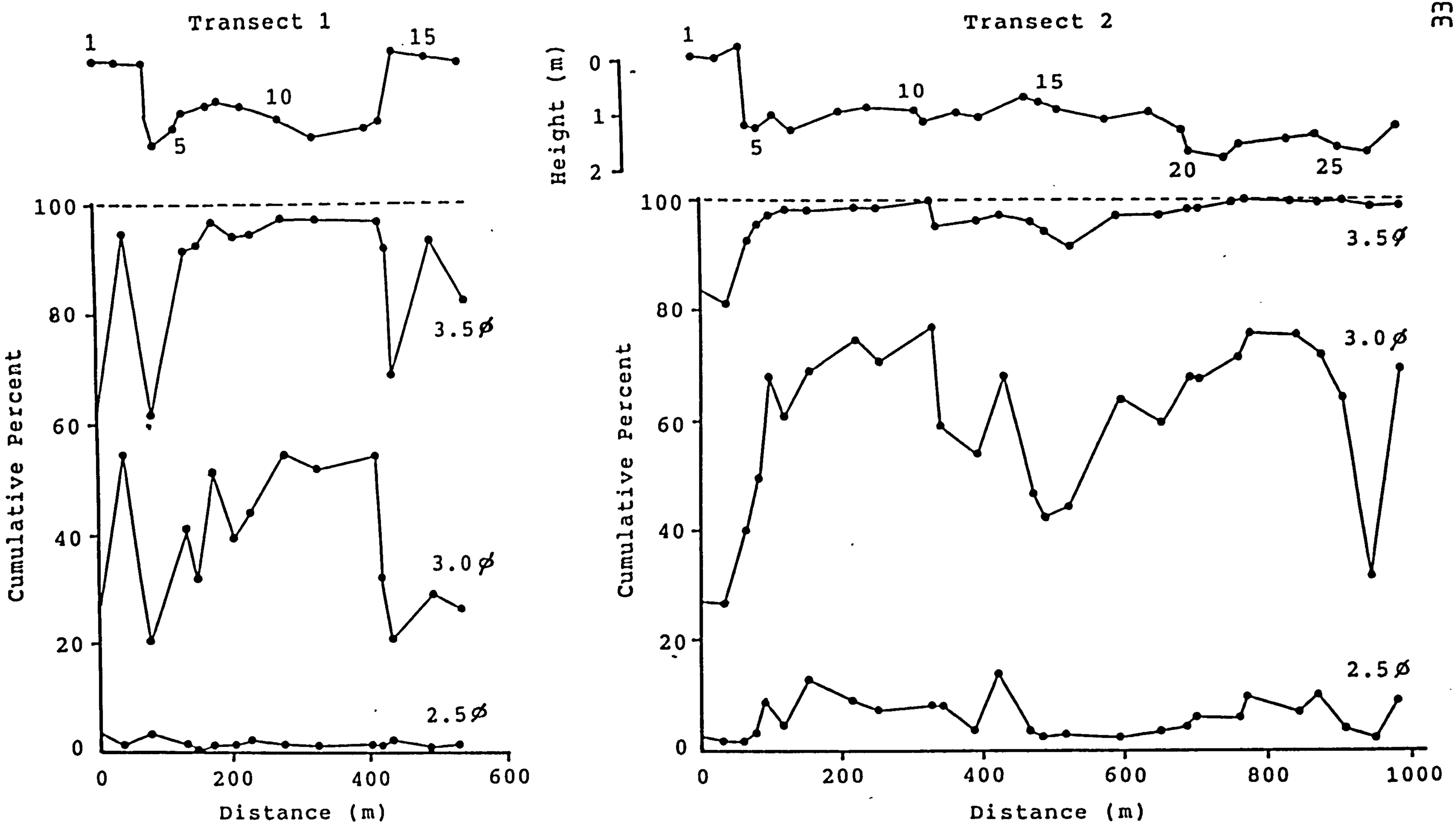

Figure 6.16. Variations of sediment coarser than 2.5ø, 3.0ø, and 3.5ø along transects 1 and 2.

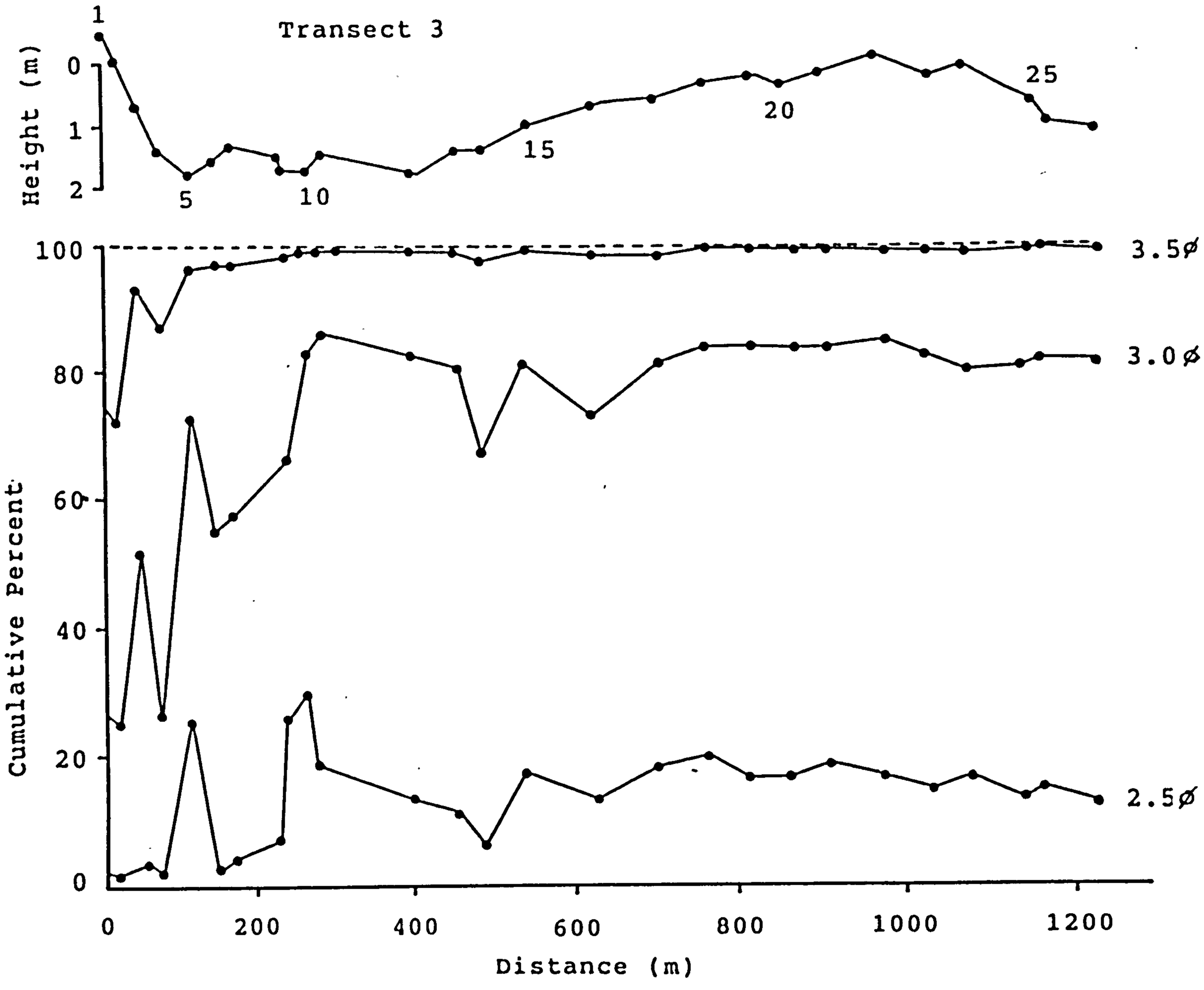

Figure 6.17. Variations of sediment coarser than 2.5ø, 3.0ø, and 3.5ø along transect 3.

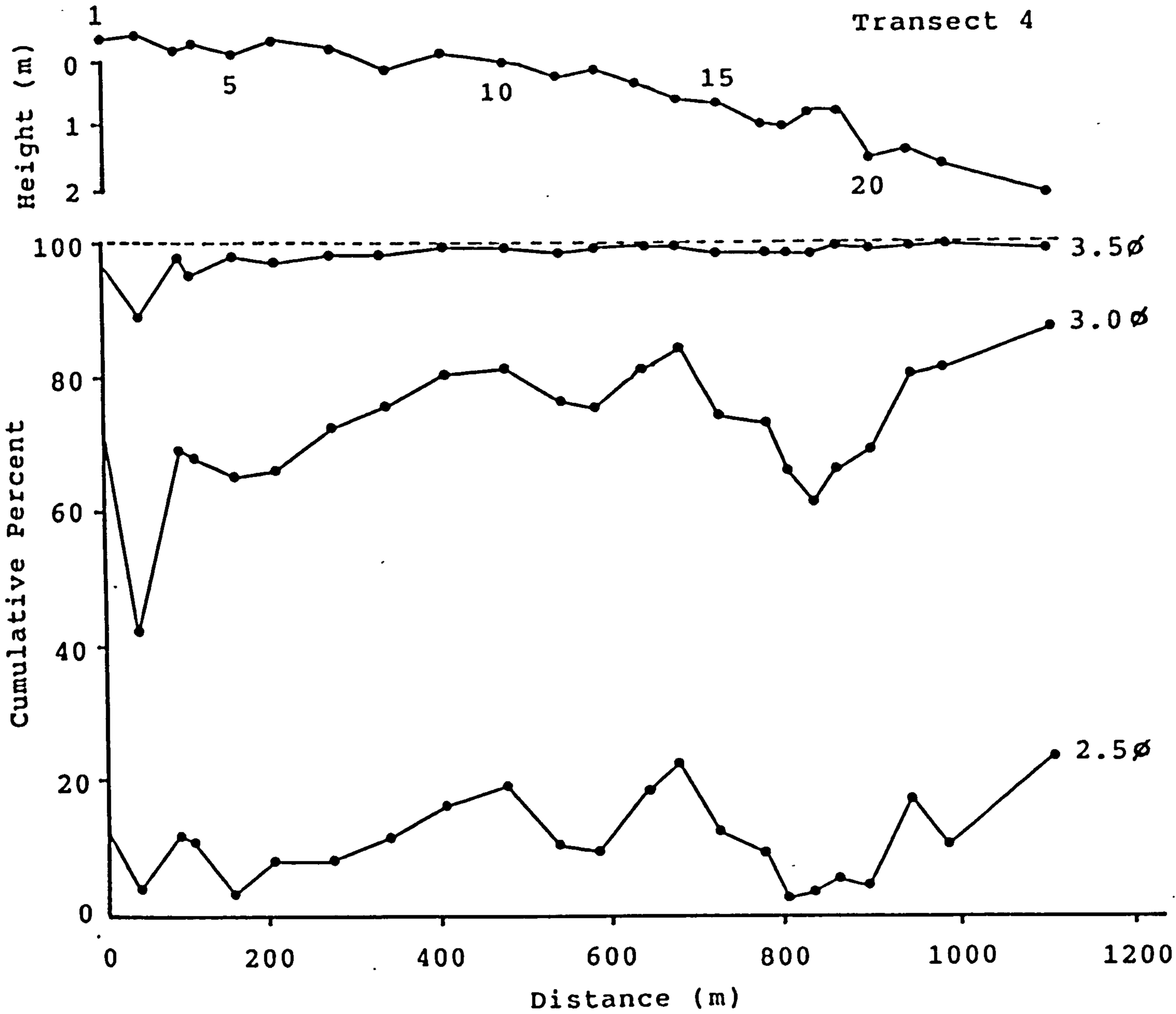

Figure 6.18. Variations of sediment coarser than 2.5ø, 3.0ø, and 3.5ø along transect 4.

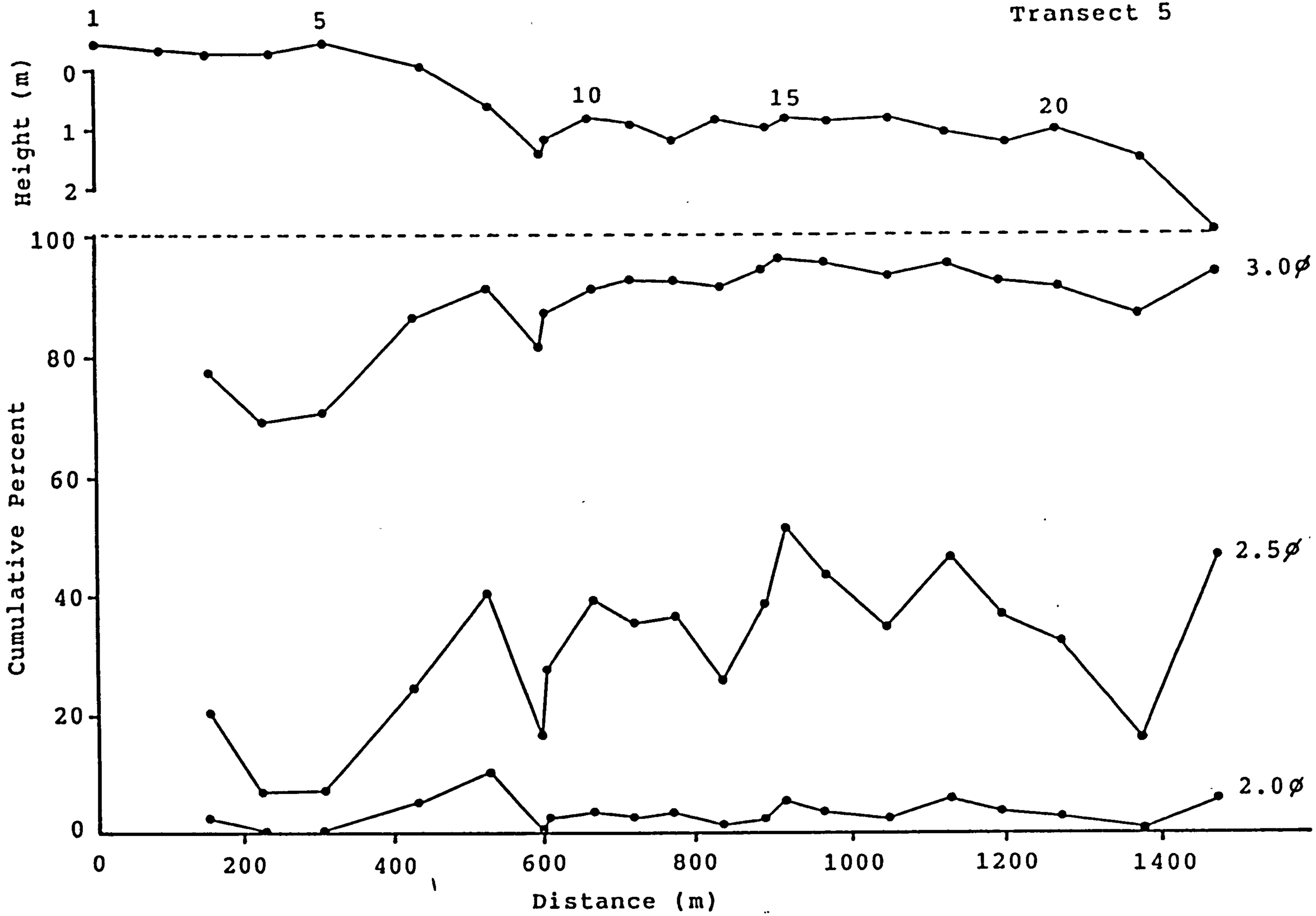

Figure 6.19. Variations of sediment coarser than 2.0ø, 2.5ø, and 3.0ø along transect 5.

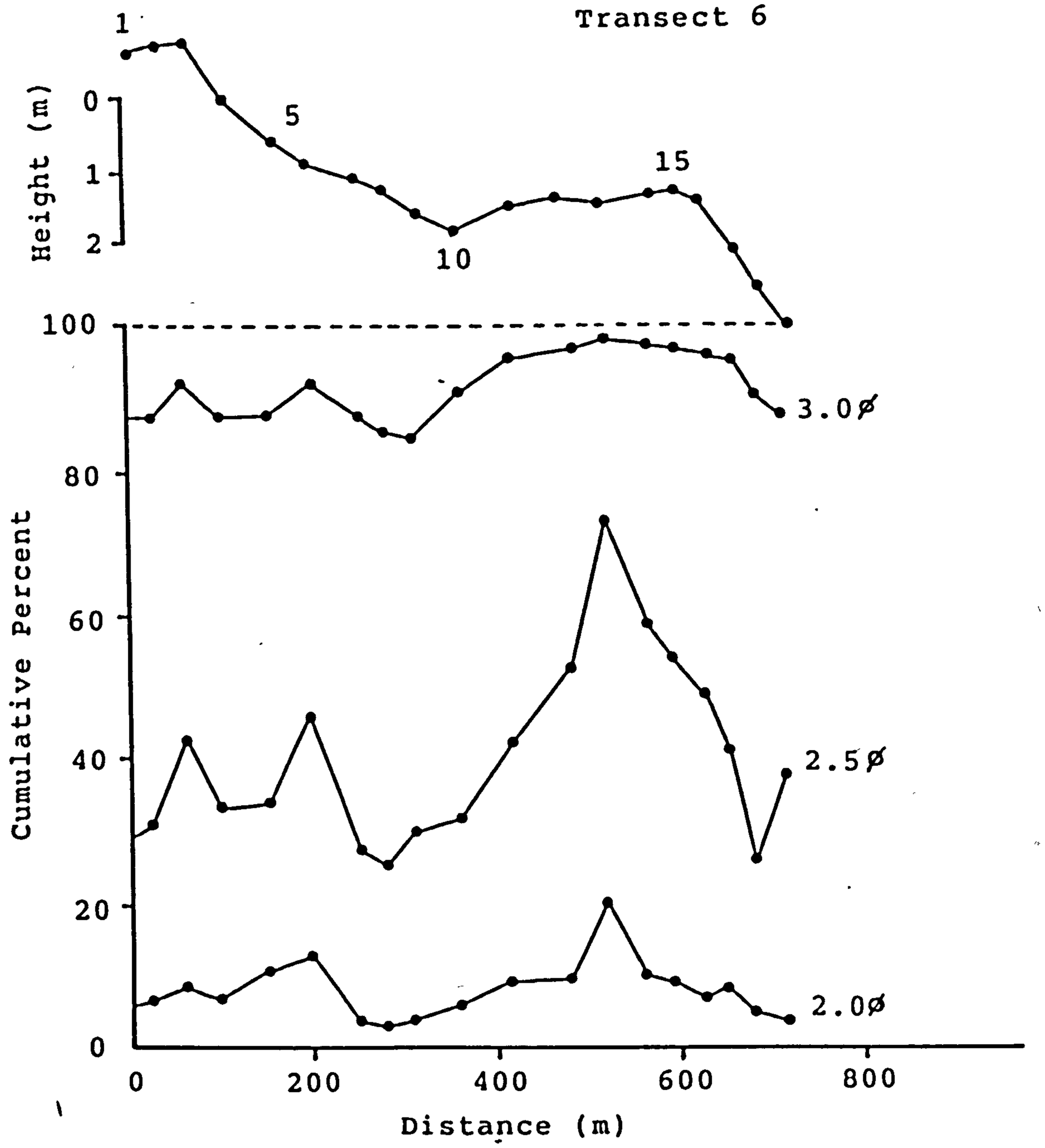

Figure 6.20. Variations of sediment coarser than 2.0ø, 2.5ø, and 3.0ø along transect 6.

amount of coarse material, the currents are powerful enough to sustain fine material in suspension and to prevent deposition. Sediments finer than 0.150mm (2.75ø) are fine enough to be transported in suspension rather than be carried along the bed (Dyer, 1984). The deposition of fine material increases in areas of slower currents such as at the margin of the estuary, so decreasing the percentage of the coarse fraction component in the sediments. In other words, intertidal flat sediment texture is a function of the strength of the tidal current . The variations of the coarse or fine fractions in sediment samples collected along each transect may possibly identify areas of high, moderate or low currents on the sand flats.

On transect 1 (Figure 6.16), most of the samples at the centre of the transect line contain more coarse material where the percentage of material coarser than 3.5ø is greater than 95% because of fast currents which prevent deposition of fine material. Samples collected at the margin (E103 and E114) contain slightly high percentage of fine material which may correspond to quiescent conditions away from the main channel ensuring a selection process in favour of deposition of fine sediment. As shown in Figure 6.21, the two samples collected from the centre of the transect (E107 and E108) are negatively skewed while the rest of the samples are positively skewed.

On transect 2 (Figure 6.16), the smallest percentage of material coarser than 3.0ø is found on the highest sand

flat (samples E214 to E219) and at the estuary margin. The fineness of sediment on the higher sand flat reflects the low energy level. Higher sand flats are submerged only close to high tide where currents approach their minimum value which facilitates settling-out of the finer material. As expected, some of the samples (E216 to E218) found in this area are positively skewed.

The existence of two tidal channels at the south end of transect 3 is clearly shown in Figure 6.17. Sample E305 collected from the edge of the outer bend of a former main channel has a higher percentage of coarse material compared to sample E306 collected from the opposite side of the channel. The percentage of coarse material in sample E305 is among the lowest found on this transect. The highest values are found at the edge of the main channel (E309 and E310). The sediment on the higher sand flats near Portmeirion shows a small variation except at the edge of the blind channel north of the transect where the percentage of coarse material is reduced.

Flood-oriented sandwaves with a wavelength of between 10 to 20 m have been observed on the low sand flats near the main channel north of transect 4 (chapter 2). These areas must represent a high energy zone where fast flood currents dominate over ebb currents. As shown in Figure 6.18, the highest percentage of coarse material is found at the edge of the main channel and at mid-elevation across the sand flats. Deposition of fine material occurs at isolated

places adjacent to the saltmarsh south of the transect line. Similar trends can be observed on transect 5 (Figure 6.19) and transect 6 (Figure 6.20).

At the estuary mouth (as represented by transect 6, Figure 6.20) the percentage of material coarser than 2.5ø is about 10%, while at the estuary head (as represented by transect 1, Figure 6.16) the percentage decreases to about 3%, while the percentage of material coarser than 3.0ø varies from 99% at the estuary mouth to less than 40% at the estuary head. These trends are similar to the variation of mean grain size which steadily decreases upstream from about 2.5ø at the estuary mouth (Figure 6.25) to about 3.0ø at the estuary head (Figure 6.21). Since tidal currents vary across the intertidal flats, we might expect the amount of coarse material also to vary across the intertidal flats.

As shown in Figures 6.21 to 6.25, the variations of textural parameters are less obvious than the variations of cumulative percent profiles (Figures 6.16 to 6.20). However, comparisons between these two sets of figures indicate that some correlation between them exists. For example, samples with high percentage of coarse material have large mean grain size, are poorer sorted, and negatively skewed.

The ranges of mean grain size for each transect plotted in the form of histogram for ease of comparison are shown

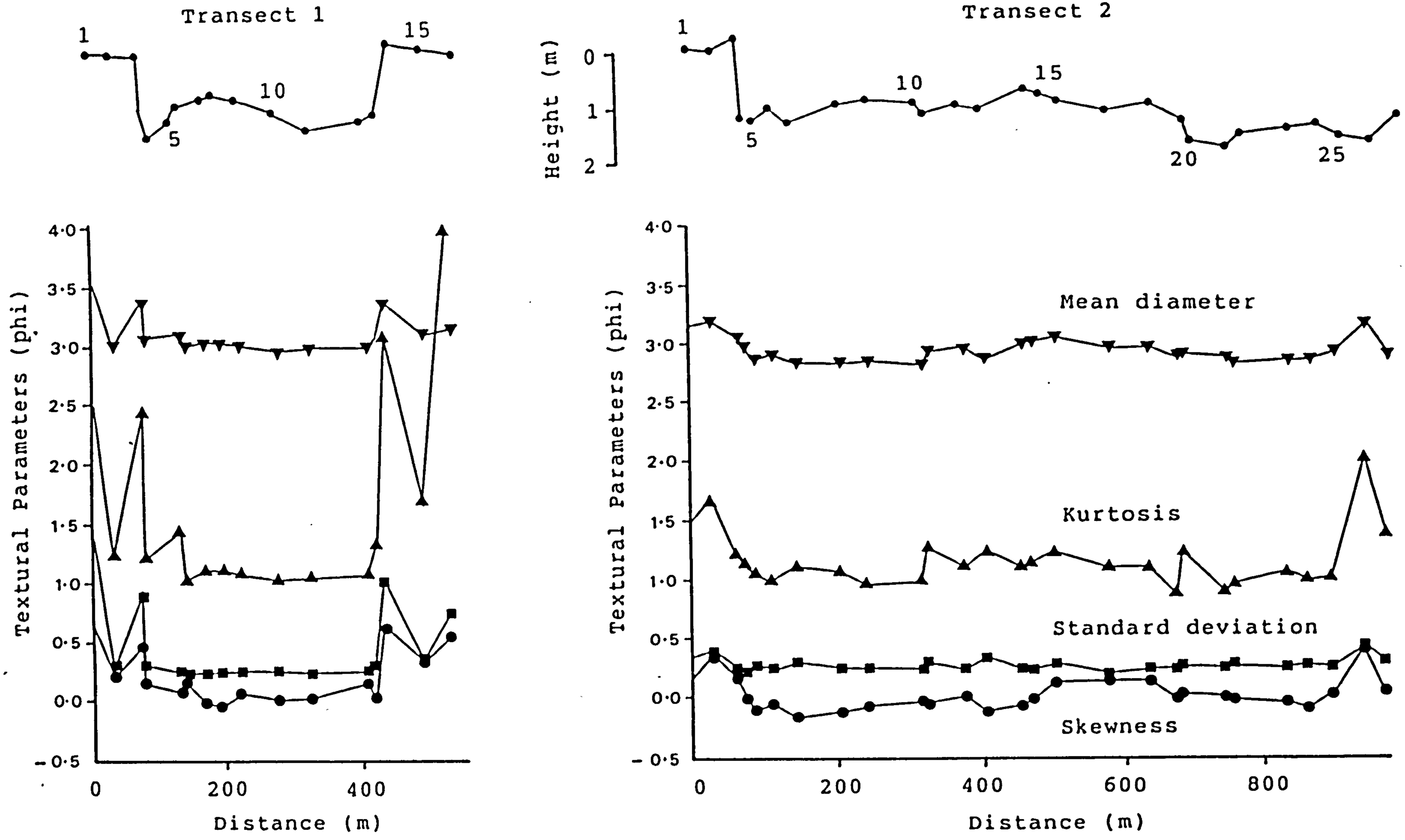

Figure 6.21. Variations of textural parameters along transects 1 and 2.

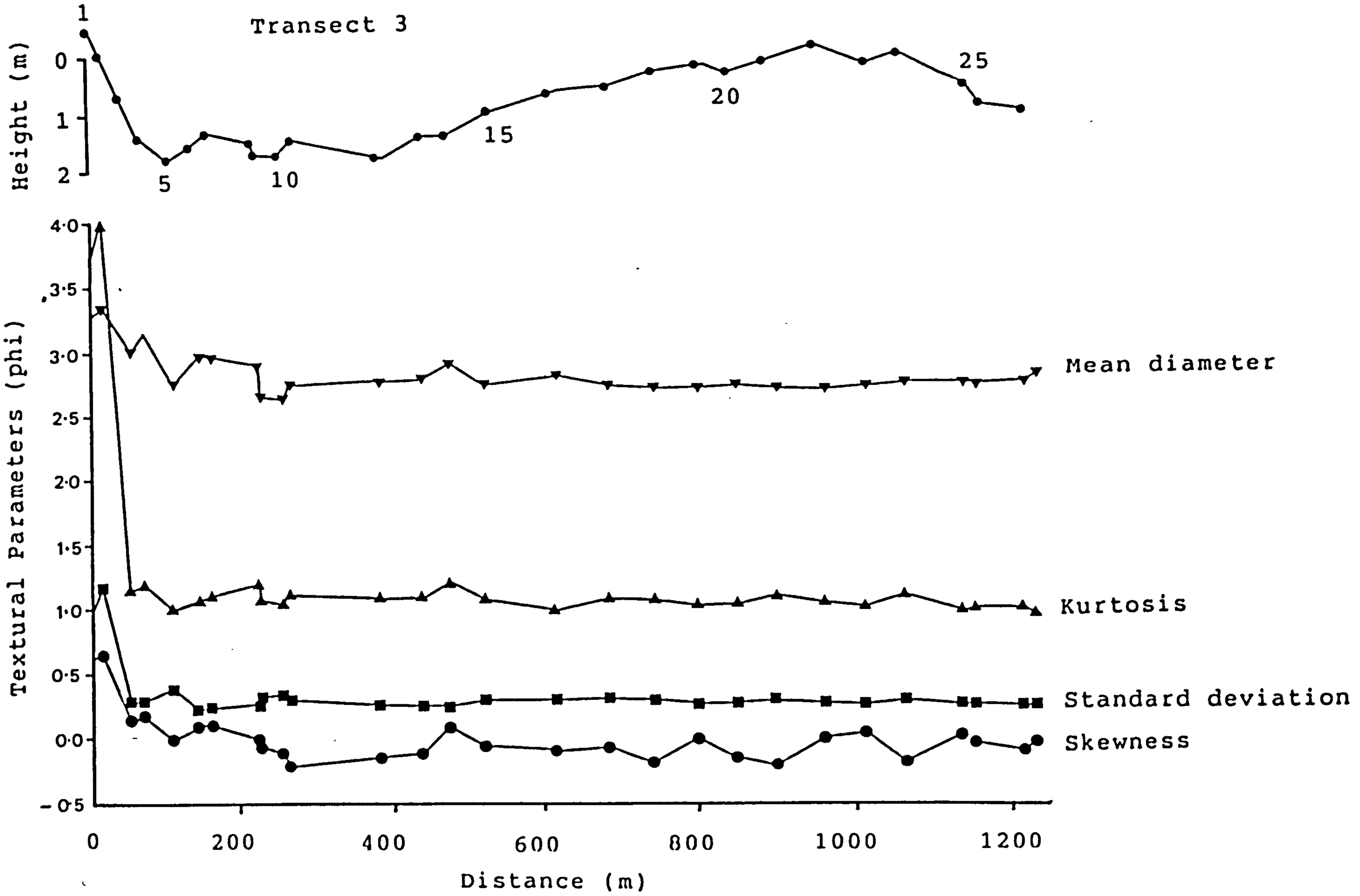

Figure 6.22. Variations of textural parameters along transect 3.

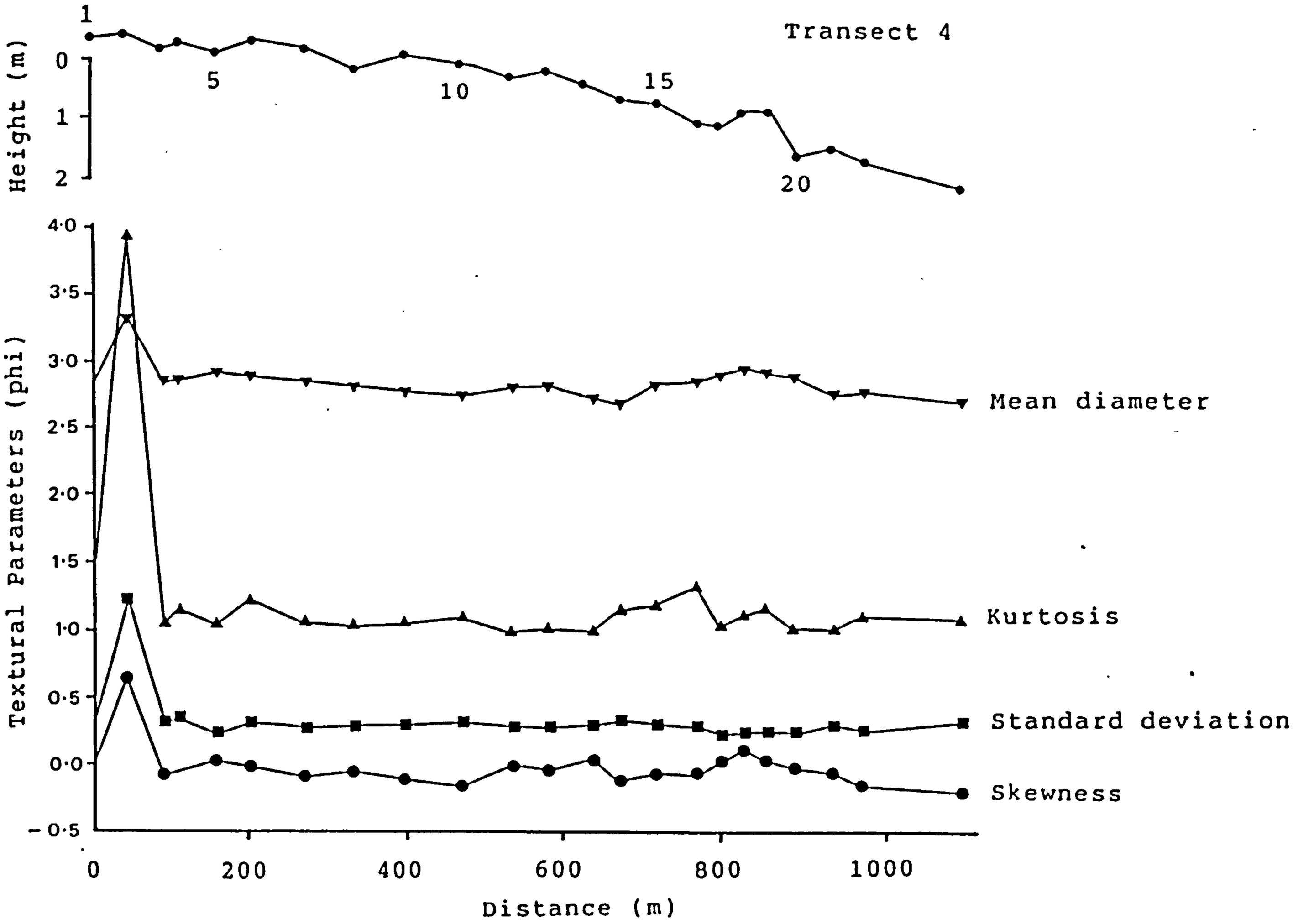

Figure 6.23. Variations of textural parameters along transect 4.

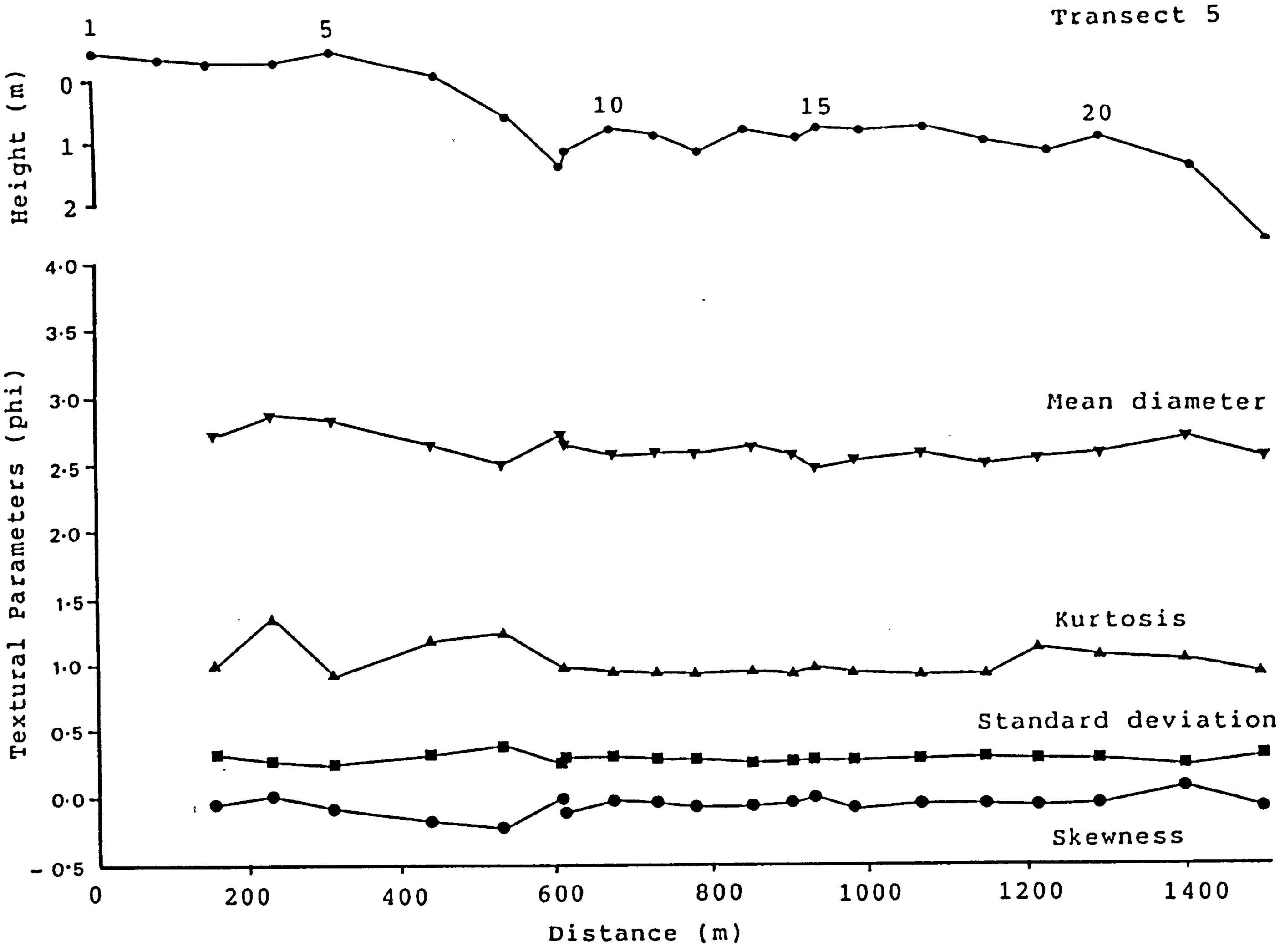

Figure 6.24. Variations of textural parameters along transect 5.

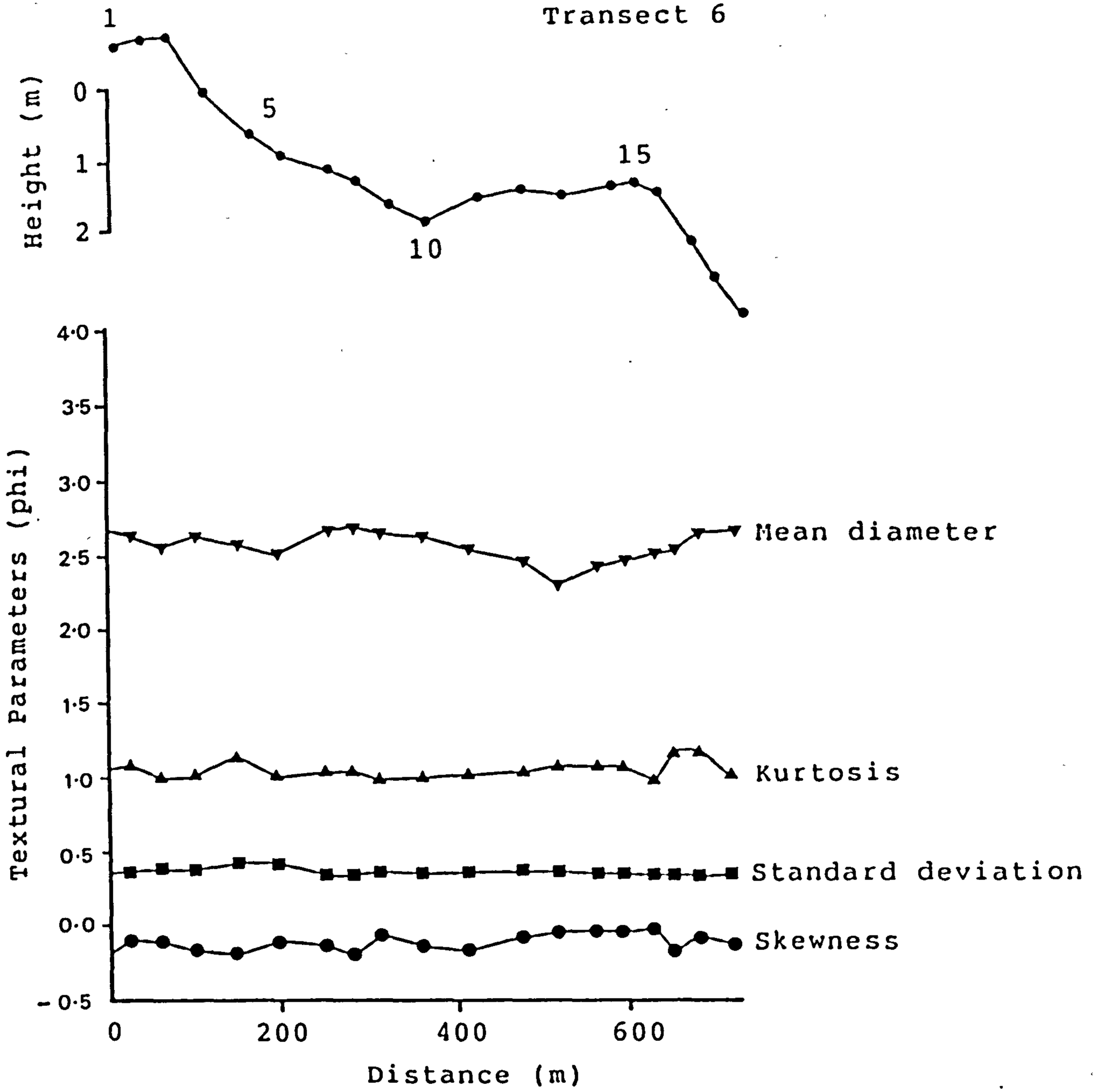

Figure 6.25. Variations of textural parameters along transect 6.

in Figure 6.26 and the average mean grain size for each transect is shown in Table 6.1. These show that there is a general trend in which mean grain size decreases from transect 6 (Figure 6.25) to transect 1 (Figure 6.21). Samples further upstream from transect 1 (E1 to E8) were not included in the comparisons because the number of samples collected in this area is small and scattered widely along the estuary. However, the average mean grain size of samples E1 to E8 is slightly finer than the average mean grain size of samples of transect 1. The progressive upstream fining of sediment over the tidal flats could be explained by the fact that fine sediments are much more easily moved than coarser sediments and will tend to travel faster and further from the mouth. The exclusion of coarse sediment from the estuary head causes the mean grain size to be finer at the head than at the mouth.

Most of the samples collected on the estuarine sand flats are very well sorted, with standard deviations ranging from 0.20 to 0.58ϕ (Figures 6.21 to 6.25). The average sorting of sand flat sediments for each transect is shown in Table 6.1 and the range of standard deviation for each transect is shown in Figure 6.27. The spatial distribution of the sorting values of estuarine sand flat sediments exhibits a general pattern in which the sediment shows a tendency to become better sorted toward the upstream part of the estuary. The progressive increase in the sorting of the estuarine sediments from the mouth to the head of the estuary together with the fining of

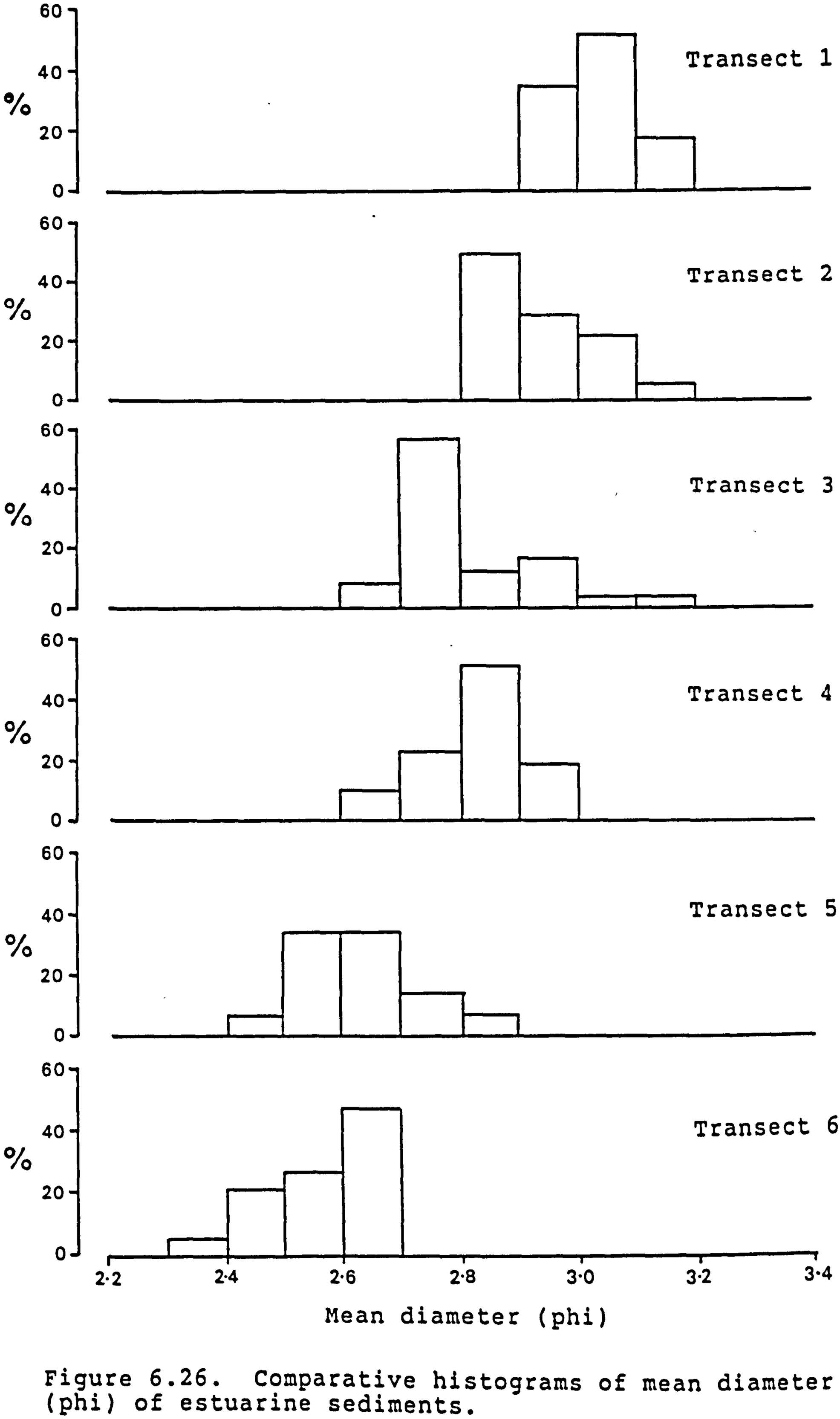

Figure 6.26. Comparative histograms of mean diameter (phi) of estuarine sediments.

Table 6.1. Average values of textural parameters for each transect.

Transect number	Mean Diameter	Standard Deviation (phi)	Skewness	Kurtosis
1	3.032	0.244	0.055	1.150
2	2.924	0.278	0.010	1.140
3	2.808	0.286	-0.033	1.094
4	2.830	0.276	-0.045	1.105
5	2.644	0.312	-0.043	1.049
6	2.566	0.349	-0.121	1.059

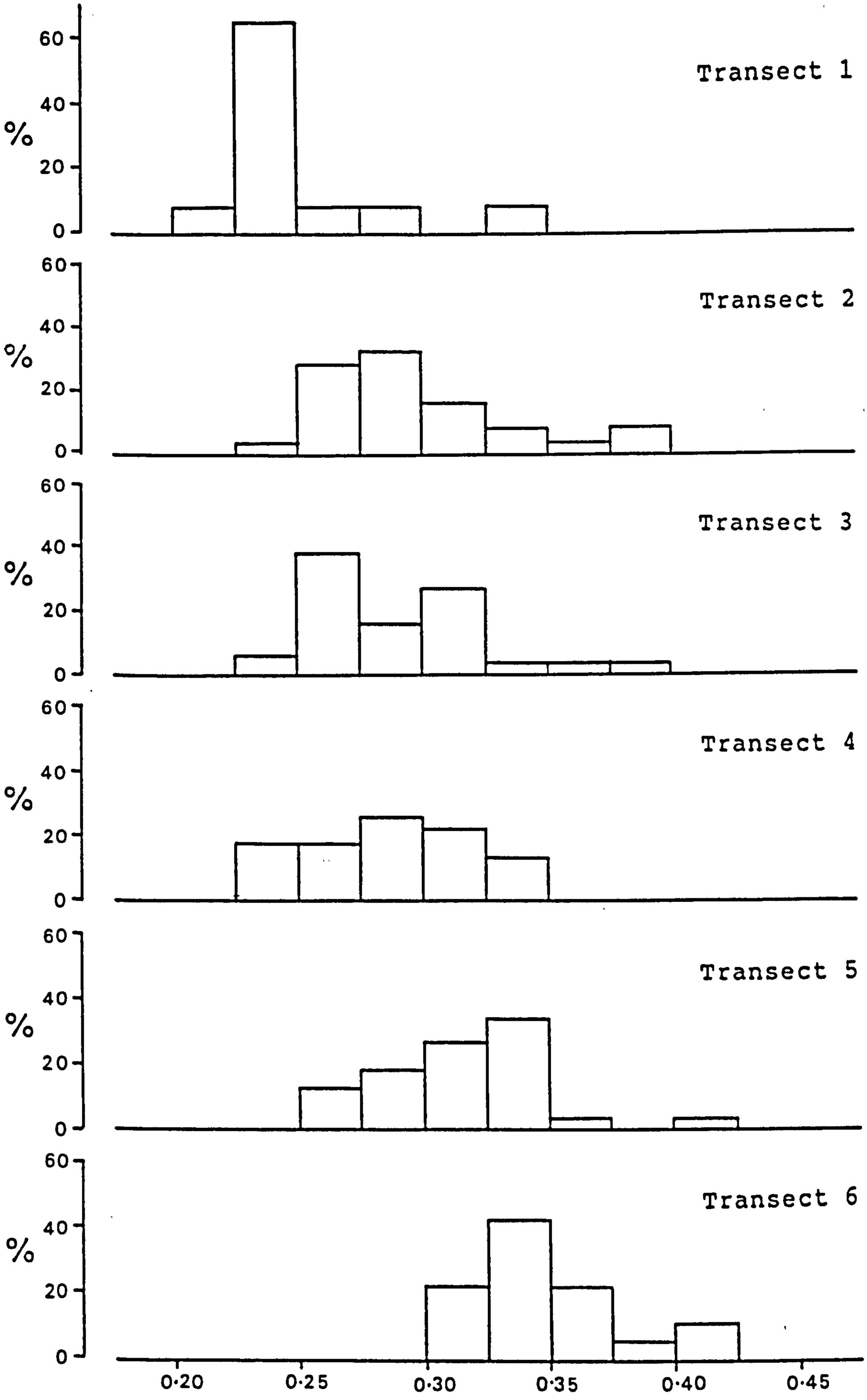

Figure 6.27. Comparative histograms of standard deviation (phi) of estuarine sediments.

sediment upstream indicate that it has been deposited from a flow which has been continually losing its energy along its transport path. These trends are in general agreement with the general trend of diminution of tidal current upstream (chapter 3).

The variations of sorting along the transects show some correlation with the variation of mean grain sizes. Samples with coarser sediments tend to show larger standard deviations probably due to fluctuating currents and turbulence on the early phase of flood and late ebb tides. Higher sorting values are observed for salt marsh samples because of deposition of fine material within this sub-environment. The quiescent conditions of these isolated place far away from the main channel ensure a selection process in favour of fine sediments. At low water level, sorting is better than the average for each transect because high current velocities near the margins of the shallow channel have removed or prevented deposition of all but a small quantity of fine material. The worst sorting occurs far away from the mobile sand zone where an increasing quantity of fine sediment occurs in response to an overall lowering of current velocity.

The sediments of the Dwyryd estuary exhibit variable values of skewness varying from -0.25 to 0.20 (Figures 6.21 to 6.25). Sediments of the upper part of the estuary show a strongly positive skewness. Negatively skewed sediments are found mostly on the sand flats in the lower

part of the estuary. Half of the samples along transect 4 are negatively skewed and almost all samples along transects 5 and 6 are negatively skewed (Figures 6.24 and 6.25) where tidal currents are more powerful than in the upper part of the estuary. Sediments with a mean grain size coarser than 2.9ø tend to have negative skewness, resulting from removal of fine material in areas of more powerfull tidal currents.

Figure 6.28 shows a general tendency for the values of skewness to increase towards the head of the estuary. The average values of skewness for each transect are as shown in Table 6.1. The increase of skewness continues upstream where the average skewness of samples E1 to E8 is about 0.15 . This trend in skewness is caused by hydraulic sorting where the range of available grain sizes is reduced at the head by continuous sorting by diminishing tidal currents. Sediments are negatively skewed at the mouth because of the absence of a fine fraction, and positively skewed sediments dominate the estuary head because of the presence of a large quantity of fine material. Almost all samples from upper sections of the estuary and salt marsh are found to be positively skewed.

Figure 6.29 indicates that a high percentage of the estuary samples have kurtosis values greater than 1.0 and smaller than 1.5 . The average values of kurtosis for each transect are as shown in Table 6.1. The range of the

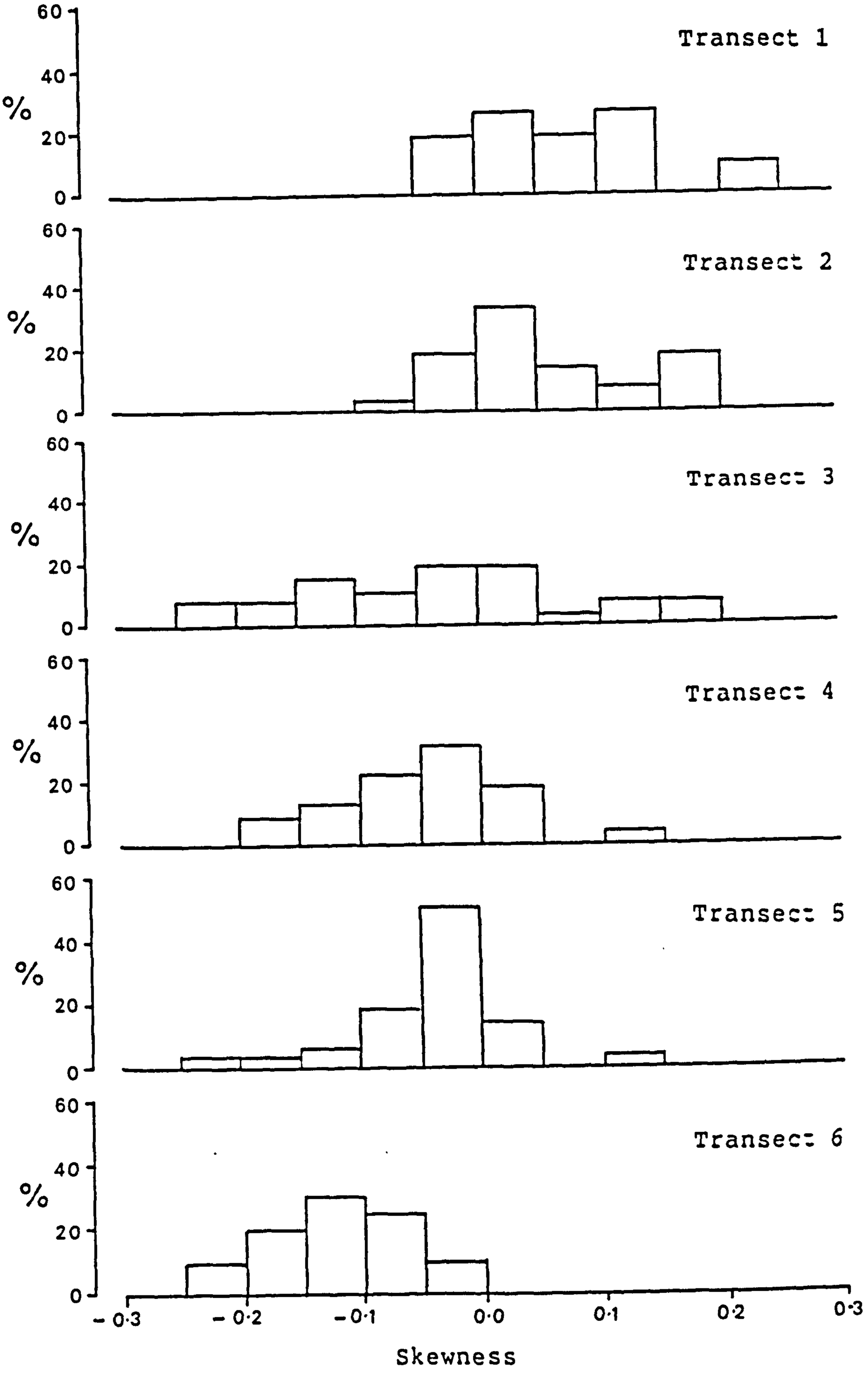

Figure 6.28. Comparative histograms of skewness of estuarine sediments.

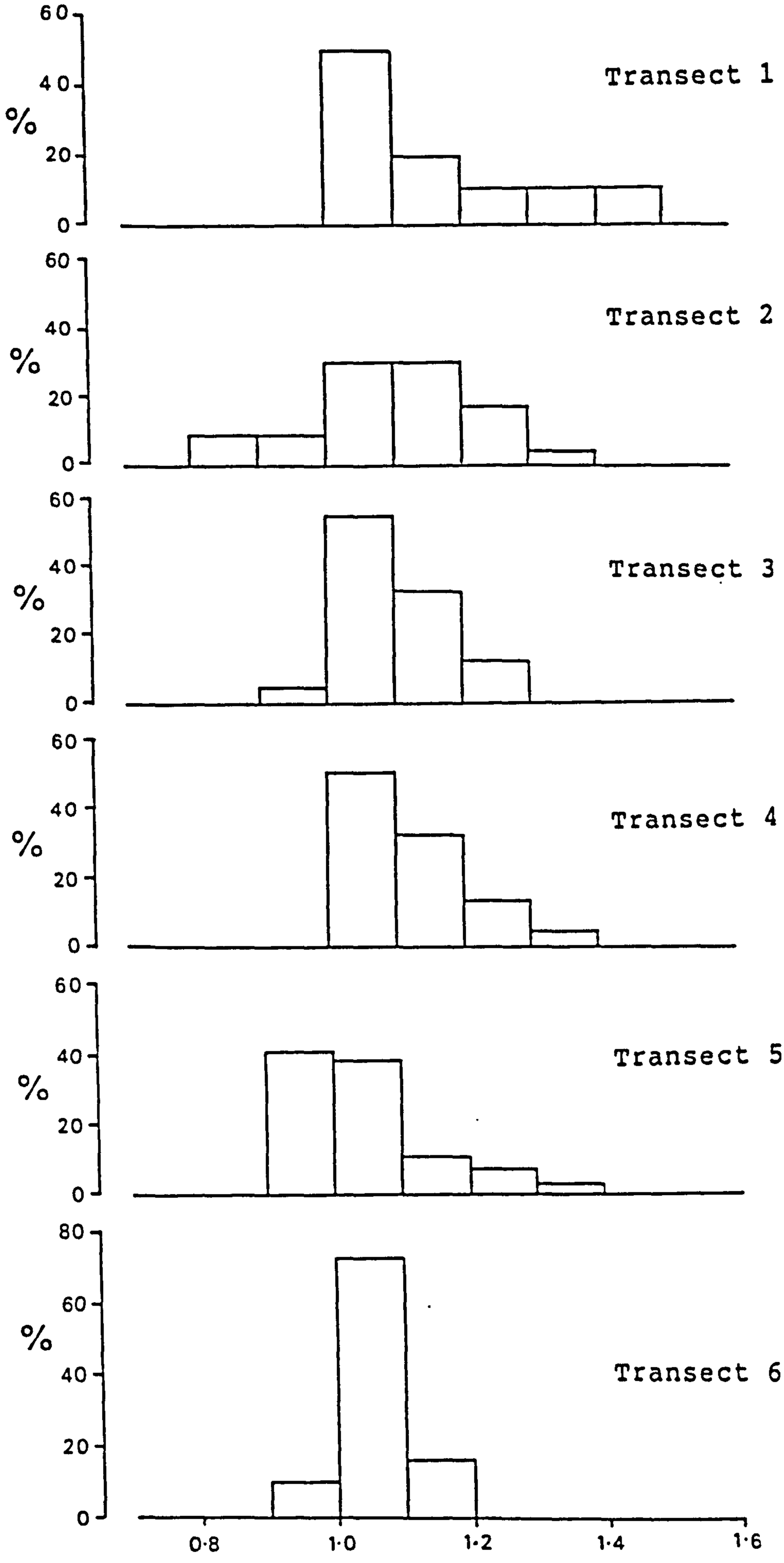

Figure 6.29. Comparative histograms of kurtosis of estuarine sediments.

averaged values is very small. There is, however, a small increase of kurtosis from the estuary mouth (transect 6) to the estuary head where the average of kurtosis of samples E1 to E8 is about 1.2 . This may be due to the increase of the fine fraction towards the head of the estuary. Since the values of kurtosis scatter erratically and no interpretable trend emerges from this parameter, kurtosis is not considered as a measure that can provide valuable information for the interpretation of grain size distribution curves (Blatt et al., 1972).

Figure 6.30 shows the variations of percentages of material coarser than 2.0, 2.5, 3.0, and 3.5ø from the beach at the estuary mouth to the upper limit of tidal intrusion (as shown in Figure 6.1) and the corresponding variations of textural parameters for the same samples as shown in Figure 6.31. All the samples plotted in Figure 6.30 are the coarsest found at each transect. Figures 6.30 and 6.31 indicate that the sediments found at the lower section of the estuary are generally coarser than found at the estuary mouth. The percentage of coarse material varies along the estuary, for example, material coarser than 2.0ø can be found only at the lower section of the estuary, i.e. from the beach to the transect 4. Upstream of transect 4, the percentage of material coarser than 2.0ø is very small. Material coarser than 2.5ø has been transported up to transect 1. Material coarser than 3.0ø exists only in very small percentages at the lower section of the estuary and gradually increases toward the estuary

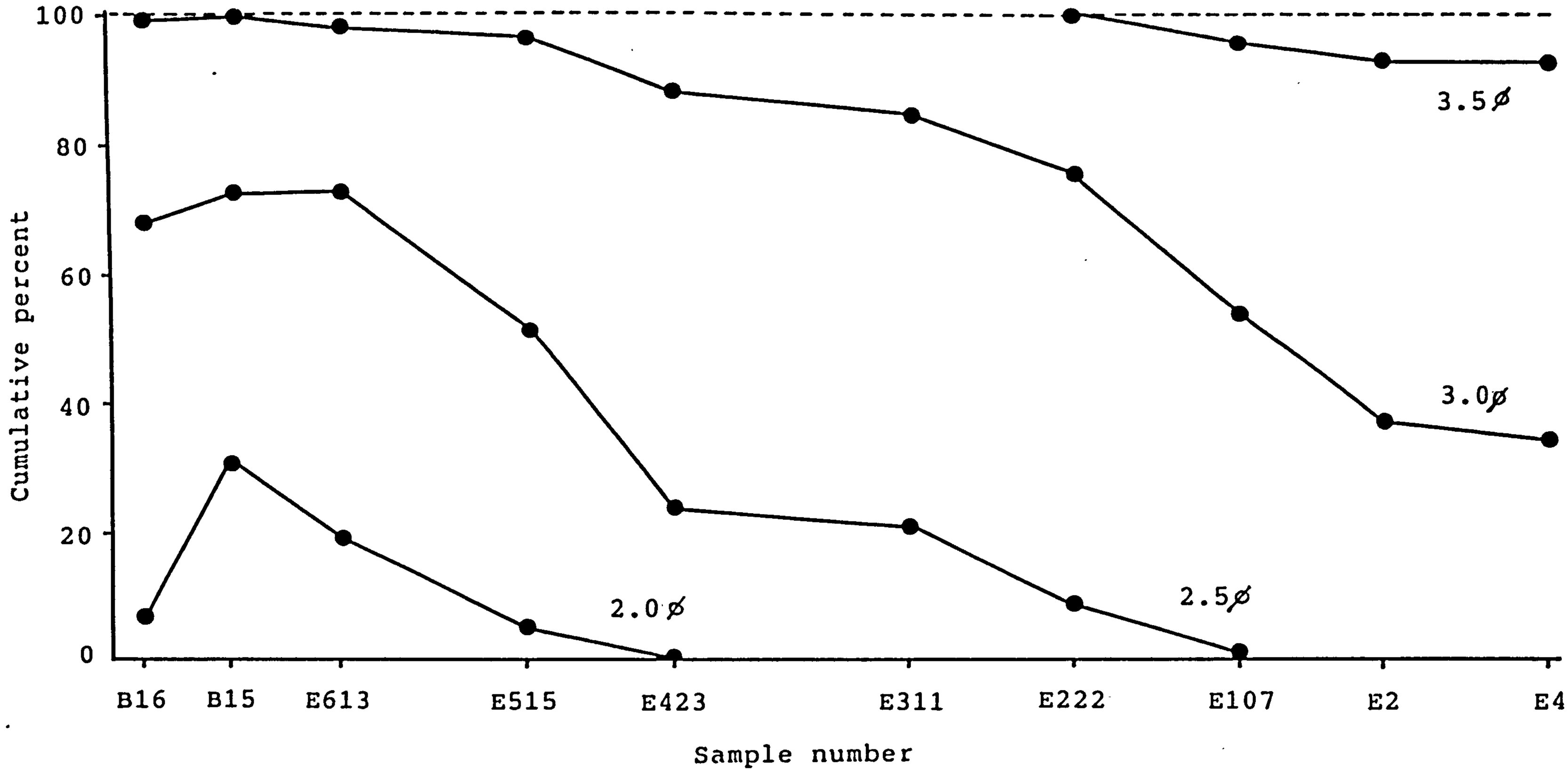

Figure 6.30. Longitudinal variation of material coarser than 2.0ø, 2.5ø, 3.0ø, and 3.5ø.

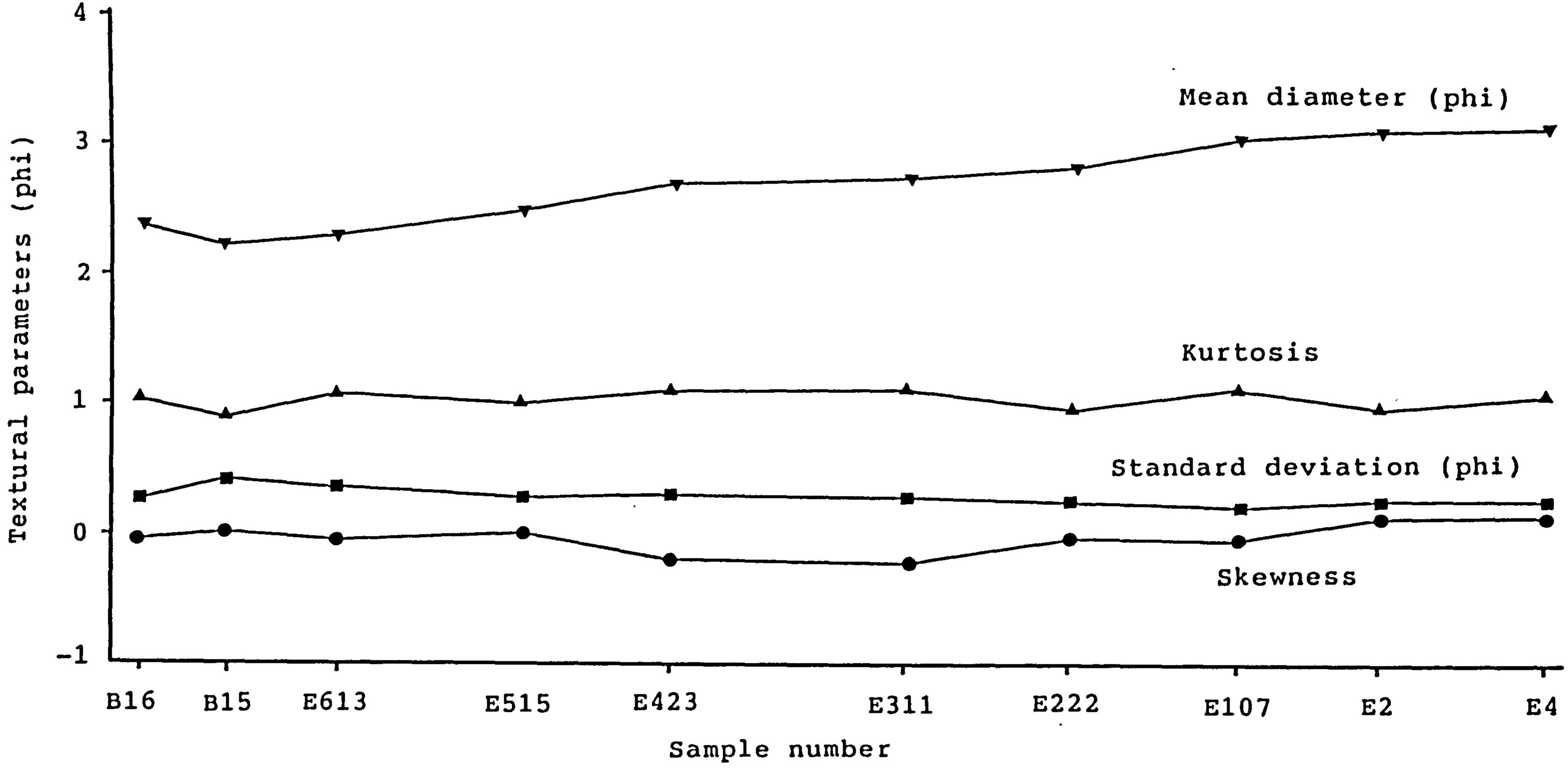

Figure 6.31. Longitudinal variation of textural parameters along the estuary.

head, where the percentage reach approximately 30% at the upper limit of tidal intrusion (sample E4). The coarseness of the material in the lower part of the estuary is attributed to high current velocities, frequently in excess of 100 cm/s (chapter 3), and probably to storm wave action, both capable of eroding and transporting away from the area all but medium-sizeparticles. Material finer than 3.5 can only be found at the upper section of the estuary where the currents are relatively slow as shown in Chapter 3.

The calcium carbonate content of 25 estuarine samples averaged about 2.5% by weight and ranged from 1.5 to 8% by weight (Figure 6.32a). In order to assess the effect of carbonate (shell) particles on the sediment size distribution parameters, some estuarine samples were re-sieved after the carbonate component had been removed by HCl digestion. Figures 6.32b and 6.33 show plots of mean diameter, standard deviation and skewness for both sets of samples (with and without carbonate component). These comparisons indicate that the differences between these two set of samples are small for the majority of the samples and we can conclude that the presence of small quantities of calcium carbonate material in the samples do not significantly alter the characteristic of the grain size distributions. The differences between these two sets of data are probably comparable to the error of the sieve analyses.

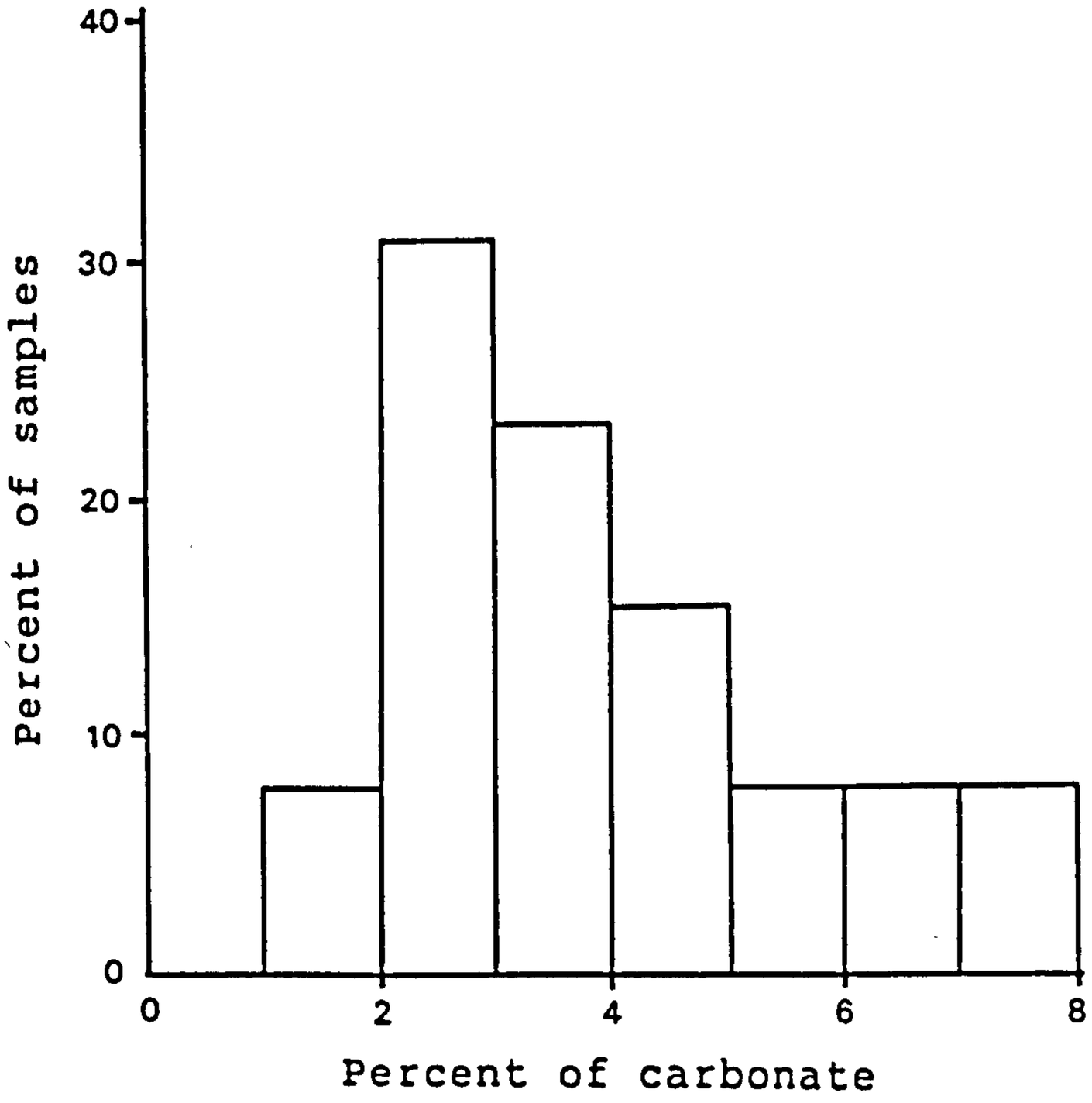

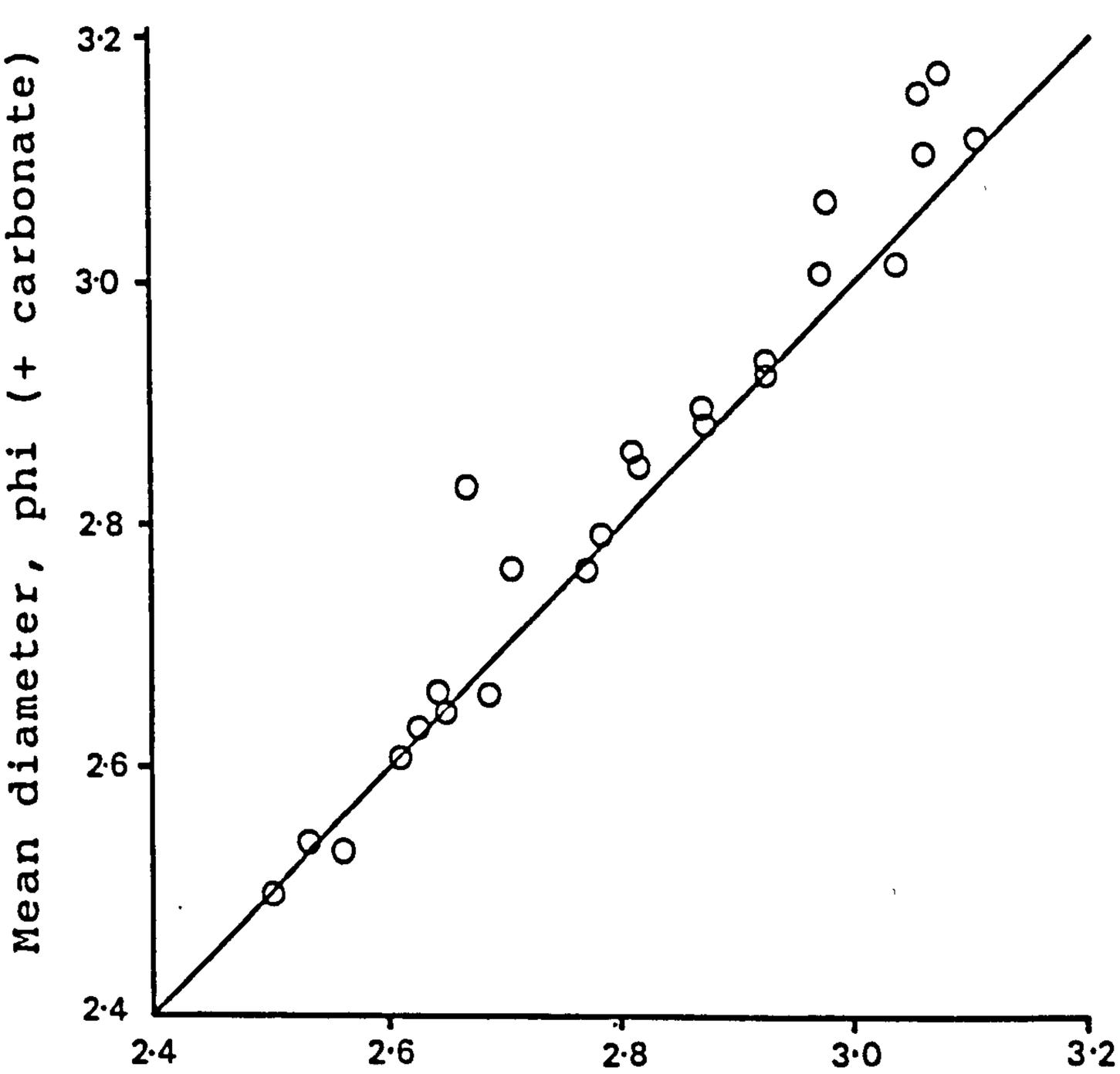

Figure 6.32. A) Histogram of distribution of percentage of carbonate in estuarine sediments. B) Comparisons between mean diameters before and after removal of carbonate, the line being that for perfect agreement.

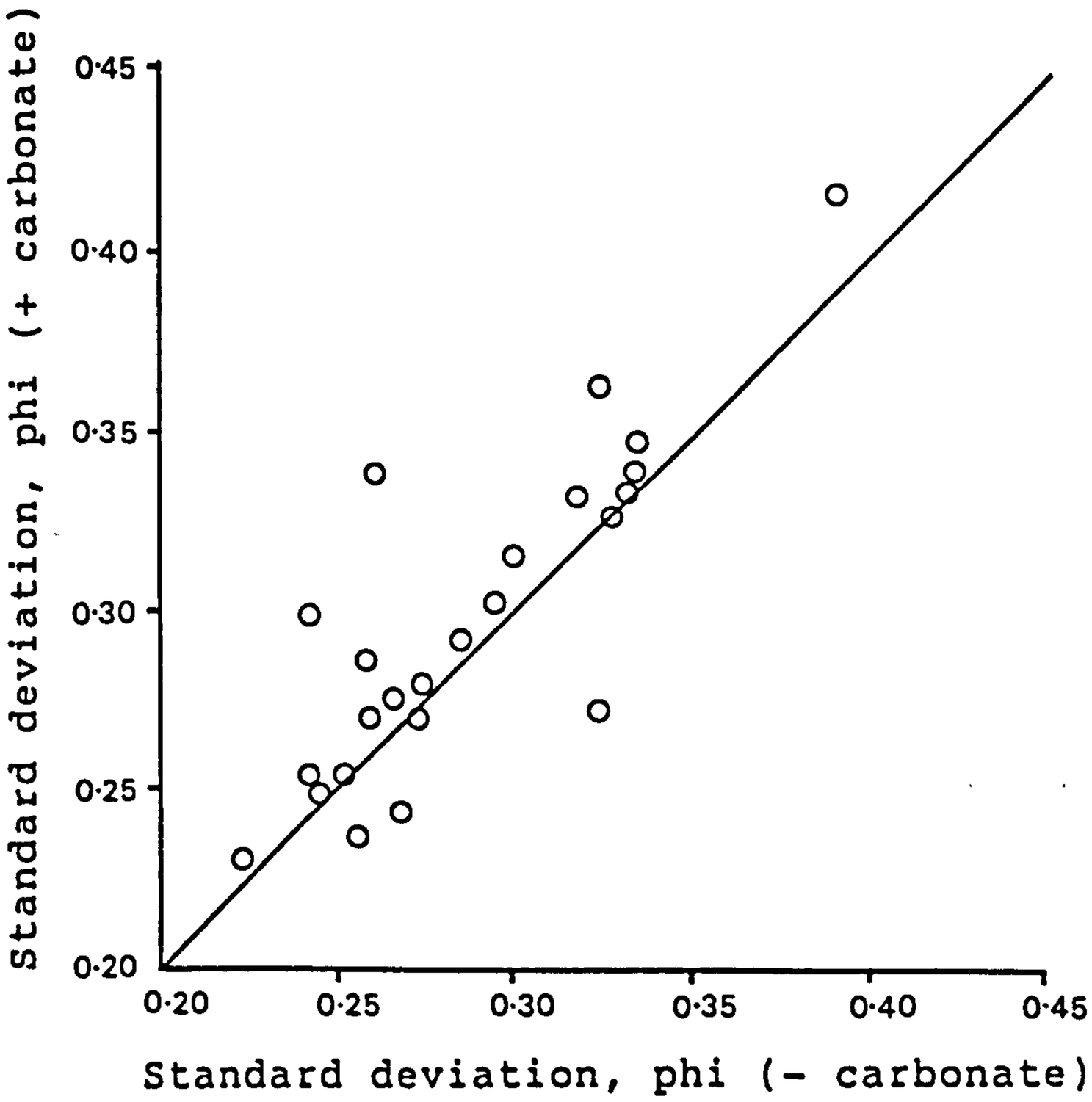

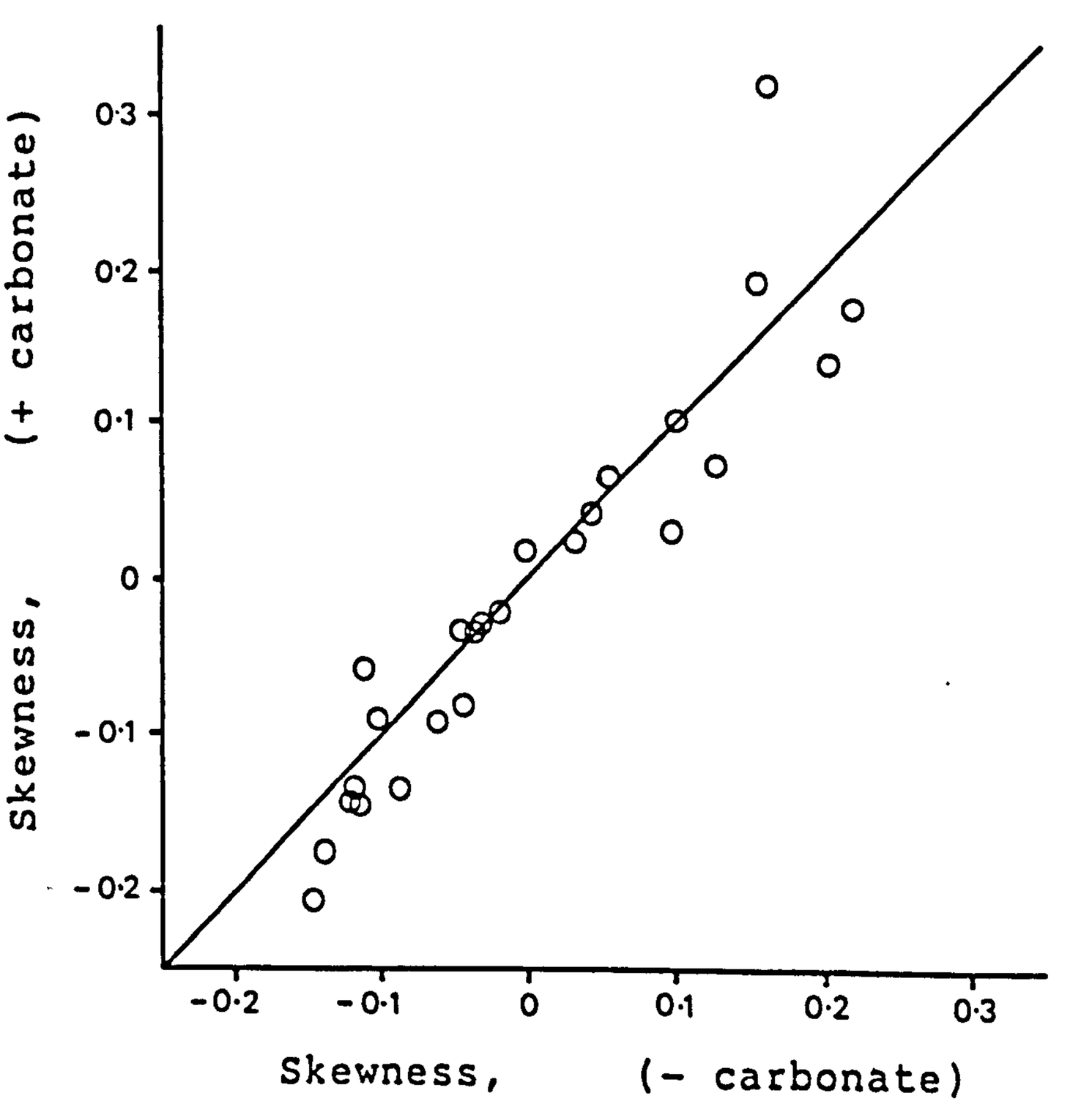

Figure 6.33. Comparisons between standard deviations (A) and skewness (B) before and after removal of carbonate. The straight lines being that for perfect agreement.

McLaren (1981), using his selective deposition model, suggested that if the sediments deposited at the head are finer, better sorted, and more positively skewed than the estuarine mouth sediments, then the net transport is landward, i.e., the source of the sediment must be marine. This study indicates that the characteristics of the estuarine samples satisfy all these three conditions; therefore, it is reasonable to suggest that the direction of sediment transport in this estuary is landwards. This is in agreement with the measured decrease of tidal currents in that direction and also in agreement with the mineralogical study of fluvial, estuarine and marine sand which proved that the estuarine sediments originate from sub-littoral parts of Tremadog Bay.

6.8. Beach Sediments

The results of sieve analyses for all beach samples are shown in Tables A7 to A9 (appendix). For ease of comparison between the estuary and beach sediments frequency histograms of mean diameter, standard deviation and skewness based on appropriate class intervals are shown in Figures 6.34 to 6.36. The characteristics of north and south beach sediments have been considered separately since it was very obvious from preliminary observations that the general characteristics of these sediments are slightly different. The mean grain size of the beach sediments is very variable compared to estuarine sediments ranging from

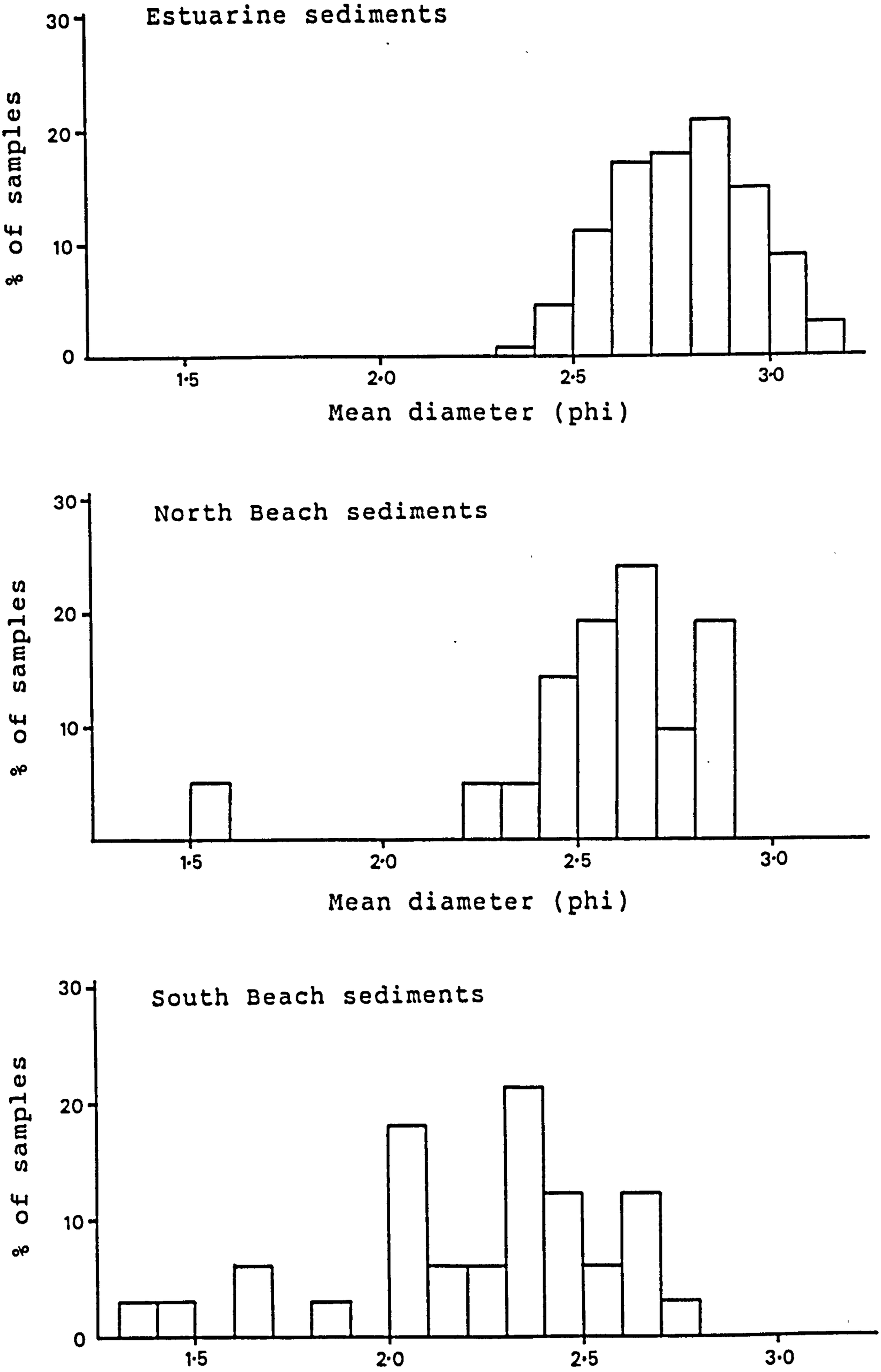

Figure 6.34. Comparison of mean diameter of estuarine and beach sediments.

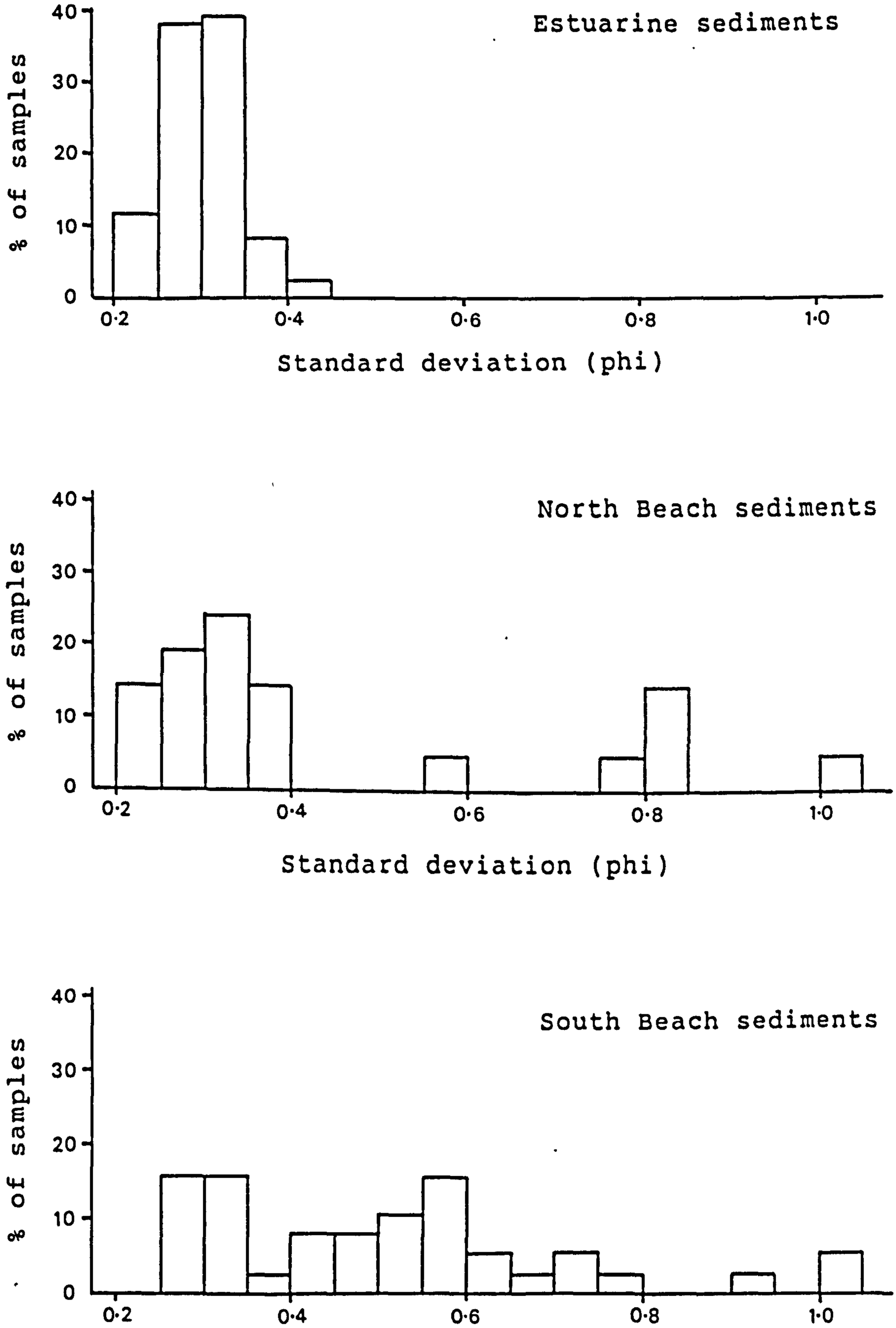

Figure 6.35. Comparison of standard deviation of estuarine and beach sediments.

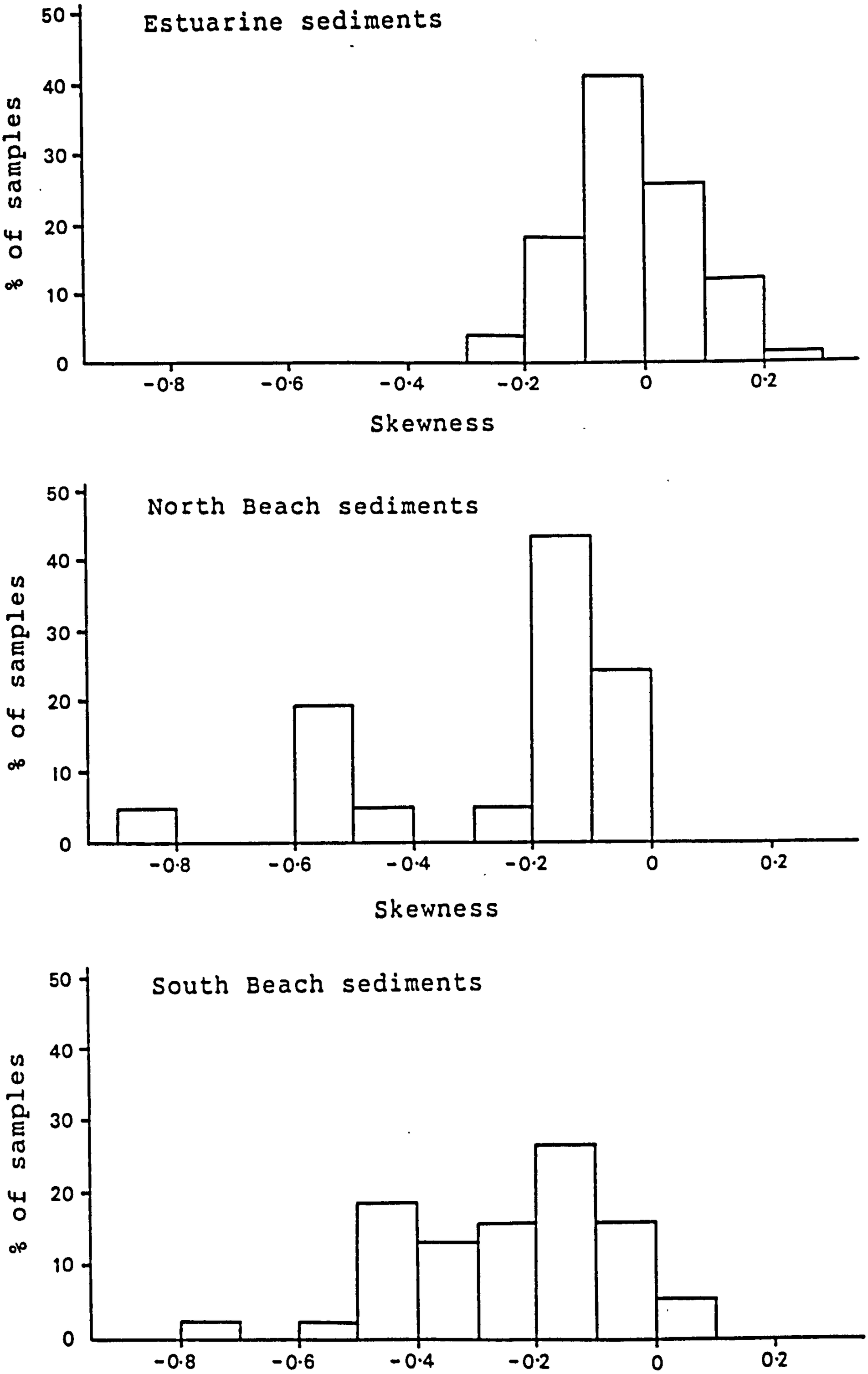

Figure 6.36. Comparison of skewness of estuarine and beach sediments.

1.3ø to 2.8ø. As shown in Figure 6.34, although the range of mean grain size of the north beach sediment is large, the majority of the samples are fairly uniform, almost similar to estuarine sediments. The beach sediments show very variable values of standard deviation (Figure 6.35) and skewness (Figure 6.36). Standard deviation varies from 0.2ø to 1.1ø whereas skewness varies from -0.8ø to 0.1ø. In general the beach sediment are poorer sorted than estuarine sediments. This study also found that almost all of the beach samples have negative skewness values which supports the conclusion reached by many previous workers (Mason an Folk, 1958; Friedman, 1961; Duan, 1964; Hail, 1967).

There is a slight tendency for the sediments to become finer towards the mouth of the estuary along both northern and southern beach. As shown in Figure 6.37 the percentages of material coarser than 2.0, 2.5, and 3.0ø change dramatically at the mouth of the estuary and at the far end of the southern beach. The variations of mean grain size (Figure 6.38),however, are less obvious compared to the variations of coarse or fine material (Figure 6.37) along the coast line. The coarseness of the sediments at the mouth of the estuary (samples NB7, B19, B18, B17, and B16) are probably due to selective deposition of coarse material in this high energy zone, while the coarseness of the sediment at the end of the southern beach (sample SB8 and SB10) are due to the presence in greater quantities of

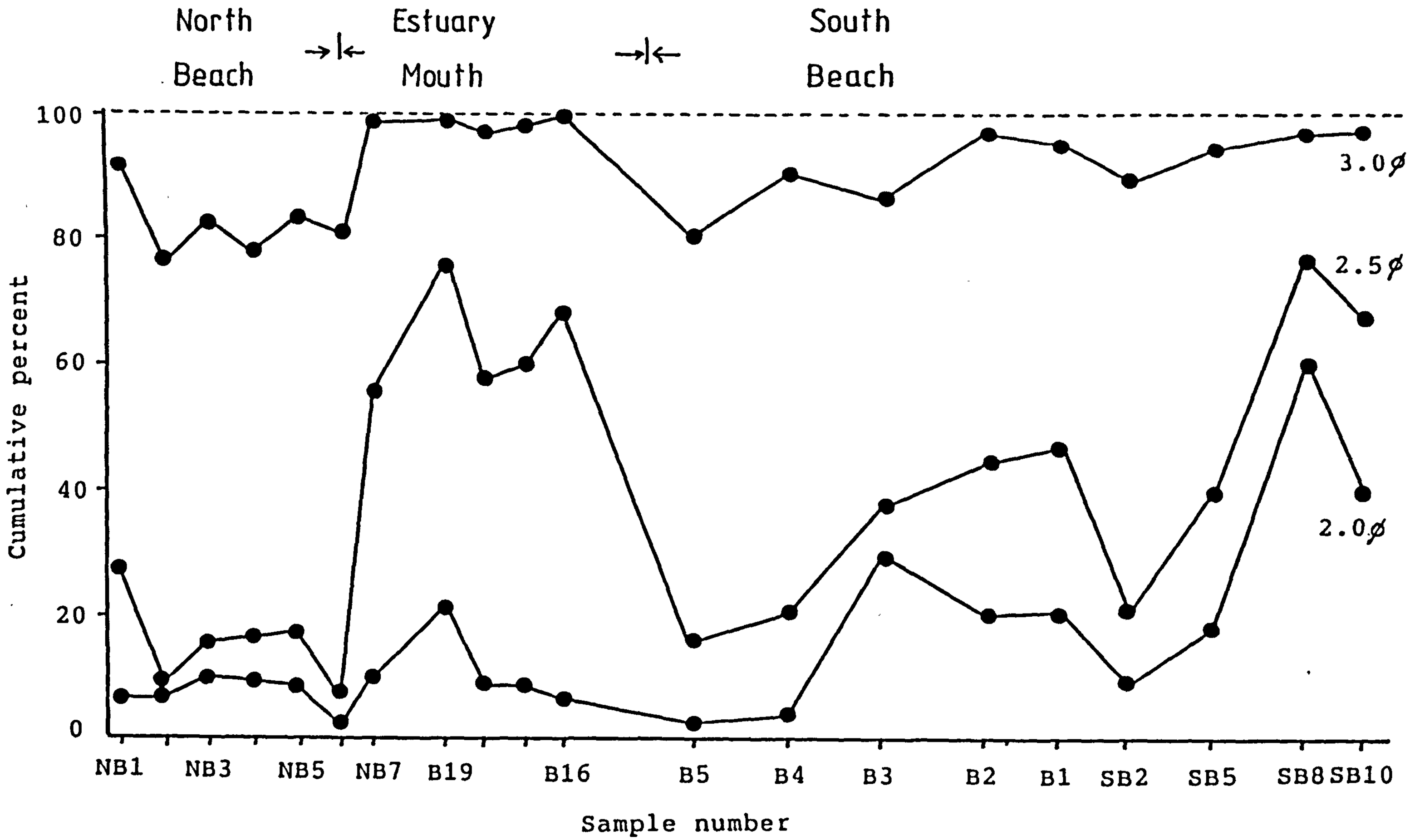

Figure 6.37. Variations of material coarser than 2.0ø, 2.5ø, and 3.0ø along the coastline from the north beach to south beach.

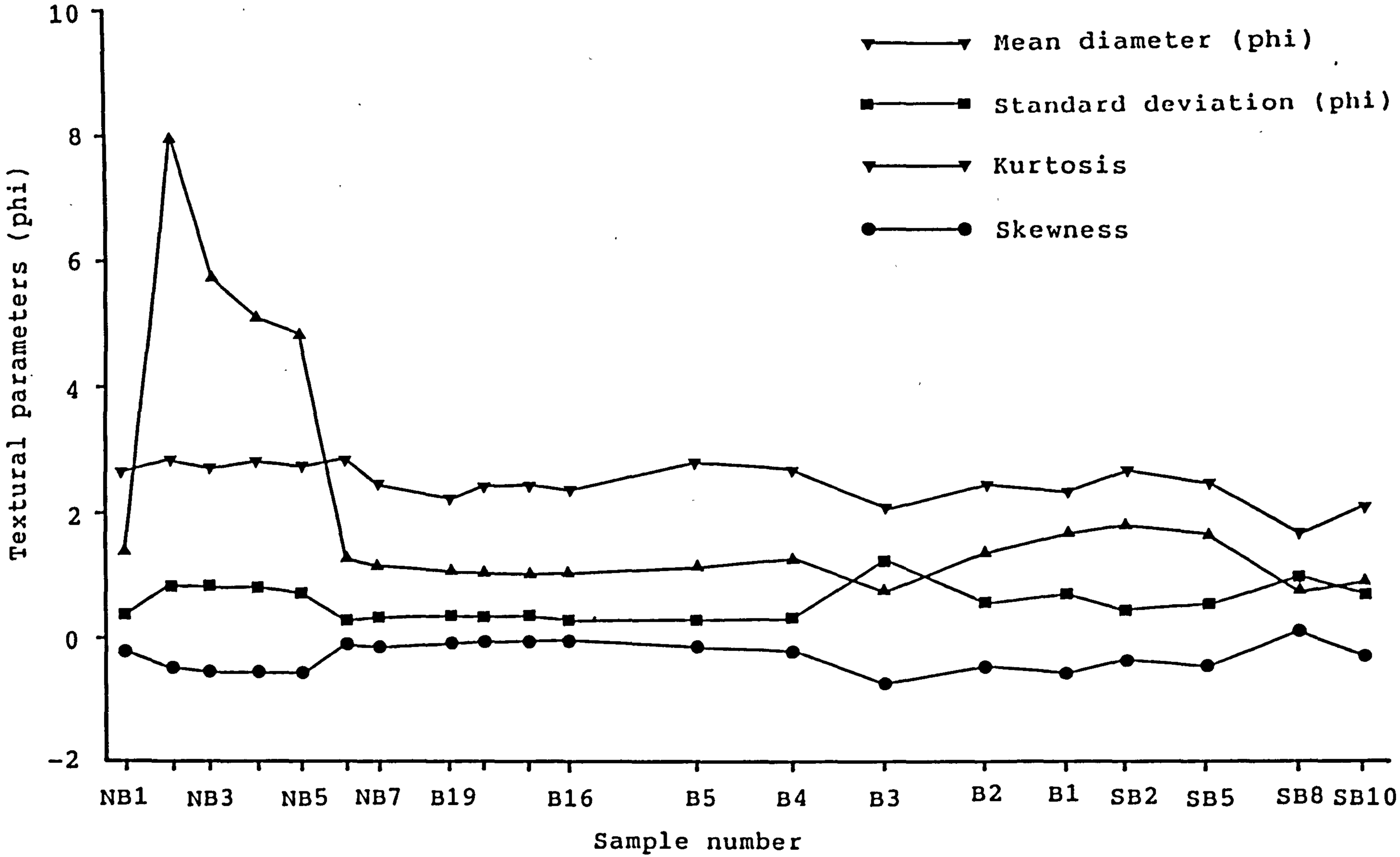

Figure 6.38. Variations of textural parameters along the coastline from the north beach to south beach.

medium (2.0 to 1.0ø) to very coarse (0 to - 1.0ø) sediments which are probably transported from the Sarn Badrig area where sediments are generally coarser (Caston, 1965).

The samples of the southern beach have an average mean grain size of 2.24ø, that is slightly coarser than the average mean size of the samples of the northern beach (2.56). These differences indicate that the level of energy along the southern beach is probably higher than at the northern beach and both energy levels decrease towards the estuary mouth. Thus a general transport in this direction must be considered responsible for these changes.

As shown in Figure 6.37, material finer than 3.0ø is present in minor quantities in all beach samples, but absent from the samples at the mouth of the estuary. The percentages of material coarser than 2.5ø vary dramatically between samples NB6 and NB7 and between Samples B16 and B6. Beach sediments at the mouth of the estuary (samples NB7, B19, B18, B17, and B16) which are from sites exposed to high current velocities have material coarser than 2.5ø greater than 50% compared to other beach sediment which have less than 25% of this material except samples at the far end of south beach. The section of beach between samples NB7 and B6 may represent the zone where the flood current forces its way into the estuary during the period of the flood tide. The presence of large flood-oriented bedforms on the intertidal flats in this area has already been discussed in chapter 2 indicating the presence of

fast flood currents which prevent deposition of material finer than 3.0ø.

Beach samples taken at the far ends of the northern and southern beaches show a different feature from other beach and estuarine samples. They are invariably bimodal with a minor second mode of medium to gravel size material as shown in Figures 6.39 and 6.40 (examples, samples NB3, B3, and SB8), probably because they were deposited by tidal currents from different sediment sources. The sediment forming the mode at -1.25 to 2.0ø is possibly derived from the area of the western and southern section of Tremadog Bay where sediments are genarally coarser, varying from medium to gravel-size material (Caston, 1965). In sample SB8, for example, the material coarser than 2.0ø makes up about 60% of the size distribution (Figure 6.40). Sample NB3 from the north beach, however, has the longest coarse tail even though the percentage of material coarser than 2.0ø is small (about 10%) compared to sample SB8 from the south beach. The presence of considerable amounts of gravel-size material in these areas indicates high turbulence, probably the result of storm-wave-induced currents close to the shore which frequently occur in these areas.

On both northern and southern beaches, it may be noted that there are trends normal to the coast line of mean grain size and the percentage of coarse material toward the

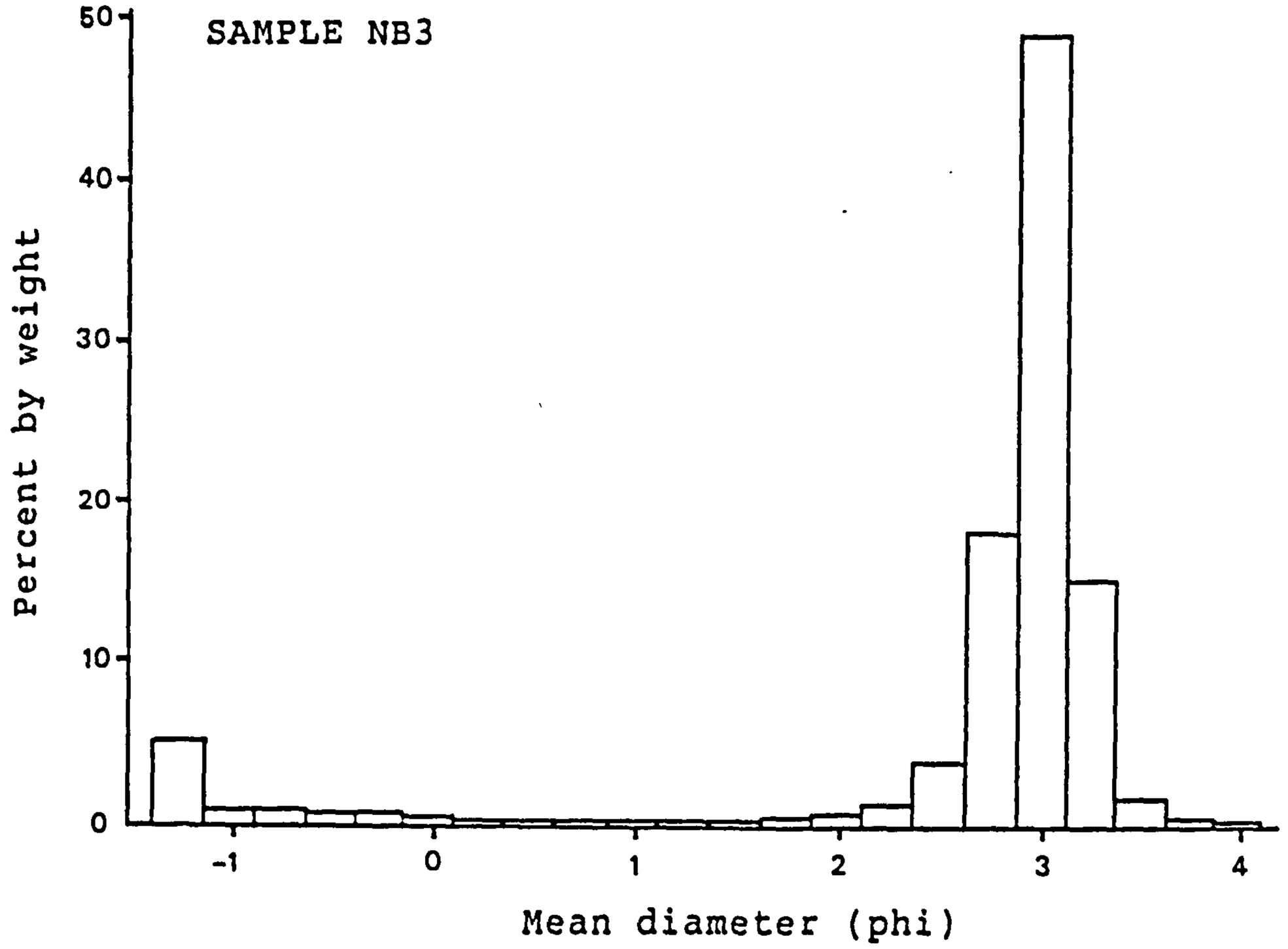

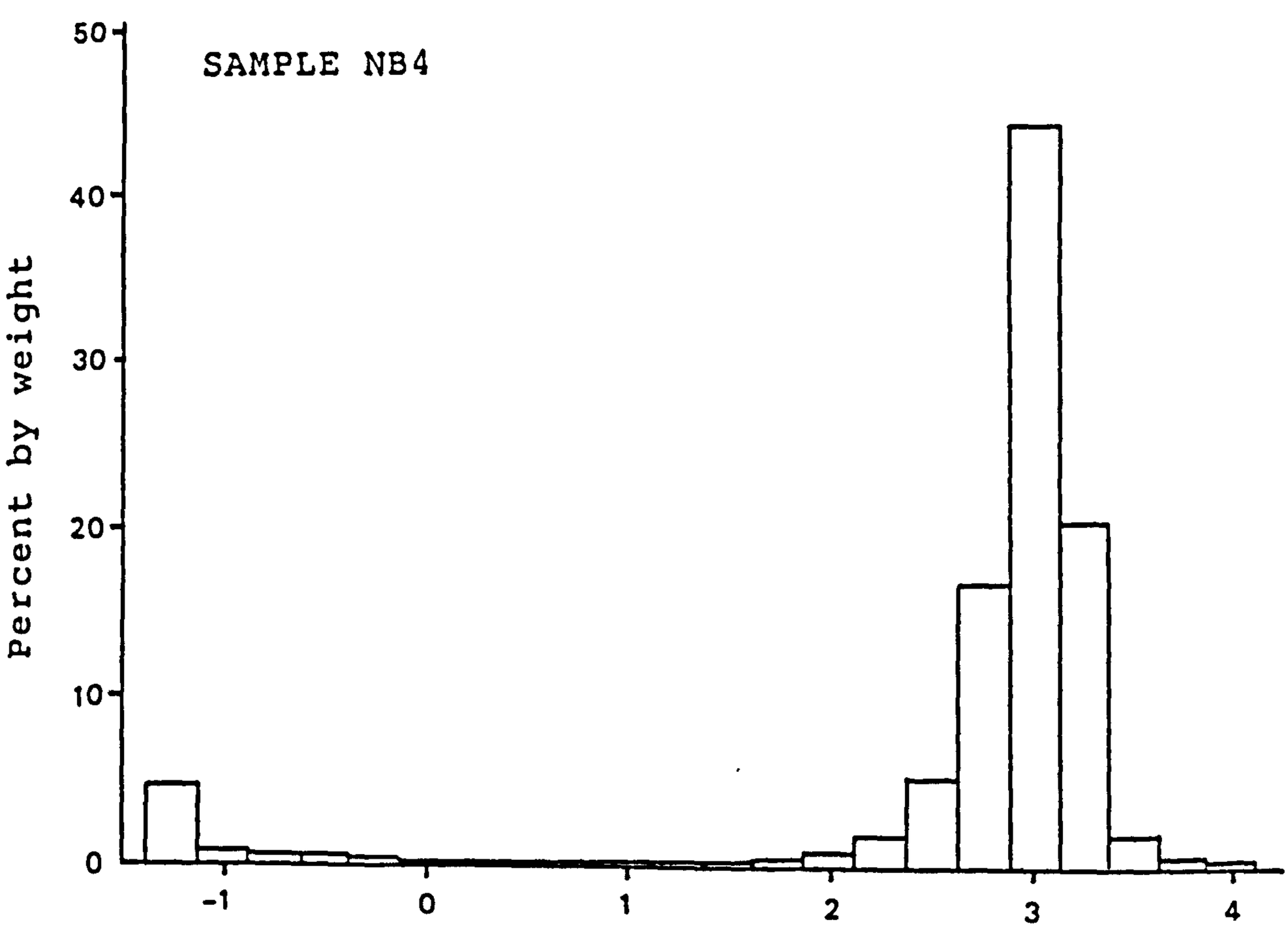

Figure 6.39. Plot of frequency by weight percentage against mean diameter for two northern beach's samples.

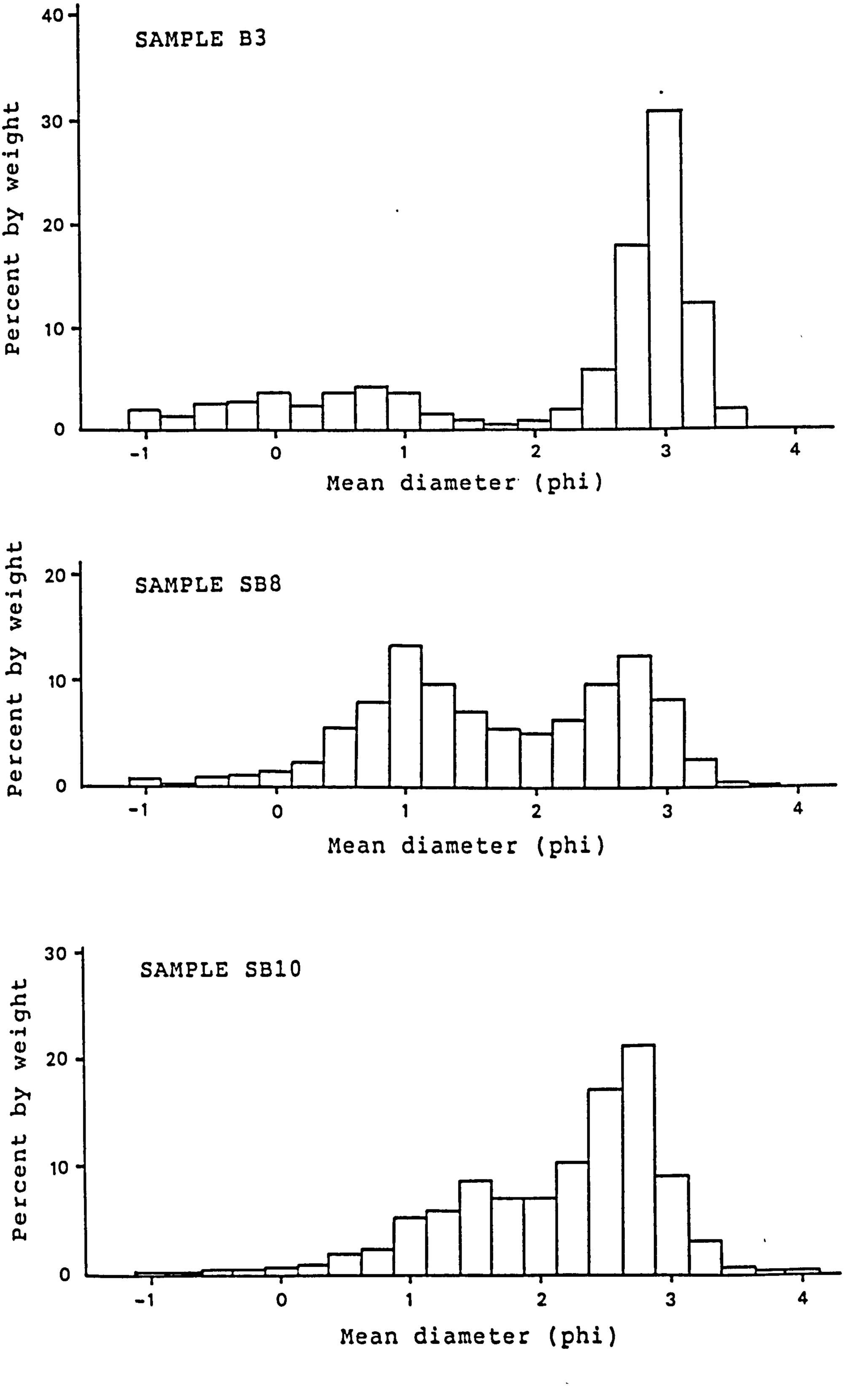

Figure 6.40. Plot of frequency by weight percentage against mean diameter for three southern beach's samples.

mid water mark from both the low and high water marks (Figures 6.41 to 6.44). The change in the amount of coarse fractions is best seen on transects 10 and 11 from the southern beach (Figure 6.42). The percentage of material coarser than 2.0ø along transect 10 increases from less than 10% at low and high water marks to approximately 80% at mid tide mark. These variations suggest that the energy level along the coast lines is the highest at mid tide. On transect 9, however, the coarsest material as indicated by a high percentage of material coarser than 2.0ø is found at both the mid and low water marks which indicates that the energy level is also higher on the lower part of the beach. Figure 6.41 shows that the fraction of material coarser than 2.0ø in northern beach samples is generally smaller (less than 30%) compared to the southern beach samples. These differences suggest that the level of energy is higher on the southern beach than that on the northern beach.

The sediments of the coastal intertidal flats show very variable values of sorting ranging from 0.23ø (very well sorted) to 1.70ø (poorly sorted). In general the beach sediment is poorer sorted than the estuarine sediment. The sediments on the southern beach exhibit the poorest sorting values with an average of 0.54ø compared to the average sorting of the northern beach sediments (0.33ø). Normal to the beach, the sediment shows a tendency to become poorer sorted toward the mid-water mark from both the low and high water marks (Figures 6.43 and 6.44). One possible reason

NORTH BEACH

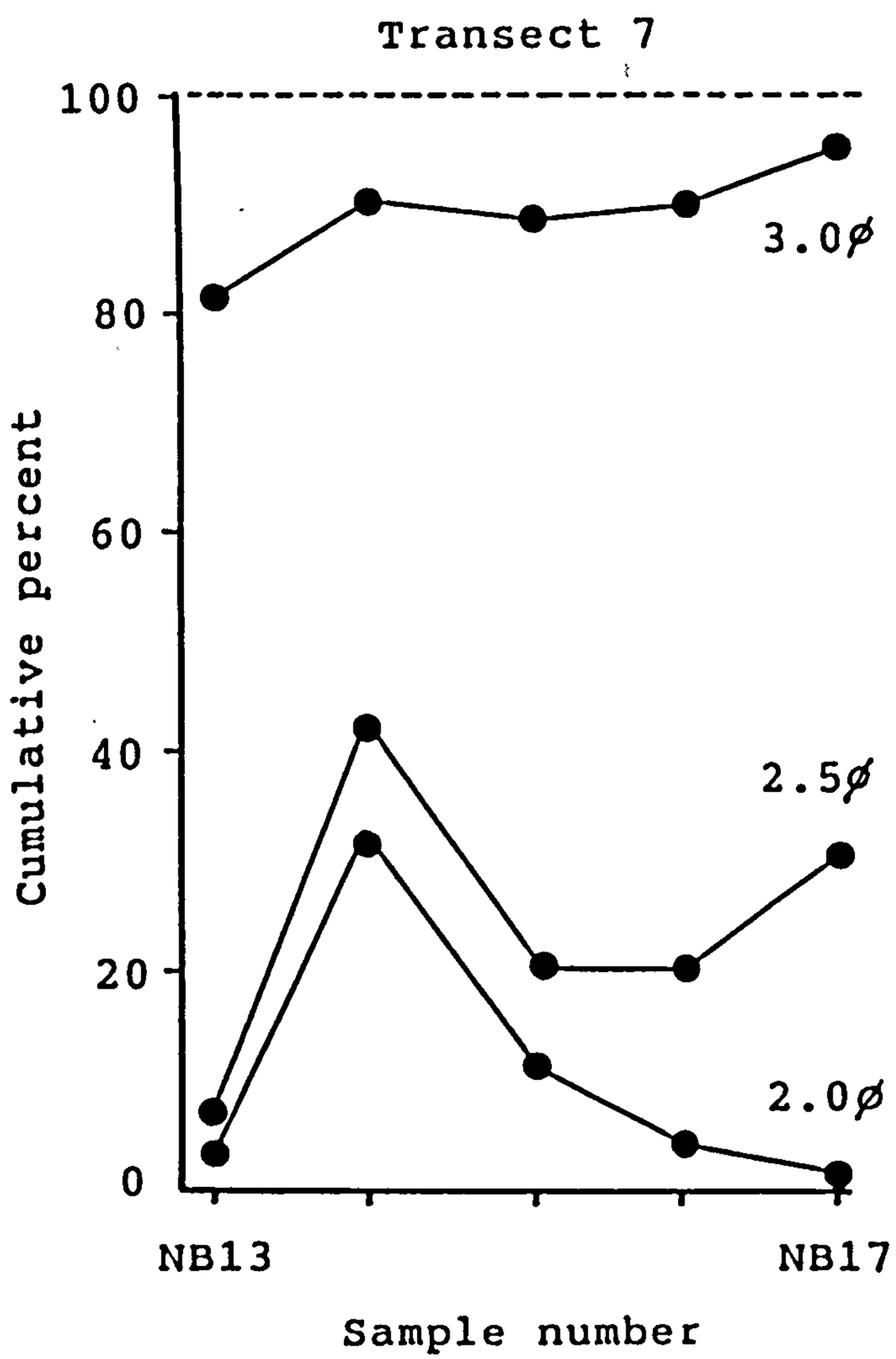

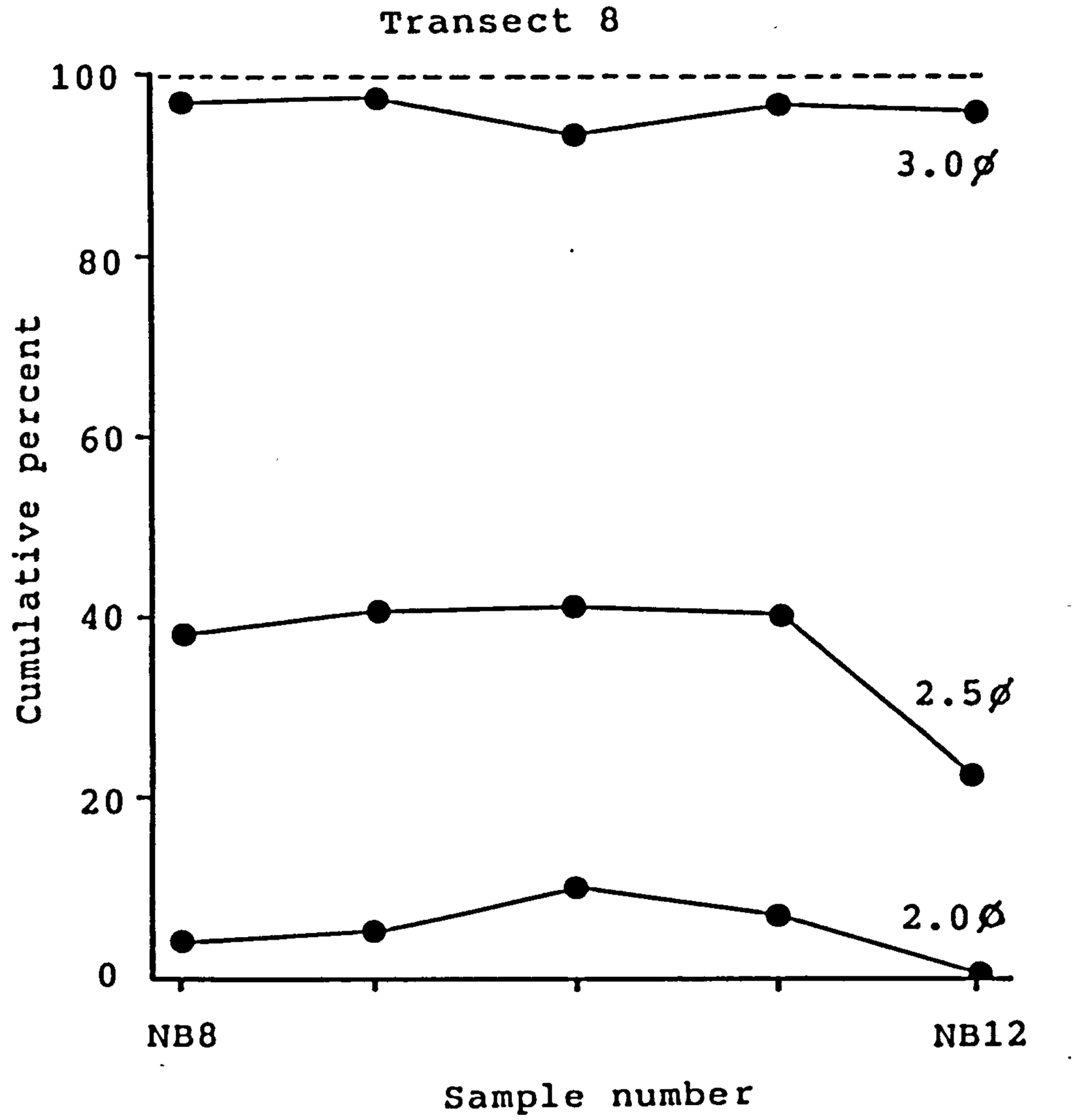

Figure 6.41. Variations of sediment coarser than 2.0ø, 2.5ø, and 3.0ø along transects 7 and 8 (North Beach).

SOUTH BEACH

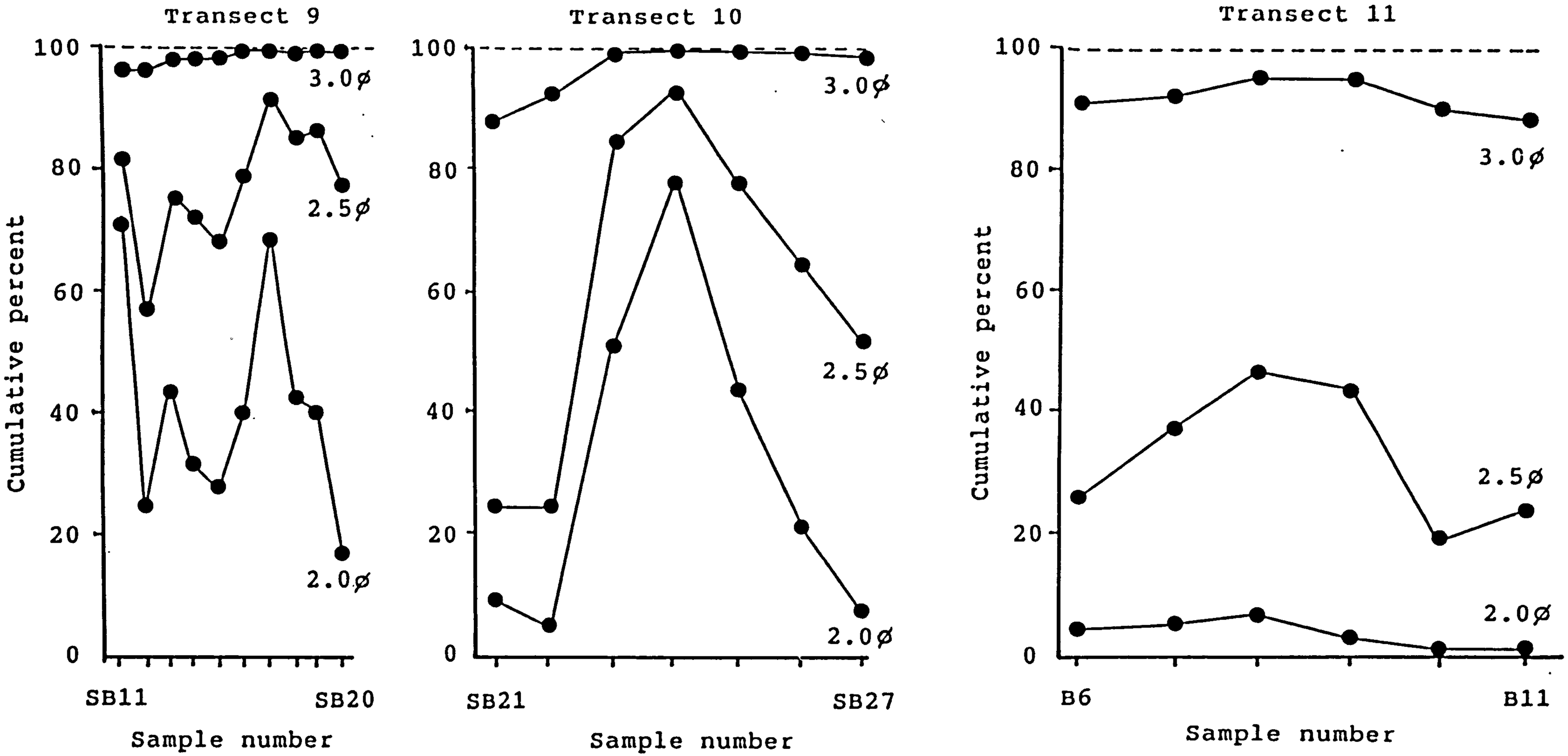

Figure 6.42. Variations of sediment coarser than 2.0ø, 2.5ø, and 3.0ø along transects 9 to 11 (South Beach).

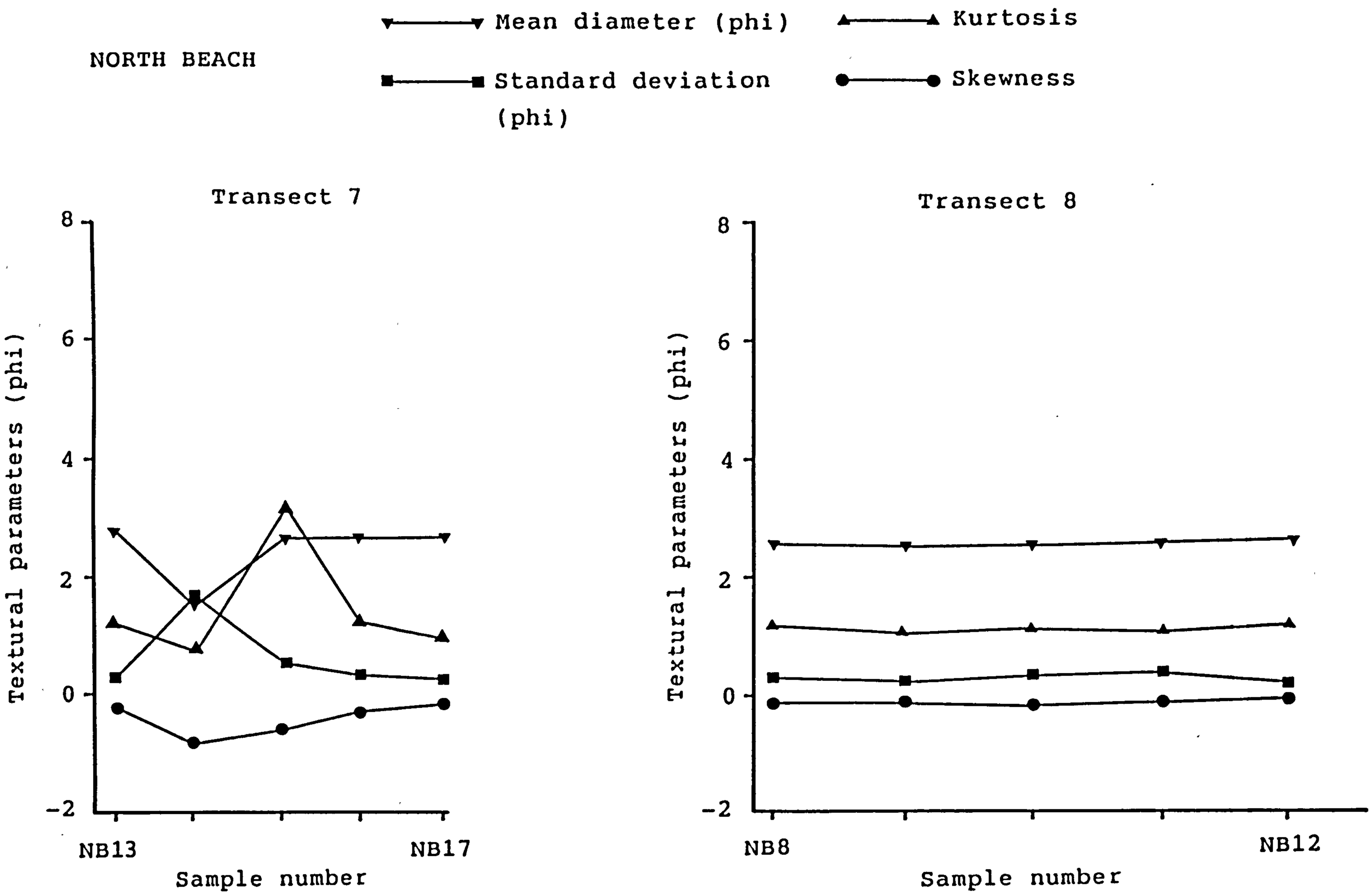

Figure 6.43. Variations of textural parameters along transects 7 and 8 (North Beach).

NORTH BEACH

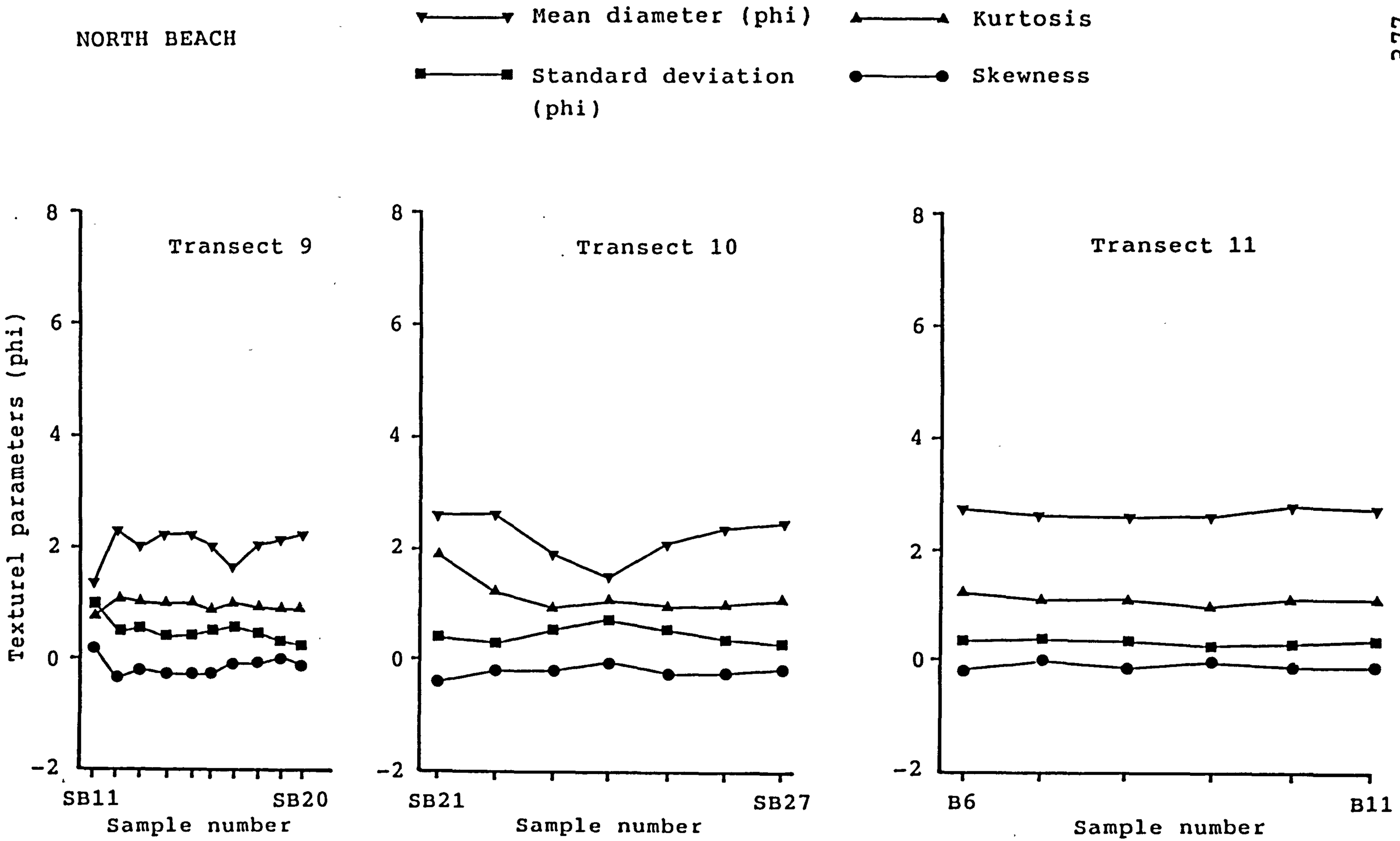

Figure 6.44. Variations of textural parameters along transects 9, 10, and 11 (South Beach).

for poor sorting values of many beach samples may be the presence of significant quantities of gravel-size sediments.

This study shows that almost all the beach samples have negative skewness values except three samples from the southern beach. The values of this parameter varies from -0.80 to 0.23 . This is in agreement with the general claim that beach sediments are negatively skewed (Mason and Folk, 1958; Friedman, 1961; Hail, 1967). Duane (1964) found that, in areas where winnowing is a dominant force as in beaches, the fine material has been removed by wave action and strong currents and as a consequence the sediments on the beach are dominantly negatively skewed.

The kurtosis values of the beach samples are more variable than those of the estuarine samples, with the values ranging from 0.71 (platykurtic) to 8.07 (very leptokurtic). All very leptokurtic samples were found at the west end of the northern beach (Figures 6.43 and 6.44). However, kurtosis of most samples was found to be near normal for beach samples.

6.9. Sediments of Tremadog Bay

The surficial sediments of the bay consist of varying proportions of mud and sand. The principal commponents of

the sand fraction include quartz, biogenic calcium carbonate and other lithic fragments (Figure 6.15). The percentage of quartz in a few samples studied was about 88% which is slightly smaller than that of estuarine sediment because the presence of slightly higher percentages of calciunm carbonate particles. The biogenic component is comprised mainly of whole and fragmented bivalves, foraminifera, and ostracods. The fragmented material is commonly of a fresh appearance but may also be abraded (which sometimes makes it difficult to differentiate from rock fragments). The present source of sediment supply is not know, but since all the rivers which discharge into Cardigan Bay supply little sediment, the sediment in this area in particular and along the coastline must be derived from erosion of unconsolidated sediments on the floor of the Irish Sea and Cardigan Bay itself.

The results of grain size analyses for all bay samples are given in Table A12 (appendix).On the percentage of mud, the sediment can be assigned to one of four groups (Folk,1974): sand (less than 20% mud), muddy sand (20 to 50% mud), sandy mud (50 to 80% mud) and mud (greater than 80% mud). Based on this classification the surface sediments of Tremadog Bay were found to consist of three textural classes,namely: Sand, muddy sand and sandy mud. Mud may be found further west of the study area in the deepest part of the bay. The geographic distribution of mud within the embayment (shown in Figure 6.45) has a similar pattern to that of the mean grain size (Figure

6.46). Mean grain size contours trend approximately parallel to the bathymetric contours, so the sediment distribution is probably in equilibrium with the present-day hydrodynamic regime. Figure 6.45 indicates that mud is widespread at the centre of Tremadog Bay and absent in shallow sub-littoral areas of the bay. The presence of a substantial quantity of mud indicates that the sediments found in this area are finer than those in the estuary and along the coast. A plot of sediment mean grain size against percentage of mud shows a decreasing in grain size with increasing percentage of mud reflecting the dominance of of mud-grade sediments in most of sea bed sediments (Figure 6.48). Obviously, the general bathymetry and current circulation in the area are affecting the overall textural characteristics of the bottom sediments. Although surficial samples were not collected in sufficiently shallow water, coarser deposits are expected to fringe the entire coastline.

Subbottom profiles indicate that a thick layer of the muddy sediments blankets most areas characterised by featureless patterns on the side-scan sonar records (chapter 2). The percentage of mud in the sediment increases with increasing water depth and distance offshore (Figure 6.45). The trend is consistent for the entire bay except for the area just north of Sarn Badrig where sediments coarser than 3.0ϕ have been observed in deeper water (samples S10, S11, and S21). The 3.0ϕ contour in the

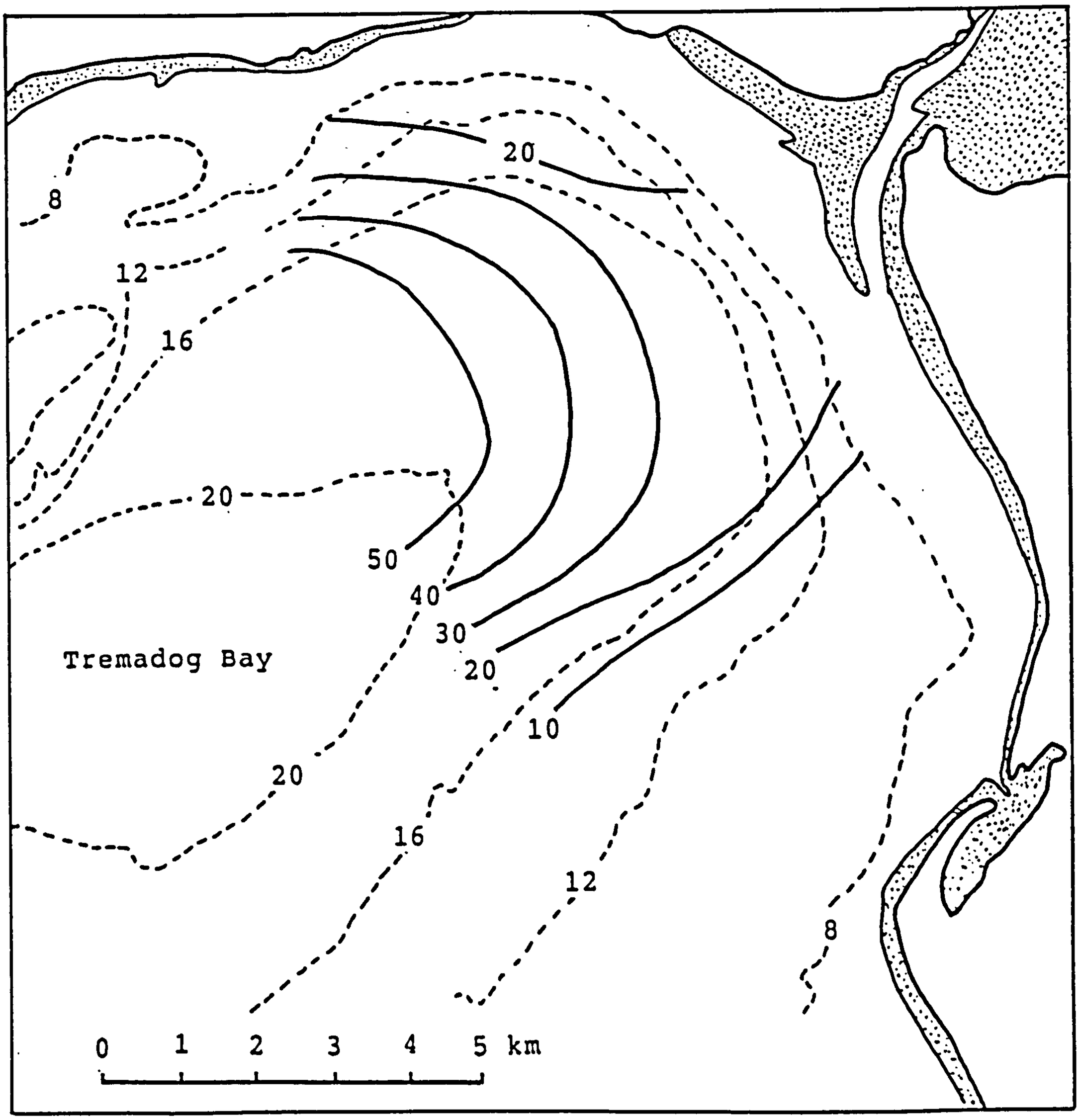

——————— Percentage of mud

---------- Depth (m)

Figure 6.45. Distribution of the mud fraction in Tremadog Bay.

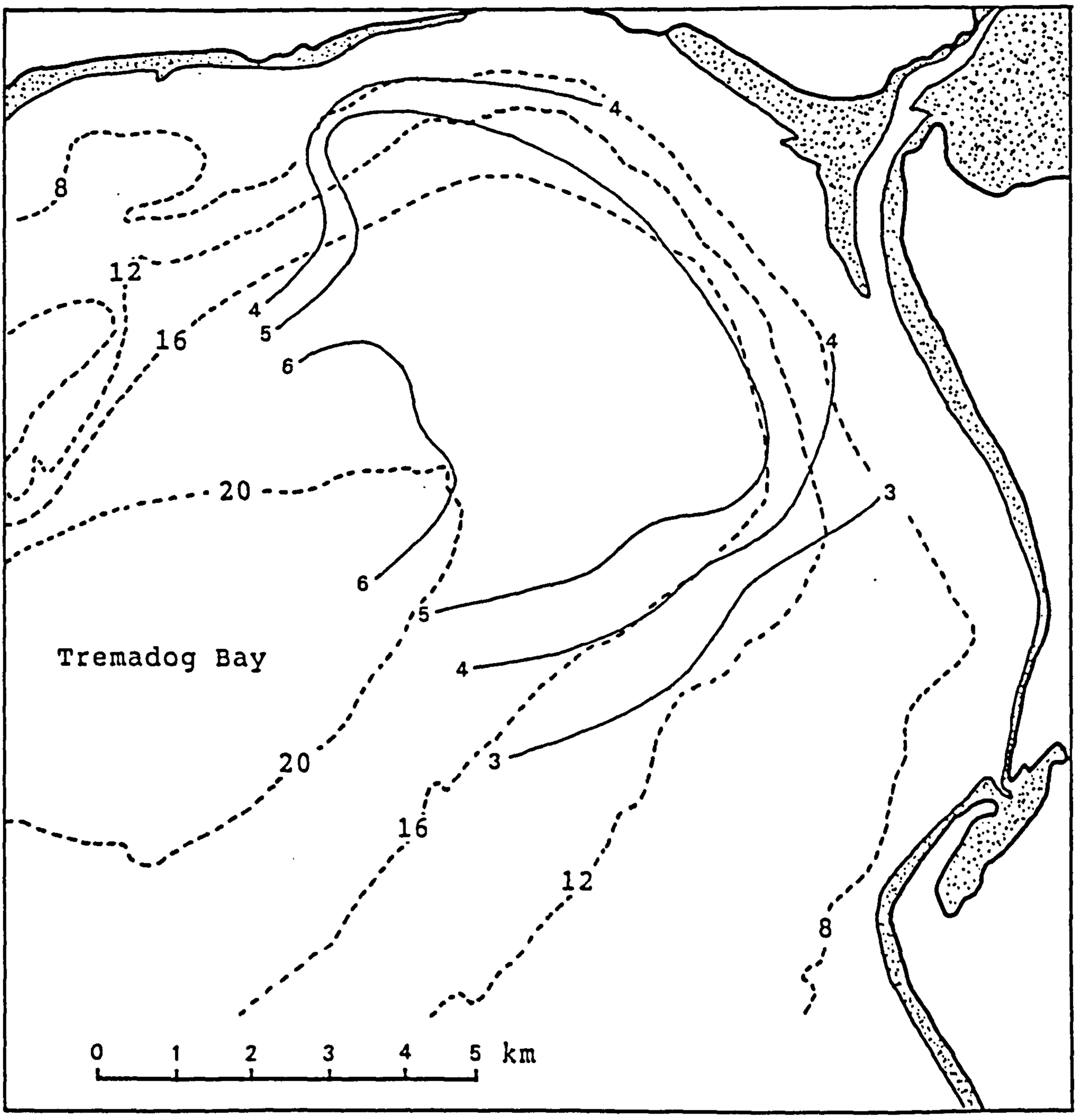

——————— Mean diameter (phi)

- - - - - - - - - - - - Depth (m)

Figure 6.46. Map showing the variation of mean grain size of sediment in Tremadog Bay.

southeast separates the area of coarse sediments from the area of muddy sediments which corresponds with a region of low, featureless topography, suggesting a quiescent depositional environment. Correlations of mean grain size and percentage of mud with water depth are shown in Figure 6.47. Most of the sediment finer than 4.0ϕ were found in water deeper than 15 meters while most of the coarser sediment were found in shallow water near the coast. The lack of coarse material is best illustrated by transects 12 to 16 (Figures 6.49 and 6.50) which indicate that the percentage of material coarser than 3.0ϕ (0.125 mm) varies from 2 to 50% and is confined mainly to the deeper water.

Sorting values of the embayment samples lie between 0.2 (very well sorted) and 3.9 (very poorly sorted). Samples from the southern region (north of Sarn Badrig) are well or very well sorted which reflect transport and deposition by waves and tidal currents. As shown in Figures 6.51, 6.52 and 6.53 the distribution of sorting values follows closely that of mean grain size. Poorest sorting is confined to the low topography at the centre of the depression. In fact current velocity in this area is moderate with a maximum velocity of about 75 cm/s at the surface (BRITISH ADMIRALTY Chart 368). Sediment in the deeper water are very poorly sorted because of their high mud content. Areas of well sorted sediments are restricted to grain sizes around 3.0ϕ and occur adjacent to the coastline and south of the area of muddy sediments. Sorting becomes poorer as mean grain size increases away from 3ϕ.

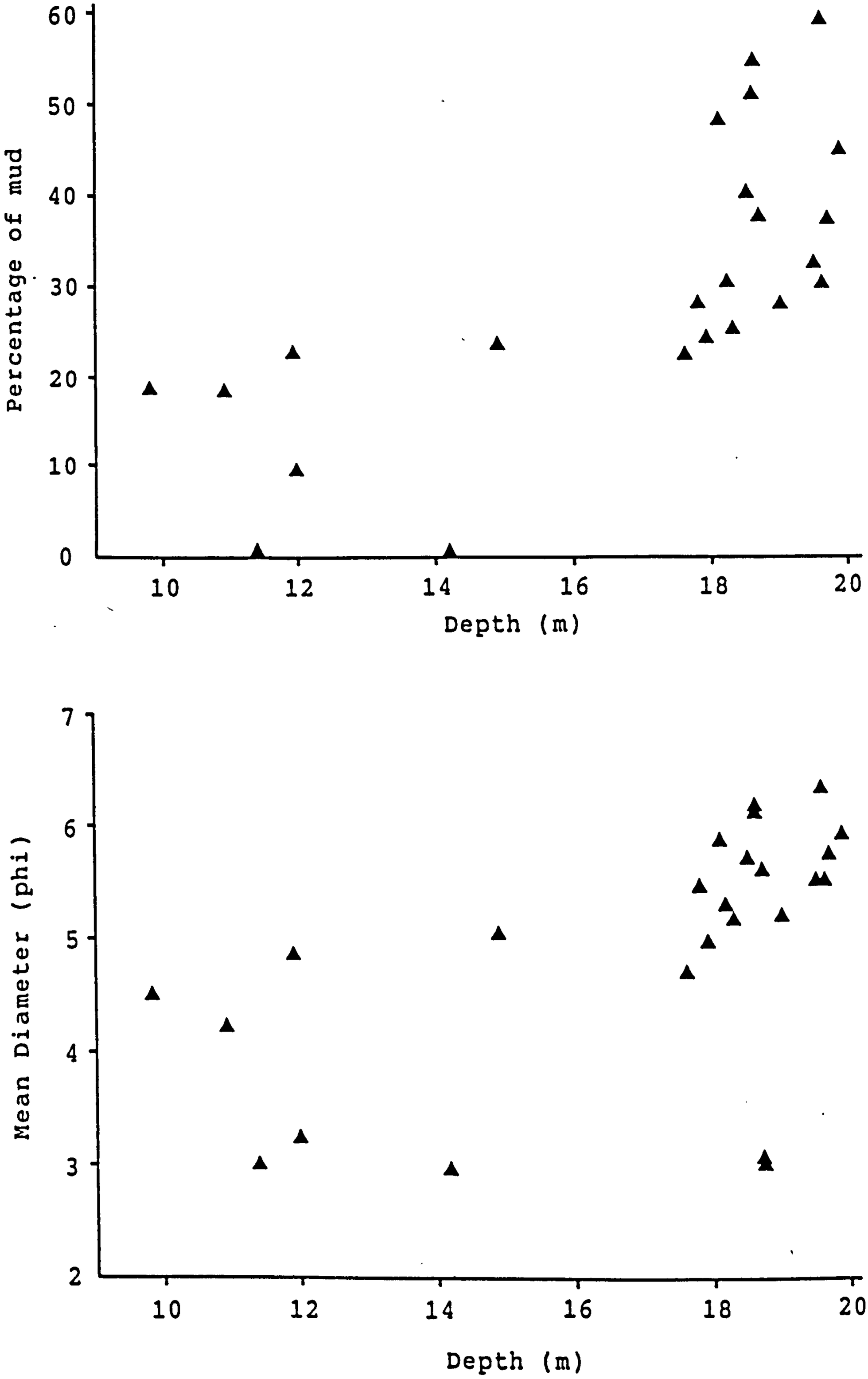

Figure 6.47. Sample percentage of mud (A) and mean grain size (B) versus water depth for Tremadog Bay sediments.

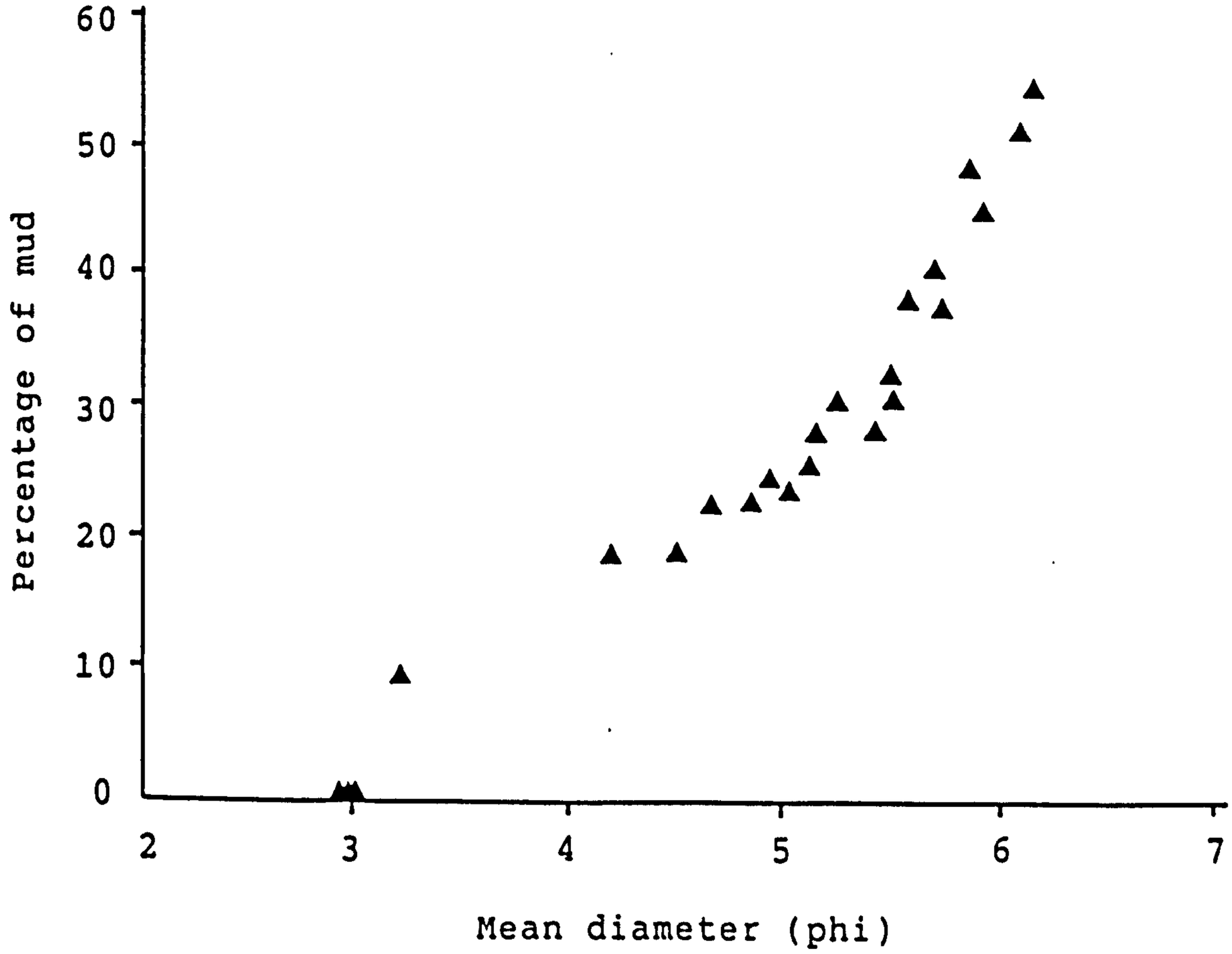

Figure 6.48. Sample percentage of mud versus mean grain size for Tremadog Bay sediments.

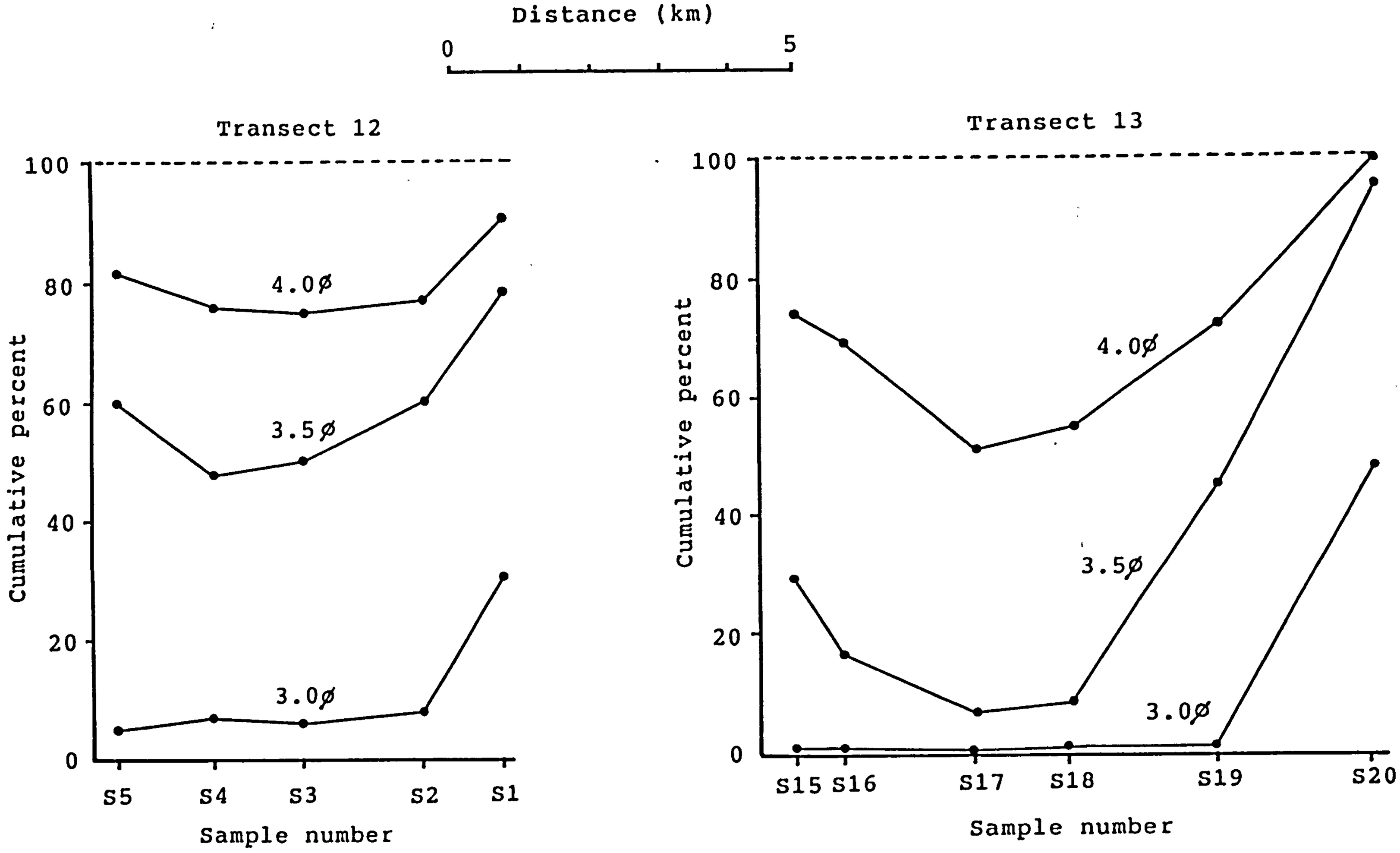

Figure 6.49. Variations of material coarser than 3.0ø, 3.5ø, and 4.0ø along transects 12 and 13.

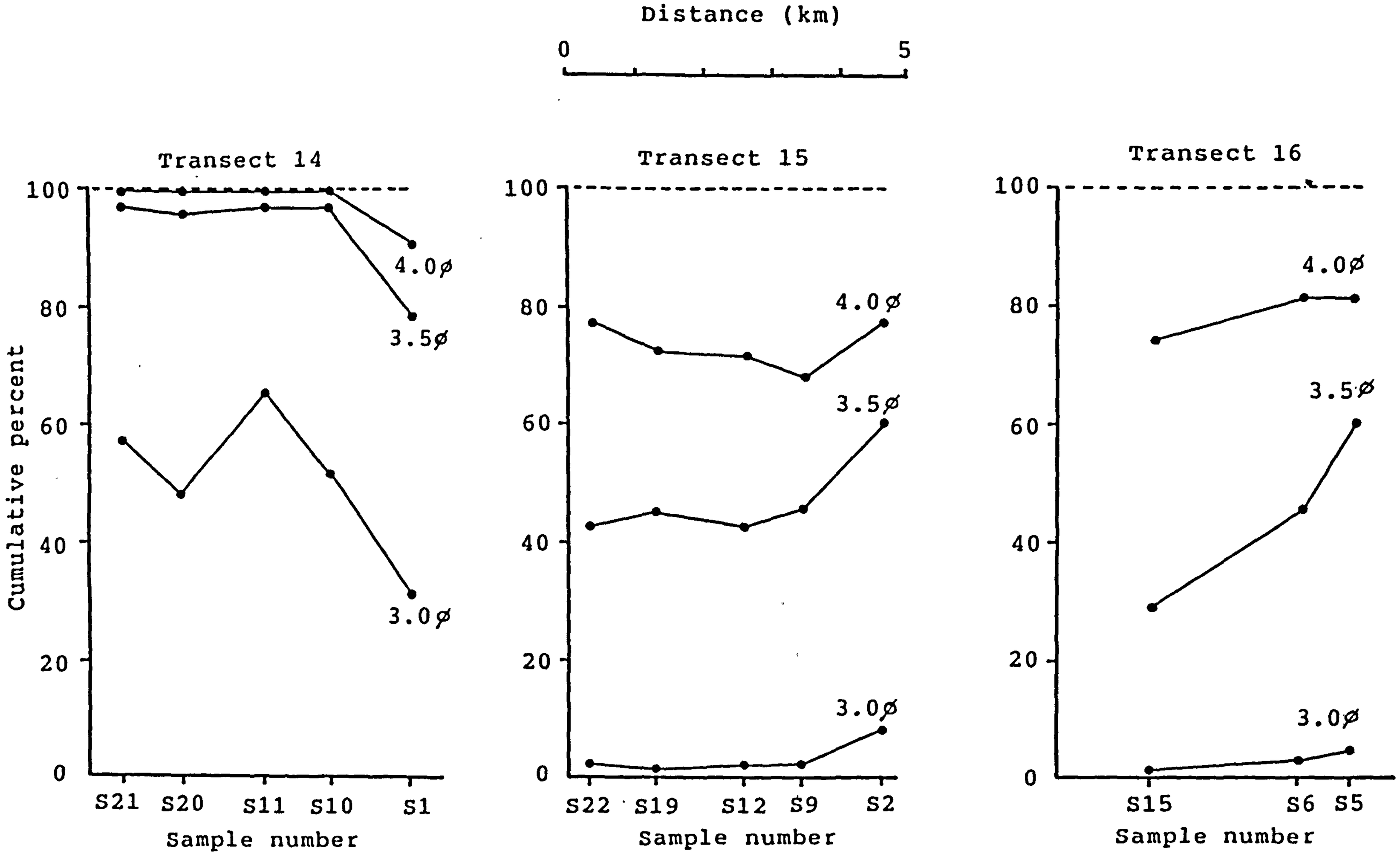

Figure 6.50. Variations of material coarser than 3.0ø, 3.5ø, and 4.0ø along transects 14, 15 and 16.

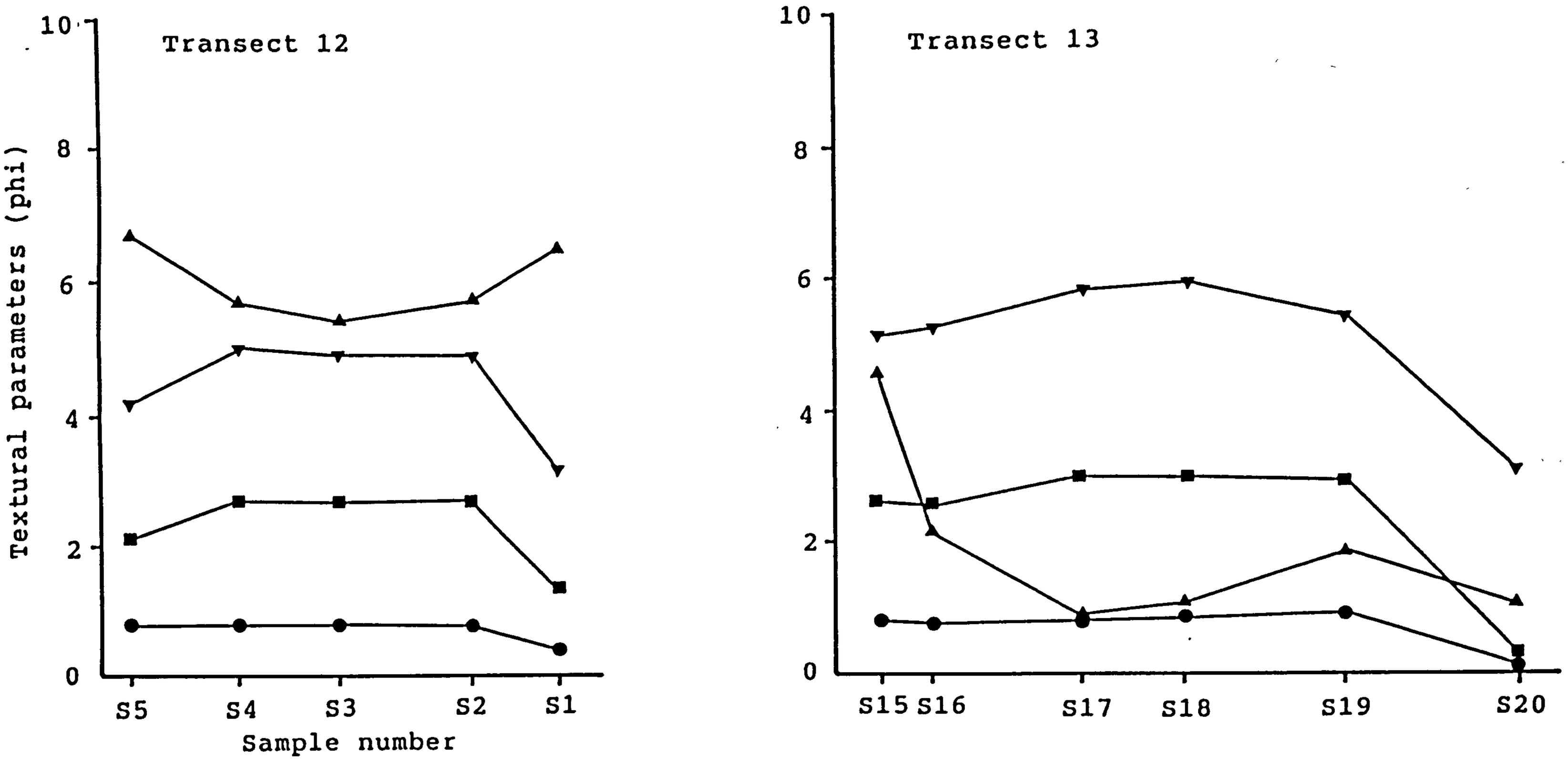

Figure 6.51. Variations of textural parameters along transects 12 and 13.

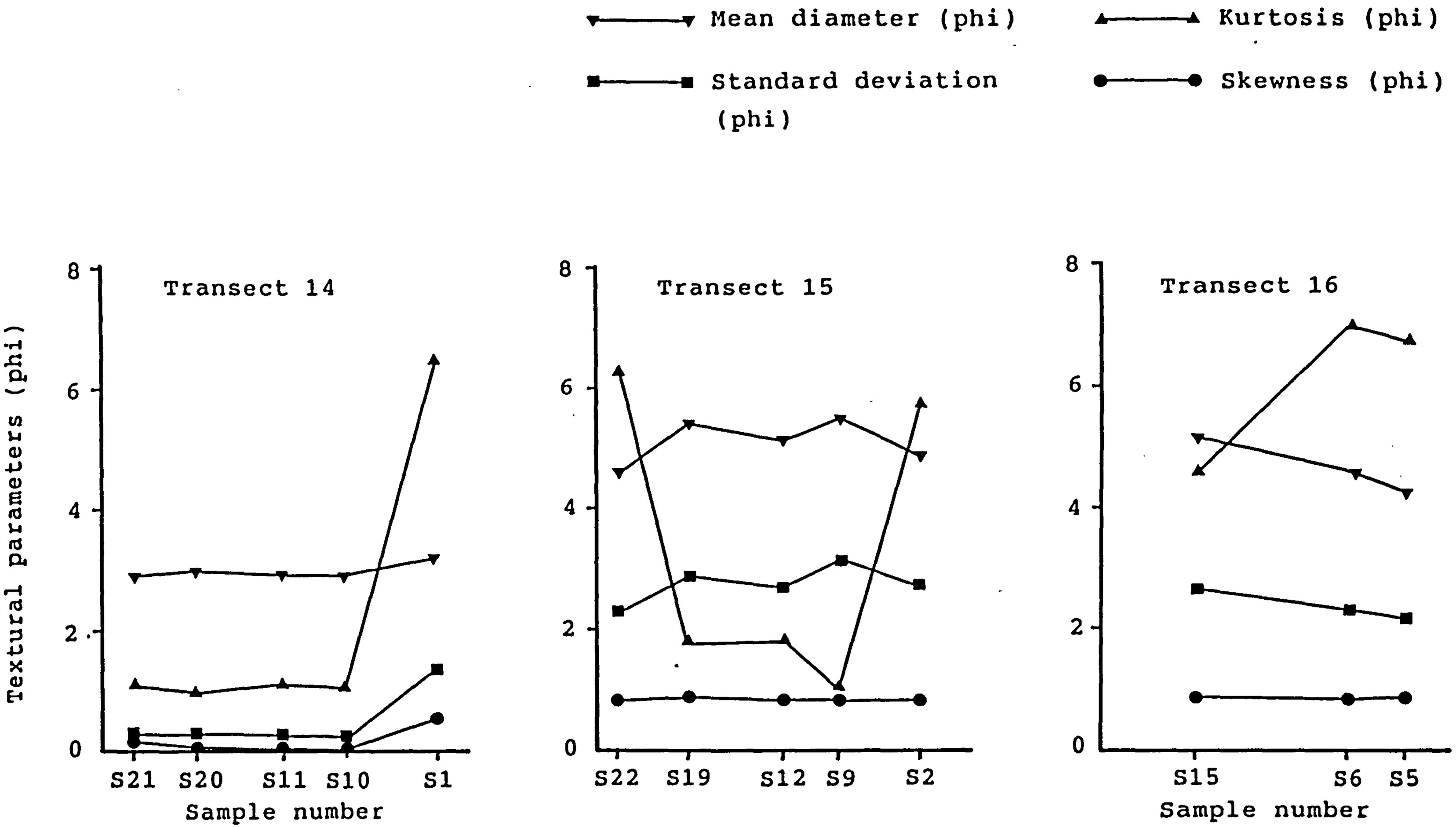

Figure 6.52. Variations of textural parameters along transects 14, 15, and 16.

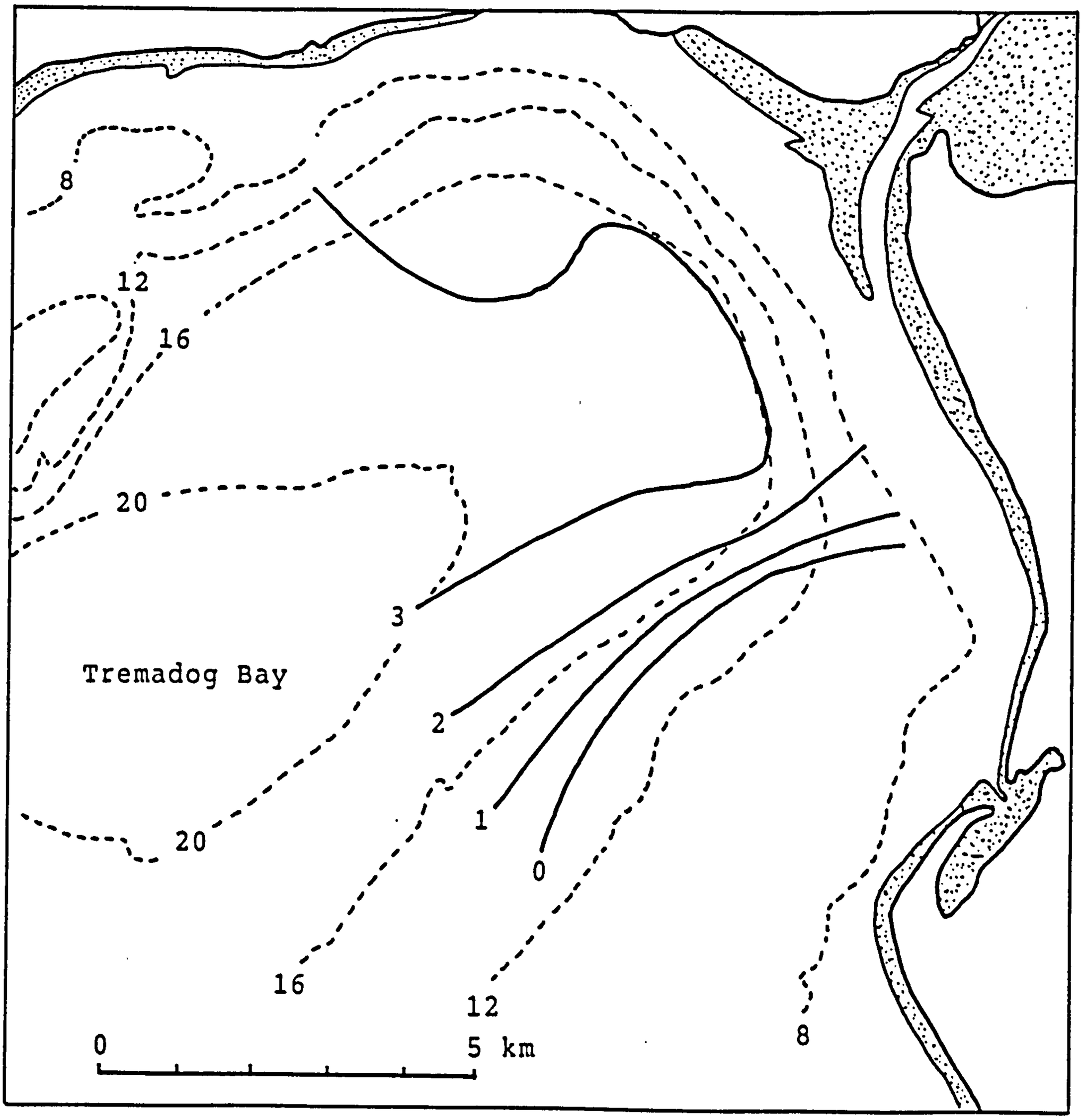

Standard deviation (phi)

Depth (m)

Figure 6.53. Map showing the variation of standard deviation of sediment in Tremadog Bay.

Skewness values for the samples are all positive as shown in Table A12 (appendix). The skewness values range from 0.0 (symmetrical) to 0.9 (extremely positive). As shown in Figures 6.51 and 6.52 the skewness of the sediments is moderately correlated with mean grain size. The near- symmetrical samples tend to have mean grain sizes around 3 , while finer sediments tend to be positively skewed. Kurtosis values vary between 0.9 (mesokurtic) to 6.9 (very leptokurtic). There is no correlation between the values of kurtosis with other textural parameters, and the results show that the values of kurtosis scatter erratically, so probably no useful information can be obtained from this parameter. For example , samples S15 and S16 which have almost similar mean grain size, sorting, and skewness have kurtosis values of 4.5 and 2.1 respectively (Table A12).

6.10. Discussion

The nature and distribution of the sediments in the Dwyryd estuary point to the powerful influence of the high velocity tidal currents in and out of the estuary. The drying and submerging of intertidal flats in the estuary create complicated water flows and patterns of sediment dispersal. The surface of the intertidal flats show signs of active sedimentation where deposition and erosion

processes have been observed throughout the estuary (chapter 5). The grain size characteristics of sediment deposited on the bed can undoubtedly be related to the characteristics of sediments being transported by water at that particular area (Middleton, 1976; Bridge and Jarvis, 1982).

As a sedimentary environment the estuary may be said to be tide dominated since the influence of the fresh water discharge is very small (see chapter 3). The principal tidal influence appears to be its role in transporting sediments from Tremadoc Bay into the estuary (chapter 5). Redistribution of the sediments result from the interaction of the tidal current with the irregular topography of the estuary. The response of deposited sediments to morphologically induced fluctuations in current velocities is evident from this study.

The textural charateristics of the sediment collected from the intertidal flat of the estuary indicate that the hydraulic conditions control sediment distribution, and that the spatial grain size distribution reflects this control . The spatial distribution of mean grain size was found to be related to the tidal current strength. This study also found that the relative proportions of coarse or fine fractions in each sample are better indicators of average hydraulic conditions than mean grain size since the variation of mean grain size is relatively small compared to the variation of coarse or fine fractions. The routes

by which sediments are transported can be postulated from the variation of coarse or fine fraction in addition to the orientation of bedforms.

There are extensive areas of aqueous dune or megaripple bedforms generally visible in the lower section of the estuary at low tide. Unfortunately field data is very limited. The presence of large bedforms in the lower section of the estuary may be due to the coarseness of its sediment in addition to strong flood current in this area, since dunes can occur only in sand coarser than 2.5ϕ or 0.180 mm (Middleton and Southard, 1978). The majority of the samples found from this area have mean grain sizes between 2.3ϕ to 2.7ϕ. The percentage of material coarser than 2.5ϕ varies between 50 to 70%. However, in the middle section of the estuary near the tip of the Penrhyndeudraeth Peninsula, where the sediment is slightly coarser (2.7ϕ), large bedforms were found to exist during or near spring tide on intertidal flats adjacent to the main channel. Similar investigation of sediment dynamics on intertidal flats of the Wash (Collin et al, 1981) found that large bedforms exist on material with medium grain size 0.150 mm. According to Middleton and Southard (1978), the bedform phases for such material are ill defined. The presence of dunes or megaripples are obvious indications of sediment movement and they show a gradual migration towards the estuary head across the intertidal flats. Landwards from the tip of the peninsula, only small scale ripples occur

because the sediment is not coarse enough for the formation of large bedforms. The percentage of material coarser than 2.5ø in all the samples found at the upper section of the estuary is less than 25%.

Chambers & Upchurch (1979) suggest that the grain-size distribution reflects both the availability of sediment and the hydrodynamic energy of its depositional environment. The sources of sediment determine the size fractions that are initially supplied to the depositional site from which the sample was obtained. In other words, initial size distribution, transportation to the depositional environment, and final processing at the site of deposition all affect the grain size distribution. The rate of accumulation depends on the capacity of the current to transport sediment from the source areas to the depositional areas.

Considerable deformation of the tidal wave has been observed in this estuary. As the tidal wave moves upstream so frictional effects cause the wave energy to be dissipated and the wave height therefore decreases since wave energy is proportional to wave height. The duration of the flood tide becomes shorter than the ebb as the tide moves upstream . The decrease in tidal current velocities towards the estuary head limits the penetration of marine material into the estuary. The differences in the flood and ebb velocities decrease inland as the channel shallows and reduces tidal energy landward.

This tidal asymmetry is of fundamental importance to estuarine morphology since it may cause more sediment to be carried into the estuary than can be carried out. Little material enters the estuary from fluvial sources and intrusion of marine sediment therefore spreads almost to the tidal limit. Most estuaries show a decrease in grain size of the bed sediment towards the estuary head (Postma, 1961; Nichols and Poor, 1967). A qualitative model describing the landward transport of sediment over a shallow intertidal flat and citing the effects of scour and settling lag has been developed by van Straaten and Keunen (1958) and Postma (1961).

The present study shows that the distribution patterns of mean grain size, sorting and skewness over the intertidal sandflats are mainly a function of the availability of tidal energy and the initial textural characteristics of the source material. The charecteristics of sediments from the estuary, beach and dunes are approximately very similar and the ranges of variation for all parameters are very small. Most of the sediments found in different environments in this study area must come from the same already well sorted source material.

Most of the estuarine and coastal samples show a lack of fine material in the sediment deposits . During flood

tides, fine material is transported in suspension upstream into the estuary into the comparatively low energy region. Coarser sand is concentrated in the middle and lower parts of the estuary. There is also a gradual differentiation of sediment load over the tidal flats which results in a decrease of grain size from the lower to upper part of the flat. Similar patterns of differentiation were reported by Evans (1965) , Pestrong (1972) Kulm and Byrne (1967), and Jago (1980). This pattern of sediment distribution is caused in large part by the variation in tidal energy across the tidal flat (van Straaten,1954; Posma,1967), as modified by tidal or estuarine circulation patterns (Dyer, 1973).

The inequality of tidal energy causes the sediment to be deposited landward from the point at which it first entered the system. Sediment from the sea probably is transported into the estuary toward the upper parts of tidal flat and saltmarsh by the process of settling lag, assuming that the water level remains upon the marsh surface long enough for the fine sediment to be deposited from suspension (Edward & Frey, 1977). The low energy environment of the saltmarsh provides ample space for the deposition of fine material. Silt and clay size material are deposited in increasing quantities as a result of a reduction of tidal current velocity towards the estuarine margin, as both currents and turbulence are reduced. Small amplitude waves (less than 5 cm) are capable of suspending fine sediment in shallow water and can increase the suspended sediment concentration

by a factor of three over calm condition (Anderson,1972).

For some defined tidal range and current strength, there exists in estuaries an energy 'barrier' which determines the distance from the mouth of the landward transport of particles of each size. The barrier, however, changes in position as the tidal range and current strength vary during the neap-spring cycle. If the sediment source entering the estuary mouth consists of particles of a broad range of sizes, we might expect that the sediment deposited on the bed must decrease in grain size from the mouth landward toward the estuary head. Flow unsteadiness during deposition may give rise to some vertical variability in grain size characteristics. Thus the bulk samples of bed sediment as obtained with the bed sampler may be looked upon as mixtures of many depositional episodes; therefore, the characteristic of the grain size distribution should reflect the average dynamic conditions.

Silt and clay size sediments are unlikely to be deposited where sand is being actively moved, as flow velocities will be large enough to sustain this fine grained sediment in suspension. Since the intensity of turbulence decreases with decreasing current velocity, the fate of silt and clay particles can be deduced.

Bouma (1963) and Macdonald (1977) have suggested that saltmarsh sediments contain a higher proportion of fine and

poorly sorted sediments than any other intertidal sandflat. On the saltmarsh, deposition of suspended material is largely restricted to periods of low current velocity and slight turbulence occuring at slack water. Sedimentation of suspended material from the water column is appreciable only if current speeds drop below 20cm/s (Einstein & Krone,1962). In this estuary these conditions occur for a period of 3 hours during spring tide . At neap tide the water lavel just barely covers the saltmarsh surface during high tide slack water.

The values of sorting or standard deviation of all the samples collected in this study are indicative of energy conditions in this depositional environment. As might be expected, the best sorted sediments are those with mean grain sizes in the fine sand range. Samples from the lower part of the estuary (transect 6) are well sorted, consistent with a combination of strong current action and the supply of well sorted material. Sediments from the upper part of the estuary are better sorted as a result of continuation of sorting processes when the lower estuary sediments were transported upstream by tidal currents. Differential transport, in which particles of one size are transported faster than particles of another, probably makes a contribution to progressive sorting of marine sediments. Sediment sorting is better at the estuary head than at the mouth because the range of available grain sizes is reduced at the head by hydraulic sorting (Lambiase,1980). This also suggests that the supply of

detritus from river discharge is negligible and all sediment deposited in this estuary come from the sea.

As stated previously, negative skewness means that the sample has a tail of coarse material and positive skewness indicatives that the sample has a tail of fine material. Negatively skewed sediments tend to be associated with higher energy environments, whereas positively skewed sediments tend to be associated with lower energy environments. All samples collected in the estuary range from negatively skewed to positively skewed while the majority of samples are approximately symmetrical.

As can be seen from Figure 4.12 skewness is moderately correlated with mean grain size. Sediments with a coarser grain size tend to have negative skewness, resulting from removal of fine material in areas of more powerful tidal currents. In this study the negatively skewed sediments are found in the peripheral areas of the estuarine mouth and along the beach. The positively skewed sediments are to be found only at the upper part of the estuary and on the saltmarsh. Sediments are negatively skewed at the mouth because of the presence of a large coarse grain population, and positively skewed sediments dominate the estuary head because the coarse population is absent (since the diminishing flood currents were unable to move coarse material further upstream). Symmetrical skewed sediments are to be found in most part of the estuary. However, the

majority of this symmetrical skewed sediment have skewness values less than zero i.e. there is a slight tendency toward negative skewness.

According to Folk & Ward (1957), skewness and kurtosis are vital clues to the bimodality of the sediment . Non-normal values of skewness and kurtosis are thought to indicate a mixing of two or more modal fractions. If one mode is dominant over the other, a leptokurtic distribution will be formed. If two subequal modes are present, a platykurtic distribution will be formed. Leptokurtic samples form the bulk of the samples in this study area. Only three samples (B3, SB8 and SB10) collected along the beach are platykurtic. These samples consist of fine sand as a dominant mode and gravel as a subordinate mode producing a slight bimodal sediment.

Beaches are the most sensitive sedimentary environments which adjust extremely quickly to changes in energy levels and these energy levels may be extremely high (Pethick, 1984). Beaches react rapidly to changes in sediment type or its supply rate. Temporal beach changes are related to long-period oscillations in mean sea level, long-term change in wave climate, and water circulation within the coastal embayments. Near-shore circulation is probably dominated by mass transport currents, rip currents and long-shore currents. The total near-shore circulation strongly depends on the mass transport associated with the waves and on the wave motion and run-up in the surf zone

(Allen,1970). Little is known about such large-scale water circulations in the Tremadog Bay.

The width of the beach in this study area which varies between 200 to 500 m is commonly associated with a large tidal range. Complex and changeable patterns of water and sediment movement are generated as the sea moves back and forth over such beaches. The beach surface is generally smooth with well sorted sand. Within the intertidal flats, a wide range of sediment has been deposited consisting of very fine sand to granules. The beach sediments which are composed of quartz sand with small fraction of lithic and biogenic components are approximately similar to the estuarine sediments. The dominance of quartz and a small amount of feldspar in beach and estuarine sediments is probably because of their physical and chemical durability with respect to other minerals.

The presence of variable amount of gravel at a few places significantly alter the textural characteristics of the beach sediments compared to the estuarine sediments. Short stretches of shingle beach further west of the northern coast and further south of the southern coast (Figures 6.2 and 6.3) probably supply most of the gravel-size material into the beach in the study area. The shape of the grain size distributions in the 1.5 to 4.0ϕ range are virtually the same for all beach and some estuarine samples. The coarser material (-2.0 to 1.5ϕ) tend to have a

different distribution for each sample, due to differences in energy level at each sample location.

The textural characteristics of the estuarine and beach sediments in the study area are very similar to the sediments along sublittoral areas of Cardigan Bay, where the majority of the sediments are of fine sand grade (Dobson, et al., 1971). Mineralogically, the Bay sediments are composed of a large fraction of quartz with a small mixture of other minerals. For example, sediments in the Dovey Estuary consist of medium to fine sand, 1.5 to 3ø. The ratio of lithic grains to quartz grains found at the mouth of the Dovey estuary is significantly similar to that found throughout most of Cardigan Bay (Haynes and Dobson, 1969). Local depressions, such as central Tremadog Bay, in the sub-littoral are filled with muddy sand. Much further south, the Taf estuary is also filling with sediment derived from adjacent sub-littoral areas of Carmarthen Bay (Jago, 1980). The intertidal flats of the Taf estuary exhibit a narrow range of grain size from 2.75 to 3.0ø which is within the range of sediment found in the Dovey and Dwyryd estuaries.

The negative skewness of the beach samples is a reflection of strong turbulence and winnowing by waves which remove the fine material from the beach (Mason and Folk, 1958; Friedman, 1961; Chappell,1967). The addition of coarse sand either in the form of terrigenous pebbles or shell material may cause the sediment to show a bimodal

distribution that will yield a poor sorting value if both populations are combined in textural analysis.

The slope of the beach was found to depend on the grain size of the sediment which is in agreement with previous findings (Bascom, 1951; Shepard, 1963; McLean and Kirk, 1969). Data on beach slopes are not available, but the relative gradient of the beach can be estimated from the width of the beach between the mean low water and mean high water and the mean tidal range. Wider beaches, as found on the northern coast with a steepness of about 0.7°consist of very fine and well sorted sand. The southern coast which is slightly steeper (1.1°) has relatively coarser and poorer sorted sand. The shingle beach nearby is steeper (2.6°) than the sandy beach in the study area.

6.11. Conclusion

The observed grain size distributions conform best to a hyperbolic distribution model than to normal distribution model. The usual interpretation of the cumulative percent curves on normal probability paper is proved to be unjustified; the presence of more than three linear segments need not necessarily reflect the three modes of sediment transport. As shown in this study, the segments and the break points are a consequent of plotting hyperbolic distribution on normal probability paper

(Bagnold & Barndorff-Nielsen, 1980; Leroy, 1981; and Christiansen et al., 1984). The common practice of using normal probability paper for plotting cummulative curves could be replace or supplimented by hyperbolic probability paper for routine study of grain size characteristics in addition to the interpretation of statistical parameters of grain size distributions.

The development of extensive intertidal flats is due to tranportation and deposition of fine sand into the estuary from the adjacent marine environment. The bulk sediments consist of quartz with small fractions of lithic and carbonate material. As deduced from the characteristics of the sediment and bedform morphology, energy conditions in the estuary vary from the highly turbulent in the sandwaves region to more tranquil conditions at the limit of tidal intrusion.

The spatial grain size distributions of sediment in the Dwyryd estuary largely reflects the characteristics of tidal flows, which control sediment transport and deposition, the source material, and the general morphology of the intertidal flats. The response of deposited sediments to morphologically induced fluctuations in current strength is evident from the variation of textural parameters and more convincely from the variations of the percentage of coarse or fine material across and along the estuary, where coarse sand (larger than 0.18 mm or 2.5ϕ) dominates where extreme current velocities occur at the

mouth of the estuary. Further upstream material finer than 0.18 mm dominates due to the inability of the flood current to transport the coarser material more than 8 km upstream from the mouth.

Similarities in the characteristics of grain size distributions and mineral compositions between the estuary, and some of beach and embayment samples are obvious evidence that the estuary is filling with marine sediment from Tremadog Bay, particularly from sub-littoral areas where sand-size material dominates. Mineralogical studies also prove that negligible amounts of river sediments enters the estuary and that the domination of marine sediment reaches up to the tidal limit, approximately 15 km from the mouth. All estuarine sediments are unimodal consisting of a very narrow grain size range from 1.5 to 4.0ø, while some of beach sediments are bimodal. Gravel-size material is probably tranported from an adjacent shingle beach and from the Sarn Badrig area where sediments are generally coarser.

SEVEN

SUMMARY AND CONCLUSIONS

7.1 Introduction

This study principally aims at a better understanding of some important sedimentary processes underlying the accumulation of fine sediment in the Dwyryd estuary and its relationships with the adjacent embayment of Tremadog Bay. This study assesses the flow characteristics and sedimentation patterns in the Dwyryd estuary and its adjacent bay and includes the assessment of the general morphology of the study area, sediment distribution, and sediment characteristics (textural and mineralogical). Interpretations are based on data from profile surveying, sediment sampling, CTD profiling at selected sites. The magnitude of sediment transport has been estimated using current measurements and sediment tranport rate formulae.

Estuarine processes are very complex and variable, temporally and spatially, so to completely describe (quantitatively) the processes involved, ideally, requires a large scientific data set covering a wide spectrum of conditions. Since only three years are available for the

planning of the research programme and for the collection and analyses of data, the amount of data which have been collected during this short period are inadequate especially for any assessment of long-term processes. Furthermore, some activities are very labour intensive creating problems which are sometimes difficult to solve. The availability of an automatic logging module for currents measurements (VGU) proved to be the best solution to the shortage of manpower.

7.2 The surface features of the Dwyryd estuary and Tremadog Bay

a) This study indicates that the sediment characteristics and surface features in the estuary is characterized by major changes of current speed and direction and water depth during the short-period flood-ebb cycle as well as over the longer spring-neap cycle.

b) Lower flow regime bedforms (ripples, megaripples, and sandwaves) are abundantly developed on the surface of the sand bodies. Sandwaves are the largest bedforms in the study area with wavelengths up to 40 m. The heights of sandwaves vary periodically reaching maximum value of about 1.0 m during spring tides. They are generally asymmetric in profile and migrate in the flood direction. Their crestlines are straight to gently sinuous. Almost all sandwaves in this study area are flood oriented when

exposed at low tide during the spring-neap cycle.

c) Megaripples occur in areas of high current velocity near the channel margins, but because of the great variability in flow velocity and water depth that occur during a tidal cycle, various modifications of basic bedform types are produced, including 2-D and 3-D megaripples and incomplete reversal of megaripples.

d) The frequency distribution of wavelengths in the lower section of the estuary is polymodal and asymmetrical, which the majority of the larger bedforms having wavelengths between 15 and 30 m. The secondary mode occur at wavelengths of 5 to 10 m. Most of these bedforms are flood-oriented.

e) The frequency distribution of wavelengths observed on the North Bank (sand spit) is bimodal. The primary mode has wavelengths less than 10 m and a secondary mode occurs at wavelengths between 10 and 20 m. The frequencies of ebb- and flood-oriented large bedforms are approximately the same.

f) The bottom topography of Tremadog Bay as revealed by analyses of side-scan, boomer, and pinger records is characterized by a broad central depression bordered by a shallow irregular seafloor on the north and west and by a ridge on the south.

g) A thick layer (up to 30 m) of fine-grained sediments (muddy sand) extends over most parts of the bay. Acoustic basement rock (boulder clay) lies deeper in the central part of the bay. Here sediments are turbid which prevent acoustic penetration. The masking effect, however, is not continuous and a reflector is detected at a few locations.

h) Sedimentation has been influenced dominantly by weak tidal currents resulting in deposition of fine-grained sediments. The lack of primary sedimentary structures reflects the fineness of sediment size and probable deposition by weak tidal currents. The sediments are bioturbated by the abundant benthic organisms.

7.3 Hydrodynamic conditions

a) Estuarine circulation patterns based on velocity and salinity structures have been used to classify the estuary using the Hansen and Rattray stratification-circulation diagram. This shows that the estuary is usually partially mixed. However, use of this diagram for estuarine classification is very limited because of large variations of both water depth and degree of stratification during the short period flood-ebb cycle as well as over the longer spring-neap cycle.

b) The estuary changes its character considerably during

the spring-neap cycle. During a spring tide, the water bodies are well-mixed as indicated by very small differences in surface and bottom water salinities. By contrast, the estuary is partially mixed to stratified during neap tides. Surface water in the main channel near the mouth of the estuary is essentially fresh, except during high tide on neaps when a prominent salt wedge develops. In the halocline salinity changes abruptly from 0.2 ‰ to 20.5 ‰ over a depth interval of 0.5 m.

c) The variation of salinity during a tidal cycle is such that highest salinities occur around high water, and lowest salinities occur several hours after low water. The greatest salinity is in the bottom waters, surface waters being 0 to 12 ‰ fresher. Near Portmeirion (at the middle of the estuary) maximum salinities often exceeded 30 and 20 ‰ during spring and neap tides respectively.

d) Throughout most of the year, river flow is low (generally less than 40.0 cumecs) compared to the volume of sea water intruded into the estuary. The average daily discharge is 4.3 cumecs. The flow rate is generally higher during the winter but very low during the summer.

e) A rough estimate of the tidal prism in the estuary for a 3.5 m tide (approaching the maximum tide range) is 13.5×10^6 m^3. This value reduces to 3.0×10^6 m^3 during a neap tide. The velocity data show conclusively that tidal

force are the principal driving mechanism for the estuary.

f) The mixing index (the ratio of the volume of fresh water to the tidal prism) for the estuary during spring and neap tides are 0.009 and 0.031 respectively. Therefore, according to Pritchard's classification scheme, the estuary can be categoried as type D estuary (mixing index less than 0.05).

g) The fastest surface currents, reaching 125 cm/s, have been recorded in the channel near the mouth of the estuary (station 6). Fast currents are not confined only to the main channel since the highest surface current recorded was 132 cm/s at 1 m above the bed during a rising spring tide at station A and B (VGU stations). It appears that in the lower section of the estuary the maximum current velocities are reached at early stages of the tide as water covers the intertidal flats. In general, therefore, flood currents are not greatly affected by morphology once inundation of intertidal sand flats has occurred. The presence of large bedforms over most of the intertidal flats near the estuary mouth reflects the strength of the tidal currents.

h) Near the mouth of the estuary, maximum flood velocities are significantly higher than maximum ebb velocities. However, at the head of the estuary the maximum flood and ebb velocities are more or less the same. Currents during spring tides are faster than during neap tides on both flood and ebb. The degree of asymmetry of the tidal wave

increased in the landward direction with the flood phase becoming shorter, e.g. 5.25 hours near the mouth and 1.25 hours at the head of the estuary. In general, the strength (or energy level) of the tidal currents decreases towards the head of the estuary .

i) Simple logarithmic velocity models are found to be inedequate for the estuarine environment since on many occasions it has been shown that the velocity profiles cab be fitted better to a linear model than to a logarithmic model. However, results show that the logarithmic model can be applied only in the region from the bed up to about 35 cm above the bed due to shallowness of the water which never exceeds 4 m in depth (over the intertidal sand flats). Above this level systematic deviation from logarithmic profiles have been observed.

j) The bed roughness length has been found to vary considerably throughout a tidal cycle. Significant differences in roughness length have been detected between flood and ebb phases. In general, the roughness lengths measured during the flood are smaller than the value measured during the ebb. At station D (the estuary head), for example, the mean flood and ebb roughness length are 0.263 and 0.801 cm respectively.

k) The mean roughness length varies from 0.54 cm to 1.27 cm. The highest value is found in the area of sandwaves

(station B). The measured value is comparable with the value calculated from the theoretical formula of Wooding et. al.(1973).

1) The depth mean velocity computed from velocity profiles was found to be equivalent to a value computed from a single current meter using the estimated average roughness length at each station.

7.4 Sediment transport

a) The dominant mode of sediment transport in the estuary is likely to be by suspension due to the fineness of its sediments (the average mean grain size is 0.15 mm) and the strong currents . This assumption was based on the threshold diagram proposed by Bagnold (1966), which suggested that suspension of sediment is likely to occur at the threshold of movement for sediment finer than 0.17 mm. Therefore, settling-lag and scour-lag mechanisms may be important in the estuary.

b) A new sediment transport rate formula (total load) has been developed in this study which is based on Guy et. al. (1966) flume data for four different sediment sizes (0.19, 0.28, 0.45, and 0.93 mm). The formula proposed is essentially in the form of a power law, where the exponent varies from 2.7 (for 0.93 mm sand) to 4.0 (for 0.19 mm). This is in contrast to the Bagnold (1966) formula and many

other formulae modified from it which are also based on a power law, but with the exponent value of 3 for all grain sizes. The new formulae are represented by

$$q = 1.383 \times 10^{-2} \left(\frac{U-U_c}{U_c}\right)^{4.18} \qquad \text{for D=0.19 mm}$$

$$q = 1.786 \times 10^{-2} \left(\frac{U-U_c}{U_c}\right)^{3.92} \qquad \text{for D=0.28 mm}$$

$$q = 4.149 \times 10^{-2} \left(\frac{U-U_c}{U_c}\right)^{3.10} \qquad \text{for D=0.45 mm}$$

$$q = 1.047 \left(\frac{U-U_c}{U_c}\right)^{2.72} \qquad \text{for D=0.93 mm}$$

where U is the depth mean velocity, and U_c is the threshold depth mean velocity. For intermediate grain sizes, an appropriate formula can be obtained from graphs of exponent vs. grain size and coefficient vs. grain size (see chapter 5).

c) For sediment with mean grain size of 0.15mm, the proposed formula is

$$q = 1.32 \times 10^{-2} \left(\frac{U-U_c}{U_c}\right)^{4.5}$$

where U is the depth mean velocity, and U_c is the

threshold depth mean velocity.

d) The values of transport rate estimates from the new formula and the Engelund and Hansen formula are of the same order of magnitude and are in good agreement with each other.

e) The magnitude of sediment transport display distinct spatial and temporal variability during both the short-term flood-ebb cycle and the longer spring-neap cycle.

f) Sediment transport is very active in the estuary. Residual sediment transport depends on differences in magnitude and duration of flood and ebb currents. The net transport near the mouth of the estuary is usually in the flood direction so that a considerable amount of sediment has been transported from the adjacent submarine areas into the estuary. At the mouth of the estuary (station A), about 99% of the material transported during the spring-neap period is transported in the flood direction. At the head (station D), only 30% of the material transported during the spring-neap period is transported in the flood direction.

g) Transport rates ranging up to 20 g/cm/s have been measured for current velocities up to 120 cm/s (depth mean velocity). This study shows that about 450 kg/m/tide (averaged over spring-neap cycle) of sediments may be transported into the estuary by flood currents and 2.6

kg/m/tide transported out of the estuary by ebb currents. An accumulation rate of 1.38 cm/year has been estimated from these transport data.

h) Changes in intertidal topography as revealed by a few survey profiles indicate that most part of the estuarine flats are areas of low stability due to active sediment movement. Large amounts of sediments were eroded and accreted from the sand flats during the period of survey. The magnitudes of erosion and accretion display distinct temporal and spatial variability. For examples, near the mouth of the estuary (transect 5), the amounts of sediments accreted and eroded during the survey period are 542 and 443 m^3 respectively, while at the head (transect 1), the amounts of sediments accreted and eroded during this period are 69 and 58 m^3 respectively. The most active areas are those which experience fast tidal currents close to the main channel. The stability of the intertidal sand flats increase with distance from the main channel. The results also show that the sand flats at the head of the estuary are more stable than those near the mouth of the estuary.

i) The net accumulation rate based on survey profiles is 4.9 cm/year which is of the same order of magnitude as the accumulation rate estimated on the basis of current measurements and transport rate formulae.

7.5. Sediment characteristics

7.5.1. Estuarine sediments

a) Sediment analysis shows that the bulk of both estuarine and beach sediments consists of quartz grains with a small admixture of lithic and carbonate grains, in contrast to the river sediments which consist predominantly of lithic grains with a small admixture of quartz grains. The percentages of quartz grains within the grain size range of 0.090 to 0.212 mm in estuarine and beach samples vary from 83 to 93% and from 89 to 93 % respectively. The river samples within the same size range, however, are composed of variable amounts of quartz grains in the range of 33 to 78%. The percentage of carbonate grains in this size range is very small making up less than 2% in estuarine samples, less than 3% in beach samples and less than 6% in sea bed samples, while in the river samples the carbonate grains are generally absent. This mineralogical evidence alone provides strong evidence that the Dwyryd estuary is filling with marine sediment from adjacent offshore areas.

b) The grain size distributions of sediment samples used in the analysis are neither log-normal nor log-hyperbolic; this reflects the great diversity of shape of the grain size distribution curves. However, this study show that in a few cases, the hyperbolic distribution is the best approximation to the true distribution of sediment grain sizes.

c) The usual interpretation of the curve shape as resulting from normal distributed subpopulations each reflecting a mode of transport must be questioned since it has been shown that deviations from a normal distribution are the direct result of plotting a non-Gaussian distribution on log-normal probability paper.

d) The surface sediment distribution within the estuary show a distinct trend, with fine sediment accumulating at the head and coarser sediment at the mouth. The mean grain size of estuarine sediments is fairly uniform varies from 2.3 phi (at the mouth) to 3.0 phi (at the head). This trend coincides with the decrease of tidal current velocity (energy level) from the mouth to the head. Therefore, the surficial sediment distribution probably reflects the prevailing hydrodynamic conditions.

e) The estuarine sediments are very well sorted, with standard deviations ranging from 0.20 to 0.58 phi. The average sorting values of estuarine sand flat sediments as measured along six transects show a tendency to become better sorted toward the head. The sorting distribution patterns of the estuarine sediments, therefore, coincide with and reflect the energy distribution. The sediments at the margin of the estuary (salt marsh) exhibit the poorest sorting due to the presence of slightly high percentage of fine material which may correspond to quiescent conditions

away from the main channel.

f) The sediments of the estuary exhibit variable skewness varying from -0.25 to 0.20 . Sediments at the head of the estuary show positive skewness, while sediments at the mouth are mostly negative skewed. Sediments with a mean grain size coarser than 2.9 phi tend to have negative skewness, resulting from removal of fine material by fast tidal currents.

g) A high percentage of estuarine sediments have kurtosis values between 1.0 and 1.5 . There is a small increase of kurtosis from the estuary mouth to the head but in general the values of kurtosis scatter erratically without any distinct trend; therefore it is not considered a valuable parameter.

h) Based on McLaren (1981) selective deposition model, the textural parameters distribution patterns of estuarine sediment suggest that the direction of sediment transport in the estuary is landwards. This is in agreement with the mineralogical study of fluvial, estuarine and marine sediments.

i) The percentage of carbonate material in the estuarine sediment is very low, averaging about 2.5% by weight and ranging from 1.5 to 8% by weight. There is no significant change in textural parameters of sediment samples before and after the removal of the carbonate material. The

difference are probably comparable to the error of the sieve analyses.

j) Cumulative weight percentage profiles plotted for each transect show a clear picture of spatial sediment distribution. The percentages of material coarser than 2.5, 3.0, and 3.5 phi show striking variations along each transect. These trends can be used to identify areas of high, moderate or low currents on the sand flats . The trends in the variation of textural parameters such as mean grain size are less convincing compared to the trends in cumulative weight percentage profiles.

k) This study shows that the mouth of estuary is dominated by material coarser than 3.0 phi, while the head is dominated by material finer than 3.0 phi except in areas of fast currents in the main channel. Transport of fine material by tidal current toward the head of the estuary causes the sediment at the mouth to become coarser, while deposition of fine material causes the sediment at the head to become finer. All estuarine sediments associated with the intertidal sand flats contain very little or no material finer than 4 phi.

7.5.2. Beach sediments

a) The sediments found on the beach are characteristically

coarser than the estuarine sediments. The mean grain size is very variable compared to estuarine sediments ranging from 1.3 phi to 2.8 phi. The presence of coarse material (grain size less than 2 phi) in many beach samples is responsible for their coarseness and bimodality. Coarse material in varying amounts are minor components in the majority of beach sediments, but in a few samples it make up the majority of the grain size distribution. The coarse material is possibly transported from the southern section of Tremadog Bay (Sarn Badrig) by storm-induced currents.

b) Beach sediments are generally poorer sorted than estuarine sediments and almost all of them have negative skewness values. The standard deviation of beach sediments varies from 0.2 phi to 1.1 phi whereas skewness varies from -0.8 to 0.1 .

c) The kurtosis values of the beach sediments are more variable than those of estuarine sediments, with the values ranging from 0.71 to 8.07. Sediments with large kurtosis values in general only confined to the northern beach. In contrast, the southern beach sediments shows less variable than the northern beach sediments.

d) The cumulative weight percentage profiles of beach sediments show very distinct features which indicate the presence of a high energy zone at a narrow stretch of beach across the mouth of the estuary. Material finer than 3.0 phi is absent in this zone compared to other section of the

beach which contain small quantities of this material. Therefore, this zone is regarded as an area where strong flood currents force their way into the estuary across the sand flats during the rising flood tide. The presence of large flood oriented bedforms (sandwaves and megaripples) also reflects fast flood currents in this zone.

e) There is a slight tendency for the sediments to become finer towards the mouth of the estuary along both the northern and southern beaches. However, the southern beach sediments are generally coarser than the northern beach sediments due to the presence of a substantial quantity of coarse material in the southern beach sediments. The percentage of material coarser than 2 phi along the southern beach varies from about 60% to 20% toward the mouth of the estuary.

f) On both northern and southern beaches, it may be noted that there are trends normal to the coastline where sediments tend to become coarser toward the mid water mark from both the low and high water marks. For example, at transect 10, the percentage of material coarser than 2.0 phi increases from less than 10% at low and high water marks to approximately 80% at the mid tide mark.

7.5.3. Sediments of Tremadog Bay

a) A thick layer of muddy sand extends over most parts of Tremadog Bay. The surface sediments of the bay consist of three classes, namely: sand, muddy sand and sandy mud. The muddy sand and sandy mud are found to occupy the deeper areas at the central part of the bay. On the other hand the relatively coarse-grained sediments (sand) occur only in the narrow belts occupying the shallow nearshore area and along the beaches. The grain size distribution of sediments indicates a deficiency of a coarse fraction. For example, material coarser than 3.0 phi is generally absent or present only in very small quantities in the central part of the bay.

b) There is a systematic decrease in grain size away from the shore, and the proportion of mud increases to values of about 60% in the central part of the bay (in the deepest depression). This is a considerably higher mud content than found elsewhere in the study area.

c) The nearshore sediments have a mean grain size of around 3.0 phi. The sediment become finer offshore to 6.5 phi. The general pattern of grain size distribution is similar to the percentage of mud distribution. The close association between bathymetry and mean grain size is also evident from the grain size distribution pattern.

d) The sorting values of the Tremadog Bay sediments are more variable than those of estuarine and beach sediments, with the values ranging from 0.23 (well-sorted) to 4.0 phi

(poorly sorted). The areal pattern of the sorting values shows the same sort of relationship to the bathymetry as the mean grain size.

e) Skewness values vary between 0.0 to 0.9. However, the majority of the samples have skewness values ranging between 0.8 to 0.9 . Strongly positive skewness sediments are generally associated with the sandy mud and muddy sand which occupy in the central part of the bay.

f) A decrease in wave-induced turbulence of the bottom waters in deeper areas provides the most favourable condition for the deposition of fine sediments. The fine material is systematically removed by winnowing towards deeper areas at the centre of the bay, leaving behind a lag deposit of coarse material on the beach.

g) Since the average velocity of both flood and ebb tidal currents in the bay is more or less of the same magnitude, the net transportation of sediments due to tides is probably very small or negligible. The absence of large bedforms over most of the seafloor may suggest that the bay, in general, represents a depositional environment with little sediment movement. However, the presence of large bedforms at various places in the bay may indicate the presence of storm-induced currents which cause disturbances at a few places on the seabed.

7.6. Summary

This study has shown that explanation of sediment distribution patterns and sediment characteristics requires consideration of sediment sources, hydrodynamic conditions, transportation, and depositional processes which among other factors will determine sediment characteristics in this study area. Because a wide range of combinations of environmental conditions and sedimentary processes can occur it is very difficult to determine which factor or parameter is the most influencial in determining the nature of sediments in this area. Although restricted to a single estuary, the study has provided a broad enough spectrum of data to permit some understanding about sedimentary processes in the Dwyryd estuary, in particular, and probably other similar estuaries in general. The results show that a reliable correlation exists between the grain size characteristics of surficial sediments and the prevailing hydrodynamic conditions, as well as the morphology of the area.

As mentioned earlier, the results derived from this are far from complete. Obviously more long-term and detailed studies are required to determine water and sediment characteristics in various critical areas not included during this study such as the sand spit (North Bank) and other offshore banks at the mouth of the estuary and also in shallow areas parallel to the coastline of Tremadog Bay.

This study shows that the estuary is not an isolated part of the coast, but instead should be regarded as an extension of it. It forms part of the general pattern of sediment transport along the Tremadog Bay coastline.

REFERENCES

Abbot,J.E. & Francis,J.R.D. 1977. Saltation and suspension trajectories of solid grains in a water stream. Phil. Trans. R. Soc. London, A284, 225-254.

Ackers,P. & White,W.R. 1973. Sediment transport: new approach and analysis. Proc. Am. Soc. Civ. Eng., J. Hydraul. Div., 99, HY11 ,2041-2060.

Adam,C.E. & Weatherby,G.L. 1981. Some effects of suspended sediment stratification on an oceanic bottom boundary layer. J. Geophys., 86, 4161-4172.

Ahnert, F. 1960. Estuarine meanders in Chesapeake Bay area. Geog. Rev., 50, 390-1.

Allen, J.R.L. (1968). Current Ripples. North-Holland, Amsterdam.

Allen, J.R.L. (1970). Physical Processes of Sedimentation. Allen & Unwin, London.

Allen, J.R.L. 1971. Mixing at turbidity current heads, and its geological implications. J. Sed. Petrol., 41, 97-113.

Allen, J.R.L. 1982a. Sedimentary Structures: Their Character and Physical Basis. Vol. 1 and 2. Elsevier, Amsterdam.

Allen, J.R.L. 1982b. Simple models for the shape and symmetry of tidal sand waves. I. Statistically-stable equilibrium forms. Mar. Geol., 48, 31-49.

Allen, J.R.L. 1982c. Simple models for the shape and symmetry of tidal sand waves. II. Dynamically-stable

symmetrical equilibrium forms. Mar. Geol.,48, 51-73.

Allen, J.R.L. 1982d. Simple models for the shape and symmetry of tidal sand waves. III. Dynamically-stable asymmetrical forms without flow separation. Mar. Geol., 48, 321-36.

Allen, G.P. 1972. Etude des processus sedimentaires dans l'estuarie de la Gironde. Thesis, Univ. Bordeaux, Bordeaux. 314 pp.

Allen,G.P., Sauzay,G., Castaing,p.,and Jouanneau,J.M. 1977. Transport and deposition of suspended sediment in the Gironde estuary, France. in: Wiley,M. (ed.), Estuarine Processes, Vol.II. Academic Press, New York.

Allen, J.R.L. 1976. Bed forms and unsteady processes: some concepts of classification and response illustrated by common one-way types. Earth surf. Proc. 1,361-74.

Allen.J.R.L. 1985. Physical Sedimentology. London, George Allen & Unwin.

Allen,G.P. & Casting,P. 1973. Suspended sediment transport from the Gironde estuary (France) onto the adjacent continental shelf. Mari. Geol., 14, M47-53.

Allen,J.R.L. & Friend,P.F. 1976. Changes in intertidal dunes during two spring-neap cycles, Lifeboat Station Bank, Wells-next-the-sea, Norfolk, England. Sedimentology, 23, 329-346.

Allen, J.R.L. et al. 1980a. Large transverse bedforms and the character of boundary-layers in shallow water environments. Sedimentology, 27, 317-323.

Allen, J.R.L. et al. 1980b. Sandwaves: a model of origin

and internal structure. Sed. Geol., 26, 281-328.

Aller, R.C. 1982. The effects of macrobenthos on chemical properties of marine sediment and overlying water, pp. 53-102. In: P.L. McCall and M.J. Tevesz (eds.), Animal- Sediment Relations. Plenum Press, New York.

Anderson,F.E. 1972. Resuspension of estuarine sediments by small amplitude waves. J. Sedim. Petrol., 42, 602-607.

Anderson, F.E. 1983. The northern muddy intertidal: a seasonally changing source of suspended sediments to estuarine waters: a review. Can. J. Fish Aquqt. sci., 40, Supp.1, 143-159.

A.S.C.E. 1975. Sedimentation Engineering. A.S.C.E., New York.

Avoine, J. et al. 1981. Suspended sediment transport in the Seine estuary, France: effect of man-made modifications on estuary-shelf sedimentology. Marine Geol., 40, 119-137.

Bagnold, R.A. 1941. Libyan Sands. Hodder and Stoughten, St.Paul's House, London, E.C. 4, 288 pp.

Bagnold, R.A. 1955. Some flume experiments on large grains but little denser than tha transporting fluid, and their implications. Proc. Inst. Civil Engng 4, pt.3, 174 pp.

Bagnold,R.A. 1956. Flow of cohesionless grains in fluids. Phil. Trans. R. Soc.,London, A249, 235-297.

Bagnold,R.A. 1963. Mechanics of marine sedimentation. In: M.N.Hill (Eds.), The Sea, 3. Wiley-Interscience, New York, 507-582.

Bagnold,R.A. 1966. An approach to the sediment transport problem from general physics. U.S. Geol. Surv. Prof. Paper, 422-I.

Bagnold, R.A. 1977. Bedload transport by natural rivers. Water Resources Research 13, 303-12.

Bagnold, R.D. & Barndorff-Nielsen, O. 1980. The pattern of natural size distributions. Sedimentology, 27, 199-207.

Barndorff-Nielsen, O. 1977. Exponentially decreasing distributions for the logarithmic of particle size. Proc. Roy. Soc. Lond. Ser. A, 353, 401-419.

Barndorff-Nielsen, O. 1982. Variations in particle size distribution over a small dune. Sedimentology, 29, 53-65.

Barndorff-Nielsen, O. 1983. Log-hyperbolic distributions encyclopedia of statistical sciences, V.3, New York, Wiley.

Bascom, W. 1951. The relationships between sand size and beachface slope. Amer. Geophys. Union Trans., 32, 866-874.

Belderson,R.H. and Stride,A.H. 1966. Tidal current fashioning of a basel bed. Marine Geol., 4, 237-257.

Belderson, R.H. et al. 1971. Holocene sediment on the continental shelf west of the British Isles. In: ICSU/SCOR Working Party 31 symposium, Cambridge, 1970, The Geology of the East Atlantic Continental Margin. 2. Europe (Ed. by F.M. Delaney). Rep. Inst. Geol. Sci., No. 70/14 pp. 157-170.

Blatt,H.and Middleton,G.V & Murray,R. 1980. Origin of Sedimentary Rocks. 2nd edn. Englewood Cliffs, NJ. Prentice-Hall.

Boersma,J.R. 1969. Internal structure of some megaripples on a shoal in Westerschedle estuary, the Netherlands. Geologie Mijnb., 48, 409-414.

Boersma, J.R. and Terwindt, J.H.J. 1981a. Neap-spring tide sequences of intertidal shoal deposits in a mesotidal estuary. Sedimentology, 28, 151-170.

Boersma, J.R. and Terwindt, J.H.J. 1981b. Berms on an intertidal shoal: shape and internal structure. In: Holocene Marine Sedimentation in the North Sea Basin (Eds. by S.-D.Nio et al.) Spec. Publs. Int. Ass. Sediment. 5, Blackwell Scientific Publications, Oxford.

Boon, J.D. 1975. Tidal discharge asymmetry in a salt marsh drainage system. Limnol. Oceanos., 20, 71-80.

Boon, J.D. and Bryne, R.J. 1981. On basin hypsometry and the morphodynamic response of coastal inlet systems. Mar. Geol., 40, 27-48.

Boothroyd, J.C. 1978. Mesotidal inlets and estuaries. In: Coastal Sedimentary Environments (Ed. by R.A. Davies Jr), pp. 287-360. Springer-Verlag, New Yark. 420 pp.

Boothroyd, J.C. and Hubbard, D.K. 1974. Bedform Developement and Distribution Pattern, Parker and Essex Estuaries, Massachusetts. Misc. Paper 1-74, Coastal Engineering Research Centre, Ft. Belvoir,VA, 39 pp.

Boothroyd,J.C. and Hubbard,D.K. 1975. Genesis of bedforms in mesotidal estuaries. In: Cronin,L.E.(Ed.),

Estuarine Research, Vol. 2, Geology and Engineering, 217-34. Academic Press, London.

Bouma,A.H. 1963. A graphical presentation of the facies model of saltmarsh deposits. Sedimentology, 2, 122-129.

Bowden,K.F. 1962. Measurements of turbulence near the sea bed in a tidal current. J. Geophys. Res., 67, 3181-3186.

Bowden, K.F. 1967. Circulation and diffusion, p. 15-36. In: Lauff (ed.), Estuaries, AAAS Publ. 83.

Braithwaite,C.J.R. 1973. Settling behaviour related to sieve analysis of skeletal sands. Sedimentology, 20, 251-62.

Bridge,J.S. and Jarvis,J. 1982. The anatomy of a river bend: a study in flow and sedimentary processes. Sedimentology, 29, 499-541.

Bridges, P.H. and Leeder, M.R. 1976. Sedimentary model for intertidal mudflat channels with examples from the Solway Firth, Scotland. Sedimentology, 23, 533-552.

Briges,S.R. 1979, A study of Middle Ground Shoal (41 28 N, 70 41 W), Sand wave migration and the local mean-velocity field. Unpublished PhD. Thesis, Woods Hole Oceanographic Institution, 291 pp.

British Admiralty, 1896, Barmouth to South Stack. British Admiralty, Chart 368.

Bruun, P. 1978. Stability of tidal inlets: Theory and Engineering, Elsevier, Amsterdam.

Bryne, R.J et al. 1975. Response characteristics of a

tidal inlet: a case study. In: Estuarine Research. Vol.II. Geology and Engineering (Ed. by L.E. Cronin).

Bull,W.B. 1979. Threshold of critical power in streams. Bull. Geol. Soc. Am., 90, 453-464.

Buller,A.T., Green,C.D. and McManus,J. 1975. Dynamics and Sedimentation: The Tay in comparison with other estuaries. In: Hails,J.& Carr,A.P.(Eds), Nearshore Sediment Dynamics and Sedimentation. John Wiley, Chichester, 201-249.

Byrne,J.V. and Kulm,L.D. 1967. Natural indicators of estuarine sediment movement. Am. Soc. of Civ. Eng., Vol. 93, 181-194.

Cameron,W.M. and Pritchard,D.W. 1963. Estuaries. In: The Sea, Vol.2,(ed.) M.N. Hill, pp. 306-24. Interscience Publishers, New York.

Carling, P.A. 1981. Sediment transport by tidal currents and waves: observations from a sandy intertidal zone (Burry Inlet, South Wales). In: Holocene Marine Sedimentation in the North Sea Basin (Eds. by S.-D.Nio et al.) Spec. Publs. Int. Ass. Sediment. 5, Blackwell Scientific Publications, Oxford.

Carver,R.E. 1971. Procedures in Sedimentary Petrology. John Wiley and Sons, New York.

Caston,V.N.D. 1965. Localised sediment transport and submarine erosion in Tremadog Bay, Northern Wales. Marine Geol., 3, 401-410.

Caston, V.N.D. 1974. Bathymetry of the Northern North Sea. Knowledge is vital for offshore oil. Offshore, February, 76-84.

Chambers, R.L. and Upchurch, S.B. 1979. Multivariate analysis of sedimentary environments using grain size frequency distributions. J. Math. Geol., 11, 27-43.

Channon,R.D. and Hamilton,D. 1971. Sea bottom velocity profiles on the continental shelf southwest of England. Nature, 231, 383-385.

Chappel,J. 1967. Recognizing fossil strand lines from grain size analysis. J. Sed. Petrol., 37, 157-165.

Charnock,H. 1959. Tidal friction from currents near the sea bed. Geophys. J. R. Astro. Soc.,2, 215-221.

Chriss,T.M. and Caldwell,D.R. 1982. Evidence for the influence of form drag on bottom boundary layer flow. J. Geophy. Res., 87, 4148-4154.

Christiansen, C. et al. 1984. Re-interpreting "segmented" grain size distributions. Geol. Mag.,121, 47-51.

Coles, S.M. 1979. Benthic microalgal populations on intertidal sediments and their role as precursors to salt marsh development. In: Jefferies,R.L., and Davy, A.J. (eds.), Ecological Processes in Coastal Environments. Blackwell, Oxford.25-42.

Coleman, J.M. 1969. Brahmaputra River: channel processes and sedimentation. Sed. Geol., 3, 129-239.

Collins, M.B.,Amos,C.L.,and Evans,G. 1981. Observations of some sediment-transport processes over intertidal flats, the Wash, U.K. In: Lolocene Marine swedimentation in the North Sea Basin (Ed. by S.-D.Nio et al.), Spec. Publ. Int. Ass. Sediment. 5, 81-98. Blackwell Scientific Publications, Oxford.

Conimos,T.J. and Peterson, D.H. 1976. Suspended-particle transport and circulation in San Francisco Bay: An overview, pp. 48-62. In: M.L.Wiley (ed.), Estuarine Processes, Vol.2, Academic Press, New York.

Costello, W.R. and Southard, J.B. 1981. Flume experiments on lower-flow-regime bedforms in coarse sand. J. sedim. Petrol., 51, 849-864.

Dalrymple, R.W. 1984. Morphology and internal structure of sandwaves in the Bay of Fundy, Sedimentology, 31, 365-382.

Dalrymple,R.W., Knight,R.J. and Lambiase,J.J. 1978. Bed-forms and their hydraulic stability relationships in a tidal environment, Bay of Fundy, Canada. Nature, 275, 100-104.

Davies, J.L. 1964. A morphogenic approach to world shore-lines. Z. Geomorph. 8, 27-42.

Dobson,M.R., Evans,W.E. and James,K.H. 1971. The sediment on the floor of the southern Irish Sea. Marine Geol., 11, 27-69.

Dronkers,J. 1986. Tidal asymmetry and estuarine morpho-logy, Netherlands. Journal of Sea Research. 20, 117-131.

Duane,D.B. 1964. Significance of skewness in recent sedi-ments. J. Sed. Petrol., 34, 846-874.

Dyer,K.R. 1970. Current velocity profiles in a tidal channel. Geophys. J.R. Astron. Soc., 22, 153-161.

Dyer,K.R. 1972. Bed shear stresses and the sedimentation of sandy gravels. Marine Geol.,13, M31-M36.

Dyer,K.R. 1973. Estuaries: A Physical Introduction.

Wiley, London, 140 pp.

Dyer,K.R. 1979 (Ed.). Estuarine hydrography and sedimentation, a handbook. Cambridge University press, Cambridge.

Dyer,K.R. 1980. Velocity profiles over a rippled bed and the threshold of movement of sand. Estuarine Coastal Mar. Sci., 10, 181-199.

Dyer, K.R. 1986. Coastal and Estuarine sediment Dynamics. John Wiley & Sons.

Dyer, K.R. and Ramamoorthy, K. 1969. Salinity and water circulation in the Vellar estuary. Limnol. Oceanog., 14, 4-15.

Edwards,G.R. 1980. Snowdonia, National Park guide no.2. Her Majesty's stationary office.

Edwards,J.M. and Frey,R.W. 1977. Substrate characteristics within a Holocene salt marsh, Sapelo Island, Georgia. Senckenberg. Marit., 9, 215-259.

Edzwald, J.K. and O'Melia, C.R. 1975. Clay distribitions in recent estuarine sediments. Clays and Clay Minerals, 23, 39-44.

Einstein,H.A. 1950. The bedload function for sediment transportation in open channel flows. Soil Conserv. Serv. U.S., Dept. Tech. Bull. No.1026, 78 pp.

Einstein,H.A. and Chien,N. 1955. Effects of heavy sediment concentration near the bed on the velocity and sediment distribution. Univ. Cal. Inst. Eng. Res. U.S. Army Corp. Engrs, Missouri River Div. M.R.D. Sediment Ser. No.8, 76 pp.

Einstein,H.A. and Krone,R.B. 1962. Experiments to determine modes of cohesive sediment transport in salt water. J. Geophy. Res., 67, 1451-1461.

Eisma,D. Kalf,J. and Veenhuis,M. 1980. The formation of small particles and aggregates in the Rhine estuaries. Neth. J. of Sea Res., 14, 172-191.

Elliott, A.J. 1978. Observations of the meteorologically induced circulation in the Potomac estuary. Est. Coastal Mar. Sci., 6, 285-299.

Elliot,T. and Gardiner, A.R. 1981. Ripple, megaripple and sandwaves bedforms in the macrotidal Loughor estuary, South Wales, U.K. In: Holocene Marine Sedimentation in the North Sea Basin (Ed. by S,-D. Nio et al.) Spec. Publ. Int. Ass. Sediment. 5, Blackwell scientific Publications. Oxford.

Emery, K.O. et al. 1957. Estuaries and Lagoons. Geol. Soc. Am. Mem. 67. vol.I, p. 673-750.

Engelund,F. and Fredsoe,J. 1982. Sediment ripples and dunes. Ann. Rev. Fluid Mech., 14, 13-37.

Engelund, F. and Hansen, E. 1966. Investigation of flow in alluvial streams. Acta Plytechnica Scandinavica, Bull. no.9, Hydr. Lab. Techn. Univ. of Denmark.

Engelund,F. and Hansen,E. 1967. A monograph on sediment transport in alluvial streams. Technisk Vorlag, Copenhagen, 62 pp.

Evans,G. 1965. Intertidal flat sediments and their environments of deposition in The Wash. Q. J. Geol. Soc., London, 121, 209-241.

Evans,G. 1976. Intertidal flat sediments and their envi-

ronments of deposition in the Wash. In: Klein,G. de V.(Ed.), Holocene Tidal Sedimentation. Benchmark papers in Geology, V.30, Dowden, Hutchinson.

Evans,G. and Collins,M.B. 1975. The transport and deposition of suspended sediment over the intertidal flats of the Wash. In: Nearshore Sediment Dynamics and Sedimentation (Ed. by J.R.Hails and A.Carr). Wiley, Chichester.

Fairbridge,R.W. 1980. The estuary, its definition and geodynamic cycle. In: Olausson,E. and Cato,I (Eds.), Chemistry and Biogeochemistry of estuaries. New York, Wiley.

Fenemore,P.R. 1976. Reflection and refraction seismics and the accoustically impenetrable or 'turbid' nature of some sediments in Tremadog Bay, North Wales, MSc. Dissertation.

Finley, R.J. 1978. Ebb-tidal delta morphology and sediment supply in relation to seasonal wave energy flux, North Inlet, South Corolina. J. Sed. Petrol., 48, 227-238.

Fischer, H.B. 1972. Mass transport mechanisms in partially stratified estuaries. J. Fluid Mech., 53, 671-687.

Fischer, H.B. 1976. Mixing and dispersion in estuaries. Ann. Rev. Fluid Mech., 8, 107-133.

Fisk,H.N. 1959. Padre Island and the laguna Madre flats, coastal south Texas. Proc. 2nd Coast. Geogr. Conf., 103-52.

Flemming, B.W. 1978. Underwater sand dunes along the south east Africa continental margin: observations and

implications. Mar. Geol., 26, 177-98.

Folk,R.L. 1974. Petrology of Sedimentary Rocks. Hemphill Publishing Co., Texas.

Folk,R.L. and Ward,W.C. 1957. Brazon River bar: a study in the significance of grain size parameters. J. Sed. Petrol., 27, 3-26.

Foster,H.D. 1968. The Glaciation of the Harlech Dome. Thesis, University of London, 375 pp., unpublished.

Frank, W.M. and Friedman, G.M. 1973. Continental-shelf sediments off New Jersey. J. Sed. Petrol.,43, 224-238.

Friedman,G.M. 1961. Distinction between dune, beach and river sands from their textural characteristics. J. Sed. Petrol., 31, 514-29.

Fuller, A.O. 1962. Systematic fractionation of sand in the shallow marine and beach environment off the South African Coast. J. Sedim. Petrol., 32, 602-6.

Gadd,P.E., Lavelle,J.W. and Swift,D.J. 1978. Estimates of sand transport on the new York shelf using near-bottom current meter observations. J. Sed. Petrol., 48, 239-52.

Gellathly,D.C. 1970. Cross-bedded tidal megaripples from King Sound (NW Australia). Sedim. Geol., 4, 185-191.

Gilbert,G.K. 1914. The transport of debris by running water. Prof. Pap. U.S. Geol. Surv., 86, 1-263.

Grace, J.T. et al. 1978. Size frequency distributions taken from within sand laminae. J. Sedim. Petrol., 48, 1193-202.

Graf,W.H. 1971. Hydraulics of Sediment Transport. McGraw-Hill, New York. 513 pp.

Grant,W.D. and Madsen,O.S. 1979. Combined wave and current interactions with a rough bottom. J. Geophys. Res., 84, 1797-1808.

Griffiths,J.C. 1967. Scientific method in analysis of sediments. McGraw Hill, New York.

Groen, P. 1967. On the residual transport of suspended matter by an alternating tidal current. Neth. J. Sea Res., 3, 564-574.

Guilcher,A. 1967. Origin of sediments in estuaries. In: Estuaries,(Ed.) G.H.Lauff, pp.149-57. Pub.83. Amer. Assoc. Adv. Sci., Washington.

Guilcher,A. and Berthois,L. 1957. Cinq annees d observations sedimentologiques daus quatre estuaires-temoins de l ouest de la Bretague. Rev. Geomorphol. Dynami., 8, 64-86.

Guy,H.P., Simmons,D.B. and Richardson,E.V. 1966. Summary of alluvial channel data from flume experiments, 1956-1961. Prof. Pap. U.S. Geol. Surv., 462, 96 pp.

Haas, L.N. 1977. The effect of the spring-neap tidal cycle on the vertical salinity structure current of the James, York and Rappahannock rivers, Virginia, U.S.A. Estuarine Coastal Mar. Sci., 5, 415-496.

Hails,J.R. 1967. Significance of statistical parameters for distinguishing sedimentary environments in New South Wales, Australia. J. Sed. Petrol., 37, 1059-1069.

Halliwell,A.R. and O'Connor,B.A. 1960. Suspended sediment in a tidal estuary. 10th Conf. Coast. Engineering, pp. 687-706. American Soc. of Civ. Engineers.

Hansen,D.V. and Rattray,M. 1966. New dimensions in estuaries classification. Lim. & Ocean., vol.11, 319-326.

Hardisty,J. 1983. An assessment and calibration of formulations for Bagnold's bedload equation. J. Sed. Petrol., 53, 1007-1010.

Harms, J.C. et al. 1974. Carbonate sand waves, Isle Majores, Yucatan. In: Field Seminar on Water and Carbonate Rocks of the Yucatan Peninsula. Mexico (Ed. by A.E. Weidie). Field Trip 2, Geol. Soc. Am. Ann. meeting. Miami, pp. 123-147.

Harms, J.C. et al. 1975. Depositional environments as interpreted from primary sedimentary structures and stratification sequences. Lecture Notes, Soc. Econ. Paleont. Mineral., Short Course 2, Dallas, TX, 161 pp.

Harms, J.C. et al. 1982. Structures and sequences in clastic rocks. Soc. Econ. Paleont. Mineral., Short Course 9, 249 pp.

Hayes, M.O.(ed.) 1969. Coastal environments of northestern Massachusetts and New Hampshire. Eastern Section Guidebook. Soc. Econ. Paleont. and Mineral., 462 pp.

Hayes, M.O. 1975. Morphology of sand accumulation in estuaries: an introduction to the symposium. In Cronin, L.E. (Ed.), Estuarine Research Vol.II, Academic Press, New York, 3-22.

Haynes,J. and Dobson,M. 1969. Physiography, foraminifera and sedimentation in the Dovey estuary. Geol. J., 6, 217-256.

Heathershaw, A.D. 1979. The turbulent structure of the

bottom boundary layer in a tidal current. Geophys. J.R. Astro. Soc., 58, 395-430.

Heathershaw, A.D. 1981. Comparisons of measured and predicted sediment transport rates in tidal currents. Marine Geol., 42, 75-104.

Heathershaw, A.D. and Carr, A.P. 1977. Measurements of sediment transport rates using radioactive tracers. Coastal Sediments '77, Am. Soc. Civ. Engrs., Charleston,S.C., USA. pp. 399-416.

Heathershaw, A.D. and Hammond, F.D.C. 1979. Swansea Bay (Sker) Project: offshore sediment movement and its relation to observed tidal current and wave data. Inst. Oceanogr. Sci. Rep. No.93, 119pp.

Heathershaw, A.D.and Langhorne, D.N. 1988. Observations of near-bed velocity profiles and seabed roughness in tidal currents flowing over sandy gravels. Estuarine, Coast. and Shelf Sci., 26, 459-482.

Hedgpeth,J.L. 1963. Ecological aspects of the loguna of Madre, a hypersaline estuary. In: Lauff (ed.), Estuaries, 408-19.

Helley, E.J. 1969. U.S. Geol. Surv., Prof. Paper, 562-G.

Hjulstrom,F. 1935. Studies of the morphological activities of rivers as illustrated by the River Fyris. Bull. Geol. Inst. Univ. Uppsala, 25, 221-527.

Hjulstrom,F. 1955. Transportation of detritus by moving water. In: Recent marine sediments, A symposium, Society of Economic Paleontologists and Mineralogists, P.D. Trask (Ed.), Special Publication, No. 4, Tulsa,

Oklahoma.

Huanting,S. et al. 1984. Flow and mixing in the mouth of Changjiang estuary. In: Acta Oceanologica Sinica (ed.), Proceedings of international symposium on "Sedimentation on the continental shelf, with special reference to the East China Sea", Hangzhou, China. China Ocean press, Beijing, China.

Hutchison,C.S. 1974. Laboratory handbook of Petrographic Techniques. Wiley and Sons.

Inglis,C.C. and Allen,F.H. 1957. The regimen of the Thames estuary as affected by currents, salinities and river flow. Proc. Inst. Civil Eng., 7, 827-868.

Inman,D.L. and Chamberlain,T.K. 1955. Particle-size distribution in nearshore sediments. In: J.L.Hough and H.W.Menard (Eds.), Finding Ancient Shorelines. Soc. Econ. Palaeontologists, Spec. Publ., 3, 106-129.

Inokuchi,M. and Takayama,S. 1973. Sci. Rep. Tokyo Kyoiku Daigaku, C11, 157-169.

Ippen,A.T.(Ed.) 1966. Estuaries and Coastline Hydrodynamics. McGraw-Hill, New York.

Ippen,A.T. and Harleman,D.R.F. 1966. Tidal dynamics in estuaries. In: Ippen,A.T.(Ed.), Estuaries and Coastline Hydrodynamics. McGraw-Hill, New York, pp. 493-545.

Irani,R.R. and Callis,C.F. 1963. Particle size: measurement, interpretation, and application, John Wiley and sons, 165 pp.

Iversen, J.D. et al. 1976. Saltation threshold on Mars: the effect of interparticle force, surface roughness,

and low atmospheric density. Icarus, 29(no.3), 381-93.

Jackson, R.G. 1976. Largescale ripples in the lower Wabash River. Sedimentlogy, 23, 593-623.

Jackson, R.G. 1977. Mechanisms and hydrodynamic factors of sediment transport in alluvial streams. In: Research in Fluvial Geomorphology (Ed. by R. Davidson-Arnott & W. Nickling), pp.9-43. GeoAbstracts, Norwich, England.

Jackson,W.H. 1964. Effect of tidal range, temperature and fresh water on the amount of silt in suspension in an estuary. Nature, London, 201,1017.

Jago, C.F. 1974. The sedimentology of estuarine and coastal plain deposits between Pendine and Wharley Points, Carmarthen Bay. Imperial College of Science and Technology, University of London, 1974.

Jago,C.F. 1980. Contemporary accumulation of marine sand in a macrotidal estuary, Southwest Wales. Sedim. Geol., 26, 21-49.

Kachel,N.V. and Sternberg,R.W. 1971. Transport of bedload as ripples during an ebb current. Marine Geology, 10, 229-244.

Kamphuis, J.W. 1977. Determination of sand roughness for fixed beds. J. Hydraul. Res., 12, 193-203.

Kelland, N.C. and Bailey, A. 1975. An underwater study of sand wave mobility in Start Bay. Rep. underwat. Ass. (New Series), 1, 74-80.

Kenyon,N.H. and Stride,A.H. 1970. The tide-swept conti-

nental shelf sediments between shetland Isles and France. Sedimentology, 14,159-173.

Kestner, F.J.T. 1975. The loose boundary regimen of the Wash. Geogr. J. 141, 388-414.

Ketchum,B.H. 1951. The exchanges of fresh and salt water in tidal estuaries. J. Mar. Res., 10, 18-38.

Kidson,C. 1977. Some problems of the Quarternary of the Irish Sea. In:Kidson,C. and Tooley,M. (Eds.), The Quartenary history of the Irish Sea. Liverpool. Seal House Press.

Kindle, E.M. 1917. Recent and fossil ripple marks. Geol. Survey Canada Mus. Bull., 25, 56 pp.

Kirby, R. and Parker, W.R. 1977. Fine sediment studies relevant to dredging practice and control. Proc. 2nd. Int. Symp. Dredging Technology. B2-15 - B2-26.

Kjerfve, B. 1979. Measurement and analysis of water current, temperature, salinity, and density. In: Estuarine Hydrography and Sedimentation: a handbook, K.R.Dyer (Ed.), Cambridge University Press. Cambridge.

Kjerfve,B.J. 1975. Tide and fair weather wind effects in a bar-built Louisiana estuary. In: Estuarine Research. Vol. 2, L.E.Cronin (Ed.), pp. 47-62. Academic Press, New York.

Klein, G de V. 1963. Bay of Fundy intertidal zone sediments. J. Sed. Petrol., 33, 844-854.

Klein,G de V. 1970. Depositional and dispersal dynamics of intertidal sandbars. J.Sedim. Petrol., 40, 1095-1127.

Krenter,F. 1921. Der Flussbau (taken from Leliovsky,S. An

Introduction to Fluvial Hydraulics. Dover Publication Inc., pp.43.

Krone, R.B. 1979. Sedimentation in the San Francisco Bay System. In: Conomoss,T.J.(Ed.), San Francisco Bay: The urbanized estuary. Amer. Assoc. Sci., Pacific Div., San Francisco, 85-96.

Krumbein, W.C. 1934. Size frequency distributions of sediments. J. Sedim. Petrol., 4, 65-77.

Krumbein,W.C. 1939. Graphic presentation and statistical analysis of sedimentary data. In: Recent Marine Sediments, P.D. Trask, (ed.), pp. 558-91. Thos. Murby, London.

Krumbein, W.C. 1953. Statistical Design for Sampling Beach Sand. Trans. Am. Geophys. Union, 34, 857-868.

Krumbein,W.C and Pettijohn,F.J. 1938. Manual of Sedimentary Petrology. Appleton-Century-Crofts, Inc., New York.

Kulm, L.D. and Byrne, J.V. 1967. Sediments of Yaquina Bay, Oregan. In: Estuaries (Ed. by G.H. Lauff). Am. Ass. Adv. Sci., Publ. No. 83, 226-238.

Lambiase, J.J. 1977. Sediment dynamics in the macrotidal Avon River Estuary, Nova Scotia. Unpublished PhD Thesis. McMaster University, Hamilton.

Lambiase, J.J. 1980. Sediment dynamics in the macrotidal Avon River estuary, Bay of Fundy, Nova Scotia. Can. J. Earth Sci., 17, 1628-1641.

Langbein, W.B. 1963. The hydraulic geometry of a small tidal estuary. Bull. Inst. Ass. Scient. Hydrol., 8,

84-94.

Langhorne,D.N. 1973. A sandwave field in the Outer Thames Estuaries, Great Britain. Mar. Geology, 14, 129-143.

Langhorne,D.N. 1977. Consideration of meteorological conditions when determining the navigational water depth over a sand wave field. Int. Hydrog. Rev., LIX, 17-30.

Langhorne,D.N. 1981. An evaluation of Bagnold's dimensionless coefficient of proportionality using measurements of sandwave movement. Marine Geology, 43,49-64.

Langhorne,D.N. 1982. A study of the dynamics of a marine sandwave. Sedimentology, 29,571-594.

Lankford,R.R. 1976. Coastal lagoons of Mexico: their origin and classification. In: Estuarine Processes, Vol.2, (ed.) M.Wiley. pp. 182-215. Academic Press, New York.

Lees, B.J. 1983. The relationship of sediment transport rates and paths to sandbanks in a tidally dominated area off the coast of East Anglia, U.K. Sedimentology, 30, 461-483.

Leeder, M.R. 1983. On the dynamics of sediment suspension by residual Reynolds stresses: confirmation of Bagnold's theory. Sedimentology, 30,485-491.

Leopold,L.B., Wolman,M.G. and Miller,J.P. 1964. Fluvial Processes in Geomorphology. Freeman, San Francisco, 522 pp.

Leroy, S.D. 1981. Grain size and moment measures: a new look at Karl Pearson's ideas on distributions. J.

Sedim. Petrol., 51, 625-630.

Lettau, H. 1969. Note on aerodynamic roughness parameter estimation on the basis of roughness-element description. J. Applied Meteorology, 8, 828-832.

Ludwick, J.C. 1972. Migration of tidal sand waves in Chesapeake Bay entrance. In: Swift,D.J.P. et al.(eds.) Shelf Sediment Transport: Processes and Pattern, Dowden, Hutchinson and Ross, Stroudsberg, PA, 377-410.

Ludwick, J.C. 1974. Tidal currents and zig-zag sand shoals in a wide estuary entrance. Geol. Soc. Amer. Bull., 85, 717-726.

Ludwick,J.C. 1975. Variations in the boundary-drag coefficient in the tidal entrance to Chesapeake Bay, Virginia. Marine Geology, 19, 19-28.

Macdonald, K.B. 1977. Coastal salt marsh. In: Barbour,M.G., and Major,J. (eds.), Terrestrial Vegetation of California. John Wiley, New York.

Mantz, P.A. 1977. Incipient transport of fine grains and flakes by fluids: extended shields diagram. J. Hydraul. Div. ASCE, 103, 601-615.

Mason,C.C. and Folk,R.L. 1958. Differentiation of beach dune, and aeilian flat environments by size analysis, Mustang Islands, Texas. J. Sedim. Petrol., 28, 211-226.

McCave,I.N. 1971. Wave effectiveness at the sea bed and its relationship to bedforms and deposition of mud. J. Sedim. Petrol.,41, 89-96.

McCave,I.N. 1973. Some boundary-layer characteristics of tidal currents bearing sands in suspension. Mem. Soc. R. des Sci. de Liege, 6, 187-206.

McCave,I.N. 1974. Discussion on Meade,R.H. Net transport of sediment through the mouths of estuaries; seaward or landward? Mem. Inst. Geol. Bassin Aquitaine, No. 7, 207-213.

McCave, I.N. and Geiser, A.C. 1978. Megaripples, ridges and runnels on intertidal flats of the Wash, England. Sedimentology, 26, 353-369.

McDowell,D.M. and O'Connor,B.A. 1977. Hydraulic behaviour of estuaries. London, MacMillan.

McLaren, P. 1981. An interpretation of trends in grain size measures. J. Sedim. Petrol., 51, 611-624.

McLean, R.F. and Kirk, R.M. 1969. Relationship between grain size sorting and foreshore slope on mixed sand-shingle beaches. New Zealand. J. Geol. Geophys. 12, 138-55.

Meade,R.H. 1969. Landward transport of bottom sediments in estuaries of the Atlantic Coastal Plain. J. Sedim. Petrol., 39, 222-34.

Meade,R.H. 1972. Transport and deposition of sediments in estuaries. Mem. Geol. Soc. Am., 133, 91-120.

Middleton,G.V. 1976. Hydraulic interpretation of sand size distributions. J. Geol., 84, 405-426.

Middleton,G.V. and Southard,J.B. 1978. Mechanics of sediment movement. SEMP Short Course No.3. Tulsa, Oklahoma.

Miller,M.C., McCave,I.N. and Komar,P.D. 1977. Threshold of

sediment motion under unidirectional currents. Sedimentology, 24, 507-28.

Moss,A.J. 1962. The physical nature of comman sandy and pebbly deposits, Part 1. Am. J. Sci., 260, 337-373.

Muller,G. 1967. Methods in Sedimentary petrology. E. Schweizerbart' sche Varlagsbuchhandlung, Stuttgart.

Myers, A.C. 1977. Sediment processing in a marine subtidal sandy bottom community: I. Physical aspects. J. Mar. Res., 35, 609-632.

Nece,R.E. and Smith,J.D. 1970. Boundary shear stress in rivers and estuaries. J. Water Ways Harb. Div. Am. Soc. Civ. Engrs., 96, 335-358.

Nelson, B.W. 1959. Transportation of colloidal sediment in the fresh water marine transition zone (abstract), pp. 640-641. In: Mary Sears (ed.), 1 st Internat. Oceanog. Cong. preprints. Am. Assoc. Adv. Sci., Washington, DC.

Nichols,M. 1972. Sediments of the James River Estuaries, Virginia. In: Nelson,B.W. (ed.), Environmental Framework of Coastal Plain Estuaries, Geol. Soc. Amer. Mem., 133, 169-212.

Nichols,M. 1974. Developement of the turbidity maximum in the Rappahannock Estuary: Summary. Proceedings International Symposium on Interrelationships of Estuarine and Continental Shelf Sedimentation. Memoires de l'Institut de Geologie de Bassin d' Aquitaine, 7,19-25.

Nichols, M. and Poor,G. 1967. Sediment transport in a

coastal plain estuary. J. Wat. Harb. Coastal Eng. Div. ASCE, 93, WW4, 83-95.

Nowell,A.R.M. 1983. The benthic boundary layer and sediment transport. Rev. Geophys. Space Phys., 21, 1181-1192.

O'Brien, M.P. 1969. Dynamics of tidal inlets. In: Castanares, A., Phleger, F.(eds.), Coastal Lagoons, A symposium, UNAM-UNESCO, Memoir Symposium Intl. Langunas Costeras, pp. 397-406.

Owen, R. 1981. Holocene sedimentation in the North-western North Sea. In: Holocene Marine Sedimentation in the North Sea Basin (Ed. by S.-D. Nio et al.) Spec. Publ. Int. Ass. Sediment. 5, Blackwell Scientific Publications, Oxford.

Okubo, A. 1973. Effect of shoreline irregularities on streamwise dispersion in estuaries and other embayments. Neth. J. Sea Res., 6, 213-224.

Passega, R. 1964. Grain size representation by CM patterns as a geological tool. J. Sed. Petrol., 34, 830-847.

Pestrong,R. 1972. San Francisco Bay tidelands. Californian Geologist, 25, 27-40.

Pethick, J. 1984. An Introduction to Coastal Geomorphology. Edward Arnold, London.

Pickrill, R.A. 1986. Sediment pathways and transport rates through a tide-diminated entrance, Rangaunu Harbour, New Zealand. Sedimentology, 33, 887-898.

Postma, H. 1950. The distribution of temperature and salinity in the Wadden Sea. Tijdschr. Kon. Ned. Aardr., 57, pp. 294-302.

Postma,H. 1954. Hydrography of the Dutch Wadden Sea. Arch. Neerl., 2001, 10, 406-511.

Postma,H. 1961. Transport and accumulation of suspended matter in the Dutch Wadden Sea. Neth. J. Sea Res., 1, 149-190.

Postma,H. 1967. Sediment transport and sedimentation in the estuarine environment. In: Estuaries, (ed.) G.H.Lauff, pp. 158-79. American Association for the Advancement of Sci., Publication 83, Washington.

Postma, H. and Kalle,K. 1955. Die Entstehung von Trubungszonen im Unterlauf der Flusse, speziall im Hinblick auf die Verhaltnisse im der Unterelbe. Deutscheu Hydrographischen Zeitschrift, 8, 137-44.

Pritchard,D. 1952. Estuarine hydrology. Advances in Geophysics 1, 243-80.

Pritchard, D.W. 1955. Estuarine circulation patterns. Proc. Amer. Soc. Civil Engr., 81, 717-1-717-11.

Pritchard, D.W. 1967. Observations of circulation in coastal plain estuaries. In: Lauff,G.H (ed.), Estuaries, Amer. Ass. Adv. Sci., Publ. 83, Washington DC, pp. 3-5.

Prych, E.A. 1970. Effects of density differences on lateral mixing in open-channel flow. Rep. KH-R-21. W.M.Keck Laboratory, California Institute of Technology.

Pryor, W.A. 1975. Biogenic sedimentation and alteration of argillaceous sediments in shallow marine environments. Geol. Soc. Amer. Bull., 86, 1244-1254.

Raudkivi, A.J. 1963. Study of sediment ripple formation. J. Hydraul. Div. ASCE, 89, HY6, 15-33.

Raudkivi,A.J. 1976. Loose Boundary Hydraulics, 2nd ed. Pergamon Press, Oxford.

Redfield, A.C. 1967. Ontogeny of a salt marsh estuary. In: G.H.Lauff (ed.), Estuaries. Amer. Ass. Adv. Sci. Publ., 83, 108-114.

Reeburg,W.S. 1969. Observations of gases in chesapeake Bay sediments. Limnol. Oceanogr., 14, 368-375.

Reed, W.E. et al. 1975. Depositional environment interpretation from settling velocity (psi) distributions. Bull. Geol. Soc. Am., 86, 1321-1328.

Reineck, H.E. 1963. Sedimentgefuge im Bereich der sudlichen Nordsee: Abhandl. Sencken. Nat. Gesell, 505, 1-138.

Reineck, H.E. 1967. Layered sediments of tidal flats, beaches and shelf bottoms of the North Sea. In: Lauff,G.H. (ed.), Estuaries. Amer. Ass. Adv. Sci. Spec. Publ. 83, 191-206.

Reineck, H.E. 1973. Bibliographie geologischer Arbeiten uber cour. Forsch. Inst. Senckenberg, 57 pp.

Reineck, H.E. and Wunderlich, F. 1968a. Classification and origin of flaser and lenticular bedding. Sedimentology, 11, 99-104.

Reineck, H.E. and Wunderlich, F. 1968b. Zeitmessungen und Bezeitenschichten. Natur und Museum, 97, 193-197.

Reineck,H.E. 1972. Tidal flats. In: Rigby, J.K, and Hamblin, W.K.,(eds.), Recognition of Ancient Sedimentary Environments. Soc. Econ. Paleont. Mineral. Spec. Publ. 16, 146-159.

Rhoads, D.C. 1974. Organism-sediment relations on the muddy sea floor. Oceanogr. Mar. Biol. Ann. Rev., 12, 263-300.

Rhoads, D.C.and Stanley,D.J. 1965. Biogenic graded bedding. J. Sed. Petrol., 35, 956-963.

Ritter, J.R. 1972. Sediment transport in a tidal inlet. Proc. 13th Coastal Engn. Conf., Vancouver 1872. 832-842.

Roberts,W.P. and Pierce,J.W. 1976. Deposition in upper Patuxent estuary, Maryland, 1968-1969. Est. and Coast. Mar. Sci., 4, 267-280.

Robinson, A.H.W. 1960. Ebb-flood channel systems in sandy bays and estuaries. j. Geogr. 45, 183-199.

Roy,P.S., Thom,B.G., & Wright,L.D. 1980. Holocene sequences on an embayed high-energy coast: an evolutionary model. Sed. Geol., 26, 1-19.

Rubin, D.M. and McCulloch, D.S. 1980. Single and superimposed bedforms: a synthesis of San Francisco Bay and flume studies. Sedimen. Geol. 26, 207-231.

Sagoe,K.M.O. and Visher,G.S. 1977. Population breakes in grain size distributions of sand. A theoritical model. J. Sedim. Petrol., 47, 285-310.

Schefer,W. 1962. Aktuopalaontolie nach studien in det Nordsee. Kramer, Frankfurt a.m. 666 pp.

Schubel, J.R. 1968. Turbidity maximum of the northern Chesapeake Bay. Science, 161, 1013-1015.

Schubel,J.R. 1971. Tidal variation of the size distribution of suspended sediment at a station in the Chesapeake Bay turbidity maximum. Neth. J. Sea Res.,

5, 252-266.

Schubel, J.R. 1972. Distribution and transportation of suspended sediment in upper Chesapeake Bay. In: Nelson, B.W (ed.), Environmental Framework of Coastal Plain Estuaries. Geol. Soc. Amer. Mem., 133, 151-167.

Schubel,J.R. 1974a. Effects of tropical storm Agnes on the suspended solids of the Northern Chesapeake Bay. In: Gibbs,R.J. (Ed.), Suspended solids in water. Plenum Marine Science, 4, 113-132.

Schubel,J.R. 1974b. Gas bubbles and the accoustically impenetrable, or turbid, character of some estuarine sediments. Mar. Sci., 3, 275-298.

Schubel,J.R. & Meade,R.H. 1977. Man's impact on estuarine sedimentation. Proc. Conf. Est. Poll. Control and Assess., Vol.1. US env. Prot. Agency, Washington, 193-209.

Schubel,J.R. and Schiemer,E.W. 1973. The cause of the accoustically impenetrable, or turbid, character of Chesapeake Bay sediment. Mar. Geophys. Res., 2, 61-71.

Sedimentation Seminar, 1981. Comparison of methods of size analysis for sands of the Amazon-Solimes rivers, Brazil and Peru. Sedimentology, 28, 123-8.

Schultz,E.A. and Simmons,H.B. 1957. Fresh water-salt water density currents, a major cause of siltation in estuaries. Tech. Bull. No.2, Comm. Tidal Hydraulics, U.S. Army, Corps of Engineers. 28p.

Shepard, F.P. 1963. Submarine Geology. 2nd ed. New York.

Harper and Row.

Shields,A. 1936. Anwendung der aehnlichkeitsmechanik und der turbulenz forshung auf die geschiebebewegung. Mitt. Preuss. Versuchsanstalt Wasserbau Schiffbau. Berlin, 26.

Siegenthaler,C. 1982. Tidal cross-strata and the sediment transport rate problem: a geologist's approach. Marine Geology, 45, 227-240.

Simmons,H.B. 1955. Some effects of upland discharge on estuarine hydraulics. Proc. Am. Soc. Civ. Engrs., 81, Paper 792.

Simmons,M.B. 1966. Field experience in estuaries. In: Estuary and coastline hydrodynamics (Ed.) A.T.Ippen. McGraw-Hill, New York.

Simons,D.B. et al. 1965. Sedimentary structures generated by flow in alluvial channels. In: Middleton,G.V. (ed.), Primary Sedimentary Structures and Their Hydrodynamic Interpretation. Soc. Econ. Paleont. and Mineral. Spec. Publ. 12, Tulsa, OK, pp.34-52.

Simpkin,P.G. 1976. Geotechnical mapping of the seabed: Final Report, Part III - Acoustics. Marine Science Laboratories, UCNW, Menai Bridge.

Sleath, J.F.A. 1984. Sea bed mechanics. John Wiley and Sons, New York.

Smith,J.D. 1969a. Geomorphology of a sand ridge. J. Geol., 77, 39-55.

Smith,J.D. 1969b. Studies of non-uniform boundary layer flows. In: Investigations of Turbulent Boundary Layer and Sediment Transport Phenomena as Related to the

Shallow Marine Environment, Part 2. Rep. Dep. Oceanog. Univ. Washington. RLO-1752-13, 13 pp.

Smith, N.P. 1978. Longshore currents on the fringe of Hurricance Anita. J. Geophy. Res., 83, 6047-6051.

Smith,B. and George,T.N. 1961. British Regional Geology, North Wales, NERC, Inst. Geol. Sci., Her Majesty's Stationary Office.

Smith, D.B. and Parsons,T.V. 1965. Silt movement investigation in the Oxcars spoil ground, Firth of Forth, using radioactive tracers, 1961 and 1964, AERE-R 4980 (HMSO, 1965)

Soulsby,R.L. 1983. The bottom boundary layer of shelf seas. In: Johns,B. (Ed.), Physical Oceanography of Coastal and Shelf Seas, Elsevior Science Publishers, Amsterdam.

Soulsby,R.L. and Dyer,K.R. 1981. The form of the near-bed velocity profile in a tidally accelerating flow. J. Geophys. Res., 86, 8067-8074.

Southard, J.B. 1971. Representation of bed configurations in depth-velocity-size diagrams. J. Sedim. Petrol., 41, 903-915.

Southard, J.B. and Dingler, J.R. 1971. Flume study of ripple propagation behind mounds on flat sand beds. Sedimentology, 16, 251-263.

Speer, P.E. & Aubrey, D.G. 1985. A study of non-linear tidal propagation in shallow inlet, estuarine systems, part II Theory- Estuarine Coast. Shelf Sci., 21, 207-224.

Spencer,D.W. 1963. The interpretation of grain size distribution curves of clastic sediments. J. Sedim. Petrol., 33, 180-190.

Sternberg,R.W. 1968. Friction factors in tidal channels with differing bed roughness. Marine Geology, 6, 243-260.

Sternberg, R.W. 1971. Measurements of the incipient motion of sediment particles in the marine environment. Marine Geol., 10, 113-119.

Sternberg,R.W. 1972. Predicting initial motion and bedload transport of sediment particles in the shallow marine environment. In: Swift,D.J.P., Duane,D.B,.& Pilkey,O.H. (Eds.), Shelf sediment transport : process and pattern. Dowdem, Hutchinson and Ross, Stroudsburg, Pa., p 61-82.

Steers,J.A. 1964. The coastline of England and Wales, 2nd ed. Cambridge University Press, London, 750 pp.

Steward, H.B.Jr. 1958. Sedimentary reflections of depositional environments in San Mignel Lagoon, Baja California, Mexico. Ame. Ass. Petroleum Geologists Bull., 42, 2567-2618.

Stokes,G.G. 1851. On the effect of the internal friction of fluids on the motion of pendulums. Trans. Camb. Philos. Soc., 9, 20-21.

Sundborg,A. 1956. The River Klarelven, a study of fluvial processes. Geografiska Annalen, Stockholm.

Swift, D.J.P. 1976. Coastal sedimentation. In: Stanley,D.J. and Swift.D.J.P. (eds.), Sediment Transport and Environmental Management. Wiley-

Interscience, New York, 255-310.

Swift, D.J.P.et al. 1979. Time and space distributions of megaripples and associated bedforms, Middle Atlantic Bight, North America Atlantic Shelf. Sedimentology, 26, 389-406.

Tanner,W.F. 1964. Modification of sediment size distributions. J. Sedim. Petrol., 34, 156-164.

Taylor Smith,D. 1975. Geophysical assessment of seafloor sediment properties. Oceanology Int. 75, 320-328.

Taylor Smith,D. 1976a. Geotechnical mapping of the seabed: Final Report, Part I- An Introduction. Marine Science Laboratories, UCNW, Menai Bridge.

Taylor Smith,D. 1976b. Geotechnical mapping of the seabed: Final Report, Part IV- General Conclusions. Marine Science Laboratories, UCNW, Menai Bridge.

Terwindt, J.H.J. 1981. Origin and sequences of sedimentary structures in inshore mesotidal deposits of the North Sea. In: Holocene Marine Sedimentation in the North SEa Basin (Ed. by. S.- D.Nio et al.) Spec. Int. Ass. Sediment. 5, 3-26. Blackwell Scientific Publications, Oxford, 524 pp.

Terwindt,J.H.J. & Breusers,H.N.C. 1972. Experiments on the origin of flaser, lenticular and sand-clay alternating bedding. Sedimentology, 19, 85-98.

Terwindt,J.H.J., De Jong,J.D. & Van der Wilk,E. 1963. Sediment movement and sediment properties in the tidal area of the lower Rhine (Rotterdam waterway). Verh. K. Ned. Geol. Mijnbouwkd. Genook., Geol. Ser., 21, 243-258.

Terwindt, J.H.J. et al. 1986. The behaviour of intertidal sandwaves during neap-spring tide cycles and the relevance for paleoflow reconstructions. Sedimentology, 33, 1-31.

Thorn,M.F.C. and Parsons,J.G. 1980. Erosion of cohesive sediments in estuaries: an engineering guide. Proc. 3rd Int. Symp. Dredging Tech., 349-358.

Udden,J.A. 1914. Mechanical composition of clastic sediments. Geol. Soc. Am. Bull., 25, 655-744.

Vanoni,V.A. and Nomicos,G.N. 1959. Resistance properties of sediment-laden streams. J. Hydraulic Div. ASCE, 85, HY5, 77-107.

van Straaten,L.M.J.V. 1950. Environment of formation and facies of the Wadden Sea sediments. Koninkl. Aardrijk. Genootsch. 67, 94-108.

van Straaten,L.M.J.V. 1952. Biogene textures and the formation of shell beds in the Dutch Wadden Sea. Proc. K. ned. Akad. Wet. B55, 500-516.

van Straaten,L.M.J.V. 1953. Megaripples in the Dutch Wadden Sea and in the Basin of Arcachon (France). Geologie Mijnb. 15, 1-11.

van Straaten,L.M.J.V. 1954. Sedimentology of recent tidal flat deposits and the psammites de Condroz (Devonian). Geologie Mijnb. 16, 25-47.

Van Straaten, L.M.J.V. 1959. Minor structures of some Recent littoral and neritic sediment. Geol. en Mujnbouw, 21, 197-216.

van Straaten,L.M.J.V. 1961. Directional effects of winds,

waves and currents along the Dutch North Sea coast. Geologie Mijnb., 40, 333-346,

van Straaten,L.M.J.V. 1964. In: A.H.Bouma & A.Brouwer (Eds.), Turbidites. Elsevier, Amsterdam, pp. 142-147.

van Straaten,L.M.J.V. and Kuenen,P.H. 1957. Accumulation of fine grained sediments in the Dutch Wadden Sea. Geol. Mijnb.,329-354.

van Straaten, L.M.J.V.and Kuenen,P.H. 1958. Tidal action as a cause of clay accumulation. J. Sedim. Petrol., 28, 406-413.

Vincent,C.E., Young,R.A. and Swift,D.J.P. 1981. Bedload transport under waves and currents. Marine Geology, 39, 71-80.

Visher,G.S. 1969. Grain size distributions and depositional processes. J. Sedim. Petrol., 39, 1074-1106.

Welder,F.A. 1959. Processes of deltaic sedimentation in the Lower Mississippi River: Louisiana State Univ., Coastal Studies Inst. Tech. Rept., 12,90pp.

Wentworth, C.K. 1922. A scale of grade and class terms for clastic sediments. J. Geol., 30, 377-392.

White, B.R. 1979. Soil transport by winds on Mars. J. Geophys. Res., 84, 4643-51.

Whitehouse,U.G., Jeffrey,L.M. and Debrecht,J.D. 1960. Differential settling tendencies of clay minerals in saline waters. Proc. 7th Conf. Clays Mins., 1-79.

Wijbenga, J.H.A. and Klassen, G.J. 1983. Changes in bedform dimensions under unsteady flow conditions in a

straight flume. Spec. Publ. Int. Ass. Sediment. 6, 35-48.

Williams,P.B. and Kemp, P.H. 1971. Initiation of ripples on flat sediment beds. J. Hydraul. Div. ASCE, 97, HY4, 505-522.

Wimbush,M. and Munk,W. 1971. The benthic boundary layer. The Sea, Vol.4 Part I, New York, Wiley, 731-758.

Wooding,R.A., Bradley,E.F. and Marshall,J.K. 1973. Drag due to regular arrays of roughness elements of varying geometry. Boundary Layer Meteorology, 5, 285-308.

Wright,L.D. 1971. Hydrography of south Pass, Mississippi River. Proc. Amer. Soc. Civil Engrs., 97, WW3, 491-504.

Wright,L.D. 1978. River deltas. In: Davies,R.A.Jr.(Ed.), Coastal Sedimentary Environments, Springer-Verlag, New York, 5-68.

Wright,L.D., Coleman,J.M. and Thom,B.G. 1973. Processes of channel developement in a high-tide range environment: Cambridge Gulf-Ord River Delta, Western Australia. J. Geol., 81, 15-41.

Wright,J.E., Hull,J.H., McQuillin,R. and Arnold,S.E. 1971. Irish Sea Investigations, 1969-1970. Institute of Geological Science Report No. 71/19.

Wright,L.D. and Sonu,C.J. 1975. Processes of sediment transport and tidal delta development in a stratified tidal inlet. In: Crinin,L.E. (ed.), Estuarine Research, Vol.2, Academic Press, New York, 63-76.

Yalin,M.W. 1963. An expression for bedload transportation.

Proc. Am. Soc. Civ. Eng., J. Hydraul. Div., HY 3, 221-250.

Yalin,M.W. 1972. Mechanics of sediment transport. Pergamon, Oxford, 290 pp.

Yang,C.S. 1986. On Bagnold's sediment transport equation in tidal marine environments and the practical definition of bedload. Sedimentology, 33, 465-486.

Zarillo, G. 1982. Stability of bedforms in a tidal environment. Mar. Geol., 48, 337-351.

APPENDIX

Sample no.	Mean Diameter (Ø)	Sorting (Ø)	Kurtosis	Skewness
E1	2.972	0.247	1.058	0.048
E2	3.109	0.276	0.957	0.147
E3	3.094	0.235	1.273	0.054
E4	3.113	0.263	1.095	0.156
E5	3.020	0.240	1.081	-0.054
E6	3.018	0.254	1.010	0.119
E7	3.325	0.313	1.055	0.360
E8	3.476	0.576	2.515	0.433
E101	3.524	1.436	2.572	0.666
E102	2.996	0.248	1.243	0.202
E103	3.403	0.936	2.457	0.473
E104	3.078	0.295	1.213	0.146
E105	3.112	0.236	1.446	0.070
E106	3.005	0.226	1.035	0.141
E107	3.039	0.230	1.121	-0.020
E108	3.032	0.237	1.117	-0.044
E109	3.012	0.243	1.081	0.064
E110	2.970	0.241	1.033	0.008
E111	2.995	0.226	1.055	0.021
E112	2.997	0.240	1.077	0.144
E113	3.088	0.275	1.330	0.024
E114	3.369	0.997	3.101	0.625
E115	3.101	0.338	1.647	0.319
E116	3.158	0.730	4.335	0.540

Table A1: Textural parameters of the estuarine samples along transect 1 and further upstream.

Sample no.	Mean Diameter (Ø)	Sorting (Ø)	Kurtosis	Skewness
E201	3.167	0.363	1.494	0.190
E202	3.210	0.433	1.705	0.408
E203	3.083	0.283	1.340	0.200
E204	3.003	0.248	1.159	0.028
E205	2.875	0.301	1.083	-0.068
E206	2.925	0.261	1.010	-0.015
E207	2.851	0.328	1.135	-0.139
E208	2.844	0.275	1.091	-0.093
E209	2.864	0.271	0.984	-0.044
E210	2.822	0.260	1.010	-0.017
E211	2.942	0.312	1.293	-0.028
E212	2.984	0.253	1.129	0.035
E213	2.869	0.361	1.255	-0.099
E214	3.005	0.250	1.114	-0.054
E215	3.029	0.248	1.164	-0.003
E216	3.063	0.298	1.248	0.137
E217	2.963	0.216	1.116	0.157
E218	2.975	0.245	1.124	0.152
E219	2.884	0.247	0.881	-0.004
E220	2.910	0.274	1.237	0.037
E221	2.880	0.253	0.898	0.016
E222	2.825	0.273	0.979	-0.013
E223	2.849	0.248	1.076	-0.041
E224	2.856	0.278	1.002	-0.091
E225	2.924	0.247	1.032	0.016
E226	3.161	0.433	2.030	0.410
E227	2.890	0.292	1.321	-0.030

Table A2: Textural parameters of the estuarine samples along transect 2.

Sample no.	Mean Diameter (Ø)	Sorting (Ø)	Kurtosis	Skewness
E301	3.282	0.934	3.710	0.600
E302	3.359	1.173	4.083	0.660
E303	3.012	0.281	1.159	0.151
E304	3.152	0.286	1.214	0.174
E305	2.746	0.392	1.020	-0.004
E306	2.987	0.232	1.092	0.105
E307	2.977	0.244	1.125	0.109
E308	2.911	0.272	1.221	0.005
E309	2.659	0.326	1.092	-0.060
E310	2.641	0.352	1.068	-0.106
E311	2.753	0.302	1.128	-0.213
E312	2.782	0.263	1.103	-0.144
E313	2.806	0.259	1.119	-0.109
E314	2.928	0.254	1.235	0.100
E315	2.752	0.303	1.096	-0.045
E316	2.826	0.303	1.013	-0.085
E317	2.745	0.314	1.103	-0.058
E318	2.727	0.305	1.097	-0.182
E319	2.732	0.271	1.052	0.009
E320	2.759	0.279	1.063	-0.138
E321	2.731	0.303	1.128	-0.205
E322	2.721	0.277	1.074	0.015
E323	2.749	0.271	1.046	0.061
E324	2.778	0.305	1.134	-0.172
E325	2.771	0.271	1.014	0.039
E326	2.764	0.270	1.035	-0.022
E327	2.780	0.263	1.039	-0.081

Table A3: Textural parameters of the estuarine samples along transect 3.

Sample no.	Mean Diameter (Ø)	Sorting (Ø)	Kurtosis	Skewness
E401	2.844	0.325	1.274	-0.025
E402	3.341	1.222	3.966	0.642
E403	2.849	0.315	1.053	-0.083
E404	2.866	0.337	1.171	0.000
E405	2.925	0.230	1.046	0.025
E406	2.897	0.305	1.240	-0.017
E407	2.857	0.270	1.071	-0.092
E408	2.823	0.283	1.042	-0.061
E409	2.783	0.288	1.065	-0.114
E410	2.754	0.314	1.111	-0.165
E411	2.817	0.277	1.001	-0.007
E412	2.828	0.272	1.028	-0.035
E413	2.739	0.290	1.014	0.039
E414	2.691	0.330	1.170	-0.112
E415	2.844	0.303	1.203	-0.060
E416	2.862	0.284	1.344	-0.069
E417	2.920	0.230	1.053	0.039
E418	2.965	0.241	1.132	0.117
E419	2.925	0.251	1.187	0.046
E420	2.895	0.231	1.038	-0.011
E421	2.764	0.295	1.027	-0.050
E422	2.788	0.253	1.122	-0.145
E423	2.703	0.311	1.107	-0.194

Table A4: Textural parameters of the estuarine samples along transect 4.

Sample no.	Mean Diameter (Ø)	Sorting (Ø)	Kurtosis	Skewness
E501	2.873	0.331	1.192	-0.004
E502	2.607	0.339	1.032	-0.035
E503	2.749	0.344	1.075	-0.033
E504	2.902	0.293	1.393	0.038
E505	2.861	0.268	0.950	-0.065
E506	2.679	0.340	1.214	-0.162
E507	2.533	0.416	1.274	-0.206
E508	2.763	0.277	1.010	0.010
E509	2.672	0.319	1.007	-0.087
E510	2.593	0.328	0.973	0.003
E511	2.614	0.306	0.971	-0.014
E512	2.609	0.313	0.963	-0.049
E513	2.668	0.278	0.982	-0.036
E514	2.592	0.294	0.963	-0.016
E515	2.496	0.302	1.005	0.021
E516	2.559	0.295	0.971	-0.016
E517	2.618	0.306	0.948	-0.062
E518	2.534	0.317	0.955	-0.027
E519	2.579	0.309	1.156	-0.041
E520	2.611	0.307	1.100	-0.030
E521	2.728	0.258	1.068	0.102
E522	2.580	0.328	0.959	-0.041

Table A5: Textural parameters of the estuarine samples along transect 5.

Sample	Mean Diameter (Ø)	Sorting (Ø)	Kurtosis	Skewness
E601	2.664	0.349	1.062	-0.196
E602	2.626	0.357	1.088	-0.100
E603	2.551	0.375	1.008	-0.112
E604	2.638	0.372	1.027	-0.178
E605	2.583	0.422	1.162	-0.200
E606	2.511	0.412	1.014	-0.112
E607	2.677	0.324	1.046	-0.146
E608	2.700	0.326	1.056	-0.206
E609	2.654	0.351	1.001	-0.069
E610	2.631	0.332	1.008	-0.147
E611	2.539	0.347	1.031	-0.177
E612	2.464	0.349	1.047	-0.088
E613	2.300	0.357	1.083	-0.051
E614	2.422	0.335	1.078	-0.046
E615	2.460	0.330	1.077	-0.050
E616	2.506	0.322	0.982	-0.029
E617	2.528	0.325	1.185	-0.186
E618	2.646	0.315	1.190	-0.082
E619	2.661	0.333	0.980	-0.135

Table A6: Textural parameters of the estuarine samples along transect 6.

Sample no.	Mean Diameter (Ø)	Sorting (Ø)	Kurtosis	Skewness
B1	2.356	0.699	1.726	-0.591
B2	2.419	0.548	1.372	-0.467
B3	2.008	1.228	0.789	-0.747
B4	2.692	0.295	1.234	-0.123
B5	2.788	0.295	1.105	-0.142
B6	2.658	0.321	1.140	-0.199
B7	2.590	0.335	1.032	-0.077
B8	2.512	0.335	1.027	-0.105
B9	2.542	0.294	0.977	-0.020
B10	2.714	0.267	1.031	-0.154
B11	2.682	0.301	1.053	-0.113
B12	2.664	0.268	1.125	-0.074
B13	2.681	0.327	1.184	-0.218
B14	2.677	0.286	1.046	-0.098
B15	2.242	0.413	0.884	0.013
B16	2.389	0.269	1.066	-0.018
B17	2.422	0.318	1.033	-0.030
B18	2.425	0.332	1.004	-0.039
B19	2.255	0.357	1.069	-0.092
B20	2.710	0.311	1.158	-0.170

Table A7: Textural parameters of the beach samples.

Sample no.	Mean Diameter (Ø)	Sorting (Ø)	Kurtosis	Skewness
NB1	2.633	0.356	1.336	-0.200
NB2	2.869	0.812	8.070	-0.460
NB3	2.784	0.837	5.777	-0.559
NB4	2.802	0.814	5.060	-0.522
NB5	2.765	0.783	4.835	-0.568
NB6	2.842	0.235	1.296	-0.108
NB7	2.423	0.324	1.154	-0.149
NB8	2.535	0.259	1.143	-0.175
NB9	2.538	0.279	1.095	-0.124
NB10	2.531	0.381	1.146	-0.184
NB11	2.540	0.338	1.046	-0.191
NB12	2.633	0.227	1.229	-0.006
NB13	2.816	0.247	1.241	-0.158
NB14	1.586	1.695	0.763	-0.802
NB15	2.689	0.597	3.106	-0.564
NB16	2.698	0.310	1.256	-0.239
NB17	2.623	0.283	0.960	-0.122

Table A8: Textural parameters of the northern beach samples.

Sample no.	Mean Diameter (Ø)	Sorting (Ø)	Kurtosis	Skewness
SB1	2.516	0.488	1.508	-0.360
SB2	2.686	0.408	1.808	-0.353
SB3	2.572	0.556	1.747	-0.448
SB4	2.492	0.573	1.579	-0.441
SB5	2.460	0.539	1.610	-0.426
SB6	2.362	0.573	1.326	-0.467
SB7	2.376	0.618	1.475	-0.498
SB8	1.601	0.928	0.711	+0.074
SB9	2.301	0.719	1.015	-0.498
SB10	2.054	0.729	0.858	-0.396
SB11	1.397	1.005	0.863	+0.232
SB12	2.319	0.504	1.118	-0.347
SB13	2.053	0.593	1.015	-0.172
SB14	2.192	0.493	1.035	-0.220
SB15	2.241	0.487	1.083	-0.277
SB16	2.094	0.514	0.979	-0.230
SB17	1.679	0.626	1.031	-0.051
SB18	2.079	0.402	0.900	-0.042
SB19	2.113	0.343	0.932	+0.066
SB20	2.290	0.293	0.942	-0.033
SB21	2.661	0.446	1.915	-0.316
SB22	2.652	0.300	1.257	-0.149
SB23	1.942	0.577	0.992	-0.163
SB24	1.459	0.750	1.110	-0.019
SB25	2.071	0.554	0.962	-0.206
SB26	2.323	0.387	0.993	-0.212
SB27	2.458	0.293	1.000	-0.132

Table A9: Textural parameters of the southern beach samples.

Sample no.	Mean Diameter (Ø)	Sorting (Ø)	Kurtosis	Skewness	Carbonate (%)
E105	3.112	0.256	1.146	0.127	3.64
E109	3.041	0.268	1.042	0.057	2.31
E115	3.066	0.260	1.184	0.162	2.91
E204	2.976	0.245	1.146	0.097	3.40
E208	2.818	0.266	1.099	-0.060	1.75
E216	2.981	0.242	1.198	0.204	6.75
E221	2.875	0.242	0.900	0.008	2.64
E227	2.873	0.286	1.262	-0.031	2.71
E304	3.061	0.258	1.104	0.220	7.47
E309	2.689	0.328	1.094	-0.113	1.80
E314	2.928	0.252	1.192	0.100	3.41
E320	2.773	0.274	1.088	-0.119	2.62
E326	2.709	0.273	1.008	-0.018	2.52
E402	2.928	0.283	1.099	0.136	7.23
E407	2.813	0.259	1.107	-0.103	4.48
E412	2.670	0.324	1.011	-0.035	4.63
E417	2.927	0.223	1.050	0.044	4.30
E422	2.786	0.252	1.107	-0.121	3.22
E502	2.613	0.334	1.091	-0.045	2.47
E507	2.562	0.391	1.171	-0.148	5.06
E515	2.501	0.295	0.991	0.033	2.14
E523	2.531	0.343	1.017	-0.006	1.29
E610	2.628	0.318	0.985	-0.116	5.20
E611	2.532	0.335	1.069	-0.140	3.34
E618	2.652	0.300	1.143	-0.043	4.18
E619	2.643	0.332	0.974	-0.088	3.47

Table A10: Textural parameters of HCl digested sediments.

Sample Station	Latitude N	Longitude W	Water Depth (Metres)
S1	52° 51.6′	04° 09.7′	12.0
S2	52.1	10.1	11.9
S3	52.9	11.1	17.9
S4	53.5	11.8	14.9
S5	54.1	12.6	10.9
S6	54.2	13.3	9.8
S7	53.3	12.5	19.7
S8	52.7	11.9	19.6
S9	51.8	11.0	19.5
S10	51.0	10.2	11.4
S11	50.6	10.7	14.2
S12	51.6	11.7	19.0
S13	52.5	12.7	18.7
S14	53.1	13.2	18.5
S15	54.1	15.2	18.3
S16	53.7	15.2	18.2
S17	52.0	14.1	18.1
S18	52.2	13.6	19.9
S19	51.2	12.7	17.8
S20	50.2	11.7	18.7
S21	49.9	12.3	18.7
S22	50.8	13.2	17.6
S23	51.7	14.2	19.6
S24	52.6	14.9	18.6
S25	53.5	15.7	18.6

Table A11: The position of sampling stations and the depth of water at each position.

Sample Station	Mean Diameter (Ø)	Sorting (Ø)	Skewness	Kurtosis	Mud (%)
S1	3.214	1.447	0.561	6.540	9.28
S2	4.852	2.719	0.874	5.766	22.41
S3	4.939	2.723	0.865	5.458	24.13
S4	5.030	2.783	0.860	5.715	23.38
S5	4.204	2.115	0.849	6.783	18.35
S6	4.503	2.272	0.856	6.912	18.49
S7	5.721	3.100	0.870	1.055	37.45
S8	5.503	3.975	0.893	1.383	30.35
S9	5.500	3.102	0.885	1.068	32.22
S10	2.992	0.254	0.029	1.115	0.29
S11	2.923	0.241	0.071	1.178	0.20
S12	5.154	2.743	0.881	1.845	28.04
S13	5.567	2.951	0.891	1.061	37.81
S14	5.682	2.932	0.875	1.055	40.29
S15	5.129	2.642	0.889	4.586	25.23
S16	5.253	2.612	0.859	2.126	30.33
S17	5.847	3.010	0.876	0.944	48.33
S18	5.900	3.068	0.881	1.024	44.93
S19	5.431	2.938	0.903	1.820	27.96
S20	3.014	0.266	0.000	1.080	0.28
S21	2.978	0.232	0.116	1.129	0.21
S22	4.676	2.346	0.868	6.283	22.46
S23	6.326	3.068	0.703	0.943	59.06
S24	6.129	3.065	0.750	0.905	54.78
S25	6.085	3.145	0.835	0.855	51.11

Table A12: The values of textural parameters of seabed sediments and the percentage of mud for each samples.

Sample no.	0.090 - 0.212 mm			0.212 - 0.425 mm		
	Quartz	Lithic	CaCO3	Quartz	Lithic	CaCO3
S1	88	8	4	37	10	53
S5	86	9	5	5	4	91
S15	87	7	6	0	3	97
S20	89	7	4	51	10	39
NB2	89	8	3	70	8	20
NB6	93	7	0	81	12	7
SB1	91	7	2	82	11	7
SB5	92	8	0	84	11	5
B15	91	9	0	83	13	4
B20	89	11	1	81	8	11
E3	91	8	1	40	51	9
E5	93	6	1	58	38	4
E7	92	7	1	15	75	10
E109	86	13	1	68	11	21
E213	90	8	2	75	10	15
E319	90	9	1	84	9	7
E408	83	15	2	81	9	10
E507	89	11	0	82	12	6
E514	90	8	2	84	9	7
E610	93	6	1	77	10	13
R1	59	41	0	4	96	0
R2	54	46	0	7	93	0
R3	73	27	0	3	97	0
R4	67	33	0	4	96	0
R5	27	73	0	11	89	0
R6	30	70	0	8	92	0
R7	22	78	0	5	95	0
R8	29	71	0	10	90	0

Table A13: Percentage of quartz, lithic, and carbonate grains in estuarine, beach, seabed, and river samples two grain size ranges.